ADVANCES IN NUCLEAR PHYSICS

VOLUME 1

Contributors to this Volume

Jorrit de Boer
Department of Physics
Rutgers, The State University
New Brunswick, New Jersey

Ian Duck
Department of Physics
Rice University
Houston, Texas

Jörg Eichler
Hahn-Meitner Institut für Kernforschung
Berlin, Germany

Malcolm Harvey
Theoretical Physics
Chalk River Nuclear Laboratories
Chalk River, Ontario, Canada

Georges Ripka
Service de Physique Théorique
Centre d'Etudes Nucléaires de Saclay
France

Erich Vogt
Department of Physics
University of British Columbia
Vancouver, B. C., Canada

ADVANCES IN NUCLEAR PHYSICS

Edited by
Michel Baranger
Department of Physics
Carnegie Institute of Technology
Pittsburgh, Pennsylvania

Erich Vogt
Department of Physics
University of British Columbia
Vancouver, B.C., Canada

VOLUME 1

PLENUM PRESS • NEW YORK • 1968

ISBN 978-1-4757-0105-0 ISBN 978-1-4757-0103-6 (eBook)
DOI 10.1007/978-1-4757-0103-6

Library of Congress Catalog Card Number 67-29001

© 1968 Plenum Press

Softcover reprint of the hardcover 1st edition 1968

A Division of Plenum Publishing Corporation
227 West 17 Street, New York, N. Y. 10011

All rights reserved

No part of this publication may be reproduced in any form without
written permission from the publisher

ARTICLES PLANNED FOR FUTURE VOLUMES

Nuclear Reactions with Polarized Beams
C. Glashausser and J. Thirion

The Two-Nucleon Potential
P. S. Signell

The Giant Dipole Resonance
B. M. Spicer

The Pairing-Plus-Quadrupole Model
D. R. Bès and R. A. Sorensen

Muonic X-Rays
S. Devons and I. Duerdoth

The Interaction of Pions with Nuclei
D. S. Koltun

In-Beam Spectroscopy with Heavy Ions
R. M. Diamond and F. S. Stephens

Shell Model Calculations with Realistic Nuclear Forces
E. C. Halbert and T. T. S. Kuo

The *j*-Dependence of Stripping Reactions
C. Mayer-Böricke

Nuclear Physics with Li-Drifted Detectors
G. T. Ewan and A. E. Litherland

PREFACE

The aim of *Advances in Nuclear Physics* is to provide review papers which chart the field of nuclear physics with some regularity and completeness. We define the field of nuclear physics as that which deals with the structure and behavior of atomic nuclei. Although many good books and reviews on nuclear physics are available, none attempts to provide a coverage which is at the same time continuing and reasonably complete. Many people have felt the need for a new series to fill this gap and this is the ambition of *Advances in Nuclear Physics*. The articles will be aimed at a wide audience, from research students to active research workers. The selection of topics and their treatment will be varied but the basic viewpoint will be pedagogical.

In the past two decades the field of nuclear physics has achieved its own identity, occupying a central position between elementary particle physics on one side and atomic and solid state physics on the other. Nuclear physics is remarkable both by its unity, which it derives from its concise boundaries, and by its amazing diversity, which stems from the multiplicity of experimental approaches and from the complexity of the nucleon–nucleon force. Physicists specializing in one aspect of this strongly unified, yet very complex, field find it imperative to stay well-informed of the other aspects. This provides a strong motivation for a comprehensive series of reviews. Additional motivation arises from outside the community of nuclear physicists, through the inevitable occurrence of the nucleus as an accessory or as a tool in other fields of physics, and through its importance for terrestrial and stellar energy sources.

We hope to provide a varied selection of reviews in nuclear physics with a varied approach. The topics chosen will range over the field, the emphasis being on physics rather than on theoretical or experimental techniques. Some effort will be made to include regularly topics of great current interest which need to be made accessible by adequate reviews. Other reviews will attempt to bring older topics into clearer focus. The aim will be to attract the interest of both the active research worker and the research student. Authors will be asked to direct their article toward the maximum number of readers by separating clearly the technical material from the more basic

aspects of the subject and by adopting a pedagogical point of view rather than giving a simple recital of recent results.

Initially, the *Advances* are scheduled to appear about once a year with approximately six articles per volume. To ensure rapid publication of the papers, we shall use the "stream" technique, successfully employed for series in other fields. A considerable number of planned future articles constitute the source of the stream. The flow of articles from the source takes place primarily to suit the convenience of the authors, rather than to include any particular subset of articles in a given volume. Any attempt at a systematic classification of the reviews would result in considerable publication delays. Instead, each volume is published as soon as an appropriate number of articles have been completed; but some effort is made to achieve simultaneity, so that the spread in completion dates of the articles in a given volume is much less than the interval between volumes.

A list of articles planned for future volumes is given on page v. The prospective articles together with those in this first volume still fall far short of our long-range aims for coverage of the field of nuclear physics. In particular, we definitely intend to present more articles on experimental topics. We shall eagerly receive and discuss outside suggestions of topics for additional papers, and especially suggestions of suitable authors to write them.

The editors owe a great deal to the authors of the present volume for their cooperation in its rapid completion, and to many colleagues who have already given advice about the series. In embarking on this venture, we have had the support of Plenum Press, a relatively new publisher in the field of physics, and of its vice-president, Alan Liss, who has an almost unmatched background in physics publications.

M. Baranger
E. Vogt

October 15, 1967

CONTENTS

Chapter 1

THE REORIENTATION EFFECT

Jorrit de Boer and Jörg Eichler

1. Introduction 1
2. Classical Estimates of Effects 3
   2.1 External Field Gradients 4
   2.2 Electronic Field Gradient 4
   2.3 Muonic X Rays 4
   2.4 Coulomb Excitation 5
3. Theory of Coulomb Excitation 5
   3.1 Approximations 6
   3.2 First-Order Perturbation Theory 6
   3.3 Second-Order Perturbation Theory as a Guide to the Exact Solution 9
   3.4 Symmetrization of the Excitation Process 13
4. Theory of the Reorientation Effect 14
   4.1 The Amplitude for the Excitation $0^+ \rightarrow 2^+$ 14
   4.2 The Excitation Probability 15
   4.3 The Angular Distribution of the De-excitation Gamma Rays 16
   4.4 Magnetic Dipole Reorientation 19
   4.5 Corrections for Multiple $E2$ Transitions 20
5. Excitation via the Giant Dipole Resonance 21
   5.1 The Transition Probability 22
   5.2 Interpretation as Polarization Effect 24
6. Experimental Methods 28
   6.1 Bombarding Conditions 28
   6.2 Measurement of Cross Sections 32
   6.3 Measurement of the Gamma-Ray Angular Distribution . 39
   6.4 Measurement of the Excitation of the Projectile 43

7. Reorientation Experiments 44
7.1 Experimental Methods Used 44
7.2 Results 46
7.3 Discussion 48
Acknowledgments 49
Appendix I. Numerical Expressions 49
Appendix II. Tables of Orbital Integrals 51
Appendix III. Approximate Formula for the Reorientation Effect. 51
References 64

Chapter 2

THE NUCLEAR SU_3 MODEL

Malcolm Harvey

1. Introduction 67
2. Basic Shell Model 69
2.1 General Theory 69
2.2 Invariance Properties 73
2.3 Approximate- and Broken-Symmetry Groups 76
2.4 Rotational Features in the $1p$ Shell 77
3. Symmetry of Oscillator Quanta — The Groups U_3 and SU_3 . . 79
3.1 Problems 79
3.2 Formal Properties of U_3 and SU_3 79
3.3 Classification According to U_3 and SU_3 83
3.4 Simultaneous Classification According to S_A and SU_3 . . 85
3.5 Classification According to SU_3 and R_3. 89
3.6 Classification According to SU_3 and $SU_2 \times U_1$ 90
3.7 Construction of States Classified According to SU_3 and R_3 94
4. The Effective Interaction 99
4.1 General Principles 99
4.2 The Quadrupole-Quadrupole Force 100
4.3 The Casimir Operator of SU_3 103
5. Application of the SU_3-Coupling Scheme to Light Nuclei . . . 105
5.1 General Remarks 105
5.2 Accuracy of the SU_3 Classification Scheme in the ($2s$, $1d$) Shell 106
5.3 Positive-Parity States of Doubly Even Nuclei in the ($2s$, $1d$) Shell 109

5.4 Positive-Parity States of Odd A and Doubly Odd Nuclei in the $(2s, 1d)$ Shell 123
5.5 Negative-Parity States in the $(2s, 1d)$ Shell 128
5.6 Multi-Excitation States in the $(2s, 1d)$ Shell 139
5.7 Multi-Excitation States in the $1p$ Shell 142

6. Summary and Developments 142

Acknowledgments 148

References 148

Appendix A. Harmonic Oscillator 152

Appendix B. Use of Groups in Quantum Mechanics 154

Appendix C. The Symmetric and Unitary Groups 157

Appendix D. Generating Operators of U_s 162

Appendix E. Classification According to SU_3 without the Harmonic Oscillator 165

Appendix F. Raising and Lowering Operators of the Group SU_3 . 166

Appendix G. Calculation of Matrix Elements 170

Appendix H. The Normalization Coefficients and Overlaps . . . 177

Appendix I. Use of the Group SU_3 in the Classification of Elementary Particles 180

Chapter 3

THE HARTREE–FOCK THEORY OF DEFORMED LIGHT NUCLEI

Georges Ripka

1. Introduction 183

2. The Hartree–Fock Equations 187

3. Symmetries of the Hartree–Fock Hamiltonian 189
3.1 Time-Reversal Symmetry 190
3.2 Parity and Axial Symmetry 191
3.3 Isospin Invariance 191
3.4 Spherical Symmetry 191
3.5 Spin and Isospin Invariance 192

4. The Choice of an Expansion for the Orbits 192
4.1 Spherical Symmetry 194
4.2 Axial Symmetry 194

4.3 Ellipsoidal Symmetry 194
4.4 Time-Reversal and Mixed-Parity Solutions 195
5. Single Major Shell Hartree–Fock Calculations 196
5.1 Spherical Solutions 196
5.2 The Use of a Reference Closed-Shell Nucleus 197
5.3 The Choice of the Interaction Strength, of the Single-Particle Energies, and of the Oscillator Constant 199
6. Solutions of the Single Major-Shell Hartree–Fock Calculations for Even–Even $N = Z$ Nuclei 203
6.1 Spherical Solutions 203
6.2 Axially Symmetric Solutions 206
6.3 Ellipsoidal Solutions 206
6.4 The Energy Gap and the Spectrum of the Hartree–Fock Orbits 207
7. Deformed Excited Equilibrium States of Spherical Nuclei . . . 210
8. A Soluble Model—The Effect of the Exchange Components of the Interaction. 213
9. The Deformation of the Hartree–Fock Field—The Quadrupole–Quadrupole Interaction 216
10. The Effect of the Spin–Orbit Splitting 224
11. The Multiplicity of Hartree–Fock Solutions 227
12. Hartree–Fock Solutions of Other Nuclei 230
13. Magnetic Moments of Odd-A Nuclei 233
14. Angular Momentum Projection 235
15. Major-Shell-Mixing Hartree–Fock Calculations—Quadrupole Polarization of Closed Shells 244
16. Conclusion 256
Acknowledgments 257
References 257

Chapter 4

THE STATISTICAL THEORY OF NUCLEAR REACTIONS

Erich Vogt

1. Introduction 261
1.1 Early Evaporation Models 262
1.2 Refinement of the Early Evaporation Models 268

2. The Model for Average Cross Sections 270
2.1 Basic Evaporation Theory 270
2.2 Extension of the Model to Differential Cross Sections . . 275
2.3 Behavior of Transmission Functions 281
3. Application of the Evaporation Model 296
3.1 Inelastic Neutron Scattering at Low Energies 297
3.2 The $C^{12} + C^{12}$ Reactions 302
3.3 Evaporation Model with Level Densities 313
3.4 The Range of Recent Applications 318
4. Basis of the Evaporation Model in Reaction Theory 321
5. Conclusions 332
Acknowledgments 333
Appendix A. Absorption Cross Section of a Complex Square Well 334
Appendix B. Effect of Finite Averaging Interval 337
References 339

Chapter 5

THREE-PARTICLE SCATTERING— A REVIEW OF RECENT WORK ON THE NONRELATIVISTIC THEORY

Ian Duck

1. Introduction 343
1.1 Resumé of Two-Particle Scattering Theory 344
1.2 Difficulties in Three-Particle Scattering Theory 355
2. The Amado Model 357
2.1 Construction of the Model 357
2.2 Nucleon–Deuteron Elastic Scattering 367
2.3 Nucleon–Deuteron Inelastic Scattering 372
3. The Faddeév Equations 378
3.1 Rearrangement Scattering 378
3.2 The Faddeév Equations 382
4. Application of the Faddeév Equations 388
4.1 Hetherington–Schick Analysis of the Multiple-Scattering Series 388
4.2 Lovelace–Phillips' Calculations of Neutron–Deuteron Scattering 390

4.3 Relativistic Faddeév Equations 391
4.4 Three-Particle Correlation Energy in Nuclear Matter . . 394
5. Concluding Remarks 396
Acknowledgments 397
References 397
Appendix A 400
Appendix B 401
Appendix C 405
Appendix D 406
Appendix E 409

INDEX 411

THE REORIENTATION EFFECT*

Jorrit de Boer and Jörg Eichler

ABSTRACT

The reorientation effect in Coulomb excitation is discussed as a tool to measure static quadrupole moments in excited nuclear states. Since the electromagnetic field produced in a Coulomb excitation is well known, the method is free from the ambiguities inherent in methods employing the fields produced by the atomic electrons. In order to furnish a basis for the interpretation of experiments an outline of the theory is given in the framework of a perturbation expansion. Even if the assumptions underlying the perturbation approach are not strictly satisfied, the explicit nature of its solutions provides an indispensable guide for designing an experiment. For the actual evaluation one has to utilize the numerical solution obtained from a direct treatment of the time-dependent Schrödinger equation. Some care is devoted to the discussion of other effects which might contribute to the excitation and thus affect the measurement of the quadrupole moment. Both magnetic dipole reorientation and excitation via the giant dipole resonance turn out to be innocuous within present experimental accuracies. Various possible experiments and experimental techniques are treated in some detail, and the results obtained so far are presented and discussed. The appendix aims to facilitate the planning of experiments by compiling numerical formulas, tables, and graphs.

1. INTRODUCTION

Among the electromagnetic properties of nuclei the static electric quadrupole moment plays a particularly significant role since it gives very direct information on the nuclear shape, which in turn may be used to discriminate among nuclear models.

The usual way to measure a nuclear quadrupole moment employs its interaction with an electric field gradient. Most experiments determine the

* Research supported in part by the National Science Foundation.

interaction energy, i.e., the product of the quadrupole moment and the electric field gradient, and therefore an independent knowledge of the latter is required. There are various ways of producing an electric field gradient at the nuclear site: (a) by external field, (b) by the electrons of the atomic or molecular environment, (c) by other charged particles such as muons or kaons in bound orbits, and (d) by bombarding the target nucleus with energetic ions.

The last method is a scattering process in which the time-dependent interaction gives rise to transitions between the nuclear levels. If the minimum distance between the projectile and the target nucleus is large enough to exclude nuclear reactions, only the electromagnetic interaction will give rise to excitations of nuclear levels. The dependence of this excitation process on the static nuclear moments is called the *reorientation effect* and is the subject of the present article.

The reorientation effect has recently become an important tool for measuring the static quadrupole moments of excited nuclear states. In particular, it has led to the striking discovery of the large quadrupole moments of some "one-phonon" states in vibrational nuclei.

The effects of the static nuclear quadrupole moments on the cross sections for Coulomb excitation and on the particle and gamma-ray angular distributions were first recognized by Breit and his collaborators.[1] These authors estimated the magnitude of the reorientation effect and pointed out that it might be of measurable size in the Coulomb excitation by heavy ions. More specific calculations[2–5] dealt with the conditions necessary to distinguish experimentally the reorientation effect from other higher-order effects which erroneously might be attributed to a static quadrupole moment. The first experimental indications of the reorientation effect were obtained in the Coulomb excitation of ^{76}Se and ^{78}Se[5] and in ^{152}Sm.[6] A more accurate verification of the effect and the actual determination of quadrupole moments were later achieved by several groups.[7–14] These experiments dealt mainly with nuclei belonging to the vibrational region.

To get some feeling for the order of magnitude of the effects which play a role in the determination of nuclear quadrupole moments, some simple estimates will first be presented. They indicate that, for Coulomb excitation processes with heavy projectiles, the cross sections and gamma-ray angular distributions may depend to a measurable degree on the static quadrupole moments of nuclear levels. Quantitative calculations are then performed using second-order perturbation theory for the excitation process. The results of these calculations are used to find the most favorable experimental conditions for reorientation experiments as well as the size of competing effects which may obscure the reorientation effect. The experimental methods (some of them have actually been used, while others are merely proposed)

are discussed in detail and the results obtained so far are summarized. The numerical formulas and tables given in the appendix should make it easy for the experimenter to determine quickly the size of effects to be expected in a given case.

2. CLASSICAL ESTIMATES OF EFFECTS

Some of the features which are important for the measurement of nuclear electric quadrupole moments can be visualized classically. A few estimates and comparisons based on classical concepts are given below for the methods mentioned under (a) to (d) in the introduction.

The quadrupole moment Q of a charge distribution $\rho(\mathbf{r})$ which is symmetric around the z axis is defined as

$$eQ \equiv \int \rho(\mathbf{r})(3z^2 - r^2)\, d^3r \tag{1}$$

where e is the electron charge. This definition leads to positive Q for prolate and negative Q for oblate shapes. The deformation parameter β of a spheroid may be defined by

$$\beta = \frac{4}{3}\left(\frac{\pi}{5}\right)^{1/2} \frac{\Delta R}{R_0} = 1.06\,\frac{\Delta R}{R_0} \tag{2}$$

where R_0 is the mean radius and ΔR is the difference between the major and minor semiaxes of the spheroid. To first order in β, the quadrupole moment of a uniformly charged spheroid may be written as

$$Q = 3(5\pi)^{-1/2}\, Z_2 R_0^2 \beta = 0.76 Z_2 R_0^2 \beta \tag{3}$$

where Z_2 is the charge number of the spheroid. For spheroidal nuclei deviating about 10% from spherical symmetry and having $Z_2 \approx 50$, values for Q in the neighborhood of 1 barn (b $= 10^{-24}$ cm^2) are thus expected.

The orientation energy of a spheroid exposed to a constant electric field gradient dE/dx (i.e., the difference in energy for orientations with the symmetry axis parallel and perpendicular to the field gradient) is given by

$$E_Q = \frac{1}{4}\, eQ \frac{dE}{dx} \tag{4}$$

If the field gradient is produced by a point charge eZ_1 at a distance d, E_Q is given by

$$E_Q(d)_{[\mathrm{eV}]} = 0.72 \times 10^8\, \frac{Z_1 Q_{[\mathrm{barn}]}}{d^3_{[\mathrm{fermi}]}} \tag{5}$$

The orders of magnitude of the orientation energies for the field gradients mentioned in the introduction will be estimated in the following subsections.

2.1 External Field Gradients

For charge distributions of nuclear dimensions the field gradients that may be produced by external electrodes are too small to yield values of E_Q which are accessible to measurement. The highest values of dE/dx produced in the laboratory[15] are of the order of 10^{+14} V/cm^2 giving rise to an orientation energy $E_Q \approx 10^{-11}$ eV for $Q = 1$ barn.

2.2 Electronic Field Gradients

For the field gradients produced at the nuclear site by the atomic or molecular charges $d \approx 1$Å and $E_Q \approx 10^{-7}$ eV for $Q = 1$ barn. (In noncubic crystals the polarization of the electronic distribution may enhance E_Q by a factor of 10 to 100.) Energy differences of this order of magnitude are measured in the hyperfine splitting of atomic transitions and by the Mössbauer effect of low-energy gamma transitions.

Another effect produced by the interaction of the nuclear quadrupole moment with the electronic field gradient is the attenuation of angular distributions in gamma–gamma angular correlations. The attenuation is, in this case, due to the random change in the nuclear orientation (precession) which takes place during the lifetime τ of the intermediate state in the gamma–gamma cascade. Effects of this type are observed only for lifetimes τ long enough to allow appreciable precession angles; i.e., $\tau \gtrsim \hbar/E_Q \approx 10^{-9}$ sec. (In noncubic crystals attenuation effects have been observed for $\tau \approx 10^{-10}$ sec.[16])

In both types of measurement the determination of Q rests on the knowledge of a field gradient, the calculation of which is based on assumptions about the electronic environment of the nucleus. The accuracy of the determination of Q is therefore limited by the accuracy with which this field gradient can be calculated.

2.3 Muonic X Rays

The charge distributions of muonic atoms produce field gradients which are larger than the corresponding electronic ones by a factor $(m_\mu/m_e)^3$, where m_μ and m_e are muon and electron masses, respectively. The "hyperfine" interaction caused by mu mesons moving in orbits of nuclear dimensions ($d \approx 10^{-12}$ cm) gives rise to energy shifts $E_Q^{(\mu)} \approx 0.1$ MeV which are comparable to the excitation energies ΔE of low-lying nuclear levels. The muonic and nuclear states and therefore strongly mixed. The complex muonic spectra can, however, be evaluated in terms of parameters including the nuclear quadrupole moments and a determination of Q may thus be achieved.[17–19]

2.4 Coulomb Excitation

In Coulomb excitation a projectile with charge number Z_1 moving on a hyperbolic orbit past the nucleus produces a time-dependent field gradient at the nuclear site. The maximum interaction energy $E_Q^{(\max)}$ may again be given by Eq. (5) if d is now interpreted as the distance of closest approach. For the example of a head-on collision between an oxygen ion of 40 MeV and a Cd nucleus, $d = 16$ fm and $E_Q^{(\max)} \approx 0.15$ MeV for $Q = 1$ barn. $E_Q^{(\max)}$ and $E_Q^{(\mu)}$ are thus of the same order of magnitude.

The time-dependent interaction causes transitions from the nuclear ground state into the excited states. The transition amplitudes for these excitations are of the order of $b \approx E_Q^{(\max)} \times \tau_{\text{coll}}/\hbar$ if the duration of the collision, $\tau_{\text{coll}} \approx d/v_\infty$, is short compared with the characteristic nuclear time $\tau_{\text{nucl}} = \hbar/\Delta E$. Here v_∞ denotes the initial velocity of the projectile and ΔE is the excitation energy of the nucleus. For the above example (40 MeV ^{16}O onto ^{114}Cd), τ_{coll} is of the order of 10^{-21} sec and the transition amplitude becomes $b \approx 0.2$, which yields a probability for excitation of about 5%.

In a first-order perturbation treatment of the electric quadrupole Coulomb excitation the transition amplitudes are proportional to the matrix elements of the electric quadrupole operator between the ground state and the excited states. In the second-order perturbation, however, the excitation amplitudes contain matrix elements between the excited states including, in particular, the diagonal elements which are proportional to the static quadrupole moments.

If, as in the above example, the transition amplitudes are not too small, these second-order contributions to the excitation may become measurable. For bombarding conditions in which only a limited number of nuclear matrix elements enter into the calculation of the measured quantities in an appreciable way, a detailed experimental study of the excitation process may yield a set of model-independent values for these matrix elements. In particular, the static electric quadrupole moment of an excited state may be determined in even–even nuclei which have no quadrupole moment in their ground state. Furthermore, the strong time-dependent field inflicted by the projectile is a well-known quantity which is free of the uncertainties in the electronic structure.

3. THEORY OF COULOMB EXCITATION

The reorientation effect is most conveniently explained in terms of a perturbation treatment of Coulomb excitation. Therefore it will be necessary to give a brief review of the theory, starting with the first order and subsequently proceeding to the second-order perturbation theory, as a guide to a more exact treatment.

3.1 Approximations

The most important approximation entering into the conventional theory of Coulomb excitation is the classical description of the projectile orbit.[20] In this approximation the electromagnetic transition in the target nucleus is induced by the time-dependent electromagnetic field of a point charge moving along a hyperbolic trajectory. This semiclassical picture is justified (a) if the particle can be described by a wave packet whose dimensions are small compared with the distance of closest approach and (b) if the energy loss of the impinging particle is small compared with the bombarding energy.

A measure for the accuracy with which condition (a) is fulfilled is provided by the parameter η, defined as the ratio of half the distance of closest approach in a head-on collision a to the de Broglie wavelength $\lambda\!\!\!^{-}$ of the projectile at infinity,

$$\eta = \frac{a}{\lambda\!\!\!^{-}} = \frac{Z_1 Z_2 e^2}{\hbar v_\infty} \tag{6}$$

where Z_1 and Z_2 are the charge numbers of the projectile and the target nucleus, respectively, and v_∞ is the asymptotic velocity of the incident particle. According to condition (a) the semiclassical approximation is justified if $\eta \gg 1$. In practice this is well fulfilled if the projectile is a heavy ion with a typical experimentally available energy (see Section 6.1.2). The strong repulsive Coulomb interaction between projectile and target nucleus implied by the condition $\eta \gg 1$ then also guarantees that the projectile will not penetrate into the target nucleus. The resulting elimination of all interactions other than electromagnetic ones is the main advantage of Coulomb excitation as a tool for nuclear spectroscopy.

In most of the present discussion we shall confine ourselves to electric quadrupole transitions in the target nucleus, since higher multipoles are much less important and magnetic transition amplitudes are hindered by a factor v/c compared with electric transitions of the same multipole order. The effects of the excitation of the projectile on the excitation of the target nucleus can also be neglected.

3.2 First-Order Perturbation Theory

Under the conditions given in the preceding subsection the angular distribution of the elastically scattered projectiles is given by the classical Rutherford expression

$$d\sigma_R = \frac{1}{4} a^2 \left(\sin \frac{\theta}{2}\right)^{-4} d\Omega \tag{7}$$

A numerical expression for a is given in the appendix.

If during the collision the target nucleus is excited from the ground state $|i\rangle$ to the final state $|f\rangle$, one has to multiply $d\sigma_R$ by the probability $P_{i\to f}$ for this process to get the cross section for Coulomb excitation[21]

$$d\sigma_f = P_{i\to f}\, d\sigma_R \tag{8}$$

The probability $P_{i\to f}$ for the excitation is given by

$$P_{i\to f} = (2I_i + 1)^{-1} \sum_{M_i M_f} |\, b_{if}\,|^2 \tag{9}$$

For small excitation probabilities the transition amplitude b_{if} may be calculated by first-order perturbation theory as

$$b_{if}^{(1)} = (i\hbar)^{-1} \int_{-\infty}^{+\infty} \langle f |\, H_{\text{int}}(t) |\, i\rangle\, e^{(i/\hbar)(E_f - E_i)t}\, dt \tag{10}$$

where $H_{\text{int}}(t)$ denotes the time-dependent electromagnetic interaction which causes the transition.

Since the monopole–monopole interaction between the charged particles is already accounted for by the prescribed motion along a classical Rutherford orbit and since, furthermore, we are not interested in the excitation of the projectile, we are justified in retaining only the monopole–multipole interaction in a multipole expansion of $H_{\text{int}}(t)$.

For an electric multipole transitton of order λ we can separate the transition amplitude into a nuclear part and an orbital part in the following way:

$$b_{if}^{(1)} = (-i)(-1)^{I_i - M_i}(2I_i + 1)^{1/2} \chi_{i\to f}^{(\lambda)} \sum_{\mu} \begin{pmatrix} I_i & \lambda & I_f \\ -M_i & \mu & M_f \end{pmatrix} \mathscr{K}_{\lambda\mu}(\theta, \xi) \tag{11}$$

The strength of the $E\lambda$ transition in the target nucleus is measured by the dimensionless real quantity[22]

$$\chi_{i\to f}^{(\lambda)} = (16\pi)^{1/2} \frac{(\lambda + 1)!}{(2\lambda + 1)!!} \frac{Z_1 e}{\hbar v_\infty} \frac{\langle I_i \,\|\mathscr{M}(E\lambda)\|\, I_f\rangle}{a^\lambda \sqrt{2I_i + 1}} \tag{12}$$

where

$$\begin{aligned} &\langle I_i \,\|\, \mathscr{M}(E\lambda)\|\, I_f\rangle \\ &\quad = (-1)^{I_i - M_i} \begin{pmatrix} I_i & \lambda & I_f \\ -M_i & \mu & M_f \end{pmatrix}^{-1} \langle I_i M_i \,|\, \mathscr{M}(E\lambda, \mu) |\, I_f M_f\rangle \\ &\quad = (-1)^{I_i - M_i} \begin{pmatrix} I_i & \lambda & I_f \\ -M_i & \mu & M_f \end{pmatrix}^{-1} \left\langle I_i M_i \,\middle|\, \int r^\lambda Y_{\lambda\mu}(\Omega)\, \rho(\mathbf{r})\, d^3\mathbf{r} \,\middle|\, I_f M_f \right\rangle \end{aligned} \tag{13}$$

is the reduced nuclear 2^λ-pole matrix element, $\rho(\mathbf{r})$ is the charge density, and the connection with the conventional $B(E\lambda)$ value is given by

$$B(E\lambda, I_i \to I_f) = (2I_i + 1)^{-1} \, |\langle I_i \| \mathscr{M}(E\lambda) \| I_f \rangle|^2 \tag{14}$$

The dependence of the nuclear transition on the parameters of the projectile orbit is contained in the real quantity

$$\mathscr{K}_{\lambda\mu}(\theta, \xi) = \sqrt{\pi} \, \frac{(2\lambda - 1)!!}{(\lambda - 1)!} \, Y_{\lambda\mu}\left(\frac{\pi}{2}, 0\right) I_{\lambda\mu}(\theta, \xi) \tag{15}$$

where

$$Y_{\lambda\mu}\left(\frac{\pi}{2}, 0\right) = \begin{cases} \left(\dfrac{2\lambda + 1}{4\pi}\right)^{1/2} \dfrac{\sqrt{(\lambda - \mu)! \, (\lambda + \mu)!}}{(\lambda - \mu)!! \, (\lambda + \mu)!!} (-1)^{\frac{\lambda+\mu}{2}} & \text{if } (\lambda + \mu) \text{ even} \\ 0 & \text{if } (\lambda + \mu) \text{ odd} \end{cases} \tag{16}$$

and $I_{\lambda\mu}(\theta, \xi)$ is the conventional orbital integral defined by Alder *et al.*[21] and tabulated in References 21 and 23. The orbital integrals depend on the scattering angle θ and on the excitation energy $\Delta E = E_f - E_i$ through the parameter ξ defined by

$$\xi = \xi_{if} = \frac{E_f - E_i}{\hbar} \frac{a}{v_\infty} \tag{17}$$

The adiabaticity parameter ξ gives the ratio between the collision time $\tau_{\text{coll}} = a/v$ and the period of the nuclear transition $\tau_{\text{nucl}} = \hbar/\Delta E$. For $\xi = 0$ the process can be considered a sudden impact, while for $\xi \gg 1$ the process becomes adiabatic so that no excitation occurs. The orbital integrals $I_{\lambda\mu}(\theta, \xi)$ are maximal for $\xi \approx 0$ and vanish exponentially like $\exp[-\xi/\sin(\theta/2)]$ for large ξ. It should be noted that a classical description would require $\xi = 0$. It has been shown,[21,24] however, that the correct quantum mechanical results can be well reproduced in a classical treatment by using orbital parameters a_{if} and ξ_{if} which are symmetrized with respect to the initial and final states. The resulting changes will be discussed in Section 3.4.

In writing Eq. (15) we have adopted the focal coordinate system[21] illustrated in Fig. 1.

From Eqs. (9), (11), and (15) we get the following expression for the excitation probability of multipole order λ

$$P_{i\to f} = [\chi^{(\lambda)}_{i\to f}]^2 \, (2\lambda + 1)^{-1} \sum_\mu [\mathscr{K}_{\lambda\mu}(\theta, \xi)]^2 \tag{18}$$

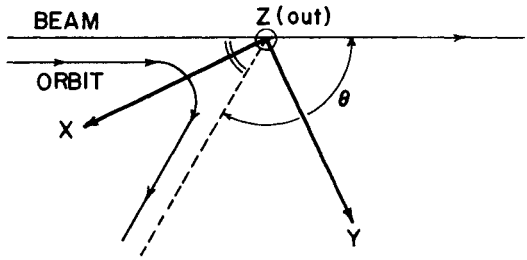

Fig. 1. The focal coordinate system, in which the x axis bisects the angle between the asymptotes of the orbit. The y axis lies in the reaction plane and points in the direction in which the projectile moves when it is closest to the target nucleus.

For a given nuclear transition the excitation probability attains a maximum for $\theta = 180°$ and $\xi \approx 0$, i.e., for a sudden impact in a head-on collision. In this case it follows from the properties[21,22] of the orbital integrals that Eq. (18) is reduced to the simple expression

$$P_{i\to f}(\theta = 180°, \xi = 0) = [\chi_{i\to f}^{(\lambda)}]^2 \tag{19}$$

which, in fact, was the original motivation for introducing the parameter $\chi^{(\lambda)}$ through Eq. (12). Due to its interpretation as the maximum transition amplitude the parameter χ is an adequate measure for the applicability of perturbation theory. Only if $\chi \ll 1$ will the first-order perturbation theory outlined in the present section approximately describe the excitation process.

3.3 Second-Order Perturbation Theory as a Guide to the Exact Solution

For projectiles with a low charge number the first-order perturbation theory will in general be an adequate description of the process. However, for the energetic heavy-ion beams now available χ may become of the order of, or even larger than, unity. For these cases it becomes necessary to solve the time-dependent Schrödinger equation for the process by direct numerical methods (see Section 4.5).

But even if χ is too large for the perturbation expansion to be accurate, some properties of the exact solution may be conveniently *discussed* in terms of higher-order perturbation theory. In particular, there are two interesting features which are common to the exact solution and the higher-order perturbation theory. These features are:

a. For large enough values of χ the collision of the projectile with the target nucleus will excite states which in first order are not excited at all or only in higher multipolarity. In the language of perturbation theory these processes are usually referred to as *multiple excitations*. They play an important role in the study of higher nuclear states.

b. For large enough values of χ the excitation of a given nuclear level $|f\rangle$ will not only depend on the *transition matrix element* between the ground state $|i\rangle$ and the state $|f\rangle$ but also on *static properties* of the state $|f\rangle$ and on transition matrix elements between other states.

The exact solution will incorporate the dependence of these effects upon the various nuclear parameters in a very complicated and implicit manner. A perturbation treatment which contains the effects (a) and (b) in the lowest nonvanishing order will therefore be extremely useful as a guide for both the physical interpretation and the setting up of suitable experimental conditions. This is true even if the conditions for the applicability of the perturbation theory are not strictly satisfied.

The simplest effects beyond the reach of first-order perturbation theory emerge in second order:

a. A second excited nuclear state may be reached from the ground state by a two-step process.

b. The excitation of the first excited state $|f\rangle$, while determined mainly by the electromagnetic transition matrix element from the ground state to the state $|f\rangle$, will be influenced also by the static quadrupole moment of the excited state $|f\rangle$. The matrix elements of the quadrupole operator between the magnetic substates of $|f\rangle$ are both diagonal and off-diagonal with respect to the magnetic quantum numbers M_f. The occurrence of off-diagonal matrix elements is responsible for the pictorial name *reorientation effect*[1] which now has been widely adopted. More generally, however, we may define the reorientation effect as the effect on the Coulomb excitation of a given state caused by the quadrupole moment of that state.

We shall now consider briefly the second-order theory[21] using again a classical description of the projectile orbit. While for larger $\chi_{i\to f}$ the second-order perturbation theory offers a convenient basis for discussing the physical situation, it will be a good approximation only for $\chi_{i\to f} \lesssim 0.1$.

To second order, the transition amplitude from an initial state $|i\rangle$ to a final state $|f\rangle$ is given by

$$b_{if}^{(2)} = b_{if}^{(1)} + \sum_n b_{inf} \tag{20}$$

with

$$b_{inf} = (i\hbar)^{-2} \int_{-\infty}^{+\infty} dt \, \langle f \mid H_{\text{int}}(t) \mid n \rangle \, e^{(i/\hbar)(E_f - E_n)t}$$

$$\times \int_{-\infty}^{t} dt' \, \langle n \mid H_{\text{int}}(t') \mid i \rangle \, e^{(i/\hbar)(E_n - E_i)t'} \tag{21a}$$

The first-order amplitude $b_{if}^{(1)}$ is defined in Eq. (10) and the sum extends over the complete set of intermediate states $\mid n\rangle$.

The double integral in Eq. (21a) may be decomposed by introducing the unit step function[21]

$$\Theta(t - t') = \lim_{\epsilon \to 0} \frac{-1}{2\pi i} \int_{-\infty}^{+\infty} \frac{\exp[-iE(t - t')/\hbar]}{E + i\epsilon} \, dE$$

$$= \begin{cases} 1 & \text{for } t > t' \\ 0 & \text{for } t < t' \end{cases} \tag{21b}$$

The integration over t and t' can now be performed independently which yields

$$b_{inf} = -\lim_{\epsilon \to +0} \frac{1}{2\pi i} \int_{-\infty}^{+\infty} \frac{b_{in}^{(1)}(E_n - E_i + E) \, b_{nf}^{(1)}(E_f - E_n - E)}{E + i\epsilon} \, dE \tag{21c}$$

With the help of the relation $(E + i\epsilon)^{-1} = \mathscr{P}E^{-1} - i\pi\,\delta(E)$ the amplitude finally is written as

$$b_{inf} = \frac{1}{2} b_{in}^{(1)}(E_n - E_i) \, b_{nf}^{(1)}(E_f - E_n)$$

$$+ \frac{i}{2\pi} \mathscr{P} \int_{-\infty}^{\infty} b_{in}^{(1)}(E_n - E_i + E) \, b_{nf}^{(1)}(E_f - E_n - E) \frac{dE}{E} \tag{22}$$

where $\mathscr{P}$ denotes the principal value of the integral. The first part of Eq. (22) consists of first-order amplitudes on the energy shell, whereas the second part represents an off-energy shell contribution. Using the definitions of Eqs. (11) to (16) and assuming that the intermediate state is reached from the initial state by the multipole order λ_1 while the final state is reached from the intermediate state by the multipole order λ_2, we can rewrite the complete second-order amplitude [Eq. (20)] in the form

$$b_{if}^{(2)} = (-1)^{I_i - M_i + 1} \sqrt{2I_i + 1} \sum_{\mu} \begin{pmatrix} I_i & \lambda & I_f \\ -M_i & \mu & M_f \end{pmatrix}$$

$$\times \Big\{ i\mathscr{K}_{\lambda\mu}(\theta, \xi_{if}) \, \chi_{i \to f}^{(\lambda)} + \frac{1}{2} \sum_{n} (-1)^{\lambda + I_i + I_f} \sqrt{2I_n + 1} \, (2\lambda + 1) \begin{Bmatrix} \lambda_1 & \lambda_2 & \lambda \\ I_f & I_i & I_n \end{Bmatrix}$$

$$\times \left[\mathscr{A}_{\lambda\mu}^{(\lambda_1\lambda_2)}(\xi_{in}, \xi_{nf}, \theta) + i\mathscr{B}_{\lambda\mu}^{(\lambda_1\lambda_2)}(\xi_{in}, \xi_{nf}, \theta) \right] \chi_{i \to n}^{(\lambda_1)} \chi_{n \to f}^{(\lambda_2)} \Big\} \tag{23}$$

where we have introduced the real functions

$$\mathscr{A}_{\lambda\mu}^{(\lambda_1\lambda_2)}(\xi, \xi', \theta) = \sum_M \begin{pmatrix} \lambda_1 & \lambda_2 & \lambda \\ M & \mu - M & -\mu \end{pmatrix} \mathscr{K}_{\lambda_1 M}(\theta, \xi)\, \mathscr{K}_{\lambda_2, \mu - M}(\theta, \xi') \tag{24}$$

and

$$\mathscr{B}_{\lambda\mu}^{(\lambda_1\lambda_2)}(\xi, \xi', \theta) = \sum_M \begin{pmatrix} \lambda_1 & \lambda_2 & \lambda \\ M & \mu - M & -\mu \end{pmatrix} \times \frac{1}{\pi} \mathscr{P} \int_{-\infty}^{+\infty} \mathscr{K}_{\lambda_1 M}(\theta, \xi + x)\, \mathscr{K}_{\lambda_2, \mu - M}(\theta, \xi' - x) \frac{dx}{x} \tag{25}$$

These functions are related in a simple way to the functions α and β defined by Alder *et al.*[21] and tabulated by Douglas[25]:

$$\mathscr{A}_{\lambda\mu}^{(\lambda_1\lambda_2)}(\xi, \xi', \theta) = \pi \frac{(2\lambda_1 - 1)!!\,(2\lambda_2 - 1)!!}{(\lambda_1 - 1)!\,(\lambda_2 - 1)!} \alpha_{\lambda, -\mu}(\lambda_1\lambda_2\xi\xi'\theta) \tag{26}$$

and

$$\mathscr{B}_{\lambda\mu}^{\lambda_1\lambda_2}(\xi, \xi', \theta) = \pi \frac{(2\lambda_1 - 1)!!\,(2\lambda_2 - 1)!!}{(\lambda_1 - 1)!\,(\lambda_2 - 1)!} \beta_{\lambda, -\mu}(\lambda_1\lambda_2\xi\xi'\theta) \tag{27}$$

The double orbital integrals $\mathscr{A}_{\lambda\mu}$ and $\mathscr{B}_{\lambda\mu}$ obey certain symmetry relations which are listed in Table I together with the symmetry of the simple orbital integrals $\mathscr{K}_{\lambda\mu}$.

TABLE I

Symmetries of Orbital Integrals

$\mathscr{K}_{\lambda\mu}(\theta, \xi)$	$=$	$\mathscr{K}_{\lambda, -\mu}(\theta, -\xi)$
$\mathscr{A}_{\lambda\mu}^{(\lambda_1\lambda_2)}(\xi_1, \xi_2, \theta)$	$=$	$(-)^{\lambda_1+\lambda_2+\lambda}\, \mathscr{A}_{\lambda\mu}^{(\lambda_2\lambda_1)}(\xi_2, \xi_1, \theta)$
$\mathscr{A}_{\lambda\mu}^{(\lambda_1\lambda_2)}(\xi_1, \xi_2, \theta)$	$=$	$(-)^{\lambda_2+\lambda-\mu}\, \mathscr{A}_{\lambda, -\mu}^{(\lambda_1\lambda_2)}(-\xi_1, -\xi_2, \theta)$
$\mathscr{B}_{\lambda\mu}^{(\lambda_1\lambda_2)}(\xi_1, \xi_2, \theta)$	$=$	$(-)^{\lambda_1+\lambda_2+\lambda+1}\, \mathscr{B}_{\lambda\mu}^{(\lambda_2\lambda_1)}(\xi_2, \xi_1, \theta)$
$\mathscr{B}_{\lambda\mu}^{(\lambda_1\lambda_2)}(\xi_1, \xi_2, \theta)$	$=$	$(-)^{\lambda_2+\lambda-\mu+1}\, \mathscr{B}_{\lambda, -\mu}^{(\lambda_1\lambda_2)}(-\xi_1, -\xi_2, \theta)$

It is interesting to note the different dependences of the on-shell and off-shell amplitudes on the energy of the intermediate state n. If the excitation energy of the intermediate state is considerably higher than the energy of the final state, then $\mathscr{A}$ is practically zero since the functions $\mathscr{K}_{\lambda_1\mu_1}(\theta, \xi_{in})$ and $\mathscr{K}_{\lambda_2\mu_2}(\theta, \xi_{nf})$ decrease exponentially as a function of $(E_n - E_i)$ and of $(E_f - E_n)$,

respectively. The amplitude $\mathscr{B}$, on the other hand, exhibits the behavior expected from time-independent perturbation theory, namely, a decrease with the inverse energy difference $(E_n - E_i)$ between the intermediate and the initial state.

The excitation probability and the differential cross section to second order may be calculated from the amplitude $b_{i\to f}^{(2)}$. The excitation probability is composed of a first-order probability $P^{(11)}$, an interference term $P^{(12)}$ between the first order and the second order, and finally a term $P^{(22)}$ which contains only second-order amplitudes. We thus may write

$$P = P^{(11)} + P^{(12)} + P^{(22)} \tag{28}$$

The last term in Eq. (28) has significance only if the interference terms between the first-order and third-order amplitudes are also taken into account.[2,3]

3.4 Symmetrization of the Excitation Parameters

The foregoing treatment assumes that v is the relative asymptotic velocity of the incoming projectile with respect to the target nucleus. If a finite energy is transferred to the target nucleus, i.e., if $\xi \neq 0$, this would lead to a violation of reciprocity and reflect the inadequacy of the classical approximation. One would expect, therefore, that a removal of this inconsistency should bring the classical calculations to a closer agreement with the accurate quantum mechanical results. The emerging improvement of the semiclassical description is considerable and has been verified by Alder and Winther.[21] The symmetrization prescription consists of the following replacements

$$a \to a_{if} = \frac{Z_1 Z_2 e^2}{M v_i v_f} \tag{29}$$

where v_i and v_f are the relative asymptotic velocities in the entrance and excit channels, respectively, and

$$\xi_{if} \to \xi_{if}^{(\text{symm})} = \frac{Z_1 Z_2 e^2}{\hbar}\left(\frac{1}{v_i} - \frac{1}{v_f}\right) \tag{30}$$

and finally

$$\chi_{i\to f}^{(\lambda)} \to \chi_{i\to f}^{(\lambda),(\text{symm})} = \frac{\sqrt{16\pi}(\lambda - 1)!}{(2\lambda + 1)!!} \frac{Z_1 e}{\hbar \sqrt{v_i v_f}} \frac{\langle i \| \mathscr{M}(E\lambda) \| f \rangle}{a_{if}^{\lambda} \sqrt{2I_i + 1}} \tag{31}$$

For each transition between any two nuclear states the relevant expressions should thus be replaced by the symmetrized expressions (29) to (31), and the expression for the cross section in the c.m. system takes the form

$$d\sigma_{i\to f} = (v_f/v_i)\, P_{i\to f}^{(\text{symm})}\, \tfrac{1}{4} a_{if}^2 \sin^{-4}(\theta/2) d\Omega$$

The latter guarantee reciprocity[26] and also represent a better approximation to the quantum mechanical solution. Typically[21] for $\lambda = 1$ and $\lambda = 2$ the symmetrized classical expressions for the total cross section are accurate within better than 5% for $n \gtrsim 3$, while a corresponding accuracy for the angular distribution of the inelastically scattered particles is only obtained for $\eta > 10$. In order to obtain the same accuracy for the angular distributions of the de-excitation γ rays from the symmetrized classical expressions, one has to use still higher values of η. A more detailed discussion can be found in References 21 and 24.

4. THEORY OF THE REORIENTATION EFFECT

From the outline of the second-order perturbation theory given in the preceding section one may easily specialize to the reorientation effect. Under the reorientation effect we understand, in the language of second-order perturbation theory, the particular case in which each of the intermediate states in Eq. (20) is one of the magnetic substates of either the ground state $|i\rangle$ or the excited state $|f\rangle$.

Physically we may visualize the reorientation effect for a rotational nucleus in the following way. The impinging particle interacts with the nucleus and excites it from the ground state $|i\rangle$ to the first excited state $|f\rangle$. Then it continues to interact with the quadrupole moment of the excited state, thus producing a change in the orientation of the excited nucleus.

4.1 The Amplitude for the Excitation $0^+ \rightarrow 2^+$

In order to simplify the presentation we shall in the following confine ourselves to the situation in which the initial state has spin $I_i = 0$ and the final state has spin $I_f = 2$. Experimentally this is by far the most important case. (More general conditions can be dealt with by going back to Section 3.3.) In the present section we also assume that the reorientation effect in the final state is the *only second-order effect* which contributes appreciably. This means in particular that there is no other 2^+ state close to the final 2^+ state which we are considering (see Section 4.5).

Under this assumption the contribution to $b_{if}^{(2)}$ in Eq. (23) is proportional to $\chi_{f\to f}^{(2)}$ and hence to the static quadrupole moment Q of the excited state:

$$b_{i\to f}^{(2)}(M_f) = -(5)^{-1/2}\chi_{i\to f}^{(2)}\Big\{i\,\mathscr{K}_{2,-M_f}(\theta, \xi) + \frac{\sqrt{5}}{2}\left[\mathscr{A}_{2,-M_f}^{(22)}(\xi_{if}, 0, \theta) + i\mathscr{B}_{2,-M_f}^{(22)}(\xi_{if}, 0, \theta)\right]\chi_{f\to f}^{(2)}\Big\} \tag{32}$$

The parameter $\chi^{(2)}_{f\to f}$ is connected with the quadrupole moment Q of the excited state by the relation

$$\chi_{f\to f} = \frac{1}{3}\sqrt{\frac{7}{10}}\, Z_1 \frac{e^2}{\hbar c} \frac{1}{V_\infty/c} \frac{Q}{a^2} \tag{33}$$

The amplitudes in Eq. (32) completely determine the excitation process in second order. They depend on two nuclear parameters, namely, the excitation matrix element $\langle i \| \mathscr{M}(E2) \| f \rangle$ and the quadrupole moment Q. In general it will be possible to determine the two quantities by two independent measurements. In the following two sections we discuss the manifestations of the reorientation effect in the excitation probability (as a function of the energy, scattering angle, and charge of the projectile) and in the angular distribution of the de-excitation gamma rays.

4.2 The Excitation Probability

The simplest sets of experiments for determining the nuclear transition matrix element and the quadrupole moment are the measurement of the excitation probability for at least two different bombarding energies E_p, scattering angles θ, or projectile charge numbers Z_1 (see Section 6.2). Retaining in the perturbation expansion only terms which are quadratic in χ (first-order term $P^{(11)}$) and cubic in χ (interference term $P^{(12)}$), we may write

$$P_{i\to f} = P^{(11)}_{i\to f} + P^{(12)}_{i\to f} \tag{34}$$

The excitation probability $P_{i\to f}$ may thus be obtained by inserting Eq. (32) into Eq. (9).

For the first-order term this yields the result

$$P^{(11)}_{i\to f} = [\chi^{(2)}_{i\to f}]^2 \times \tfrac{1}{5} \sum_\mu [\mathscr{K}_{2\mu}(\theta, \xi_{if})]^2 \tag{35}$$

The quantity $(\frac{1}{5}) \sum [\mathscr{K}_2(\theta, \xi)]^2$ is given in Table VII in the Appendix. In terms of the functions tabulated in Reference 21 one obtains

$$P^{(11)}_{i\to f} = \frac{9\pi}{5} [\chi^{(2)}_{i\to f}]^2 \sum_\mu \left[Y_{2\mu}\left(\frac{\pi}{2}, 0\right) I_{2\mu}(\theta, \xi_{if}) \right]^2 \tag{36}$$

or

$$P^{(11)}_{i\to f} = \frac{225}{4\pi} [\chi^{(2)}_{i\to f}]^2 \frac{df_{E2}(\theta, \xi_{if})}{d\Omega} \sin^4\left(\frac{\theta}{2}\right) \tag{37}$$

for the excitation probability to first order.

The interference term $P^{(12)}$, obtained from Eqs. (32) and (9), is the term which is proportional to χ^3. Since the function $\mathscr{K}_{2\mu}(\theta, \xi)$ defined by Eq. (15) is real, the real part $\mathscr{A}_{2\mu}(\xi_{if}, 0, \theta)$ of the second-order orbital function in Eq. (23) does not contribute to $P^{(12)}$ and we obtain

$$P^{(12)}_{i\to f} = (5)^{-1/2}[\chi^{(2)}_{i\to f}]^2 \chi^{(2)}_{f\to f} \sum_{\mu} \mathscr{K}_{2\mu}(\theta, \xi_{if}) \mathscr{B}^{(22)}_{2\mu}(\xi_{if}, 0, \theta) \tag{38}$$

The quantity $(5)^{-1/2} \sum \mathscr{K}_{2\mu}(\theta, \xi) \mathscr{B}_{2\mu}(\xi, 0, \theta)$ is given in Table VIII in the Appendix. In terms of the functions tabulated in References 21 and 25, Eq. (38) may be written as

$$P^{(12)}_{i\to f} = \frac{27\pi^{3/2}}{\sqrt{5}} [\chi^{(2)}_{i\to f}]^2 \chi^{(2)}_{f\to f} \sum_{\mu} Y_{2\mu}\left(\frac{\pi}{2}, 0\right) I_{2\mu}(\theta, \xi_{if}) \beta_{2,-\mu}(\xi_{if}, 0, \theta) \tag{39}$$

The differential cross section in the center-of-mass system is then obtained from $P_{i\to f}$ by Eq. (8).

4.3 The Angular Distribution of the De-excitation Gamma Rays

A more complicated experiment than the measurement of the excitation probability discussed in the preceding section is a measurement in which the angular distribution of the de-excitation gamma rays is observed in coincidence with the scattered projectiles (see Section 6.3). Since the projectile orbit determines a scattering plane, the gamma angular distribution depends on the polar angle θ_γ and the azimuth ϕ_γ, or on $\Omega_\gamma = \{\theta_\gamma, \phi_\gamma\}$. All angles are defined with respect to the focal coordinate system as illustrated in Fig. 2.

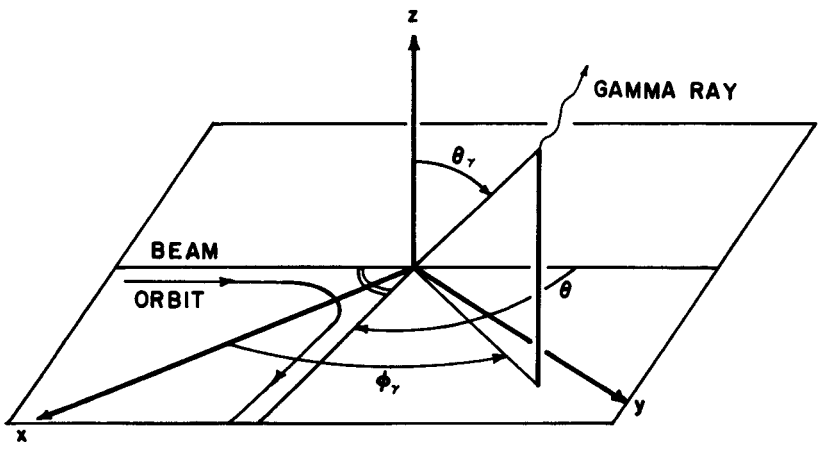

Fig. 2. Illustration of the angles θ_γ and ϕ_γ in terms of which the gamma-ray angular distributions are given.

The angular distribution, furthermore, depends on the scattering angle θ and on the parameter ξ.

If the polarization of the gamma rays is not observed (see Section 6.3.4), the angular distribution is given by

$$W(\Omega_\gamma) = \sum_P \sum_{M_i} \left| \sum_{M_f} b_{if}(M_i M_f) \langle I_i M_i \mid H_\gamma(\Omega_\gamma P) \mid I_f M_f \rangle \right|^2 \tag{40}$$

where the first sum denotes the summation over the polarizations $P = \pm 1$ and H_γ is the electromagnetic interaction. For the particular spin sequence $0^+ \to 2^+ \to 0^+$, only electric quadrupole matrix elements can contribute in the multipole expansion of $H_\gamma(\Omega_\gamma, P)$ and the correlation assumes the form

$$W(\Omega_\gamma) = -5(4\pi)^{1/2} \sum_{k \text{ even}} (2k+1)^{1/2} \sum_{\kappa \text{ even}} \sum_M \Big[b_{if}(M)\, b_{if}^*(\kappa + M) \times \begin{pmatrix} 2 & 2 & k \\ -M & \kappa + M & -\kappa \end{pmatrix} \begin{pmatrix} 2 & 2 & k \\ 1 & -1 & 0 \end{pmatrix} Y_{k\kappa}(\Omega_\gamma) \Big] \tag{41}$$

Here and in the following equations we use a normalization in which the isotropic term is equal to the excitation probability. We now insert the excitation amplitude [Eq. (32)], and, for convenience of evaluation, we express the correlation in terms of real angular functions, using the symmetry properties of the various orbital integrals given in Table I. We obtain

$$W(\Omega_\gamma) = [\chi_{i\to f}^{(2)}]^2 \sum_{\substack{k=0 \\ 2 \\ 4}} \sum_{\substack{\kappa=0 \\ 0,2 \\ 0,2,4}} \{(\mathscr{R}_{k\kappa}^{(11)} + \chi_{f\to f}^{(2)} \mathscr{R}_{k\kappa}^{(12)}) \times \frac{1}{2} [Y_{k\kappa}(\Omega_\gamma) + Y_{k,-\kappa}(\Omega_\gamma)] + \chi_{f\to f}^{(2)} \mathscr{T}_{k\kappa}^{(12)} \frac{1}{2i} [Y_{k\kappa}(\Omega_\gamma) - Y_{k,-\kappa}(\Omega_\gamma)] \tag{42}$$

where the coefficients $\mathscr{R}_{k\kappa}$ and $\mathscr{T}_{k\kappa}$ depend on θ and ξ. The term arising from the first order, $\mathscr{R}_{k\kappa}^{(11)}$, is given by

$$\mathscr{R}_{k\kappa}^{(11)} = -(4\pi)^{1/2} (2k+1)^{1/2} \begin{pmatrix} 2 & 2 & k \\ 1 & -1 & 0 \end{pmatrix} (2 - \delta_{\kappa 0}) \times \sum_M \begin{pmatrix} 2 & 2 & k \\ M & \kappa - M & -\kappa \end{pmatrix} \mathscr{K}_{2M}(\theta, \xi)\, \mathscr{K}_{2,M-\kappa}(\theta, \xi) \tag{43}$$

where $\delta_{\kappa 0}$ is the Kronecker symbol. The interference between first order and second order gives rise to the terms $\mathscr{R}_{k\kappa}^{(12)}$ and $\mathscr{T}_{k\kappa}^{(12)}$ given by

$$\mathscr{R}_{k\kappa}^{(1,2)} = -\sqrt{4\pi}\,\sqrt{2k+1}\begin{pmatrix} 2 & 2 & k \\ 1 & -1 & 0 \end{pmatrix}(2-\delta_{\kappa 0})$$
$$\times \frac{1}{2}\sqrt{5}\sum_M \left\{\begin{pmatrix} 2 & 2 & k \\ M & \kappa - M & -\kappa \end{pmatrix}\right.$$
$$\left.\times\,[\mathscr{K}_{2M}(\theta,\xi)\,\mathscr{B}_{2,M-\kappa}^{(22)}(\xi,0,\theta) + \mathscr{K}_{2,M-\kappa}(\theta,\xi)\,\mathscr{B}_{2M}^{(22)}(\xi,0,\theta)]\right\} \tag{44}$$

and

$$\mathscr{T}_{k\kappa}^{(12)} = \sqrt{4\pi}\,\sqrt{2k+1}\begin{pmatrix} 2 & 2 & k \\ 1 & -1 & 0 \end{pmatrix}\sqrt{5}\sum_M \left\{\begin{pmatrix} 2 & 2 & k \\ M & \kappa - M & -\kappa \end{pmatrix}\right.$$
$$\left.\times\,[\mathscr{K}_{2M}(\theta,\xi)\,\mathscr{A}_{2,M-\kappa}^{(22)}(\xi,0,\theta) - \mathscr{K}_{2,M-\kappa}(\theta,\xi)\,\mathscr{A}_{2,M}^{(22)}(\xi,0,\theta)]\right\} \tag{45}$$

The three orbital functions given by Eqs. (43) to (45) are tabulated in Appendix B.

The coefficients $\mathscr{T}_{k\kappa}^{(12)}$ arise from the interference between the imaginary first-order amplitude and the real part of the second-order amplitude. This behavior of the phases is reflected in the angular distributions, which have a structure quite different from the first-order angular distribution. While $\frac{1}{2}(Y_{k\kappa} + Y_{k,-\kappa})$ is proportional to $\cos(\kappa\phi)$, we have

$$(1/2i)(Y_{k\kappa} - Y_{k,-\kappa}) \propto \sin(\kappa\phi).$$

This effect can be used in principle[27] to distinguish the second-order contribution from the first-order part and hence to measure directly the quadrupole moment of the excited state. The isolation of the reorientation effect can be achieved by choosing two positions for the gamma-counters in such a way that the cosine terms vanish and the sine terms have opposite signs in both counters (see Section 6.3.) Then the difference between the coincidence counting rates in the two counters is proportional to the quadrupole moment.

This arrangement has one additional advantage[27]: Since the double integral $\mathscr{A}$ vanishes exponentially with the energy of the intermediate state and since $\mathscr{B}$ is always connected with the angular distribution $\cos(\kappa\phi)$, an isolation of the term $\sin(\kappa\phi)$ eliminates not only first-order transitions but also contributions due to higher-lying intermediate states (e.g., the electric dipole resonance or higher 2^+ states).

In general the angular distribution of the de-excitation gamma rays is more strongly affected by the shortcomings of the classical approximation than are transition probabilities. But in the quantum mechanical as well as the classical calculation of the angular distribution there can be only $\cos(\kappa\phi)$

terms in first order. Classically, the terms proportional to $\sin(\kappa\phi)$ arise from the phase difference of $\pi/2$ between the first-order transition amplitude and the off-energy shell part of the second-order amplitude [Eq. (22)]. This is also true for the quantum mechanical calculation. Thus, if the first-order angular dependence is eliminated experimentally, the inaccuracy of the classical theory enters only as a small correction of the reorientation effect.

The present considerations are based on second-order perturbation theory. It is clear that for values of $\chi_{i\to f}$ close to unity, a more detailed computer calculation has to be used (see Section 6.5) for the evaluation of experiments. The optimum geometry for a specific experiment is, however, indicated by the results of perturbation theory.

4.4 Magnetic Dipole Reorientation

In addition to the reorientation due to the electric quadrupole moment, there is also the possibility of magnetic dipole reorientation[28] which arises from the interaction of the static magnetic moment $\mu e\hbar/2M_pc$ of the excited state with the magnetic field produced by the projectile. The ratio ϵ of the $M1$ and $E2$ interference terms is given by

$$\epsilon = \frac{P^{(12)}(M1)}{P^{(12)}(Q)} = -\frac{4}{15}\frac{Z_1e^2}{a}\frac{1}{M_pc^2}\frac{\mu}{\chi^{(2)}_{f\to f}}\cot\frac{\theta}{2}$$

$$\times \frac{\sum_{M=\pm 2}\frac{M}{2}\mathscr{K}_{2,-M}(\theta,\xi)\frac{\mathscr{P}}{2\pi}\int_{-\infty}^{+\infty}\mathscr{K}_{2,-M}(\theta,\xi+x)\,\mathscr{K}_{20}(\theta,-x)\frac{dx}{x}}{\sum_M \mathscr{K}_{2M}(\theta,\xi)\,\mathscr{B}^{(22)}_{2M}(\xi,0,\theta)} \tag{46}$$

The quantity ϵ is very small (less than 1%) for cases of practical interest, since the main factor is the ratio between the Coulomb energy e^2Z_1/a per proton of the target at half the distance of closest approach and the proton rest mass. Furthermore, the two terms in the sum of the numerator tend to cancel.[28] Upon inserting Eq. (33) for $\chi_{f\to f}$ into Eq. (46), the energy dependence of ϵ is seen to be governed by two factors (aside from the energy dependence of the orbital integrals): (a) the factor v/c, giving the ratio between the amplitudes of the magnetic and the electric fields generated by the projectile, and (b) the factor a, accounting for the fact that the quadrupole field decreases by one power of the radial distance faster than the dipole field. The resulting velocity dependence is thus $\epsilon \sim 1/v$. Since a measurement of Q requires a high projectile velocity, the magnetic dipole reorientation can be neglected in such cases.

4.5 Corrections for Multiple *E*2 Transitions

In the theory of the reorientation effect presented above only the first-order term $P^{(11)}$ and the interference term $P^{(12)}$ of the perturbation expansion have been considered. Higher-order terms would have to include multiple transitions between the magnetic sublevels of the 2^+ state[2,3] as well as transitions involving higher excited nuclear levels. The higher-lying states can contribute to the population of the first 2^+ state in two ways: (a) by multiple transitions involving the higher states as intermediate states for the excitation of the 2^+ state, and (b) by gamma (or conversion) cascades feeding the 2^+ state from higher states. Contributions of this type involve, in general, a large number of nuclear parameters, and explicit expressions for, and tabulation of, these effects are therefore impractical.

In the final analysis of any experiment, however, these effects must be included. The basis for such a numerical analysis is a computer program[26] developed by Winther and de Boer. For this program the time-dependent Schrödinger equation governing the excitation process is written as a set of coupled differential equations for the amplitudes of the unperturbed states of the target nucleus. With the initial conditions set to represent the target in its ground state, the computer integrates the differential equations, advancing in small steps of time along the relevant portion of the hyperbolic orbit. From the final amplitudes thus obtained, any property of the excited nucleus or its decay that may be measured can be computed.

The input for this program consists of all the known parameters of the target nucleus (excitation energies, spins, and $E2$ matrix elements) and the parameters of the bombardment (projectile energy, mass, charge, and scattering angle). The dependence of the experimentally determined quantity on any unknown parameter may then be determined by performing several computer runs for different values of this parameter.

From such calculations it has been found[12] that, in most cases, the largest contributions to the excitation of the 2^+ state, apart from the first-order and the reorientation terms, arise from interference terms involving higher-lying $2'^+$ levels as intermediate states.

In lowest-order perturbation these interference terms are given by an expression similar to Eq. (38), namely,

$$P^{(12)}_{i\to f}(z) = (5)^{-1/2}\chi^{(2)}_{i\to f}\chi^{(2)}_{i\to z}\chi^{(2)}_{z\to f}\sum_{\mu}\mathscr{K}_{2\mu}(\theta, \xi_{if})\,\mathscr{B}^{(22)}_{2\mu}(\xi_{iz}, \xi_{zf}, \theta) \tag{47}$$

where z denotes the intermediate $2'^+$ state. The product of the three χ values in Eq. (47) is proportional to the product of the three matrix elements $\langle i\|\mathscr{M}(E2)\|f\rangle$, $\langle i\|\mathscr{M}(E2)\|z\rangle$, and $\langle z\|\mathscr{M}(E2)\|f\rangle$. Since most experiments (excitation probability of state z, gamma-ray branching ratio from state z

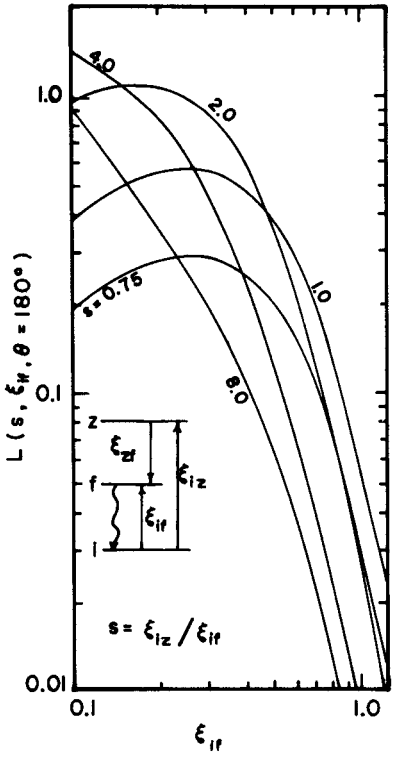

Fig. 3. The function

$$L(s, \xi_{if}, \theta) = \sum_{\mu} \mathscr{K}_{2\mu}(\theta, \xi_{if}) \mathscr{B}_{\mu}^{(22)}(\xi_{iz}, \xi_{zf}, \theta),$$

which gives the contribution to the excitation of a 2^+ state $|f\rangle$ via a second $2'^+$ state $|z\rangle$ as an intermediate state. The function is shown for the experimentally most important case of backward scattering ($\theta = 180°$). The variable is the ξ value for the excitation of the state $|f\rangle$, ξ_{if}. The parameter $s \equiv \xi_{iz}/\xi_{if}$ is the ratio of the ξ values leading to the 2^+ states. The parameter is approximately equal to the ratio of the excitation energies of the two 2^+ states.

to states i and f, respectively) determine the *square* of the $E2$ matrix elements in question, the sign of this term is normally not known. The ambiguity in the sign of $P_{i\to f}^{(12)}(z)$ can therefore introduce a large uncertainty in the interpretation of experiments in terms of the quadrupole moment of an excited state.[12]

To facilitate an estimate of the size of these effects, the sum appearing in Eq. (47), denoted by $L(s, \xi_{if}, \theta)$, has been calculated for a backscattering orbit ($\theta = 180°$)with the ratio $s = \xi_{iz}/\xi_{if}$ as a parameter. The result is shown in Fig. 3. Due to the symmetry of $\mathscr{B}_{2\mu}^{(22)}$ (see Table I), $L(s = 0.5, \xi_{if}, \theta) = 0$. The case $s = 1.0$ corresponds to the usual reorientation effect. For $\xi_{if} \gtrsim 0.3$, $L(s, \xi_{if}, \theta)$ has a maximum at $s \approx 3.0$, dropping off slowly for still higher energies of the intermediate state z (see end of Section 3.3).

5. EXCITATION VIA THE GIANT DIPOLE RESONANCE

With increasing experimental accuracy it might be possible to measure other second-order effects which accompany the reorientation effect. Aside

from corrections due to multiple $E2$ transitions, virtual excitations via the giant dipole resonance[29] are of particular interest, both because they may limit the accuracy with which quadrupole moments may be obtained from the reorientation effect and because they constitute an interesting problem by themselves. Since the $E1$ matrix elements between the ground state and the giant resonance are quite large, one may expect a sizable effect.

5.1 The Transition Probability

Let us again consider the particular case $i \to n \to f$, where the initial state $|i\rangle$ is the 0^+ ground state, $|n\rangle$ is one of the highly excited 1^- states in the giant resonance, and $|f\rangle$ is the final 2^+ state. Since the probability of actually populating the high-lying states $|n\rangle$ is vanishingly small (as has been discussed in Section 3, we can safely neglect the term $\mathscr{A}$ in the second-order transition amplitude given by Eq. (23) and thus write

$$b_{if}^{(2)} = -i(5)^{-1/2} \Big\{ \mathscr{K}_{2,-M_f}(\theta, \xi_{if})\, \chi_{i\to f}^{(2)} + \tfrac{1}{2}(5)^{1/2} \sum_n \mathscr{B}_{2,-M_f}^{(11)}(\xi_{in}, \xi_{nf}, \theta)\, \chi_{i\to n}^{(1)} \chi_{n\to f}^{(1)} \Big\} \tag{48}$$

The orbital integrals $\mathscr{K}$ and $\mathscr{B}$ and the parameters χ have been defined in Section 3. The sum over intermediate states is a sum over energies only, since the sum over magnetic substates has already been carried out. Using the definition of Eq. (12) for $\chi_{i\to f}^{(\lambda)}$ and introducing the double integral of Eq. (25) for $\mathscr{B}_{2,-M_f}^{(11)}$ explicitly, we may rewrite the sum over intermediate states in Eq. (48) as

$$\sum_n b_{inf}(M_f) = i\,\frac{8\pi}{9\sqrt{3}}\,\frac{Z_1{}^2 e^2}{\hbar v_\infty a^3} \sum_n \frac{\langle i \,\|\, \mathscr{M}(E1) \,\|\, n\rangle \langle n \,\|\, \mathscr{M}(E1) \,\|\, f\rangle}{E_n - E_i} \times \sum_{\mu_1\mu_2} \begin{pmatrix} 1 & 1 & 2 \\ \mu_1 & \mu_2 & M_f \end{pmatrix} Y_{1\mu_1}\left(\frac{\pi}{2}, 0\right) Y_{1\mu_2}\left(\frac{\pi}{2}, 0\right) \rho_{\mu_1,-\mu_2}(\theta, \xi_{if}) \tag{49}$$

where $\rho_{\mu\mu'}(\theta, \xi)$ is the double orbital integral defined[29] by

$$\rho_{\mu_1\mu_2}(\theta, \xi) = \int_{-\infty}^{+\infty} I_{1\mu_1}(\theta, x)\, I_{1\mu_2}(\theta, x - \xi)\, dx \tag{50}$$

In writing down Eqs. (49) and (50) we have made use of the fact that $\xi_{in} \approx -\xi_{nf} \gg 1$ and $E_n - E_i \gg E_f - E_i$, so that the error involved in Eq. (49) is of the order of $(E_f - E_i)/(E_n - E_i)$, or a few percent. It is conven-

ient to relate the sum over intermediate states to an experimentally known quantity by introducing a reference parameter η_0 through the relation

$$\sum_n \frac{\langle i \| \mathscr{M}(E1) \| n \rangle \langle n \| \mathscr{M}(E1) \| f \rangle}{E_n - E_i}$$

$$\equiv \eta_0 (5/2)^{1/2} \sum_n \frac{\langle i \| \mathscr{M}(E1) \| n \rangle \langle n \| \mathscr{M}(E1) \| i \rangle}{E_n - E_i} \tag{51}$$

which permits a comparison with the (−2)-moment of the photonuclear absorption cross section

$$\sigma_{-2} = \int \frac{\sigma(E)}{E^2} dE$$

$$= \frac{16\pi^3}{9\hbar c} \sum_n \frac{\langle i \| \mathscr{M}(E1) \| n \rangle \langle n \| \mathscr{M}(E1) \| i \rangle}{E_n - E_i} \tag{52}$$

Since the giant dipole resonance is a nuclear-size effect, σ_{-2} is approximately independent of details of the nuclear structure and empirically given by[30]

$$\sigma_{-2} \approx 3.5 A^{5/3} \qquad \mu\text{b/MeV} \tag{53}$$

While η_0 would be of the order of 1 if the electromagnetic coupling of the final state $|f\rangle$ and the initial state $|i\rangle$ to the dipole resonance were the same, it may be smaller in actual cases.[31] We shall come back to this question in the next section.

Inserting Eqs. (52) and (51) into Eq. (49), we obtain the transition amplitude

$$\sum_n b_{inf}(M_f) = \frac{i}{2\pi^2} \sqrt{\frac{5}{6}} \frac{Z_1{}^2 e^2}{a^3 v/c} \eta_0 \sigma_{-2} \mathscr{B}^{(E1)}_{-M_f}(\theta, \xi_{if}) \tag{54}$$

with

$$\mathscr{B}^{(E1)}_{-M_f}(\theta, \xi_{if}) = \sum_{\mu_1 \mu_2} \begin{pmatrix} 1 & 1 & 2 \\ \mu_1 & \mu_2 & M_f \end{pmatrix} Y_{1\mu_1}\left(\frac{\pi}{2}, 0\right) Y_{1\mu_2}\left(\frac{\pi}{2}, 0\right) \rho_{\mu_1, -\mu_2}(\theta, \xi_{if}) \tag{55}$$

The quantity $\mathscr{B}^{(E1)}_{M_f}(\theta, \xi_{if})$ is tabulated in Appendix B.

From Eq. (54) we may derive the interference between first-order and second-order transitions

$$P^{(12)}_{i \to f}(E1) = -\frac{1}{\pi^2 \sqrt{6}} \frac{Z_1{}^2 e^2}{a^3 v_\infty/c} \eta_0 \sigma_{-2} \chi^{(2)}_{i \to f} \sum_{M_f} \mathscr{K}_{2M_f}(\theta, \xi) \mathscr{B}^{(E1)}_{M_f}(\theta, \xi) \tag{56}$$

or the ratio

$$\frac{P_{i\to f}^{(12)}(E1)}{P_{i\to f}^{(11)}} = -\frac{5}{8\pi^{7/2}}\frac{\hbar c e Z_1 \sigma_{-2}}{a}\frac{\eta_0}{\langle i \| \mathscr{M}(E2) \| f\rangle}\phi(\theta, \xi_{if})$$

$$= -3.12\frac{E\sigma_{-2}}{(1 + A_1/A_2)\, Z_2}\frac{e\eta_0}{\langle i \| \mathscr{M}(E2) \| f\rangle}\phi(\theta, \xi_{if}) \tag{57}$$

where E is the bombarding energy in MeV. The ratio $\phi(\theta, \xi)$, given by

$$\phi(\theta, \xi) = \frac{\sum_M \mathscr{K}_{2M}(\theta, \xi)\, \mathscr{B}_M^{(E1)}}{\sum_\mu [\mathscr{K}_{2\mu}(\theta, \xi)]^2} \tag{58}$$

varies between 0.05 and 0.1 for most cases of interest and is shown in Fig. 4 for various values of θ and ξ_{if}.

The angular distribution of the de-excitation γ rays may be obtained conveniently by the following substitutions in Eqs. (42) to (45):

$$\mathscr{R}_{k\kappa}^{(11)} \to \mathscr{R}_{k\kappa}^{(11)} \tag{59}$$

$$\mathscr{T}_{k\kappa}^{(12)} \to 0 \tag{60}$$

$$\mathscr{B}_{2,M}^{(22)}(\xi, 0, \theta) \to \mathscr{B}_M^{(E1)}(\theta, \xi) \tag{61}$$

$$\chi_{i\to f}^{(2)}\chi_{f\to f}^{(2)} \to -(\pi)^{-2}\,(5/6)^{1/2}\,\frac{Z_1{}^2 e^2}{a^3\, v_\infty/c}\,\sigma_{-2}\eta_0 \tag{62}$$

5.2 Interpretation as Polarization Effect

With the purpose of obtaining an estimate for the parameter η_0 one may look at the excitation via the giant dipole resonance from a different point of view. Classically, the dipole interaction between the projectile and the target nucleus consists of a dipole polarization of the target nucleus[32] (if $\tau_{\text{coll}} \gg \tau_{\text{nucl}}$). For a spherical target nucleus, the dipole polarization leads only to a small change in the monopole interaction. For a deformed nucleus, however, the induced dipole moment of the target nucleus is not in the direction of the field. The resulting torque acting on the target nucleus causes it to rotate and thus contributes to the excitation of the 2^+ state.

In a model in which the nucleus is described as a uniformly charged body whose shape is given by

$$R = R_0\left[1 + \sum_\mu \alpha_\mu Y_{2\mu}(\theta, \phi)\right] \tag{63}$$

and whose degrees of freedom consist of rotations or surface vibrations,

the interaction energy between the induced dipole moment of the nucleus and the projectile is obtained[32,33] in second-order perturbation theory as

$$V_{\text{pol}} = -\frac{4\pi}{9}\frac{Z_1{}^2e^2}{r^4}\sum_n \frac{|\langle i \| \mathscr{M}(E1) \| n\rangle|^2}{E_n - E_i}\left[1 + 2\sum_\mu \alpha_\mu Y_{2\mu}(\theta, \phi)\right] \tag{64}$$

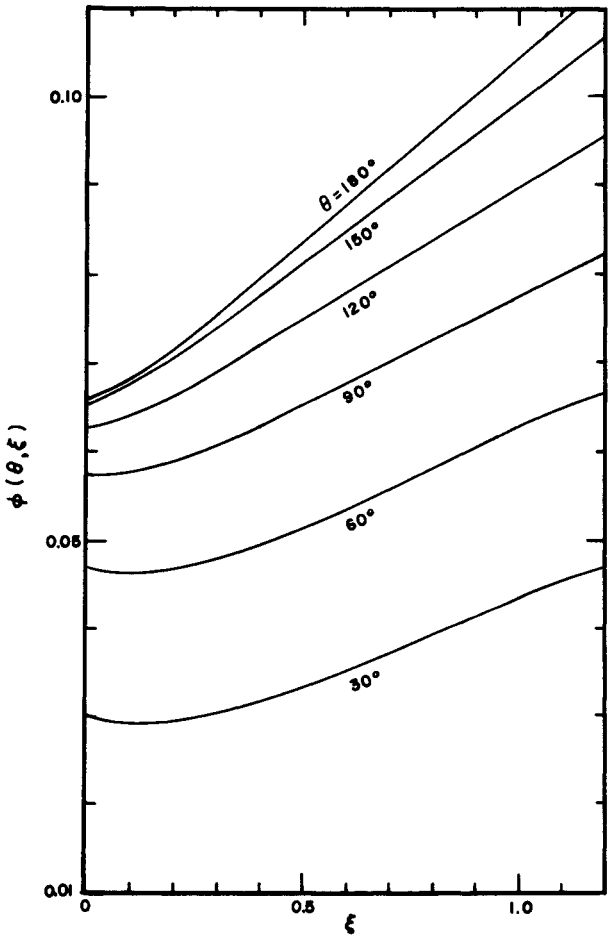

Fig. 4. The relative contribution to the $E1$ effect [see Eqs. (57) and (58)]. The ratio

$$\phi(\theta, \xi) = \sum_M \mathscr{K}_{2M}(\theta, \xi)\,\mathscr{B}_M^{(E1)}(\theta, \xi) \Big/ \sum_\mu [\mathscr{K}_{2\mu}(\theta, \xi)]^2$$

is plotted as a function of θ with ξ as parameter.

Adding this polarization potential to $H_{\text{int}}(t)$ in Eq. (10) leads to a correction of the first-order transition amplitude due to the dipole polarization. The approximations entering in Eq. (64) are identical[33] to those involved in deriving Eq. (49), and the results are completely equivalent. (The connection with the polarization suggests that the symmetrization of the parameters ξ, a, etc., should be made with respect to the initial and final states and not with respect to the virtual intermediate state.) This is most easily verified for backward scattering. Inserting Eq. (64) into Eq. (22) and observing that the relevant orbital integral

$$I_{3,\mu-\mu'}(\theta, \xi) = (1/2\pi)\rho_{\mu\mu'}(\theta, \xi)$$

we get back the excitation amplitude in Eq. (49) if we identify

$$\eta_0 = \tfrac{4}{3}\sqrt{\pi}\,\frac{\langle i \| \mathcal{M}(E2) \| f \rangle}{Z_1 e R_0^2} \tag{65}$$

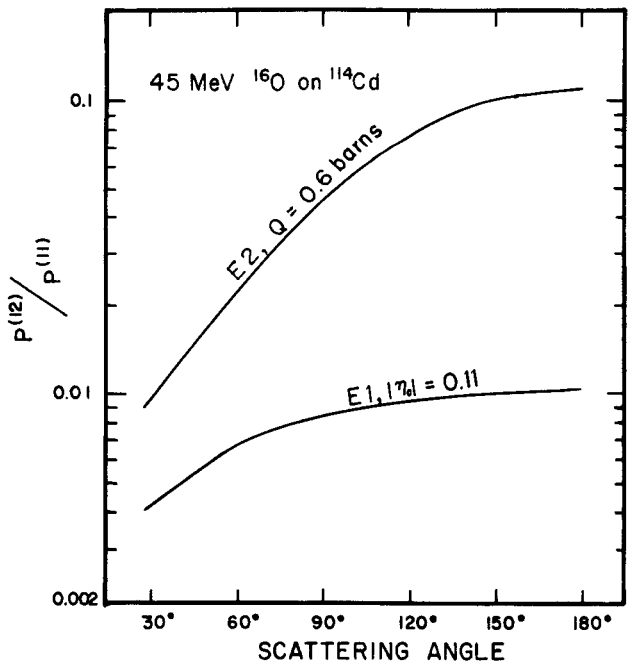

Fig. 5. The relative contributions of the reorientation effect ($E2$) and the giant dipole interference effect ($E1$) to the $E2$ excitation probability of the first 2^+ state in ^{114}Cd by 40-MeV ^{16}O ions scattered through an angle θ.

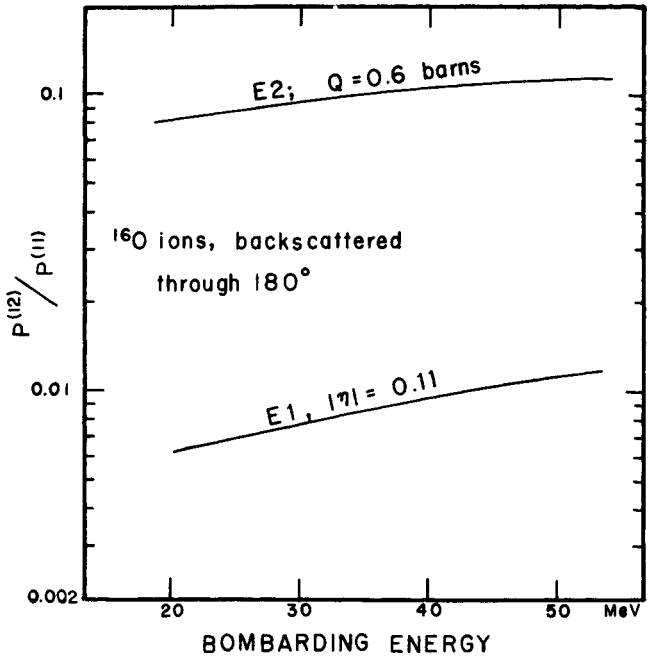

Fig. 6. The relative contributions of the reorientation effect ($E2$) and the giant dipole interference effect ($E1$) to the $E2$ excitation probability of the first 2^+ state in ^{114}Cd by ^{16}O ions of energy E_p, backscattered through an angle $\theta = 180°$.

This relation is valid for rotational and vibrational nuclei but may also provide a useful estimate for the more general case, since the polarization is essentially a nuclear-size effect.

Taking ^{114}Cd as an example, one obtains from the measured $B(E2)$ value the estimate η_0 (^{114}Cd) ≈ 0.11, which is in approximate agreement with more detailed model calculations.[34,35]

From Eqs. (57) and (65) we furthermore derive the estimate

$$\frac{P_{i\to f}^{(12)}(E1)}{P_{i\to f}^{(11)}} \approx -1.8 \times 10^{-3} \frac{A_2 E_{[\mathrm{MeV}]}}{Z_1 Z_2} \phi(\theta, \xi)\,(1 + A_1/A_2)^{-1} \tag{66}$$

which is considerably smaller than the reorientation effect. The comparison between the reorientation effect and the excitation via the giant dipole resonance is shown in Figs. 5 and 6 for the typical case of ^{114}Cd. With increasing experimental accuracy both effects may become separately measurable.

6. EXPERIMENTAL METHODS

In this section we shall discuss the experimental possibilities which offer themselves as a means of measuring the reorientation effect. The choice among these must, of course, not only take into account the way in which the static quadrupole moment affects the measured quantity but also the accuracy and ease with which an experiment can be performed. Since an explicit dependence of the measurable quantities on the nuclear parameters can be given in a perturbation analysis, the choice of the best conditions for a reorientation experiment may be obtained from such a treatment. The results of perturbation theory may, in many circumstances, not be sufficiently accurate for a final analysis, but the accuracy usually suffices to compare the effectiveness of various experimental possibilities. Such a comparison will be presented below in Sections 6.2 and 6.3. The final analysis of the results will, in most cases, have to be performed with the help of a computer program in which the perturbation expansion is avoided.

The foremost requirement for all reorientation experiments is the absence of nuclear reactions. Our treatment furthermore assumes a classical orbit for the projectile, i.e., $\eta \gg 1$. Also, if we want to discuss the reorientation effect in terms of perturbation theory, we must have $\chi < 1.0$. The following subsection will deal with the bombarding conditions which must be met in order to fulfill these requirements.

The ways in which the reorientation effect can be singled out from a series of measurements of the cross sections and of the angular distributions are discussed in Sections 6.2 and 6.3, respectively. Section 6.4 deals with the reorientation effect occurring in the excitation of the projectile.

6.1 Bombarding Conditions

6.1.1 "Safe" Bombarding Energies

For reorientation experiments where one attempts to measure a small interference term in the presence of a large first-order term, one has to rely to a high degree on the accuracy of the calculated Coulomb excitation cross sections. In typical reorientation measurements effects of the order 10% may be expected in the cross sections, requiring an accuracy within 1% or better for the calculations.

Due to proper nuclear interactions, deviations of the experimentally determined quantities from those predicted by a pure Coulomb interaction will always be observed for sufficiently high bombarding energies. The nuclear interactions are, in general, not sufficiently well understood to be amenable to accurate calculations, so that the range of "safe" bombarding energies can only be determined by a series of experiments.

In order to obtain a rough estimate of the maximum value ϵ_s of the safe bombarding energy we have, somewhat arbitrarily, chosen the following requirements: (a) The minimum distance Δ between the two nuclear surfaces in a head-on collision must be larger than 3 fermi, and (b) the minimum distance Δ must be larger than the de Broglie wavelength λ of the projectile at infinity.

The first of these requirements applies to heavy projectiles for keeping the two surfaces sufficiently far apart to avoid proper nuclear interactions. The second one applies to lighter projectiles which may, even at larger classical distances, interact through the quantum mechanical penetration. Although the definite choices made in (a) and (b) are based on somewhat scanty experiments,[12,21,36] they might still serve as useful guides for the maximum bombarding energy to be used in a particular experiment.

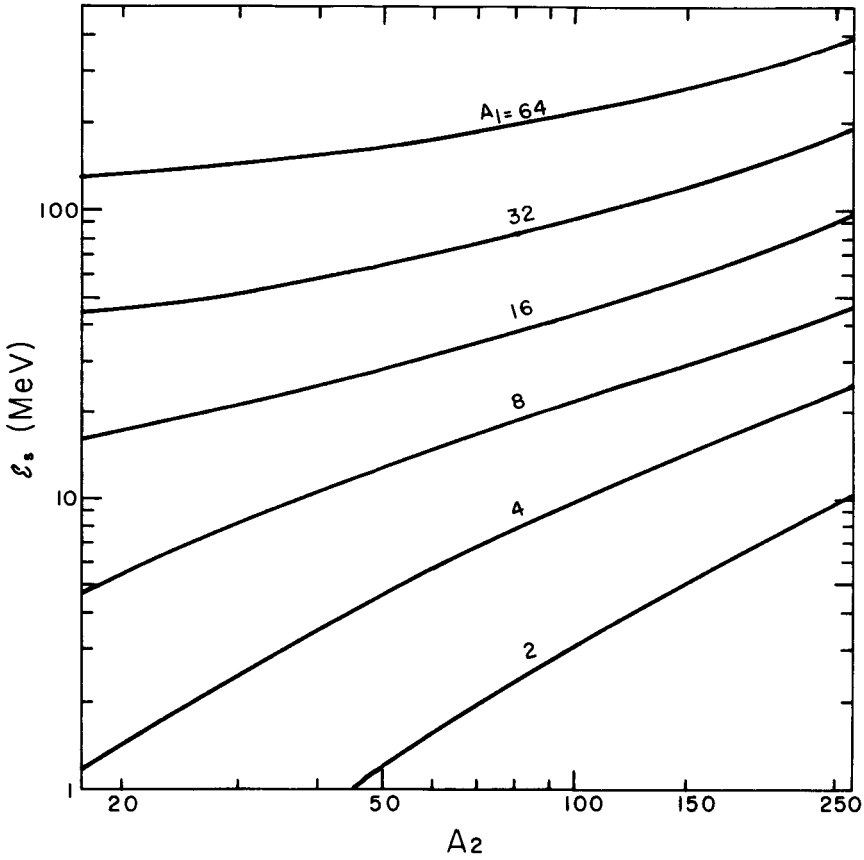

Fig. 7. A rough estimate of the maximum energy ϵ_s that may be used in the Coulomb excitation of target nuclei with mass A_2 by projectiles of mass A_1.

If we assume a value of $R = 1.25A^{1/3}$ fm for the nuclear radius, $Z_1 = 0.5A_1$ for the projectile, and $Z_2 = 0.4A_2$ for the target, ϵ_s may be calculated as a function of A_1 and A_2. The result of this calculation is shown in Fig. 7. Modern machines, capable of accelerating a large variety of projectiles to energies in this range, are thus particularly suited for reorientation experiments.

6.1.2 Validity of the Semiclassical Approximation

As discussed in Sections 3.1 and 3.4 the parameter η is a measure for the quality of the semiclassical approximation. For bombarding energies equal to the maximum safe value ϵ_s, η has been calculated as a function of A_2 and

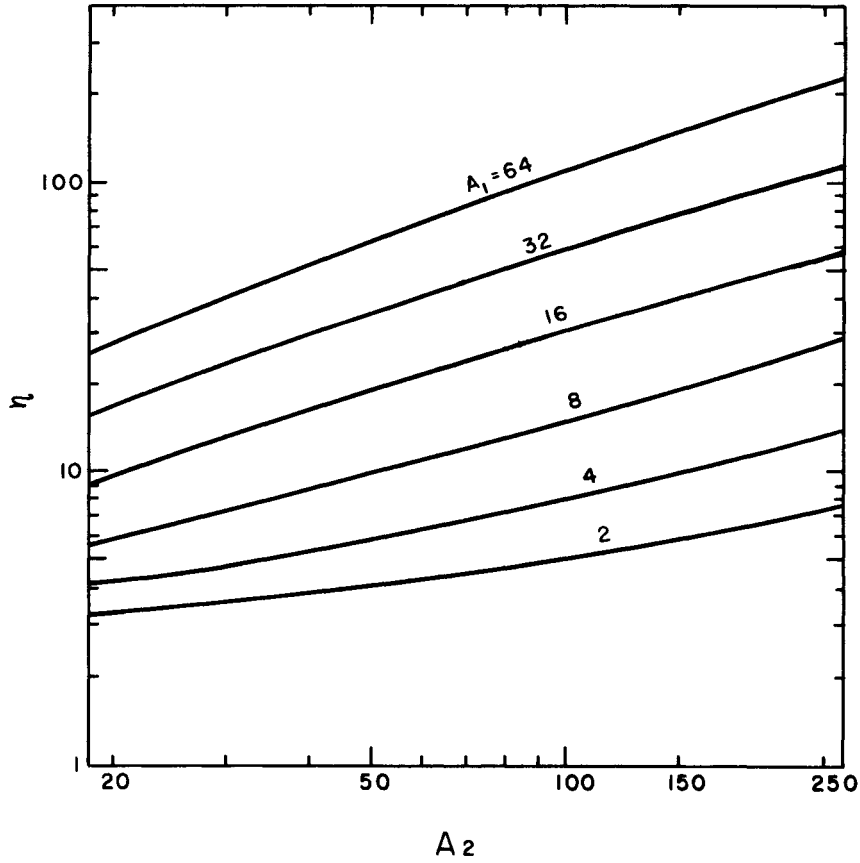

Fig. 8. The parameter η, which is a measure for the validity of a semiclassical description, calculated for the bombardment of nuclei with mass A_2 by projectiles of mass A_1 and having energies ϵ_s (see Fig. 7).

A_1 by using again $Z_1 = 0.5A_1$ and $Z_2 = 0.4A_2$. It can be seen from Fig. 8 that, for most combinations of A_1 and A_2, $\eta > 5$, so that a semiclassical picture is justified.

6.1.3 The Interaction Strength χ

The order of magnitude of the excitation probability [Eq. (35)] as well as of the reorientation effect [Eq. (38)] depend on the quantities $\chi_{i\to f}$ and $\chi_{f\to f}$. Figure 9 gives χ as a function of A_2 and A_1 calculated under the following assumptions: bombarding energy $= \epsilon_s$, $Z_1 = 0.5A_1$, $Z_2 = 0.4A_2$, and a value of $1.0e$ barn for all matrix elements.

For $\chi \gtrsim 1/10$, the second-order perturbation expansion gives values for $P_{i\to f}$ which are accurate within $\gtrsim 1\%$. For χ values $\lesssim 1$ the perturba-

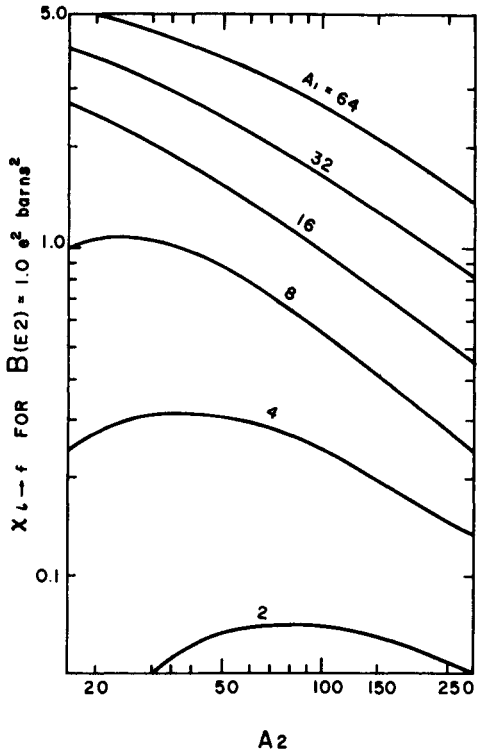

Fig. 9. The interaction strength $\chi_{i\to f}$, which is a measure for the applicability of perturbation theory, calculated for the excitation of a 2^+ state in an even-even nucleus of mass A_2 and a value of $B(E2, O^+ \to 2^+) = 1.0$ $(e \cdot \text{barn})^2$ by projectiles of energy ϵ_s (Fig. 7), and mass A_1.

tion expansion can, however, still serve as a valid guide in the choice of suitable experimental conditions.

6.1.4 The Spectrum of the Target Nucleus

The interpretation of reorientation experiments becomes easier the smaller the number of levels involved in the excitation. In nuclei belonging to the vibrational region, e.g., only the first 2^+ state is strongly excited. It is for this reason that most reorientation experiments performed so far have dealt with nuclei belonging to this region.

In odd mass nuclei more than one state can usually be strongly excited by single $E2$ transitions. In addition to the transition matrix elements between these states, the static quadrupole moments of the excited states as well as of the ground state will affect the measured cross sections. It will therefore be hard, in general, to interpret a series of experiments in terms of a specific matrix element.

Finally, the excitation energy ΔE may not be too small since the sensitivity of the reorientation effect [see Eq. (67)] is approximately proportional to ΔE. This is just the opposite of the requirement imposed by Mössbauer or muonic X-ray studies, where low-excitation energies are required. This is also the reason that it is difficult to measure by reorientation the static quadrupole moment Q of the 2^+ state in a rotational nucleus. Because of the high accuracy with which Q may be predicted by the rotational model, one might otherwise be tempted to check one's experimental method by such a measurement.

6.2 Measurement of Cross Sections

The center-of-mass cross section $d\sigma_f/d\Omega$ for the excitation of state f is calculated by multiplying the Rutherford cross section $d\sigma_R/d\Omega$ with the excitation probability $P_{i\to f}$. Since in most cases the transition to the laboratory system involves only small changes in the cross sections and solid angles, we shall discuss the experiments in terms of P rather than in terms of the actually measured elastic and inelastic cross sections.

6.2.1 Approximate Formula for the Reorientation Effect

The best experimental conditions for determining the reorientation effect from a series of measurements of cross sections can most easily be found from the approximate expression for the reorientation coefficient $r \equiv P^{(12)}/P^{(11)}$ derived in the Appendix:

$$r \equiv \frac{P^{(12)}_{i\to f}}{P^{(11)}_{i\to f}} \approx \frac{A_1}{Z_2}\,\frac{\Delta E}{1 + A_1/A_2}\,\langle I_f \,\|\, \mathscr{M}(E2) \|\, I_f\rangle\, K(\xi, \theta) \tag{67}$$

Here ΔE is the excitation energy in MeV and $\langle I_f \| \mathscr{M}(E2) \| I_f \rangle$ is the static reduced $E2$ matrix element of the final 2^+ state f in e barn, which is related to the static quadrupole moment Q of the excited 2^+ state by

$$eQ = 4/5(2\pi/7)^{1/2} \langle I_f \| \mathscr{M}(E2) \| I_f \rangle \tag{68}$$

Figure 10 shows $K(\xi, \theta)$ as a function of ξ with θ as a parameter.

For typical cases, r lies between 0.05 and 0.20, and the major part in the excitation probability arises from the first-order term $P^{(11)}$, which is proportional to $B(E2, i \to f)$. If the $B(E2)$ value is known to sufficient accuracy

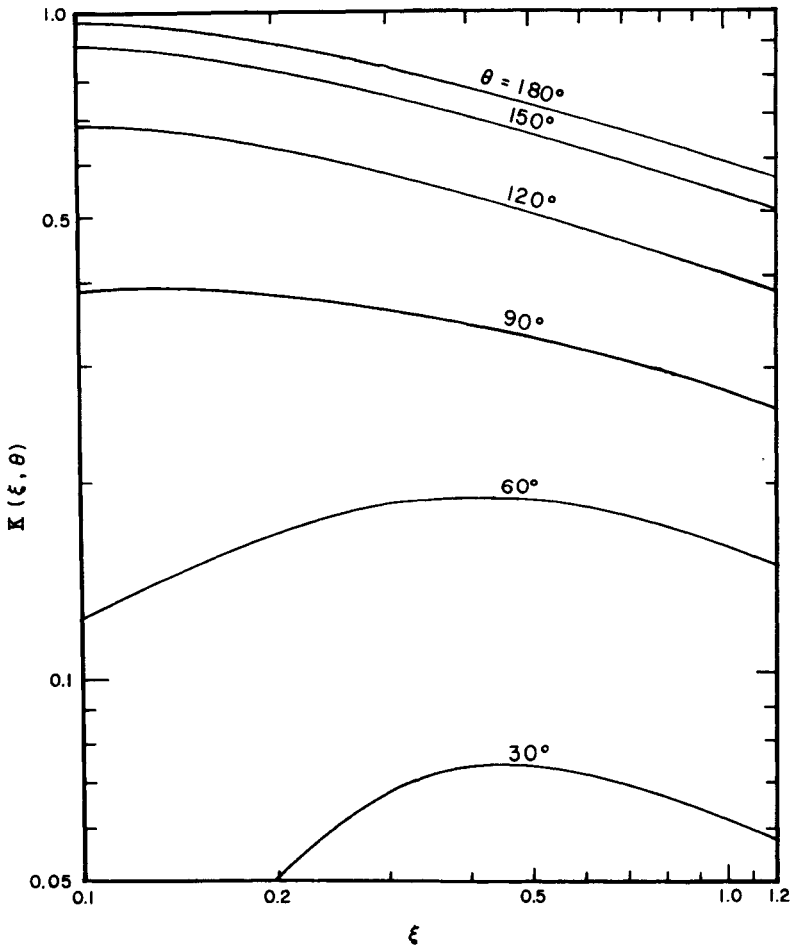

Fig. 10. The function $K(\xi, \theta)$, defined in Eq. (89), and used in the approximate formula (67) for the reorientation effect.

from an independent measurement (e.g., from the lifetime of the 2^+ state), an absolute determination of the excitation probability $P \approx P^{(11)}(1 + r)$ will yield r, since $P^{(11)}$ can be calculated. Experiments of this type are, however, difficult, since both the independent determination of $B(E2)$ values and the measurement of absolute cross sections typically involve errors on the order of 10%.

One can get around this difficulty by not measuring absolute but relative excitation probabilities. The ratio of two excitation probabilities P_α and P_β for different bombarding conditions α and β can be determined more accurately experimentally, because the large uncertainties of absolute calibrations cancel out. We may write the ratio P_α/P_β in terms of r as

$$\frac{P_\alpha}{P_\beta} \approx \frac{P_\alpha^{(11)}}{P_\beta^{(11)}} \frac{1 + r_\alpha}{1 + r_\beta} \approx \frac{P_\alpha^{(11)}}{P_\beta^{(11)}} (1 + r_\alpha - r_\beta) \tag{69}$$

The ratio of the first-order probabilities in Eq. (69) is independent of the nuclear matrix element $B(E2, i \to f)$ and can therefore be calculated. The deviation of the experimental ratio P_α/P_β from this calculated value is proportional to $(r_\alpha - r_\beta)$, which is proportional to the quadrupole moment of the excited state.

The sensitivity of the experimentally determined quantity P_α/P_β on the static quadrupole moment is given by the size of $(r_\alpha - r_\beta)$. If we set $1 + A_1/A_2 \approx 1$ in Eq. (67), we may write

$$r_\alpha - r_\beta = \frac{\Delta E \langle f \| \mathscr{M}(E2) \| f \rangle}{Z_2} [A_1^{(\alpha)} K(\xi_\alpha, \theta_\alpha) - A_1^{(\beta)} K(\xi_\beta, \theta_\beta)] \tag{70}$$

Since the first term of Eq. (70) contains parameters of the target only, one must choose the parameters for the bombardments α and β in such a way as to give a large value for the term between brackets. There are three different ways to achieve this, corresponding to the various choices of the three parameters A_1, θ, and ξ. The following three paragraphs deal with each case separately.

6.2.2 Comparison of Excitation Probabilities for Different Projectiles

In this type of experiment the ratio of the excitation probabilities P_α and P_β is measured. If similar orbits are chosen for the projectiles $A_1^{(\alpha)}$ and $A_1^{(\beta)}$, the two values $K(\xi_\alpha, \theta_\alpha)$ and $K(\xi_\beta, \theta_\beta)$ are approximately equal and $(r_\alpha - r_\beta)$ is roughly proportional to $(A_1^{(\alpha)} - A_1^{(\beta)})$, the mass difference of the projectiles. From Fig. 10 it can be seen that $K(\xi, \theta)$ is largest for small ξ (high bombarding energies) and backward scattering angles. In actual experiments projectiles of masses 4, 12, 16, and 32 have so far been used (see Section 7.1).

There are two ways of measuring excitation cross sections: (a) by detection of the inelastically scattered projectiles and (b) by detection of the decay of the excited nucleus (emission of a gamma ray or internal conversion). These two types of experiments will be discussed below. (The method involving internal conversion will not be discussed here since the conversion coefficients are very small in most important cases.)

a. Magnetic Separation of Inelastic and Elastic Particle Groups. The most straightforward way of measuring excitation probabilities is by comparing the number of particles scattered inelastically with those scattered elastically. In terms of the laboratory cross sections for inelastic and elastic scattering labeled by indices f and i, respectively, the measured ratio $R^{(a)}$ is given by

$$R^{(a)} = \frac{(d\sigma_f/d\Omega)_{\text{lab}}}{(d\sigma_i/d\Omega)_{\text{lab}}} \tag{71}$$

For most practical cases, the cross sections and solid angles in the laboratory system (lab) are almost equal to those of the center-of-mass system (*cm*), so that

$$R^{(a)} \approx \frac{(d\sigma_f/d\Omega)_{\text{cm}}}{(d\sigma_i/d\Omega)_{\text{cm}}} \tag{72}$$

In perturbation theory, this last expression is equal to the excitation probability $P_{i\to f}$, so that $R^{(a)} \approx P_{i\to f}$. The experiment may therefore be discussed in terms of $P_{i\to f}$ rather than $R^{(a)}$.

The main experimental problem in this type of measurement lies in the separation of the inelastic and elastic peaks. For nuclei with high excitation energy, $P_{i\to f}$ is small and it is hard to detect the small inelastic peak in the low-energy tail of the intense elastic peak. For nuclei with low-excitation energies the difficulty usually lies in resolving the inelastic and elastic peaks. Extremely thin targets (a few micrograms per square centimeter) must therefore be used in experiments where heavy ions are scattered through large angles. In a magnetic analysis, one has furthermore to account for the energy dependence of the charge-state distribution of the scattered ion. The resolving power of solid-state detectors for heavy ions has, so far, not made it possible to separate the two particle groups.

b. Gamma Rays in Coincidence with Backscattered Particles. A typical setup for this type of experiment is shown in Fig. 11. The gamma detector, in coincidence with the annular counter, counts the de-excitation gamma rays $f \to i$, which are produced in excitations by backward-scattered particles

The measured quantity $\epsilon_\gamma R^{(b)}$, expressed in terms of the cross sections, is given by

$$\epsilon_\gamma R^{(b)} = \epsilon_\gamma \frac{\sum_{n=2}^{\infty} f_n (d\sigma_n/d\Omega)_{\text{lab}}}{\sum_{n=1}^{\infty} (d\sigma_n/d\Omega)_{\text{lab}}} \tag{73}$$

In this expression, ϵ_γ is the fraction of emitted gamma rays giving rise to a count in the photopeak of the pulse-heights spectrum and f_n is the fraction of decays of state n which give rise to a gamma ray $f \rightarrow i$.

If only one state is strongly excited, then $R^{(b)} \approx P_{i\rightarrow f}$, and the discussion given above for the choice of the best conditions for a reorientation measurement applies also to this type of experiment.

The fraction ϵ_γ of gamma rays detected in the gamma counter is, for an isotropic source, given by the overall efficiency multiplied with the photopeak fraction of the counter. The gamma rays emerging from the target are, however, not isotropically distributed and appropriate corrections have to be applied.

If the particle (or gamma) counter possesses rotational symmetry around the beam axes, the angular distribution of the gamma rays can be written as

$$W(\theta_{\text{beam}}) = W_0[1 + A_2(\xi, \theta)\, P_2(\cos\theta_{\text{beam}}) + A_4(\xi, \theta)\, P_4(\cos\theta_{\text{beam}})] \tag{74}$$

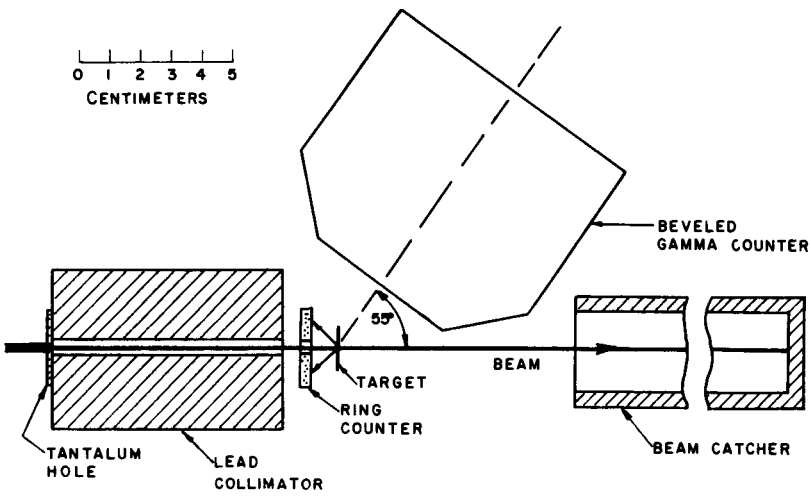

Fig. 11. Schematic view of a typical setup in which the gamma rays are detected by a NaI counter in coincidence with the projectiles backscattered into an annular solid-state counter.

where θ_{beam} is the angle between the direction of the emitted gamma ray and the beam axes. If one chooses the *angle* between the symmetry axis of the gamma counter and the beam direction to be 55°, $P_2(\cos\theta_{\text{beam}})$ vanishes. The *distance* from the target to the counter can be chosen in such a way that $P_4(\cos\theta_{\text{beam}})$ almost averages zero for some (low) gamma energies (see Reference 37).

In measuring the ratio of probabilities, ϵ_γ cancels out to a large extent because A_2 and A_4 are very nearly the same for projectiles of similar ξ and are independent of the excitation process altogether for exact backward scattering. The overall photopeak efficiency for an isotropic source drops out of the ratio completely if the geometry of the gamma detector remains unchanged.

The targets used in this type of experiment can be much thicker than those in which the particle groups must be separable. This advantage is, however, partly canceled by the relatively low efficiency of a coincidence experiment. This experimental method has been used for most reorientation experiments.

If the gamma-ray yields for two different projectiles are measured without particle coincidences, the sensitivity of the yield to the static quadrupole moment is appreciably reduced owing to the drop-off of the reorientation effect for forward angles (see next subsection). The increased accuracy which may be achieved in this simpler type of experiment may, however, largely compensate for the smaller sensitivity.

6.2.3 Comparison of Excitation Probabilities for Different Scattering Angles

Another way to obtain large values for $(r_\alpha - r_\beta)$ is by using the angular dependence of $K(\xi, \theta)$. For $\theta_\alpha = 60°$, $K(\xi, \theta)$ is about five times smaller than for $\theta_\beta = 180°$, and $(r_\alpha - r_\beta)$ can thus be made large if heavy ions are used.

An experimental problem, however, is brought about by the rapid decrease of the excitation probability for forward angles.

a. Magnetic Separation of Inelastic and Elastic Particle Groups. For backward angles, the comments made in Section 6.2.(a) hold also for this section. For forward directions, however, one may use thicker targets because all particles now traverse the entire target and the straggling of the energy loss in the target rather than the energy loss itself determines the observed widths of the particle groups.

In heavy-ion bombardments, the kinematic spread of the lines is appreciable and small solid angles or compensating devices or both have to be used. The split-pole spectrographs now in use or under construction[38] might conveniently perform these tasks, especially if they can be equipped with position-sensitive counters in their focal plane.[39]

b. Particle-Gamma Coincidences. If the angular distribution of the inelastic particles is to be measured by coincidence methods, the gamma counter is conveniently placed with its symmetry axis perpendicular to the reaction plane. Figure 12 shows a possible setup for this type of experiment.

The fraction ϵ_γ of the gamma rays recorded in the gamma detector now depends on the particle scattering angle θ because of the change in the gamma-ray angular distribution with θ. The dependence of ϵ_γ on θ is, however, not very pronounced if a large gamma counter with a solid angle close to 2π (which would give ϵ_γ = constant) is used. In any case, the dependence of the efficiency of a gamma counter on the angle of incidence of the gamma ray can be measured and appropriate corrections can be applied.

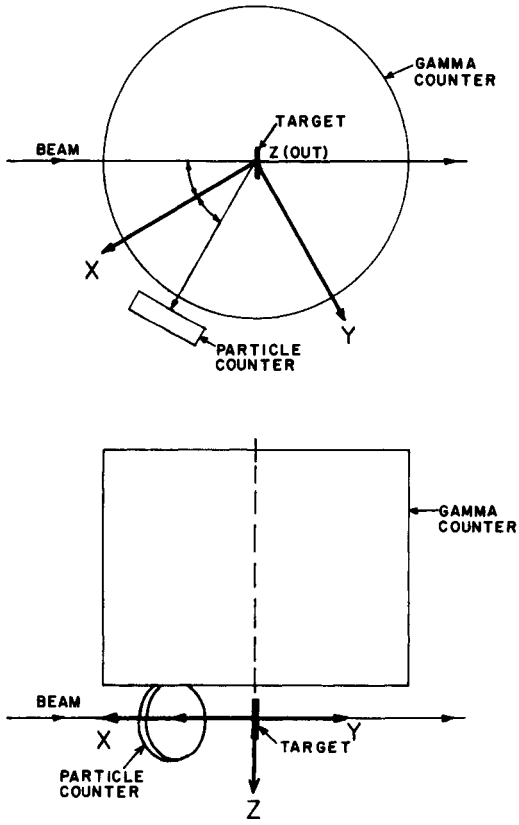

Fig. 12. Schematic view of a setup in which gamma rays are recorded in coincidence with projectiles, scattered through various angles. This experiment measures the variation of the excitation probability with scattering angle.

The lower limit for the scattering angle θ is set by the increasing number of random coincidences occurring for the high particle counting rates at forward angles.

6.2.4 Comparison of Excitation Probabilities for Different Energies

The weak dependence of $K(\xi, \theta)$ (see Fig. 10) on ξ makes $(r_\alpha - r_\beta)$ very small for experiments in which identical projectiles with different bombarding energies are chosen for α and β. Experiments of this type are therefore rather insensitive to the value of Q, and high experimental accuracies are required for an adequate determination of the reorientation effect. Despite these difficulties, the interpretation of the energy variation of the excitation probability in terms of the reorientation effect has been possible in a few cases.[6,12,40]

6.3 Measurement of the Gamma-Ray Angular Distributions

In this section we discuss the measurement of the reorientation effect as it manifests itself in the angular distribution of the de-excitation gamma rays recorded in coincidence with projectiles moving on a specific orbit. Experiments of this type are in general worthwhile only if the measured gamma anisotropies are more sentitive to the value of the quadrupole moment than are the cross section themselves, because the angular-distribution measurement is intrinsically a more difficult one. If Eq. (42) is evaluated numerically for realistic cases, it is found that the above condition is fulfilled only for the second term in the sum which is proportional to $[Y_{k\kappa}(\Omega_\gamma) - Y_{k,-\kappa}(\Omega_\gamma)]$. A possible experiment determining the amplitude of this term, which is proportional to the static quadrupole moment, will be discussed in this section.

6.3.1 Discussion of a Specific Experimental Arrangement

If the amplitude of the imaginary term in Eq. (42) is to be determined experimentally, one has to look for oscillations in the angular distribution which vary as $\sin(\kappa\phi)$. The calculation of realistic numerical values for the amplitudes of these terms shows that: (a) The amplitude of $\sin(4\phi)$ is larger than that of $\sin(2\phi)$; (b) the amplitude of $\sin(4\phi)$ is largest for $\theta_\gamma = 90°$, i.e., for an arrangement in which the gamma counters lie in the reaction plane; (c) for $\theta_\gamma = 90°$, the amplitudes of $\cos(2\phi)$ and of $\sin(2\phi)$ vanish for all projectile orbits; and (d) the amplitude of $\sin(4\phi)$ is largest for projectile orbits with $\theta \approx 90°$.

Two possible experimental arrangements for a measurement of the amplitude of $\sin(4\phi)$ are illustrated in Figs. 13 and 14. For a definition of

the angles θ, ϕ, and θ_γ, see Fig. 2. In the first arrangement (Fig. 13) two particle counters P_1 and P_2 and one gamma counter G are used, whereas the second one (Fig. 14) consists of two gamma counters G_1 and G_2 and one particle counter P. In the first experiment, the two coincidence counting rates P_1G and P_2G are compared, whereas one compares G_1P with G_2P in the second experiment. In each case, the counting rate difference is proportional to the amplitude of sin (4ϕ).

The angular distribution has been calculated for this geometry and for 40-MeV ^{16}O ions bombarding ^{114}Cd, assuming a quadrupole moment equal to 1 barn. An amplitude of sin (4ϕ) of 5% relative to the isotropic term has been computed resulting in a counting rate difference of 10% for the two coincidence rates. Anisotropies of this size may well be measured with reasonable accuracy, especially if multiple-counter systems can be used.

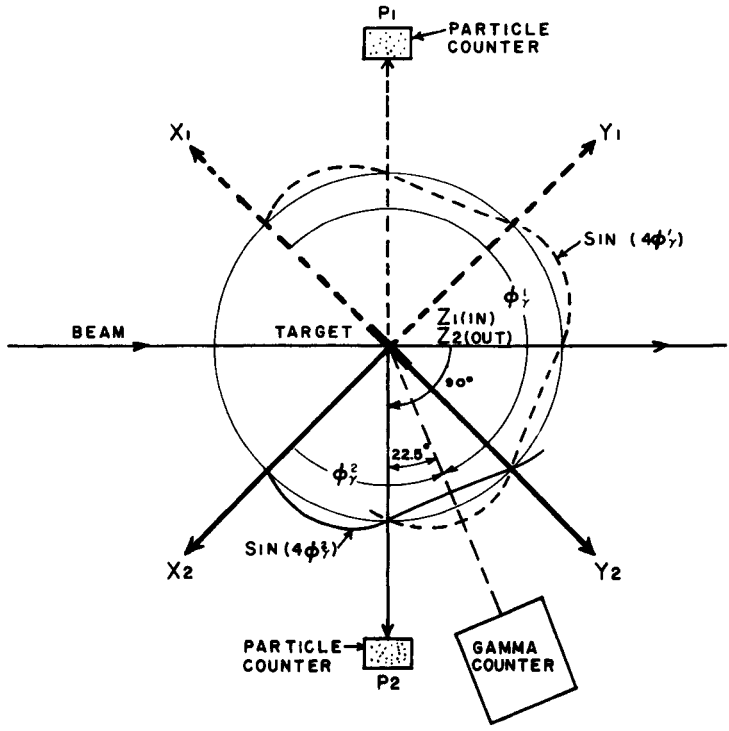

Fig. 13. Schematic view of an experimental arrangement in which the influence of the reorientation process on the angular distribution of the de-excitation gamma rays is studied. The gamma counter is in coincidence with either one of the two particle counters. All three counters lie in a plane.

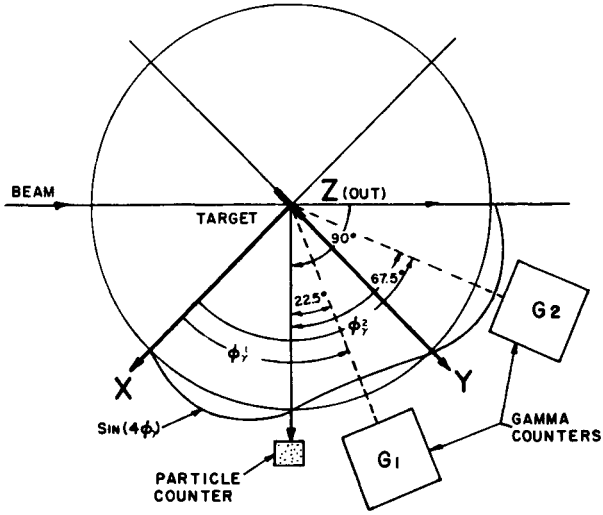

Fig. 14. Similar to Fig. 13, but using one particle counter in coincidence with either one of two gamma counters. All three counters lie in the reaction plane.

6.3.2 Nuclear Deorientation

The word *deorientation* was introduced by Breit[1] to denote the effects of the random change in the nuclear orientation which takes place during the time between Coulomb excitation and gamma de-excitation. Effects of this kind are observed in gamma–gamma angular correlation experiments and are found to be appreciable in general for nuclear lifetimes $\tau \gtrsim 10^{-10}$ sec.[16]

For experiments of the type described in the previous subsection, the target nucleus may receive several MeV of recoil energy. A fraction of the excited nuclei will therefore leave the target and decay in the vacuum. These nuclei may find themselves exposed to strong electric field gradients or magnetic fields, depending on their highly ionized electronic configuration. In such an atom the outermost electronic orbits will have smaller radii than those of a neutral atom and deorientation effects may therefore be enhanced.

A measurement of the importance of these attenuations may be obtained from a determination of the highly anisotropic distribution of gamma rays stemming from nuclei that recoil into the vacuum from backscattered projectiles.

6.3.3 Corrections Due to the Recoil Motion of the Target Nucleus

The orientation of the coordinate system in which the gamma-ray angular distributions [Eq. (42)] are calculated is shown in Fig. 2. The origin

of this coordinate system is located in the target nucleus and may therefore move with an appreciable velocity in the laboratory system if the recoil velocity V is sufficiently high.

For the special case of backscattered projectiles the recoil moves in the direction of the beam with a velocity which is, for small excitation energies, given by

$$\frac{V}{c} = 0.0086 E_{p\,[\mathrm{MeV}]}(A_1)^{1/2}(A_1 + A_2)^{-1} \tag{75}$$

where c is the velocity of light. (For 40-MeV ^{16}O ions bombarding ^{114}Cd, $V/c = 1\%$.) In this case the angular distribution depends only on one angle, the angle θ_{beam} between the beam direction and the direction of the gamma ray, and is given by Eq. (74) for a coordinate system in which the target nucleus is at rest. If the target nucleus decays in flight, the angular distribution in the laboratory system also contains odd Legendre polynomials and is given, to first order in V/c, by

$$W(\theta_{\mathrm{beam}}) = 1 + A_2P_2 + A_4P_4 + \left(\frac{2V}{c}\right)\left\{\left(1 - \tfrac{1}{5}A_2\right)P_1 + \left(\tfrac{5}{6}A_2 - \tfrac{2}{3}A_4\right)P_3 + \tfrac{5}{3}A_4P_5\right\} \tag{76}$$

The odd terms are of the order of V/c and may give rise to efficiency corrections[41] in experiments of the type described in Section 6.2.2(b).

In the general case the emission angles $\phi_{\gamma L}$ and $\theta_{\gamma L}$ in the laboratory system must be computed from the recoil velocity **V** by vectorially adding **V** to the vector **c** (see Fig. 15).

In general, these effects are of importance only for projectile excitation or if light target nuclei are excited by heavy ions.

In addition to changing the pattern of the angular distribution of the gamma rays in the laboratory system, the recoil motion introduces a Doppler shift in the energy of the emitted gamma rays.

6.3.4 Polarization of the Gamma Rays

The circular polarization of the de-excitation gamma rays can be calculated from Eq. (40) by not carrying out the summation over the polarization $P = \pm 1$. The angular dependence then contains four angular functions, namely, Y_{10}, Y_{30}, and $Y_{3,\pm 2}$. Only the linear combination $(Y_{32} - Y_{3,-2})$ is free from first-order contributions. Thus the isolation of the reorientation effect by measuring the polarization of gamma rays is even more difficult than by merely measuring the angular distribution, and hence polarization measurements do not appear very promising for this purpose.

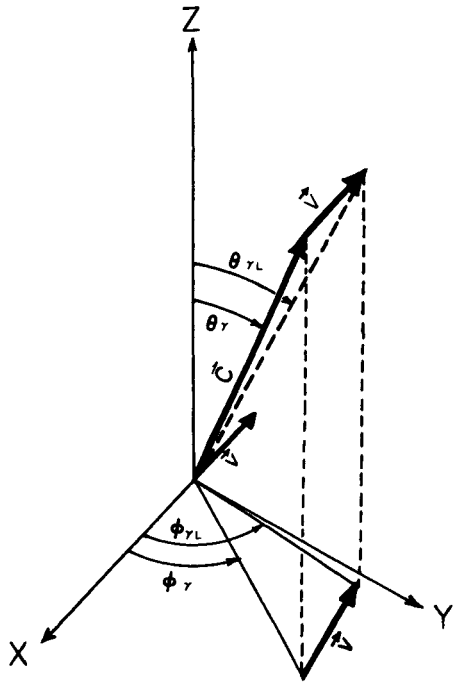

Fig. 15. Effect of the recoil motion of the target. The angular distribution, given as a function of θ_γ and ϕ_γ in Eq. (42), refers to a coordinate system in which the emitting target nucleus is at rest. The emission angles $\theta_{\gamma L}$ and $\phi_{\gamma L}$ observed in the laboratory are obtained by adding vectorially the recoil velocity **V** to **c**.

6.4 Measurement of the Excitation of the Projectile

In the description of the Coulomb excitation of the *target* nucleus we have neglected contributions that might arise from an excitation of the projectile because such contributions would involve multipole–quadrupole interactions, which are much weaker than the dominant monopole–quadrupole interaction responsible for the excitation of the target.

For the excitation of the *projectile* the interaction strength $\chi_{i\to f}^{(\lambda)}$ is obtained from Eq. (31) by exchanging the projectile charge number Z_1 for the charge number of the target Z_2. The formula for ξ [Eq. (30)] remains unchanged.

For projectile excitation the approximate formula for r is

$$r \approx \frac{A_1}{Z_1} \frac{\Delta E_{[\mathrm{MeV}]}}{1 + A_1/A_2} \langle I_f \| \mathscr{M}(E2) \| I_f \rangle_{[\mathrm{ebarn}]} K(\xi, \theta) \tag{77}$$

as obtained from Eq. (67) by replacing Z_2 with Z_1.

In comparing the two formulas we can make the following statements: (a) Since the projectile is studied, we can only vary A_2, ξ, and θ. (b) For light projectiles the dependence of r on the target mass A_2 is not a very pronounced one. (c) The dependence of r on ξ and θ is given by the function $K(\xi, \theta)$. Therefore the arguments given in Section 6.2 also hold for the measurements of the excitation of the projectile. (d) For given values of ΔE, $\langle I_f \| \mathscr{M}(E2) \| I_f \rangle$, and $K(\xi, \theta)$, the reorientation coefficient r in the projectile is enhanced over the one in the target by a factor of about Z_2/Z_1.

The difficulty with experiments involving projectile excitation usually lies in the experimental complications in producing beams of the desired ions with energies high enough to yield easily measurable excitation probabilities.

7. REORIENTATION EXPERIMENTS

Not many reorientation experiments have been performed so far. The main reason for this might be that most accelerators were, until recently, mostly used for bombardments with light ions not leaving sufficient time for experimenters to develop the high-precision heavy-ion techniques required for reorientation experiments.

We shall in this section give a list of all reorientation experiments known to us by mid 1967. We shall briefly discuss the experimental methods employed and the results obtained. For more thorough discussions we refer the reader to the original papers.

7.1 Experimental Methods Used

A list of the nuclei for which reorientation experiments have been performed is given in Table II. In the first experiment listed the dependence of the cross section for one projectile on the bombarding energy was analyzed in terms of the reorientation effect (see Section 6.2.4). Most of the other experiments used the dependence of the reorientation effect on the projectile mass A_1. Except for two measurements on ^{114}Cd, the gamma rays were recorded in coincidence with the backscattered ions (see Section 6.2.2b).

TABLE II

List of Reorientation Experiments

Nucleus	Projectile	Bombarding energies, MeV	Experimental method used[a]	Type of analysis of results	Refs.
^{152}Sm	^{16}O	17–42	6.2.4	Computer	6, 37, 40
^{114}Cd	^{4}He ^{16}O	10 41	6.2.2a	Computer	12
^{114,116}Cd	^{4}He ^{12}C ^{16}O	8–10 25–30 33–42	6.2.2b	Computer	12
^{114}Cd ^{130}Ba ^{148,150}Sm	^{16}O ^{32}S	19–27 41–54	6.2.2b	Computer and Perturbation	7
^{112,114,116}Cd ^{104}Ru ^{110}Pd ^{122}Te ^{63}Cu	^{4}He ^{16}O	8 23	6.2.2b	Perturbation	9
^{126,128}Te	^{4}He ^{16}O	8–10 33–41	6.2.2b	Computer	13
^{116,124}Sn	^{4}He ^{16}O ^{32}S	10 40 56	6.2.2b	Perturbation	14
^{114}Cd	^{16}O	40	6.2.3a	Computer	39
^{114}Cd	^{16}O	40	6.2.3b	Computer	42

[a] The quoted numbers refer to the section in this paper in which the particular experimental method is described.

In two recent experiments[39,42] the dependence of the excitation probability on the scattering angle was measured.

The merits and disadvantages of the two principal methods, namely, recording the gamma rays in coincidence with the backscattered ions and separating the inelastically and elastically scattered particles, are summarized in Table III. The drawbacks of very thin targets and of small solid angles

encountered in experiments using magnetic analysis may well be offset by the small efficiency of gamma counters for high energies and by the fact that the product of two solid angles is involved in a coincidence experiment.

TABLE III

Comparison of Experimental Methods

	Gamma-particle coincidences	Magnetic separation of elastic and inelastic particle groups
Beam	Variations in intensity may give counting rate effects.	Highest beam that target can stand is all right.
Target	Should be thin enough to give an energy loss of less than about 10% of the full energy.	Must be thin enough to allow separation of elastic and inelastic groups.
Target backing	Particles backscattered from backing must be separable from those backscattered from target; must not give excessive gamma-ray background.	Must allow kinematic separation of the backscattered ions.
Solid angles	Maximum attainable value is about 10% of sphere for each detector.	Maximum value about 0.05% of sphere.
Efficiency	Dependent on gamma energy; corrections because of gamma angular distributions have to be applied.	Dependent on how many charge states can simultaneously be recorded with spectrograph.
Charge states	. . . . .	Owing to the energy dependence of the charge-state distribution of the backscattered ions, corrections must be applied before comparing inelastic and elastic peaks.

7.2 Results

The results of the experiments listed in Table II are summarized in Table IV. Average values are quoted in those cases where several measurements have been made on the same nucleus. In addition to the static quadrupole moments $eQ = 0.758\,\langle 2\|\mathscr{M}(E2)\|2\rangle$ [see Eq. (68)], the values of the transition moments $\langle 0\|\mathscr{M}(E2)\|2\rangle = [B(E2, 0 \to 2)]^{1/2}$ are given in

units of e barn as well as in single particle units (s.p.u.) with 1 unit = $5.5 \times 10^{-3} A^{2/3} e$ barn.

The next column gives the experimental value for the absolute value of the ratio

$$\langle 2 \mathscr{M}(E2) \| 2 \rangle / \langle 0 \| \mathscr{M}(E2) \| 2 \rangle.$$

TABLE IV

Experimental Results

Nucleus	Q,[a] barns	$\lvert\langle 0 \| \mathscr{M}(E2) \| 2\rangle\rvert$, e barns[b]	s.p.u.[c]	$\dfrac{\lvert\langle 2 \| \mathscr{M}(E2) \| 2\rangle\rvert^{d}}{\lvert\langle 0 \| \mathscr{M}(E2) \| 2\rangle\rvert}$	β^{e}
$^{104}_{44}$Ru	-0.63 ± 0.20	0.96	7.9	0.86	+0.18
$^{110}_{46}$Pd	-0.82 ± 0.18	0.92	7.3	1.18	+0.21
$^{112}_{48}$Cd	$+0.12 \pm 0.35$	0.72	5.6	0.22	−0.03
$^{114}_{48}$Cd	-0.60 ± 0.15	0.75	5.8	1.05	+0.14
$^{116}_{48}$Cd	-0.78 ± 0.14	0.79	6.0	1.30	+0.19
$^{116}_{50}$Sn	$+0.6 \pm 0.3$	0.46	3.5	1.72	−0.14
$^{124}_{50}$Sn	-0.46 ± 0.25	0.46	3.4	1.32	+0.10
$^{122}_{52}$Te	-0.50 ± 0.22	0.81	5.9	0.82	+0.11
$^{126}_{52}$Te	-0.33 ± 0.17	0.73	5.3	0.60	+0.07
$^{128}_{52}$Te	-0.20 ± 0.20	0.64	4.6	0.41	+0.04
$^{130}_{56}$Ba	-1.10 ± 0.34	0.87	6.2	1.67	+0.21
$^{148}_{62}$Sm	-0.73 ± 0.38	0.94	6.1	1.02	+0.11
$^{150}_{62}$Sm	-1.22 ± 0.22	1.15	7.4	1.40	+0.19
$^{152}_{62}$Sm	-1.8 ± 0.6	1.85	11.7	1.28	+0.28

[a] From the references quoted in Table II.

[b] From Paul H. Stelson and Lee Grodzins, *Nucl. Data Tables, U.S. At. Energy Comm.* **1**, 29 (1965).

[c] Single particle unit = $5.5 \times 10^{-3} A^{2/3} e$ barn.

[d] In the pure rotational model this ratio is equal to 1.195.

[e] Calculated from Q with the help of Eqs. (78), (68), and (3), assuming for the nuclear radius $R_0 = 1.3 \text{ fm} \times A_2^{1/3}$.

In a purely rotational description both of these $E2$ matrix elements are expressed in terms of the intrinsic quadrupole moment Q_0 by the equation

$$\langle I_i \| \mathscr{M}(E2) \| I_f \rangle = (-1)^{K+1} \left\{ (2I_i + 1)(2I_f + 1) \frac{5}{16\pi} \right\}^{1/2} Q_0 \begin{pmatrix} I_i & I_f & 2 \\ K & -K & 0 \end{pmatrix} \quad (78)$$

where K is the spin of the level upon which the rotational band is built. The ratio between two matrix elements is independent of Q_0 and is, for the two matrix elements in columns 1 and 2, equal to

$$\frac{\langle 2 \| \mathscr{M}(E2) \| 2 \rangle}{\langle 0 \| \mathscr{M}(E2) \| 2 \rangle} = -\left(\frac{10}{7}\right)^{1/2} \quad (79)$$

Although most of the nuclei listed in Table IV do not exhibit rotational features in their spectra, the ratio between the two $E2$ matrix elements is nevertheless found to be close to the rotational value.

In order to obtain a better feeling for the size of the quadrupole moments involved, we have, in the last column, also listed the values of the deformation parameter β which, by Eq. (3), would yield intrinsic quadrupole moments Q_0 which are, through Eqs. (68) and (78), consistent with the measured values of Q. (The nuclear radius R_0 has been taken as $R_0 = 1.3A^{1/3}$ fm.)

7.3 Discussion

The quadrupole moments of first excited 2^+ states in spherical nuclei measured by the reorientation effect establish a very striking fact. While the conventional vibrational model of spherical nuclei[43] predicts a vanishing quadrupole moment for the one-phonon states, the experiments reveal a quadrupole moment of collective magnitude. In fact one may say that the quadrupole moment exhibits the same degree of enhancement compared with single-particle values as does the $E2$ transition amplitude. A similar situation is encountered in the region of strongly deformed nuclei.

The results show that the vibrational picture must be modified to include large anharmonicities. Various attempts have been made to understand the larger measured quadrupole moments. Tamura and Udagawa[44,45] propose that the first excited 2^+ state should be described as a mixture of a one-phonon and a two-phonon state. DoDang *et al.*[46] try to correct the current microscopic random phase approximation (R.P.A.) theory by incorporating density fluctuations between the ground state and the 2^+ state. By means of a self-consistent perturbation theory these fluctuations lead to a change in the excited-state density and hence to a deformation. Kumar and Baranger[47,48] attribute the effect to the presence of strong nonlinearities in Bohr's collective Hamiltonian. They calculate the macroscopic functions

entering into this Hamiltonian with a microscopic theory based on the pairing-plus-quadrupole model of two-nucleon effective interaction.[47,48] The calculated enhancement of quadrupole moments is of the correct order of magnitude. B. Sørensen[49] treats the anharmonicities in ^{114}Cd by taking into account nonlinear terms in a boson expansion of fermion pair operators. In a pairing-plus-quadrupole model he obtains reasonable agreement with experimental values for the energies, the $E2$ transition matrix elements, and the static quadrupole moment. Numerous further theoretical investigations are in progress.[50,51]

Perhaps the most obvious merit of the reorientation experiments is that they have stimulated an intense activity among theorists which may add a good deal to our understanding of nuclei.

Acknowledgments

The authors would like to thank Dr. G. M. Temmer for his interest in and generous support of the present work. In particular J. E. is grateful to the Rutgers staff for the hospitality extended to him during his stay at Rutgers. We also appreciate our valuable discussions with Dr. L. S. Kisslinger on the magnetic dipole reorientation. The invaluable assistance rendered by Dr. Gregory G. Seamen in the computer programming for the tables in the Appendix is also gratefully acknowledged. Thanks are due to Mrs. Ruth Freeswick for the careful typing of the manuscript.

APPENDIX A. NUMERICAL EXPRESSIONS

The first part of the Appendix consists of a collection of numerical expressions for the quantities introduced in Sections 3, 4, and 5. Although many of the formulas are contained in other references,[12,21,22,24,26,29] they are given here for completeness of this text. Table V gives a list of the input quantities and the units in which they must be entered in the numerical expressions given below.

1. The reduced bombarding energy ϵ_f defined by

$$\epsilon_f = E_p - (1 + A_1/A_2)\,\Delta E_f \tag{80}$$

is used in the symmetrized expressions.

2. The symmetrized expression for half the distance of closest approach (see Eq. 29) in a head-on collision is given by

$$a_{fn} = 0.07199 Z_1 Z_2 (1 + A_1/A_2)(\epsilon_f \epsilon_n)^{-1/2}\, 10^{-12}\ \text{cm} \tag{81}$$

TABLE V

Input Quantities and their Units

Name of Quantity	Symbol	Unit
Bombarding energy	E_p	MeV
Projectile mass	A_1	amu
Projectile charge number	Z_1	
Scattering angle in c-m. system	θ	degrees
Target mass	A_2	amu
Target charge number	Z_2	
Index of states: initial	i	
intermediate	n	
final	f	
Excitation energy of state n	ΔE_n	MeV
Reduced $E\lambda$ matrix element[a]	$\langle n \parallel \mathscr{M}(E\lambda) \parallel f \rangle$	$e(10^{-12}\ \mathrm{cm})^\lambda$
Spin of state n	I_n	$\hbar$

[a] For definition see Eq. (13).

3. The symmetrized expression [see Eq. (31)] for the strength of the transition $n \to f$ is given for $E1$ excitation by

$$\chi_{n\to f}^{(1)} = \frac{5.169 A_1^{1/2}(\epsilon_n \epsilon_f)^{1/2}}{Z_2(1 + A_1/A_2)} \frac{\langle n \parallel \mathscr{M}(E1) \parallel f \rangle}{(2I_n + 1)^{1/2}} \tag{82}$$

and for $E2$ excitation by

$$\chi_{n\to f}^{(2)} = \frac{14.360 A_1^{1/2}(\epsilon_n \epsilon_f)^{3/4}}{Z_1 Z_2^2(1 + A_1/A_2)^2} \frac{\langle n \parallel \mathscr{M}(E2) \parallel f \rangle}{(2I_n + 1)^{1/2}} \tag{83}$$

4. The symmetrized expression for the adiabaticity parameter [see Eq. (30)] is given by

$$\xi_{nf}^{(\mathrm{symm})} = \frac{Z_1 Z_2 A_1^{1/2}}{6.325} (\epsilon_n^{-1/2} - \epsilon_f^{-1/2}) \tag{84}$$

If $(1 + A_1/A_2)\, \Delta E_f \ll E_p$, then $\xi_{nf}^{(\mathrm{symm})}$ may be approximated by

$$\xi_{nf}^{(\mathrm{symm})} \approx \frac{Z_1 Z_2 A_1^{1/2}(1 + A_1/A_2)(\Delta E_f - \Delta E_n)}{12.65\, E_p^{3/2}} \tag{85}$$

5. The first-order symmetrized differential cross section in the center-of-mass system in units of barn per steradian is given by

$$\frac{d\sigma_f}{d\Omega} = 2.592 \times 10^{-4} \left(\frac{E_p}{\epsilon_f}\right)^{1/2} \left\{\frac{(1 + A_1/A_2)\, Z_1 Z_2}{E_p}\right\}^2 \times [\chi_{i\to f}^{(2)}]^2 \sum_{\mu} [\mathscr{K}_{2\mu}(\theta, \xi)]^2 \left(\sin\frac{\theta}{2}\right)^{-4} \tag{86}$$

APPENDIX B. TABLES OF ORBITAL INTEGRALS

In this appendix the orbital integrals which are needed for the calculation of first-order processes and for first- to second-order interference effects are tabulated. The calculations were performed on the Rutgers-Bell SDS 925 computer. Table VI gives a list of the tabulated quantities, the numbers of the defining equations, and the numbers of the equations in which the tabulated values are used.

TABLE VI

List of Tabulated Orbital Integrals

Tabulated quantity	Table	Defined in Eq.	Used in Eq.
$\frac{1}{5}\sum_{\mu} [\mathscr{K}_{2\mu}(\theta, \xi)]^2$	VII	(15)	(35)
$(\frac{1}{5})^{1/2} \sum_{\mu} \mathscr{K}_{2\mu}(\theta, \xi)\, \mathscr{B}_{2\mu}^{(22)}(\xi, 0, \theta)$	VIII	(15), (25)	(38)
$\mathscr{B}_{k\kappa}^{(11)}(\xi, 0, \theta)$	IX	(43)	(42)
$\mathscr{B}_{k\kappa}^{(12)}(\xi, 0, \theta)$	X	(44)	(42)
$\mathscr{T}_{k\kappa}^{(12)}(\xi, 0, \theta)$	XI	(45)	(42)
$\mathscr{B}_{M}^{(E1)}(\theta, \xi)$	XII	(55), (50)	(54), (58), (61)

APPENDIX C. APPROXIMATE FORMULA FOR THE REORIENTATION EFFECT

The relative contribution r of the reorientation effect to the excitation probability is given by

$$r = \frac{P_{i\to f}^{(12)}}{P_{i\to f}^{(11)}} \tag{87}$$

Inserting Eqs. (35) and (38) into (87), one obtains an expression for r which is independent of $\chi^{(2)}_{i\to f}$ and proportional to $\chi^{(2)}_{f\to f}$.

A good estimate for r may be obtained in those cases where

$$(1 + A_1/A_2)\,\Delta E_f \ll E_p$$

i.e., $\epsilon_f \simeq E_p$. The dependence of $\chi^{(2)}_{f\to f}$ on the bombarding energy E_p is then simply given by a factor $E_p^{3/2}$ [see Eq. (83)]. If $E_p^{3/2}$ is eliminated with the help of the approximate expression in Eq. (85) for ξ, the ratio r can be written as

$$r = \frac{A_1\,\Delta E\langle 2^+ \| \mathscr{M}(E2) \| 2^+\rangle}{Z_2(1 + A_1/A_2)}\,K(\theta, \xi_{if}) \tag{88}$$

where $K(\theta, \xi_{if})$ is given by

$$K(\theta, \xi) = 1.135\,\frac{\sum_\mu \mathscr{K}_{2\mu}(\theta, \xi)\,\mathscr{B}^{(22)}_{2\mu}(\xi, 0, \theta)}{\xi \sum_\mu [\mathscr{K}_{2\mu}(\theta, \xi)]^2} \tag{89}$$

The function $K(\theta, \xi)$ is shown in Fig. 10.

TABLE VII

The Quantity $\frac{1}{5} \sum_{\mu} [\mathscr{K}_{2\mu}(\theta, \xi)]^2$, used for the Calculation of the First-Order Excitation Probability

THETA	XI= 0.0	XI= 0.1	XI= 0.2	XI= 0.3	XI= 0.4
10.0	.1431E-03	.1450E-03	.5384E-04	.1146E-04	.1847E-05
20.0	.1918E-02	.2094E-02	.1654E-02	.9416E-03	.4360E-03
30.0	.8254E-02	.8736E-02	.7878E-02	.5750E-02	.3594E-02
40.0	.2244E-01	.2310E-01	.2138E-01	.1701E-01	.1199E-01
50.0	.4752E-01	.4780E-01	.4412E-01	.3620E-01	.2694E-01
60.0	.8596E-01	.8478E-01	.7720E-01	.6382E-01	.4858E-01
70.0	.1393E 00	.1350E 00	.1208E 00	.9944E-01	.7620E-01
80.0	.2080E 00	.1985E 00	.1743E 00	.1419E 00	.1085E 00
90.0	.2912E 00	.2740E 00	.2362E 00	.1895E 00	.1437E 00
100.0	.3864E 00	.3594E 00	.3040E 00	.2402E 00	.1801E 00
110.0	.4900E 00	.4510E 00	.3750E 00	.2916E 00	.2158E 00
120.0	.5974E 00	.5448E 00	.4460E 00	.3416E 00	.2492E 00
130.0	.7026E 00	.6358E 00	.5136E 00	.3878E 00	.2792E 00
140.0	.7998E 00	.7194E 00	.5744E 00	.4282E 00	.3046E 00
150.0	.8828E 00	.7902E 00	.6254E 00	.4616E 00	.3250E 00
160.0	.9464E 00	.8442E 00	.6638E 00	.4862E 00	.3396E 00
170.0	.9864E 00	.8782E 00	.6878E 00	.5014E 00	.3486E 00
180.0	.1000E 01	.8896E 00	.6960E 00	.5066E 00	.3516E 00

TABLE VII

(continued)

THETA	XI= 0.5	XI= 0.6	XI= 0.7	XI= 0.8	XI= 0.9
10.0	.2524E-06	.3096E-07	.3516E-08	.3772E-09	.3874E-10
20.0	.1766E-03	.6520E-04	.2250E-04	.7376E-05	.2324E-05
30.0	.2016E-02	.1044E-02	.5098E-03	.2378E-03	.1069E-03
40.0	.7728E-02	.4654E-02	.2660E-02	.1459E-02	.7740E-03
50.0	.1857E-01	.1207E-01	.7490E-02	.4480E-02	.2600E-02
60.0	.3462E-01	.2344E-01	.1523E-01	.9570E-02	.5850E-02
70.0	.5514E-01	.3812E-01	.2540E-01	.1642E-01	.1035E-01
80.0	.7882E-01	.5498E-01	.3708E-01	.2434E-01	.1561E-01
90.0	.1041E 00	.7268E-01	.4924E-01	.3252E-01	.2104E-01
100.0	.1295E 00	.9002E-01	.6088E-01	.3950E-01	.2610E-01
110.0	.1536E 00	.1060E 00	.7128E-01	.4696E-01	.3038E-01
120.0	.1753E 00	.1198E 00	.7996E-01	.5232E-01	.3368E-01
130.0	.1940E 00	.1312E 00	.8672E-01	.5630E-01	.3598E-01
140.0	.2092E 00	.1400E 00	.9166E-01	.5896E-01	.3738E-01
150.0	.2210E 00	.1464E 00	.9500E-01	.6060E-01	.3810E-01
160.0	.2292E 00	.1507E 00	.9706E-01	.6148E-01	.3840E-01
170.0	.2342E 00	.1532E 00	.9816E-01	.6186E-01	.3846E-01
180.0	.2358E 00	.1539E 00	.9850E-01	.6198E-01	.3846E-01

TABLE VII

(*continued*)

THETA	XI= 1.0	XI= 1.2	XI= 1.4	XI= 1.6	XI= 2.0
10.0	.3842E-11	.3486E-13	.2918E-15	.2302E-17	.1261E-21
20.0	.7084E-06	.6108E-07	.4882E-08	.3688E-09	.1862E-11
30.0	.4668E-04	.8296E-05	.1373E-05	.2152E-06	.4714E-08
40.0	.3996E-03	.9988E-04	.2334E-04	.5188E-05	.2294E-06
50.0	.1472E-02	.4440E-03	.1258E-03	.3400E-04	.2234E-05
60.0	.3494E-02	.1180E-02	.3756E-03	.1143E-03	.9586E-05
70.0	.6384E-02	.2308E-02	.7904E-03	.2594E-03	.2542E-04
80.0	.9814E-02	.3700E-02	.1326E-02	.4566E-03	.4954E-04
90.0	.1336E-01	.5160E-02	.1900E-02	.6742E-03	.7800E-04
100.0	.1664E-01	.6496E-02	.2426E-02	.8756E-03	.1053E-03
110.0	.1936E-01	.7572E-02	.2842E-02	.1033E-02	.1268E-03
120.0	.2138E-01	.8318E-02	.3116E-02	.1133E-02	.1397E-03
130.0	.2270E-01	.8742E-02	.3250E-02	.1175E-02	.1441E-03
140.0	.2340E-01	.8898E-02	.3272E-02	.1173E-02	.1418E-03
150.0	.2368E-01	.8876E-02	.3224E-02	.1143E-02	.1356E-03
160.0	.2370E-01	.8774E-02	.3150E-02	.1104E-02	.1285E-03
170.0	.2364E-01	.8672E-02	.3088E-02	.1074E-02	.1231E-03
180.0	.2360E-01	.8632E-02	.3064E-02	.1063E-02	.1211E-03

TABLE VIII

The Interference Term $(\frac{1}{5})^{1/2} \sum_{\mu} \mathscr{K}_{2\mu}(\theta, \xi)\, \mathscr{B}_{2\mu}^{(22)}(\xi, 0, \theta)$

THETA	XI= 0.0	XI= 0.1	XI= 0.2
30.0	.000E 00	-.365E-04	.158E-03
60.0	.000E 00	.208E-02	.510E-02
90.0	.000E 00	.211E-01	.351E-01
120.0	.000E 00	.736E-01	.110E 00
150.0	.000E 00	.141E 00	.202E 00
180.0	.000E 00	.173E 00	.245E 00

THETA	XI= 0.4	XI= 0.8	XI= 1.2
30.0	.205E-03	.244E-04	.111E-05
60.0	.712E-02	.252E-02	.405E-03
90.0	.392E-01	.149E-01	.310E-02
120.0	.106E 00	.361E-01	.745E-02
150.0	.181E 00	.554E-01	.106E-01
180.0	.215E 00	.629E-01	.116E-01

TABLE IX

The Gamma-Ray Angular-Distribution Coefficients $\mathscr{R}_{k\kappa}^{(11)}(\xi, 0, \theta)$.

(The two numbers in brackets denote k and κ, respectively, $[k, \kappa]$)

THETA	XI	[0,0]	[2,0]	[2,2]	[4,0]	[4,2]	[4,4]
30.0	.00	.293E-01	.173E-02	.130E-01	-.110E-01	.150E-01	-.951E-02
30.0	.10	.310E-01	-.248E-02	.118E-01	-.847E-02	.136E-01	-.783E-02
30.0	.20	.279E-01	-.523E-02	.807E-02	-.541E-02	.932E-02	-.440E-02
30.0	.40	.127E-01	-.339E-02	.236E-02	-.172E-02	.272E-02	-.896E-03
30.0	.80	.843E-03	-.254E-03	.893E-04	-.912E-04	.103E-03	-.208E-04
30.0	1.20	.294E-04	-.914E-05	.219E-05	-.299E-05	.253E-05	-.365E-06
60.0	.00	.305E 00	-.884E-02	.137E 00	-.950E-01	.158E 00	-.132E 00
60.0	.10	.301E 00	-.238E-01	.124E 00	-.824E-01	.143E 00	-.117E 00
60.0	.20	.274E 00	-.386E-01	.971E-01	-.624E-01	.112E 00	-.837E-01
60.0	.40	.172E 00	-.373E-01	.457E-01	-.296E-01	.528E-01	-.323E-01
60.0	.80	.339E-01	-.927E-02	.595E-02	-.440E-02	.687E-02	-.298E-02
60.0	1.20	.418E-02	-.122E-02	.553E-03	-.482E-03	.638E-03	-.213E-03
90.0	.00	.103E 01	-.949E-01	.446E 00	-.273E 00	.515E 00	-.530E 00
90.0	.10	.971E 00	-.109E 00	.401E 00	-.243E 00	.463E 00	-.470E 00
90.0	.20	.837E 00	-.118E 00	.316E 00	-.191E 00	.365E 00	-.357E 00
90.0	.40	.509E 00	-.968E-01	.160E 00	-.977E-01	.185E 00	-.163E 00
90.0	.80	.115E 00	-.279E-01	.271E-01	-.176E-01	.313E-01	-.223E-01
90.0	1.20	.183E-01	-.489E-02	.348E-02	-.245E-02	.401E-02	-.240E-02

TABLE IX

(continued)

THETA	XI	[0,0]	[2,0]	[2,2]	[4,0]	[4,2]	[4,4]
120.0	.00	.212E 01	-.279E 00	.872E 00	-.498E 00	.101E 01	-.119E 01
120.0	.10	.193E 01	-.268E 00	.778E 00	-.444E 00	.899E 00	-.106E 01
120.0	.20	.158E 01	-.237E 00	.612E 00	-.350E 00	.707E 00	-.820E 00
120.0	.40	.884E 00	-.153E 00	.312E 00	-.180E 00	.360E 00	-.400E 00
120.0	.80	.185E 00	-.386E-01	.555E-01	-.330E-01	.641E-01	-.644E-01
120.0	1.20	.295E-01	-.680E-02	.772E-02	-.476E-02	.892E-02	-.818E-02
150.0	.00	.313E 01	-.479E 00	.124E 01	-.686E 00	.143E 01	-.184E 01
150.0	.10	.280E 01	-.433E 00	.111E 01	-.611E 00	.128E 01	-.164E 01
150.0	.20	.222E 01	-.349E 00	.866E 00	-.479E 00	.100E 01	-.128E 01
150.0	.40	.115E 01	-.188E 00	.439E 00	-.244E 00	.506E 00	-.642E 00
150.0	.80	.215E 00	-.376E-01	.778E-01	-.436E-01	.898E-01	-.111E 00
150.0	1.20	.315E-01	-.582E-02	.109E-01	-.615E-02	.126E-01	-.151E-01
180.0	.00	.355E 01	-.566E 00	.139E 01	-.760E 00	.160E 01	-.212E 01
180.0	.10	.315E 01	-.504E 00	.123E 01	-.676E 00	.142E 01	-.188E 01
180.0	.20	.247E 01	-.394E 00	.965E 00	-.529E 00	.111E 01	-.147E 01
180.0	.40	.125E 01	-.199E 00	.488E 00	-.267E 00	.563E 00	-.745E 00
180.0	.80	.220E 00	-.351E-01	.860E-01	-.471E-01	.993E-01	-.131E 00
180.0	1.20	.306E-01	-.489E-02	.120E-01	-.656E-02	.138E-01	-.183E-01

TABLE X

The Gamma-Ray Angular-Distribution Coefficients $\mathscr{R}_{k\kappa}^{(12)}(\xi, 0, \theta)$

THETA	XI	[0,0]	[2,0]	[2,2]	[4,0]	[4,2]	[4,4]
30.0	.00	.000E 00	.000E 00	.000E 00	.000E 00	.000E 00	.000E 00
30.0	.10	-.129E-03	-.228E-03	-.136E-03	.213E-03	-.157E-03	-.767E-04
30.0	.20	.559E-03	-.401E-03	-.815E-04	.113E-03	-.941E-04	-.163E-03
30.0	.40	.728E-03	-.292E-03	-.202E-04	-.249E-04	-.234E-04	-.673E-04
30.0	.80	.864E-04	-.293E-04	-.115E-06	-.699E-05	-.132E-06	-.287E-05
30.0	1.20	.395E-05	-.129E-05	.247E-07	-.354E-06	.286E-07	-.728E-07
60.0	.00	.000E 00	.000E 00	.000E 00	.000E 00	.000E 00	.000E 00
60.0	.10	.736E-02	-.629E-02	.105E-02	.224E-02	.122E-02	-.827E-02
60.0	.20	.181E-01	-.992E-02	.197E-02	.137E-02	.228E-02	-.107E-01
60.0	.40	.252E-01	-.101E-01	.204E-02	-.914E-03	.236E-02	-.723E-02
60.0	.80	.894E-02	-.303E-02	.572E-03	-.722E-03	.660E-03	-.117E-02
60.0	1.20	.143E-02	-.467E-03	.749E-04	-.130E-03	.865E-04	-.355E-04
90.0	.00	.000E 00	.000E 00	.000E 00	.000E 00	.000E 00	.000E 00
90.0	.10	.747E-01	-.261E-01	.217E-01	-.548E-02	.251E-01	-.561E-01
90.0	.20	.125E 00	-.408E-01	.325E-01	-.111E-01	.375E-01	-.770E-01
90.0	.40	.139E 00	-.428E-01	.300E-01	-.144E-01	.346E-01	-.614E-01
90.0	.80	.529E-01	-.158E-01	.900E-02	-.589E-02	.104E-01	-.145E-01
90.0	1.20	.110E-01	-.326E-02	.162E-02	-.123E-02	.187E-02	-.214E-02

TABLE X

(continued)

THETA	XI	[0,0]	[2,0]	[2,2]	[4,0]	[4,2]	[4,4]
120.0	.00	.000E 00	.000E 00	.000E 00	.000E 00	.000E 00	.000E 00
120.0	.10	.261E 00	-.572E-01	.910E-01	-.443E-01	.105E 00	-.169E 00
120.0	.20	.390E 00	-.861E-01	.132E 00	-.659E-01	.152E 00	-.237E 00
120.0	.40	.376E 00	-.849E-01	.118E 00	-.621E-01	.137E 00	-.201E 00
120.0	.80	.128E 00	-.303E-01	.357E-01	-.201E-01	.412E-01	-.547E-01
120.0	1.20	.264E-01	-.647E-02	.670E-02	-.398E-02	.774E-02	-.939E-02
150.0	.00	.000E 00	.000E 00	.000E 00	.000E 00	.000E 00	.000E 00
150.0	.10	.499E 00	-.860E-01	.190E 00	-.102E 00	.219E 00	-.304E 00
150.0	.20	.717E 00	-.124E 00	.271E 00	-.146E 00	.313E 00	-.430E 00
150.0	.40	.643E 00	-.113E 00	.239E 00	-.130E 00	.276E 00	-.374E 00
150.0	.80	.196E 00	-.357E-01	.708E-01	-.389E-01	.817E-01	-.108E 00
150.0	1.20	.377E-01	-.705E-02	.132E-01	-.731E-02	.152E-01	-.197E-01
180.0	.00	.000E 00	.000E 00	.000E 00	.000E 00	.000E 00	.000E 00
180.0	.10	.612E 00	-.977E-01	.239E 00	-.131E 00	.276E 00	-.366E 00
180.0	.20	.869E 00	-.139E 00	.340E 00	-.186E 00	.393E 00	-.519E 00
180.0	.40	.761E 00	-.122E 00	.298E 00	-.163E 00	.344E 00	-.455E 00
180.0	.80	.223E 00	-.356E-01	.873E-01	-.478E-01	.101E 00	-.133E 00
180.0	1.20	.413E-01	-.659E-02	.161E-01	-.885E-02	.186E-01	-.247E-01

TABLE XI

The Gamma-Ray Angular-Distribution Coefficients $\mathscr{T}_{k\kappa}^{(12)}(\xi, 0, \theta)$

THETA	XI	[0,0]	[2,0]	[2,2]	[4,0]	[4,2]	[4,4]
30.0	.00	.000E 00	.000E 00	.000E 00	.000E 00	.000E 00	.000E 00
30.0	.10	.000E 00	.000E 00	.300E-03	.000E 00	.347E-03	.411E-03
30.0	.20	.000E 00	.000E 00	.187E-03	.000E 00	.216E-03	.383E-03
30.0	.40	.000E 00	.000E 00	-.324E-05	.000E 00	-.374E-05	.131E-03
30.0	.80	.000E 00	.000E 00	-.560E-05	.000E 00	-.647E-05	.529E-05
30.0	1.20	.000E 00	.000E 00	-.274E-06	.000E 00	-.316E-06	.132E-06
60.0	.00	.000E 00	.000E 00	.000E 00	.000E 00	.000E 00	.000E 00
60.0	.10	.000E 00	.000E 00	.345E-02	.000E 00	.398E-02	.996E-02
60.0	.20	.000E 00	.000E 00	.291E-02	.000E 00	.336E-02	.122E-01
60.0	.40	.000E 00	.000E 00	-.118E-04	.000E 00	-.137E-04	.782E-02
60.0	.80	.000E 00	.000E 00	-.580E-03	.000E 00	-.669E-03	.121E-02
60.0	1.20	.000E 00	.000E 00	-.112E-03	.000E 00	-.129E-03	.118E-03
90.0	.00	.000E 00	.000E 00	.000E 00	.000E 00	.000E 00	.000E 00
90.0	.10	.000E 00	.000E 00	.197E-02	.000E 00	.228E-02	.420E-01
90.0	.20	.000E 00	.000E 00	-.455E-03	.000E 00	-.525E-03	.556E-01
90.0	.40	.000E 00	.000E 00	-.556E-02	.000E 00	-.642E-02	.421E-01
90.0	.80	.000E 00	.000E 00	-.354E-02	.000E 00	-.409E-02	.931E-02
90.0	1.20	.000E 00	.000E 00	-.816E-03	.000E 00	-.943E-03	.132E-02

TABLE XI

(continued)

THETA	XI	[0,0]	[2,0]	[2,2]	[4,0]	[4,2]	[4,4]
120.0	.00	.000E 00	.000E 00	.000E 00	.000E 00	.000E 00	.000E 00
120.0	.10	.000E 00	.000E 00	-.122E-01	.000E 00	-.141E-01	.757E-01
120.0	.20	.000E 00	.000E 00	-.191E-01	.000E 00	-.221E-01	.103E 00
120.0	.40	.000E 00	.000E 00	-.200E-01	.000E 00	-.231E-01	.833E-01
120.0	.80	.000E 00	.000E 00	-.736E-02	.000E 00	-.850E-02	.211E-01
120.0	1.20	.000E 00	.000E 00	-.155E-02	.000E 00	-.179E-02	.344E-02
150.0	.00	.000E 00	.000E 00	.000E 00	.000E 00	.000E 00	.000E 00
150.0	.10	.000E 00	.000E 00	-.184E-01	.000E 00	-.212E-01	.643E-01
150.0	.20	.000E 00	.000E 00	-.259E-01	.000E 00	-.299E-01	.887E-01
150.0	.40	.000E 00	.000E 00	-.225E-01	.000E 00	-.260E-01	.736E-01
150.0	.80	.000E 00	.000E 00	-.657E-02	.000E 00	-.759E-02	.197E-01
150.0	1.20	.000E 00	.000E 00	-.121E-02	.000E 00	-.140E-02	.339E-02
180.0	.00	.000E 00	.000E 00	.000E 00	.000E 00	.000E 00	.000E 00
180.0	.10	.000E 00	.000E 00	.000E 00	.000E 00	.000E 00	.000E 00
180.0	.20	.000E 00	.000E 00	.000E 00	.000E 00	.000E 00	.000E 00
180.0	.40	.000E 00	.000E 00	.000E 00	.000E 00	.000E 00	.000E 00
180.0	.80	.000E 00	.000E 00	.000E 00	.000E 00	.000E 00	.000E 00
180.0	1.20	.000E 00	.000E 00	.000E 00	.000E 00	.000E 00	.000E 00

TABLE XII

The Quantity $\mathscr{B}_M^{(E1)}(\theta, \xi)$ Used in Electric Dipole Interference Terms

THETA	M	XI= 0.0	XI= 0.1	XI= 0.2	XI= 0.4	XI= 0.8	XI= 1.2
30.0	-2	.00312	.00440	.00489	.00404	.00133	.00029
	0	-.00415	-.00373	-.00295	-.00152	-.00029	-.00004
	+2	.00312	.00193	.00117	.00041	.00005	.00001
60.0	-2	.01711	.02066	.02252	.02158	.01207	.00497
	0	-.01910	-.01819	-.01614	-.01127	-.00416	-.00130
	+2	.01711	.01315	.00980	.00523	.00133	.00032
90.0	-2	.04053	.04529	.04712	.04382	.02642	.01240
	0	-.03928	-.03790	-.03457	-.02597	-.01162	-.00443
	+2	.04053	.03393	.02742	.01698	.00575	.00179
120.0	-2	.06520	.06917	.06923	.06149	.03613	.01717
	0	-.05746	-.05572	-.05143	-.03994	-.01934	-.00800
	+2	.06520	.05789	.04947	.03386	.01362	.00491
150.0	-2	.08383	.08503	.08200	.06894	.03799	.01745
	0	-.06977	-.06778	-.06288	-.04955	-.02483	-.01064
	+2	.08383	.07804	.06971	.05159	.02354	.00941
180.0	-2	.09073	.08820	.08194	.06484	.03280	.01419
	0	-.07408	-.07202	-.06691	-.05294	-.02678	-.01159
	+2	.09073	.08820	.08194	.06484	.03280	.01419

REFERENCES

1. G. Breit and J. P. Lazarus, *Phys. Rev.* **100**:942 (1955).
   G. Breit, R. L. Gluckstern, and J. E. Russell, *Phys. Rev.* **103**:727 (1956).
   G. Breit and R. L. Gluckstern, *in* "Handbuch der Physik," (S. Flügge, ed.), Vol. XLI/1, p. 496, Springer-Verlag, Berlin (1959).
2. J. F. Masso and D. L. Lin, *Phys. Rev.* **140**:B1182 (1965).
3. D. L. Lin and J. F. Masso, *in* "Proceedings of the Third Conference on Reactions Between Complex Nuclei" (A. Ghiorso, R. M. Diamond, and H. E. Conzett, eds.), p. 267, University of California Press, Berkeley (1963).
4. D. S. Beder, *Can. J. Phys.* **41**:547 (1963).
5. A. C. Douglas, W. Bygrave, D. Eccleshall, and M. J. L. Yates, *in* "Proceedings of the Third Conference on Reactions Between Complex Nuclei" (A. Ghiorso, R. M. Diamond, and H. E. Conzett, eds.), p. 274, University of California Press, Berkeley (1963).
6. G. Goldring, J. de Boer, and H. Winkler, *in* "Proceedings of the Third Conference on Reactions Between Complex Nuclei" (A. Ghiorso, R. M. Diamond, and H. E. Conzett, eds.), p. 278, University of California Press, Berkeley (1963).
7. J. J. Simpson, D. Eccleshall, M. J. L. Yates, and N. J. Freeman, *Nucl. Phys.* **A94**:177 (1967).
8. P. H. Stelson, W. T. Milner, J. L. C. Ford, Jr., F. K. McGowan, and R. L. Robinson, *Bull. Am. Phys. Soc.* **10**:427 (1965).
9. P. H. Stelson, *in* "Proceedings of the Summer Study Group on the Physics of the Emperor Tandem Van de Graaff Region," Vol. III, p. 1005, Brookhaven National Laboratory (1965), and *private communication.*
10. J. de Boer, R. G. Stokstad, G. D. Symons, and A. Winther, *Bull. Am. Phys. Soc.* **9**:718 (1964).
11. J. de Boer, R. G. Stokstad, G. D. Symons, and A. Winther, *Phys. Rev. Letters*, **14**:564 (1965).
12. R. G. Stokstad, I. Hall, G. D. Symons, and J. de Boer, *Nucl. Phys.* **A92**:319 (1967).
13. R. G. Stokstad and I. Hall, *Bull. Am. Phys. Soc.* **12**:35 (1967).
14. A. Kleinfeld, R. Covello-Moro, J. de Boer, and H. P. Lie, *Bull. Am. Phys. Soc.* **12**:564 (1967).
15. E. Mueller, *in* "Advances in Electronics and Electron Physics" (L. Martin, ed.), Vol. 8, p. 83, Academic Press, Inc., New York (1960).
16. E. Karlsson, E. Matthias, and K. Siegbahn, eds., "Perturbed Angular Correlations" North-Holland Publishing Company, Amsterdam (1964).
17. R. J. Powers, V. L. Telegdi, *Z. Physik* **202**:214 (1967).
18. H. L. Acker, H. Marschall, G. Backenstoss, and D. Quitmann, *Nucl. Phys.* **62**:477 (1965).
19. R. C. Barrett, S. Bernow, I. Duerdoth, S. Devons, D. Hitlin, E. R. Macagno, J. Rainwater, K. Runge, and C. S. Wu, *to be published.*
20. K. A. Ter-Martirosyan, *Zh. Eksperim. i Teor. Fiz.* **22**:284 (1952).
21. K. Alder, A. Bohr, T. Huus, B. Mottelson, and A. Winther, *Revs. Mod. Phys.* **28**:432 (1956).
    K. Alder and A. Winther, "Coulomb Excitation" *in* "Perspectives in Physics," Academic Press, Inc., New York (1966).
22. K. Alder and A. Winther, *Kgl. Danske Videnskab. Selskab, Mat.-Fys. Medd.* **32**(8) (1960).

23. K. Alder and A. Winther, *Kgl. Danske Videnskab. Selskab, Mat.-Fys. Medd.* **31**(1) (1956).
24. L. C. Biedenharn and P. J. Brussaard, "Coulomb Excitation," Clarendon Press, Oxford (1965).
25. A. C. Douglas, *Nucl. Phys.* 42:428 (1963) and "Atomic Weapons Research Establishment Report NR/P-2/62," Aldermaston, England, *unpublished.* Also: B. Greiner and H. Arenhövel, *to be published in Nucl. Phys.*
26. A. Winther and J. de Boer, "A Computer Program for Multiple Coulomb Excitation," Progress Report, Rutgers, The State University, and California Institute of Technology, Nov., 1965.
27. J. Eichler, *Bull. Am. Phys. Soc.* **9**:152 (1964).
28. L. Kisslinger, *private communication.*
29. J. Eichler, *Phys. Rev.* **133**:B1162 (1964).
30. J. S. Levinger, "Nuclear Photo-Disintegration" Oxford University Press, Inc., New York (1960).
31. N. McDonald, *Phys. Letters* **10**:334 (1964).
32. A. Bohr and B. Mottelson, *private communication.*
33. A. Winther, *in* "Proceedings of the International Symposium on Nuclear Physics with Tandems," Heidelberg, Germany (1966).
34. A. C. Douglas and N. McDonald, *Phys. Letters* **24B**:447 (1967).
35. H. Nebel and D. L. Lin, *Phys. Rev.* **156**:1133 (1967).
36. G. G. Seaman, N. Benzer-Koller, and M. Bertin, *Bull. Am. Phys. Soc.* **12**:491 (1967).
37. J. de Boer, G. Goldring, and H. Winkler, *Phys. Rev.* **134**:B1032 (1964).
38. J. E. Spencer and H. H. Enge, *Nucl. Instr. Meth.* **49**:181 (1967).
39. J. E. Glenn and J. X. Saladin, *Phys. Rev. Letters* **19**:33 (1967).
40. G. Goldring and U. Smilansky, *Phys. Rev. Letters* **16**:151 (1965).
41. B. Herskind and Y. Yoshizawa, *Nucl. Instr. Meth.* **27**:104 (1964).
42. G. Schilling, R. P. Scharenberg, and J. W. Tippie, *Phys. Rev. Letters* **19**:318 (1967).
43. A. Bohr and B. R. Mottelson, *Kgl. Danske Videnskab. Selskab, Mat.-Fys. Medd.* **27**:16 (1953).
44. T. Tamura and T. Ugadawa, *Phys. Rev. Letters* **15**:765 (1965).
45. T. Tamura and T. Ugadawa, *Phys. Rev.* **150**:783 (1966).
46. G. DoDang, R. Dreizler, A. Klein, and C. S. Wu, *Phys. Rev. Letters* **17**:709 (1966).
47. K. Kumar and M. Baranger, *Phys. Rev. Letters* **17**:1146 (1966).
48. K. Kumar and M. Baranger, *Nucl. Phys.* **A92**:608 (1967).
49. B. Sørensen, *Phys. Letters* **24B**:328 (1967).
50. L. Kisslinger and K. Kumar, submitted to *Phys. Rev. Letters.*
51. Proceedings of the "International Conference on Nuclear Structure," Tokyo (1967).

THE NUCLEAR SU_3 MODEL

M. Harvey

1. INTRODUCTION

The shell model, despite a somewhat checkered career, has emerged as a useful approximation to the many-particle description of the atomic nucleus (E57*b*, S63). In principle it is perhaps the closest of all nuclear models to being unified, i.e., to describing all properties of all states of all nuclei. Unfortunately, even with the restriction to a shell structure, the number of possible states is often very large and there are few nuclei whose properties can be described without a prohibitive amount of computational labor. Thus several submodels of the shell model have been constructed to reduce the number of states and hence also the computational difficulty. These submodels describe more of the physical structure of states in terms of well-defined quantum numbers. It is as a submodel of the shell model that we can classify the "SU_3 model."

The SU_3 model is both very elegant and very useful. This article is aimed at making the model widely accessible to physicists at a time when it has become firmly established.

Simultaneous with the development of the shell model has been the construction of various collective models (M57, B60*b*). In their simplest forms, however, these two types of models seem to have little in common: the shell model is based on the assumption of independent particle motion, whereas the collective models rely on the coherent motion of many nucleons. Neither model in its simplest form is very successful; qualitative features of nuclear energy levels can be described, but quantitative precision is lacking. In the extreme form of the shell model, the single-particle submodel (in which the properties of states are given by the shell model orbit of the last odd nucleon), estimates can be made for electromagnetic transition probabilities (Weisskopf estimates, W60) and magnetic moments (Schmidt values, B56) which, while often of the correct order of magnitude, yet lack precision. For the collective models, on the other hand, (e.g., one based on the rotation of a nucleus deformed into a nonspherical shape) the observed approximate $J(J+1)$

dependence of "bands" of energy states of some nuclei can be explained and electromagnetic transitions predicted to be proportional to the square of a Clebsch–Gordan coefficient; the "moment of inertia" and "deformation" have to be treated as parameters, however.

With the development of both types of model, it soon becomes apparent that they may not in fact be different. The shell model goes beyond its single-particle features with the introduction of "configuration mixing," while the rotational model gains some individual-particle features in the construction of the rotating "intrinsic state."

The impetus for the development of the SU_3 model was the observation of collective features in such nuclei as ^{19}F and ^{24}Mg (cf. the review in G60). These nuclei were light enough for a shell model description, and hence attempts could be made to study the many-particle and the collective nature of states at the same time.

The classification of shell-model states according to the group SU_3 has excited considerable interest, since its introduction by J. P. Elliott (E58), for several reasons:

a. It appears to be of physical interest in that the states so constructed possess many of the gross properties of states of light nuclei, at least for mass $A \leqslant 24$.
b. It has the important property of exhibiting simultaneously both the collective and single-particle aspects of a many-body state.
c. It is an extremely elegant approach carrying with it the power of group theory, the resulting simplification in calculations, and the *understanding* of the results of such calculations.

Basically the SU_3 model is a shell model and much of the background is therefore similar. In this article we have tried to cut back to a minimum the discussion on the pure shell aspect of the problem with, we hope, adequate references to articles and books already written on the subject. In Part 2 we review some of the main features of the shell model to make the article reasonably self-contained and to clarify the position occupied by the SU_3 scheme in the general shell theory.

The general classification and structure of states according to SU_3 is contained in Part 3. There are actually several approaches (e.g., B60*a*, B61, M62, K66*b*) one can take in establishing the SU_3 scheme but, to avoid an article with an amorphous character and enormous length, we present here only the approach (E58, E59, H61*a*, E62, E63*a*) with which the author is most familiar. We hope our references adequately cover the other methods.

The validity of any model of course depends on the character of the

internucleon force or the *effective* force present in the nucleus. This point is discussed in Part 4.

In Part 5 we shall review some of the applications of the SU_3 scheme. These applications set out to answer either or both of the questions: (a) Are the states classified according to SU_3 indeed the eigenfunctions of a realistic Hamiltonian, and (b) does the SU_3 model successfully predict observable data in the real nucleus? As we shall show, very few calculations yield answers to both questions.

Part 6 is devoted to a summary and developments stemming from the SU_3 model and a discussion on related work.

In Parts 5 and 6 we have tried to give an objective view of the worth of the SU_3 classification scheme and a review of the papers from which we have drawn our conclusions. With the present rate of production of scientific papers we feel certain that some papers concerned directly with the SU_3 scheme have been missed. We hope that the papers we do quote present a fair cross section of the calculations that have been done.

It has been our intention to make the text of this article readable to everyone remotely interested in the field. For this reason many of the mathematical proofs have been relegated to appendices. In the appendices also are given those parts of the shell model theory which are necessary for a complete appreciation of the SU_3 scheme but which would detract from the main arguments if included in the text. These appendices are not meant to be complete but only to serve as a step between the main text and the detailed literature.

The group SU_3 has perhaps caught the imagination of contemporary physicists in its application in the field of elementary particles. Its use there, however, has no physical relationship with its use in nuclear structure theory—the three-dimensional spaces are different! The abstract properties of the group can of course be applied in both fields. In Appendix I we briefly give the classification of the elementary particles (and quarks) according to the group SU_3 and its subgroups SU_2 and U_1 and show the abstract connection with the classification of the *intrinsic* states in the nuclear model.

2. BASIC SHELL MODEL

2.1 General Theory

The fundamental principle on which the shell model is based is that the interactions of any nucleon with all the other nucleons may be approximated by an average single-particle potential (*E*57*b*, *S*63). Initially we assume this field to be spherically symmetric. In practice this field is rarely derived from

any self-consistent (e.g., Hartree–Fock) arguments but rather from considerations of the basic physics of the problem. Thus, since the nucleons are bound together in a finite region of space (of the order of 10^{-13}-cm radius), the average field is expected to be attractive throughout the region occupied by the nucleus and to vanish everywhere else. For spin-independent forces then the central potential is expected to have roughly the form illustrated in Fig. 2.1a. (We ignore here any repulsion due to the Coulomb forces between protons.) The lowest bound states of an A-particle system are then formed by filling the lowest bound orbits in the central well obeying the Pauli principle. Since each nucleon can have spin and isospin projections of $\pm\frac{1}{2}$, each single-particle orbital state will be occupied by at most four particles.

As long as we are concerned only with the lowest bound states, the single-particle orbits of the actual finite potential are similar to those of an appropriate infinite potential, e.g., the harmonic oscillator well (Fig. 2.1*b*). The advantage of using harmonic oscillator functions is that they are more amenable to mathematical manipulation. We can thus concentrate on the physical many-body aspect of the problem without additional complication in the mathematics. Some of the properties of the harmonic oscillator pertinent to the SU_3 model are reviewed in Appendix A.

Recent Hartree–Fock calculations, which set out to determine the single-particle wave functions self-consistently, show that the harmonic-oscillator assumption is quite good (M65*b*). Harmonic-oscillator functions

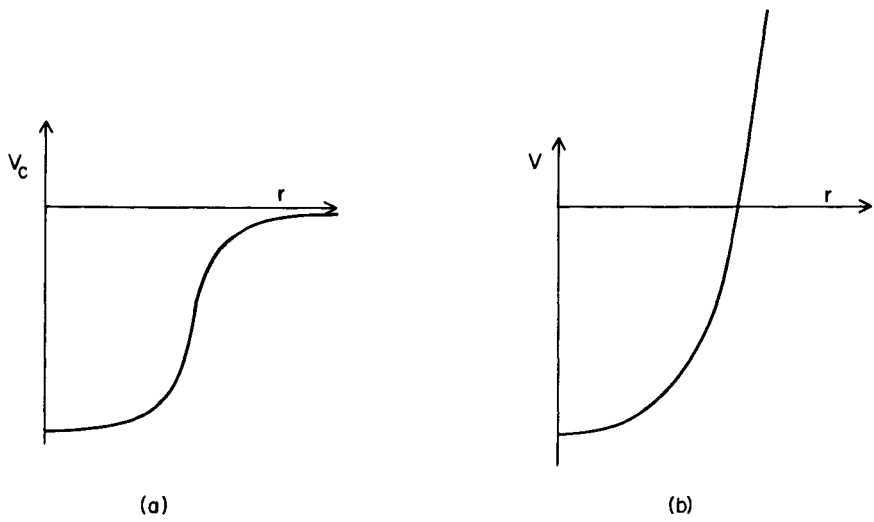

Fig. 2.1. A comparison between the single-particle well one might construct from intuitive arguments (*a*), and the harmonic-oscillator well (*b*) which has the same "shape" for bound states.

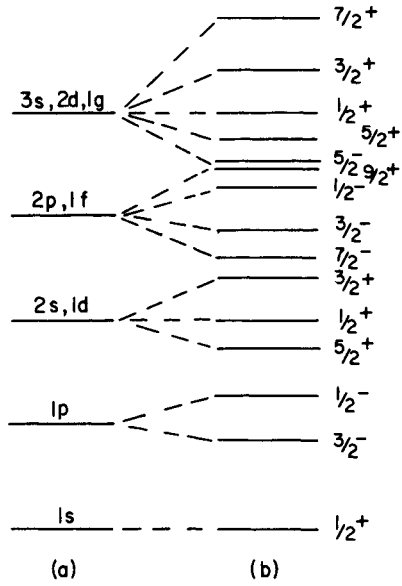

Fig. 2.2. Single-particle spectrum of the harmonic oscillator (*a*) with no spin-orbit force, (*b*) with a spin-orbit force $\xi \sum_i s_i l_i$ with $\xi = 0.27\hbar\omega$.

are most inaccurate in determining the "tail" of the nucleus (i.e., the region of large radii where the wave functions approach zero) since they decay with a Gaussian form instead of the more realistic exponential form. As long as we are not considering nuclear properties which are sensitive to the tail (e.g., electromagnetic transitions of high multipole order), then the use of the harmonic-oscillator functions is a reasonable approximation for bound states. Even in higher excited states few people use the more correct wave function from a well such as shown in Fig. 2.1*a*, often with the argument (but not the justification) that the single-particle character of these states is small (see however B65*b*, B66*f*, W66*a*).

The oscillator parameter can be treated as a variational parameter or alternatively it can be determined so that the lowest functions in the well have the correct mean square radius, as determined for example from electron scattering experiments (H57, see Appendix A).

The lowest orbits in the harmonic oscillator are shown schematically in Fig. 2.2*a*, where each energy level is characterized by the number of quanta. The spacing between levels is a constant proportional to the frequency of oscillation $\hbar\omega$. In light nuclei the filling of each shell corresponds to the "magic number" of particles 2, 8, 20 for neutrons and protons separately,

observed, for example, through discontinuities in binding energies and excitation energies of first excited states as a function of particle number (L60). For heavy nuclei the observed magic numbers can be reproduced if a spin-dependent single-particle potential $V_s = \xi(s \cdot l)$ is assumed to be part of the average well.[1] The splitting of the harmonic oscillator levels is shown in Fig. 2.2*b* for the strength parameter $\xi = 0.27\hbar\omega$.

For a nucleus which has more than the number of particles required to close a shell, the lower states are assumed to be formed by filling as many of the lower orbits as possible and then allowing the remaining "extra core" particles to partially fill the next lowest orbit. The next orbit usually has a large degeneracy; e.g., even with the single-particle levels in Fig. 2.2*b* the degeneracy per level is at least $(2j + 1)$. Because of this degeneracy the number of many-body functions which can be formed is large: the number of ways W of putting p like-particles into an orbit of degeneracy d is $W = d!/[(d-p)!\,p!]$. Since a large degeneracy is not observed in nuclei clearly the model as it stands is not sufficient. The shell model is extended by allowing the extra core particles to interact and thus split the degeneracy of the wave functions.

The two basic problems in the shell model then are: (a) The introduction of the appropriate residual interaction. (One makes the assumption that the residual interaction simply splits the degeneracy of the average field without lifting particles from one orbit to another.) (b) Finding the configurations of extra core nucleons which form the eigenfunctions.

The residual interaction which is introduced is supposed to take account of the effects of the nucleon–nucleon interaction which have not been included in the average central field. The effective residual interaction differs from the nuclear force between free nucleons for several reasons: (a) The presence of other nucleons inhibits the final states which may result from any interaction—quite generally this effect of the Pauli principle causes the effective residual interaction to have a longer range than the free force; (b) the nucleons polarize other nucleons, so it may be considered that the interaction is taking place between "quasi particles" which are not real nucleons. Thus one has some freedom in choosing the effective residual interaction (cf. Part 4) which will lead to eigenfunctions possessing the observed features of the lowest energy levels, e.g., energies, moments, transition probabilities, etc.

The problem of finding the eigenfunctions of a given residual interaction in terms of a finite set W of shell model states is in principle easy to solve. It is only necessary to set up and diagonalize the energy matrix with the many-body functions as basis states. Such a problem can be and has been

[1] One also needs a single-particle orbital term to split the oscillator degeneracy; this is equivalent to having a "squarer" well (cf. E57*b*).

set up on fast electronic computers, e.g., (N65*a*, G66). Although solutions can be determined by such an approach and the answer found to whether or not the properties of the nucleus can be reproduced in the basic scheme, the properties are not immediately obvious; they can only be obtained after extensive calculations on the computer. Thus, even if the solution is found numerically, there is still a need to understand the results by referring perhaps to more restrictive models. In this way we can hope to learn more about the physical structure.

In many cases the speed and size of present-day computers are not sufficient to tackle the problem, e.g., calculations when there are many particles in a highly degenerate orbit. Here one is forced to make a simplification by referring to a more restrictive model. This simplification may be to consider only the number of many-body functions that the computer can accept and ignore the rest. Another approach is to consider submodels of the shell model as, e.g., in the present discussion on the SU_3 model.

As an example of the difficulties encountered in the straightforward use of the shell model we might consider the nucleus ^{20}Ne for which the SU_3 model provides a useful description. We choose the configurations $(1s)^4$, $(1p)^{12}$, $(2s, 1d)^4$ in which we have two protons and two neutrons in the unfilled (active) $(2s, 1d)$ shell. The number of degenerate magnetic substates available to each proton or neutron is 12, and the number of states W for two neutrons and two protons is therefore 66. The total number of states is $66 \times 66 = 4356$. These 4356 can easily be enumerated into 640 different energy levels of various values of total angular momentum J and parity π (cf. Section 2.2). The distribution of the 640 levels (with $J\pi$ in brackets) is: 4 (8+), 12 (7+), 36 (6+), 64 (5+), 109 (4+), 129 (3+), 143 (2+), 97 (1+), and 46 (0+). Any residual interaction could split the degeneracy of these 640 states; however, it requires a formidable amount of calculation to diagonalize, e.g., the matrix based on the 143 levels for $J\pi = 2+$. These 143 levels have various spatial symmetries and the SU_3 model is simply a classification according to this symmetry. In the following sections we shall discuss why the SU_3 symmetry is of physical importance.

2.2 Invariance Properties

The problem we are faced with is that of finding the eigenfunctions in terms of a finite set W of states of a given Hamiltonian without using the numerical matrix diagonalization method. In our case the nuclear Hamiltonian can be written in the form

$$H = H_0 + U_R \tag{2.1}$$

Here H_0 is the average single-particle Hamiltonian which may or may not include spin-orbit terms:

$$H_0 = \sum_i h_0(i) \tag{2.2}$$

The *residual* interaction U_R is assumed to include at most two-body forces

$$U_R = \sum_i V_i^{(1)} + \sum_{i<j} V_{ij}^{(2)} \tag{2.3}$$

The simplification technique often used in all many-body problems is to apply the invariance properties of the Hamiltonian with respect to a group G (H64*a*, T64). How these invariance properties can be utilized in the general case is briefly reviewed in Appendix B.

Since the nucleus is to be considered isolated in space, it is clear that the Hamiltonian will not be changed by any rotation of the coordinate system, i.e., it will be invariant with respect to the group of rotations in three dimensions, R_3. According to the representation theory of groups (cf. Appendix B), we can say immediately that the eigenfunctions of H can belong to a definite irreducible representation of R_3. Thus we can "label" the eigenvalues by an integral or half integral number J describing the irreducible representations. It is important to remember that to each eigenvalue there corresponds a degeneracy of eigenfunctions corresponding at least to the dimension $(2J + 1)$ of the representation. Each of these functions can be labeled with the quantum number J of the eigenvalue. The number J we call a quantum number and in this particular case it is better known as the angular momentum label (E57*a*).

If we select the basic set of shell model states so that each belongs to a definite representation J and reorder the set according to the J values, then, from the argument in Appendix *B*, the energy matrix will have the "reduced" form shown in Appendix B, Fig. B.1. Matrix elements between the sets of states of different J, are zero. Clearly the energy matrix has been partially diagonalized without resorting to numerical means; in the process we have also learned something about the (angular momentum) structure of the eigenfunctions.

Since the Hamiltonian is invariant with respect to R_3, it is also clearly invariant with respect to the subgroups of R_3, e.g., R_2. The eigenfunctions then can also be classified according to R_2 and hence each can have an M label. Thus, since M is also conserved in nuclear interactions, we can use arguments entirely analogous to those above to further reduce the energy matrix according to the M labels. As far as finding the energy levels of a given J is concerned, it is only necessary to diagonalize the diagonal submatrix with a single M value. Because of the invariance of H with respect

to R_3, in order to find the other eigenfunctions of different M values of the same J value it is necessary only to operate on the eigenfunctions resulting from the diagonalization with the raising and lowering operators $J_{\pm 1}$ of R_3. It is *not* necessary to diagonalize each submatrix of a given J but different M. Thus, even if we resort in the final instance to numerical diagonalization of a submatrix with basis states having the same J and M labels, the number of submatrices to be considered is severely reduced.

Having learned how the invariant group R_3 can help in the simplification of the problem, we may pertinently enquire about other invariant groups. Ideally of course one would like to reduce the energy matrix to completely diagonal form. Actually we now have a restriction on the problem since the new group G must be such that eigenfunctions can still be classified according to R_3. This restricts G to being a subgroup of R_3 or R_3 to being a subgroup of G or G to being invariant with respect to R_3. The first of these possibilities has already been used with $G = R_2$.

In looking for groups which are invariant with respect to R_3 the one that immediately springs to mind is the space-inversion, or parity, group. This group is finite dimensional, having just two elements—the unit element and the space-inversion operator (H64*a*, T64). For such a finite Abelian group only two irreducible representations ($\pi = \pm 1$) exist in contrast to the infinite number for a continuous group like R_3 (T64, Eq. 3-16 and page 13). Assuming nuclear forces to be parity conserving (as is usually done in this study) the eigenfunctions can be labeled with one of the two representations π.

With one exception the above groups are the only ones considered as "good" symmetry groups leading to good classifications or quantum numbers. The one exception is almost trivial at this stage; it is the group of permutations of particle number. Since nucleons are fermions, they must obey the Pauli principle and hence it is possible to represent the many body eigenfunctions of the nuclear Hamiltonian in terms of the complete set of completely antisymmetric functions. In group language the eigenfunctions belong to the totally antisymmetric representation of the permutation group S_A, where A is the number of particles. Since physically we are restricted to one representation of S_A, the problem is not simplified by this realization; however, it does place a limitation on the representations and the number available to us from other groups to be considered. Much of the work in the analysis of states using group theory is in the discovery of representation labels of sets of groups (like R_3) which are compatible with the total wave function being antisymmetric. This study is worthy of an article in itself, but to keep this present article bounded we relegate the relevant discussion on the permutation group to Appendix C.

As mentioned, we have now exhausted the groups under which the general nuclear Hamiltonian can be considered invariant. Further study of

the application of groups necessitates making some assumption about the specific form of the nuclear Hamiltonian. This leads to submodels of the shell model, with nuclear states classified according to either approximate-symmetry or broken-symmetry groups or to both.

2.3 Approximate- and Broken-Symmetry Groups

An approximate-symmetry group G is one for which the Hamiltonian H is approximately invariant with respect to G. This means that:

1. The matrix elements of H are negligibly small between states transforming according to *different* representation of G;
2. The matrix elements of H are the *same* between states transforming according to the *same* representation of G.

A broken symmetry group is one for which only the condition (1) above is true. In this case the Hamiltonian is not invariant with respect to the group G, but its eigenfunctions still transform according to a definite representation of G. Functions belonging to the same representation are, however, not degenerate.

In looking for additional groups it must still be remembered that these must always allow a simultaneous classification according to R_3, i.e., states must still have a definite angular momentum.

Nuclear forces are considered largely charge independent. Thus nuclear states will transform according to the representations of the group SU_2 of two-dimensional special unitary transformations (det $= 1$) between the two basic isospin components $t_0 = \pm\frac{1}{2}$ (i.e., the neutron and the proton). Eigenfunctions can thus be labeled with the representation label T of SU_2, and functions belonging to the same representation will be degenerate in energy. It is as well to point out that functions of the same isospin T but different projections T_0 belong to nuclei of the same mass number but different charge. Thus at this stage all nuclei of the same mass can be treated at the same time as long as we consider all possible isospin components.

For nuclear forces the isospin classification is treated as an approximate symmetry. In actual nuclei, however, there exists the Coulomb repulsion between protons, which of course is not charge independent. In light nuclei it is usual to treat the Coulomb force as a "breaking-symmetry" term. Thus, states can still be classified according to isospin, but now states of the same isospin in different nuclei of the same mass number will not be degenerate in energy. Isospin then is a broken-symmetry (R66a).

Another example of an approximate symmetry arises in the Wigner supermultiplet theory (W37, E57*b*). In this case it is assumed that nuclear

forces are not only charge (isospin) independent but also largely spin independent, i.e., the dominant part of the nuclear force operates only in orbital space. Nuclear eigenfunctions can thus be considered to transform according to the representations of the group U_4 of four-dimensional unitary transformations in charge and spin space. As can be shown (cf. Appendix C), functions which have a definite symmetry according to U_4 also have a definite symmetry according to the group of permutations S_A between the particle numbers of charge-spin states. Remembering that the complete functions representing nuclear states must be totally antisymmetric with respect to permutations of S_A between particle numbers in the full charge-spin-orbit space, we shall find it perhaps not hard to accept the fact that symmetry with respect to S_A in charge-spin space automatically defines the symmetry in the orbital space. The symmetry of the orbital functions is said to be *adjoint* to the symmetry of the charge-spin functions

Thus for a purely central force eigenfunctions will have a definite orbital symmetry and, if the force is attractive, as it is in the nuclear problem, the states of maximum orbital symmetry will be lowest in energy. Note that all the orbital functions that transform between themselves according to a definite representation of S_A go together with the charge-spin functions of adjoint symmetry to form *one* totally antisymmetric nuclear state.

There may be different *sets* of orbital functions which transform among themselves in the same way. At this stage we have no way of knowing which of these sets will be lowest in energy. The decision on this can be made: (a) By numerical diagonization of the energy matrix between the sets of functions transforming in the same way. (Note that the size of this matrix is certainly much less than that of the full energy matrix between all shell model states.) (b) By making some further assumption concerning the nature of the central force.

The classification according to SU_3 arises from a further assumption about the nuclear force in the Wigner supermultiplet theory.

We should point out for completeness the existence of other classification schemes of the nucleus, e.g., one when the spin-orbit force is considered nonnegligible. Discussions on these other models can be found elsewhere (E57*b*, S63). We restrict ourselves here to the assumptions which lead to the SU_3 classification scheme.

2.4 Rotational Features in the 1*p* Shell

In the Introduction we noted the existence of rotational features in light nuclei. These features manifest themselves not only in the energy-level spacing but also in the transition probabilities between levels. The classification scheme we seek is one that exhibits these features. In this section

we discuss how one might intuitively expect such collective features to arise from the SU_3 classification scheme.

In the nuclear $1p$ shell it was realized by Feenberg and Phillips (F37) that states belonging to the same orbital symmetry, but with different orbital angular momentum L, have energies proportional to $L(L+1)$ if the interaction is central. A simple way (E62, E63*a*) to see this $L(L+1)$ structure is to note that for two particles in the $1p$ shell there are only three orbital states having angular momentum $L = 0, 1$, and 2. Thus there are only three two-body matrix elements which completely determine the spectrum of all the many-body functions in the $1p$ shell. Whatever the value of these matrix elements, they can be derived (with suitable choice of parameters) from a potential of the form

$$V = aI + bM + c\mathscr{L} \tag{2.4}$$

with

$$I = \sum_{i<j} 1 \qquad \text{the two-body unit operator}$$

$$M = \sum_{i<j} P_{ij} \qquad \text{the Majorana operator}$$

$$\mathscr{L} = \sum_{i<j} (l_i \cdot l_j) = \tfrac{1}{2}\left(L^2 - \sum_i l_i^2\right)$$

and parameters a, b, and c. Here l_i is the orbital angular momentum operator of the ith particle and $L = \sum_i l_i$, the total orbital angular momentum operator. The operator P_{ij} is the permutation operator between particles i and j.

For a k particle state with orbital permutation symmetry $[f]$ (cf. Appendix C) and angular momentum L we have

$$\langle V \rangle = a\frac{k(k-1)}{2} + b\langle M \rangle + \frac{c}{2}\{L(L+1) - 2k\} \tag{2.5}$$

where the expectation value $\langle M \rangle$ depends only on the representation label $[f]$ [cf. Eq. (5.2)]. Equation (2.5) clearly exhibits the rotational $L(L+1)$ structure of spectra in the $1p$ shell for a purely spin-independent potential.

One might expect some similarity between the classification scheme in the $1p$ shell and in the $(2s, 1d)$ shell to bring out the collective features explicitly. Unfortunately the Wigner supermultiplet classification is much too general in the $(2s, 1d)$ shell to demonstrate these collective effects immediately. It is possible to construct many states which have the same

orbital symmetry and the same angular momentum; e.g., there are two $L = 0$ states with orbital symmetry $[f] = [2]$ having the structure s^2 and d^2.

The orbital symmetry classification is equivalent to the classification of states according to the group U_s of unitary transformations between the s single-particle orbits available to the particles. In the nuclear $1p$ shell $s = 3$. It was realized by Elliott (E58) that, since each particle in the $1p$ shell carries *one* oscillator quantum, the supermultiplet classification is there equivalent to the symmetry of the oscillator quanta. In the nuclear $(2s, 1d)$ shell each particle carries *two* oscillator quanta and hence the orbital and quantum symmetries are not the same; it is possible to construct functions which have the same particle symmetry but different quantum symmetries. Thus one is lead to the classification of states in the $(2s, 1d)$ shell according to the symmetry of their quanta as well as the orbital symmetry. We shall see that this scheme does possess collective characteristics.

3. SYMMETRY OF OSCILLATOR QUANTA—THE GROUPS U_3 AND SU_3

3.1 Problems

For clarity we begin by stating the problems involved in the classification of nuclear states according to the group U_3 as well as the groups S_A and R_3. This classification leads to the introduction of a subgroup SU_3 of U_3 whose use with oscillator wave functions forms the basis of the SU_3 model.

In the shell model, with just one partially filled (active) oscillator shell, it is possible to construct in general a large number W of A particle states, each having N quanta. One problem is *how* to construct, from the W set, the states which transform according to the irreducible representations of S_A, U_3, and R_3. Associated with this is the *existence* problem of finding to which representations of U_3 can belong states that have a definite orbital symmetry and, again, of finding which angular momentum labels can be given to states of definite U_3 symmetry.

This section discusses the formal properties of the groups U_3 and SU_3 and the structure and classification of states according to the groups.

3.2 Formal Properties of U_3 and SU_3

The study of the *infinite* group of unitary transformation in s dimensions (R51, B60*b*, H64*a*) can be simplified by considering only a linearly independent *finite* set s^2 of *generating*, or *shift* operators (cf. Appendix D). For the symmetry group U_3 of the harmonic oscillator, these operators can conveniently be written in terms of the *creation* and *destruction* operators of

oscillator quanta. In a Cartesian representation the explicit definition of the *creation* and *destruction* operators in the x direction are, respectively,

$$a_x^\dagger = \sqrt{\frac{1}{2}}\,\frac{x - ib^2p_x}{b}$$
$$a_x = \sqrt{\frac{1}{2}}\,\frac{x + ib^2p_x}{b} \tag{3.1}$$

with similar definitions in the y and z directions.

Oscillator quanta are "bosons" and as such have the commutation relations

$$[a_\alpha^\dagger, a_\beta^\dagger] = [a_\alpha, a_\beta] = 0$$
$$[a_\alpha, a_\beta^\dagger] = \delta_{\alpha\beta} = \begin{cases} 0 & \text{for } \alpha \neq \beta \\ 1 & \text{for } \alpha = \beta \end{cases} \tag{3.2}$$

These expressions can easily be checked from the explicit construction of the operators in Eq. (3.1).

The nine shift operators of the group U_3 can conveniently be written (B63*a*, E63*b*) in terms of the nine operators

$$\mathscr{A}_{\alpha\beta} = \tfrac{1}{2}(a_\alpha^\dagger a_\beta + a_\beta a_\alpha^\dagger) \qquad \alpha, \beta = x, y, \text{ or } z \tag{3.3}$$

which *shift a* quanta from the β to the α direction.

The commutation relation of the shift operators defined in Eq. (3.3) can easily be deduced from those of their constituent creation and destruction operators [Eq. (3.2)]

$$[\mathscr{A}_{\alpha\beta}, \mathscr{A}_{\gamma\delta}] = \mathscr{A}_{\alpha\delta}\delta_{\beta\gamma} - \mathscr{A}_{\gamma\beta}\delta_{\alpha\delta} \tag{3.4}$$

For completeness we can define the nine Hermitian generating matrices (cf. Appendix D)

$$\mathscr{G}_{\alpha\beta}^{\pm} = (\mathscr{A}_{\alpha\beta} + \mathscr{A}_{\beta\alpha}) \pm i(\mathscr{A}_{\alpha\beta} - \mathscr{A}_{\beta\alpha}) \tag{3.5}$$

In terms of the shift operators the single-particle harmonic-oscillator Hamiltonian [cf. Appendix A, Eq. (A.1)] can be written

$$\mathscr{H}_0 = \mathscr{A}_{xx} + \mathscr{A}_{yy} + \mathscr{A}_{zz} \tag{3.6}$$

It is now almost trivial to verify that the harmonic oscillator is indeed invariant (*J*40) with respect to the group U_3:

From Eqs. (3.4) and (3.6) it can be shown that $[\mathscr{H}_0, \mathscr{A}_{\alpha\beta}] = 0$ for all α, β.

Hence for all unitary transformations $U = \exp(i \sum_{\alpha\beta\pi} C^{\pi}_{\alpha\beta} \mathscr{G}^{\pi}_{\alpha\beta})$, with real coefficients $C^{\pi}_{\alpha\beta}$, we clearly have

$$[\mathscr{H}_0, U] = 0 \tag{3.7}$$

Because of the invariance of the harmonic oscillator with respect to U_3, each eigenvalue of the Hamiltonian can be labeled with an irreducible representation label of U_3. Each eigenvalue has the degeneracy of the dimension of the representation; e.g., the states of the oscillator $n = 2$ shell belong to a six-fold representation of U_3. In the next section we discuss the *labeling* of the various representations of U_3 in terms of Young tableaux (cf. Appendix C), but it can be seen that for one particle in a harmonic oscillator the one number n, giving the number of quanta, is sufficient to distinguish states of different representations.

At the beginning of this section, in Eq. (3.1), the expressions for the *creation* and *destruction* operators of oscillator quanta were given. It is a trivial matter now to show that these operators actually have the properties ascribed to them:

From the commutation properties in Eq. (3.2) and the harmonic-oscillator Hamiltonian in Eq. (3.6) it can be shown that

$$\begin{aligned} [\mathscr{H}_0, a_\alpha^\dagger] &= a_\alpha^\dagger \\ [\mathscr{H}_0, a_\alpha] &= -a_\alpha \qquad \text{for } \alpha = x, y, \text{ or } z \end{aligned} \tag{3.8}$$

Thus, if $|n_\alpha\rangle$ is a wave function having n_α quanta in the α direction, then $a_\alpha^\dagger|n_\alpha\rangle$ and $a_\alpha|n_\alpha\rangle$ have $(n_\alpha + 1)$ and $(n_\alpha - 1)$quanta,respectively, in the α direction from Eq. 3.8.

Similar arguments to the above can be used to show that the many-body harmonic oscillator

$$H_0 = \sum_i \mathscr{H}_0(i) \tag{3.9}$$

where i is the particle number, is invariant with respect to the group U_3 described by the nine shift operators

$$A_{\alpha\beta} = \sum_i \mathscr{A}_{\alpha\beta}(i) \tag{3.10}$$

These many-body operators have similar commutation relations to the single-particle operator as given in Eq. (3.4). Corresponding Hermitian generating operators can be defined

$$G^{\pm}_{\alpha\beta} = (A_{\alpha\beta} + A_{\beta\alpha}) \pm i(A_{\alpha\beta} - A_{\beta\alpha}) \tag{3.11}$$

TABLE 3.I

Transformation Matrix between the Shift Operators in a Cartesian Basis and Those with Spherical Tensor Properties

	Q_{+1}	Q_{-1}	$\sqrt{3}L_{+1}$	$\sqrt{3}L_{-1}$	$\sqrt{3}L_0$	Q_{+2}	Q_{-2}	$\sqrt{2}H_0$	Q_0
$\sqrt{6}A_{xz}$	$-\frac{1}{2}$	$\frac{1}{2}$	$\frac{1}{2}$	$\frac{1}{2}$					
$\sqrt{6}A_{zx}$	$-\frac{1}{2}$	$\frac{1}{2}$	$-\frac{1}{2}$	$-\frac{1}{2}$					
$i\sqrt{6}A_{yz}$	$-\frac{1}{2}$	$-\frac{1}{2}$	$\frac{1}{2}$	$-\frac{1}{2}$					
$i\sqrt{6}A_{zy}$	$-\frac{1}{2}$	$-\frac{1}{2}$	$-\frac{1}{2}$	$\frac{1}{2}$					
$i\sqrt{6}A_{yx}$					$\sqrt{\frac{1}{2}}$	$\frac{1}{2}$	$-\frac{1}{2}$		
$i\sqrt{6}A_{xy}$					$-\sqrt{\frac{1}{2}}$	$\frac{1}{2}$	$-\frac{1}{2}$		
$\sqrt{6}A_{xx}$						$\frac{1}{2}$	$\frac{1}{2}$	$\sqrt{\frac{1}{3}}$	$-\sqrt{\frac{1}{6}}$
$\sqrt{6}A_{yy}$						$-\frac{1}{2}$	$-\frac{1}{2}$	$\sqrt{\frac{1}{2}}$	$-\sqrt{\frac{1}{6}}$
$\sqrt{6}A_{zz}$								$\sqrt{\frac{1}{3}}$	$\sqrt{\frac{2}{3}}$

It is sometimes useful to define the basic set of nine shift operators of U_3 so that they have definite spherical tensor properties instead of the Cartesian properties given above (E58). In Table 3.I is shown the transformation between the Cartesian set and a new set consisting of H_0, L_q, and Q_q, which are tensors of rank zero, one, and two, respectively. The operator H_0 is simply the harmonic-oscillator Hamiltonian defined in Eq. (3.9). The operator L_q is the orbital angular momentum operator

$$L_q = \sum_i l_q(i)$$

with

$$l_q = (r \times p)_q \tag{3.12}$$

The tensor of rank two can be written explicitly

$$Q_q = \sum_i \tilde{Q}_q(i)$$

with

$$\tilde{Q}_q = \sqrt{\frac{4\pi}{5}} \left(\frac{r^2 Y_q^2(\theta_r \phi_r) + b^4 p^2 Y_q^2(\theta_p \phi_p)}{b^2}\right) \tag{3.13}$$

The commutation relations of the spherical tensor set can be deduced from Eq. (3.4) to be

$$
\begin{aligned}
[L_q, L_{q'}] &= -\sqrt{2}\,(11qq' \mid 1\; q+q')\, L_{q+q'} \\
[Q_q, L_{q'}] &= -\sqrt{6}\,(21qq' \mid 2\; q+q')\, Q_{q+q'} \\
[Q_q, Q_{q'}] &= 3\sqrt{10}\,(22qq' \mid 1\; q+q')\, L_{q+q'}
\end{aligned}
\tag{3.14}
$$

with H_0 commuting with all L_q and Q_q.

The subset of eight operators $L_q (q = \pm 1, 0)$ and $Q_q (q = \pm 2, \pm 1, 0)$ commute among themselves and are therefore associated with a subgroup of U_3— actually the group SU_3 of special unitary transformations of determinant $+1$. The unitary transformations $U = \exp iC_0H_0$ for arbitrary real coefficients C_0 are simply phase transitions and are of no physical interest. Thus in the shell model we are, strictly speaking, interested only in the classification according to SU_3.

Another obvious subgroup of U_3 and SU_3 is the group R_3 generated from the operators L_q. It is because R_3 is a *subgroup* of SU_3 that it is possible to effect a simultaneous classification.

In Section 3.5 we shall return to the discussion of subgroups when considering the explicit construction of states.

3.3 Classification According to U_3 and SU_3

Any solution of A independent harmonic oscillators can be written in terms of the set of states

$$
\begin{aligned}
\mid pqr\rangle_{i_1 \cdots i_{p+q+r}} = {} & a_x^\dagger(i_1)\, a_x^\dagger(i_2) \cdots a_x^\dagger(i_p)\, a_y^\dagger(i_{p+1}) \cdots a_y^\dagger(i_{p+q})\, a_z^\dagger(i_{p+q+1}) \\
& \cdots a_z^\dagger(i_{p+q+r}) \mid 0\rangle
\end{aligned}
\tag{3.15}
$$

where $\mid 0\rangle$ is the "vacuum" state of no quanta (i.e., the $1s$ state) and $a_\alpha^\dagger(i)$, the *creation* operator that gives the ith particle an oscillator quantum in the α direction. In the expression (3.15) the function $\mid pqr\rangle_{i_1 \cdots i_{p+q+r}}$ has $p(q$ or $r)$ quanta in the $x(y$ or $z)$ directions. The numbers $i_1 \cdots i_{p+q+r}$ each take on the values $1, 2, \ldots, A$, where A is the number of particles; a particle number may appear more than once or not at all, depending on how many quanta are on that particular particle.

In Appendix C we have briefly reproduced the arguments from which the classification scheme in the symmetric group S_A (the Young tableau) can be carried over to describe the symmetry with a unitary group U_s. There it is supposed that s single-particle states are occupied by A particles. If one

assumes that each member of the set $i_1 \cdots i_{p+q+r}$ in Eq. (3.15) takes on one value only from the set 1, 2,..., A (i.e. each particle has *one* quantum), then collections of states like $|pqr\rangle_{i_1 \cdots i_A}$, which have a definite permutation symmetry with respect to the group S_A of particle numbers 1, 2,..., A, will also have definite symmetry according to the group U_s ($s = 3$) of unitary transformations between quanta.

As an example consider the two-particle states in which one particle has a quantum in the x direction and the other a quantum in the y direction. Two such states can be constructed, e.g., $a_x^\dagger(1)\, a_y^\dagger(2)$ and $a_x^\dagger(2)\, a_y^\dagger(1)$. These two states do not have definite symmetry, so we consider instead:

$$\begin{aligned} \psi_s &= a_x^\dagger(1)\, a_y^\dagger(2) + a_x^\dagger(2)\, a_y^\dagger(1) \\ \psi_a &= a_x^\dagger(1)\, a_y^\dagger(2) - a_x^\dagger(2)\, a_y^\dagger(1) \end{aligned} \tag{3.16}$$

The function ψ_s is symmetrical with respect to interchange of particle number and is said to belong to the [2] (or the Young tableau $\square\square$) representation of S_2. This function also belongs to a definite representation of U_3 (cf. Appendix C), and we can also conveniently use the particle symmetry label [now written (2)] to describe this symmetry. The function ψ_a is antisymmetrical with respect to interchange of particle number and belongs to the [11] (or Young tableau $\begin{smallmatrix}\square\\\square\end{smallmatrix}$) representation of S_2, or equivalently to the (11) representation of U_3. One can demonstrate explicitly that the shift operators of U_3, defined in Eq. (3.10), only transform symmetrical states into symmetrical states, etc., i.e., that symmetrical functions like the ψ_s in Eq. (3.16) (e.g., $a_x^\dagger(1)\, a_x^\dagger(2)$, etc.) all belong to the *same* representation of U_3.

Suppose now that just *one* particle has two quanta, one in the x and one in the y direction. The states of this particle can be taken from Eq. (3.16) simply by putting 1 in place of 2. Thus

$$\begin{aligned} \psi_s &\approx a_x^\dagger(1)\, a_y^\dagger(1) \\ \psi_a &\approx 0 \end{aligned} \tag{3.17}$$

For a single particle having two quanta, only the (2) representation of U_3 exists. The state ψ_s in Eq. (3.17) is a *single-particle state* and thus belongs to the [1] representation of the symmetry group S_1. We have then demonstrated explicitly how the quantum symmetry and particle symmetry are equivalent in the $1p$-shell which has only one oscillator quantum. All higher shells have more oscillator quanta and therefore this equivalence does not hold.

Since quanta can only be created in one of *three* directions, it is impossible to construct a totally antisymmetric state of more than three quanta. Thus general tableaux representing quantum symmetry must have N squares in, at most, three rows, where N is the total number of quanta,

or equivalently the representation can be described by three numbers (p_1, p_2, p_3) which measure the length of the rows in the Young tableau. The single-particle states having $n = 0, 1, 2,...$, etc., quanta belong to the (0, 0, 0), (1, 0, 0), (2, 0, 0),..., etc., representations of U_3, respectively, i.e., in this case the number of quanta n is a labeling sufficient to describe representations of U_3.

Functions which transform according to an irreducible representation of U_3 also transform according to an irreducible representation of SU_3. However, sets belonging to representations described by tableaux differing only in the number of completed columns (of three squares) all belong to the *same* representation under SU_3. Thus only two *numbers* are needed to classify states according to SU_3 and these can conveniently[2] be defined as $\lambda = (p_1 - p_2)$ and $\mu = (p_2 - p_3)$.

3.4 Simultaneous Classification According to S_A and SU_3

From the definition of representation in Appendix *B* it will be seen that states can be simultaneously classified according to two groups only if the elements of the two groups operate in different spaces or if one is a subgroup of the other. The group elements of S_A operate in particle-number space, while those of SU_3 operate in the different function space; thus it is possible to classify states simultaneously according to S_A and U_3. In Appendix C it is shown that the classification according to S_A is equivalent to that according to all the unitary transformations of U_s between the s single-particle basis states. A subset of these transformations forms the group U_3 (cf. Appendix E). Thus the classification according to S_A and U_3 can be considered as one according to U_s and its subgroup U_3.

The existence problem of finding to which representations of SU_3 states having a definite symmetry with respect to S_A can belong can be solved by a chain procedure, which can be conveniently illustrated by the example of particles in the $n = 2$ oscillator shell.

In the last section it was shown that single-particle states in the oscillator $n = 2$ shell belong to the (2, 0, 0) representation of U_3. Consider now the two-particle states. Under the transformations of the permutation group S_2, two-particle states can be classified according to representations described by Young tableaux consisting of two squares (two being the number of particles), i.e., $\square\square \equiv [2]$ and $\begin{smallmatrix}\square\\\square\end{smallmatrix} \equiv [11]$. These diagrams are arrived at simply by adding one square to one square and describe symmetrical and antisymmetrical functions, respectively (cf. The section on Outer Product in

[2] We follow here the notation in Reference E58. Other numbers are used, e.g., $K_1 = (p_1 - p_3)$ and $K_2 = p_2 - p_3$ (F65*b*).

TABLI

Classification of Some States in the Oscillato

[Taken fron

	$(\lambda\mu)$...	(10, 2)	(75)	(48)	(11, 0)	(83)	(56)	(29)	(91)	(64)	(37)	(0, 10)	(72)	(45)
k	$[f]$													
1	[1]	.	.	.	.	.	.	.	.	.	.	.	.	.
4	[4]	.	.	.	.	.	.	.	.	.	.	.	.	.
	[31]	.	.	.	.	.	.	.	.	.	.	.	.	.
	[22]	.	.	.	.	.	.	.	.	.	.	.	.	.
	[211]	.	.	.	.	.	.	.	.	.	.	.	.	.
	[1111]	.	.	.	.	.	.	.	.	.	.	.	.	.
7	[43]	.	.	.	.	1	.	.	.	1	.	.	1	1
	[421]	.	.	.	.	.	.	.	1	1	.	.	2	1
10	[442]	1	1	1	.	1	1	.	2	4	2	1	3	3
	[4411]	.	1	.	.	1	1	.	1	2	1	.	3	3

	$(\lambda\mu)$...	(11, 1)	(84)	(57)	(2, 10)	(92)	(65)	(38)	(10, 0)	(73)	(46)	(19)	(81)	(54)
k	$[f]$													
2	[2]	.	.	.	.	.	.	.	.	.	.	.	.	.
	[11]	.	.	.	.	.	.	.	.	.	.	.	.	.
5	[41]	.	.	.	.	.	.	.	.	.	.	.	1	.
	[32]	.	.	.	.	.	.	.	.	.	.	.	.	.
8	[44]	.	1	.	.	.	.	.	.	1	1	.	1	1
	[431]	.	.	.	.	1	1	.	.	2	1	.	2	3
11	[443]	1	1	1	1	1	1	1	1	3	3	1	2	4
	[4421]	.	1	1	.	1	2	1	1	4	4	1	3	6

	$(\lambda\mu)$...	(12, 0)	(93)	(66)	(39)	(0, 12)	(10, 1)	(74)	(47)	(1, 10)	(82)	(55)	(28)	(90)	(63)	(36)
k	$[f]$															
3	[3]	.	.	.	.	.	.	.	.	.	.	.	.	.	.	.
	[21]	.	.	.	.	.	.	.	.	.	.	.	.	.	.	.
	[111]	.	.	.	.	.	.	.	.	.	.	.	.	.	.	.
6	[42]	.	.	.	.	.	.	.	.	.	1	.	.	.	1	.
	[411]	.	.	.	.	.	.	.	.	.	.	.	.	.	1	.
9	[441]	.	1	1	.	.	.	1	.	.	2	2	1	1	3	2
	[432]	.	.	.	.	.	1	1	1	.	2	2	1	1	4	2
12	[444]	1	1	1	1	1	.	.	.	.	2	2	2	.	2	2
	[4431]	.	1	1	1	.	1	2	2	1	3	5	3	1	6	6

V

= 2 Shell According to S_A (or U_6) and SU_3
iott (E58)]

18)	(80)	(53)	(26)	(61)	(34)	(07)	(42)	(15)	(50)	(23)	(31)	(04)	(12)	(20)	(01)
.	.	.	.	.	.	.	.	.	.	.	.	.	.	1	.
.	1	.	.	.	.	.	1	.	.	.	.	1	.	1	.
.	.	.	.	1	.	.	1	.	.	1	1	.	1	1	.
.	.	.	.	.	.	.	1	.	.	.	1	1	.	1	.
.	.	.	.	.	.	.	.	.	1	1	1	.	1	.	1
.	.	.	.	.	.	.	.	.	.	.	.	.	1	.	.
.	1	2	1	2	1	.	3	1	1	2	2	1	1	1	.
.	1	3	1	3	3	.	5	2	2	4	4	2	3	2	1
1	3	6	5	4	5	.	8	4	1	4	4	4	2	3	.
1	1	5	2	4	5	1	5	3	3	5	4	1	3	1	1

27)	(62)	(35)	(08)	(70)	(43)	(16)	(51)	(24)	(32)	(05)	(40)	(13)	(21)	(02)	(10)
.	.	.	.	.	.	.	.	.	.	.	1	.	.	1	.
.	.	.	.	.	.	.	.	.	.	.	.	.	1	.	.
.	1	.	.	.	1	.	1	1	1	.	1	1	1	1	
.	1	.	.	.	1	.	1	1	1	.	2	1	1	1	.
.	2	1	1	.	1	.	2	2	1	.	2	1	.	1	.
1	4	3	.	3	6	2	5	4	6	2	2	4	4	1	1
2	5	5	2	1	5	3	4	6	4	1	3	3	2	2	.
3	8	8	2	3	10	5	8	10	9	3	5	7	5	3	1

09)	(71)	(44)	(17)	(52)	(25)	(60)	(33)	(06)	(41)	(14)	(22)	(30)	(03)	(11)	(00)
.	.	.	.	.	.	1	.	.	.	.	1	.	.	.	1
.	.	.	.	.	.	.	.	.	1	.	1	.	.	1	.
.	.	.	.	.	.	.	.	.	.	.	.	1	1	.	.
.	1	2	.	1	.	2	2	1	2	1	3	.	.	1	1
.	.	.	.	1	1	1	1	.	1	.	1	1	1	.	.
.	3	4	1	4	2	3	5	2	3	2	4	1	1	1	1
.	4	6	2	6	5	3	7	2	6	5	6	2	2	3	.
.	1	4	1	1	1	3	3	3	1	1	3	.	.	.	2
1	5	9	5	9	9	4	11	4	7	7	8	3	3	3	.

Appendix C). The two functions can also belong to representation of U_3 described by four squares (four being the total number of quanta). The diagrams in this case can be derived by adding one symmetric pair of squares to another symmetric pair (cf. Outer Product in Appendix C). This leads to the three tableaux of U_3:

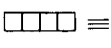 $\equiv (4, 0, 0)$ $\equiv (3, 1, 0)$ and $= (2, 2, 0)$ (3.18a)

(Note that the tableau cannot exist since one of the constituent pairs would have to be antisymmetric.) Thus states can belong to the

$$(\lambda\mu) = (4, 0), (2, 1) \text{ and } (0, 2) \tag{3.18b}$$

representations of SU_3.

Having now discovered to which representations of S_A and SU_3 the two-particle states in the $n = 2$ shell *can* belong, the problem is to find the permutation symmetry of the states transforming according to a definite representation of U_3.

It is clear that the two pairs of squares in the (4, 0, 0) representation of U_3 are symmetrically placed; thus states belonging to this representation also belong to the [2] representation of S_2. The orbital symmetry of the other representation of U_3 can be found by dimensionality arguments.

First we note again that the S_A ($A = 2$) classification is equivalent to that by U_s ($s = 6$) of transformations between the six ($2s$, $1d$) orbitals. The number of sets of two-particle states which transform according to a definite symmetry of S_2 is just the dimension of the equivalent representation of U_6. A formula for the dimension of the representation $[f]$ of the unitary group U_s has been given by Weyl (W28, p. 383; also H64*a*, Eq. 10-25 and Sec. 10-4)

$$\dim[f] = \prod_{1 \leqslant i < j \leqslant s} \frac{(f_i - f_j + j - i)}{(j - i)} \tag{3.19}$$

where f_i is the number of squares in the ith row. Thus we find

$$\begin{aligned} \dim[2] &= 21 \\ \dim[11] &= 15 \end{aligned} \tag{3.20}$$

One can immediately check that this is correct by noting that the total dimension ($21 + 15 = 36$) must be just the total number of states formed by putting two particles in the six possible ($2s$, $1d$) orbitals (i.e., $6^2 = 36$).

Equation (3.19) can also be used to find the dimension of the represen-

tation of U_3 in Eq. (3.18a) and hence of SU_3 in Eq. (3.18b). This can be written in the general form

$$\dim(\lambda\mu) = \tfrac{1}{2}(\lambda + 1)(\mu + 1)(\lambda + \mu + 2) \tag{3.21a}$$

Thus we find

$$\begin{aligned} \dim(40) &= 15 \\ \dim(21) &= 15 \\ \dim(02) &= 6 \end{aligned} \tag{3.21b}$$

It is already known that the 15 states of $(\lambda\mu) = (40)$ are to be included in the 21 states of permutation symmetry [2]; the remaining 6 states must therefore transform according to $(\lambda\mu) = (02)$ of SU_3. (Note that a *complete* representation of SU_3 must be contained in the representation of U_6 because SU_3 is a subgroup.)

The above arguments can be extended to any number of particles in any oscillator shell or any mixed shells. Tables 3.II and 3.III reproduce the reductions derived by Elliott (E58) for some of the orbital symmetries of particles in the oscillator $n = 2$ and $n = 3$ shells into representations of SU_3.

TABLE 3.III

Classification of Some States in the Oscillator $n = 3$ Shell According to S_A (or U_6) and SU_3 [Taken from Elliott (E58)]

n	$[f]$														
0	[0]	(00)													
1	[1]	(30)													
2	[2]	(60)	(22)												
	[11]	(41)	(03)												
3	[3]	(90)	(52)	(33)	(30)	(03)									
	[21]	(71)	(52)	(33)	(41)	(14)	(22)	(11)							
	[111]	(60)	(33)	(22)	(00)										
4	[4]	(12, 0)	(82)	(63)	(44)	(60)	(33)	(41)	(06)	(22)	(00)				
	[31]	(10, 1)	(82)	$(63)^2$	(71)	(44)	$(52)^2$	(60)	$(25)^2$	$(32)^2$	$(41)^2$	(14)	$(22)^2$	(30)	(03)	(11)
	[22]	(82)	(71)	$(44)^2$	(52)	(60)	(33)	(41)	(06)	(14)	$(22)^2$	(11)			
	[211]	(90)	(63)	(71)	(44)	$(52)^2$	(25)	$(33)^2$	$(41)^2$	$(14)^2$	(22)	$(30)^2$	(03)	(11)	
	[1111]	(52)	(33)	(06)	(22)	(30)									

3.5 Classification According to SU_3 and R_3

Arguments similar to those in the previous section can be used to derive the simultaneous classification according to SU_3 and to the three-dimensional orthogonal group R_3, whose irreducible representation are labeled by the

orbital angular momentum L. One starts from the knowledge that a one-quantum state transforms with respect to SU_3 according to $(\lambda\mu) = (1, 0)$ and has angular momentum $L = 1$. Two-quantum states can belong to the representations $(\lambda\mu) = (20)$ and (01) of SU_3 (cf. the section on Outer Product in Appendix C) and to the representation $L = 1 \times 1 = (0, 1, \text{and } 2)$ of R_3 according to the well-known angular momentum vector coupling rules. Dimensionality arguments [cf. Eq. (3.21a)] show that

$$\begin{aligned} \dim(20) &= 6 \\ \dim(01) &= 3 \end{aligned} \tag{3.22}$$

The dimension of the representation L of R_3 is of course just $(2L + 1)$. Thus one must conclude that functions transforming according to the $(\lambda\mu) = (20)$ representation of SU_3 can have $L = 0$ and 2 and those transforming according to $(\lambda\mu) = (01)$ can only have $L = 1$.

For this reduction Elliott (E58) has derived the general rule that for any representation $(\lambda\mu)$ of SU_3, the orbital angular momenta are given by

$$\begin{aligned} L &= K, K + 1, \ldots, K + \bar{\lambda} \qquad & K \neq 0 \\ &= \bar{\lambda}, \bar{\lambda} - 2, \ldots, 1 \text{ or } 0 \qquad & K = 0 \end{aligned}$$

with the interger K taking on the values

$$K = \bar{\mu}, \bar{\mu} - 2, \ldots, 1 \text{ or } 0 \tag{3.23}$$

Here $\bar{\lambda}$ is the maximum of the numbers λ and μ, and $\bar{\mu}$, the minimum of these numbers.

3.6 Classification According to SU_3 and $SU_2 \times U_1$

In the explicit construction of states, to be described in Section 3.7, it is found convenient to use the classification of states with respect to SU_3 and its subgroups SU_2 and U_1.

The SU_2 group is the group of special unitary transformations in two dimensions, which can conveniently be chosen as the xy plane. The shift operators for the group U_2 can be chosen as the four operators

$$A_{\alpha\beta} \qquad \text{for } \alpha, \beta = x, y \tag{3.24}$$

The commutation relations are of course again those given in Eq. (3.4). The group SU_2 is a subgroup of U_2 formed from the shift operators in Eq. (3.24) with the exception of the one operator $A_{xx} + A_{yy}$, which has

nonzero trace and is associated with phase transitions in the two-dimensional space. The three operators of SU_2 can be chosen to be

$$\begin{aligned}
\omega_0 &= \tfrac{1}{2}(A_{xx} - A_{yy}) = \tfrac{1}{2}\sqrt{\tfrac{1}{6}}\,(Q_2 + Q_{-2}) \\
\omega_{+1} &= -\sqrt{\tfrac{1}{2}}\,A_{xy} = \frac{i}{4\sqrt{3}}(-\sqrt{2}\,L_0 + 2Q_2 - 2Q_{-2}) \\
\omega_{-1} &= +\sqrt{\tfrac{1}{2}}\,A_{yx} = -\frac{i}{4\sqrt{3}}(+\sqrt{2}\,L_0 + 2Q_2 - 2Q_{-2})
\end{aligned} \tag{3.25}$$

The commutation relation of the ω operators can easily be deduced from Eq. (3.4) to be

$$[\omega_{+1}, \omega_{-1}] = -\omega_0 \qquad \text{and} \qquad [\omega_0, \omega_{\pm 1}] = \pm\omega_{\pm 1}$$

The commutation relations are just those of the group R_3, and what we have done is simply to demonstrate the isomorphism between the groups SU_2 and R_3. This is not to say, of course, that the group SU_2 is *in fact* the group R_3 that was discussed in Section 3.4. The groups SU_2 and R_3 simply have a similar group structure.

The similarity between the classifications according to the groups R_3 and SU_2 is well known (E57*a*, H64*a*). Thus we define a quantum number Λ to describe the symmetry with respect to SU_2 to correspond to the angular momentum label J describing the classification with respect to R_3. States will be defined which are eigenfunctions of the operator ω_0 with eigenvalue $\nu/2$ (by convention) corresponding to the quantum number M for the eigenvalue of L_0 in R_3. Clearly $\nu/2$ will take on the values

$$\frac{\nu}{2} = \Lambda, \Lambda - 1, \ldots, -\Lambda \tag{3.27}$$

within a representation Λ of SU_2. In an argument analogous to that in R_3, for states belonging to the representation Λ of SU_2,

$$\langle \omega^2 \rangle = \langle \omega_0{}^2 - \omega_{+1}\omega_{-1} - \omega_{-1}\omega_{+1} \rangle = \Lambda(\Lambda + 1) \tag{3.28}$$

The group U_1 is described simply by the one shift operator

$$Q_0 = 2A_{zz} - A_{xx} - A_{yy} \tag{3.29}$$

This one operator of U_1 commutes with all the operators of SU_2 and thus a simultaneous classification can be achieved for both groups. The group U_1 being of only one dimension needs but one *number* to define its representations fully; this number is conveniently chosen to be the eigenvalue ϵ of Q_0.

The complete classification according to SU_3 and its subgroups SU_2 and U_1 has been given by Elliott (E58). Within a representation $(\lambda\mu)$ of SU_3 it is found that ϵ can take on the values

$$\epsilon = 2\lambda + \mu, 2\lambda + \mu - 3,..., -\lambda - 2\mu \tag{3.29}$$

For definite representations $(\lambda\mu)$ and ϵ of SU_3 and U_1, the group SU_2 has representations described by

$$\begin{aligned} \Lambda = {} & \tfrac{1}{6}|\, 2\lambda - 2\mu - \epsilon \,|, \tfrac{1}{6}|\, 2\lambda - 2\mu - \epsilon \,| + 1,..., \\ & \min\{\tfrac{1}{6}(2\lambda + 4\mu - \epsilon), \tfrac{1}{6}(2\lambda + 4\lambda + \epsilon)\} \end{aligned} \tag{3.30}$$

Structures of States in the Harmonic Oscillator

States classified according to the chain $SU_3 \rightarrow SU_2 \times U_1$ have a very simple structure in the harmonic oscillator. From the definition of the shift operators it will be seen that the operator $A_{\alpha\alpha}$ ($\alpha = x, y$, or z) simply *counts* the number of quanta, N_α, in the α direction. Thus states having a definite number of quanta in each of the three directions in space will have a definite value of ν and ϵ from Eqs. (3.25) and (3.29)

$$\begin{aligned} \nu &= \langle 2\omega_0 \rangle = N_x - N_y \\ \epsilon &= \langle Q_0 \rangle = 2N_z - N_x - N_y \end{aligned} \tag{3.31}$$

To construct such many-body states having definite ϵ and ν values, it is only necessary to define single-particle harmonic-oscillator states in a Cartesian representation (cf. Appendix A); such states have a definite number of quanta in each spatial direction and thus have definite ϵ and ν values. In view of the linear structure of the $A_{\alpha\alpha}$ operators [cf. Eq. (3.10)], it is clear that the ϵ and ν values of the many-body system are simply the *sum* of the ϵ_i and ν_i values of the single-particle constituents

$$\epsilon = \sum_i \epsilon_i \qquad \nu = \sum_i \nu_i \tag{3.32}$$

Table 3.IV lists the six single-particle states in Cartesian coordinates for the oscillator $n = 2$ shell, according to their ϵ and ν labels.

For single-particle states the Λ classification is unnecessary since it is related to ϵ and the total number of quanta n

$$\Lambda = \max \frac{\nu}{2} = \frac{1}{2}(n_x + n_y) = \frac{1}{6}(2n - \epsilon) \tag{3.33}$$

The A-particle functions with definite particle symmetry and with the

maximum possible value of ϵ, $\tilde{\epsilon}_{\max}$, are formed by putting as many particles as possible into the single-particle orbits (e.g., in Table 3.IV) with the largest ϵ_i compatible with the particle symmetry. Since these functions do have the maximum possible value of ϵ, it is clear that $\tilde{\epsilon}_{\max} = 2\tilde{\lambda} + \tilde{\mu}$ [cf. Eq. (3.29)] for the *particular* representation $(\tilde{\lambda}\tilde{\mu})$ of SU_3, giving the maximum possible value for this quantity. [The *existence* problem, to determine which representation $(\lambda\mu)$ actually occur for a given particle symmetry, was discussed in Section 3.3].

TABLE 3.IV

The Six Single-Particle States in the Oscillator $n = 2$ Shell Described Either by the Number of Quanta n_x, n_y, and n_z in the x, y, or z Direction or Equivalently by the Quantum Numbers ϵ and ν

n_x	n_y	n_z	ϵ	ν	Notation
0	0	2	4	0	ϕ_0
1	0	1	1	1	ϕ_{+1}
0	1	1	1	-1	ϕ_{-1}
2	0	0	-2	2	ϕ_{+2}
1	1	0	-2	0	ϕ_0'
0	2	0	-2	-2	ϕ_{-2}

The $(\tilde{\lambda}\tilde{\mu})$ representation of SU_3 for maximum orbital symmetry is of special significance in nuclear physics, as will be shown in Section 4.3. It is just the states classified in this way which are often expected to be low in energy.

The states having $\epsilon = \epsilon_{\max} = 2\lambda + \mu$ are of significance in the explicit construction of states having a definite angular momentum within a general representation $(\lambda\mu)$ of SU_3, as will be shown in Section 3.7. Since the state having $\epsilon = \tilde{\epsilon}_{\max}$ is especially easy to construct and the representation $(\tilde{\lambda}\tilde{\mu})$ is of physical importance in the study of low-energy nuclear spectra, the significance of the construction of states to be described in the next section will be apparent.

If the structure of the state having $\epsilon = \tilde{\epsilon}_{\max}$ and $\nu = \tilde{\nu}_{\max}$ is known, other states of the $(\tilde{\lambda}\tilde{\mu})$ representation can be constructed using the lowering operators given in Appendix F. Once all the states of this *leading* representation are obtained, the states with $\epsilon = \epsilon_{\max}$ of a different representation can be found by orthogonality arguments. By continuing in this way all states classified according to $SU_3 \rightarrow SU_2 \times U_1$ could in principle be constructed. [An alternative approach to constructing states of a definite symmetry uses Young operators (H64a). Since the states of physical interest are especially easy to construct by the chain procedure, we shall not discuss this alternative approach].

3.7 Construction of States Classified According to SU_3 and R_3

In the previous section was discussed the classification according to $SU_3 \to SU_2 \times U_1$ of states which we shall here denote by $\phi((\lambda\mu)\,\gamma\epsilon\Lambda\nu)$. The invariance of the nuclear Hamiltonian with respect to R_3 means that the states of more *physical* interest have a definite angular momentum. The states having a definite *orbital* angular momentum in the representation $(\lambda\mu)$ of SU_3 will be written $\psi((\lambda\mu)\alpha LM)$. The γ and α labels in the states ϕ and ψ are put in to describe the properties of these states not explicitly given by the other quantum numbers.

In this section we review the generalized analysis originally given by Elliott (E58), which shows simultaneously the explicit structure of the states ψ and their rotational characteristics.

Since there is only a finite set of states within a representation $(\lambda\mu)$ of SU_3, it is possible to expand any one of the functions ϕ in terms of the set ψ

$$\phi((\lambda\mu)\,\gamma\epsilon\Lambda\nu) = \sum_{\alpha LK_L} a((\lambda\mu)\,\gamma\epsilon\Lambda\nu,\, \alpha LK_L)\,\psi((\lambda\mu)\,\alpha LK_L) \tag{3.34}$$

where $a(\lambda\mu)\,\gamma\epsilon\Lambda\nu,\, \alpha LK_L)$ are expansion coefficients.

In the construction of states ψ it is convenient to consider the above expansion taking place in a frame rotated through the Euler angles Ω relative to the laboratory frame

$$\phi_\Omega((\lambda\mu)\,\gamma\epsilon\Lambda\nu) = \sum_{\alpha LK_L} a((\lambda\mu)\,\gamma\epsilon\Lambda\nu,\, \alpha LK_L)\,\psi_\Omega((\lambda\mu)\,\alpha LK_L) \tag{3.35}$$

From the well-known properties of rotations of states with angular momentum L we can write

$$\psi_\Omega((\lambda\mu)\,\alpha LK_L) = \sum_{K'_L} \mathscr{D}^{L*}_{K'_L K_L}(\Omega)\,\psi((\lambda\mu)\,\alpha LK'_L) \tag{3.36}$$

where $\mathscr{D}$ is a rotation matrix element (E57*a*). By substituting Eq. (3.36) in Eq. (3.35), multiplying by $\mathscr{D}^L_{M_L K_L}$, and integrating over all Euler angles Ω, we find

$$\int \mathscr{D}^L_{M_L K_L}(\Omega)\,\phi_\Omega((\lambda\mu)\,\gamma\epsilon\Lambda\nu)\,d\Omega = \sum_\alpha \frac{a((\lambda\mu)\,\gamma\epsilon\Lambda\nu,\, \alpha LK_L)}{(2L+1)}\,\psi((\lambda\mu)\,\alpha LM_L) \tag{3.37}$$

using the notation

$$\int d\Omega \equiv \frac{1}{8\pi^2}\int_0^\pi \int_0^\pi \int_0^{2\pi} d\theta_1 \sin\theta_2\, d\theta_2\, d\theta_3$$

for the integration over the Euler angles $\Omega = (\theta_1, \theta_2, \theta_3)$ and the known orthogonality relations for the rotation matrix elements.

In Eq. (3.37) the functions ψ are undefined with regard to the quantum number α. The states ψ will now be *defined* as those states of definite L and K_L in the expansion of the *maximum-weight* state ϕ of maximum ϵ $(=\epsilon_{\max} = 2\lambda + \mu)$ and ν $(=\nu_{\max} = \mu)$ in a representation $(\lambda\mu)$ of SU_3

$$\phi_\Omega((\lambda\mu)\,\gamma(\epsilon\Lambda\nu)_{\max}) = \sum_{K_L L} a((\lambda\mu)\,\gamma(\epsilon\Lambda\nu)_{\max}\,, LK_L)\,\psi_\Omega((\lambda\mu)\,\gamma K_L L K_L) \tag{3.38a}$$

Since the $(\epsilon\Lambda\nu)_{\max}$ numbers are given uniquely by λ and μ [cf. Eqs. (3.29), (3.30), and (3.27)], we simplify the notation a little to write Eq. (3.38a)

$$\phi_\Omega((\lambda\mu)\,\gamma) = \sum_{K_L L} a((\lambda\mu)\,LK_L)\,\psi_\Omega((\lambda\mu)\,\gamma K_L L K_L) \tag{3.38b}$$

where the symbol α of Eq. (3.35) has now been split into γ (carrying the properties of ϕ over to ψ that are not involved in the expansion) and the number K_L.

The *important* property of the state of maximum weight $\phi(\lambda\mu)$ is that the functions $\psi((\lambda\mu)\,K_L L M_L)$, $M_L = L, L-1, \ldots, -L$, so defined in Eq. (3.38b), span *all* the states of the representation $(\lambda\mu)$. The proof involves a *reductio ad absurdum* argument which can be found in Reference E58.

Thus *any* state of the representation $(\lambda\mu)$ of SU_3 with angular momentum L can be written in terms of the projection (H53) of L and K_L from the state of maximum weight $\phi((\lambda\mu)\,\gamma)$

$$\psi((\lambda\mu)\,\gamma K_L L M_L) = \frac{2L+1}{a((\lambda\mu)\,LK_L)} \int \mathscr{D}^L_{M_L K_L}(\Omega)\,\phi_\Omega((\lambda\mu)\,\gamma)\,d\Omega \tag{3.39}$$

Thus functions with a definite angular momentum L in a representation $(\lambda\mu)$ of SU_3 can be written in a way very similar to states of the collective model (*M*57) with the *intrinsic state* being the state $\phi((\lambda\mu)\,\gamma)$. The quantum number K_L is simply the projection of orbital angular momentum L on the intrinsic z axis (cf. Eq. 3.38b).

The intrinsic state ϕ is an oscillator state with the number of quanta N in the x, y, and z direction given by

$$\begin{aligned} N_x &= a + \mu \\ N_y &= a \\ N_z &= a + \mu + \lambda \end{aligned} \tag{3.40}$$

with

$$3a + 2\mu + \lambda = N_x + N_y + N_z = N$$

To illustrate the deformed structure of such a state we shown in Fig. 3.1 the contours of the particle probability density distribution in the $x = 0$, $y = 0$, and $z = 0$ planes for $(\lambda\mu) = (84)$; this representation is expected to describe the lowest states in Mg^{24}(cf. Section 5.3).

Note that the above construction of states ψ is not unique. It is also possible to generate the same *set* of states by projecting from the state $\bar{\phi}(\lambda\mu)$ of minimum weight, ($\epsilon_{\min} = -2\mu - \lambda$, $\nu = -\lambda$). Elliott (E58) has suggested that, when $\lambda \geqslant \mu$ states should be projected from the state of maximum weight and when $\lambda < \mu$, the projection from the minimum weight states should be performed. Actually the lack of uniqueness of the intrinsic state is far greater than that discussed above. If $F(A)$ is *any* function of the

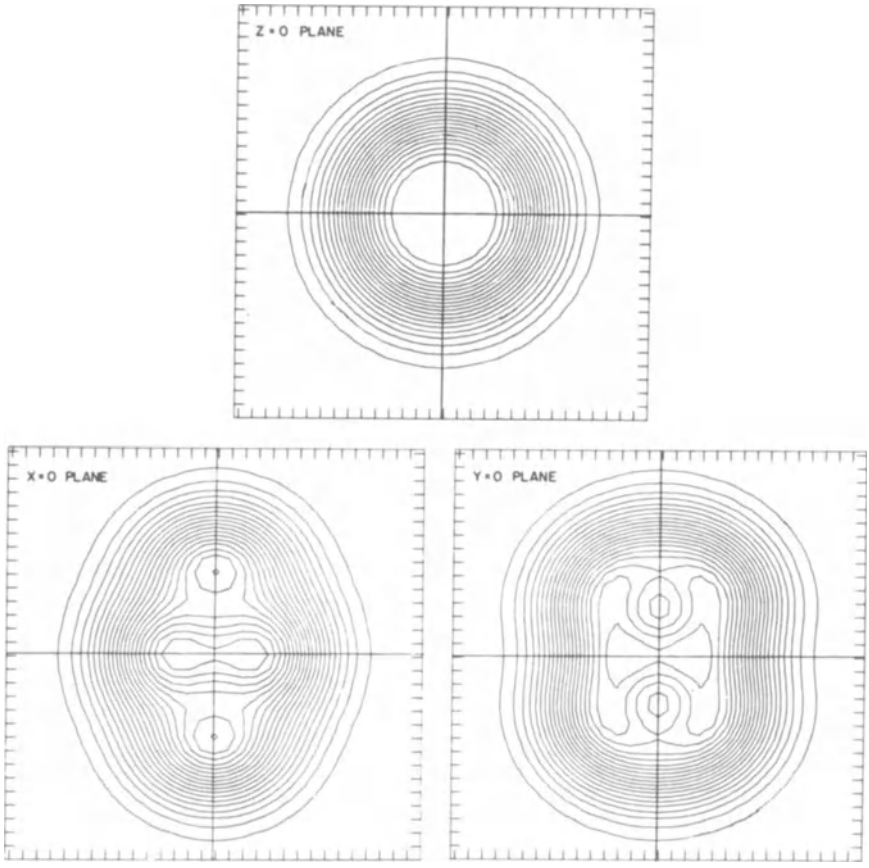

Fig. 3.1. Contours for the particle probability density in the state of maximum weight for $(\lambda\mu) = (84)$.

SU_3-group operators, then $\phi' = F(A)\phi(\lambda\mu)$ is a function belonging to the same representation of SU_3. Thus the projection of angular momentum states $\psi'(L)$ from ϕ' can only lead to the *same set* of functions $\psi'(L)$ as can be projected from ϕ. *All the functions like ϕ' are said to be spurious.* The spurious states ϕ' have a very simple physical interpretation. In Appendix F we show how any function of the SU_3-group operators acting on the state of maximum weight can be written equivalently in terms of a function of angular momentum operators only. These latter operators are associated with the rotations of the group R_3, i.e., the set ϕ' above can simply be written in terms of the functions which have the same shape as the state $\phi(\lambda\mu)$ but different orientations with respect to the "intrinsic axis." Clearly there is no physical difference between the rotation of (projection from) an intrinsic frame having a state ϕ at an orientation Ω or $\Omega + \Omega'$ to it. The state $\tilde{\phi}(\lambda\mu)$ of minimum weight is actually the state of maximum weight $\phi(\lambda\mu)$ rotated in the *intrinsic frame* through $\pi/2$ about the intrinsic x axis, i.e., if the number of quanta in the x, y, or z direction for $\tilde{\phi}(\lambda\mu)$ are $\tilde{N}_x$, $\tilde{N}_y$, $\tilde{N}_z$, then $\tilde{N}_x = N_x$, $\tilde{N}_y = N_z$, and $\tilde{N}_z = N_y$, with N_x, N_y, and N_z defined in Eq. (3.38).

When $\lambda \gg \mu$, the intrinsic state has the characteristics of a prolate (or "cigar") shape and the function $\phi(\lambda\mu)$ has the symmetry axis in the intrinsic z direction; if $\lambda \ll \mu$, the intrinsic state takes on the characteristics of an oblate (or "pancake") shape and it is the function $\tilde{\phi}(\lambda\mu)$ that has the symmetry axis in the intrinsic z direction.

It must be emphasized that it is not necessarily the *same* state that can be projected with definite L and K_L from $\phi(\lambda\mu)$ and from a spurious state ϕ'. Simply from classical arguments it can be seen, e.g., that it is the $L = 2$, $K_L = 0$ state projected from $\phi(\lambda\mu)$, which is closely related to the $L = 2$, $K_L = 2$ state projected from $\tilde{\phi}(\lambda\mu)$.

These *spurious* states of rotational motion arise in any model involving an intrinsic state.

Although the functions ψ in Eq. (3.39) span the complete space of functions classified according to SU_3, i.e., the label K_L gives a linearly independent set of states of given L, the states so defined are *not orthogonal* with respect to K_L. This is the price that must be paid for writing the function ψ in the form closest to that of functions of the rotational model. Actually this nonorthogonality is not a serious problem as far as calculations are concerned (see Appendix G); Appendix H shows how the overlap and the normalization coefficients $a((\lambda\mu)\, K_L L)$ are related and gives a method for calculating them. The states with different K_L and with small L [compared with $\max(\lambda, \mu)$] are almost orthogonal and, in the calculations that have been done, K_L turn out to be a good quantum number.

The complete antisymmetric wave function actually consists of com-

binations of an orbital function ψ and a charge-spin function $\Gamma(\gamma' SM_S)$ with the total angular momentum $J = L + S$ defined.

A complete set of states can be written

$$\overline{\Psi}(\gamma\gamma'(\lambda\mu)\, K_L LSJM) = \sum_{M_L(M_S)} (LSM_L M_S \mid JM)\{\psi((\lambda\mu)\,\gamma K_L M_L)\, \Gamma(\gamma' SM_S)\} \tag{3.41}$$

where { } denotes an antisymmetric state and $\gamma\gamma'$ absorb all quantum numbers not explicitly defined; e.g., γ includes the orbital symmetry $[f]$, while γ' includes the charge-spin symmetry $[\tilde{f}]$ (adjoint to $[f]$) and the isotopic spin T. The Clebsch–Gordan coefficient $(\ldots.|..)$ is defined in References E57*a* and R59.

Functions like $\overline{\Psi}$ will be referred to as *L-projected functions*. An equivalent set can be defined if the *total* angular momentum J is projected directly from an intrinsic state

$$\Phi(\gamma\gamma'(\lambda\mu)\, SK_S) = \{\phi((\lambda\mu)\,\gamma)\; \Gamma(\gamma' SK_S)\} \tag{3.42}$$

Thus

$$\tilde{\Psi}(\gamma\gamma'(\lambda\mu)\, K_L KSJM) = \frac{2J+1}{A((\lambda\mu)\, SK_S KJ)} \int \mathscr{D}^J_{MK}(\Omega)\, \Phi(\gamma\gamma'(\lambda\mu)\, SK_S)\, d\Omega \tag{3.43}$$

where $K = K_L + K_S$.

The relationship between the J-projected set of states of Eq. (3.41) and the L-projected set in Eq. (3.39) can be derived in the following manner:

$$\Phi(\gamma\gamma'(\lambda\mu)\, SK_S) = \sum_{KJ} A((\lambda\mu)\, SK_S KJ)\, \tilde{\Psi}(\gamma\gamma'(\lambda\mu)\, K_L KSJK) \tag{3.44a}$$

[by definition from Eq. (3.43)]

$$= \sum_{K_L L} a((\lambda\mu)\, K_L L)\{\psi((\lambda\mu)\,\gamma K_L LK_L)\, \Gamma(\gamma' SK_S)\}$$

$$= \sum_{K_L LJ} a((\lambda\mu)\, K_L L)\, (LSK_L K_S \mid JK)\, \overline{\Psi}(\gamma\gamma'(\lambda\mu)\, K_L LSJK) \tag{3.44b}$$

Thus

$$\tilde{\Psi}(\gamma\gamma'(\lambda\mu)\, K_L KSJK) = \sum_L \frac{a((\lambda\mu)\, K_L L)\, (LSK_L K_S \mid JK)}{A((\lambda\mu)\, SK_S KJ)}\, \overline{\Psi}(\gamma\gamma'(\lambda\mu)\, K_L LSJK) \tag{3.45}$$

With the a coefficients (Appendix H) and the Clebsch–Gordan coefficients known, the A coefficients defined in Eq. (3.44a) can be determined by the normalization conditions from Eq. (3.45). Alternatively the A coefficients

can be calculated directly by using arguments similar to those in Appendix H (e.g., W65).

It is clear from Eq. (3.45) that functions like $\tilde{\Psi}$ do not have orbital angular momentum defined but, in its place, the label K has been introduced to represent the projection of total angular momentum J on the intrinsic z axis. Functions like $\tilde{\Psi}$ are not orthogonal with respect to either K_L or K, but the overlaps can be determined from the overlaps of functions like $\overline{\Psi}$ (cf. Appendix H). Again, for small angular momentum J, overlaps are usually negligible.

It is perhaps appropriate at this stage to think a little about the applications of such function $\overline{\Psi}$ in Eq. (3.41) or $\tilde{\Psi}$ in Eq. (3.41). If spin-dependent forces are negligible in the nuclear Hamiltonian H, then the orbital angular momentum L will be a good quantum number. It is therefore more appropriate to use the functions $\overline{\Psi}$ in attempting to describe eigenfunctions of H. If, on the other hand, spin-dependent forces are not negligible, then orbital angular momentum is not preserved and it is therefore more appropriate to use the functions $\tilde{\Psi}$. Whether the admixtures of states of different L [as defined for $\tilde{\Psi}$ in Eq. (3.45)] which go together to form a state with definite K is appropriate for the spin-dependent force chosen is a fact to be discovered numerically (cf. Chapter 5).

Finally we note that for states which have zero total spin ($S = 0$), the functions $\overline{\Psi}$ and $\tilde{\Psi}$ are actually identical.

4. THE EFFECTIVE INTERACTION

4.1 General Principles

In the previous section we reviewed the rather formal theory of the simultaneous classification and construction of states belonging to definite irreducible representations of the group S_A, U_3, and R_3. We return now to the physical problem of deciding on the structure of real nuclear states, i.e., of the eigenfunction of the nuclear Hamiltonian.

The structure of nuclear states depends of course on the assumption concerning nuclear forces. It is important to remember, however, that the form of the nuclear Hamiltonian need not be unique; i.e., the explicit form of two Hamiltonians may look entirely different, but they can still have the same eigenvalues and eigenfunctions. Such a situation can arise in the following way. Suppose a Hamiltonian is constructed with an assumed two-body interaction. Because we are dealing with a many-body problem, the effective force between two nucleons is not just the force put into the Hamiltonian but also includes second- and higher-order effects through the the interactions with other nucleons. For example, the Pauli principle modifies

the free two-body force between nucleons in a nucleus into an effective force. Thus one could redefine the original two-body interaction to take into account some of these higher-order effects. The force we have now is said to be *effective* and will lead to the same physical structure as the original force, but it could lead to a Hamiltonian which is easily soluble.

It is very difficult to derive an easily soluble *effective* Hamiltonian H_{eff} from a *realistic* one H_{real} derived, e.g., from the two-body scattering data. What is often done is to resort to some gross feature actually observed in nuclei and, by using a force which could produce this feature, set up an effective Hamiltonian. Thus the observation of an energy gap has suggested the importance of an effective pairing force (N65*c*) and, as we shall discuss in the rest of this chapter, the observation of rotational features suggests an effective quadrupole–quadrupole potential (M58, B60*a*, H61*a*, E62, M62, W62).

The solution of the effective Hamiltonian H_{eff} leads to effective wave functions which one hopes possess the gross properties (e.g., transitions) of real nuclear states. It is a questionable point whether the energy spectrum should be determined from the effective Hamiltonian or from the realistic Hamiltonian with the effective wave functions; if we write $H_{\text{real}} = H_{\text{eff}} + (H_{\text{real}} - H_{\text{eff}})$, then it is a question of the magnitude of $\langle H_{\text{real}} - H_{\text{eff}} \rangle$ between effective wave functions. Of course if H_{eff} is derived from H_{real} in some self-consistent sense, then it should not matter which we use.

A word of caution! There is no reason to believe that an observed nuclear property belongs uniquely to *one* particular effective potential, however plausable the arguments leading to its construction. In Chapter 6 we shall discuss other "collective" models of the nucleus for which other criteria are used to define a rotational state. In these models the effective force is not necessarily the quadrupole–quadrupole force.

4.2 The Quadrupole-Quadrupole Force

In the Introduction it was noted that light nuclei in the mass $A \approx 20$ region exhibit collective features. It is to be expected that such collective features can only occur if there is some communication between opposite sides of the nucleus, or, in other words, an *effective two-body force* must have a long range compared with the size of the nucleus.

The problem now is to decide on the important parts of the effective force. This problem can be tackled by making a long-range expansion (in terms of the range parameters a) of any two-body central force, e.g., one having a Gaussian or Yukawa radial dependence (H61*a*, E62, E63*a*).

$$V^{(2)} = \sum_{i<j} V\left(\frac{r_{ij}}{a}\right) = \sum_{i<j} \left(\xi_0 + \xi_2 \frac{r_{ij}^2}{a^2} + \xi_4 \frac{r_{ij}^4}{a^4} + \cdots +\right) \tag{4.1}$$

For a very long range the matrix of $V^{(2)}$ is diagonal and all the diagonal elements in the A-body problem are approximately $\xi_0[A(A-1)/2]$ from the first term in the expansion of Eq. (4.1). The first correction to this comes from the second term, which is proportional to

$$\sum_{i<j} r_{ij}^2 \equiv \sum_{i<j} (r_i - r_j)^2 = \sum_{i<j} (r_i^2 + r_j^2 - 2r_i r_j \cos\theta_{ij})$$
$$= (A-1)\sum_i r_i^2 - 2\sum_{i<j} r_i r_j \cos\theta_{ij} \tag{4.2}$$

The first term in Eq. (4.2) is just proportional to the oscillator potential which verifies the fact that the average spherical potential has a long-range character and can be approximated by the harmonic oscillator. Many-body states are thus ordered by this term according to their oscillator quanta, and states with the same number of quanta are degenerate in energy. The splitting of the degeneracy can only come from other terms in the expansion of $V^{(2)}$ [Eq. (4.1)].

All of the orbits of a single oscillator shell have the same parity. Thus, in a shell model with only one active shell, all the matrix elements of the term $\sum_{i<j} r_i r_j \cos\theta_{ij}$ in Eq. (4.2) are zero. For more than one active shell we can write

$$\sum_{i<j} r_i r_j \cos\theta_{ij} = \sum_{i<j} (r_i \cdot r_j) = \frac{b^2}{2}\sum_{i<j} (\{a_{(i)}^+ + a_{(i)}\} \cdot \{a_{(j)}^+ + a_{(j)}\}) \tag{4.3}$$

using the oscillator creation- and destruction-operator formalism and the notation $(\cdot)$, implying scalar product. The matrix elements between states with the same number of quanta are just given by the matrix elements of

$$\frac{b^2}{2}\sum_{i<j} \{(a_{(i)}^+ \cdot a_{(j)}) + (a_{(i)} \cdot a_{(j)}^+)\} = \frac{b^2}{2}\{\bar{H} - H_0\} \tag{4.4}$$

where H_0 is the many-body harmonic oscillator defined in Eq. (3.9) and $\bar{H}$ is the harmonic-oscillator Hamiltonian of the center of mass.

$$\bar{H} = \tfrac{1}{2}\{(\bar{a}^+ \cdot \bar{a}) + (\bar{a} \cdot \bar{a}^+)\}$$

with

$$\bar{a}^+ = \sum_i a^+(i) \qquad \text{etc.} \tag{4.5}$$

Thus from Eq. (4.4) the matrix elements of $\sum_{i<j}(r_i \cdot r_j)$ are constants between states with the same number of oscillator quanta and the same excitation of the center of mass and therefore do not contribute to any splitting of degeneracy.

The next term in the expansion of $V^{(2)}$ in Eq. (4.1) is proportional to

$$\sum_{i<j} r_{ij}^4 \equiv \sum_{i<j} (r_i^2 + r_j^2 - 2r_i r_j \cos\theta_{ij})^2$$
$$= \sum_{i<j} \{r_i^4 + r_j^4 + \tfrac{8}{3} r_i^2 r_j^2 + \tfrac{4}{3} r_i^2 r_j^2 P_2(\cos\theta_{ij})$$
$$- 4(r_i^2 + r_j^2)\, r_i r_j \cos\theta_{ij}\} \qquad (4.6)$$

Again the last term in Eq. (4.6) has zero matrix elements in a shell model with one active shell from parity considerations. The first three terms are either constants or single-particle terms that do not lead to significant splittings in the energy of the degeneracy of many-body states. Thus the first term that really leads to any splitting of the oscillator degeneracy is proportional[3] to

$$r_i^2 r_j^2 P_2(\cos\theta_{ij}) \equiv \left(r_i^2 Y^2(\theta_i\phi_i) \cdot r_j^2 Y^2(\theta_j\phi_j)\right) \qquad (4.7)$$

This term is referred to as the "P_2 potential" or "quadrupole–quadrupole potential" or simply the "QQ-potential" (M58).

This QQ-potential will actually couple many-body harmonic-oscillator states having different numbers of oscillator quanta. These couplings are to be ignored in the SU_3 scheme with the argument that the splitting between oscillator shells is large enough from first-order effects to make such couplings negligible. Thus the potential in Eq. (4.7) is to be considered to operate only within one oscillator shell. Within an oscillator shell

$$r_i^2 Y_q^2(\theta_i\phi_j) \equiv \frac{b^2}{4}\sqrt{\frac{5}{\pi}}\, Q_q \qquad (4.8)$$

where Q_q is the SU_3 operator introduced in Eq. (3.13). Thus the splitting of the harmonic-oscillator degeneracy is simply proportional to $\sum_{i<j} (Q(i)\cdot Q(j))$. We shall show in Section 4.3 that the eigenfunctions of such an operator are closely related to those classified according to SU_3.

We note that the above arguments included the assumption of only one active oscillator shell. For more than one active shell of mixed parity the SU_3 classification need not be a consequence of the long-range part of a central force because of such terms as $\sum_{i<j} (r_i^2 + r_j^2)\, r_i r_j \cos\theta_{ij}$ [cf. Eq. (4.6)] in the potential. The consequences of such terms have not yet been fully investigated.

[3] See Reference A65 for a discussion on the sign of this part of the potential.

4.3 The Casimir Operator of SU_3

In Section 3.2 it was shown that the harmonic oscillator is invariant with respect to U_3 and SU_3. Other invariant operators can be constructed from the group operators and these go under the name of *Casimir operators* (R51, H64*a*).

The Casimir operator of the group U_3 of bilinear form can bewritten

$$C_2 = \sum_{\alpha\beta} A_{\alpha\beta} A_{\beta\alpha} \tag{4.9}$$

with the SU_3 shift operators defined in Eq. (3.10).

It is trivial to prove that C_2 is invariant with respect to U_3 by using the commutation relations in Eq. (3.4).

The Casimir operator $\tilde{C}_2$ of SU_3 can be extracted from C_2 simply by removing all dependence on the shift operator H_0 [cf. Eq. (3.9)]

$$\begin{aligned} \tfrac{1}{6}\tilde{C}_2 &= \sum_{\alpha\neq\beta} A_{\alpha\beta} A_{\beta\alpha} + \tfrac{1}{6}\{2A_{zz} - A_{xx} - A_{yy}\}^2 + \tfrac{1}{2}\{A_{xx} - A_{yy}\}^2 \\ &= \tfrac{1}{6}\{(Q\cdot Q) + 3(L\cdot L)\} \end{aligned} \tag{4.10}$$

In the last expression we make use of the spherical tensor form for the shift operators defined in Eqs. (3.12) and (3.13). Equation (4.10) immediately shows the scalar character of $\tilde{C}_2$ under R_3; this is as it should be, of course, since the invariance of $\tilde{C}_2$ with respect to SU_3 immediately implies its invariance with respect to its subgroup R_3.

We note that $\tilde{C}_2$ includes the term

$$(Q\cdot Q) = \sum_i (Q(i)\cdot Q(i)) + 2\sum_{i<j} (Q(i)\cdot Q(j)) \tag{4.11}$$

with particle numbers i and j. The two-body part of this operator is to be considered as an important term for the long-range force in the harmonic oscillator model with one active shell (cf. Section 4.2). The self-energy term leads to a splitting of the single-particle orbits and can also be included with the two-body term to take into account interactions with closed shells. [In O^{17}, e.g., the $2s$ and $1d$ levels are not actually degenerate and can be considered split by the single-particle potential proportional to $\sum_i (Q(i)\cdot Q(i))$.]

Rewriting Eq. (4.10), we find that a *typical attractive* long-range force (with a single-particle term) contains a term proportional to

$$-(Q\cdot Q) = -\tilde{C}_2 + 3L^2 \tag{4.12}$$

$\tilde{C}_2$ is invariant with respect to SU_3 and therefore cannot couple states belonging to different representations. Within a representation only the

diagonal matrix elements (expectation values) are nonzero and have a value depending only on the representation labels λ and μ. The operator L^2 consists of operators of SU_3 and therefore cannot couple different representations, but it is not *invariant* with respect to the group. SU_3 is a typical *broken-symmetry* group (cf. Section 2.3) for a Hamiltonian having a $(Q \cdot Q)$ potential.

From Eq. (4.12) it is immediately seen that within a representation of SU_3 the eigenvalues of $(Q \cdot Q)$ are proportional to $L(L+1)$; this is exactly the collective feature that it was hoped the SU_3 scheme would provide. Equation (4.12) also provides another important piece of information. The states which are lowest in energy will belong to the representation of SU_3 which maximizes $\langle C_2 \rangle$; this representation is often referred to as the *leading representation.*

Since $\tilde{C}_2$ is invariant with respect to SU_3, its expectation value $\langle \tilde{C}_2 \rangle$, between states classified according to the group, only depends on the representation labels λ and μ. Thus *any* state belonging to the $(\lambda\mu)$ representation can be used to determine $\langle \tilde{C}_2 \rangle$. It is convenient to use the state of maximum weight in the chain classification $SU_3 \rightarrow SU_2 \times U_1$ (cf. Section 3.6). Within a representation the state of maximum weight $\phi(\lambda\mu)$ has the maximum number of quanta in the z direction and, for this number, the maximum number in the x direction (cf. Section 3.7). Clearly then

$$A_{xy}\phi(\lambda\mu) = A_{zx}\phi(\lambda\mu) = A_{zy}\phi(\lambda\mu) = 0 \tag{4.13}$$

Terms like $A_{xy}A_{yx}$ in Eq. (4.7) can be rewritten

$$A_{xy}A_{yx} = A_{yx}A_{xy} + A_{xx} - A_{yy} \qquad \text{etc.}$$

and for the state $\phi(\lambda\mu)$

$$\begin{aligned} (2A_{zz} - A_{xx} - A_{yy})\,\phi(\lambda\mu) &= \epsilon_{\max}\phi(\lambda\mu), \qquad \epsilon_{\max} = 2\lambda + \mu \\ (A_{xx} - A_{yy})\,\phi(\lambda\mu) &= \nu_{\max}\phi(\lambda\mu), \qquad \nu_{\max} = \mu \end{aligned} \tag{4.14}$$

cf. Eq. (3.29), (3.30), and (3.27).
Thus we deduce

$$\langle \tilde{C}_2 \rangle_{\lambda\mu} = 4[\lambda^2 + \mu^2 + \lambda\mu + 3\lambda + 3\mu] \tag{4.15}$$

Representations which maximize $\langle \tilde{C}_2 \rangle$ turn out to have the maximum value for $(2\lambda + \mu)$. Thus, in view of the discussion in Section 3.7, the states which are expected to be low in energy are actually the easiest to construct in the projection of angular momentum technique.

Before closing this section we note the existence of another invariant operator of U_3, which has the trilinear form

$$C_3 = \sum_{\alpha\beta\gamma} A_{\alpha\beta} A_{\beta\gamma} A_{\gamma\alpha} \tag{4.16}$$

This too leads to another invariant operator $\tilde{C}_3$ of SU_3. An alternative way of defining representation labels of SU_3 is to use the expectation value of $\tilde{C}_2$ and $\tilde{C}_3$ instead of the numbers λ and μ. Of course, the two schemes are related in such expressions as Eq. (4.15).

The second Casimir operator C_3 (or $\tilde{C}_3$) involves three-body operators. To the author's knowledge no use of these operators has been made in discussions of effective potentials.[4]

5. APPLICATION OF THE SU_3-COUPLING SCHEME TO LIGHT NUCLEI

5.1 General Remarks

In the SU_3 model the lowest nuclear states are described by functions having maximum orbital symmetry and transforming according to the leading representation of SU_3. It must be remembered, however, that the SU_3 scheme is designed specifically to describe collective effects in nuclei. If the actual forces in a particular nucleus do not cooperate to give collective effects, then naturally the SU_3 classification will fail. If collective effects are present but are due partly to spin-dependent forces, then the SU_3-classification scheme can also fail. As we have discussed at some length, it is not possible in most cases to discover the validity of the SU_3 scheme by theoretical calculations in the shell model alone because of the size of the problem. Some cases where reasonably full shell model calculations have been made are discussed in Section 5.2. In general the validity of the SU_3 scheme has been gauged by its ability to describe observed features in "real" nuclei. In assessing the success of the model one should also keep in mind the successes of other models predicting different structures for the same states [cf. The discussion on pseudonium (C66*b*)]. Some data are model independent!

In this section we discuss the predictions and consequences of assuming the exact classification according to the leading representations of SU_3. The attempts to explain the deviations from the observed data will be described in Part 6.

In the discussions of normal-parity states with one active shell in the $0 < A \leqslant 16$ region (i.e., the filling of the $1s$ and $1p$ shells), the SU_3 scheme

[4] Note Added in Proof: The trilinear operator has been used by F. Nash [*Nuovo Cimento* **42**:8 (1966).] in the discussion of three-body forces in the *ip*-shell.

adds little to the shell model (*K*56, B66*a*) that is not already there in the Wigner supermultiplet scheme apart may be from some ease in calculations (K61). For nuclei of mass much above $A = 40$ even the single-particle picture seems to imply large nontrivial spin-orbit effects in the average central well and the complicated situation of several shells being filled at the same time. Thus to date the applications of the SU_3-classification scheme has been mainly restricted to nuclei of mass $16 \leqslant A \leqslant 40$ [the filling of the $(2s, 1d)$ shell], although in principle it can be applied to any set of oscillator orbits. Some general predictions of the model in the oscillator $(2s, 1d)$ shell and comparisons with observed systematics in nuclear data are discussed in Sections 5.3 and 5.4.

Since the SU_3 scheme is specifically set up to describe collective features, it has been used to try to describe nuclear states which have observed collective effects but which are thought to have more than one active shell. Here, however, there is very little theoretical evidence available to indicate the validity of the scheme. Even the analysis of long-range forces in Part 4 does not lead unambiguously to the SU_3 scheme for more than one active shell. In Section 5.5 we review the calculations done on the single-excitation negative-parity states in the $(2s, 1d)$ shell, and in Section 5.6, the work on the double-excitation states. In Section 5.7 we briefly mention the very recent work on nonnormal parity states in the $1p$ shell.

It is not possible here to review in detail every piece of work remotely connected with the SU_3 scheme, neither do we think this is desirable. Our intention is only to give a reasonably broad survey of the abilities and uses of the model and to try to establish the regions in which the predictions can be expected to be valid. We hope our references adequately cover the papers giving detailed calculations using the SU_3 scheme.

5.2 Accuracy of the SU_3 Classification in the $(2s, 1d)$ Shell

For the SU_3 scheme to be valid it is necessary for the central part of the residual potential to dominate the interaction and then for this part to lead to an effective long-range potential. The central dominance leads to the classification according S_A (W37), and the effective long range, to the classification according to SU_3.

The full shell-model calculations with only the $(2s, 1d)$ shell active have been made for normal parity states of nuclei of mass 18 and 19 (E55). On introducing the SU_3 scheme Elliott (E58) showed for ^{18}F, ^{18}O, and ^{19}F the similarity between the zero-excitation positive-parity states, classified according to the leading representations of SU_3, and the eigenfunctions within the shell model of a realistic Hamiltonian which had been used to describe the properties of light nuclei. The interaction used had a Yukawa

radial dependence, Rosenfeld exchange, and a single-particle potential to reproduce the splitting of the single-particle levels observed in O^{17}. In Table 5.I we quote the overlaps between the calculated and predicted states. Shown also in this table is the percentage of states of maximum orbital symmetry in the variational state (see also I64, I66).

TABLE 5.I

Percentage of Those Parts of the Wave Functions from a Standard Shell Model Calculation Which Have Maximum Orbital Symmetry (% $L-S$) and Which Belong to the Leading Representation of SU_3 (% SU_3) [Taken from Elliott (E58)][a]

Nucleus	T	J	$(\lambda\mu)$	L	% $(L-S)$	% SU_3	
^{18}F	0	1	(40)	S	97	92	
	0	3	(40)	D	98	96	
	0	5	(40)	G	100	100	(trivial)
^{18}O	1	0	(40)	S	86	72	
	1	2	(40)	D	80	72	
^{19}F	$\frac{1}{2}$	$\frac{1}{2}$	(60)	S	92	92	
	$\frac{1}{2}$	$\frac{5}{2}$	(60)	D	86	74	
	$\frac{1}{2}$	$\frac{3}{2}$	(60)	D	84	74	
	$\frac{1}{2}$	$\frac{9}{2}$	(60)	G	87	85	
^{20}Ne	0	0	(80)	S	100	92	
	0	2	(80)	D	100	99	
	0	4	(80)	G	100	92	
	0	6	(80)	I	(100)	99	
	0	8	(80)	L	(100)	100	(trivial)

[a] In ^{20}Ne the shell model calculation was only performed for states of maximum orbital symmetry.

The striking point about the results in Table 5.I is the large percentage of states of maximum orbital symmetry in the variational state, indicating the dominance of the spin-independent forces. The states of maximum orbital symmetry also turn out to be given very well by the states of the leading representation of SU_3, which indicates effective collective phenomena.

One can justifiably question the use of overlaps to determine the validity of the SU_3-classification scheme, it being well known that even small changes in wave functions can often seriously change the gross properties possessed by these states. Actually, in the cases were it has been checked, it has been found that, if the states of the leading representation of SU_3 dominate the

shell-model eigenstates, then the gross properties of the latter are indeed determined by the SU_3 structure.

The above results on $A = 18$ have essentially been verified by Flores *et al.* (F65*b*, L65). In this series of papers a phenomenological force is used consisting of a long-range (QQ), short-range (orbital pairing), and single-particle spin-orbit parts. The reason for choosing these types of potentials is that combinations of them contain the properties of any reasonably general potential. Each part of the phenomenological potential is exactly soluble by group theoretical means: QQ using SU_3, orbital pairing using R_6, spin orbit by jj coupling. By calculating the "transformation brackets" between the sets of states classified according to the different schemes, the complete energy matrix can be set up with just one as a basis. For greater information on this method we suggest References F65*b* and L65. The strengths of the various components of the force and the possibility of exchange mixtures are determined by a least squares fitted to observed data.[5]

In heavier nuclei in the ($2s$, $1d$) shell the full variational calculations have not been made because of the size of the problem, although attempts are being made (see G66). Some attempts have been made however to check on the assumption that the effective part of the spin-*independent* force leads to the SU_3-coupling scheme. In principle this can be done by considering the variational calculation, using only the states of maximum orbital symmetry and a potential, say, of the Yukawa type. (Remember that for a charge-spin independent force the orbital symmetry is an exact classification). The results obtained by Elliott for ^{20}Ne are also shown in Table 5.I where again the SU_3 classification is largely verified. These results have also been obtained by Kalman *et al* (K67) using a Gaussian potential and by Engeland and Kallio (E64) using a hard-core, cutoff potential. With the phenomenological potential, however, De Llano *et al.* (L65) find much smaller overlaps with the SU_3 functions ($\sim$25%). This is a puzzling result in view of the other calculations.

Again because of the size of the problem few of the above calculations have been attempted. Rather, the emphasis has been put on calculating the admixtures into the states of the leading representation of SU_3 by either a restricted variational procedure or a perturbation approach.

In ^{24}Mg early calculations using only states of maximum orbital symmetry found about a 10% admixture of the states of the (46) representation into the states of the leading (84) representation (E63*b*). Very little change was found however in the energies and other gross properties of the states. These results have recently been verified in a larger calculation using

[5] For a discussion of the four-particle problem using a QQ plus pairing model, see Broglia and Maqueda, B66*g*.

all the states of maximum orbital symmetry (W67) and thus suggest that the central part of the nuclear force still tends to favor the SU_3 structure. In these calculations spin-orbit effects are identically zero, however, because of the assumption of maximum orbital symmetry. Bannerjee *et al.* (B63*b*) have considered an approximation treatment of a perturbation method suggested by Feingold to take into account spin-dependent effects through the admixture of states of less than maximum orbital symmetry. The results show quite large changes in the energy spectrum (in better agreement with experiment), although the resulting changes in the wave functions were not computed. These calculations seem to indicate the growing effect of the spin-dependent forces as particles are added into the $(2s, 1d)$ shell.

Recent calculations (B67) on ^{28}Si show similar but more dramatic features than those in ^{24}Mg. The admixture of states of maximum orbital symmetry into the states of the leading representations is quite small through the central force, but no agreement can be reached with experiment. Here again the spin-orbit force has been used to explain away the discrepancy (cf. D67 and Chapter 6).

At the beginning of the $(2s, 1d)$ shell the indications from the above mentioned calculations are that a large fraction of the shell model states arising from one active shell can be classified according to the leading representation of SU_3 having maximum orbital symmetry. This scheme appears to break down later in the $(2s, 1d)$ shell because of the growth of spin-dependent parts of the interaction. By a detailed comparison of the prediction of the scheme with experimental data one can discover which data can be explained by the model and in which areas the model breaks down. These aspects we discuss in Sections 5.3 through 5.6. By studying the deviations of the predictions of the model from experimental results one can discover the effects of those parts of the nuclear interaction not contributing to the effective spin-independent long range potential.

5.3 Positive-Parity States of Doubly Even Nuclei in the $(2s, 1d)$ Shell

Doubly even nuclei are particularly interesting to study. In the first place, the density of low-energy states is quite small so there should be fewer ambiguities in theoretical fits and a greater chance of observing gross features. On the theoretical side the Wigner supermultiplet classification shows that all states of maximum orbital symmetry have zero intrinsic spin (i.e., $S = 0$) (J51*a*, *b*); thus, if we restrict ourselves to this class of functions, spin-dependent forces have zero matrix elements, the total angular momentum J of a state will simply be given by the orbital angular momentum L, and L-projected and J-projected states of Section 3.7 are equivalent.

To compare the gross properties derived from the SU_3 scheme with experimental data, it is first necessary to decide on the ordering, with respect to energy, of states classified according to SU_3. The comparison can then be made by a one-to-one correspondence. The effective Hamiltonian for this purpose need only possess properties allowing the exact supermultiplet and SU_3 classification. It is useful to consider a potential of the form (B63*b*)

$$V = aM + \frac{b}{4}(Q \cdot Q) \tag{5.1}$$

Here $M = \sum_{i<j} P_{ij}$ is the Majorana operator, which orders states according to their orbital symmetry $[f]$. If the parameter a is negative, then states of maximum orbital symmetry will be lowest in energy, as is the case for any central potential.

If the orbital symmetry $[f]$ is represented by a tableau with four columns of length n_1, n_2, n_3, and n_4, then the expectation value of the Majorana operator can be written

$$\langle M \rangle_{[f]} = (n_2 + 2n_3 + 3n_4) - \tfrac{1}{2} \sum_{i=1}^{4} n_i(n_i - 1) \tag{5.2}$$

which can be interpreted as the number of symmetric pairs (in the rows) in the representation $[f]$ minus the number of antisymmetric pairs (in the columns) (S63, p. 469).

The quadrupole–quadrupole operator in Eq. (5.1) is that discussed in Section 4.3 where it was shown that

$$\frac{b}{4}(Q \cdot Q) = \frac{b}{4}\tilde{C}_2 - \frac{3}{4}bL^2 \tag{5.3}$$

Here $\tilde{C}_2$ is the Casimir operator of bilinear form of SU_3 with expectation values within a representation $\langle \tilde{C}_2 \rangle_{\lambda\mu}$ given by Eq. (4.15).

Such a potential in Eq. (5.1) reproduces the features of a two-body central (Yukawa) potential with a Serber exchange and strength $V_0 = 40$ MeV for (B63*b*)

$$a \approx -1.053 \text{ MeV} \qquad b \approx -0.211 \text{ MeV} \tag{5.4}$$

Note that the single-particle part of the potential in Eq. (5.1) leads to an *s-d* splitting of $4.5b \approx 1$ MeV, which is of the correct order of magnitude of that observed in ^{17}O.

Spectra for ^{18}O, ^{20}Ne, ^{22}Ne, ^{24}Mg, ^{26}Mg, and ^{28}Si derived from the potential in Eq. (5.1) with the parameters in Eq. (5.4) are given in Figs. 5.1

through 5.6. Since the potential used is charge-independent, these figures should also be considered for the mirror nuclei. In these figures has been

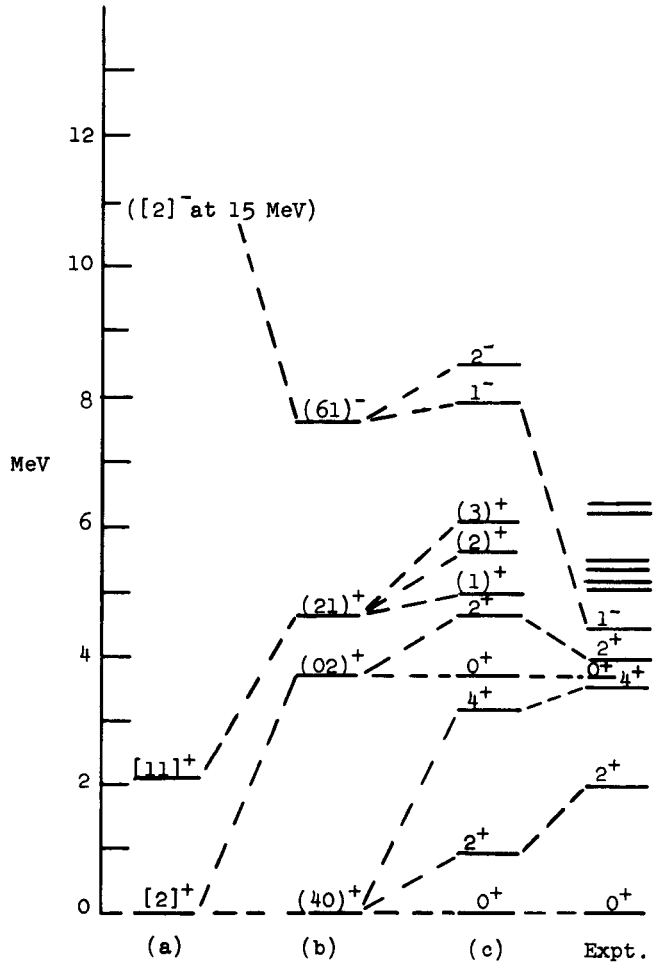

Fig. 5.1. Spectra for ^{18}O (or ^{18}Ne) (*a*) with a pure Majorana potential and highly degenerate levels labeled with the particle symmetry $[f]$; (*b*) with the addition of the SU_3 Casimir operator $\tilde{C}_2$ and degenerate levels labeled with the SU_3 symmetry $(\lambda\mu)$; and (*c*) the Majorana potential plus an attractive QQ potential. The labels in (*a*) and (*b*) are to be carried across to spectrum (*c*); thus the ground state in (*c*) has particle symmetry $[f] = [2]$, SU_3 symmetry $(\lambda\mu) = (40)$ and orbital angular momentum $L = 0$. The zero-order of energy of the negative-parity (single-excitation) states is at 15 MeV. (For general shell-model approach, see Ref. E55*a*. Experimental spectrum from Ref. H61*b*).

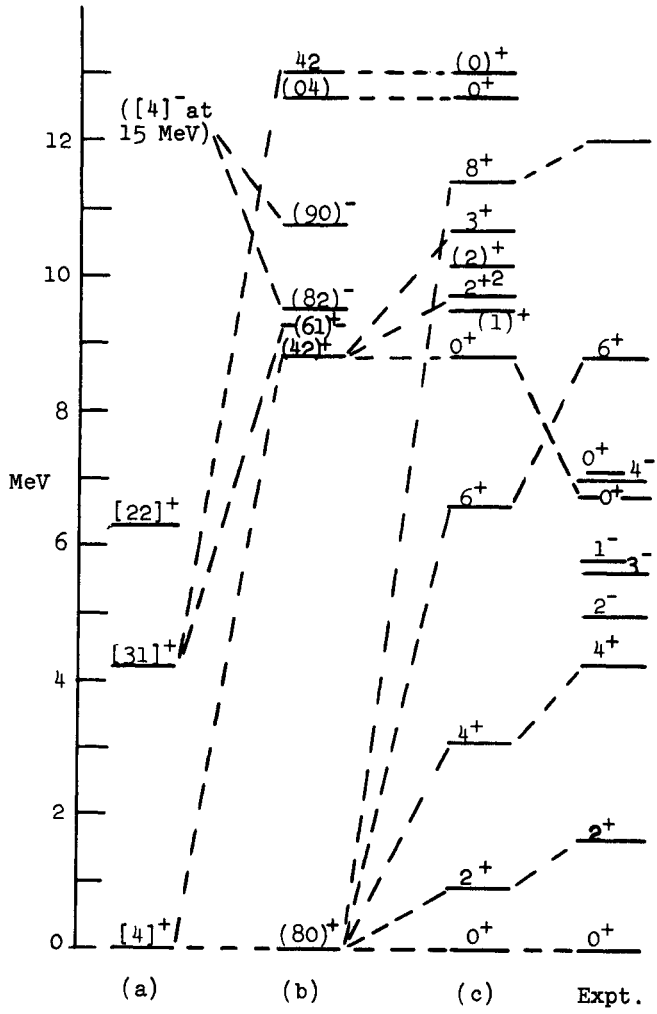

Fig. 5.2. Spectra for ^{20}Ne. See caption to Fig. 5.1 for the meaning of the spectra (a), (b), and (c). (Experimental spectrum from Ref. H61*b*. For later experimental work see Ref. A66*c*. For additional more general theoretical work see Refs. A66*a*, P64, E64).

shown how the orbital symmetry, Casimir operator of SU_3, and L^2 terms of the assumed potential go together to construct the final spectrum, shown in each figure as the spectrum *c*. Thus in each figure the Majorana operator splits the degeneracy of oscillator states according to orbital symmetry (spectrum *a*), the Casimir operator makes a further split according to SU_3

symmetry (spectrum *b*), and finally, the L^2 operator makes a split according to R_3 symmetry, or orbital angular momentum (spectrum *c*).

The spectra in Figs. 5.1 through 5.6 are intended only to establish a one-one correspondence with experiment and show how the various parts of the effective potential in Eq. (5.1) contribute to the energy splitting. These spectra *must not* be regarded as a verification or disproof of the SU_3

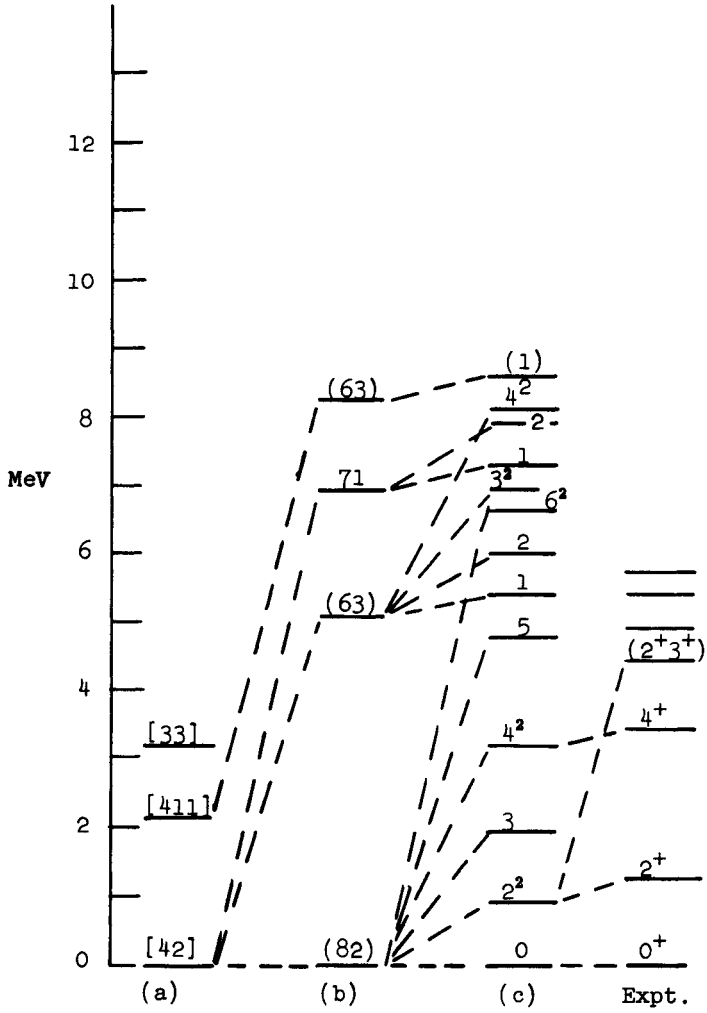

Fig. 5.3. Spectra for ^{22}Ne (or ^{22}Mg). See caption to Fig. 5.1 for the meaning of the spectra (*a*), (*b*), and (*c*). (Experimental spectrum from Ref. H61*b*.)

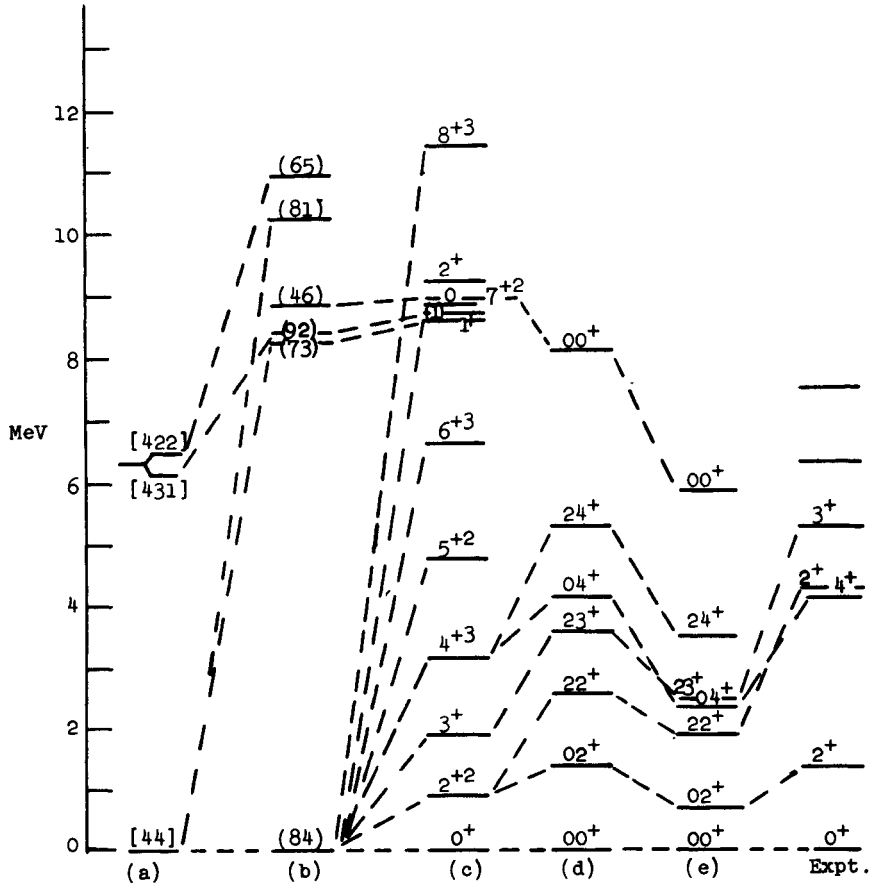

Fig. 5.4. Spectra for ^{24}Mg. See caption to Fig. 5.1 for the meaning of the spectra (*a*), (*b*), and (*c*). Spectra (*d*) and (*e*) are taken from Ref. E63*b* for a Gaussian two-body potential with Serber or Rosenfeld exchanges, respectively. The labels in (*d*) and (*e*) are KJ^{π}. (Experimental spectrum from Ref. H61*b*).

structure of real nuclear states. It is for this reason that no attempt has been made to determine the values of the parameters a and b in Eq. (5.1) that give the best fit. [It is often possible to generate spectra having similar features but with states having vastly different characteristics (C66*b*)]. It is gratifying, however, that the spectra derived under these very crude arguments are not too dissimilar from those observed, at least at the beginning of the shell. The model can explain such gross features as why only one $J = 2^+$ state is observed in the low-energy spectrum of ^{20}Ne but two are seen in ^{22}Ne, ^{24}Mg, and ^{26}Mg. In ^{24}Mg the model predicts three $J = 4^+$ states of low energy but

only two $J = 4^+$ states in ^{22}Ne and ^{26}Mg and only one in ^{20}Ne. These features are simply a consequence of the properties of the particular representation which is *leading* in the various nuclei [cf. Eq. (3-23)].

The observed $J(J+1)$ dependence of the low-energy spectrum also comes out of the model with the effective Hamiltonian of Eq. (5.1). Actually it is found (cf. Appendix G) that, for any central potential, the energy of

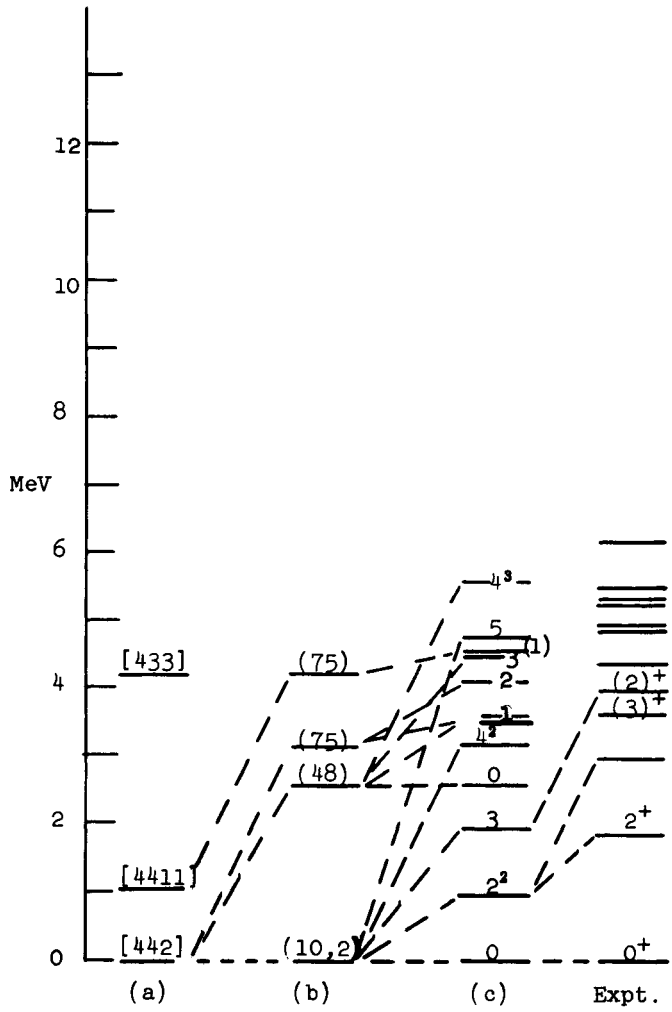

Fig. 5.5. Spectra for ^{26}Mg (or ^{26}Si). See caption to Fig. 5.1 for the meaning of the different spectra (*a*), (*b*), and (*c*). Experimental spectrum from Ref. H61*b*.

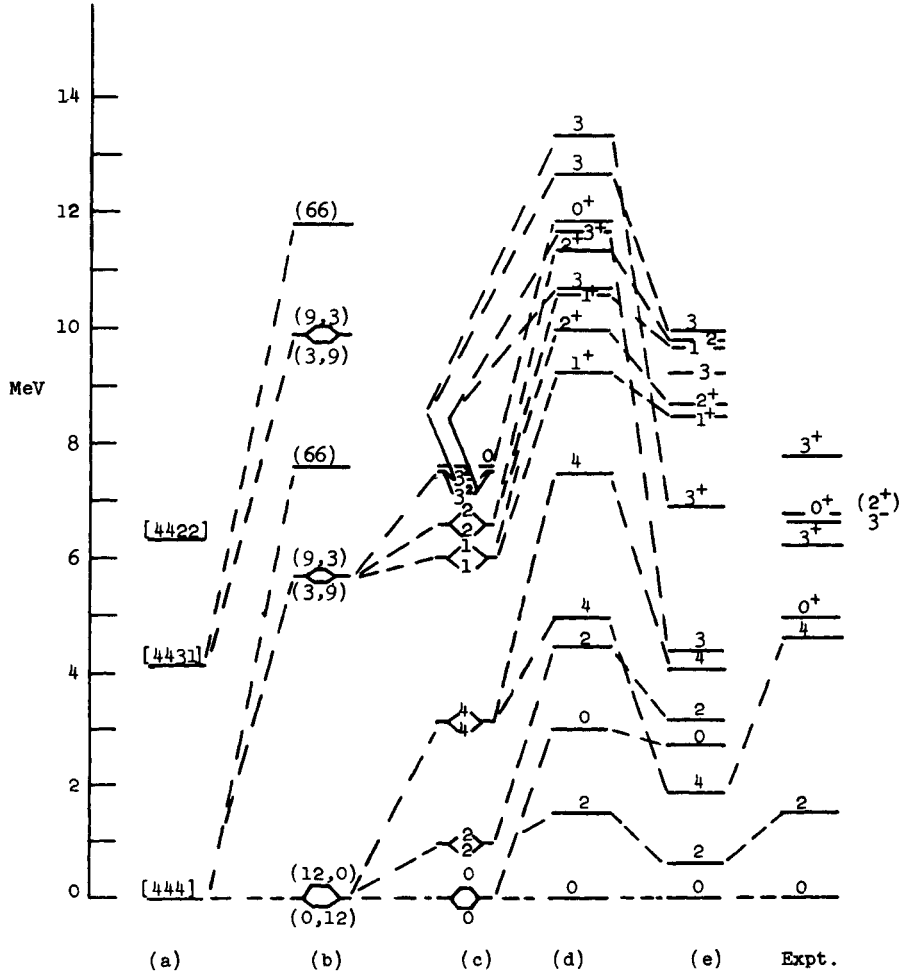

Fig. 5.6. Spectra for ^{28}Si. See caption to Fig. 5.1 for the meaning of the spectra (*a*), (*b*), and (*c*). Spectra (*d*) and (*e*) are taken from Ref. B67 for a Gaussian two-body potential with Serber or Rosenfeld exchanges, respectively. (Experimental spectrum from Ref. H61*b*; later experiments from Ref. A66*c*).

states within an SU_3 representation can always have this collective feature. For nuclei where it may be possible to construct more than one state of a given angular momentum in an SU_3 representation (cf. Table 3.I), a degeneracy still remains in the energy spectrum for the potential of Eq. (5.1), which is not seen experimentally. For a more conventional force this final degeneracy can be lifted. In Fig. 5.4, spectra (d) and (e), we show the results

of Elliott and Harvey (E63*b*) for the leading representation of ^{24}Mg using a potential with a Gaussian radial dependence and either a Serber or a Rosenfeld exchange. Here it is found that the final degeneracy is lifted so that states are defined with a definite $K = K_L$ projection of angular momentum on the intrinsic z axis (cf. Section 3.7). There seems to be no *a priori* reason in this analysis that the K quantum number should be as good as it is, although one might expect it to be so from the rotational model. The disturbing feature about these calculations is that the density of states is too large. As is discussed in Section 5.2 and Reference B63*b*, this failure appears to be caused by the neglect of states of lower orbital symmetry. It would be nice, however, to have further experimental data on ^{24}Mg to test the inadequacy of SU_3 here, since the only observed electromagnetic transition rates (see later) seem to be explained by the model.

For one nucleus in the $(2s, 1d)$ shell, i.e., ^{28}Si, there are many accidental degeneracies of *representations of* SU_3 with the simple potential in Eq. (5.1). What is disturbing about this is that even the ground state is predicted to be degenerate and it is not observed to be so! Here the admixture of states of maximum orbital symmetry using a more realistic potential has been found to be negligible and so leads to no improvement in the calculated spectrum (B67). As we shall briefly discuss in Part 6, the failure of the model may be corrected by taking into account the spin-orbit force, but this certainly destroys the SU_3 symmetry (D67).

From energy systematics alone it appears that states do not have pure SU_3 symmetry for nuclei near the center of the $(2s, 1d)$ shell. We shall return to this point in Part 6. Data on the latter half of the $(2s, 1d)$ shell are really too inadequate to show the growth or waning of SU_3 symmetry. The lack of symmetry between the properties of nuclei at the beginning and end of the shell indicates that SU_3 symmetry probably does not exist at the end of the shell.

To test the validity of the SU_3 model early in the $(2s, 1d)$ shell, where the gross features of the energy spectrum appear to be reproduced, one would like to consider the predictions and observations of all types of experimental data. Here, however, one is limited to the experimental data available. Since the SU_3 scheme has been specifically set up to exhibit collective features, the examination of $E2$ transition rates is of particular interest and there are fortunately enough of these known to discuss systematics.

Using the methods given in Appendix G, Svenne and Harvey (S64) have calculated $E2$ transition rates between states belonging to the leading representation of SU_3 (cf. Table 3.I) for ^{20}Ne, ^{24}Mg, and ^{28}Si, among others. In Table 5.II their results are reproduced with an effective charge of $\frac{1}{2}$ introduced to account for small polarization effects of the ^{16}O core. Comparisons are made in Table 5.II between the predictions of the SU_3 model and

those of a pure rotator. (In this latter case the reduced transition probability $B(E2)$ is simply proportional to the square of the Clebsch–Gordan coefficient $(J_i 2 K_i K_f - K_i \mid J_f K_f)$ where $\mid K_i J_i\rangle$ and $\mid K_f J_f\rangle$ are the initial and final states,

TABLE 5.IIa

$E2$ Transition Probabilities in ^{20}Ne with the Energy Levels Assumed to Have the Pure SU_3 Symmetry[a]

$(\lambda\mu)$	$K_i J_i^\pi$	$K_f J_f^\pi$	E_γ(expt)	$B(E2)_{SU_3}$	$\mid M \mid^2_{SU_3}$	$\mid M \mid^2_{\text{rot}}$	$\mid M \mid^2_{\text{expt}}$	Γ_{sp}
(80)	0 2+	0 0+	1.63	62.54	19.39	(19.39)	17.4 ± 1.7[b]	30.80
	0 4+	0 2+	2.62	79.19	24.56	27.7	15.1 ± 1.4[b]	32.59
	0 6+	0 4+	4.54	67.09	20.80	30.5	28 ± 7[b]	
	0 8+	0 6+	3.20	39.80	12.34	31.9		
(82)	2 3−	2 2−	0.66	131.00	40.62	37.47		0.33
	2 4−	2 3−	1.39	97.82	30.33	27.98	29[c]	13.80
	2 5−	2 4−		65.52	20.32	20.03		
	2 6−	2 5−		50.53	15.67	14.76		
	2 7−	2 6−		31.56	9.79	11.24		
	2 8−	2 7−		29.82	9.25	8.82		
	2 9−	2 8−		13.43	4.17	7.09		
	2 10−	2 9−		20.04	6.21	5.81		
	2 4−	2 2−	2.05	40.29	12.49	(12.49)	11.0 ± 3.5[b]	143.2
	2 5−	2 3−		58.69	18.20	20.03		
	2 6−	2 4−		66.56	20.64	24.65		
	2 7−	2 5−		61.25	18.99	27.67		
	2 8−	2 6−		58.24	18.06	29.76		
	2 9−	2 7−		38.68	11.99	31.26		
	2 10−	2 8−		33.36	10.34	32.39		
	0 2−	0 0−		74.16	22.99	(23.00)		
	0 4−	0 2−		96.92	30.05	32.86		
	0 6−	0 4−		89.06	27.62	36.19		
	0 8−	0 6−		67.13	20.81	37.88		
	0 0−	2 2−		22.58	7.00			
	0 2−	2 2−		5.91	1.83			
	0 2−	2 3−		9.30	2.88			
	0 2−	2 4−		8.27	2.57			

[a] The ground-state $K = 0$ band is assumed to belong to $(\lambda\mu) = (80)$, and the lowest observed negative-parity $K = 2^-$ band, to the $(\lambda\mu) = (82)$ symmetry. (The observed odd $K = 0^-$ band has not been considered here). Columns 2 and 3 label the initial and final states differing from the observed energies as given in column 4. Columns 5 and 6 are the calculated $B(E2)$ and $\mid M \mid^2$ (Weisskopf unit, Ref. W60) with an effective charge of $\frac{1}{2}$; the single-particle Weisskopf unit Γ_{sp} is given in column 9. The calculated $\mid M \mid^2$ given by the rotational model is in column 7 normalized in a band to the numbers in brackets. Experimental numbers are given in column 8.

[b] Skorka (S65*b*).

[c] Alexander *et al.* (A66*c*).

TABLE 5.IIb

$E2$ Transition Probabilities in ^{24}Mg with the Lowest Positive-Parity Energy Levels Assumed to Have the $(\lambda\mu) = (84)$, SU_3 Symmetry[a]

$(\lambda\mu)$	$K_iJ_i^\pi$	$K_fJ_f^\pi$	E_γ(expt)	$B(E2)_{SU_3}$	$\lvert M\rvert^2_{SU_3}$	$\lvert M\rvert^2_{\text{rot}}$	$\lvert M\rvert^2_{\text{expt}}$	Γ_{sp}
(84)	0 2+	0 0+	1.37	104.81	25.49	(25.49)	~25[b]	0.163
	0 4+	0 2+	2.75	140.84	34.25	36.41	41[b]	
	0 6+	0 4+		138.09	33.58	40.11		
	0 8+	0 6+		120.35	29.26	41.98		
	2 3+	2 2+	0.98	182.48	44.37	43.41		0.031
	2 4+	2 3+		138.17	33.60	32.41		
	2 5+	2 4+		86.28	20.98	23.20		
	2 6+	2 5+		72.68	17.67	17.10		
	2 7+	2 6+		36.25	8.82	13.02		
	2 8+	2 7+		45.77	11.13	10.21		
	2 9+	2 8+		11.24	2.73	8.21		
	2 10+	2 9+		35.73	8.69	6.74		
	2 4+	2 2+	1.77	59.53	14.47	(14.47)	6.7[c]	
	2 5+	2 3+		87.36	21.24	23.20		
	2 6+	2 4+		106.51	25.90	28.56		
	2 7+	2 5+		99.12	24.10	32.06		
	2 8+	2 6+		110.82	26.95	34.47		
	2 9+	2 7+		79.51	19.33	36.22		
	2 10+	2 8+		96.73	23.52	37.53		
	4 5+	4 4+		163.09	39.66	33.35		
	4 6+	4 5+		170.16	41.38	35.83		
	4 7+	4 6+		146.20	35.55	32.02		
	4 8+	4 7+		118.90	28.91	27.40		
	4 9+	4 8+		93.52	22.74	23.24		
	4 10+	4 9+		72.73	17.69	19.76		
	4 11+	4 10+		50.93	12.38	16.91		
	4 12+	4 11+		37.66	9.16	14.59		
	4 6+	4 4+		26.37	6.41	(6.41)		
	4 7+	4 5+		45.50	11.07	12.32		
	4 8+	4 6+		54.50	13.25	16.95		
	4 9+	4 7+		54.71	13.30	20.50		
	4 10+	4 8+		48.43	11.78	23.24		
	2 11+	2 9+		35.88	8.72	25.37		
	2 12+	2 10+		22.21	5.40	27.06		
	2 2+	0 0+	4.24	15.70	3.82		14[b], 10.9[c]	46.480
	2 2+	0 2+	2.87	20.66	5.02		>1.4[b], 2.1[c]	6.638
	2 4+	0 2+	4.63	15.44	3.76		0.38[c]	
	2 4+	0 4+		15.22	3.70			
	2 6+	0 4+		29.04	7.06			
	2 6+	0 6+		3.73	0.91			
	4 4+	2 2+		14.52	3.53			
	4 4+	2 4+		3.75	0.91			
	0 6+	2 4+		15.14	3.68			
	0 6+	2 5+		23.88	5.81			
	2 6+	0 4+		29.04	7.06			

[a] See footnotes to Table 5.IIa for the labeling of the columns and experimental references.

TABLE 5.IIc

$E2$ Transition Probabilities in ^{28}Si Assuming the Lowest States Belong to Either the Pure $(\lambda\mu) = (12, 0)$ or $(0, 12)$ Representations of SU_3 [a]

$(\lambda\mu)$	$K_iJ_i^\pi$	$K_fJ_f^\pi$	E_γ	$B(E2)_{SU_3}$	$\lvert M\rvert^2_{SU_3}$	$\lvert M\rvert^2_{\text{rot}}$	$\lvert M\rvert^2_{\text{expt}}$	Γ_{sp}
(12, 0)	0 2+	0 0+	1.78	161.36	31.95	(31.95)	~12[b]	0.744
or	0 4+	0 2+	2.84	217.71	43.10	45.64	~20[b], 6.7[c]	
(0, 12)	0 6+	0 4+		214.40	42.45	50.27		
	0 8+	0 6+		186.04	36.83	52.62		
	0 10+	0 8+		139.53	27.62	54.05		
	0 12+	0 10+		77.17	15.28	55.01		

[a] See captions to Table 5.IIa for the labeling of the columns and experimental references.

respectively, belonging to bands K_i and K_f). It will be noticed that the transitions between the low angular momentum states in a band exhibit the same features in both the SU_3 and rotator models. For large angular momentum states the transitions decrease for the SU_3 model (eventually going to zero at the band cutoff), while those in the pure rotator model increase indefinitely.

In the SU_3 scheme the reduced $E2$ transition between the lowest $J = 2^+$ state and the ground state increases for nuclei nearer the center of the $(2s, 1d)$ shell at ^{28}Si; observations show a maximum for the transitions near ^{24}Mg. The calculated $B(E2;\ 2 \rightarrow 0)$ in ^{20}Ne and ^{24}Mg are in fair agreement with experiment (with an effective charge of $\frac{1}{2}$), but that in ^{28}Si is more than a factor of 2 too large. This last piece of information is additional evidence for the apparent failure of the SU_3 scheme for ^{28}Si. Further evidence can be found in References B67 and D67.

The nucleus for which there is a considerable amount of experimental data on $E2$ transitions is ^{20}Ne(L61, K63, E65*c*, A66). Here all the states of the ground-state $K = 0$ "band" have been identified (L61, K64, K66*a*) up to the band cutoff for the leading SU_3, (80) representation at $J = 8^+$. Recent experiments (A66) have given *estimates* for all the $B(E2)$ transitions in the ground-state band from $J = 6^+$ down. The preliminary analysis of this data is not too encouraging from the point of view of SU_3 classification, but the erros in the data are perhaps too large for much weight to pe placed on them just yet (see K67). The evidence at the moment (cf. Table 5.II) shows the SU_3 scheme capable of explaining the enhancement of the $B(E2; 2^+ \rightarrow 0^+)$, but the observed result that $B(E2; 2^+ \rightarrow 0^+) > B(E2; 4^+ \rightarrow 2^+)$ is in contradiction to either the SU_3 or rotation models. The observed $B(E2;\ 6^+ \rightarrow 4^+)$ (with *large* errors!) is much greater than could be predicted in *any* model assuming a closed ^{16}O core. If this last transition is verified, it seem to imply large deformations of the ^{16}O core, at least for high angular

momentum states, and the disappearance of spherical shell effects. In consequence of the latter result the $K = 0$ band should not be cut off and the ^{20}Ne nucleus should become more like a classical rotator.

An important property of the SU_3 model is that, for $T = 0$ states with the same number of quanta, $E2$ transitions can only exist between states belonging to the same representation of SU_3 (cf. Appendix G). Thus in ^{20}Ne, if the $J = 2^+$ (1.63 MeV) level does belong to the (80) representation of SU_3, the only $E2$ transition to it must be from other states of the (80) representation of from $T = 1$ states or from states having a different number of oscillator quanta (i.e., more than one active shell). With these points in mind the observed $B(E2)$ transition of the $J = 0^+$ (6.72 MeV, $T = 0$) state to the $J = 2^+$ (1.63 MeV, $T = 0$) of 3.7 Weisskopf unit is of particular interest (S65*b*). This implies either nonpurity of representations of SU_3 or admixtures of states with more than one active shell. This datum has yet to be explained.

The above selection rule of the model does not exist in general for $T \neq 0$ states. In ^{18}O, however, it is true for the single active shell model because both particles in the $(2s, 1d)$ shell are the same (i.e., neutrons). Here the observed $B(E2)$ for the decay of the $J = 0^+$ (3.63 MeV, $T = 1$) state to the $J = 2^+$ (1.98 MeV, $T = 1$) of $\sim$8 Weisskopf unit is of interest (S65*b*). Actually this enhancement cannot come from *any* admixture of states with one active shell; thus it is not simply the breakdown of the SU_3 scheme but, rather, the invalidity of the single active shell (zero excitation) assumption. This datum can actually be explained by the admixture of double excitation states with the zero excitation states (cf. Section 5.6). Whether such admixtures are necessary to explain the decay of other excited $J = 0^+$ states in other nuclei (e.g., ^{20}Ne) remains to be seen. A study of this point (with more experimental information) would be of interest in assessing the validity of the closed shell assumption of the ^{16}O core as particles are added into the $(2s, 1d)$ shell.

Apart from $E2$ transitions, few other data on doubly even nuclei are available or have been examined in detail to check the validity of the SU_3 scheme. Spectroscopic factors are now beginning to be collected, but the errors in these figures are usually too great for a comparison to point out anything but gross features. Thus the calculated spectroscopic factors for ^{20}Ne from the SU_3 model agree qualitatively with those extracted from experiment (cf. Table 5.III), but so do the factors from the Nilsson model in which a spin-orbit force has been included. With more data on other nuclei and better accuracy in the extraction of spectroscopic factors from experiment, these spectroscopic factors should prove useful in determining the relative structure of nuclear states. (For a discussion of direct reactions using the SU_3 scheme, see References G64 and R66*b*).

TABLE 5.III

Single-Particle (Proton) Spectroscopic Factors for ^{20}Ne Levels; Experimental Values in Column 4; Predictions from the Nilsson Model in Column 5 [Taken from Siemssen *et al.* (S65*a*)]; Predictions from the Pure SU_3 Model in Column 6[a]

Excitation energy (MeV)	J	L	S_{expt}	Nilsson model	SU_3 model
					$K = 0^+$
					$(\lambda, \mu) = (8,0)$
0.000	0^+	0	0.31	0.41	0.43
1.632	2^+	2	0.63	0.32	0.24
4.248	4^+	4	$\leqslant 0.21$	0.0	0.0
					$K = 2^-$
					$(\lambda, \mu) = (8,2)$
4.969	2^-	1	$\leqslant 0.001$	0.0	0.0
		3	$\leqslant 0.06$	0.0	0.0
5.631	3^-	3	$\leqslant 0.042$	0.0	0.0
7.02	4^-	3	$\leqslant 0.026$	0.0	0.0
					$K = 0^-$
					$(\lambda, \mu) = (9,0)$
5.80	1^-	1	0.051	0.08	0.031
7.17	3^-	3	$\leqslant 0.092$	0.11	0.014
					$K = 0^+$
					$(\lambda, \mu) = (4,2)$
6.72	0^+	0	0.47	0.22	0.17
7.43	2^+	2	0.16	0.15	0.007
					$K = 0^+$
					$(\lambda, \mu) = (0,4)$
					(2,0)
7.20	0^+	0	$\leqslant 0.027$	0.0	0.0

[a] The $J = \frac{1}{2}^+$ ground state of ^{19}F is assumed to be the zero excitation state belonging to the $(\lambda\mu) = (60)$ (see Ref. H64*b*) and the states in ^{20}Ne have the symmetry given in column 6.

We note the recent calculation (T66) on the positive-parity states of ^{20}O. This nucleus is of interest because of the large value of its isotopic spin ($T = 2$)—the other nuclei discussed in this section had $T = 0$. Here it is shown that, even allowing for a limited amount of configuration mixing with the conventional Gaussian potential and single-particle spin-orbit force, the SU_3 classification remains meaningful. The gross features of the

spectrum (five levels) and spectroscopic factors [^{18}O (t, p) ^{20}O] can be understood. Predictions are made for $E2$ transitions probabilities but lack of experimental data prevents any comparison. It would be of interest to consider other large T nuclei, to examine in general their collective properties and in particular the possibility of a description within the SU_3 scheme. This latter problem is of particular significance in nuclei with $A > 40$.

5.4 Positive-Parity States in Odd A and Doubly Odd Nuclei in the $(2s, 1d)$ Shell

States of maximum orbital symmetry of odd A and doubly odd nuclei need not have zero total intrinsic spin (i.e., $S \neq 0$). Here then, unlike the conditions for doubly even nuclei, the spin-orbit force cannot be ignored even in the first approximation and there is some ambiguity as to what are to be called the SU_3 states. If the *effective* spin-orbit force can be neglected, the suggested structure for the nuclear states is the L-projected LS-coupled states of Eq. (3.41). For a slightly larger spin-orbit force preserving collective features, the suggested states are the J-projected states of Eq. (3.43). For very large spin-orbit effects of course the supermultiplet scheme breaks down and the states are better described in a jj-coupled model.

A recent attempt has been made by Wilsdon (W65) to understand how far into the $(2s, 1d)$ shell the spin-orbit effects can be treated as small and hence the SU_3 classification preserved. Wilsdon assumed either L-projected states of the leading representations of SU_3 and calculated approximate spectra and such properties as spectroscopic factors, quadrupole and magnetic moments, and electromagnetic transition probabilities.

As in the case of doubly even nuclei the assignment of SU_3 labels to the low-lying states is made according to the effective potential in Eq. (5.1). Because of the nonzero value of the total spin S however, there are many states of the same total angular momentum J in the leading representation of SU_3. These can be distinguished either by their orbital angular momentum L in the L-projected scheme or by the K label in the J-projected scheme. The possible S, K_L, and K labels in the J-projected scheme for the considered are given in Table 5.IV: the (overly complete) J values are given by

$$J = |K|, \ |K| + 1 \cdots |K| + \lambda \tag{5.5a}$$

except for $K = K_s = K_L = 0$ when

$$\begin{aligned} J &= 0, 2, 4, \ldots, \lambda \quad \text{or} \quad \lambda - 1 \qquad \text{if } \lambda + S \text{ is even} \\ &= 1, 3, 5, \ldots, \lambda \quad \text{or} \quad \lambda - 1 \qquad \text{if } \lambda + S \text{ is odd} \end{aligned} \tag{5.5b}$$

Before any comparison can be made with experiment, some idea must be

TABLE 5.IV

Proposed Classification for the Lowest-Lying Positive-Parity States (Zero Excitation) of Some Odd A Nuclei in the $(2s, 1d)$ Shell[a]
[after Wilsdon, (W65)]

Nucleus	$[f]$	$(\lambda\mu)$	T	S	K_L	K
^{17}O (^{39}K)	[1]	(20)	$\frac{1}{2}$	$\frac{1}{2}$	0	$\frac{1}{2}$
^{19}O (^{37}Cl)	[21]	(41)	$\frac{3}{2}$	$\frac{1}{2}$	1	$\frac{1}{2}, \frac{3}{2}$
^{19}F	[3]	(60)	$\frac{1}{2}$	$\frac{1}{2}$	0	$\frac{1}{2}$
^{20}F	[31]	(61)	1	1	1	0, 1, 2
				0	1	1
^{21}Ne (^{35}Cl)	[41]	(81)	$\frac{1}{2}$	$\frac{1}{2}$	1	$\frac{1}{2}, \frac{3}{2}$
^{21}F (^{35}S)	[32]	(62)	$\frac{3}{2}$	$\frac{1}{2}$	0	$\frac{1}{2}$
					2	$\frac{3}{2}, \frac{5}{2}$
^{22}Na	[42]	(82)	0	1	0	0, 1
					2	1, 2, 3
			1	0	0	0
					2	2
^{23}Na (^{33}S)	[43]	(83)	$\frac{1}{2}$	$\frac{1}{2}$	1	$\frac{1}{2}, \frac{3}{2}$
					3	$\frac{5}{2}, \frac{7}{2}$
^{24}Na	[431]	(92)	1	0	0	0
					2	2
			1	1	0	0, 1
					2	1, 2, 3
		(65)	1	0	1	1
					3	3
					5	5
			1	1	1	0, 1, 2
					3	2, 3, 4
					5	4, 5, 6
^{25}Mg (^{31}P)	[441]	(93)	$\frac{1}{2}$	$\frac{1}{2}$	1	$\frac{1}{2}, \frac{3}{2}$
					3	$\frac{5}{2}, \frac{7}{2}$
		(66)	$\frac{1}{2}$	$\frac{1}{2}$	0	$\frac{1}{2}$
					2	$\frac{3}{2}, \frac{5}{2}$
					4	$\frac{7}{2}, \frac{9}{2}$
					6	$\frac{11}{2}, \frac{13}{2}$
^{27}Al (^{29}Si)	[443]	(11,1)	$\frac{1}{2}$	$\frac{1}{2}$	1	$\frac{1}{2}, \frac{3}{2}$
		(2,10)	$\frac{1}{2}$	$\frac{1}{2}$	0	$\frac{1}{2}$
					2	$\frac{3}{2}, \frac{5}{2}$
		(8,4)	$\frac{1}{2}$	$\frac{1}{2}$	0	$\frac{1}{2}$
					2	$\frac{3}{2}, \frac{5}{2}$
					4	$\frac{7}{2}, \frac{9}{2}$
		(5,7)	$\frac{1}{2}$	$\frac{1}{2}$	1	$\frac{1}{2}, \frac{3}{2}$
					3	$\frac{5}{2}, \frac{7}{2}$
					5	$\frac{9}{2}, \frac{11}{2}$

[a] Column 2 gives the orbital particle symmetry, column 3 the SU_3 symmetry, column 4 the isotopic spin, and column 5 the total particle spin which are taken directly from the work of Jahn (J51*a*,*b*), the orbital particle symmetry being known; column 6 gives the number K_L for the (approximate) projection of the orbital angular momentum L on the intrinsic z axis; the classification is for the particle states for the unbracketed nuclei in column 1, and for the hole states for the bracketed nuclei.

sought as to the best construction for the states in the SU_3 scheme. Thus one must somehow judge the balance of the strength of the central and spin-orbit forces. This Wilsdon did using the approximate form as given in Eq. (G.22) for the contribution of the central force to the energy spectrum within a representation in the L-projected scheme. The parameter a_3 was either calculated using the methods in Appendix G and a realistic (Yukawa) potential or assumed to have the value $a_3 \approx 0.1$ MeV; the latter value is of the order of magnitude for the realistic calculation. The parameter ξ of the single-particle spin-orbit force $\xi \sum_i s_i l_i$ was chosen to be $\xi = -2$ MeV to give the $d_{3/2} - d_{5/2}$ splitting in ^{17}O. For greater information on the methods involved in this calculation we suggest to the reader Reference W65.

The results of Wilsdon's energy calculation cannot be expected to give good agreement with experiment. In the first place, the value for the parameter a_3 for the conventional force is known to lead to too dense a spectrum in doubly even nuclei. It would thus be surprising if the value were correct for the neighboring odd A and doubly odd nuclei. The second inaccuracy is in the choice of the spin-orbit parameter ξ. This choice really only describes the effective spin-orbit interaction of the active shell particles with the ^{16}O core. One should still add spin-orbit effects from the spin-dependent interaction *between* the active shell particles. As a first guess one might try to do this by choosing an effective value for the parameter ξ.

Wilsdon's calculations as they stand show that often the favored coupling scheme within an SU_3 representation is the J-projected one. The results provide a prescription for labeling the lowest observed states. In Fig. 5.7 we show the *observed* energy spectra for some of the nuclei considered in the $(2s, 1d)$ shell and the assigned labels. All that really can be said about this labeling from the spectrum point of view is that the angular momenta for the low-lying states from the calculations are consistent with those observed. Where two representations of SU_3 are low in energy (i.e., near the center of the shell) and agreement with other data cannot be reached, Wilsdon has suggested the possible predominant representation mixing shown in Fig. 5.7. We note that in these cases the suggested admixtures involve states of the same (maximum) orbital symmetry. From the work on doubly even nuclei however (e.g., ^{24}Mg and more recently ^{28}Si) one suspects that admixtures of states of different orbital symmetries are of equal importance.

The calculated tables of magnetic moments, quadruple moments, $M1$ transitions, and $E2$ transitions are reproduced here in Tables 5.V through 5.VIII.

In Table 5.V the magnetic moments calculated in both the L-projected schemes are shown. It is seen that the experimental data available here are really insufficient for selecting the best structure. The magnetic moments

of two nuclei in the list are given poorly by the model in both the L-projected and J-projected schemes. In ^{20}F Wilsdon notes, however, that only a *small* admixture of the $S = 0$, $K = 1$ band of states, from the (61) representation, into the $S = 1$, $K = 2$ band will result in a drastic change of magnetic moment. Thus SU_3 symmetry can be preserved, but the labeling with respect

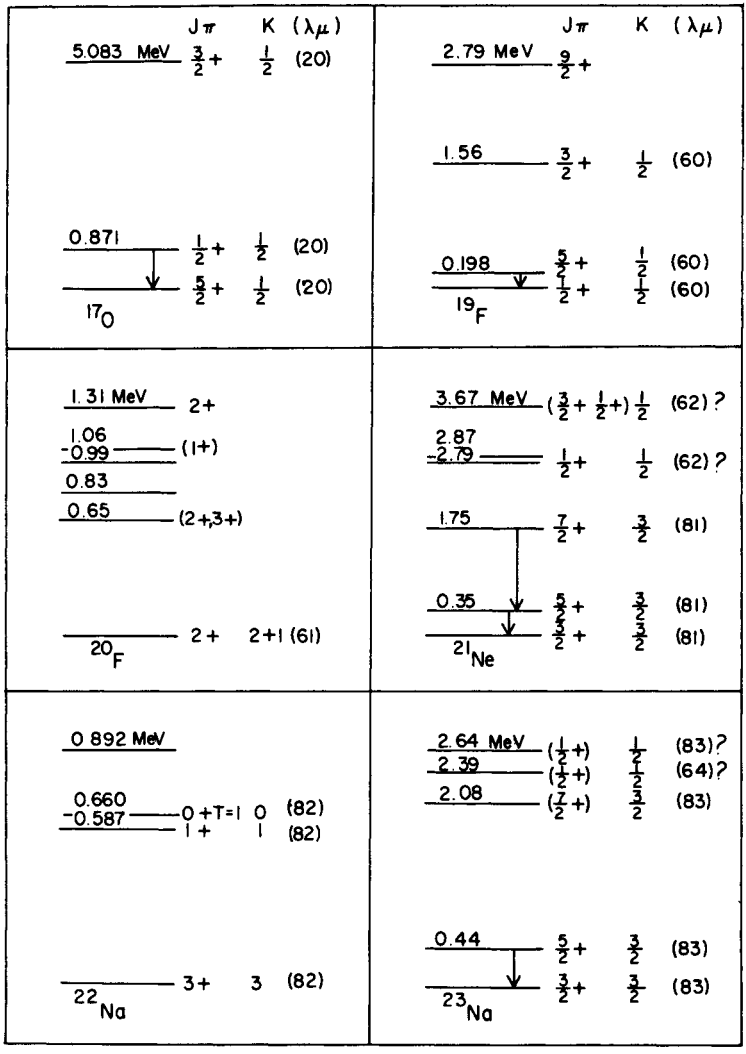

Fig. 5.7. Experimental spectra for some odd A nuclei in the ($2s$, $1d$) shell. The labeling is that given by Wilsdon (W65) based on calculations of energy, moments, and electromagnetic transitions. Values for the transitions indicated are given in Tables 5.VII and 5.VIII. [Taken from Wilsdon (W65).]

to S is destroyed. For ^{21}Ne no such simple explanation has been offered for the discrepancy which is presumably caused by representation mixing. The calculated magnetic moments for nuclei at the end of the $(2s, 1d)$ shell differ too much from experiment for any faith to be placed in the proposed structure.

The calculated quadrupole moments in Table 5.VI are in reasonable qualitative agreement with experiment at the beginning of the $(2s, 1d)$ shell

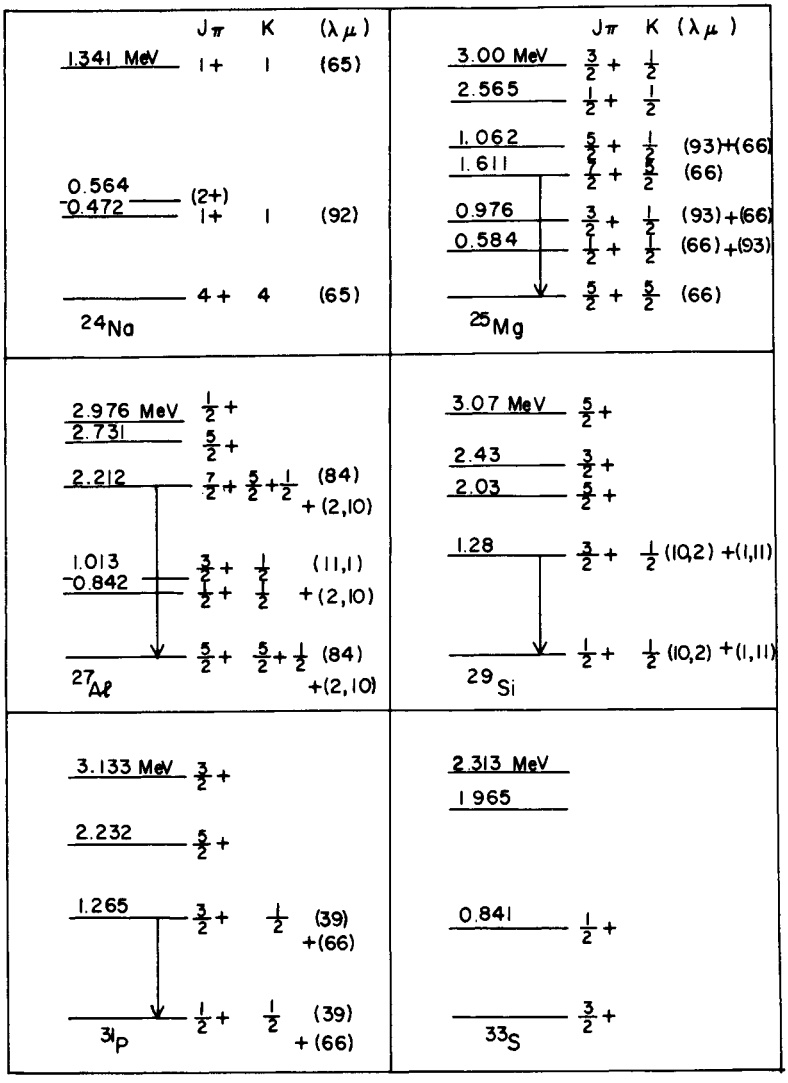

Fig. 5.7. B

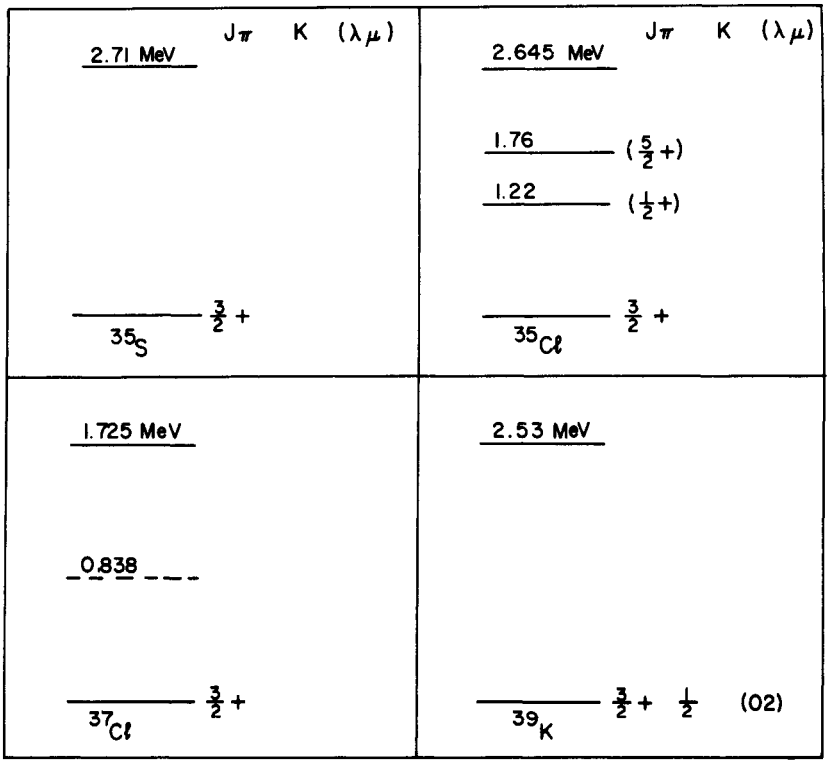

Fig. 5.7. C

and verify the K labeling of the states, as suggested from the energy calculations. We note that the agreement with experiment deteriorates for nuclei near the center of the shell and for those nuclei in the second half of the shell.

Some $M1$ and $E2$ transitions in the odd A and doubly odd nuclei are given in Tables 5.VII and 5.VIII. Here again the failure of the model toward the middle and at the end of the $(2s, 1d)$ shell is apparent.

5.5 Negative-Parity States in the (2s, 1d) Shell

The lowest negative-parity states in the $(2s, 1d)$ shell are assumed to be single-excitation states with either a particle excited from the $1p$-shell into $(2s, 1d)$ shell or a particle excited from the $(2s, 1d)$ shell into the $(2p, 1f)$ shell. The observation of collective properties of these single-excitation states has prompted discussions of these within the framework of the SU_3 model. As we have already noted, however, one is not led unambiguously to the SU_3 scheme by arguments on the effective force alone.

TABLE 5.V

Magnetic Moments for Nuclei in the $(2s,1d)$ Shell in the J-Projected and L-Projected SU_3 Schemes and the jj-Coupled Model[a]
[from Wilsdon (W65, Table XIV)]

			J-projected			$L-S$ coupled			$j-j$	Expt	Ref
	J	$(\lambda\mu)$	K	μ_0 n.m.	$\Delta\mu_0$ n.m.	K_L	L	μ_0 n.m.	μ_0 n.m.	μ_0 n.m.	
^{17}O	$\frac{5}{2}$	(20)	$\frac{1}{2}$	−1.91	0	0	2	−1.91	−1.91	−1.89	
^{19}F	$\frac{1}{2}$	(60)	$\frac{1}{2}$	2.79	0	0	0	2.79	2.74	2.63	b
	$\frac{5}{2}$		$\frac{1}{2}$	3.46	0	0	2	3.46	3.51	3.5	
^{20}F	2	(61)	2	0.8	0.06	1	1	1.01		2.09	c
^{21}Ne	$\frac{3}{2}$	(81)	$\frac{3}{2}$	−1.02	−0.14	1	1	−1.71	3.71	−0.66	b
^{22}Na	3	(82)	3	1.78						1.75	b
^{23}Na	$\frac{3}{2}$	(83)	$\frac{3}{2}$	2.32	0.16	1	1	3.18	−1.99	2.22	b
^{24}Na	4	(65)	4	1.59						1.69	b
^{25}Mg	$\frac{5}{2}$	(66)	$\frac{5}{2}$	−0.64	−0.15	0	2	−0.73	−0.63	−0.85	b
			$\frac{1}{2}$	−0.73		0	2	−0.73			
		(93)	$\frac{1}{2}$	1.50		1	2	−0.87			
^{27}Al	$\frac{5}{2}$	(84)	$\frac{5}{2}$	3.22	0.15	0	2	3.79	4.79	3.64	b
		(2,10)	$\frac{1}{2}$	3.68		0	2	3.68			
		(84)	$\frac{1}{2}$	3.79		0	2	3.79			
		(11,1)	$\frac{1}{2}$	0.88		1	2	3.97			
		(57)	$\frac{1}{2}$	0.79		1	2	3.80			
^{29}Si	$\frac{1}{2}$	(10,2)	$\frac{1}{2}$	−1.91	0	0	0	−1.91	−1.91	−0.55	d
		(1,11)	$\frac{1}{2}$	0.82	0	1	1	0.82			
		(48)	$\frac{1}{2}$	−1.91	0	0	0	−1.91			
		(75)	$\frac{1}{2}$	0.96	0	1	1	0.96			
^{31}P	$\frac{1}{2}$	(66)	$\frac{1}{2}$	2.79	0	0	0	2.79	2.79	1.13	b
		(39)	$\frac{1}{2}$	−0.63	0	1	1	−0.63			
^{33}S	$\frac{3}{2}$	(38)	$\frac{1}{2}$	1.09	−0.15	1	1	−1.30	1.15	0.64	b
^{35}S	$\frac{3}{2}$	(26)	$\frac{1}{2}$	2.41		0	2	2.41	1.15	±1.0	b
			$\frac{3}{2}$	2.79							
^{35}Cl	$\frac{3}{2}$	(18)	$\frac{1}{2}$	0.54	0.18	1	1	3.59	0.26	0.82	b
^{37}Cl	$\frac{3}{2}$	(14)	$\frac{1}{2}$	1.35	0.31	1	1	3.79	0.12	0.68	b
^{39}K	$\frac{3}{2}$	(02)	$\frac{1}{2}$	0.12	0	0	2	0.12	0.12	0.39	b

[a] Experimental values are given in column 11. In each case μ_0 gives the nuclear magnetic moment. (In the SU_3 scheme this number is calculated assuming orthogonality of states with respect to the K_L and K quantum numbers; the correction taking the nonorthogonality into account is given by $\Delta\mu_0$.)

Experimental references:

[b] Endt *et al.*, *Nucl. Phys.* **34**:1 (1962).

[c] Tsang *et al.*, *Phys. Rev.* **132**:1141 (1963).

[d] Nuclear data sheets.

TABLE 5.VI

Quadrupole Moments for Nuclei in the $(2s,1d)$ Shell[a]
[from Wilsdon (W65, Table XV)]

	$(\lambda\mu)$	K	J	Q (bns) SU_3	Q (bns) Expt	Ref.
^{17}O	(20)	$\frac{1}{2}$	$\frac{5}{2}$	−0.032	−0.027	[b]
^{19}F	(60)	$\frac{1}{2}$	$\frac{5}{2}$	−0.12	±0.11	[c]
^{21}Ne	(81)	$\frac{3}{2}$	$\frac{3}{2}$	0.13	0.09	[d]
^{23}Na	(83)	$\frac{3}{2}$	$\frac{3}{2}$	0.14	0.10	[d]
^{25}Mg	(66)	$\frac{5}{2}$	$\frac{5}{2}$	0.26	0.22	[e]
		$\frac{1}{2}$	$\frac{5}{2}$	−0.21		
^{27}Al	(84)	$\frac{5}{2}$	$\frac{5}{2}$	0.27	0.14	[d]
		$\frac{1}{2}$	$\frac{5}{2}$	−0.21		
	(2,10)	$\frac{1}{2}$	$\frac{5}{2}$	0.22		
^{33}S	(38)	$\frac{1}{2}$	$\frac{3}{2}$	0.15	−0.064	[d]
		$\frac{3}{2}$	$\frac{3}{2}$	−0.15		
^{35}S	(26)	$\frac{1}{2}$	$\frac{3}{2}$	0.15	0.045	[d]
		$\frac{3}{2}$	$\frac{3}{2}$	−0.15		
^{35}Cl	(18)	$\frac{1}{2}$	$\frac{3}{2}$	0.13	−0.079	[d]
		$\frac{3}{2}$	$\frac{3}{2}$	−0.13		
^{37}Cl	(14)	$\frac{1}{2}$	$\frac{3}{2}$	0.12	−0.062	[d]
		$\frac{3}{2}$	$\frac{3}{2}$	−0.12		
^{39}K	(02)	$\frac{1}{2}$	$\frac{3}{2}$	0.10	0.07	[d]
					0.11	

[a] Calculated in the J-projected SU_3 scheme in column 5; experimental values are given in column 6.

Experimental references:

[b] Barker, *Nucl. Phys.* **59**:513 (1964).

[c] Sugimoto *et al.*, *Phys. Rev.* **B134**:539 (1964).

[d] Endt *et al.*, *Nucl. Phys.* **34**:1 (1962).

[e] Nuclear data sheets.

In Table 5.IX we show the table by Elliott and Harvey (E63*b*) of leading representation for the single-excitation states of doubly even nuclei throughout the $(2s, 1d)$ shell. For a pure QQ potential, as defined in Eq. (4.12), the lowest single-excitation states for nuclei lighter than ^{20}Ne are formed by the excitation of a $1p$ particle; for nuclei heavier than ^{20}Ne the lowest single-excitation states have a particle excited to the $2p$, $1f$ shell. For ^{20}Ne, states of two representations are competing in energy. The lowest belong to an (82) representation with a hole in the $1p$ shell and close in energy lie the states of a (90) representation.

TABLE 5.VII

$M1$ Transition Rates in the $(2s,1d)$ Shell[a]
[from Wilsdon (W65, Table XVI)]

	$(\lambda\mu)$	K	J	J'	SU_3 per second	Expt* per second	Ref.
^{21}Ne	(81)	$\frac{3}{2}$	$\frac{5}{2}$	$\frac{3}{2}$	4.1×10^{11}	$>5 \times 10^{9}$	b
			$\frac{7}{2}$	$\frac{5}{2}$	2.3×10^{13}	$5^{+9.3}_{-2.5} \times 10^{12}$	c
^{23}Na	(83)	$\frac{3}{2}$	$\frac{5}{2}$	$\frac{3}{2}$	7.0×10^{11}	7.7×10^{11}	d
^{25}Mg	(66)	$\frac{5}{2}$	$\frac{7}{2}$	$\frac{5}{2}$	3.8×10^{13}	4.1×10^{13}	e
^{27}Al	(84)	$\frac{5}{2}$	$\frac{7}{2}$	$\frac{5}{2}$	8.5×10^{13}	3.1×10^{13}	f
	(2,10)	$\frac{1}{2}$	$\frac{7}{2}$	$\frac{5}{2}$	forbidden		
^{29}Si	(1,11)	$\frac{1}{2}$	$\frac{3}{2}$	$\frac{1}{2}$	8.8×10^{12}	6.7×10^{12}	f
	(10,2)	$\frac{1}{2}$	$\frac{3}{2}$	$\frac{1}{2}$	forbidden		
^{31}P	(66)	$\frac{1}{2}$	$\frac{3}{2}$	$\frac{1}{2}$	forbidden	4.5×10^{12}	f
	(39)	$\frac{1}{2}$	$\frac{3}{2}$	$\frac{1}{2}$	2.4×10^{13}		

[a] For the J-projected SU_3 scheme in column 6; the experimental value in column 7 is the total transition rate for the level concerned; J and J' in columns 4 and 5 are the angular moment of the initial and final states, respectively, and the appropriate transitions are shown in Fig. 7*a* and *b*.

Experimental references:

[b] Khubakhpashev *et al.*, *JETP*, **37** (10):705 (1960).

[c] Bent *et al.*, *Proc. Conf. Low and Medium Energy Nuclear Physics, Manchester*, 1963.

[d] Swann, *Nucl. Phys.* **42**:602 (1963).

[e] Berkes *et al.*, *Res. Inst. Phys.*, Hungarian Academy of Sciences, 1963.

[f] Booth *et al.*, *Nucl. Phys.* **35**:472 (1962).

Actually there are two sets of single-excitation states in ^{20}Ne transforming according to the (90) representation of SU_3 which arise from the excitation of a $1p$ particle and from the excitation of a $(2s, 1d)$ particle. One combination of these two types form a spurious set of states of excitation of the center of mass (E55*b*) of the zero-excitation states transforming according to the (80) representation of SU_3.

Since an oscillator quantum transforms according to the (10) representation of SU_3, the classification of single excitation, spurious states of excited center of mass motion can be determined from the outer product of (10) with *all* the zero-excitation states. Thus, e.g., in ^{20}Ne the ground-state band is assumed to transform according to (80) representation: associated with these states are spurious states of excited centre of mass transforming according to the $(80) \times (10) = (90) + (71)$ representations of SU_3.

One must always consider the spuriousness associated with the excitation of the center of mass in any problem involving more than one active shell.

TABLE 5.VIII

Some $E2$ Transition Rates in Odd A Nuclei[a]
[from Wilsdon (W65, Table XVII)]

	$(\lambda\mu)$	K	$J \to J'$	SU_3 per second	Expt per second	Ref.
^{17}O	(20)	$\frac{1}{2}$	$\frac{1}{2} \to \frac{5}{2}$	3.8×10^9	3.9×10^9	[b]
^{19}F	(60)	$\frac{1}{2}$	$\frac{5}{2} \to \frac{1}{2}$	1.2×10^7	8×10^6	[c]
^{19}Ne	(60)	$\frac{1}{2}$	$\frac{5}{2} \to \frac{1}{2}$	6.1×10^7	5.6×10^7	[c]
^{21}Ne	(81)	$\frac{3}{2}$	$\frac{5}{2} \to \frac{7}{2}$	3.4×10^9	1.1×10^9	[d]
^{23}Na	(83)	$\frac{3}{2}$	$\frac{5}{2} \to \frac{3}{2}$	3.2×10^9	1.9×10^9	[e]
^{25}Mg	(66)	$\frac{5}{2}$	$\frac{7}{2} \to \frac{5}{2}$	2.4×10^{12}	1.3×10^{12}	[f]
^{27}A	(84)	$\frac{5}{2}$	$\frac{7}{2} \to \frac{5}{2}$	1.2×10^{13}	4.8×10^{12}	[g]
	(2,10)	$\frac{1}{2}$	$\frac{7}{2} \to \frac{5}{2}$	9.0×10^{11}		
^{31}P	(66)	$\frac{1}{2}$	$\frac{3}{2} \to \frac{1}{2}$	3.2×10^{11}	2.2×10^{11}	[d]
	(93)	$\frac{1}{2}$	$\frac{3}{2} \to \frac{1}{2}$	5.0×10^{11}		

[a] Theoretical values are given in column 5, assuming the J-projected, SU_3 symmetry, experimental values are given in column 6, and the appropriate transitions are shown in Fig. 7*a* and *b*.

Experimental references:
[b] Becker *et al.*, *Phys. Rev.* **B134**:1200 (1964).
[c] Endt *et al.*, *Nucl. Phys.* **34**:1 (1962).
[d] Gove (G60).
[e] Hooten, *Nucl. Phys.* **59**:332 (1964).
[f] Rasmussen *et al.*, *Phys. Rev.* **123**:1386 (1961).
[g] Bhatt, *Nucl. Phys.* **39**:375 (1962).

TABLE 5.IX

Lowest Representations of SU_3 with Their Configurations for Zero- and Single-Excitation States of Doubly Even Nuclei in the $(2s,1d)$ Shell
[taken from Ref. E63*b*, Table 5]

Configuration	Parity	^{16}O	^{18}O	^{20}Ne	^{22}Ne	^{24}Mg	^{26}Mg	^{28}Si
$s^4p^{12}(d,s)^{A-16}$	+	(00)	(40)	(80)	(82)	(84)	(10,2)	(12,0)
$s^4p^{11}(d,s)^{A-15}$	−	(21)	(61)	(82)	(84)	(94)	(11,2)	(1,12)
$s^4p^{12}(d,s)^{A-17}(f,p)$	−		(50)	(90)	(11,1)	(11,3)	(12,3)	(14,1)
		^{30}Si	^{32}S	^{34}S	^{36}A	^{38}A	^{40}Ca	
$s^4p^{12}(d,s)^{A-16}$	+	(2,10)	(48)	(28)	(08)	(04)	(00)	
$s^4p^{11}(d,s)^{A-15}$	−	(3,10)	(39)	(19)	(07)	(03)		
$s^4p^{12}(d,s)^{A-17}(f,p)$	−	(4,11)	(69)	(68)	(48)	(36)	(32)	

At first it is perhaps surprising that negative-parity states are observed as low in energy as they are; e.g., in ^{19}F the lowest negative-parity state has an energy of only 110 keV compared with the shell spacing of 15 to 17 MeV. In the SU_3 scheme this phenomenon is explained by the greater deformation energy possessed by the negative-parity states over the lowest positive-parity states. This we have illustrated in Figs. 5.1 and 5.2 for ^{18}O and ^{20}Ne, respectively. Here it is seen how, for the simple QQ potential of Eq. (4.12), the energy of the negative-parity states is considerably lowered from the 15 MeV assumed for the shell spacing. This lowering is caused mainly by the difference in $\langle \tilde{C}_2 \rangle$ between the positive- and negative-parity states, i.e., by their difference in deformation (cf. Section 3.7).

Calculations of the energies of the states of the leading representations

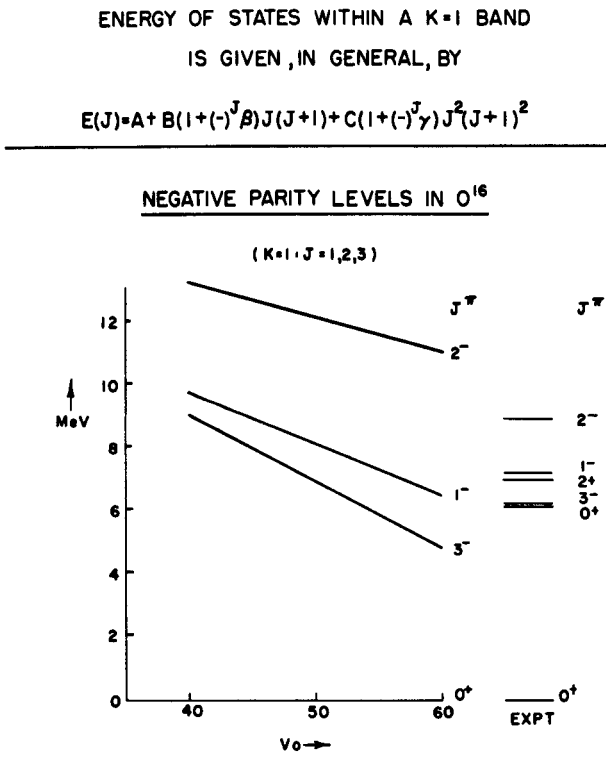

Fig. 5.8. Negative-parity single-excitation states of ^{16}O having $(\lambda\mu) = (21)$ and belonging to a decoupled $K^\pi = 1^-$ band. Energies determined for a Gaussian two-body potential, Rosenfeld exchange, and single-particle energies from ^{15}O (^{15}N), ^{16}O, ^{17}O (^{17}F) with spin-orbit effects subtracted. Spectrum shown as a function of the strength of the two-body force V_0. [Taken from Harvey (H64c).]

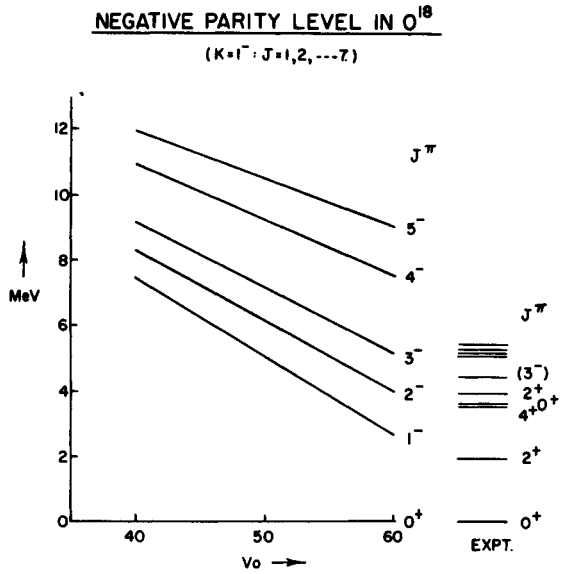

Fig. 5.9. Negative-parity single-excitation states of ^{18}O having $(\lambda\mu) = (61)$ and belonging to a slightly decoupled $K = 1$ band; calculation details as in caption to Fig. 5.8. [Taken from Harvey (H64c).]

of SU_3 for ^{16}O, ^{18}O and ^{19}F have been performed (H63, H64b, H64c) using a conventional Gaussian two-body potential, Rosenfeld exchange, and the single-particle and hole energies deduced from ^{15}O (^{15}N), ^{16}O, and ^{17}O (^{17}F). Results are reproduced in Figs. 5.8 to 5.10 for the energies of the negative-parity states relative to the positive-parity ground states as a function of the strength of the central force. Here it is seen that for $V_0 \approx 50$ MeV the calculated excitation of the lowest negative-parity state is comparable with that observed. [In these calculations the positive-parity ground state is assumed to have the pure SU_3 structure (cf. Sections 5.3 and 5.4)].

In ^{16}O the negative-parity states (Fig. 5.8) belong to the $K = 1$ band of (21) representation of SU_3 ($J = 1, 2$, and 3). As discussed in Appendix G (Eq. G.22b) the energies of states in $K = 1$ bands are "decoupled" and, in the case of ^{16}O, the calculated decoupling parameter $\beta > 1$. Thus the calculated ordering of states ($J = 3^-, 1^-, 2^-$) is as observed. The $J = 2^-$ level has in fact too high an energy, which indicates configuration mixing.

The results on ^{16}O in the SU_3 model are not really new; they merely provide a different way of interpreting the particle-hole calculations of Elliott and Flowers (E57*b*). In these latter calculations all particle-hole states were considered, but it was found that the lowest states were described predomi-

nantly by states of maximum orbital symmetry. All of the single-excitation states of maximum orbital symmetry which are nonspurious belong to the (21) representation of SU_3.

In ^{18}O the negative-parity states (Fig. 5.9) also belong to a $K = 1$ band, this time transforming according to the (61) representation of SU_3 ($J = 1, 2, \ldots, 7$). In this case the calculated decoupling parameter β is negligibly small. Thus the lowest predicted nagative-parity state has $J^\pi = 1^-$ (in agreement with experiment in Reference Z65), which forms the base for a conventional $K = 1$ band. The second negative-parity state (predicted at $\sim$5 MeV) should have $J = 2^-$ but this appears to be in contradiction to the

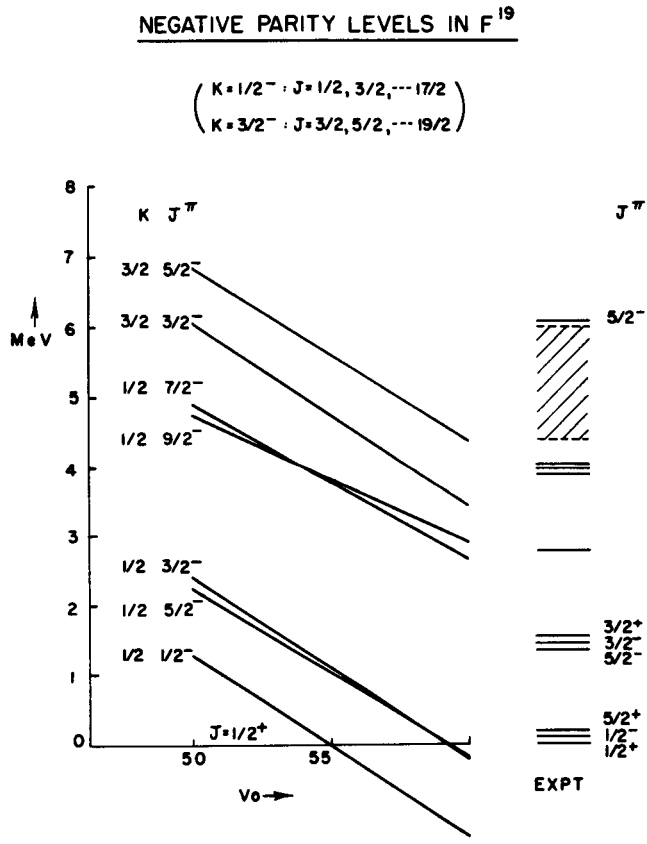

Fig. 5.10. Negative-parity single-excitation states of ^{19}F having $(\lambda\mu) = (81)$ and belonging to $K = \frac{1}{2}$ and $\frac{3}{2}$ bands; calculation details as in caption to Fig. 5.8 with the $p_{1/2} - p_{3/2}$ spin-orbit splitting for the hole in the p shell deduced from ^{15}O and ^{15}N. [Taken from Harvey (H64*b*).]

recent tentative $J = 3^-$ assignment for the level at 5.07 MeV (L66, M64*b*, and W66*c*). More data is needed here, however, for a clear picture to be seen.

In ^{19}F the lowest single-excitation states (Fig. 5.10) of maximum orbital symmetry transform according to the (81) representation of SU_3 and have intrinsic spin $S = \frac{1}{2}$. In the J-projected scheme the states can belong to either a $K = \frac{1}{2}$ or $K = \frac{3}{2}$ band. These negative-parity states have the structure of four particles (two neutrons and two protons) in the $(2s, 1d)$ shell in a singlet–singlet state and a proton hole in the $1p$ shell. Since the total spin S is nonzero, the spin-orbit splitting must be considered, but, because of the singlet–singlet structure for the particles in the $(2s, 1d)$ shell, only the $p_{3/2}$–$p_{1/2}$ splitting of the proton hole actually contributes to the calculation. In Fig. 5.11 we show how the spectrum changes from the L-projected scheme (with orbital angular momentum L a good quantum number) to the J-projected scheme (with K defined) as the strength of the spin-orbit parameter ξ_p increases. For the value of the parameter $\xi_p = -4.2$ MeV, which will give the $p_{3/2}$–$p_{1/2}$ splitting in ^{15}O, the observed features of the negative-parity spectrum in ^{19}F can be reproduced. We note the predictions of a $K = 3/2^-$ band starting at about 5.5 MeV and a negative-parity doublet $[J^\pi = (7/2)^-, (9/2)^-]$ at about 4 MeV.

The observed lowest negative-parity states in ^{20}Ne appear to lie in either a $K = 2^-$ or an odd $K = 0^-$ ($J = 1^-, 3^-, \ldots$) band (see e.g., Reference L61).

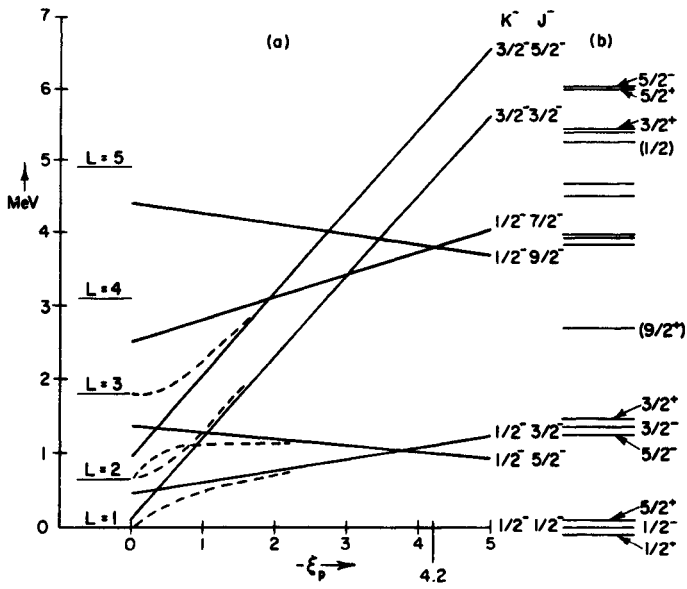

Fig. 5.11. As in Fig. 5.10, but with the energies now shown as a function of the strength of the spin-orbit force $\xi_p \sum_i s_i l_i$.

In the SU_3 scheme the leading representation is the $(\lambda\mu) = (82)$ with an even $K = 0^-$ ($J = 0^-, 2^-, \ldots$) and a $K = 2^-$ band. With a conventional Gaussian potential and Rosenfeld exchange it can be shown (E63*b*) that the bands in the (82) representation are split by about 6 MeV, with the $K = 2^-$ lowest. The observed odd $K = 0^-$ band is assumed to belong to the (non-spurious) (90) representation of SU_3.

As for the positive-parity states the real test of the model comes in the calculation of data other than energy levels. Unfortunately very few additional data are available. In Table 5.X we list some electric quadrupole and octopole transitions that have been observed and compare them with the model predictions. With such few data it is impossible to tell whether or not gross features are being described. We note that the $E2$ transition observed in ^{16}O between $J = 1^-$ (7.12 MeV) and $J = 3^-$ (6.13 MeV) is not given too well by the model. Observed $E2$ transitions in the other nuclei are not given too badly if an effective charge of $\frac{1}{2}$ is assumed. Of the four observed $E3$ transitions, only that one in ^{19}F is in violent disagreement with experiment if, again, an effective charge of $\frac{1}{2}$ is assumed. If this enhancement of the E3 transition in ^{19}F is a consequence of octopole vibrations, as has been suggested (L63), then it is not surprising that a model specifically constructed to describe quadrupole effects (i.e., the SU_3 scheme) should fail. What is of interest is why these octopole-vibrations do not appear to exist in other nuclei in the region, e.g., in ^{20}Ne where the SU_3 scheme can explain the qualitative features of the data. Clearly more data on $E3$ transitions are needed to study the problem.[6]

In ^{17}O the negative-parity states have been studied in the full generality of the shell model with all single-excitation states considered (M65*a*). It was shown that the features of the lowest observed negative-parity spectrum could be reproduced. The structure of the lowest states is given mainly by the excitation of a neutron from the $1p$ shell into the $(2s, 1d)$ shell. Such a configuration does not have maximum orbital symmetry, so we see here the breakdown of the supermultiplet scheme. Actually, in this example, the SU_3 classification could still be valid. The single-excitation states of ^{17}O are somewhat unique in having two sets of states transforming according to the leading (41) representation of SU_3; one set has maximum orbital symmetry $[f] = [44441]$, and the other, the lower symmetry [44432]. An investigation is now in progress to see whether the admixture of these two sets producing the configuration with just a neutron excitation yields just the set of states lowest in energy from the complete calculation.

[6] We note the observation of an $E3$ transition in ^{28}Si (N65*b*), but to date the SU_3 scheme has not been used to describe this feature because of the uncertainty associated with structure of the ground state.

TABLE 5.X

Some $E2$ and $E3$ Transition Probabilities Associated with Negative Parity States in ^{16}O, ^{19}F, and ^{20}Ne[a]
[theoretical numbers taken from Ref. S64 and, for ^{19}F, from H64*b*; experimental numbers taken from S65*b*]

Nucleus	λ_i	μ_i	K_i	J_i^π	E_i, MeV	λ_f	μ_f	K_f	J_f^π	E_f, MeV	Mode	$\lvert M \rvert_{SU_3}$	$\lvert M \rvert_{\text{expt}}$	$\Gamma_{sp} \times 10^{-q}$ eV	q
^{16}O	2	1	1	1^-	7.12	2	1	1	3^-	6.13	$E2$	7.2	26.6	1.89	6
	2	1	1	3^-	6.13	0	0	0	0^+	0	$E3$	12.0	14 ± 1.5	1.9	6
^{19}F	8	1	$\frac{1}{2}$	$\frac{3}{2}^-$	1.46	8	1	$\frac{1}{2}$	$\frac{1}{2}^-$	0.11	$E2$	23.77	18 ± 8	11.14	6
	8	1	$\frac{1}{2}$	$\frac{5}{2}^-$	1.35	6	0	$\frac{1}{2}$	$\frac{1}{2}^+$	0	$E3$	0.87	12 ± 4	67.85	12
^{20}Ne	8	2	2	4^-	7.01	8	2	2	2^-	4.97	$E2$	12.49	11^{+4}_{-3}	14.32	6
	8	2	2	4^-	7.01	8	2	2	3^-	7.19	$E2$	30.33	29^{+12}_{-10}	13.8	6
	8	2	2	3^-	5.63	8	0	0	0	0	$E3$	4.44	7^{+3}_{-2}	1.65	6
	8	2	2	3^-	5.63	8	0	0	2^+	1.63	$E3$	0.38	<2.3	0.15	6

[a] The classification of states is according to the assumed SU_3 symmetry. In both the $E2$ and $E3$ calculations an effective charge of $\frac{1}{2}$ has been assumed.

5.6 Multi-Excitation States in the (2*s*, 1*d*) Shell

The formal problem of considering states with more than one quantum of excitation in the SU_3 model is basically no more difficult than the problem with zero- and single-excitation states. The main differences are that there are far more states to consider and one is farther away from the zero-excitation calculations (cf. Section 5.2) that give some faith in the SU_3 classification for the lowest states. The number and type of spurious states of excited center of mass motion has also increased; one must not only consider the spurious states which have the relative nucleon structure of the zero-excitation states and excited center of mass, but also those that have the relative nucleon structure of *real* single- and multi-excitation states and excited center of mass. Only in the few places therefore where the experimental data demands unambiguously the presence of multi-excitation states have these been considered.

In ^{16}O the closed 1*s* and 1*p* shells yield only one state (having $J = 0^+$), which presumably describes the main features of the ground state. The higher positive-parity state at only 6 to 7 MeV must have at least the structure of a double-excitation state. Recent experiments (C64) show that these excited positive-parity states possess collective quadrupole features, so there is some reason to expect an SU_3 classification to be valid. What is not apparent is whether these exicted states should be dominated by doubly or quadruply excited states.

The possible double excitation structure for these states has been discussed by Brink and Nash (B63*d*) and by Borysowicz (B66*c*). These authors consider only states of maximum orbital symmetry and in Reference B66*c* the possibility of representation mixing. The ordering of representations arising from these calculations was found to be the same as that given by the QQ potential, the lowest states transforming mainly according to the leading $(\lambda\mu) = (42)$ representation. Although the observed relative energy spectrum could be reproduced for these excited positive-parity states above 6 MeV, the absolute energy was determined very poorly. Predictions of $E2$ transition probabilities are also poor.

Brown and Green (B66*d*, B66*e*) have argued that quadruple-excitation states with large deformation should lie low in energy in ^{16}O and they have suggested that these are actually the predominant components in the positive-parity states at 6 to 7 MeV. (Hartree–Fock calculations on the same problem indicate directly the favoring of quadruple over double excitation (B65).) In Reference B66*d* the lowest deformed quadruple-excitation states are selected such that they transform according to the leading $(\lambda\mu) = (82)$ representation of SU_3 in the limit of zero spin-orbit force. (Actually the states are assumed to be projections from intrinsic states formed from

Nilsson-like orbits (cf. Part 6), but the calculations of energies rely heavily on the asymptotic SU_3 structure of these states). The crude estimates of relative and absolute energies can give agreement with experiment and the resulting wave functions for the lowest states can explain many of the gross features in $E2$ transition probabilities.[7]

The lowest positive-parity states in ^{17}O have also been considered by Brown and Green with the single-particle zero-excitation states admixed by deformed double- and quadruple-excitation states. Again the crude estimates for the lowest energy spectrum are in fair agreement with experiment. Calculations of the ground-state quadrupole moment and lowest $E2$ transition, however, are too small compared with experiment which shows that not all the collective effects have been included. Estimates of single-particle strengths in ^{17}O using the ^{16}O and ^{17}O wave functions are on the whole not in good agreement with experiment, especially when these are observed to be small. This is not so surprising, since the small spectroscopic factors arise from near cancellation of many terms and are thus very sensitive to the detailed description of the states.

In ^{18}O measurements (S65*b*) of the $B(E2; 0^+ \rightarrow 2^+)$ from the level at 3.63 MeV to that at 1.98 MeV reveal this to be much larger than can be predicted in the shell model with single active shell, even after assuming an effective charge (cf. Section 5.3). Engeland (E65*b*) has shown that the double-excitation states belonging to the nonspurious leading representations $(\lambda\mu) = (82)$ and (44) lie low in energy, and admixtures into the zero-excitation states are nonnegligible; e.g., the ground state ($J = 0_1^+$) has a 25% component transforming according to $(\lambda\mu) = (82)$, while the excited $J = 0_2^+$ state has a 15% component belonging to $(\lambda\mu) = (82)$ and (44). Similar admixtures are to be found in $J \neq 0$ states. These admixtures can change $B(E2)$ values for low-lying states drastically, as is shown in Table 5.XI taken from Reference E65*b*. In this way much of the discrepancy between experiment and the single active shell model can be explained.

As is clear, the above calculations in the $A = 16$-, 17-, and 18-particle nuclei are very much of an exploratory nature and are not meant to be the last word or to imply that they are the best way to consider the effects of highly deformed states in the low-energy spectrum. They do give an idea, however, of the type of properties to expect from low-energy multi-excitation states. Alternative ways using the Hartree–Fock scheme can be found in the article by G. Ripka.

[7] In view of the title of this article we have restricted ourselves entirely to the attempts made to understand the structure of the ^{16}O states using the SU_3 model. For further latest discussions on these states see References B65, K65, C66*a*, H66, and S66.

TABLE 5.XI

$B(E2)$ Values for Transitions in ^{18}O[a]
[taken from Engeland (E65*b*)]

Type of configuration			Calculation without effective charge			Calculation with an effective 0.5 proton charge		
			$(2^+)_1 \to (0^+)_1$	$(0^+)_2 \to (2^+)_1$	Branching ratio	$(2^+)_1 \to (0^+)_1$	$(0^+)_2 \to (2^+)_1$	Branching ratio
A	Two-neutron wave function					3.4	0.8	0.24
B	Wave function	$\lambda = 12.5$ MeV	2.0	26.4	13.2	15.8	79.4	5.0
	with the (82)	$\lambda = 13.0$ MeV	0.7	9.6	13.7	10.0	32.4	3.3
	configuration only	$\lambda = 13.5$ MeV	0.3	2.8	9.3	7.2	12.1	1.7
C	Wave function with	$\lambda = 12.5$ MeV	2.0	16.8	8.4	15.9	52.2	3.3
	both (82) and (44)	$\lambda = 13.0$ MeV	0.7	5.6	8.0	10.2	20.2	2.0
	configuration	$\lambda = 13.5$ MeV	0.3	1.7	5.7	7.3	7.8	1.1

[a] *A*. The two-neutron wave functions are those from a shell-model variational calculation with two neutrons in the single active $(2s,1d)$ shell. *B*. The wave functions used here are those of *A* with admixtures of the double-excitation states belonging to the (82) representation of SU_3. *C*. The wave functions used are those of *A* with admixtures of the double-excitation states belonging to both the (82) and (44) representations of SU_3. Here λ refers to the spacing between the $1p$ and $(2s,1d)$ shells and 0_1^+ refers to the ground state. Experimental values are $B(E2; (2^+)_1 \to (0^+)_1) = 9.0 \pm 1.7$ and $B(E2; (0^+)_2 \to (2^+)_1) = (30 \pm 10)$; values are given in $e^2 fm^4$.

5.7 Multi-Excitation States in the 1*p* Shell

The lowest states of nuclei with mass $4 < A \leqslant 16$ are assumed to be zero-excitation states (K56, E57*c*, B66*a*) having only the 1*p* shell active. The classification of such states according to SU_3 is therefore equivalent to that of the Wigner supermultiplet theory (cf. Section 3.3). The SU_3 notation and methods have been used in the discussion of these states by Koltun (61). With more than one active shell, however, the classification according to SU_3 is not trivial even in this region of nuclei. Again in the discussions of multi-excitation states care must be taken to avoid the spurious states of excited center of mass motion.

Nash (N63) has discussed single-excitation (negative-parity) states in the mass 8 nuclei and calculated the energy spectrum with the force suggested by Brink (B63*c*); this force is diagonal in the SU_3 scheme. It is shown that reasonable agreement can be reached with the known data; an observed dipole state in ^{9}Be can be described and two further dipole states are predicted.

The single- and double-excitation states of ^{12}C have also been considered by Nash (N64). Energies of dipole and quadrupole states were examined and the strength of electric transitions to the ground state calculated. Again the agreement with the available data seems to be good.

The zero-excitation (negative-parity) and single-excitation (positive-parity) states of ^{9}Be have been considered by Adler *et al.* (A66*b*). In this paper the energy spectrum was parameterized within the framework of the SU_3 model and the sets of parameters chosen to get the best agreement with experiment. The work on the zero-excitation states is largely a repeat of that by Koltun (K61), however with the advantage of more experimental data. We note that the absence of a low-lying $J = \frac{1}{2}^-$ state in the observed spectrum leads to much of the ambiguity in the parameter fit. For the single-excitation states only those transforming according to the leading representation of SU_3 were considered, but systematics of the lowest positive-parity spectrum could be reproduced. The inhibited $E1$ transition from the ground state $[J = (\frac{3}{2})^-, (\lambda\mu) = (31)]$ to the lowest positive-parity state $[J = \frac{1}{2}^+$, 1.7 MeV, $(\lambda\mu) = (60)]$ can be explained in the model. [The dipole operator transforms according to SU_3 as $(\lambda\mu)_D = (10) + (01)$, and $(\lambda\mu)_D$, (31), and (60) do not satisfy the triangular condition for the group SU_3 (cf. Appendix C, Inner Product)]. More data are required on this nucleus, however, before the SU_3 scheme is unambiguously established.

6. SUMMARY AND DEVELOPMENTS

In the discussions in the previous section it was shown that the SU_3 model can describe in a qualitative way many (but not all) of the observed collective

properties in light nuclei. In many cases the qualitative features of many of the low-energy natural parity states of nuclei with mass $A < 24$ can be understood with a single active shell structure, as can the characteristics of other low-energy states which are suspected of having more than one active shell.

The quantitative agreement with experiment is not nearly so good, however, and, in the cases where good agreement has been reached, one suspects this is due to a lack of data rather than to the complete success of the model. Notable quantitative failures are the model's inability to reproduce the correct density of states (e.g., in ^{24}Mg), to explain the enhanced $E2$ transition for nuclei heavier than ^{24}Mg (the use of an effective charge of 1/2 being assumed correct for nuclei lighter than ^{24}Mg), and to explain the observed enhanced $E3$ transitions, in particular in ^{19}F.

The quantitative failure of the SU_3 scheme is not to say that it should be abandonned! On the contrary, the qualitative agreement with experiment suggests that we are not too far from the truth in assuming that the long-range QQ potential plays an important role in determining the structure of states, at least for some light nuclei. By a careful analysis of the deviation of the model predictions from experiment, one can hope to learn the causes of these failures. Thus one could treat the SU_3 model in much the same way that the single-particle model has been used in the study of collective features, i.e., as a baseline from which to compare experimental data. (This approach has been taken e.g., by Kalman *et al.* (K67) in analyzing energies and transitions in ^{20}Ne).

The calculations which attempt to check the accuracy of the SU_3 scheme for central forces in the single active ($2s$, $1d$) shell (see Section 5.2) tend to show that it is remarkably good here despite the fact that agreement with experiment deteriorates the more particles are in the shell. One suspects then that it is the assumed potential which is at fault and that noncentral forces cannot be entirely neglected.

If noncentral forces are important, one must study the best way of taking them into account. One can of course return to the general shell-model variational approach, possibly limiting the basis states according to some prescription based on the SU_3 model (see e.g., References I64 and I66). This has the standard disadvantages of not having a simple, concise description of the lowest eigenfunctions, as discussed in the Introduction. In ^{24}Mg Bannerjee *et al.* (B63*b*) considered including the effects of the noncentral forces by an approximate treatment of a perturbation method of Feingold; they were able to derive much improved spectrum with such a method (including a better density of states), but changes in other properties were not computed. Wilsdon's recent study (W65) of the spin-orbit force

strictly within the SU_3 scheme, as suggested by Elliott (E62, E63*a*), tended to show this approach was not sufficient to describe the main effects (see Section 5.4). Bouten *et al.* (B64) have attempted to extrapolate energy levels between the SU_3 limit and the *jj* coupling extreme. Here one tries to get agreement with the experimental energy spectra in some intermediate region without attempting to predict where this point should be. It is shown that agreement with the observed spectra can often be reached by this method, but, since the wave functions are not constructed for this intermediate region, no other properties can be studied.

The persistent observation of collective features, even when the SU_3 model fails to give good qualitative agreement with experiment, suggests that it is the parts of the noncentral potential contributing to the collective effects which are the next most important possibility to be taken into account. It would thus be nice to have a collective model which is spin dependent. To the author's knowledge this problem has not been solved using group techniques, however some success has been gained along other lines. In the remainder of this section we shall briefly discuss these other approaches concentrating on their relationships with the SU_3 model.

In the development of the SU_3 model (as presented in this article) collective features arose from the assumption of the dominance of an effective QQ potential. It was shown in Section 3.7, however, that every state of a given angular momentum within a representation of SU_3 could be projected by a Hill–Wheeler integral from a single intrinsic state; this state has definite SU_3 symmetry but does not have definite angular momentum. It should be noted that the existence of rotational bands in the model (see Section 4.3) does not rely on the existence of this intrinsic state, however.

The alternative approach to collective phenomena is the more conventional one of assuming that these arise because of the presence of the intrinsic state, or, in other words, the existence of the intrinsic state is *necessary*. The emphasis here then is to construct the suitable intrinsic state from which the real (collective) nuclear states are assumed to be projected by a Hill–Wheeler integral (H53). The general problem has been discussed by Peierls and Yoccoz (P57). It is assumed that the single particles in the intrinsic state move predominantly in the single-particle, self-consistent field generated by all the other particles. This field one can either guess (e.g., as in the Nilsson model, Reference N55) or, better, actually construct following the Hartree–Fock theory (see the article in this present volume by G. Ripka).

In the latter approach, any (well-behaved) potential can be used, including a spin-dependent one. Thus, in this sense, it is an extension to the SU_3 scheme if we can show that the two approaches are equivalent (i.e., lead to the *same* collective states) for spin-independent potentials. This we can do

by demonstrating that the Hartree–Fock procedure leads to the SU_3 intrinsic state as defined in Section 3.20.

The straightforward Hartree–Fock theory leads to a simple Slater determinant for the intrinsic state; thus equivalence between the two approaches can only be reached if the SU_3 intrinsic state is also a determinant. When there is only one set of states belonging to the leading representation of SU_3, then it can indeed be projected from a determinantal intrinsic state: as a rule this occurs for even–even and odd-A nuclei. When there is more than one set of states belonging to the leading representation (e.g., for odd-odd nuclei) some other criteria must be used to select those which are lowest in energy. The Majorana component of the nuclear potential will favor states of maximum orbital symmetry and thus in the SU_3 model we impose this further condition; here states of the leading representation with maximum orbital symmetry cannot be projected from a single Slater determinant. In this case, however, there is also an ambiguity in the Hartree–Fock solution of what is to be considered the best intrinsic state; additional considerations of particle symmetry will again lead to a state which is not a Slater determinant but which has a structure similar to the intrinsic state of the SU_3 model.

We now briefly consider the problem of whether the Hartree–Fock and the SU_3 schemes actually lead to the *same* intrinsic state for spin-independent forces. This we demonstrate first in an approximate way, assuming the simple two-body QQ potential (see Section 4.3), which is closely diagonalized in the SU_3 scheme to within a single-particle term. We shall show that the SU_3 intrinsic state of maximum weight is in fact a self-consistent solution to the Hartree–Fock single-particle potential without exchange, i.e., the Hartree potential:

The Hartree–Fock self-consistent single-particle potential that is derived from a general two-body potential $V^{(2)}$ can be written (see the article by G. Ripka):

$$V_{H-F} = \sum_{\alpha\beta} \left\{ \sum_{\gamma\delta} \bar{V}^{(2)}_{\alpha\gamma\beta\delta} \langle a_\gamma{}^+ a_\delta \rangle \right\} a_\alpha{}^+ a_\beta \tag{6.1}$$

using a general representation for the nucleon creation operators $a_\alpha{}^+$, etc. Here $\bar{V}^{(2)}_{\alpha\gamma\beta\delta} = \langle \alpha\gamma \mid V^{(2)} \mid \beta\delta - \delta\beta \rangle$ and expectation values $\langle \cdots \rangle$ are taken with respect to the Hartree–Fock ground state. If we assume the potential $V^{(2)} = V_0 \sum_{i<j} (Q(i) \cdot Q(j))$ (see Section 4.3) and take just the direct term in Eq. (6.1), the resulting Hartree potential can be written

$$V_H = \sum_{\alpha\beta} \left\{ V_0 \sum_q (-)^q \sum_{\gamma\delta} \langle \alpha \mid Q_q \mid \beta \rangle \langle \gamma \mid Q_{-q} \mid \delta \rangle \langle a_\gamma{}^+ a_\delta \rangle \right\} a_\alpha{}^+ a_\beta \tag{6.2}$$

Remembering that in second quantized notation we can write the quadrupole operator

$$Q_q = \sum_{\alpha\beta} \langle a \mid Q_q \mid \beta \rangle \, a_\alpha^+ a_\beta \tag{6.3}$$

Eq. 6.2 can be written:

$$V_H = V_0 \sum_q (-)^q \langle Q_{-q} \rangle \, Q_q \tag{6.4}$$

If we now assume that the SU_3 intrinsic state $\phi(\lambda\mu)$ of maximum weight is the Hartree state in order to construct V_H, then we can show that V_H actually has $\phi(\lambda\mu)$ as an eigenfunction, i.e., we have reached self-consistency for the state $\phi(\lambda\mu)$. For the state $\phi(\lambda\mu)$

$$\langle Q_0 \rangle = 2\lambda + \mu \qquad \langle Q_{+1} \rangle = \langle Q_{-1} \rangle = 0$$

$$\langle Q_2 \rangle = \langle Q_{-2} \rangle = \tfrac{1}{2}\sqrt{6}\,\mu$$

(see Section 3.6). Equation (6.4) can thus be written

$$V_H = V_0\{(2\lambda + \mu)\, Q_0 + \tfrac{1}{2}\sqrt{6}\,\mu(Q_2 + Q_{-2})\} \tag{6.5}$$

V_H is given in terms of operators diagonal in the intrinsic representation ($SU_3 \rightarrow SU_2 \times U_1$, see Section 3.6) and thus indeed has the state $\phi(\lambda\mu)$ as an eigenstate. An equivalent argument can be made using the state of minimum weight $\tilde{\phi}(\lambda\mu)$, as defined in Section 3.6).

For $\mu = 0$ [i.e., for axial symmetry, see Eq. (3.40) and related discussion], the Hartree potential V_H is just the Nilsson potential after ignoring the single-particle terms or, equivalently, in the region of large deformation δ. For $\mu \neq 0$, V_H is a nonaxially symmetric potential, as considered e.g. by Newton (N60).

For a general two-body central potential the Hartree–Fock theory also tends to yield the intrinsic state of the SU_3 model. In ^{28}Si, e.g., the Hartree–Fock calculations in the ($2s$, $1d$) shell have been made by Das Gupta and Harvey (D67) among others. For a Yukawa two-body potential with Rosenfeld exchange, two Hartree–Fock minima are found; these lead to two intrinsic states which have overlaps of over 99 % with the intrinsic states belonging to the (12,0) and (0,12) representations of SU_3.

One should not really be too surprised at the similarity of the Hartree–Fock and SU_3 approaches! The Hartree–Fock procedure picks out the field effects from a given potential and these are necessarily of a long-range character. From the arguments in Chapter 4, one of the dominant terms of a long-range potential has the QQ form which is closely associated with the Casimir operator of SU_3.

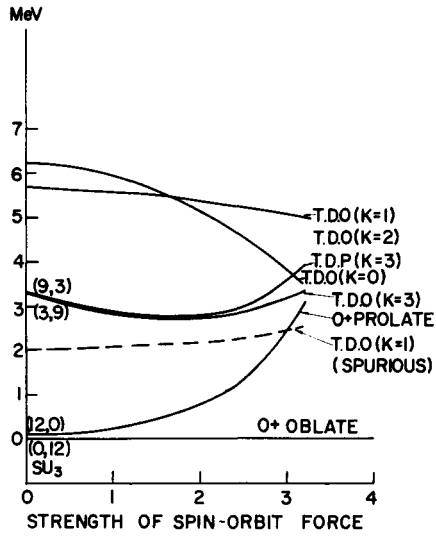

Fig. 6.1. Variation in energy of the lowest prolate P and oblate O Hartree–Fock minima and the Tamm–Dancoff (TD) particle-hole excitations from these minima with definite projection of angular momentum K. Shown relative to the oblate Hartree–Fock solution as a function of the strength of the single-particle spin-orbit force. The SU_3 symmetry of the states for zero-spin orbit force is given on the left. The broken curve refers to the spurious $K = 1$ Tamm–Dancoff particle-hole state $J_{+1} \mid \text{oblate}\rangle$ based on the oblate Hartree–Fock state $\mid \text{oblate}\rangle$. [Taken from Das Gupta and Harvey (D67).]

The above considerations leads us to assume that, for central potentials, the SU_3 scheme and Hartree–Fock scheme will lead to essentially the same collective states.[8] With spin-dependent potentials, however, the two approaches can deviate in their prescriptions for generating the lowest collective state. We can illustrate the deviation of the Hartree–Fock approach away from the SU_3 scheme, with the introduction of the single-particle spin-orbit force, by again considering the example of ^{28}Si (D67). For zero spin-orbit force (i.e., in the SU_3 extreme) there are two Hartree–Fock minimums which largely belong to the representations (12,0) and (0,12) of SU_3 and which are essentially degenerate in energy [see discussion in

[8] It would be interesting to check this statement in, say, the $2p$, $1f$ shell.

Section 5.3 and (B67)]. On the introduction of the spin-orbit force the two Hartree–Fock states loose their SU_3 symmetry and also their degeneracy. In Fig. 6.1 is shown the change in the energy of the Hartree–Fock states as a function of spin-orbit force strength. One certainly needs this degeneracy split to get any agreement with experiment, and it has been suggested by Das Gupta and Harvey (D67) that it is the spin-orbit interaction in the average field which largely accounts for the deviations of the SU_3 predictions in ^{28}Si from experiment.

As an extension to the pure Hartree–Fock approach, the structure of excited bands of states can be assumed to be projections from Tamm–Dancoff particle-hole excitations from the Hartree–Fock state (D67). In the limit of zero spin-orbit force these Tamm–Dancoff states are found to be either intrinsic states of SU_3 representation of symmetry lower than the leading representations or spurious states of rotational motion (see Section 3.7). For nonzero spin-orbit force the Tamm–Dancoff states loose their SU_3 symmetry with the Hartree–Fock state, but spurious states remain spurious.

In summary, it is our feeling that, although exact agreement with experiment should not be expected of the SU_3 model, the scheme is realistic enough for a comparison to be fruitful. A systematic study of the disagreements between model and experiment should be a useful way of determining their causes and of pointing out the direction in which the model should be extended.

Acknowledgments

It is a pleasure to thank J. P. Elliott for past discussions concerning the SU_3 model and to E. W. Vogt and the Chalk River group for their criticisms of this article. The permission to publish from the various authors whose work has been quoted in detail is gratefully acknowledged.

REFERENCES

W28 Weyl, H., "Group Theory and Quantum Mechanics," Dover Publications, New York, 1928.

F37 Feenberg, E., and M. Phillips, *Phys. Rev.* **51**:597 (1937).

W37 Wigner, E. P., *Phys. Rev.* **51**:106 (1937).

J40 Jauch, J. M., and E. L. Hill, *Phys. Rev.* **57**:641 (1940).

R42 Racah, G., *Phys. Rev.* **62**:438 (1942).

J51*a* Jahn, H. A., *Proc. Roy. Soc.* **205**:192 (1951).

J51*b* Jahn, H. A., and H. van Wieringen, *Proc. Roy. Soc.* **A209**:502 (1951).

R51 Racah, G., "Lecture Notes on Group Theory in Spectroscopy," Princeton University, 1951.

H53 Hill, D. L., and J. A. Wheeler, *Phys. Rev.* **89**:1102 (1953).

E55*a* Elliott, J. P., and B. H. Flowers, *Proc. Roy. Soc.* **A229**:536 (1955).

E55*b* Elliott, J. P., and T. H. R. Skyrme, *Proc. Roy. Soc.* **A232**:561 (1955).

N55 Nilsson, S. G., *Dan. Mat. Fys. Medd.* **29**:16 (1955).

B56 Blin-Stoyle, R. J., *Rev. Mod. Phys.* **28**:75 (1956).

K56 Kurath, D., *Phys. Rev.* **101**:216 (1956).

E57*a* Edmonds, A. R., "Angular Momentum in Quantum Mechanics," Princeton University Press, Princeton, N. J., 1957.

E57*b* Elliott, J. P., and B. H. Flowers, *Proc. Roy. Soc.* **A242**:57 (1957).

E57*c* Elliott, J. P., and A. M. Lane, *in* "Encyclopedia of Physics" S. Flügge, ed., Vol. 39. Springer-Verlag, Berlin-Göttingen-Heidelberg, 1957.

H57 Hofstadter, R., *Ann. Rev. Nucl. Sci.* **7**:231 (1957).

M57 Moszkowski, S. A., *in* "Encyclopedia of Physics," S. Flügge, ed. Springer-Verlag, Berlin-Göttingen-Heidelberg, 1957.

P57 Peierls, R. E., and J. Yoccoz, *Proc. Phys. Soc.* **A70**:381 (1957).

E58 Elliott, J. P., *Proc. Roy. Soc.* **A245**:128 and 562 (1958).

M58 Moskowski, S., *Phys. Rev.* **110**:403 (1958).

E59 "Nuclear Reaction *I*," P. M. Endt and M. Demeur, eds. North Holland Publishing Co., Amsterdam, 1959.

R59 Rotenberg, M., R. Bivins, N. Metropolis, and J. K. Wooten, Jr., "The 3-*j* and 6-*j* Symbols," The Technology Press, Massachusetts Institute of Technology, Cambridge, Mass, 1959.

B60*a* Bargman, V., and M. Moshinsky, *Nucl. Phys.* **18**:697 (1960).

B60*b* Bayman, B. F., "Groups and Their Application to Spectroscopy," Lectures delivered in 1957 at NORDITA. Nordisk Institute for Teoretisk Atom Fysik, Copenhagen, 1960.

B60*c* Bohr, A., and B. R. Mottelson, *in* "Nuclear Spectroscopy B," Fay Ajzenberg-Selove, ed. Academic Press, New York-London VI, C, 1960.

G60 Gove, H. E., Proc. Internl. Conf. Nuclear Structure, Kingston: D. A. Bromley and E. W. Vogt, eds. University of Toronto Press, p. 438, 1960.

L60 Lawson, R. D., *in* "Nuclear Spectroscopy B," Fay Ajzenberg-Selove, ed. Academic Press, New York-London VI, A, 1960.

N60 Newton, T. D., "Energy Levels of a Completely Anistropic Oscillator," *Chalk River Nucl. Labs. Rept., CRT-886*, 1960.

W60 Wilkinson, D. H., *in* "Nuclear Spectroscopy B," Fay Ajzenberg-Selove, ed. Academic Press, New York-London, V.F., 1960.

B61 Bargman, V., and M. Moshinsky, *Nucl. Phys.* **23**:177 (1961).

H61*a* Harvey, M., Ph.D. Thesis, Southampton, 1961.

H61*b* Hellwege, K. H., ed., "Energy Levels in Light Nuclei," Springer-Verlag, Berlin-Göttingen-Heidelberg, 1961.

K61 Koltan, D. S., *Phys. Rev.* **124**:1162 (1961).

L61 Litherland, A. E., J. A. Kuehner, H. E. Gove, M. A. Clarke, and E. Almqvist, *Phys. Rev. Letters* **7**:98 (1961).

N61 Ne'eman, Y., *Nucl. Phys.* **26**:222 (1961).

E62 Elliott, J. P., "Escuela Latino Americana De Fisca." Universidad de Mexico, 1962.

G62 Gell-Mann, M., *Phys. Rev.* **125**:1067 (1962).

M62 Moshinsky, M., "Escuela Latino Americana De Fisca." Universidad de Mexico, 1962.

W62 Willey, R. S., *Phys. Rev.* **126**:1127 (1962).

B63*a* Bannerjee, M. K., and C. Levinson, *Phys. Rev.* **130**:1036 (1963).

B63*b* Bannerjee, M. K., C. Levinson, and S. Meshkov, *Phys. Rev.* **130**:1064 (1963).

B63*c* Brink, D. M., *Nucl. Phys.* **40**:593 (1963).

B63*d* Brink, D. M., and G. F. Nash, *Nucl. Phys.* **40**:608 (1963).
E63*a* Elliott, J. P., "Selected Topics in Nuclear Theory." International Atomic Energy Agency, Vienna, 1963.
E63*b* Elliott, J. P., and M. Harvey, *Proc. Roy. Soc.* **A272**:557 (1963).
L63 Litherland, A. E., M. A. Clark, and C. Broude, *Phys. Rev. Letters* **3**:204 (1963).
H63 Harvey, M., *Phys. Rev. Letters* **3**:209 (1963).
N63 Nash, G. F., *Nuovo Cimento* **30**:1064 (1963).
S63 de Shalit, A., and I. Talmi, "Nuclear Shell Theory," Academic Press, New York-London, 1963.
B64 Bouten, M. C., J. P. Elliott, and J. A. Pullen, Comptes Rendus du Congrès International de Physique Nucléaire, pré Madame P. Gugenberger, Centre National de la Recherche Scientifique, Paris, 1964, Vol. II, p. 413. Also preprint, 1966.
C64 Carter, E. B., G. E. Mitchell, and R. H. Davies, *Phys. Rev.* **133B**:1421 and 1434 (1964).
E64 Engeland, T., and A. Kallio, *Nucl. Phys.* **59**:211 (1964).
G64 Guiaşu, I., and M. Micu, *Rev. Roum. Physics* **9**:911 (1964).
H64*a* Hamermesh, M., "Group Theory and its Application to Physical Problems," Addison-Wesley, Reading, Mass., 1964.
H64*b* Harvey, M., *Nucl. Phys.* **52**:542 (1964).
H64*c* Harvey, M., *Symp. Structure of Low-Medium Mass Nuclei*, Kansas, 1964.
H64*d* Hecht, K. T., *in* "Selected Topics in Nuclear Spectroscopy," B. J. Verhaar, ed. North-Holland and John Wiley, 1964.
H64*e* Horie, H., *J. Phys. Soc. Japan* **19**:1783 (1964).
I64 Inoue, T., T. Sebe, H. Hagiwara, and A. Arima, *Nucl. Phys.* **59**:1 (1964).
K64 Kuehner, J. A., and J. D. Pearson, *Can. J. Phys.* **42**:477 (1964).
M64*a* McKellar, B. H. J., *Phys. Rev.* **134**:B1190 (1964).
M64*b* Middleton, R., and D. J. Pullen, *Nucl. Phys.* **51**:63 (1964).
N64 Nash, G. F., *Nuovo Cimento* **32**:727 (1964).
P64 Pandya, S. P., and I. M. Green, *Nucl. Phys.* **57**:658 (1964).
S64 Svenne, J. P., and M. Harvey, *unpublished.*
T64 Tinkham, M., "Group Theory and Quantum Mechanics," McGraw-Hill Book Co., New York, 1964.
A65 Arima, A., M. Nomura, and H. Kawarada, *Phys. Rev. Letters* **19**:400 (1965).
B65*a* Bassichis, W. H., and G. Ripka, *Phys. Rev. Letters* **15**:320 (1965).
B65*b* Block, C., and V. Gillet, *Phys. Rev. Letters* **16**:62 (1965) and **18**:58 (1965).
E65*a* Engeland, T., *Nucl. Phys.* **72**:68 (1965).
E65*b* Evans, H. C., M. A. Eswaren, H. E. Gove, A. E. Litherland, and C. Broude, *Can. J. Phys.* **43**:82 (1965).
F65 Flores, J., E. Chacon, P. A. Mello, and M. de Llano, *Nucl. Phys.* **72**:352 (1965).
H65 Hecht, K. T., *Nucl. Phys.* **62**:1 (1965).
K65 Kelson, I., *Phys. Rev. Letters* **16**:143 (1965).
L65 de Llano, M., P. A. Mello, E. Chacon, and J. Flores, *Nucl. Phys.* **72**:379 (1965).
M65*a* Margolis, B., and N. de Takacsy, *Phys. Rev. Letters* **15**:329 (1965).
M65*b* Muthukrishnan, R., and M. Baranger, *Phys. Rev. Letters* **18**:160 (1965).
N65*a* Newton, T. D., NUSTAT—An Apex Program for Fully Mechanized Shell Model Calculations, *Chalk River Nucl. Labs.*, Ontario, Canada, *CRT*-1213, 1965.
N65*b* Nordhagen, R., M. Hoffman, F. Ingelretsen, and A. Tveter, *Phys. Rev. Letters* **16**:163 (1965).
N65*c* Nathan, O., and S. G. Nilsson, *in* "Alpha-Beta- and Gamma-Ray Spectroscopy," Chap. 10, Kai Siegbahn, ed. North-Holland Publishing Co., Amsterdam, 1965.

S65*a* Siemssen, R. H., L. L. Lee, Jr., and D. Cline, *Phys. Rev.* **140**:B1258 (1965).

S65*b* Skorka, S. J., "Compilation of Electromagnetic Transition Strengths in Light Nuclei ($A \leqslant 40$)," II Institute für Experimental physik, der Universität Hamburg, 1965.

W65 Wilsdon, C. E., Ph.D. Thesis, 1965, Sussex.

Z65 Zeidman, B., and T. H. Braid, *Phys. Rev. Letters* **16**:139 (1965).

A66*a* Abulaffio, C., *Nucl. Phys.* **81**:71 (1966).

A66*b* Adler, C., T. Carocoran, and C. Most, *Nucl. Phys.* **88**:145 (1966).

A66*c* Alexander, T. K., C. Broude, A. J. Ferguson, J. A. Kuehner, A. E. Litherland, R. W. Ollerhead, and P. J. M. Smulders, *Gatlinburg Conf. Nucl. Phys.*, 1966.

B66*a* Barker, F. C., *Nucl. Phys.* **83**:418 (1966).

B66*b* Bernier, J.-P., and M. Harvey, *unpublished.*

B66*c* Borysowicz, J., *Nucl. Phys.* **82**:321 (1966).

B66*d* Brown, G. E., and A. M. Green, *Nucl. Phys.* **75**:401 (1966).

B66*e* Brown, G. E., and A. M. Green, *Nucl. Phys.* **85**:87 (1966).

B66*f* Bauer, M., and F. Prats, *Nucl. Phys.* **89**:230 (1966).

B66*g* Broglia, R. A., and E. E. Maqueda, *Nucl. Phys.* **86**:457.

C66*a* Celenza, L. S., R. M. Dreizler, A. Klein, and G. J. Dreiss, *Phys. Rev. Letters* **23**:241 (1966).

C66*b* Cohen, S., R. D. Lawson, and J. M. Soper, *Phys. Rev. Letters* **21**:306 (1966).

F66 Flores, J., and M. Moshinsky, "Studies on Nuclear Structure in the 2*s*,1*d* Shell, III Group Theory and Particle-Hole States." Instituto de Fisica, Universidad de México, Preprint, 1966.

G66 Glaudemans, P. W. M., B. H. Wildenthal, and J. B. McGrory, *Phys. Rev. Letters* **21**:427 (1966).

H66 Hughes, D. J., and A. B. Volkov, *Phys. Rev. Letters* **23**:113 (1966).

I66 Inoue, T., T. Sebe, H. Hagiwara, and A. Arima, *Nucl. Phys.* **85**:184 (1966).

K66*a* Kuehner, J. A., and R. W. Ollerhead, *Phys. Rev. Letters* **20**:301 (1966).

K66*b* Kramer, P., and M. Moshinsky, *Nucl. Phys.* **82**:241 (1966).

L66 Lopas, J. S., O. Häusser, R. D. Gill, and H. J. Rose, *Nucl. Phys.* **89**:127 (1966).

R66*a* Robson, D., Annual Reviews of Nuclear Science **16**:119 (1966).

R66*b* Reif, R., *Phys. Rev. Letters* **23**:125 (1966).

S66 Seaborn, J. B., and J. M. Eisenberg, *Nucl. Phys.* **82**:308 (1966).

T66 Trlifaj, L., M. Gmitro, and M. Sotana, *Nucl. Phys.* **86**:681 (1966).

W66*a* Wahsweiler, H. G., M. Danos, and W. Greiner, *Phys. Rev. Letters* **17**:395, and **23**:257 (1966).

W66*c* Wiza, J. L., R. Middleton, and P. V. Hewka, *Phys. Rev.* **141**:975 (1966).

Z66 Zichichi, A., ed., "Recent developments in particle Symmetries," Academic Press, New York and London, 1966.

A67 Akiyamu, Y., Private Communication, Tokyo University, Japan.

B67 Bernier, J.-P., and M. Harvey, *Nucl. Phys.* **A94**:593 (1967).

D67 Das Gupta, S., and M. Harvey, *Nucl. Phys.* **A94**:602 (1967).

I67 Iosifescu, M., and F. Stancu, *Nucl. Phys.* **B8**:471 (1967).

K67 Kalman, C., J.-P. Bernier, and M. Harvey, *Can. J. Phys.* **45**:1297 (1967).

S67 Sebe, T., Preprint, Hosei University, Japan, and Chalk River Nuclear Laboratories, Canada.

V67 Vergados, J. D., Preprint, University of Michigan, Ann Arbor.

W67 Wathne, C., and T. Engeland, *Nucl. Phys.* **A94**:129 (1967).

APPENDIX A—HARMONIC OSCILLATOR

General Properties

The Hamiltonian for a single particle in the harmonic oscillator in three dimensions and can be written

$$\mathscr{H}_0 = \frac{1}{2m} p^2 + \frac{1}{2} m\omega^2 r^2 \tag{A.1}$$

where p is the momentum operator. Eigenvalues of $\mathscr{H}_0$ are characterized by the number of oscillator quanta and can be written $E_n = (n + \frac{3}{2})\hbar\omega$. In general these eigenvalues are multiply-degenerate (see the discussion in Section 3.2) and the eigenfunctions can be written in several ways. We quote below the structure of these eigenfunctions in the spherical, cylindrically polar, and Cartesian coordinate systems. In all of these expressions the oscillator parameter b is related to the frequency ω by $\omega = \hbar/mb^2$ with m the mass of the particle.

A. Spherical

$$\psi_{nlm} = R_{\bar{n}l}\left(\frac{r}{b}\right) Y_{lm}(\theta\phi) \tag{A.2}$$

with r, θ, and ϕ sherical coordinates. Here $2\bar{n} + l = n$, $Y_{lm}(\theta\phi)$ is a spherical harmonic, and

$$R_{\bar{n}l}(x) = \sqrt{\frac{2\bar{n}!}{b^3\,\Gamma(\bar{n} + l + \frac{3}{2})}}\, x^l \mathscr{L}_{\bar{n}}^{l+\frac{1}{2}}(x^2) \exp(-x^2/2)$$

with $\mathscr{L}_n^\alpha(y)$ a Laguerre polynomial with normalization as defined in Reference B53, Vol. 2, Section 10.12.

B. Cylindrical

$$\chi_{nn_\perp m} = \mathscr{N}_{n_z n_\perp m}\, e^{im\phi} \left(\frac{\rho}{b}\right)^{|m|} \mathscr{L}^{|m|}_{(n_\perp - |m|)/2}\, H_{n_z}\left(\frac{z}{b}\right) e^{-r^2/2b^2} \tag{A.3}$$

where $n_z = n - n_\perp$ and ρ, z, and ϕ are cylindrical polar coordinates. Here $\mathscr{N}$ is a normalization coefficient

$$\mathscr{N}_{n_z n_\perp m} = \sqrt{\frac{\{(n_\perp - |m|)/2\}!}{2^{n_z} n_z!\,\{(n_\perp + |m|)/2\}!\, b^3\pi^{3/2}}}$$

$\mathscr{L}$ is a Laguerre polynomial, and H is a Hermite polynomial. (c.f. Reference B53 Vol. II).

C. Cartesian

$$\phi_{n_x n_y n_z} = \sqrt{\frac{1}{2^n n_x!\, n_y!\, n_z!\, \pi^{3/2} b^3}}\, H_{n_x}\left(\frac{x}{b}\right) H_{n_y}\left(\frac{y}{b}\right) H_{n_z}\left(\frac{z}{b}\right) e^{-r^2/2b^2} \tag{A.4}$$

where x, y, and z are Cartesian coordinates. Here $n = n_x + n_y + n_z$, and H is a Hermite polynomial. as defined in Reference B53 Vol. II.

The many-body harmonic oscillator

$$H_0 = \sum_i \mathscr{H}_0(i) \tag{A.5}$$

has eigenvalues $\sum_i E_n(i)$ with eigenfunctions the product of single-particle functions.

Mean Square Radius

The oscillator parameter b can be determined by imposing the condition that the mean square radius of the many-body functions of lowest body energy (observing the Pauli principle),

$$\tfrac{3}{5}R^2 = \frac{1}{A}\left\langle \sum_i r_i^2 \right\rangle \tag{A.6}$$

has at least the average value with

$$R = r_0 A^{1/3} \times 10^{-13}\ \text{cm} \tag{A.7}$$

as determined from, say, electron scattering experiments (H57). The expectation value in Eq. (A.6) is simply the sum of $\langle r^2 \rangle$ between single-particle harmonic-oscillator states. Remembering that within an oscillator shell $\langle p^2 \rangle = \langle r^2 \rangle$, we can immediately write

$$\tfrac{3}{5}R^2 = \frac{1}{A} b^2 \sum_i [n(i) + \tfrac{3}{2}] \tag{A.8}$$

where $n(i)$ is the oscillator number of the ith particle. Equation (A.8) with Eq. (A.7) immediately give an estimate of the oscillator parameter

$$b^2 = \frac{3}{5} \frac{A^{5/3} r_0^2}{\sum_i [n(i) + \tfrac{3}{2}]} \times 10^{-26}\ \text{cm} \tag{A.9}$$

The parameter r_0 of Eq. (A.7) can be taken to be of the order of $r_0 = 1.2$.

APPENDIX B—USE OF GROUPS IN QUANTUM MECHANICS

Basic Theory

In the text we have assumed the reader to be familiar with the basic ideas of group theory, but for clarity we review here some of the more important ideas leading to a simplification and understanding of the physical problem. For greater detail we suggest to the reader References R51, S63, H64*a*, T64.

A group G is defined as a set of objects (e.g., transformations) g_i with a law of association defined (e.g., multiplication) and having the properties:

a. A product (under the law of association) of two of the elements, g_i and g_j, yields a third elements g_k of the set

$$g_i g_j = g_k$$

b. The set includes a unit, or identity element, e such that

$$eg_i = g_i e = g_i$$

for all g_i in the set G.

c. For each element g_i there exists an "inverse" element g_i^{-1} such that

$$g_i g_i^{-1} = g_i^{-1} g_i = e$$

d. For three elements g_i, g_j, and g_k the associative law holds

$$g_i(g_j g_k) = (g_i g_j)\, g_k = g_i g_j g_k$$

As an example pertinent to our present study we quote the infinite set of unitary matrices in three dimensions which are said to form the group U_3. (Unitary matrices are those with determinant ± 1 such that $U^{-1} = \tilde{U}'$, where the tilde and prime denote complex conjugation and transposition, respectively).

Representation

Assume now that the elements g_i are transformations operating on a complete set of functions ψ_α

$$g_i \psi_\alpha = \sum_\beta R_{\alpha\beta}(i)\, \psi_\beta \tag{B.1}$$

The matrix $R_{\alpha\beta}(i)$ is said to be the *representation* of the transformation g_i with respect to the basic set ψ_α. If the set ψ_α is orthonormal, then the matrices will be unitary.

If we can find a finite subset r of dimension d of the functions ψ_α such that *none* of the group elements of G transform outside the set and, furthermore, this set cannot be reduced to smaller dimensions, then the representation is said to be *irreducible* and of dimension d. The functions of the subset r are said to transform according to (or belong to) the irreducible representation r of the group G. Thus Eq. (B.1) could be rewritten

$$g_i \psi_\alpha{}^r = \sum_\beta R^r_{\alpha\beta}(i)\, \psi_\beta{}^r \tag{B.2}$$

where α and β label the particular functions of the finite irreducible set r. A set of *operators* $T_\alpha{}^r$ is said to transform according to the αth row of the rth representation of the group G if

$$g_i T_\alpha{}^r g_i^{-1} = \sum_\beta R^r_{\alpha\beta}(i)\, T_\beta{}^r \tag{B.3}$$

Physical Application

To understand how the idea of representation helps to simplify the many-body problem, suppose a Hamiltonian is invariant with respect to a group G, i.e., for every element of the group g_i

$$Hg_i = g_i H \tag{B.4}$$

If ψ_0 is an eigenfunction of H with eigenvalue E, i.e.,

$$H\psi_0 = E\psi_0 \tag{B.5}$$

then all the functions $\psi_i = g_i\psi_0$ are also eigenfunctions with the same eigenvalue E

$$[H\psi_i = Hg_i\psi_0 = g_i H\psi_0 = E\psi_i] \tag{B.6}$$

If ψ_0 transforms according to a definite irreducible representation r of G, then, by definition, so do all the functions ψ_i. Thus the above arguments show that functions are degenerate that belong to the same irreducible representation of a group under which the Hamiltonian is invariant. The important point is that eigenfunctions of H can *always* be defined so that they belong to an irreducible representation of the invariant group G. The proof of this statement simply involves showing that the matrix elements

$$(\psi_{\alpha'}^{r'} \mid H \mid \psi_\alpha{}^r) = 0 \qquad \text{for all } r \neq r' \tag{B.7}$$

This second proof uses the property that functions transforming according

to different representation are orthogonal (cf. H64*a*, Sec. 3–15) and that the function $\phi_\alpha = H\psi_\alpha{}^r$ transforms according to the same representation r as the function $\psi_\alpha{}^r$

$$\left[g_i\phi_\alpha = g_i H\psi_\alpha{}^r = Hg_i\psi_\alpha{}^r = \sum_\beta R^r_{\alpha\beta}(i)\, H\psi_\beta{}^r = \sum_\beta R^r_{\alpha\beta}\phi_\beta\right] \tag{B.8}$$

We see that we have learned a property of the eigenfunctions of H without actually having solved the Schrödinger equation. Properties such as these can be of use, e.g., in telling immediately whether transitions are allowed or forbidden (see discussion of inner product in Appendix C).

The knowledge of the transformation properties of the eigenfunctions of H is also of use in actually finding approximations to the eigenfunctions in terms of a given finite set of states, e.g., those with a given number of quanta in the oscillator shell model. If we divide the basic set of states ψ into sets each of which transform according to a represention r of G and if we collect together sets transforming in a similar way, then the energy matrix of H will have the form shown in Fig. B.1. The matrix elements of the off-diagonal matrices are zero because of Eq. (B.6). (For an *assumed* invariant group the size of the off-diagonal matrices is a measure of the goodness of the assumption.) Clearly Fig. B.1 shows that the diagonalization of the energy matrix has been partially done. It is only necessary now to diagonalize each submatrix M_i separately. This one may hope to do by seeking further groups G' under which H is invariant but which transform only between the states which belong to the same representation r of G. To respect the latter restriction one seeks chains of subgroups $G_1G_2G_3 \ldots$ such that G_{i+1} is a subgroup of G_i. Pertinent to this discussion is the classification of nuclear states according to R_3 and R_2, which is discussed in Part 2.

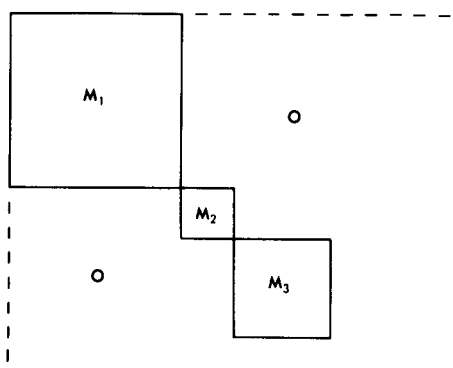

Fig. B.1. A reduced matrix consisting of uncoupled submatrices M_1, M_2, etc.

Actually the classification according to R_3 and R_2 is not sufficient to diagonalize completely the general energy matrix in the nuclear shell model and, as discussed in Part 2, several other groups have been proposed. Of importance to the present work are the symmetric group, the group of unitary transformations U_s between s single-particle states, and the group U_3 of unitary transformation between the oscillator quanta in three dimensions.

APPENDIX C—THE SYMMETRIC AND UNITARY GROUPS

Much has already been written on the symmetric and unitary groups and on their application to physical problems (S63, H64*a*). In this appendix we restrict ourselves to establishing notation and reviewing some of the fundamental concepts referred to in the text.

In the whole of this appendix it is assumed that we are given the set of d functions of k particles distributed over s single-particle orbits. Thus, if there are $s = 6$ orbits, denoted by ϕ_i ($i = 1, 2,..., 6$) and $k = 2$ particles, the $d = 36$ ($=s^k$) functions can be written

$$\phi_i(1)\,\phi_j(2) \qquad i, j = 1, 2,..., 6 \tag{C.1}$$

Classification According to S_k

The set of all $k!$ permutations of k objects form a group (cf. Appendix B) called the symmetric group and denoted here by the symbol S_k. The problem we consider the subdivision of the set of d functions so that the permutations of the group S_k transform within the smallest set possible, i.e., we wish to study the irreducible representation of S_k.

When $k = 2$, the group S_k has just two elements, the identity I and the transposition P_{12}. It is clear that, if the 36 functions of Eq. (C.1) are divided into the two sets $\mathscr{S}$ and $\mathscr{A}$ containing elements

$$\psi_{ij}^{\mathscr{S}} = \phi_i(1)\,\phi_j(2) + \phi_i(2)\,\phi_j(1)$$

and (C.2)

$$\psi_{ij}^{\mathscr{A}} = \phi_i(1)\,\phi_j(2) - \phi_i(2)\,\phi_j(1)$$

then neither of the elements of S_2 will transform from the set $\mathscr{A}$ to the set $\mathscr{S}$. In fact each of the states $\psi_{ij}^{\mathscr{S}}$ and $\psi_{ij}^{\mathscr{A}}$ transform to themselves within a factor of ± 1. Thus we say that the 21 states like $\psi_{ij}^{\mathscr{S}}$ all transform in the same way as the *one*-dimensional *symmetric* representation of S_2; the 15 states like $\psi_{ij}^{\mathscr{A}}$ all transform like the *one*-dimensional *antisymmetric* representation.

In this example for S_2 there are only two irreducible representations. For $k \neq 2$ it is natural for us to ask how the complete set of s^k functions

can be subdivided into irreducible sets, how many irreducible sets there will be, and what their dimensions will be. The problem of the number of irreducible sets in existence is known to be the same as the number of partitions $[f_1 f_2 \cdots]$ of k into integral parts f_i such that $f_1 \geqslant f_2 \geqslant \cdots$, etc., with $f_1 + f_2 + \cdots$, etc., $= k$. The partition $[f_1 f_2 \cdots]$ we shall here simply denote by $[f]$. It can be used to *label* the representations. The partition $[f]$ can be illustrated by a Young pattern in which there are f_i squares in the ith row. For example, the partition [432] has the Young pattern

$$[432] \equiv \tag{C.3}$$

The *dimension* of the representation is given simply by the number of ways the numbers $1, 2, \ldots, k$ can be placed into the squares of the Young pattern so that they form an increasing sequence in both rows and columns. This set of numbered patterns can be used to label the various functions of an irreducible representation. Thus in the example for S_2 there are just two one-dimensional irreducible representations

$$[2] \equiv \qquad \text{and} \qquad [11] \equiv \tag{C.4}$$

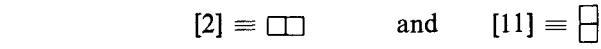

For three particles there are in general three tableaux

$$[3] \equiv \qquad\qquad [111] \equiv \tag{C.5a}$$

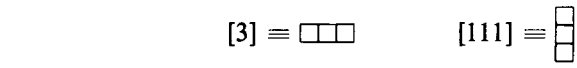

and

$$[21] = \tag{C.5b}$$

The representation in Eq. (C.5a) are both one-dimensional, while that in Eq. (C.5b) has two dimensions. Note that, if there are only $s = 2$ orbits, it is not *possible* to form a totally antisymmetric state of more than three particles, i.e., the partition [111] does not exist; for $s > 2$ the three partitions in Eq. (C.5) are the *only* ones that exist.

The general ways of constructing states from the basic $d = s^k$ set which have a definite symmetry are well known (see discussion on Young operators in Reference H64*a*, Sec. 7.10). In practice we can often construct states having the required symmetry by other means, so we shall not discuss this branch of the subject.

Classification According to U_s

The set of all unitary transformations between the s single-particle orbits forms the unitary group U_s of dimension s. These transformations induce corresponding transformations $\{U_s = \sum_{\alpha=1}^{k} U_s(i)\}$ between the $d = s^k$ functions of k particles in s orbits. The problem now is the subdivision of the set of $d = s^k$ functions so that transformations of U_s act between the smallest sets possible, i.e., we wish to construct irreducible sets. This problem is actually related to the classification according to S_k. Suppose the $d = s^k$ functions are defined so that each belongs to a definite symmetry $[f]$ with respect to S_k. Since the transformation U_s is symmetric (invariant) with respect to S_k, it cannot change the symmetry label of a function $\psi[f]$). Thus the transformations of U_s only act within the states of the same symmetry. Actually the transformation of U_s will only operate between functions $\psi([f]\,\alpha)$ belonging to the same particular row α (or numbered Young pattern) of the representation $[f]$, and these functions form an irreducible set. In the set of functions defined in Eq. (C.2) (with $s = 6$. $k = 2$), the transformations of U_2 will only operate within the set of states $\psi^{\mathscr{S}}$ or $\psi^{\mathscr{A}}$ but not between the two.

If $\psi([f]\,\alpha i)$ is a function (say, one of the $\psi^{\mathscr{S}}$ states in Eq. C.2) transforming according to the α row of the $[f]$ representation of S_k and it transforms under an element U of U_s as

$$U\psi([f]\,\alpha i) = \sum_j u_{ij}\psi([f]\,\alpha j) \tag{C.6}$$

then the functions $\psi([f]\,\alpha' i) = P\psi([f]\,\alpha i)$, with P a permutation of S_k, will transform under the operation U in *exactly the same way* because of the invariance of U_s with respect to S_k (i.e., $UP = PU$). Thus the transformation properties of the state $\psi([f]\,\alpha i)$ under U_s is *independent* of α. It can thus be concluded that for the irreducible representation label for U_s we may simply use the label $[f]$ of S_k.

The dimension of the representation $[f]$ of U_s is of course not the same as the dimension of $[f]$ of S_k; the representations are made up from different basis states. Weyl has given a general formula [W28, p. 383 also H64*a*, Eq. (10-25) and Sec. 10-4] for the dimension $[f]$ of U_s, which can be written

$$d([f]\,U_s) = \prod_{1 \leqslant i < j \leqslant s} \frac{(f_i - f_j + j - i)}{j - i} \tag{C.7}$$

In the example of $s = 6$, $[f] = [2]$ or $[11]$ and

$$d([2]\,U_6) = 21$$
$$d([11]\,U_6) = 15$$

Outer Product

Suppose we are given a set of d states $\psi([f]\,\alpha)$, where $\alpha = 1,\ldots, d$ of k particles in s orbits which transform between themselves according to the αth row of the d-dimensional representation $[f]$ of S_k. Here $[f]$ will be a Young tableau with k squares and at most s rows. Suppose that $\psi[[f']\,\alpha']$ ($\alpha' = 1, 2,\ldots, d'$) are states of *another* set of k' particles transforming according to the $[f']$ representation of $S_{k'}$, where $[f']$ has k' squares. The set of product states $\psi([f]\,\alpha)\,\psi([f']\,\alpha')$ will transform between themselves according to the group $S_{k+k'}$, if we allow for permutations between the two sets k and k', and therefore form the basis for a representation; this representation is not necessarily irreducible however. We are here dealing with the *outer product* representation (symbol $\otimes$) of the two representations $[f]$ and $[f']$, which have to be revolved into irreducible representations of $S_{k+k'}$ (H64*a*, Sec. 7-12).

The total number of functions in the outer product representation $[f] \otimes [f']$ of $S_{k+k'}$ is the product of the number of ways of dividing $k + k'$ particles into two parts having k and k' particles, respectively (i.e., $C_{kk'} = (k + k')!/k!k'!$), with the number of possible functions $\psi[f]$ and $\psi[f']$ of the respective parts, i.e., d and d'. Then the total number of states is

$$d([f] \otimes [f']) = \frac{(k + k')!}{k!\,k'!}\,dd' \tag{C.8}$$

The outer product must now be resolved into irreducible representations $[f'']$ of $S_{k+k'}$, which we write schematically by the equation

$$[f] \otimes [f'] = \sum_{f''} n_{f''}\,[f''] \tag{C.9}$$

where $n_{f''}$ is an integer giving the number of times the representation $[f'']$ appears in the resolution.

Rules for generating the representation $[f'']$ are given, e.g., by Hammermesh (H64*a*, Sec. 7.12) and simply involve the addition of the squares $[f']$ to those of $[f]$, preserving the symmetry of both in the final tableau $[f'']$; this can be achieved by putting the number i in all the squares of the ith row in $[f']$ and only constructing tableau $[f'']$, in which the same number does not occur in the same column. To illustrate this process, if

$$[f] = \begin{array}{|c|c|c|}\hline & & \\ \hline \\ \cline{1-1}\end{array} = [31]$$

and

$$[f'] = \begin{array}{|c|c|}\hline 1 & 1 \\ \hline\end{array} = [2]$$

then

$[f] \otimes [f'] =$ 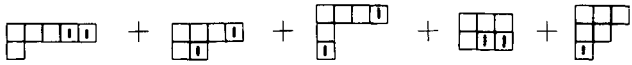

$$= [51] + [42] + [411] + [33] + [321] \tag{C.10}$$

A check can now be placed on this procedure by comparing the dimensions on both sides. Thus the total dimension of $[f] \otimes [f']$ from Eq. (C.8) is 45. The dimension of the right hand side of Eq. (C.10) is just the sum of the dimensions of each representation, i.e., $5 + 9 + 10 + 5 + 16 = 45$.

The concept of the outer product has been used in Section 3.4 in deducing the simultaneous symmetries of functions according to the group S_k (or U_s) and U_3.

Inner Product

If a set of functions $\psi([f]\,\alpha)$ ($\alpha = 1, 2,..., d$) of k particles transform according to the α row of the $[f]$ representation of S_k and likewise the functions $\psi([f']\,\alpha')$ of the *same* k particles transform according to the α' row of the $[f']$ representation, then the functions

$$\phi = \psi([f]\,\alpha) \cdot \psi([f']\,\alpha')$$

will in general transform according to the mixed representations of S_k present in the *inner product* (symbol $\times$) of $[f]$ and $[f']$

$$[f] \times [f'] = \sum_{f''} n_{f''}\,[f''] \tag{C.11}$$

Here the integer $n_{f''}$ is the number of times the representation $[f'']$ appears in the inner product $[f] \times [f']$.

An example of the use of this concept is found in the Wigner supermultiplet theory (W37 and H64*a*, Sec. 11-7), where the complete antisymmetric nuclear wave function of k particles is made up of an orbital function $\psi([f]\,\alpha)$ with symmetry $[f]$ of S_k and a charge-spin function $\Gamma([\tilde{f}]\,\tilde{\alpha})$ of the same k particles with symmetry $[\tilde{f}]$. General rules for giving the representations resulting from the inner product (H64*a*, Chap. 7) show that the totally antisymmetric representation of S_k *only* appears in the inner product $[f] \times [f']$ if $[f']$ is the adjoint of $[f]$ (written $[f'] = [\tilde{f}]$ with the definition that the number of squares in the ith row of $[f]$ is equal to the number in the ith column of $[\tilde{f}]$). Thus, since the total nuclear states are antisymmetric (to describe the Fermi character of the nucleons), the symmetry

of the orbital and charge-spin functions must be adjoint. As indicated in Eq. (C.11), a simple product of an orbital function $\psi([f]\,\alpha)$ with a charge-spin function $\Gamma([\tilde{f}]\,\tilde{\alpha})$ is not sufficient to give a totally antisymmetric state. This state is only formed from a sum over the row labels α with appropriate coefficients

$$\Psi([f]) = \sum_{\alpha(\tilde{\alpha})} c([f]\,\alpha\tilde{\alpha})\{\psi([f]\,\alpha)\,\Gamma([\tilde{f}]\,\tilde{\alpha})\} \tag{C.12}$$

It is usual to label the complete antisymmetric state Ψ with the symmetry of its orbital part.

Another use of the concepts of *inner* product is to be found when considering transition probabilities. Suppose that a transition *operator* $T([f']\,\alpha')$ belongs to the α' row of the $[f']$ representation of S_k in orbital space. Then the transition from a state $\Psi([f])$ to a state $\Psi([f'']$ will only exist if there is nonzero overlap between $\Psi[f'']$ and the state

$$\phi = T([f']\,\alpha')\,\Psi([f]) \tag{C.13}$$

The state ϕ transforms according to the mixed symmetries of the *inner* product $[f'] \times [f]$. Because of the orthogonality of functions belonging to different representation (H64*a*, Sec. 3-15), it follows that a transition to a state of symmetry $[f'']$ will be allowed *only* if this symmetry occurs in the inner product $[f'] \times [f]$. If the transition is allowed, then it is proportional to a generalized concept of the Clebsch–Gordan coefficient in angular momentum theory, written $([f]\,[f'] \mid [f''])$.

Thus one has a powerful tool for deciding on the allowed and forbidden transitions without any numerical calculation.

The relationship between the classification of the groups S_k and U_s allows one to carry the concept of inner product from one to the other.

For the calculation of inner product we refer the reader to Hammermesh (H64*a*, Chap. 7.13). Clebsch–Gordan coefficients for the SU_3 group in the classification $SU_3 \rightarrow SU_2 \times U_1$ have been considered by Hecht (H65). Clebsch–Gordan coefficients for the SU_3 group in the $SU_3 \rightarrow R_3$ classification have been considered in References H64*e*, E65*a*, A67, I67, S67, and V67.

APPENDIX D—GENERATING OPERATORS OF U_s

In this approach to generating operators we follow Bayman (B60*b*, p. 178).

If a matrix U is unitary, then it can be diagonalized by means of a unitary matrix S and its eigenvalues will be of unit modulus. Thus *any* unitary matrix can be written

$$U = S \begin{bmatrix} e^{i\phi_1} & & & \\ & e^{i\phi_2} & & \\ & & \ddots & \\ & & & e^{i\phi_s} \end{bmatrix} S^{-1}$$

$$= S \left\{ \sum_n \frac{1}{n!} \begin{bmatrix} i\phi_1 & & & \\ & i\phi_2 & & \\ & & \ddots & \\ & & & i\phi_s \end{bmatrix}^n \right\} S^{-1}$$

$$= \sum_n \frac{1}{n!} \left\{ iS \begin{bmatrix} \phi_1 & & & \\ & \phi_2 & & \\ & & \ddots & \\ & & & \phi_s \end{bmatrix} S^{-1} \right\}^n$$

$$= \exp \left\{ iS \begin{bmatrix} \phi_1 & & & \\ & \phi_2 & & \\ & & \ddots & \\ & & & \phi_s \end{bmatrix} S^{-1} \right\} \tag{D.1}$$

Since S is unitary and the real diagonal matrix $[\phi_1 \cdots \phi_s]$ is Hermitian, it follows that the matrix

$$S \begin{bmatrix} \phi_1 & & \\ & \ddots & \\ & & \phi_s \end{bmatrix} S^{-1} = H \tag{D.2}$$

where H is an Hermitian matrix. Thus any matrix U can be written in terms of an Hermitian matrix.

$$U = \exp\{iH\} \tag{D.3}$$

The matrix H is as yet undetermined by U since $e^{i\phi_\alpha}$ is undetermined by ϕ_α. However, if we specify that $0 \leqslant \phi_\alpha \leqslant 2\pi$, there will be a one-to-one correspondence between the matrices U and H.

Clearly the Hermitian null matrix corresponds to the unitary matrix I. Any unitary transformation differing from I by a small amount can be written

as a Hermitian matrix with small elements; thus, in this case we can expand the exponential in Eq. (D.3) and write

$$U \approx I + iH \qquad \text{for small matrix elements of } H. \tag{D.4}$$

Thus the H can be considered the first-order infinitesimal changes to the unit matrix I leading to a unitary matrix U. Actually there is little need to use the approximate Eq. (D.4) in defining H when we have the exact Eq. (D.3).

The Hermitian matrices H can themselves be written as a linearly independent set of s^2 Hermitian matrices

$$G_{ij}^{\pm} = (E_{ij} + E_{ji}) \pm i(E_{ij} - E_{ji}) \tag{D.5}$$

where E_{ij} is a matrix with a single one in the ijth element. [We sometimes refer to the E_{ij} as shift operators since the result of operating on a column vector with a one in the jth position is to shift the one to the ith position.]

Thus

$$U = \exp i \left\{\sum_{\alpha} C_{\alpha} G_{\alpha}\right\} \tag{D.6}$$

with the G_{α} defined in Eq. (D.5). The operators (matrices) G are known as the *generating operators* of the group U_s or, in view of Eq. (D.4), as the *infinitesimal operators.*

The (group) property (cf. Appendix B) that the *product* of two unitary matrices is a unitary matrix implies that the *commutators* of the generating matrices G are expandable in terms of generating matrices. Alternatively, if the members of a subset of the generating matrix G commute among themselves, then the unitary matrices based on this set form a group. Thus, when looking for subgroups of the infinite set of unitary matrices of U_s, it is easier to consider only the finite s^2 set of generating matrices G and their commutation relations.

If the unitary matrix U is supposed to operate in the space of k particles, then

$$\begin{aligned} U &= U(1)\, U(2) \cdots U(k) \\ &= \exp i \left\{\sum_{\alpha} c_{\alpha} G_{\alpha}(i)\right\} \exp i \left\{\sum_{\alpha} c_{\alpha} G_{\alpha}(2)\right\} \cdots \exp i \left\{\sum_{\alpha} c_{\alpha} G_{\alpha}(k)\right\} \\ &= \exp i \left\{\sum_{\alpha} c_{\alpha} [G_{\alpha}^{(1)} + G^{(2)} + \cdots + G_{\alpha}(k)]\right\} \end{aligned}$$

the last line following from the fact that generating operators G of different particles commute. Thus the generating operators of the unitary trans-

formation in the states of k particles are symmetric functions of the particle numbers.

APPENDIX E—CLASSIFICATION ACCORDING TO SU_3 WITHOUT THE HARMONIC OSCILLATOR

In the main text the emphasis has been placed on using harmonic oscillator functions and on classifying states according to their quantum symmetry. The reason for this is simply that most applications of the classification scheme have been made in this way. Actually the classification according to SU_3 can exist even if the basic sets of states do not have the radial functions of the harmonic oscillator.

The complete set of unitary transformations U_s between s states $|\alpha\rangle$ can be written (cf. Appendix D) in terms of s^2 generating Hermitian matrices or in terms of the s^2 shift operators $E_{\alpha\beta}$, where

$$E_{\alpha\beta}|\gamma\rangle = \delta_{\beta\gamma}|\alpha\rangle \tag{E.1}$$

From this definition it can be seen in general that the commutators of the shift operator are

$$[E_{\alpha\beta}, E_{\gamma\delta}] = E_{\alpha\delta}\,\delta_{\beta\gamma} - E_{\gamma\beta}\,\delta_{\alpha\delta} \tag{E.2}$$

If each state $|\alpha\rangle$ has angular momentum l_α and projection m_α, then an equivalent set of tensor, shift operators can be defined (following Racah, R42, and Elliott, E58)

$$U_q^{\,t}(l_\alpha l_\beta) = \sqrt{\frac{1}{2l_\alpha + 1}} \sum_{m_\alpha(m_\beta)} (l_\beta t m_\beta q \mid l_\alpha m_\alpha)\, E^{l_\alpha l_\beta}_{m_\alpha m_\beta} \tag{E.3}$$

where $(\cdots \mid \cdot\cdot)$ is an R_3-group, vector-coupling coefficient. The commutators of the set in Eq. (E.3) can be derived from Eq. (E.2) and have been given by Elliott (E58) in the form

$$\begin{aligned}[U_q^{\,t}(ll'), U_p^{\,s}(kk')] = \sum_{r\nu} &\sqrt{2r+1}\,(tsqp \mid r\nu) \\ &\times \{(-)^{t+s-r}\,\delta(l'k)\,W(tslk' : rl')\,U_\nu^{\,r}(lk') \\ &\quad - \delta(lk')\,W(tsl'k : rk')\,U_\nu^{\,r}(kl')\}\end{aligned} \tag{E.4}$$

where W is a Racah function.

As discussed in Appendix D, subgroups of the full unitary group U_s can be found by seeking the subsets of the shift operators which are closed

under the commutation relations. This general procedure has been discussed by Elliott (E.58). In particular the set of three operators

$$L_q = \sum_l \{l(l+1)(2l+1)\}^{1/2}\, U_q^1(ll) \tag{E.5}$$

are tensors of rank one and have the properties of the orbital angular momentum operators; they are therefore the appropriate operators for the subgroup R_3 of U_s.

If the set of s orbits has $l = n, n-2, \ldots, 0$ or 1, then the three operators L_q, together with the five operators of second rank

$$Q_q = \sum_l -(2n+3)\left\{\frac{l(l+1)(2l+1)}{(2l-1)(2l+3)}\right\}^{1/2} U_q^2(ll)$$
$$+ \left\{\frac{6(l+1)(l+2)(n-l)(n+l+3)}{(2l+3)}\right\}^{1/2} \{U_q^2(l, l+2) + U_q^2(l+2, l)\} \tag{E.6}$$

form a subgroup SU_3 of U_s. Notice that in the definitions of the operators no reference has been made at all to radial functions. If the radial functions happen to be those of the harmonic oscillator, then the operators Q_q have the explicit form of Eq. (3.13).

APPENDIX F—RAISING AND LOWERING OPERATORS OF THE GROUP SU_3

For the group R_3, any function $|JM\rangle$ of the representation J can be generated from the state of maximum weight $|JM = J\rangle$ of the same representation by suitable operator of the *lowering* operator J_{-1} of R_3. Thus

$$N(J, M)|JM\rangle = J_{-1}^{J-M}\,|JM = J\rangle$$

where

$$N(JM) = \prod_{K=J}^{M+1} \{\tfrac{1}{2}(J+K)(J-K+1)\}^{1/2} \qquad M \neq J$$
$$N(JJ) = 1 \tag{F.1}$$

The operator J_{+1} can be referred to as a raising operator of R_3.

In an analogous way the operators $\omega_{\pm 1}$ of Eq. (3.24) are the raising and

lowering operators for the quantum number ν in a representation Λ of the SU_2 subgroup of SU_3:

$$\omega_{\pm 1}(\phi(\lambda\mu)\,\epsilon\Lambda\nu) = \mp\sqrt{\frac{1}{2}}\sqrt{\left(\Lambda \mp \frac{\nu}{2}\right)\left(\Lambda \pm \frac{\nu}{2} + 1\right)}\,\phi((\lambda\mu)\,\epsilon\Lambda\nu \pm 2) \tag{F.2}$$

We have included in the function ϕ above the representation labels $\lambda\mu$ of SU_3 and ϵ of U_1 to emphasize that the operators $\omega_{\pm 1}$ do not change their values.

In the array below (Eq. F.3) we show the values of 2Λ that a state can possess (in general) with a definite ϵ (deduced from Eq. 3.27 and 3.28). Of course parts of the array may be missing.

$$\begin{array}{cc} \underline{\epsilon} & \underline{2\Lambda} \\ 2\lambda + \mu & \mu \\ 2\lambda + \mu - 3 & (\mu - 1)\,(\mu + 1) \\ 2\lambda + \mu - 6 & (\mu - 2)\,\mu\,(\mu + 2) \\ 2\lambda + \mu - 9 & (\mu - 3)\,(\mu - 1)\,(\mu + 1)\,(\mu + 3) \\ & \ldots, \text{etc.} \end{array} \tag{F.3}$$

It is clear from this array that operators which change ϵ must simultaneously change 2Λ and also, possibly, ν ($\nu = 2\Lambda, 2\Lambda - 1, \ldots, -2\Lambda$). This leads to a certain complexity and ambiguity in the construction of the raising and lowering operators for SU_3. In general the raising and lowering operators cannot be written simply in terms of linear operators. We quote below a set of raising and lowering operators which are certainly adequate for our present purposes (H61):

$$[A_{yx}A_{xz} + (\Lambda - \tfrac{1}{2}\nu)\,A_{yz}]\,\phi(\epsilon\Lambda\nu) = \phi'(\epsilon - 3, \Lambda + \tfrac{1}{2}, \nu - 1) \tag{F.4a}$$
$$[A_{yx}A_{xz} - (\Lambda + \tfrac{1}{2}\nu + 1)\,A_{yz}]\,\phi(\epsilon\Lambda\nu) = \phi'(\epsilon - 3, \Lambda - \tfrac{1}{2}, \nu - 1) \tag{F.4b}$$
$$[A_{xy}A_{yz} - (\Lambda + \tfrac{1}{2}\nu)\,A_{xz}]\,\phi(\epsilon\Lambda\nu) = \phi'(\epsilon - 3, \Lambda + \tfrac{1}{2}, \nu + 1) \tag{F.4c}$$
$$[A_{xy}A_{yz} - (\Lambda - \tfrac{1}{2}\nu + 1)\,A_{xz}]\,\phi(\epsilon\Lambda\nu) = \phi'(\epsilon - 3, \Lambda - \tfrac{1}{2}, \nu + 1) \tag{F.4d}$$

$$[A_{zx}A_{xy} + (\Lambda - \tfrac{1}{2}\nu)\,A_{zy}]\,\phi(\epsilon\Lambda\nu) = \phi'(\epsilon + 3, \Lambda + \tfrac{1}{2}, \nu + 1) \tag{F.5a}$$
$$[A_{zx}A_{xy} - (\Lambda + \tfrac{1}{2}\nu + 1)\,A_{zy}]\,\phi(\epsilon\Lambda\nu) = \phi'(\epsilon + 3, \Lambda + \tfrac{1}{2}, \nu + 1) \tag{F.5b}$$
$$[A_{zy}A_{yx} + (\Lambda + \tfrac{1}{2}\nu)\,A_{zx}]\,\phi(\epsilon\Lambda\nu) = \phi'(\epsilon + 3, \Lambda - \tfrac{1}{2}, \nu - 1) \tag{F.5c}$$
$$[A_{zy}A_{yx} - (\Lambda - \tfrac{1}{2}\nu + 1)\,A_{zx}]\,\phi(\epsilon\Lambda\nu) = \phi'(\epsilon + 3, \Lambda + \tfrac{1}{2}, \nu - 1) \tag{F.5d}$$

By the function ϕ' is implied an unnormalized state. The representation label

$\lambda\mu$ is understood. The above properties of the operators in Eqs. (F.4) and (F.5) can be checked by calculating the commutators with

$$Q_0 = 2A_{zz} - A_{xx} - A_{yy} \tag{F.6a}$$

$$\omega^2 = \omega_0{}^2 - \omega_{+1}\omega_{-1} - \omega_{-1}\omega_{+1} \tag{F.6b}$$

and

$$\omega_0 = \tfrac{1}{2}(A_{xx} - A_{yy}) \tag{F.6c}$$

since these operators are diagonal in the $\epsilon\Lambda\nu$ representation (cf. Section 3.5).

In the practical use of the raising and lowering operators it is necessary to construct operators which will generate any function $\phi(\epsilon\Lambda\nu)$ from the function of maximum weight[1] $\phi(\lambda\mu)$. It is possible to do this using only three of the raising and lowering operators.

Note first that, if the state $\phi(\epsilon\Lambda\nu = 2\Lambda)$ can be constructed, then any state $\phi(\epsilon\Lambda\nu)$ can be generated with the lowering operator ω_{-1} of the SU_2 subgroup. Any function $\phi(\epsilon\Lambda_{\max}\nu = 2\Lambda_{\max})$ can be generated from the state of maximum weight by the appropriate numbers of applications of the operator in Eq. (F.4c). This operator can be written

$$E_+ \approx A_{yz}A_{xy} - (\Lambda + \tfrac{1}{2}\nu - 1)\, A_{xz} \tag{F.7}$$

On any state with $\nu = 2\Lambda$, the first term of E_+ gives zero contribution

$$[A_{xy}\phi(\Lambda\nu = 2\Lambda) \approx \omega_{+1}\phi(\Lambda\nu = 2\Lambda) = 0] \tag{F.8}$$

Thus any function $\phi(\epsilon\Lambda_{\max}\nu = 2\Lambda_{\max})$ can be generated from the state of maximum weight by the appropriate number of applications (H61) alone of

$$E_+ = A_{xz} \tag{F.9}$$

On any state $\phi(\epsilon\Lambda\nu = 2\Lambda)$ the function $\phi'(\epsilon - 3, \Lambda - \tfrac{1}{2}, \nu = 2\Lambda - 1)$ can be generated with the application of the operator in Eq. (F.4b), which can be written, in this case, in the complete operator form

$$E_- = [A_{yx}A_{xz} - A_{yz}(2\omega_0 - 1)] \tag{F.10}$$

Using the operators in Eqs. (F.2), (F.7), and (F.10), a general state $\phi(\epsilon\Lambda\nu)$ within the representation $\lambda\mu$ of SU_3 can be written (H61)

$$\begin{aligned}\phi(\epsilon\Lambda\nu) &= N(pqr)\,\omega_{-1}^{r}E_-{}^{q}E_+{}^{p}\phi(\lambda\mu)\\ &= F(\epsilon\Lambda\nu)\,\phi(\lambda\mu)\end{aligned} \tag{F.11}$$

[1] For a definition of maximum weight, see discussions preceding Eq. (3.38a) and (3.38b).

Equivalents operator changing ϵ by 0 and 6 [taken from Ref. H61*a* and E63*b*]

$$F(\lambda\mu\epsilon\Lambda\nu;\mathbf{L}) = \tfrac{1}{2}N\sum_i L_0^{2i}\{A_i + B_iL^2 + C_i(L_{+1}^2 + L_{-1}^2) + D_iL_0(L_{+1}^2 - L_{-1}^2)\}$$

WHERE $3(p+q) = 2\lambda + \mu - \epsilon$, $(p-q) = 2\Lambda - \mu$, $2r = 2\Lambda - \nu$

rqp	i	A_i	B_i	C_i	D_i
200	0	2μ	—	—	—
	1	-2	—	—	—
400	0	$6\mu(\mu-2)$	—	—	—
	1	$-4(3\mu-4)$	—	—	—
	2	2	—	—	—
002	0	2λ	-1	1	—
	1	1	—	—	—
202	0	$2\lambda(\mu+2)$	$-(\mu+2)$	$(\mu+2)$	—
	1	$\mu+2-2\lambda$	1	-1	—
	2	-1	—	—	—
402	0	$6\lambda\mu(\mu+2)$	$-3\mu(\mu+2)$	$3\mu(\mu+2)$	—
	1	$3\mu^2+6\mu-12\lambda\mu-8\lambda$	$2(3\mu+2)$	$-2(3\mu+2)$	—
	2	$2(\lambda-3\mu-2)$	-1	1	—
	3	1	—	—	—
111	0	—	—	—	$(\mu+2)$
	1	$-(2\lambda+\mu+2)$	1	-1	—
	2	-1	—	—	—
311	0	—	—	—	$(\mu+2)(3\mu-2)$
	1	$(2\lambda+\mu+2)(2-3\mu)$	$(3\mu-2)$	$(2-3\mu)$	$-(\mu+2)$
	2	$2(\lambda-\mu+2)$	-1	1	—
	3	1	—	—	—
020	0	$2\mu^2(\lambda+\mu+1)$	$-\mu^2$	$-\mu(\mu+2)$	$2(\mu+1)$
	1	$-(2\lambda+2\mu-\mu^2+2)$	1	-1	—
	2	-1	—	—	—
220	0	$2\mu^2(\mu-2)(\lambda+\mu+1)$	$-\mu^2(\mu-2)$	$-\mu(\mu-2)(\mu+2)$	$2(\mu+1)(\mu-2)$
	1	$-(2\lambda+\mu)(\mu-1)(\mu+2)$ $-5\mu^2+4$	$(\mu-1)(\mu+2)$	$(\mu^2+\mu+2)$	$-2(\mu+1)$
	2	$2\lambda+\mu+4-\mu^2$	-1	1	—
	3	1	—	—	—

where

$$\epsilon = 2\lambda + \mu - 3(p + q)$$
$$2\Lambda = \mu + p - q$$
$$\nu = \mu + p - q - 2r$$

and the normalization coefficient is found to be

$$N(pqr) = \left\{\frac{\lambda!\,\mu!\,p!\,q!\,r!\,(\mu + p + 1)!\,(\lambda + \mu + 1)!}{2^r(\lambda - p)!\,(\mu - q)!\,(\lambda + \mu - q + 1)!\,(\mu + p - q - r)!\,(\mu + p - q + 1)}\right\}^{-1/2} \tag{F.12}$$

Equivalent Operators

Of the eight shift operators of SU_3 operating on the state of maximum weight, two are diagonal (Q_0 and ω_0), three give zero

$$[A_{zx}\phi(\lambda\mu) = A_{zy}\phi(\lambda\mu) = A_{xy}\phi(\lambda\mu) = 0] \tag{F.13}$$

and the remaining three are equivalent to the operation of the orbital angular momentum operators

$$A_{xz}\phi(\lambda\mu) \equiv (A_{xz} - A_{zx})\,\phi(\lambda\mu) = \tfrac{1}{2}(L_{+1} + L_{-1})\,\phi(\lambda\mu) \tag{F.14a}$$
$$A_{yz}\phi(\lambda\mu) \equiv (A_{yz} - A_{zy})\,\phi(\lambda\mu) = -i\tfrac{1}{2}(L_{+1} - L_{-1})\,\phi(\lambda\mu) \tag{F.14b}$$
$$A_{yx}\phi(\lambda\mu) \equiv (A_{yx} - A_{xy})\,\phi(\lambda\mu) = -iL_0\phi(\lambda\mu) \tag{F.14c}$$

These results occur using the results of Eq. (F.13) and Table 3.I. Using the commutation relation it is therefore possible to write *any function* of the shift operators, operating on the state of maximum weight, completely in terms of orbital angular operators. In particular the equivalence of the lowering operators $F(\epsilon\Lambda\nu) \equiv F(\epsilon\Lambda\nu : L)$ can be found. Tables of these equivalences have been given in Reference H61*a*. In table *F.I* we present some equivalences for changes of ϵ by 0 and 6 as given in References H61*a* and E63*b*.

APPENDIX G—CALCULATION OF MATRIX ELEMENTS

The matrix elements between states classified according to SU_3 can be calculated using the standard method of fractional parentage. In this appendix we describe an alternative method designed to make full use of the projection properties of states with definite angular momentum of a representation of

SU_3 and the simplicity of the intrinsic states (H61, E63*b*, B63*a*, H64*d*). We derive the matrix elements for a *general tensor* operator of rank p. For a scalor ($p = 0$) the method is appropriate for calculating matrix elements of the nuclear Hamiltonian.

Consider the operation of a tensor T_r^p on the J-projected wave function

$$\tilde{\Psi}((\lambda\mu)\,\gamma S K_L K J M) = \frac{2J+1}{A((\lambda\mu)\,S K_L K J)} \int \mathscr{D}^J_{MK}(\Omega)\,\Phi(\lambda\mu\gamma S K_S)\,d\Omega \tag{G.1}$$

To simplify the notation below we shall use the symbol α to describe the symmetry given above by $(\lambda\mu)\,\gamma S$. Using the rotation properties of tensor operators (E57*a*) we have

$$T_q^p\tilde{\Psi}(\alpha K_L K J M) = \frac{2J+1}{A(\alpha K_L K J)} \sum_q \int \mathscr{D}^J_{MK}(\Omega)\,\mathscr{D}^p_{rq}(\Omega)\,T_q^p(\Omega)\,\Phi(\alpha K_S)\,d\Omega \tag{G.2}$$

where now $T_q^p(\Omega)$ operates on the intrinsic function ϕ in the rotated frame Ω. Expanding this operation in terms of the complete set of *all* states in the intrinsic frame:

$$T_q^p\Phi(\alpha K_S) = \sum_{\alpha' K_S'' \epsilon' \Lambda' \nu'} h(pq;\alpha K_S, \alpha' K_S'', \epsilon'\Lambda'\nu')\,\Phi(\alpha' K_S'' \epsilon' \Lambda' \nu') \tag{G.3}$$

where, because of orthonormality,

$$h(pq;\alpha K_S, \alpha' K_S'' \epsilon' \Lambda' \nu') = \langle \alpha' K_S'' \epsilon' \Lambda' \nu' \mid T_q^p \mid \alpha K_S \rangle \tag{G.4}$$

and $\epsilon'\Lambda'\nu'$ are the U_1 and SU_2 labels within the representation $\lambda'\mu'$, the labels of which have been absorbed into α'. Making use now of the raising and lowering operators of SU_3 and their equivalences when operating on a state of maximum weight, Eq. (G.3) can be written

$$T_q^p\Phi(\alpha K_S) = \sum_{\alpha' K_S''} G(pq;\alpha K_S, \alpha' K_S'', L)\,\Phi(\alpha' K_S'') \tag{G.5}$$

where we define the *function* of orbital angular momentum operators

$$G(pq;\alpha K_S, \alpha' K_S'', L) = \sum_{\epsilon'\Lambda'\nu'} h(pq;\alpha K_S, \alpha' K_S'' \epsilon' \Lambda' \nu')\,F(\alpha'\epsilon'\Lambda'\nu'; L) \tag{G.6}$$

Expanding $\Phi(\alpha' K_S'')$ in Eq. (G.5) in terms of orbital angular momentum

states[1] $\Psi(\alpha' K_S'' K_L' L' K_L')$ from Eq. (3.38b) and applying the operator G, we have

$$T_q^p \Phi(\alpha K_S) = \sum_{\alpha} \sum_{K_S''} \sum_{K_L' L' K_L''} g(pq; \alpha K_S, \alpha' K_S'', L' K_L' K_L'') \, a(\alpha' K_L' L') \times \Psi(\alpha' K_S'' K_L' L' K_L'') \tag{G.7}$$

where

$$G(\beta L) \, \Psi(K_L' L' K_L') = \sum_{K_L''} g(\beta, L K_L' K_L'') \, \Psi(K_L' L' K_L'') \tag{G.8}$$

with an obvious simplification of notation. Now, however,

$$\begin{aligned} \Psi_\Omega(\alpha' K_S'' K_L' L' K_L'') &= \sum_{J' M''} (L' S' K_L'' K_S'' \mid J' K'') \, \mathscr{D}_{M'' K''}^{J'}(\Omega) \, \overline{\Psi}(\alpha' K_L' L' J' M'') \\ &= \sum_{J' M'' K'} \frac{(2L'+1)}{(2J'+1)} \frac{A(\alpha' K_L' K' J')}{a(\alpha' K_L' L')} (L' S' K_L'' K_S'' \mid J' K'') \\ &\quad \times (L' S' K_L'(K' - K_L') \mid J' K') \times \tilde{\Psi}(\alpha' K_L' K' J' M'') \, \mathscr{D}_{M'' K''}^{*J'}(\Omega) \end{aligned} \tag{G.9}$$

using the properties of the rotation matrix elements and the relation between the L-projected states $\overline{\Psi}$ and J-projected states $\tilde{\Psi}$ from Eq. (3.45).

Substituting Eq. (G.9) in Eq. (G.7) and this in turn in Eq. (G.2), it will be seen that the integration over the Euler angles Ω involves only $\mathscr{D}$ functions and can easily be performed. Thus

$$\begin{aligned} T_r^p \tilde{\Psi}(\alpha K_L K J M) = \sum_{q J' K' K_L' \alpha'} & \frac{(2J+1)}{(2J'+1)} \frac{A(\alpha' K_L' K' J')}{A(\alpha K_L K J)} (J p M r \mid J' M + r) \\ & \times (J p K q \mid J' K + q) \, \tilde{g}(pq; \alpha(K - K_L), \alpha'(K' - K_L') \, J' K' K) \\ & \times \tilde{\Psi}(\alpha' K_L' K' J'(M + r)) \end{aligned} \tag{G.10a}$$

with the definition

$$\begin{aligned} \tilde{g}(pq; \alpha K_S, \alpha' K_S' J' K' K) = \sum_{L' K_L''} & \frac{(2L'+1)}{(2J'+1)} (L' S' K_L'' K_S'' \mid J' K + q) \\ & \times (L' S' K_L' K_S' \mid J' K') \, g(pq; \alpha K_S, \alpha' K_S'' L' K_L' K_L'') \end{aligned} \tag{G.11a}$$

[1] In Eq. (3.38b) the function ψ referred only to an orbital function. By including the charge-spin function Γ (see Eq. 3.42) and antisymmetrizing, however, the expansion of Φ required here involves the same coefficients $a(\lambda\mu K_L L)$ as in the expansion of the orbital function ϕ if ψ is now interpreted as including the charge-spin function.

and

$$K_S'' = K + q - K_L''$$

The summation in Eq. (G.10) involves both positive and negative value of K. Using the relation in Eq. (H.13b) and Eq. (H.13c), we can write Eq. (G.10) in terms of a summation over *positive* and *zero* values of K only

$$T_r^p \tilde{\Psi}(\alpha K_L K J M) = \sum_{qJ'K'K_L'\alpha'}{}' \frac{2J+1}{2J'+1} \frac{A(\alpha' K_L' K' J')}{A(\alpha K_L K J)} (JpMr \mid J'M+r)$$
$$\times (JpKq \mid J'K+q)\, \tilde{g}'(pq; \alpha(K-K_L)\alpha'(K'-K_L')\, J'K'K)$$
$$\times \tilde{\Psi}(\alpha' K_L' K' J' M+r) \qquad \text{(G.10b)}$$

where $\sum'$ implies the sum over values of $K \geqslant 0$ only and

$$\tilde{g}'(pq; \alpha K-K_L \alpha' K'-K_L' J'K'K)$$
$$= \tilde{g}(pq; \alpha K-K_L \alpha' K'-K_L' J'K'K) + (-)^{\lambda'+\mu'+S'+J'-2K'}$$
$$\times \tilde{g}(pq; \alpha K-K_L\,, \alpha'-K'+K_L' J' - K' + K) \qquad \text{for } K' \neq 0 \qquad \text{(G.11b)}$$

and

$$\tilde{g}'(pq; \alpha K-K_L \alpha' K'-K_L' J'K'K)$$
$$\equiv \tilde{g}(pq; \alpha K-K_L \alpha' K'-K_L' J'K'K) \qquad \text{for } K = 0 \qquad \text{(G.11c)}$$

In examining the structure of Eq. (G.10) we first consider the overlaps of functions with respect to K_L and K to be small. From Eq. (G.10), then, the probability for a transition from the state $\tilde{\Psi}(\alpha K_L K J M)$ to $\Psi(\alpha' K_L' K' J' M+c)$ via the operator T_q^p is proportional to the reduced matrix element

$$(\alpha' K_L' K' J' \| T^p \| \alpha K_L K J) = \frac{(2J+1)}{\sqrt{(2J'+1)}} \frac{A(\alpha' K_L' K' J')}{A(\alpha K_L K J)} \sum_q (JpKq \mid J'K+q)$$
$$\times \tilde{g}'(pq; \alpha(K-K_L), \alpha'(K'-K_L')\, J'K'K) \qquad \text{(G.12)}$$

To evaluate this matrix element one needs to know values for the A coefficients (cf. Eq. (3.43) and Appendix H), vector-coupling coefficients, and the $\tilde{g}'$ functions. The last are defined in Eqs. (G.11) in terms of g functions, which are in turn given in Eq. (G.8). The construction of the G operator in Eq. (G.8) is given in Eq. (G.6) in terms of equivalent operators of SU_3 (discussed in Appendix F) and matrix elements h in the intrinsic frame (Eq. G.4). Since there is no vector coupling in the intrinsic frame, these matrix elements h are simply matrix elements between determinantal

states or, at most, a sum over a small number of such matrix elements. Note that the only matrix elements that need to be calculated are those between states $\phi(\alpha' K_s'' \epsilon \Lambda \nu)$ and the *single* state $\phi(\alpha K_s)$, i.e., *only one row* of the matrix of $T_q{}^p$ in the intrinsic frame has to be calculated. Clearly many of these matrix elements are identically zero, e.g., when $T_q{}^p$ is a one body operator and $\phi(\alpha' K_s'' \epsilon \Lambda \nu')$ differs from $\phi(\alpha K_s)$ by more than one particle. In practice actually only very few matrix elements need to be calculated.

This method is fully amenable to use on a computer and has been programmed for the G-20 computer at Chalk River Nuclear Laboratories by Bernier and Harvey (B66*b*).

In the rotational model the J dependence of the reduced matrix element in Eq. (G.12) is described by

$$\sqrt{(2J+1)}\,(JpKK'-K \mid J'K') \tag{G.13a}$$

Clearly Eq. (G.12) will only yield such a relationship if

$$\sqrt{\frac{(2J+1)}{(2J'+1)}}\,\frac{A(\alpha' K_L' K' J')}{A(\alpha K_L K J)}\,\tilde{g}'(pq;\alpha K-K_L\,,\,\alpha'(K'-K_L')\,J'K'K) \tag{G.13b}$$

is proportional to $\delta(K'-K-q)$ and independent of J and J'. This result is by no means obvious and indeed only approximately true in many cases.

Energy Matrix

The formula for these matrix elements (H61, E63*b*) can be deduced from Eq. (G.10) with $p = 0$ (and hence $r = q = 0, J = J'$) and $T_0{}^0 \equiv H$ (the Hamiltonian). Thus

$$H\tilde{\Psi}(\alpha K_L K J M) = \sum_{\alpha' K_L' K'} \frac{A(\alpha' K_L' K' J)}{A(\alpha K_L K J)}\,\tilde{g}'(00;\alpha K_S\,,\,\alpha' K_S' J K' K)\,\tilde{\Psi}(\alpha' K_L' K' J M) \tag{G.14}$$

with $K_S = K - K_L$, etc.

The approximate solution of the Hamiltonian (in terms of the finite set of states $\tilde{\Psi}$) is *not* found simply by diagonalizing the matrix with elements $(\alpha' K_L' K' J M \mid H \mid \alpha K_L K J M)$ because of the nonorthogonality between the functions $\tilde{\Psi}$ with respect to K_L and K. The functions $\tilde{\Psi}$ do define a complete set, however, from which we can deduce that the diagonalization of the nonsymmetric matrix $\tilde{g}'$ actually yields the eigenvalues and vectors, as follows:

Consider a nonnormalized, nonorthogonal complete set of functions $\tilde{\Psi}_\alpha'$, where

$$H\tilde{\Psi}_\alpha' = \sum_\beta \tilde{g}'(\alpha\beta)\,\tilde{\Psi}_\beta' \tag{G.15}$$

If the eigenfunctions of H are expanded in terms of the $\tilde{\Psi}'_\alpha$, we have

$$\chi_i = \sum_\alpha a_{i\alpha}\tilde{\Psi}'_\alpha \qquad \text{with} \qquad H\chi_i = E_i\chi_i \tag{G.16}$$

Thus

$$H\chi_i = \sum_\alpha a_{i\alpha}H\tilde{\Psi}'_\alpha = \sum_{\alpha\beta} a_{i\alpha}\tilde{g}'(\alpha\beta)\,\tilde{\Psi}'_\beta$$
$$= E_i \sum_\beta a_{i\beta}\tilde{\Psi}'_\beta$$

or

$$\sum_\beta \Big(\sum_\alpha a_{i\alpha}\tilde{g}'(\alpha\beta) - E_i a_{i\beta}\Big)\,\tilde{\Psi}'_\beta = 0 \tag{G.17}$$

Since the $\tilde{\Psi}'_\beta$ are supposed to form a linearly independent set,

$$\sum_\alpha a_{i\alpha}\tilde{g}'(\alpha\beta) - E_i a_{i\beta} = 0 \tag{G.18}$$

This is an eigenvalue problem; the eigenvalues of the (nonsymmetric) matrix $\tilde{g}$ are the eigenvalues E_i of H, and the eigenfunctions $a_{i\alpha}$ are the coefficients in the expansion of the eigenfunctions χ_i of H in Eq. (G.16).

The above proof can be applied to the present case if we define non orthogonal, nonnormalized functions

$$\tilde{\Psi}'(\alpha K_L KJM) = A(\alpha K_L KJ)\,\tilde{\Psi}(\alpha K_L KJM) \tag{G.19}$$

If the matrix $\tilde{g}'$ is closely diagonal, the eigenfunctions are given to a good approximation by the functions $\tilde{\Psi}$ and the eigenvalues are approximately

$$(\alpha K_L KJM|\, H\, |\alpha K_L KJM = \tilde{g}'(00;\alpha K_S \alpha K_S JKK) \tag{G.20}$$

These matrix elements have been examined in References H61 and E63*b* for a central force and in H64*b* and W65 for a spin-orbit force.

When $S = 0$, the spin-orbit force can be ignored and the J-projected states $\tilde{\Psi}$ and L-projected states $\bar{\Psi}$ of Eqs. (3.43) and (3.41) are equivalent. In this case the $\tilde{g}'$ functions in Eq. (G.20), as defined in Eq. (G.11), is exactly the function g', where

$$g'(00;\alpha 0, \alpha 0, LK_L K_L) = g(00;\alpha 0\,\alpha 0, LK_L K_L)$$
$$+ (-)^{\lambda+\mu+L}\, g(00;\alpha 0\,\alpha 0, L\,-K_L K_L) \tag{G.21}$$

with the g functions defined in Eq. (G.20). From the structure of the G

operator in Eq. (G.8), using the equivalent operators, it can be shown that $\tilde{g}'$ has the structure

$$\begin{aligned}\tilde{g}'(00;\alpha0\alpha0;JKK) &\equiv g'(00;\alpha0,LK_LK_L)\\ &= a_0 + a_2K_L^2 + a^4K_L^4 + (b_0 + b_2K_L^2)\,L(L+1)\\ &\quad + [\text{smaller terms including those}\\ &\qquad \text{proportional to } L^2(L+1)] \quad K_L \neq 1 \qquad \text{(G.22a)}\end{aligned}$$

For $K_L = 1$, the quadratic terms in the operators L from the equivalent operators of SU_3 lead to a decoupling such that

$$\begin{aligned}\tilde{g}'(00;\alpha0,\alpha0,J11) &\equiv g'(00;\alpha0,\alpha0L11)\\ &= A + B_0(1+\beta(-)^L)\,L(L+1) + (\text{smaller terms})\end{aligned} \qquad \text{(G.22b)}$$

We see from Eq. (G.22a) that, if $\lambda\mu$ and $K_L(\neq 1)$ are good quantum numbers, the energy spectrum will have the familiar rotational form.

When $S \neq 0$ and spin-orbit forces cannot be ignored, there is a competition between the central and spin-orbit forces over the structure of states even within an SU_3 representation. Often it turns out that within a representation of SU_3 the orbital angular momentum quantum is destroyed in favor of the K quantum number defined in the J-projected states. Whether this situation actually occurs in a nucleus is very hard to predict. We note that, if the spin orbit force is strong enough to define the K number, it must not be too strong for the supermultiplet scheme to break down. Discussions of the interplay between the spin-orbit and central forces can be found in References E62, E63*a*, H64*b*, W65, and D67.

E2 Transitions

The electric quadrupole transition operator may be written

$$T_q^2 = \tfrac{1}{2}e(1+2\alpha)\sum_i r_i^2 Y_q^2(\theta_i\phi_i) - \tfrac{1}{2}e\sum_i \tau_z(i)\, r_i^2 Y_q^2(\theta_i\phi_i) \qquad \text{(G.23)}$$

in terms of sums over particle numbers i and the isospin operator τ_z ($\langle\tau_z\rangle = +1$ for neutron and -1 for proton); the parameter α represents an effective charge.

The last term in Eq. (G.23) is a tensor of rank one in isospin space and matrix elements of it can be evaluated in the SU_3 scheme using the methods discussed in this appendix. For transitions, however, between $T = 0$ states (e.g., between low-energy states of doubly even nuclei), the contribution from such a term is zero.

The matrix elements of the first term of Eq. (G.23) can also be found by using the methods of this appendix; however, here there is a great simplification. This term is directly proportional to the quadrupole operator of the group SU_3 from Eq. (3.13)

$$\sum_i r_i^2 Y_q^2 = \frac{b^2}{4}\sqrt{\frac{5}{\pi}}\, Q_q \tag{G.24}$$

A closed expression can be found for the matrix elements of the Q operator between states classified according to SU_3. In the L-projected scheme this takes the form (E58, H61)

$$\begin{aligned} Q_q^2\psi(\alpha K_L LM) = \sum_{L'} \frac{2L+1}{2L'+1} \frac{(L2Mq \mid L'M+q)}{a(\alpha K_L L)} \Big[&(L2K0 \mid L'K)\, a(\alpha KL') \\ &\times \{2\lambda + \mu + \tfrac{1}{2}(L'(L'+1) + 6 - L(L+1))\}\, \Psi(\alpha KL'M) \\ &+ \sum_{\pm} (L2K_L \pm 2 \mid L'K\pm 2)\{\tfrac{3}{2}(\mu \mp K)(\mu \pm K + 2)\}^{1/2} \\ &\times a(\alpha K\pm 2L')\, \Psi(\alpha K\pm 2L'M) \end{aligned} \tag{G.25}$$

The expression in Eq. (G.25) is applicable when the functions ψ are projected from the states of maximum weight. A similar expression (E58) can be derived for projection from minimum weight.

To calculate the matrix elements in the J-projected scheme use can be made of Eq. (G.25) in conjunction with Eq. (3.43), or again an expression similar to Eq. (G.25) can be derived directly (W65).

Note that, since the operator Q_q is a generator of SU_3, it cannot couple states belonging to different representations. Thus, when the effect of the last term in Eq. (G.21) is negligible, there is a powerful selection rule in the SU_3 model for $E2$ transitions.

APPENDIX H—THE NORMALIZATION COEFFICIENTS AND OVERLAPS

a Coefficients

The normalization coefficient $a(\lambda\mu K_L L)$ of Eq. (3.39) for L-projected functions is defined in the expansion of the state of maximum weight $\phi(\lambda\mu)$ in Eq. (3.38b). These coefficients may be calculated (H61, E63) by considering the function

$$P(\lambda\mu LKK') = \big(\phi(\lambda\mu) \mid \psi(\lambda\mu KLK')\big)\, a(\lambda\mu KL) \tag{H.1}$$

Since

$$\phi(\lambda\mu) = \sum_{K'L'} a(\lambda\mu K'L')\,\psi(\lambda\mu K'L'K') \tag{H.2}$$

we clearly have

$$P(\lambda\mu LKK) = a^2(\lambda\mu KL) \tag{H.3a}$$

$$P(\lambda\mu LKK') = a(\lambda\mu KL)\,a(\lambda\mu K'L)\big(\psi(\lambda\mu KLK')|\,\psi(\lambda\mu K'LK')\big) \tag{H.3b}$$

Thus, by calculating the P functions, we can determine all the a coefficients from Eq. (H.3a) (to within a phase) and hence all the overlaps of the function $\psi(\lambda\mu KLK')$ from Eq. (H.3b). The phase of $a(\lambda\mu KL)$ is defined so that

$$a(\lambda\mu KL) > 0 \qquad \text{for } K \geqslant 0 \tag{H.4a}$$

using the relation

$$a(\lambda\mu KL) = a(\lambda\mu - KL)(-)^{\lambda+\mu+L} \qquad \text{for } K < 0 \tag{H.4b}$$

which ensures that

$$\psi(\lambda\mu - KLM) = \psi(\lambda\mu KLM) \tag{H.4c}$$

Using the projection form of the function ψ from Eq. (3.39) we write

$$P(\lambda\mu LKK') = (2L+1)\int \mathscr{D}^{L}_{K'K}(\Omega)(\phi(\lambda\mu)|\,\phi_\Omega(\lambda\mu))\,d\Omega \tag{H.5}$$

The values of the expansion coefficients $a(\lambda\mu KL)$ and overlaps

$$\big(\psi(\lambda\mu KLK)|\,\psi(\lambda\mu K'LK)\big)$$

depend only on the properties of the group SU_3. Thus we can use any convenient form for the function $\phi(\lambda\mu)$ to determine them. From the discussion in Section 3.3 we see that the function

$$\begin{aligned}\phi(\lambda\mu) = {} & \sqrt{\tfrac{1}{2}}\,\{\phi_z(1)\,\phi_x(2) - \phi_x(1)\,\phi_z(2)\}\,\sqrt{\tfrac{1}{2}}\,\{\phi_z(3)\,\phi_x(4) - \phi_x(3)\,\phi_z(4)\}\cdots \\ & \sqrt{\tfrac{1}{2}}\,\{\phi_z(2\mu-1)\,\phi_x(2\mu) - \phi_x(2\mu-1)\,\phi_z(2\mu)\} \\ & \times \phi_z(2\mu+1)\,\phi_z(2\mu+2)\cdots\phi_z(2\mu+\lambda)\end{aligned} \tag{H.6}$$

does indeed have the property of being the maximum-weight state of the representation $(\lambda\mu)$ of SU_3; here $\phi_\alpha(i)$ is the single-particle state of the ith particle having *one* quanta in the α direction.

The overlap function $(\phi(\lambda\mu)|\phi_\Omega(\lambda\mu))$ in Eq. (H.5) then involves such overlaps as

$$(\phi_z|(\phi_z)_\Omega) = \cos\beta \tag{H.7a}$$

and

$$\left(\sqrt{\tfrac{1}{2}}\,(\phi_z(1)\,\phi_x(2) - \phi_x(1)\,\phi_z(2))\,|\,\sqrt{\tfrac{1}{2}}\,(\phi_z(1)\,\phi_x(2) - \phi_x(1)\,\phi_z(2)_\Omega\right)$$
$$= \cos\alpha\cos\gamma - \cos\beta\sin\alpha\sin\gamma \tag{H.7b}$$

Thus

$$(\phi(\lambda\mu)\,|\,\phi_\Omega(\lambda\mu)) = (\cos\alpha\cos\gamma - \cos\beta\sin\alpha\sin\gamma)^\mu\,(\cos\beta)^\lambda \tag{H.8}$$

With the expansion

$$(\cos\alpha\cos\gamma - \cos\beta\sin\alpha\sin\gamma)^\mu$$
$$= \sum_{n=0}^{\mu} \frac{\mu!\,(-)^n}{n!\,(\mu-n)!}\,(\sin\alpha\sin\gamma\cos\beta)^n\,(\cos\alpha\cos\gamma)^{\mu-n} \tag{H.9a}$$

and

$$\mathscr{D}^L_{K'K}(\Omega) = e^{iK'\alpha}e^{iK\gamma}\,d^L_{K'K}(\beta) \tag{H.9b}$$

(E57*a*, Eq. 4.1.12) we can write the P function from Eq. (H.5)

$$P(\lambda\mu LKK') = \frac{(2L+1)}{2^{\mu+L}}\,\mu!\sum_{n=0}^{\mu}\bar{A}_n(\mu K')\,\bar{A}_n(\mu K)\,\bar{B}_n(\lambda LK'K)\,n!(\mu-n)! \tag{H.10}$$

with

$$\bar{A}_n(\mu K) = \frac{(-i)^n\,2^\mu}{2\pi n!(\mu-n)!}\int_0^{2\pi} d\alpha\,e^{iK'\alpha}\sin^n\alpha\cos^{\mu-n}\alpha$$
$$= \sum_p \frac{(-)^p}{p!(n-p)!\left(\dfrac{\mu-K}{2}-p\right)!\left(\dfrac{\mu+K'}{2}+p\right)!} \tag{H.11a}$$

$$\bar{B}_n(\lambda LK'K) = 2^{L-1}\int_{-1}^{1} dZ\,d^L_{K'K}(\beta)\,Z^{\lambda+n},\ Z = \cos\beta$$
$$= [(L+K')!\,(L-K)!\,(L+K)!\,(L-K)!]^{1/2}$$
$$\times\sum_\sigma (-)^{L-K'-\sigma}\frac{(\sigma+k)!\,(L-\sigma-k)!}{(L-K'-\sigma)!\,(2k+\sigma)!\,\sigma!\,(L-K-\sigma)!}$$
$$\times\sum_{p=0}^{\sigma+k}\sum_{q=0}^{L-\sigma-k}\frac{(-)^q}{\left(p!\,(\sigma+k-p)!\,q!\,(L-\sigma-k-q)!\,(\lambda+n+p+q+1)\right)}$$

with $\lambda+n+p+q$ even and $2k = K+K'$.

A Coefficients

The normalization coefficients $A(\lambda\mu K_L KJ)$ of Eq. (3.41) for J-projected functions can be found in a way analogous to that for the a coefficients. Alternatively, using Eq. (3.43) we can write

$$\begin{aligned}
&\tilde{P}(\lambda\mu JK_L KK'_L K') \\
&\quad = A(\lambda\mu SK_S KJ)\, A(\lambda\mu SK'_S K'J)(\tilde{\Psi}(\lambda\mu K'_L K'SJK) \mid \tilde{\Psi}(\lambda\mu K_L KSJK)) \\
&\quad = \sum_L a(\lambda\mu K_L L)\, a(\lambda\mu K'_L L)(LSK_L K_S \mid JK)(LSK'_L K'_S \mid JK') \\
&\qquad\qquad \times (\Psi(\lambda\mu K_L LK_L) \mid \Psi(\lambda\mu K'_L LK_L)) \\
&\quad = \sum_L P(\lambda\mu LK_L K'_L)(LSK_L K_S \mid JK)(LSK'_L K'_S \mid JK') \qquad K = K_L + K_S \text{ etc.,}
\end{aligned} \tag{H.12}$$

When $K_L = K'_L$, $K = K'$, Eq. (H.12) defines the A coefficients to within a phase factor. We define the convention

$$A(\lambda\mu SK_S KJ) \geqslant 0 \qquad \text{if} \quad K \geqslant 0 \tag{H.13a}$$

using the relation

$$A(\lambda\mu SK_S KJ) = (-)^{\lambda+\mu+S+J-2K} A(\lambda\mu S - K_S - KJ) \qquad \text{for } K < 0 \tag{H.13b}$$

which ensures that

$$\tilde{\Psi}(\lambda\mu - K_L - KSJM) = \tilde{\Psi}(\lambda\mu K_L KSJM) \tag{H.13c}$$

APPENDIX I—USE OF THE GROUP SU_3 IN THE CLASSIFICATION OF ELEMENTARY PARTICLES

The use of the SU_3 classification for the elementary particles[1] has no *physical* connection with the use of the group in nuclear structure theory. The pure abstract group properties as discussed in this article can of course be applied in elementary particle physics. In this brief appendix we merely point out the relationship between the isobaric spin and strangeness quantum numbers and the ϵ and Λ labels used in Section 3.6 to describe the representation of the subgroup U_1 and SU_2 of SU_3.

In the SU_3 model of elementary particles it is assumed that each particle (baryon, meson, or quark) belong to a definite representation of SU_3 (space

[1] See, e.g., Reference Z66.

undefined). The representations are described by their dimensions rather than with the Young-tableau $(\lambda\mu)$ labeling used in this article. The dimensions of the representation $(\lambda\mu)$ of SU_3 has already been given by Eq. (3.21a) as

$$\dim(\lambda\mu) = \tfrac{1}{2}(\lambda + 1)(\mu + 1)(\lambda + \mu + 2) \tag{I.1}$$

Thus the "eight-fold way" is the $(\lambda\mu) = (11)$ representation.

The subclassification according to SU_2 and U_1 (as discussed in Section3.6) is assumed to be that of the isobaric-spin group and the strangeness. The irreducible representation of SU_2 in Section 3.6 were described by the quantum number Λ; in elementary particle physics it is usual to use the isobaric-spin label T. The representation according to U_1 were described in Section 3.6 by a quantum number ϵ; for elementary particles it is more usual to use the strangeness label S related to ϵ by

$$S = \frac{\epsilon}{3} - B \tag{I.2}$$

TABLE I.I

List of Some Elementary Particles[a]

Name	Mass, MeV	B	D	T	S	$(\lambda\mu)$	Λ	ϵ
N	939	1	8	$\frac{1}{2}$	0	(1,1)	$\frac{1}{2}$	3
Σ	1193			1	-1		1	0
Λ	1115			0	-1		0	0
Ξ				$\frac{1}{2}$	2		$\frac{1}{2}$	-3
Ω	(1679)	1	10	0	1	(3,0)	0	6
Ξ_δ	1535			$\frac{1}{2}$	0		$\frac{1}{2}$	3
Σ_δ	1385			1	-1		1	0
N_δ	1238			$\frac{3}{2}$	-2		$\frac{3}{2}$	-3
$\bar{K}$	496	0	8	$\frac{1}{2}$	1	(1,1)	$\frac{1}{2}$	3
π	138			1	0		1	0
η	548			0	0		0	0
K	496			$\frac{1}{2}$	-1		$\frac{1}{2}$	-3
Λ_q		$\frac{1}{3}$	3	0	$\frac{1}{3}$	(1,0)	0	2
N_q				$\frac{1}{2}$	$-\frac{2}{3}$		$\frac{1}{2}$	-1

[a] Here the quantum numbers at the head of the columns refer to the baryon number B; dimension of the irreducible representation of SU_3, D; isobaric spin T; strangeness S; Young tableau representation of SU_3, $(\lambda\mu)$; the representation of the SU_2 subgroup of SU_3, $\Lambda \equiv T$; and the representation of the U_1 subgroup ϵ. The quarks have been given Λ_q and N_q symbols.

where B is the baryon number ($B = 1$ for baryons, 0 for mesons, and $\frac{1}{3}$ for quarks).

With these relationships it is straightforward from Eqs. (3.29) and (3.30) to find the isobaric-spin and strangeness labels for particles belonging to a definite representation of SU_3,

In Table I-I we give a short list of elementary particles with their isobaric T, strangeness S, and baryon B labels and the equivalent set $SU_2(\Lambda)$, $U_1(\epsilon)$ and baryon (B) labels.

The charge Q is related to the third component of isobaric spin in elementary particle physics by

$$Q = +T_3 + \frac{S+B}{2} \equiv + \frac{\Lambda_3 + \epsilon}{6} \tag{I.3}$$

[We note that this relates the neutron with isobaric-spin projection $T_3 = -\frac{1}{2}$. In nuclear physics the neutron is often associated with $T_3 = +\frac{1}{2}$, i.e., in this notation $Q = -T_3 + (S + B)/2$].

In the quark model of elementary particles it is assumed that baryons are made up of at least three quarks. Thus the three quark baryons can belong to SU_3 representations

$$(10) \otimes (10) \otimes (10) = (3,0) + (1,1) + (0,0) \tag{I.4}$$

using the outer product of representation as discussed in Appendix C. Mesons are assumed to be made up from a quark and antiquark $((\lambda\mu) = (01))$ and can thus belong to representation of SU_3

$$(10) \otimes (01) = (1,1) + (0,0) \tag{I.5}$$

The references will be found on page 148 preceding the Appendixes.

THE HARTREE–FOCK THEORY OF DEFORMED LIGHT NUCLEI

Georges Ripka

1. INTRODUCTION

The existence of rotational bands in nuclei of the $2s$-$1d$ shell ($16 < A < 40$) and to a lesser extent in those of the $1p$ shell ($4 < A < 16$) has been recognized for a long time. The main features of such bands are the approximate proportionality to $J(J + 1)$ of the energy levels and the strong quadrupole transition moments and static moments. Although these aspects are not as striking in a light nucleus as they are among the heavy deformed ones, the interpretation of the experimental data in terms of a rotating deformed intrinsic state seems unescapable. This article is concerned with the calculation and the study of the deformations in light nuclei with the Hartree–Fock (H.F.) method.

As is well known from atomic physics, the H.F. approximation consists in assuming that each nucleon of the nucleus moves independently in a potential field that is the sum of the interactions of this nucleon with all the other nucleons of the nucleus, averaged over the wave functions of these other nucleons. This description of the nucleus in terms of an independent particle wave function gives rise to the following objection. It is currently thought that the interaction between nucleons contains a short-range strong repulsive core. Such a repulsive cove will produce short-range two-body correlations which are not described by an independent particle wave function. The success with which the independent particle model has met in explaining a large number of experimental data suggests that the short-range correlations do not play an important role in many nuclear properties. It is therefore believed that H.F. wave functions are significant and that they must be calculated with an effective nucleon–nucleon interaction from which the repulsive core has been removed.

The explicit calculation of the effective interaction in terms of the real nucleon–nucleon interaction is still a subject of much debate,[35] and it will not be treated in this article. Such a calculation, which leads to what may

be called radial H.F. calculations, will neccessarily concentrate on explaining the total binding energy and the equilibrium radius of a nucleus, in other words, on the study of the saturation properties of nuclei.

This article concentrates mostly (though not exclusively) on calculating what happens within a major shell, in which case the radial dependence of the wave functions is given *a priori* and the problem of radial stability does not arise. The H.F. method will be shown to be a particularly convenient and physically meaningful way of treating configuration interaction inside one major shell. It will also be used to calculate the configuration interaction between major shells which produces the quadrupole deformations and the effective charge. For these calculations the choice of the two-body interaction is much less critical then for the calculation of the nuclear saturation properties, which are not treated in this article.

Theoretical discussions of the rotational spectra are usually based on the unified model of Bohr and Mottelson[1] in which single-particle and collective rotational motions are distinguished and uncoupled. In this model, e.g., the state of spin J belonging to the ground-state rotational band of an even–even nucleus is described by the product wave function

$$|JM\rangle = \sqrt{\frac{2J+1}{8\pi^2}}\, D^{J*}_{M0}(\Omega)|\varphi_0\rangle \qquad J = 0, 2, 4,... \tag{1}$$

The rotational motion is described by the symmetric top wave function[2]

$$D^{J*}_{M0}(\Omega) = \sqrt{\frac{4\pi}{2J+1}}\, Y_M{}^J(\beta, \gamma) \tag{2}$$

The single-particle motion is described by the intrinsic state $|\varphi_0\rangle$. The wave function of the nucleus is only expected to factorize when the particle excitation energy (or the spacing of intrinsic states) is larger than the energy of collective excitation (or level spacing in a rotational band). The conditions are met in even–even $N = Z$ nuclei in which, as will be seen in Section 6, the single-particle excitations are hindered by an energy gap of approximately 8 MeV, while the 2^+ and 4^+ levels of the ground-state rotational bands lie at about 1.7 and 4 MeV, respectively. However, large single-particle excitation energy is not a sufficient condition for the validity of the wave function of Eq. (1), and in Section 14 it will be shown that the collective variable Ω is not very well defined in light nuclei.

The simplest assumption that can be made about the intrinsic state $|\varphi\rangle$ is that it is a Slater determinant of single nucleon orbits in a deformed nonspherical) field.

$$|\varphi\rangle = b^\dagger_{\lambda_1} b^\dagger_{\lambda_2} \cdots b^\dagger_{\lambda_A}\,|0\rangle \tag{3}$$

The notation of second quantization is used here, and $b_\lambda^\dagger$ is the fermion operator which creates a particle in the orbit λ. It obeys the anticommutation rules

$$[b_\lambda, b_\mu^\dagger]_+ = \delta_{\lambda\mu} \qquad [b_\lambda, b_\mu]_+ = 0 \tag{4}$$

The orbits λ described by the nucleons are eigenstates of a single-particle Hamiltonian h

$$h \mid \lambda\rangle = e_\lambda \mid \lambda\rangle \tag{5}$$

This Hamiltonian h, which represents the deformed field, may be either guessed or calculated explicitly in terms of the two-body effective interactions between the nucleons. The choice of a deformed harmonic oscillator with a spin orbit and an l^2 correction,

$$h = -\frac{\hbar^2}{2m}\nabla^2 + \tfrac{1}{2}m[\omega_x^2x^2 + \omega_y^2y^2 + \omega_z^2z^2] + a\mathbf{l}\cdot\mathbf{s} + Dl^2 \tag{6}$$

has often been made, and it has met with considerable success.[4] The resulting orbits (5) are Nilsson orbits.[4] The choice of the Hamiltonian h and of which orbits λ are occupied by nucleons determines entirely the intrinsic wave function (3). The parameters of the Hamiltonian (6) are phenomenological, and they may be chosen so as to fit many of the experimental data such as ground-state spins, β decays, nuclear moments, single-particle stripping strengths, etc. The parameters of the Hamiltonian (6) may also be determined by a variational procedure in the following sense: The intrinsic state $\mid \varphi\rangle$ is a function of the parameters of the Hamiltonian h. These are varied so as to minimize the mean value in the state $\mid \varphi\rangle$, not of the one-body Hamiltonian h, but of the many-body nuclear Hamiltonian

$$H = \sum_{i=1}^{A} \frac{P_i^2}{2m} + \frac{1}{2}\sum_{i\neq j} v(ij) \tag{7}$$

In this procedure the single-particle Hamiltonian is only used to generate the orbits (5) of the intrinsic state. Equilibrium shapes of nuclei have been investigated by using this method both in p shell[5] and $2s$-$1d$ shell nuclei.[6] This variational approach actually constitutes a restricted form of H.F. calculations.

This article is devoted to the unrestricted H.F. approach, in which full

consistency is achieved between the single-particle potential and the single-particle orbits. In Sections 2 to 4 the H.F. theory and the symmetries of the H.F. solutions are discussed. The first explicit application to deformed nuclei of the $2s$-$1d$ shell was made by Kelson.[7] In Sections 5 and 6, detailed calculations of the even–even $N = Z$ nuclei of this shell are presented. An important new feature, namely, the appearance of a large energy gap between filled and empty orbits, is shown in Section 8 to be related to the nonlocality of the H.F. field.[10,11] This energy gap is one of the main differences between H.F. and Nilsson orbits. Its calculation leads to reasonable estimates of the neutron separation energies. It has also permitted a more reliable calculation of excited particle-hole vibrations of the intrinsic states.[9] The deformation of the field is shown in Section 9 to be similar to that produced by a quadrupole–quadrupole interaction. A similarity is found between H.F. wave functions obtained with a gaussian nucleon-nucleon interaction and the states which diagonalize the quadrupole–quadrupole interaction in a given major shell. The latter states have been obtained by group theoretical methods of J. P. Elliott and M. Moshinsky.[13] Differences between H.F. wave functions and the ones obtained by group theoretical methods are mainly due to the effect of the spin–orbit interaction, which is discussed in Section 10. The spin–orbit interaction becomes increasingly important in the second half of the $2s$–$1d$ shell where the H.F. theory does not always give a well-defined equilibrium state (Section 11). Section 12 discusses H.F. calculations of nuclei other than even–even $N = Z$. The H.F. theory has also been extended to high-order particle-hole excitations in nuclei with excited equilibrium shapes, i.e., ^{16}O, ^{18}O, and ^{19}F.[14–16] In Section 13 the magnetic moments of odd-A nuclei are calculated by using the H.F. wave functions.[30] The rotations of the intrinsic states are studied in Section 14. In particular, the validity of wave functions of the type of Eq. (1), in which the rotational and intrinsic motions are factorized is analyzed by using the Peierls–Yoccoz method[25] of angular momentum projection.[15] Finally in Section 15 it is shown that the H.F. theory may be successfully applied to the quadrupole polarizations of closed shells.

This article is concerned with deformations in light nuclei. Radial H.F. calculations of spherical closed-shell nuclei are not discussed. Hartree–Fock calculations are quite simple with present-day computers and have recently become very popular, so that the author is certain to have omitted many references, for which he wishes to apologize.

This article is an attempt to illustrate most of the important results of the H.F. calculations in light nuclei and also to show the limitations of the method. The theory is presented in a manner that is suitable for actual numerical calculations. Sufficient details are given so that the reader may pursue his own calculations.

2. THE HARTREE–FOCK EQUATIONS

The purpose of the H.F. theory is to determine the wave functions of the orbits λ of the Slater determinant Eq.(3). This is achieved by requiring the energy of the system described by the wave function in Eq. (3) to be stationary and minimum for infinitesimal variations of the orbits λ. The energy of the system is obtained by taking the expectation value of the Hamiltonian equation (7) in the state of Eq. (3):

$$E_{\mathrm{HF}} = \langle \varphi \mid H \mid \varphi \rangle = \sum_{\lambda=1}^{A} \langle \lambda \mid t \mid \lambda \rangle + \tfrac{1}{2} \sum_{\lambda,\mu=1}^{A} \langle \lambda\mu \mid v \mid \lambda\mu \rangle \tag{8}$$

where E_{HF} is called the H.F. energy; $\langle \lambda \mid t \mid \lambda \rangle$ is the kinetic energy of the orbit λ, and

$$\langle \lambda\mu \mid v \mid \lambda\mu \rangle = -\langle \lambda\mu \mid v \mid \mu\lambda \rangle \tag{9}$$

is an antisymmetrized matrix element of the two-body interaction $v(ij)$.

It is advantageous to expand the orbits on a basis j of known wave functions

$$\mid \lambda \rangle = \sum_{j} c_j^{\lambda} \mid j \rangle \tag{10}$$

The basis j may be e.g., the set $\mid nljm\tau \rangle$ of shell model states in a harmonic oscillator. Any basis may be used to expand the orbits, provided one is able to calculate matrix elements of the interaction v with the basis states. The set of orbits λ (both filled and empty) is assumed to form an orthonormal set of wave functions

$$\sum_{j} C_j^{\lambda^*} C_j^{\lambda'} = \delta_{\lambda\lambda'} \qquad \sum_{\lambda} C_j^{\lambda^*} C_{j'}^{\lambda} = \delta_{jj'} \tag{11}$$

The wave function $\mid \varphi \rangle$ is determined by the coefficients c_j^{λ}, which become variational parameters. The energy will be stationary with the normalization condition (11) when

$$\frac{\partial}{\partial C_j^{\lambda^*}} \left[\langle \varphi \mid H \mid \varphi \rangle - e_\lambda \sum_{j} C_j^{\lambda^*} C_j^{\lambda} \right] = 0 \tag{12}$$

Here e_λ is introduced as a Lagrange multiplier. With the help of expansion (10) of the orbits, the energy $\langle \varphi \mid H \mid \varphi \rangle$ in Eq. (12) may be expressed in terms of the known matrix elements of t and v in the known basis j. The derivative (12) may then be calculated directly, and one obtains

$$\sum_{j'} \left[\langle j \mid t \mid j' \rangle + \sum_{\lambda=1}^{A} \sum_{j_1 j_2} C_{j_1}^{\lambda^*} \langle j j_1 \mid v \mid j' j_2 \rangle C_{j_2}^{\lambda} \right] C_{j'}^{\lambda} = e_\lambda C_j^{\lambda} \tag{13}$$

Equations (13) have the form of an eigenvalue problem

$$\sum_{j'} \langle j \mid h \mid j' \rangle C_{j'}^{\lambda} = e_{\lambda} C_{j}^{\lambda} \tag{14}$$

where h is a Hamiltonian given by its matrix elements

$$\begin{aligned} \langle j \mid h \mid j' \rangle &= \langle j \mid t \mid j' \rangle + \sum_{\lambda=1}^{A} \langle j\lambda \mid v \mid j'\lambda \rangle \\ &= \langle j \mid t \mid j' \rangle + \sum_{\lambda=1}^{A} \sum_{j_1 j_2} C_{j_1}^{\lambda *} \langle jj_1 \mid v \mid j'j_2 \rangle C_{j_2}^{\lambda} \end{aligned} \tag{15}$$

where h is the H.F. Hamiltonian. Equation (14) is the same as Eq. (5) expressed in the basis j. Equations (14) and (15) are the H.F. equations for the orbits λ. They may be solved by the well-known iteration procedure:

a. An initial set of coefficients c_j^{λ} is guessed, and also which orbits are occupied.
b. With this set of coefficients c_j^{λ}, the matrix elements of Eq. (15) of the H.F. Hamiltonian are calculated.
c. Equation (14) is solved by diagonalizing the Hamiltonian matrix (15). A new set of coefficients c_j^{λ} is obtained, and A orbits are chosen to be filled by nucleons (often the ones with lowest energy). One returns to step *b*. This process is repeated until successive diagonalizations produce the same set of coefficients c_j^{λ}.

The iteration process is somewhat complicated by the fact that there are many local minimums of the energy (8) and therefore many solutions of the H.F. equations (see Section 11). Various minimums may be reached by various initial guesses, which therefore become crucial. Furthermore, after each diagonalization of the Hamiltonian matrix (15) one must decide which orbits to fill and it will be seen that the energies of the orbits vary from one solution to another. Finally, in Section 3 it will be shown that the H.F. Hamiltonian h may have various symmetries, which, when assumed in a given step of the iteration process (and in particular in the initial guess), are preserved in the successive iterations. Such a symmetry, axial symmetry, e.g., may not be the symmetry of the solution with lowest energy. Hence some control over the iteration process is neccessary. Simple models help to suggest an "educated" initial guess. For example, the quadrupole–quadrupole interaction is known to play an important role in producing nuclear deformations (Section 9). Thus a good initial guess may be obtained by choosing

a set of occupied orbits (n_x, n_y, n_z) in a deformed harmonic oscillator. After each iteration, one must decide which orbits to fill.

The time involved in solving the H.F. equations depends on the possibility of storing the matrix elements of the interaction in the fast memories of the computer. The calculation of the matrix elements is usually longer than the iteration process. It is convenient to write the H.F. equations in terms of the density matrix defined by

$$\rho_{ij} = \sum_{\lambda=1}^{A} C_i^{\lambda} C_j^{\lambda *} \tag{16}$$

When the density matrix is real at each step of the iteration process, the H.F. Hamiltonian matrix (15) may be written

$$\langle j \mid h \mid j' \rangle = \langle j \mid t \mid j' \rangle + \sum_{j_1 j_2} R(jj'; j_1 j_2)\, \rho_{j_2 j_1} \tag{17}$$

where

$$R(jj'; j_1 j_2) = \tfrac{1}{2} [\langle jj_1 \mid v \mid j'j_2 \rangle + \langle jj_2 \mid v \mid j'j_1 \rangle] \tag{18}$$

In the usual case where matrix elements are real numbers, R has the following symmetry properties:

$$R(jj'; j_1 j_2) = R(j'j; j_1 j_2) = R(jj'; j_2 j_1) = R(j_1 j_2; jj')$$

These are very useful for storing purposes. The symmetry properties of h discussed in the following section are also easily exploited when the H.F. Hamiltonian is written in the form of Eq. (17).

3. SYMMETRIES OF THE HARTREE–FOCK HAMILTONIAN

It is well known that the H.F. Hamiltonian (15) does not necessarily have the same symmetry properties as the nuclear Hamiltonian (7). Also, a given symmetry is not necessarily preserved in successive iterations. For example, axial symmetry is always possible, but not spherical symmetry. The possible symmetries of the H.F. Hamiltonian are governed by the following theorem:

Theorem: Let U be a unitary operator that commutes with the nuclear Hamiltonian (7)

$$U^{-1} H U = H \tag{19}$$

Then, if U leaves the set of occupied orbits invariant, it commutes with the H.F. Hamiltonian (15)

$$U^{-1}hU = h \tag{20}$$

The operator U leaves the set of occupied orbits invariant whenever the state obtained by operating on any occupied orbit λ may be expressed as a linear combination of occupied orbits only

$$|\bar{\lambda}\rangle \equiv U\,|\lambda\rangle = \sum_{\mu=1}^{A} X_{\mu}{}^{\lambda}\,|\mu\rangle \qquad \lambda = 1, 2,..., A$$

$$\sum_{\lambda=1}^{A} X_{\lambda}^{\mu^*} X_{\lambda}{}^{\nu} = \delta_{\mu\nu} \tag{21}$$

Proof: Since the nuclear Hamiltonian commutes with U, the H.F. Hamiltonian (15) may be written as

$$\langle i\,|\,h\,|\,j\rangle = \langle i\,|\,U^{-1}tU\,|\,j\rangle + \sum_{\lambda=1}^{A} \langle i\lambda\,|\,U^{-1}vU\,|\,j\lambda\rangle$$

With the help of Eq. (21), the above expression becomes

$$\begin{aligned}
\langle i\,|\,h\,|\,j\rangle &= \langle \bar{\imath}\,|\,t\,|\,\bar{\jmath}\rangle + \sum_{\lambda=1}^{A} \langle \bar{\imath}\bar{\lambda}\,|\,v\,|\,\bar{\jmath}\bar{\lambda}\rangle \\
&= \langle \bar{\imath}\,|\,t\,|\,\bar{\jmath}\rangle + \sum_{\lambda=1}^{A} \sum_{\mu,\nu=1}^{A} X_{\mu}^{\lambda^*} \langle \bar{\imath}\mu\,|\,v\,|\,\bar{\jmath}\nu\rangle\, X_{\nu}^{\lambda} \\
&= \langle \bar{\imath}\,|\,t\,|\,\bar{\jmath}\rangle + \sum_{\mu=1}^{A} \langle \bar{\imath}\mu\,|\,v\,|\,\bar{\jmath}\mu\rangle \\
&= \langle \bar{\imath}\,|\,h\,|\,\bar{\jmath}\rangle = \langle i\,|\,U^{-1}hU\,|\,j\rangle
\end{aligned} \tag{22}$$

Hence Eq. (20) is satisfied.

In the proof of this theorem the orbits λ may be the ones obtained in any iteration. Some of the most frequently met symmetries will serve to illustrate the theorem.

3.1 Time-Reversal Symmetry

With real C_j^{λ} coefficients, time-reversal symmetry is equivalent to the symmetry of a rotation of π about the y axis times the parity operation (because of the spherical harmonics definition[2])

$$U = e^{-i\pi J_y} P \tag{23}$$

In an even-even nucleus, if for any orbit λ the orbit $|\bar{\lambda}\rangle = e^{-i\pi J_y}|\lambda\rangle$ is also filled, then the H.F. field commutes with the time-reversal operator, the orbits $|\lambda\rangle$ and $|\bar{\lambda}\rangle$ are degenerate, and

$$Pe^{-i\pi J_y}|\varphi\rangle = |\varphi\rangle \tag{24}$$

3.2 Parity and Axial Symmetry

These are always possible symmetries, for, if each orbit λ has a definite parity or a good projection of J_z, the component of the angular momentum along the z axis, then the operators

$$U = P \qquad \text{or} \qquad U = e^{i\varphi J_z} \tag{25}$$

leave the set of occupied orbits invariant. P is the parity operator.

3.3 Isospin Invariance

If a nucleus has an equal number of protons and neutrons, then a state $|\varphi\rangle$ may be constructed such that neutrons and protons fill the same orbits. The three components of the total isospin operator will then leave the set of occupied orbits invariant. If the Coulomb interaction is neglected, the H.F. field is an isospin scalar, neutron and proton orbits are degenerate, and the state $|\varphi\rangle$ has zero isospin (it is formed of closed isospin shells). In even–even $N = Z$ nuclei, time-reversal and isospin invariance may be combined so as to obtain a fourfold degeneracy of the orbits: A given neutron orbit is degenerate with its time-reversed orbit and with the corresponding two proton orbits. Such H.F. states are lowest in energy for even–even $N = Z$ nuclei.

3.4 Spherical Symmetry

The H.F. Hamiltonian does not in general commute with the three components J_x, J_y, and J_z of the total angular momentum, for, if one assumes as an initial guess that the orbits λ are eigenstates of the angular momentum operator,

$$|\lambda\rangle = |j_\lambda m_\lambda\rangle \tag{26}$$

then J_x and J_y, which raise and lower the magnetic quantum number m_λ, will leave the set of occupied orbits invariant only if for each j_λ all the magnetic quantum numbers m_λ are filled or empty. Hence spherical symmetry can exist only in nuclei that have the right number of particles to form closed shells.

3.5 Spin and Isospin Invariance

When the spin–orbit interaction is neglected, the orbits of even–even $N = Z$ nuclei may be factorized into space, spin, and isospin wave functions

$$|\lambda\rangle = |\lambda_x, \sigma_\lambda, \tau_\lambda\rangle \tag{27}$$

When four nucleons fill the four spin and isospin states of each orbit λ_x in configuration space, the H.F. Hamiltonian is a spin and an isospin scalar provided only central forces are used in the nuclear Hamiltonian (7). The intrinsic state $|\varphi\rangle$ is then an L-S coupling wave function with total spin and isospin $S = T = 0$ (it is formed of closed spin and isospin shells). Although the spin-orbit interaction may not be neglected in $2s$-$1d$ shell nuclei, its neglect leads to very useful models which illustrate the nature of H.F. calculations[11] (Sections 8 and 9).

Further symmetries will be discussed below. It should be stressed, however, that the theorem quoted above gives only a necessary condition for the existence of a given symmetry of the H.F. field. When a solution with a given symmetry is obtained, there may be another solution with lower energy and without this particular symmetry. Examples will be found below.

4. THE CHOICE OF AN EXPANSION FOR THE ORBITS

The basis j on which the H.F. orbits of Eq. (10) are expanded is arbitrary in principle. In practice the convergence of the expansion, the convenience of calculating the matrix elements (18) of the two-body interaction, and the symmetries of the H.F. field suggest useful expansions. The convergence of the expansion has been studied for spherical closed-shell nuclei,[18] and harmonic-oscillator orbits were found to give excellent convergence for the expansion of the bound orbits which determine the H.F. state $|\varphi\rangle$. Thus harmonic-oscillator wave functions will be used for the radial part of the basis states j. Shell model states

$$|j\rangle \equiv |nljm\tau\rangle \tag{28}$$

are convenient to use because of the general availability of matrix elements of the two-body interaction in this representation; n and l are the radial and orbital angular momentum quantum numbers of the harmonic-oscillator wave function; j and m are the total angular momentum and its projection on the z axis of the intrinsic frame of reference attached to the nucleus; and τ, the third component of isospin, distinguishes proton and neutron states. The basis Eq. (28) will be used here, but it is by no means essential to use this

representation. Much may be said, e. g., in favor of using the (n_x, n_y, n_z) representation of a deformed oscillator (see Section 9).

Expansion (10) of the H.F. orbits on basis (28) is

$$|\lambda\rangle = \sum_{jm} C^{\lambda}_{jm} \, | jm\tau_\lambda\rangle \tag{29}$$

In Eq. (29) as well as in what follows, j stands for the three quantum numbers n, l, and j. The mixing of neutron and proton states in a given orbit has not been considered, so that the expansion of Eq. (29) is limited to a single value of τ_λ, in which, as previously noted, proton and neutron orbits are distinguished. In the basis (28) the H.F. Hamiltonian matrix (15) becomes

$$\langle jm\tau \mid h \mid j'm'\tau\rangle = \langle jm\tau \mid t \mid j'm'\tau\rangle + \sum_{\lambda=1}^{A} \langle jm\tau, \lambda \mid v \mid j'm'\tau, \lambda\rangle \tag{30}$$

where

$$\langle jm\tau, \lambda \mid v \mid j'm'\tau, \lambda\rangle = \sum_{j_1m_1} \sum_{j_2m_2} C^{\lambda *}_{j_1m_1} \langle jm\tau, j_1m_1\tau_\lambda \mid v \mid j'm'\tau, j_2m_2\tau_\lambda\rangle \, C^{\lambda}_{j_2m_2} \tag{31}$$

The interaction matrix element in (31) is given in terms of antisymmetrized coupled matrix elements[1] by

$$\langle jm\tau, j_1m_1\tau_\lambda \mid v \mid j'm'\tau, j_2m_2\tau_\lambda\rangle$$
$$= \sum_{JM} \sum_{TM_T} \begin{bmatrix} j & j_1 & J \\ m & m_1 & M \end{bmatrix} \begin{bmatrix} j' & j_2 & J \\ m' & m_2 & M \end{bmatrix} \begin{bmatrix} \frac{1}{2} & \frac{1}{2} & T \\ \tau & \tau_\lambda & M_T \end{bmatrix}^2 \langle jj_1 \mid v \mid j'j_2\rangle_{JT} \tag{32}$$

In the expression above,

$$\begin{bmatrix} j_1 & j_2 & J \\ m_1 & m_2 & M \end{bmatrix}$$

is a Clebsch–Gordan coefficient[2] and not a three-j symbol.

[1] The coupled antisymmetrized matrix elements $\langle j_1j_2 \mid V \mid j_3j_4\rangle_{JT}$ are often divided by $\sqrt{2}$ whenever $j_1 = j_2$ or $j_3 = j_4$ so that they should represent matrix elements between normalized two-nucleon states. These factors of $\sqrt{2}$ should not be used in Eq. (32).

[2] $\begin{bmatrix} j_1 & j_2 & J \\ m_1 & m_2 & M \end{bmatrix}$ is exactly equal to the Clebsch–Gordan coefficient $\langle j_1 \, j_2 \, m_1 \, m_2 \mid JM\rangle$ defined in Appendix C of Ref. 2.

The density operator (16) may be written in the basis (28)

$$\rho^{(\tau)}_{j_1m_1,j_2m_2} = \sum_{\lambda=1}^{A} C^{\lambda}_{j_1m_1} C^{\lambda^*}_{j_2m_2} \tag{33}$$

It is trivial to rewrite Eq. (17) and (18) in the basis (28).

The expansion (29) of the orbits is further limited by the symmetry properties of the solution (Section 3).

4.1 Spherical Symmetry

Orbits of closed-shell spherical solutions have the following expansion:

$$|\lambda\rangle = \sum_{nl} C^{\lambda}_{nl} \,|\, nlj_\lambda m_\lambda \tau_\lambda\rangle \tag{34}$$

and the orbits which differ only by m_λ are degenerate. Here j stands for the total angular momentum quantum number only.

4.2 Axial Symmetry

In axially symmetric solutions the orbits are eigenstates of J_z, and the expansion equation (29) of an orbit λ is limited to states of a given m_λ

$$|\lambda\rangle = \sum_{j} C_j^{\lambda} \,|\, jm_\lambda \tau_\lambda\rangle \tag{35}$$

4.3 Ellipsoidal Symmetry

Even–even nuclei which do not have axial symmetry may have ellipsoidal symmetry, i.e., a symmetry with respect to reflections in the (x, y), (y, z), and (z, x) planes. Such a reflection is equivalent to a parity operation P followed by a rotation about the axis perpendicular to the plane

$$U_1 = e^{-i\pi J_z}P \qquad U_2 = e^{-i\pi J_y}P \qquad U_3 = e^{-i\pi J_x}P \tag{36}$$

With real C^{λ}_{jm} coefficients, a solution with ellipsoidal symmetry has time-reversal symmetry. When the expansion (29) of each orbit is limited to states $|\, nljm\tau\rangle$ such that all its components have $l + m + \frac{1}{2}$ even (or odd), the orbits are eigenfunctions of U_1, and the H.F. field is symmetric with respect to a reflection in the (x, y) plane. Each orbit $|\lambda\rangle$ is then orthogonal to the orbit

$$|\bar{\lambda}\rangle = U_2\,|\lambda\rangle = \sum_{nljm} (-)^{l+j-m} C^{\lambda}_{nljm} \,|\, nlj - m\rangle$$

so that, if both the orbits $|\lambda\rangle$ and $|\bar{\lambda}\rangle$ are filled, the H.F. Hamiltonian will commute with U_2. Finally, the H.F. Hamiltonian will commute with U_3 only if the orbits have a good parity, because then $U_3 = U_2 U_1$. The H.F. state $|\varphi\rangle$ is then an eigenfunction of U_1, U_2, and U_3

$$U_1 |\varphi\rangle = U_2 |\varphi\rangle = U_3 |\varphi\rangle = |\varphi\rangle$$

4.4 Time-Reversal and Mixed-Parity Solutions

In even–even nuclei, time-reversal symmetry is obtained by requiring that, for each occupied orbit,

$$|\lambda\rangle = \sum_{nljm} C^{\lambda}_{nljm} \, | nljm\tau_{\lambda}\rangle$$

the time-reversed orbit

$$|\bar{\lambda}\rangle = T|\lambda\rangle = \sum_{nljm} C^{\lambda *}_{nljm} (-)^{l+j-m} \, | nlj - m\rangle$$

is also occupied and orthogonal to $|\lambda\rangle$. The phase conventions of Reference 2 are used here. In axially symmetric solutions the orbits $|\lambda\rangle$ and $|\bar{\lambda}\rangle$ are always orthogonal. In other solutions they are orthogonal if all the components of the orbits have $m + l + \frac{1}{2}$ even (or odd). Real coefficients C^{λ}_{nljm} may be used. Then the time-reversal symmetry is equivalent to a reflection in the (x, z) plane.

The deformed intrinsic state of Eq. (3) can be expanded on states with good parity and with total angular momentum J and projection K on the z axis of the intrinsic frame

$$|\varphi\rangle = \sum_{JK} \alpha_{JK} \, | JK^{+}\rangle + \beta_{JK} \, | JK^{-}\rangle$$

Here $|JK^{+}\rangle$ and $|JK^{-}\rangle$ are the positive and negative parity members of the rotational band K generated by the deformed intrinsic state $|\varphi\rangle$. They necessarily involve even and odd powers of spherical harmonics and so they have the following time-reversal properties:

$$T|JK^{+}\rangle = (-)^{J-K} \, | J - K^{+}\rangle \qquad T|JK^{-}\rangle = -(-)^{J-K} \, | J - K^{-}\rangle$$

Hence the time-reversal symmetry of $|\varphi\rangle$ implies that the $K = 0$ rotational band involves only states of natural parity, i.e., 0^{+}, 2^{+}, 4^{+},... and 1^{-}, 3^{-}, 5^{-},... states.

Hartree–Fock calculations made so far can be divided into two classes according to the number of terms included in expansion (29) of the orbits.

a. Single major-shell calculations in which expansion (29) of each orbit is limited to states $|jm\tau\rangle$ belonging to a major shell of the spherical oscillator.
b. Major-shell mixing calculations which include states of several major shells in the expansion of the orbits.

The results obtained from H.F. calculations of both types will be reviewed separately.

5. SINGLE MAJOR-SHELL HARTREE–FOCK CALCULATIONS

In single major-shell H.F. calculations the expansion (29) of each orbit is limited to states of one major shell,

$$|\lambda\rangle = \sum_{jm} C_{jm}^{\lambda} \, |jm\tau_{\lambda}\rangle$$

$$\begin{aligned} j &= 1s_{1/2} && \text{for } 1s \text{ shell orbits} \\ &= 1p_{3/2} \text{ and } 1p_{1/2} && \text{for } 1p \text{ shell orbits} \\ &= 1d_{5/2}, 2s_{1/2}, \text{ and } 1d_{3/2} && \text{for } 2s\text{-}1d \text{ shell orbits} \\ &= 1f_{7/2}, 2p_{3/2}, 2p_{1/2}, \text{ and } 1f_{5/2} && \text{for } 2p\text{-}1f \text{ shell orbits} \\ &\text{etc.} \end{aligned} \tag{37}$$

5.1 Spherical Solutions

Since there is only one state of a given angular momentum in any major shell, the restrictions of Eq. (37) reduce the expansion (34) of the orbits to one term. The H.F. Hamiltonian is then diagonal in the $|jm\tau\rangle$ representation. For nuclei with equal numbers of protons and neutrons, the sums over magnetic quantum numbers may be made explicitly and H.F. Hamiltonian (30) becomes

$$\langle jm\tau \,|\, h \,|\, j'm'\tau\rangle = \epsilon_j \delta_{jj'} \delta_{mm'}$$

with

$$\epsilon_j = \langle jm \,|\, t \,|\, jm\rangle + \frac{1}{2(2j+1)} \sum_{j_\lambda} \sum_{JT} (2J+1)(2T+1) \langle jj_\lambda \,|\, v \,|\, jj_\lambda\rangle_{JT} \tag{38}$$

In Eq. (38) $\sum_{j_\lambda}$ is a sum over the quantum numbers j of occupied orbits only. The ϵ_j are the single-particle energies in the spherical field of the closed-shell nucleus. They are commonly used in shell model calculations.

The wave functions of the orbits are the basis states $|jm\tau\rangle$ themselves. Such a solution is called a *spherical solution.*

Furthermore, if a nucleus has a *filled major shell,* such as ^{16}O and ^{40}Ca, e.g., then the spherical solution is also the H.F. solution of the nucleus obtained by adding (or subtracting) one particle to (or form) the closed-shell nucleus. Indeed, let $|\varphi_0\rangle$ be the spherical solution of the closed-shell nucleus. Adding one particle to an unknown orbit μ yields the state $b_\mu^\dagger|\varphi_0\rangle$, whose energy is

$$E_{\mathrm{HF}} = \langle\varphi_0 | b_\mu H b_\mu^\dagger | \varphi_0\rangle = E_0 + \langle\mu | t | \mu\rangle + \sum_{\lambda\epsilon\varphi_0} \langle\mu\lambda | v | \mu\lambda\rangle \tag{39}$$

E_0 is the H.F. energy $\langle\varphi_0 | H | \varphi_0\rangle$ of the closed-shell nucleus. Because of the restrictions of (37) the sum $\sum_{\lambda\epsilon\varphi_0}$ over the orbits filled in the state $|\varphi_0\rangle$ is independent of the coefficients C_{jm}^λ. Equation (38) yields

$$E_{\mathrm{HF}} = E_0 + \sum_{jm} |C_{jm}^\mu|^2 \epsilon_j \tag{40}$$

and the variational problem, Eq. (12), reduces to $(\epsilon_j - e_\mu) C_j^\mu = 0$. Hence the orbit μ is just one of the empty $|jm\tau\rangle$ states of the closed-shell nucleus. Indeed, when a nucleus has a filled major shell, the interaction of the extra particle with the closed shell can only mix occupied orbits among themselves and such a mixing leaves the Slater determinant invariant.

Hence the restrictions of (37) prevent the description of polarizations of closed-shell cores.

5.2 The Use of a Reference Closed-Shell Nucleus

Because the wave functions of orbits in nuclei which have a filled major shell are known, it is convenient to use them as reference nuclei. For example, let us choose ^{16}O as a reference nucleus.

In ^{16}O the four $1s$-shell orbits and the twelve $1p$-shell orbits are filled. The filling of the orbits in another nucleus may be compared with the filling in ^{16}O by writing the sum over occupied orbits in Eq. (30) thus[14]

$$\sum_{\lambda=1}^{A} = \sum_{\lambda=1s,1p} + \sum_{\mu=1}^{M} - \sum_{\nu=1}^{N} \tag{41}$$

The orbits μ are the orbits that are filled in the nucleus under consideration but empty in ^{16}O. These are called *particle orbits,* and they belong to the $2s$-$1d$ shell or higher shells. The orbits ν, called *hole orbits,* are empty in the

nucleus under consideration but filled in ^{16}O, and they belong to the $1p$ or $1s$ shell. Thus ^{20}Ne would consist of $M = 4$ particle orbits and no hole orbits in its ground state; ^{12}C would consist of $N = 4$ hole orbits. A negative parity state of ^{19}F, say, may be constructed with $M = 4$ particle orbits and $N = 1$ hole orbit; etc. The H.F. Hamiltonian matrix of Eq. (30) would then become

$$\begin{aligned}\langle jm\tau \mid h \mid j'm'\tau\rangle = \langle jm \mid t \mid j'm'\rangle &+ \sum_{\lambda\epsilon 1s,1p} \langle jm\tau, \lambda \mid v \mid j'm'\tau, \lambda\rangle \\ &+ \sum_{\mu=1}^{M} \langle jm\tau, \mu \mid v \mid j'm'\tau, \mu\rangle \\ &- \sum_{\nu=1}^{N} \langle jm\tau, \nu \mid v \mid j'm'\tau, \nu\rangle \qquad (42)\end{aligned}$$

The first line of Eq. (42) is just the H.F. Hamiltonian of the closed-shell solution of ^{16}O.

Thus the H.F. Hamiltonian takes the simple form

$$\begin{aligned}\langle jm\tau \mid h \mid j'm'\tau\rangle = \epsilon_j \delta_{jj'}\delta_{mm'} &+ \sum_{\mu=1}^{M} \langle jm\tau, \mu \mid v \mid j'm'\tau, \mu\rangle \\ &- \sum_{\nu=1}^{N} \langle jm\tau, \nu \mid v \mid j'm'\tau, \nu\rangle \qquad (43)\end{aligned}$$

where only particle and hole orbits appear and where the kinetic energy term in (30) is replaced with the single-particle energies ϵ_j of the ^{16}O field. In terms of the ^{16}O closed-shell Slater determinant $\mid \varphi_0\rangle$ the H.F. state of Eq. (3) may be written thus

$$\mid \varphi\rangle = b^\dagger_{\mu_1} b^\dagger_{\mu_2} \cdots b^\dagger_{\mu_M} b_{\nu_1} b_{\nu_2} \cdots b_{\nu_N} \mid \varphi_0\rangle \qquad (44)$$

and the H.F. energy of Eq. (8) becomes

$$\begin{aligned}E_{\mathrm{HF}} = E_0 &+ \sum_{\mu} \langle \mu \mid K \mid \mu\rangle - \sum_{\nu} \langle \nu \mid K \mid \nu\rangle \\ &+ \tfrac{1}{2} \sum_{\mu\mu'} \langle \mu\mu' \mid v \mid \mu\mu'\rangle + \tfrac{1}{2} \sum_{\nu\nu'} \langle \nu\nu' \mid v \mid \nu\nu'\rangle - \sum_{\mu\nu} \langle \mu\nu \mid v \mid \mu\nu\rangle \qquad (45)\end{aligned}$$

where E_0 is the ^{16}O ground-state energy

$$E_0 = \langle \varphi_0 \mid H \mid \varphi_0\rangle$$

and K is the ^{16}O spherical field operator defined by its matrix elements

$$\langle jm\tau \mid K \mid j'm'\tau \rangle = \epsilon_j \delta_{jj'} \delta_{mm'} \tag{46}$$

The density matrix formulation of Section 2 may be maintained provided the density operator of Eq. (33) is replaced by the operator

$$\rho^{(\tau)}_{j_1m_1,j_2m_2} - \rho^0_{j_1m_1,j_2m_2}$$

where

$$\rho^0_{j_1m_1,j_2m_2} = \sum_{\lambda=1s,1p} C^{\lambda}_{j_2m_2} C^{\lambda^*}_{j_1m_1} \tag{47}$$

is the density operator of the ^{16}O spherical field. Thus the H.F. problem is formulated with reference to the ^{16}O closed shell. This formulation is suitable for the description of $2s$-$1d$ shell nuclei in which one assumes an inert ^{16}O closed-shell core and $A - 16$ valence nucleons occupying orbits μ which are expanded on the $1d_{5/2}$, $2s_{1/2}$, and $1d_{3/2}$ states of the $2s$-$1d$ shell. The inert ^{16}O core simply produces a spherical field, and all the deformation is due to the valence particles (or holes). Hartree–Fock calculations of this type are used as an approximation to the diagonalization of the Hamiltonian (7) among the $A - 16$ nucleon configurations in the $2s$-$1d$ shell. They are simple and much may be learned from them about the structure of nuclei.

5.3 The Choice of the Interaction Strength, of the Single-Particle Energies, and of the Oscillator Constant

Since the mean square radii $\langle jm\tau \mid r^2 \mid jm\tau \rangle$ of all orbits belonging to a given major shell of an oscillator are equal, the mean square radius of a H.F. wave function obtained by a single major-shell calculation depends on the oscillator constant $\alpha = \sqrt{m\omega/\hbar}$ only and not on the variational parameters C_j^{λ}. The oscillator constant α is thus determined for each nucleus by the mean square radius known from electron-scattering experiments.[20] The values of α for each nucleus are given in Table I.

It has been shown that in a single major-shell calculation the states of ^{17}O and ^{15}O are just the $\mid jm\tau \rangle$ states themselves. Thus the single-particle energies may be obtained from the binding-energy differences

$$\begin{aligned} [^{17}\mathrm{O}]_j - [^{16}\mathrm{O}] &= \epsilon_j \\ &= \langle \varphi_0 \mid b_{jm\tau} H b^{\dagger}_{jm\tau} \mid \varphi_0 \rangle - \langle \varphi_0 \mid H \mid \varphi_0 \rangle \end{aligned}$$

$j = 1d_{5/2}, 2s_{1/2}, 1d_{3/2}$

and

$$[^{16}\mathrm{O}] - [^{15}\mathrm{O}]_j = \epsilon_j$$
$$= \langle \varphi_0 \mid H \mid \varphi_0 \rangle - \langle \varphi_0 \mid b^{\dagger}_{jm\tau} H b_{jm\tau} \mid \varphi_0 \rangle$$

$j = 1s_{1/2}, 1p_{3/2}, 1p_{1/2}$

TABLE I

Root Mean Square Radii of Charge Distributions of Various Nuclei, Obtained from Electron Scattering[19] Experiments, and the Value of the Oscillator Constant $\alpha = \sqrt{m\omega/\hbar}$, Which Yields the Experimental Charge Radius in Single Major-Shell Calculations

Nucleus	Root mean square radius, fm	α, fm^{-1}
^{4}He	1.62	0.756
^{12}C	2.37	0.620
^{16}O	2.64	0.568
^{24}Mg	2.98	0.547
^{28}Si	3.04	0.548
^{32}S	3.19	0.531
^{40}Ca	3.52	0.492

where $[^{16}\mathrm{O}]$ is the binding energy of ^{16}O, and $[^{17}\mathrm{O}]_j$ and $[^{15}\mathrm{O}]_j$ are, respectively, the binding energies of a state of ^{17}O and ^{15}O with spin j. Assuming that the ground state $5/2^+$ with the lowest $1/2^+$ and $3/2^+$ states of ^{17}O and the ground state $1/2^-$ with the lowest $3/2^-$ state of ^{15}O have unit single-particle strength, the following values of ϵ_j in the $1p$ shell and $2s$-$1d$ shell are obtained:

$$\begin{aligned} &\epsilon_{d_{5/2}} = -4.14 \text{ MeV} \qquad \epsilon_{s_{1/2}} = -3.27 \text{ MeV} \qquad \epsilon_{d_{3/2}} = 0.94 \text{ MeV} \\ &\epsilon_{p_{1/2}} = -15.67 \text{ MeV} \qquad \epsilon_{p_{3/2}} = -21.83 \text{ MeV} \end{aligned} \tag{48}$$

One of the advantages of using form (43) of the H.F. Hamiltonian resides in the use of experimental values (48) of single-particle energies. Indeed, most calculations use simple forces, which do not yield the correct values of ϵ_j when they are calculated explicitly with expression (38). No spin-orbit splitting is obtained with central forces, for example. It is hoped that some of the missing terms in the interaction v that is used and possibly some of the effects of the restrictions of Eq. (37) are counterbalenced by the use of experimental values of single-particle energies. Nonetheless it should

not be forgotten that the ϵ_j used in Eq. (43) represents the value of Eq. (38) calculated with the oscillator constant α of the nucleus under consideration. The values in (48) are the ones obtained with the ^{16}O value of α. As α varies from one nucleus to another, the ϵ_j's also vary, and this effect may be taken into account by considering the ^{40}Ca closed-shell solution in which the energies of the orbits are

$$e_j = \epsilon_j + \sum_{\mu=1}^{24} \langle jm\tau, \mu \mid v \mid jm\tau, \mu \rangle \tag{49}$$

In ^{40}Ca all the $2s$-$1d$ shell orbits are filled, so that e_j is independent of the C_{jm}^{μ} coefficients. The energies e_j may be estimated from pickup experiments on ^{40}Ca[21]

$$e_{d_{5/2}} = -21.73 \text{ MeV} \qquad e_{s_{1/2}} = -18.20 \text{ MeV} \qquad e_{d_{3/2}} = -15.73 \text{ MeV} \tag{50}$$

Assume a given interaction $V_0 v$ has been chosen, with the strength V_0 only to be determined. The difference between the binding energies of ^{40}Ca and ^{16}O is

$$[^{40}\text{Ca}] - [^{16}\text{O}] = 2 \sum_j (2j+1)\, \epsilon_j + \tfrac{1}{2} V_0 \sum_{\mu\mu'=1}^{24} \langle \mu\mu' \mid v \mid \mu\mu' \rangle = -274 \text{ MeV} \tag{51}$$

The experimental value is taken from Table VI. Equation (49) becomes

$$e_j = \epsilon_j + V_0 \sum_{\mu=1}^{24} \langle jm\tau, \mu \mid v \mid jm\tau, \mu \rangle \tag{49a}$$

Equations (49a) and (51) may be solved for the ϵ_j and for V_0. In these equations the oscillator constant α appropriate to ^{40}Ca should be used and the ϵ_j values obtained will be those corresponding to the ^{40}Ca value of α.

For example, if a Rosenfeld force is chosen,

$$v = V_0 e^{-(r/\mu)^2} \frac{\boldsymbol{\tau}_1 \cdot \boldsymbol{\tau}_2}{3} [0.3 + 0.7\, \boldsymbol{\sigma}_1 \cdot \boldsymbol{\sigma}_2] \tag{52}$$

with $\mu = 1.48$ fm, Eqs. (49) and (51) yield strength $V_0 = {}_{+}70.82$ MeV and single-particle energies ϵ_j to be used in ^{40}Ca:

$$\epsilon_{d_{5/2}} = -6.19 \text{ MeV} \qquad \epsilon_{s_{1/2}} = -3.22 \text{ MeV} \qquad \epsilon_{d_{3/2}} = -0.25 \text{ MeV} \tag{53}$$

Values (53) of the single-particle energies ϵ_j in ^{40}Ca are quite similar to values (48) in ^{16}O. It should be reasonable to extra-polate them linearly for values of α in intermediate nuclei. The set of values thus obtained for each nucleus when the Rosenfeld force of Eq. (52) is used is shown in Table II. This method has the advantage of giving ^{16}O and ^{40}Ca compatible roles as reference nuclei.

If, instead of a Rosenfeld force, a Serber force had been used,

$$v = V_0 e^{-(r/\mu)^2} \tfrac{1}{8}[3 - \sigma_1 \cdot \sigma_2 - \tau_1 \cdot \tau_2 - (\sigma_1 \cdot \sigma_2)(\tau_1 \cdot \tau_2)] \tag{54}$$

with $\mu = 1.48$ fm, Eqs. (49a) and (51) would yield the strength $V_0 = -35$ MeV and single-particle energies ϵ_j to be used in ^{40}Ca:

$$\epsilon_{d_{5/2}} = -8.16 \text{ MeV} \qquad \epsilon_{s_{1/2}} = -4.97 \text{ MeV} \qquad \epsilon_{d_{3/2}} = -2.16 \text{ MeV} \tag{55}$$

TABLE II

Values of the Oscillator Constant and of the Single-Particle Energies ϵ_j Used in the Single Major-Shell H.F. Calculations with a Rosenfeld Force[a]

Nucleus	α, fm^{-1}	$\epsilon_{d_{5/2}}$	$\epsilon_{s_{1/2}}$	$\epsilon_{d_{3/2}}$
^{16}O	0.568	−4.14	−3.27	0.93
^{20}Ne	0.559	−4.38	−3.26	0.79
^{24}Mg	0.547	−4.71	−3.26	0.61
^{28}Si	0.548	−4.68	−3.26	0.62
^{32}S	0.531	−5.14	−3.25	0.36
^{36}A	0.496	−6.09	−3.22	−0.19
^{40}Ca	0.492	−6.19	−3.22	−0.25

[a] The energies of the p-shell single-particle states were those obtained from ^{15}O as given by Eq. (48). In ^{12}C the values of (48) were also used for p shell and $2s-1d$ shell states. The values of α for ^{20}Ne and ^{36}A were extrapolated from the values of neighboring nuclei given in Table I.

There are no radial variations in single major-shell calculations, so that the problem of radial stability is not encountered. But the solutions are sensitive to the exchange mixture of the force. In Section 8 it is shown that solutions of even-even $N = Z$ nuclei depend essentially on two combinations of the exchange components of the interaction, namely,

$$S = 4W + 2B - 2H - M \qquad \text{and} \qquad G = W + 2B - 2H - 4M \tag{56}$$

where W, B, H, and M are the strengths of the Wigner, Bartlett, Heisenberg, and Majorana components of the interaction written in the form

$$v = e^{-(r/\mu)^2}[W + BP_\sigma - HP_\tau + MP_x]$$

$$P_\sigma = \frac{1 + \sigma_1 \cdot \sigma_2}{2} \qquad P_\tau = \frac{1 + \tau_1 \cdot \tau_2}{2} \qquad P_x = -P_\sigma P_\tau \tag{57}$$

It will be shown that, for a given binding energy, large gaps are only obtained with large values of G compared with those of S. Experimental data suggest large gaps (Table VI), so that in this theory a Rosenfeld force which has

$S = 0$, $G > 0$ is a preferable effective interaction to a Serber force which has $S = -G$ and produces small gaps (see Fig. 3).

6. SOLUTIONS OF THE SINGLE MAJOR-SHELL HARTREE–FOCK CALCULATIONS FOR EVEN–EVEN $N = Z$ NUCLEI

In this section the energies and the wave functions of the orbits obtained by diagonalizing the H.F. Hamiltonian equation (43) for even–even $N = Z$ nuclei are given.

The orbits are fourfold degenerate, as discussed in Section 3. Neutrons and protons are in the same orbits, and time-reversal symmetry is assumed. The Coulomb interaction is neglected. If its effect is to shift the proton levels all by the same amount above the neutron levels, it has no effect on the orbital wave functions.[10] The single-particle energies and the oscillator constants shown in Table II are used as well as the Rosenfeld force (52). The single-particle energies of $1p$ shell states are those of Eqs. (48) for all nuclei. The results are classified according to their symmetry. Only the solution with the lowest energy of a stated symmetry is given for each nucleus. The question of other solutions is discussed in Section 11.

6.1 Spherical Solutions

These are shown in Table III. Only the energies of the orbits need be shown, since the wave functions are pure $|jm\tau\rangle$ states. The spherical solutions

TABLE III

Energies of the H.F. Orbits in the Spherical Field of Closed-Shell Solutions of Various Nuclei

Orbits \ Nucleus	^{12}C	^{16}O[a]	^{28}Si	^{32}S	^{36}Ar	^{40}Ca[a]
$1d_{3/2}$	5.12	+0.93	−10.12	−11.59	−14.36[b]	−15.73[b]
$2s_{1/2}$	−1.20	−3.27	−8.92	−17.00[b]	−11.16	−18.20[b]
$1d_{5/2}$	0.84	−4.15	−14.35[b]	−16.13[b]	−20.26[b]	−21.73[b]
$1p_{1/2}$	−8.43	−15.67[b]	−28.13[b]	−29.29[b]	−32.23[b]	−33.66[b]
$1p_{3/2}$	−13.25[b]	−21.83[b]	−33.32[b]	−34.58[b]	−38.39[b]	−39.82[b]
E_{HF}[c]	48.57	0	−114.22	−168.08	−216.25	−274.30

[a] The ^{16}O and ^{40}Ca values are taken from experiment (except for the p-shell states of ^{40}Ca); they are used to determine the single-particle energies and the interaction strength (Section 5).

[b] The shells that are closed in each nucleus.

[c] The bottom line indicates the H.F. energy relative to ^{16}O.

TABLE IV

Axially Symmetric Solutions

	^{12}C	^{20}Ne	^{24}Mg	^{28}Si prol.	^{28}Si obl.	^{32}S obl.	^{32}S prol.	^{36}Ar
1p Shell orbits	−18.29*	−27.62*	−32.03*	−36.37*	−35.09*	−35.30*	−37.21*	−38.29*
	−14.80*	−0.9626	−0.9480	−0.9356	−32.13*	−34.11*	−0.9776	−36.32*
	0.7343	0.2710	0.3184	0.3530	0.8344	0.9874	0.2107	0.9534
	0.6789	−23.81*	−26.95*	−29.92*	0.5511	0.1582	−34.38*	0.3019
	−1.84	−18.69*	−22.29*	−25.08*	−24.07*	−29.03*	−29.66*	−30.54*
	0.6789	0.2710	0.3184	0.3530	0.5511	0.1582	0.2107	0.3019
	0.7343	0.9626	0.9480	0.9356	−0.8344	−0.9874	0.9776	0.9534
2s-1d Shell orbits	−2.71	−14.58*	−16.25*	−19.37*	−18.53*	−17.95*	−19.74*	−20.92*
	−1.64	−0.7576	−0.7904	−0.7763	−17.98*	−0.7536	−0.8856	−19.78*
	−0.2450	0.5273	0.5452	0.6188	−0.5783	−0.5904	0.4641	0.9941
	−0.9652	0.3847	0.2794	0.1203	−0.7596	0.2891	0.0203	0.1084
	0.0914	−6.58	−11.94*	−17.53*	0.2977	−17.61*	−19.91*	−18.80*
	0.13	−0.9932	−0.9706	−0.9531	−14.99*	−16.48*	−0.9753	0.8054
	0.8521	0.1167	0.2406	0.3027	0.6935	−0.5655	0.2209	0.5873
	0.5234	−5.19	−9.81	−14.67*	0.7204	0.8064	−15.51*	0.0801
	3.41	−0.6357	−0.5436	−0.4572	−8.32	0.1729	−0.2985	−15.83*
	0.9493	−0.7298	−0.4139	−0.4212	0.7204	−15.07*	−0.5350	−0.4393
	−0.2196	−0.2516	−0.7302	−0.7833	−0.6935	0.9081	−0.7903	0.6822

	0.2251	−5.14	−7.50	−9.26	−8.11	0.4187	−14.33*	−0.5844
	4.35	−2.35	−4.89	−6.50	0.8044	−11.37	−10.23	−14.74*
	0.5234	−0.1481	0.2825	0.4340	−0.4702	0.4187	0.2209	0.1084
	−0.8521	0.4351	0.7290	0.6630	0.3630	−0.9081	0.9753	−0.9941
	8.01	−0.8881	−0.6235	−0.6099	−4.10	−10.03	−10.03	−10.14
	0.1972	−0.25	−2.99	−4.70	0.1358	0.3352	0.3559	0.3979
	−0.1419	0.1167	0.2406	0.3027	−0.4494	0.0332	0.7060	−0.4355
	−0.9700	0.9932	0.9706	0.9531	−0.8830	0.9416	−0.6123	−0.8075
E_{HF}	41.06	−35.78	−72.91	−122.01	−123.00	−168.44	−168.80	−220.48
$\langle J^2 \rangle$	7.24	16.33	18.73	26.74	23.50	16.92	14.85	14.07

The underlined numbers are the energies e_λ of the H.F. orbits. The energy of each orbit is followed by its components C_j^λ. The first three orbits are $1p$-shell negative-parity orbits. The next six orbits are positive-parity orbits of the $2s$-$1d$ shell. The energies of $K = \frac{1}{2}$ negative-parity orbits are followed by their components on the $p_{1/2}^{3/2}$ and $p_{1/2}^{1/2}$ states. The $K = \frac{3}{2}$ negative-parity orbits have no indicated components, and they are pure $p_{3/2}^{3/2}$ states. The $K = \frac{1}{2}$ positive-parity orbits are followed by their components on the $d_{1/2}^{5/2}$, $2s_{1/2}^{1/2}$, $d_{1/2}^{3/2}$ states, in that order. The $K = \frac{3}{2}$ positive-parity orbits are followed by their components on the $d_{1/2}^{5/2}$ and $d_{1/2}^{3/2}$ states. The $K = \frac{5}{2}$ positive-parity orbits have no indicated components, and they are pure $d_{5/2}^{5/2}$ states. The last two lines give the H.F. energy E_{HF} and the mean value $\langle J^2 \rangle$ of the total angular momentum operator in the H.F. state. Asterisks indicate which orbits are filled.

of ^{20}Ne and ^{24}Mg are not shown because they are much higher in energy than the deformed solutions and because they are of no particular interest.

6.2 Axially Symmetric Solutions

These are shown in Table IV. Expansion (35) of the orbits in an axially symmetric field makes it possible to label the orbits according to their component m_λ of J_z. Two solutions of ^{28}Si and ^{32}S are shown, one with prolate shape (positive quadrupole moment) and one with oblate shape (negative quadrupole moment). The near degeneracy of these solutions will be discussed below.

6.3 Ellipsoidal Solutions

These are found to have a lower energy than the axially symmetric solutions in ^{24}Mg and ^{32}S.[12] The orbits may no longer be labeled by m_λ, because J_z does not commute with the H.F. Hamiltonian in this case. But, in order to ensure the reflection symmetries (36), the orbits must be expanded over the $2s$-$1d$ shell states (Table V)

$$d^{5/2}_{-3/2}\,,\ d^{5/2}_{1/2}\,,\ d^{5/2}_{5/2}\,,\ 2s^{1/2}_{1/2}\,,\ d^{3/2}_{1/2}\,,\ d^{3/2}_{-3/2} \tag{58}$$

The time-reversed orbit

$$|\,\bar{\lambda}\rangle = e^{-i\pi J_y}\,|\,\lambda\rangle = \sum_{jm} C^{\lambda}_{jm}(-)^{j-m}\,|\,j-m\rangle \tag{59}$$

is then orthogonal to the orbit $|\,\lambda\rangle$ expanded on the states in (58). With this expansion the x, y, and z axes are automatically the principal axes of the ellipsoid. If an axially symmetric solution is rotated by a finite angle about an axis other than the z axis, the H.F. state will consist of orbits which do not have good m_λ but it still will not represent a different solution. This difficulty is avoided by the proper choice of principal axes. With expansion (58) one still has the possibility of obtaining an axially symmetric solution but with the z axis interchanged with one of the other two axes. Such a solution will appear ellipsoidal, but it is in fact spurious. These spurious solutions may easily be recognized by the fact that the energies of the H.F. state and of the orbits are the same as those of an axially symmetric solution oriented along the z direction. The ellipsoidal solutions of ^{24}Mg and ^{32}S are given in Table V.

TABLE V

Ellipsoidal Solutions of ^{24}Mg and ^{32}S[a]

Magnesium 24	$\alpha = 0.547$	$d^{5/2} = -4.71$	$s^{1/2} = -3.26$	$d^{3/2} = 0.61$	$E = -76.73$	
e_λ	$d^{5/2}_{-3/2}$	$d^{5/2}_{1/2}$	$d^{5/2}_{5/2}$	$2s^{1/2}_{1/2}$	$d^{3/2}_{1/2}$	$d^{3/2}_{-3/2}$
−16.89*	−0.2118	−0.7794	0.1213	0.5327	0.1544	−0.1595
−14.48*	0.7553	0.1051	0.0870	0.3343	0.5201	0.1690
−7.90	0.3945	−0.5034	−0.6553	−0.3544	−0.1644	0.0945
−6.94	−0.3558	0.2971	−0.7253	0.3311	0.3828	−0.0545
−4.92	−0.2788	−0.1976	0.1486	−0.5581	0.6951	0.2577
−2.45	−0.1570	−0.0294	−0.0120	0.2403	−0.2212	0.9315
Sulfur 32	$\alpha = 0.531$	$d^{5/2} = -5.14$	$s^{1/2} = -3.24$	$d^{3/2} = 0.35$	$E = -171.84$	
−20.70*	0.0938	−0.1597	0.9382	−0.2869	0.0374	−0.0412
−19.36*	0.5274	−0.5734	−0.3161	−0.5185	0.0086	−0.1555
−17.51*	−0.7117	−0.2047	−0.1184	−0.4973	0.3509	0.2592
−15.14*	−0.0546	0.4208	−0.0477	−0.2478	0.3541	−0.7943
−9.90	−0.4060	−0.6023	0.0410	0.3799	−0.2393	−0.5188
−6.50	−0.1969	0.2528	−0.0431	−0.4426	−0.8323	−0.0829

[a] The heading lines give the oscillator constant, the single-particle energies ϵ_j used, and the H.F. energy E. The first column gives the energies e_λ of the H.F. orbits, and the following columns give the components on the $2s$-$1d$ shell states shown. Asterisks indicate which orbits are filled.

6.4 The Energy Gap and the Spectrum of the Hartree–Fock Orbits

Figure 1 shows the spectrum of the H.F. orbits of the lowest-energy solutions. The most remarkable features of the single-particle spectrum of the H.F. field are the constancy of the Fermi level, defined as the energy of the highest filled orbit, and the energy gap separating filled and empty orbits.

The wave function of the Fermi level changes constantly as more particles are added. In ^{12}C and ^{16}O the Fermi level is a p shell orbit and between ^{20}Ne and ^{40}Ca it is a $2s$-$1d$ shell orbit. Odd-A nuclei obtained by adding or removing one nucleon from an even-even $N = Z$ nucleus may in a first approximation be described as a particle or a hole in the H.F. wave function of the even nucleus

$$\begin{aligned} |\varphi_\mu\rangle &= b_\mu^\dagger\,|\varphi\rangle \qquad \text{for the } A+1 \text{ nucleus} \\ |\varphi_\lambda\rangle &= b_\lambda\,|\varphi\rangle \qquad \text{for the } A-1 \text{ nucleus} \end{aligned} \tag{60}$$

where $|\varphi\rangle$ is the H.F. state (44) of the even nucleus. Then the difference in binding energies between the even and odd nuclei is according to Eq. (43)

$$\begin{aligned} E(A+1) - E(A) &= e_\mu \\ E(A) - E(A-1) &= e_\lambda \end{aligned} \tag{61}$$

Thus the neutron separation energies of the even–even nucleus A and of the odd $A+1$ nucleus are equal to the Fermi level and to the energy of the lowest empty orbit, respectively. The gap is therefore given by

$$G = E(A+1) - E(A) - [E(A) - E(A-1)] \tag{62}$$

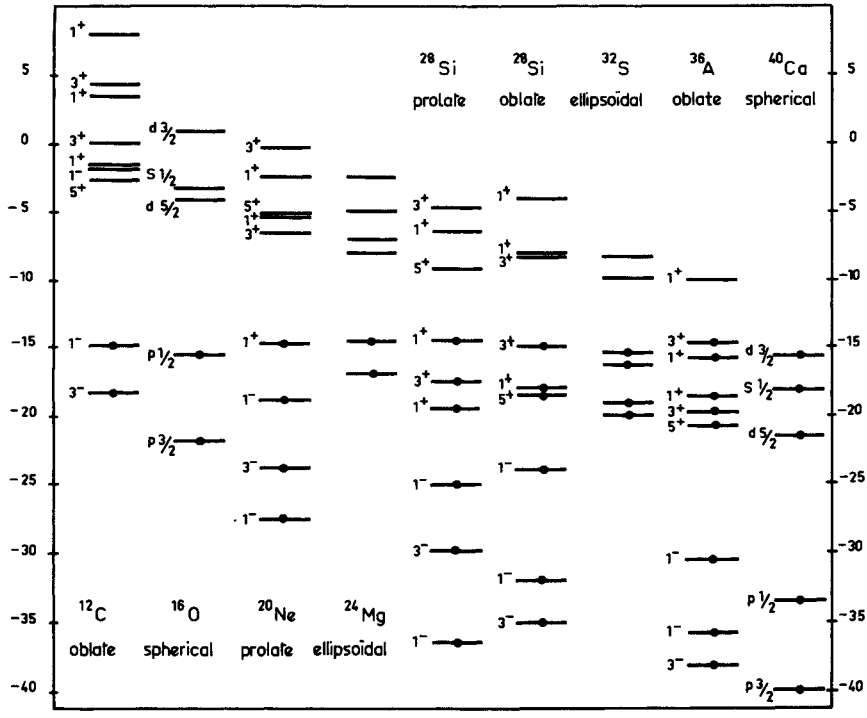

Fig. 1*a*. Spectrum of the H.F. orbits of lowest-energy solutions of even-even $N = Z$ nuclei between ^{12}C and ^{40}Ca. The levels are fourfold degenerate, and occupied orbits are marked with a dot. The additional symmetry of each solution is indicated and also the shape (prolate or oblate) of the axially symmetric solutions. The axially symmetric solutions are labeled by $(2k)^\pi$; e.g., 3^+ means a $k = \frac{3}{2}$ orbits of the $2s$-$1d$ shell and 1^- means a $k = \frac{1}{2}$ orbit of the p shell. For spherical and axially symmetric solutions the $1p$ and $2s$-$1d$ shell orbits are shown. For ellipsoidal solutions only $2s$-$1d$ shell orbits are shown.

TABLE VI

Experimental Values of Binding Energies and Neutron Separation Energies[a]

Nucleus	A	$E(A)$	$E(A) - E(A-1)$ Fermi level	Gap	$\frac{E(A) - E(16)}{A - 16}$
^{12}C	12	−101.38	−18.72	13.77	10.37
^{16}O	16	−142.88	−15.67	11.53	0
^{20}Ne	20	−181.98	−16.87	10.11	−9.77
^{24}Mg	24	−228.71	−16.54	9.21	−10.73
^{28}Si	28	−277.26	−17.17	8.69	−11.20
^{32}S	32	−323.23	−15.08	6.43	−11.27
^{36}A	36	−369.42	−15.27	6.48	−11.33
^{40}Ca	40	−416.97	−15.63	7.27	−11.42

[a] The binding energies are corrected for the Coulomb energy assumed to be of the form $E_c = \alpha[Z(Z-1)/A^{1/3}]$; the value of α was deduced from the difference in binding energies of the mirror $A - 1$ nuclei. $E(A) - E(A-1)$ is the neutron separation energy of the even–even A nucleus. The gap is $G = E(A+1) - E(A) - [E(A) - E(A-1)]$. The last column gives the binding energy per particle relative to the ^{16}O binding energy.

Table VI gives the experimental values of the binding energies, the Fermi level, and the gap defined by Eqs. (61) and (62). Table VII gives the corresponding quantities obtained from the H.F. solutions with lowest energy.

TABLE VII

The Fermi Level (Energy of the Highest Occupied Orbit), the Energy Gap between the Fermi Level and the Lowest Empty Orbit, and the H.F. Energy Divided by the Number of Nucleons in the $2s$-$1d$ Shell[a]

Nucleus	Shape	Fermi level	Gap	$E_{HF}/(A-16)$
^{12}C	oblate	−14.80	12.09	10.26
^{16}O	spherical	−15.67*	11.53*	0
^{20}Ne	prolate	−14.58	8.00	−8.94
^{24}Mg	ellipsoïdal	−14.48	6.58	−9.59
^{28}Si	prolate	−14.67	5.41	−10.17
^{28}Si	oblate	−14.99	6.67	−10.25
^{32}S	ellipsoïdal	−15.14	5.24	−10.74
^{36}A	oblate	−14.74	4.60	−11.02
^{40}Ca	spherical	−15.73*	7.27*	−11.42*

[a] The results are obtained from a single major-shell calculation using a Rosenfeld force. The numbers marked by an asterisk are those which were used to determine the single-particle energies and the interaction strength.

It should be borne in mind that the description of odd-A nuclei given by Eq. (60) can only be a rough approximation. For example, angular momentum effects are completely neglected. Nonetheless a comparison of Tables VI and VII shows that the constancy of the Fermi level is very well reproduced by the H.F. calculation. The agreement of the binding energies is simply an illustration of the saturation property of the Rosenfeld force. Table VI shows that the gap is a slowly decreasing function of the mass number A. Compared with experiment, the H.F. calculations yield a slightly smaller gap which decreases somewhat faster with mass number. Calculations show that the gap is reduced by the spin–orbit splitting between the $d_{5/2}$ and $d_{3/2}$ states. The gap will be shown to be due to the large Majorana exchange component of the force. As the mass number increases, the gap becomes smaller because the matrix elements of the force become smaller, whereas the spin–orbit splitting increases somewhat. In the second half of the $2s$-$1d$ shell, the spin–orbit splitting becomes comparable to the gap and the intrinsic states become less stable. It will be seen that some trouble is encountered in this region in trying to explain nuclear properties with H.F. wave functions.

A comparison between the spherical and deformed solutions in Tables III and IV shows that deformed solutions are strongly favored for ^{12}C and ^{28}Si. The deformed solutions have, respectively, 7.5 MeV and 9 MeV more binding. The gaps of the spherical solutions of ^{12}C and ^{28}Si are, respectively, 4.82 MeV and 5.43 MeV, which are much smaller than the experimental values shown in Table VI. In the spherical solutions the gap is the splitting between the $p_{3/2}$ and $p_{1/2}$ states in ^{12}C and between the $d_{5/2}$ and $2s_{1/2}$ states in ^{28}Si. Calculations of particle-hole excitations which assume closed-shell ground states are led to use single-particle energies for the $p_{3/2}$ and $p_{1/2}$ states in ^{12}C and for the $d_{5/2}$ and $2s_{1/2}$ states in ^{28}Si, which are separated by 13.77 and 8.69 MeV, respectively. With reasonable forces, such splittings are incompatible with the splittings observed in ^{15}O and ^{17}O. A reasonable gap is obtained in the deformed H.F. solution by using single-particle energies observed in ^{15}O and ^{17}O. Furthermore, the spherical solutions would imply that the 2^+ excited states in ^{12}C and ^{28}Si are particle-hole vibrations. But the large experimental energy gap makes it difficult to obtain a low enough excitation energy in using such configurations. On the other hand, it will be seen in Section 14 that one easily obtains low 2^+ states with deformed solutions.

7. DEFORMED EXCITED EQUILIBRIUM STATES OF SPHERICAL NUCLEI

It is well known that rotational bands have been observed[38] among the excited states of ^{16}O. In particular the 0^+ (6.05 MeV), 2^+ (6.92 MeV),

4^+ (10.36 MeV), and 6^+(~15 MeV) and also the 1^- (9.59 MeV), 3^- (11.63 MeV), and 5^-(~15 MeV) states appear to form $K = 0$ positive and negative parity rotational bands.

Positive-parity particle-hole configurations[39] do not successfully account for the low-lying positive-parity states of ^{16}O. They consist of a particle jumping two major shells (neighboring shells have opposite parity), and they lie too high in energy. Negative-parity particle-hole configurations[36] can only account for the 3^- (6.13 MeV), 1^- (7.12 MeV), and 2^- (8.88 MeV) states, but there are no further particle-hole configurations for the negative-parity states that are assumed to form a rotational band. Two-particle, two-hole ($2p$-$2h$) configurations[40] yield positive-parity states of 12 to 15 MeV excitation. The strong particle–particle and particle–hole residual interactions (especially when the pair of particles and the pair of holes are each coupled to an isospin $T = 1$[41]) lower the $2p$-$2h$ states by about 10 MeV below their unperturbed energy of 23 MeV. But the electromagnetic transitions between the excited states of ^{16}O cannot be accounted for by particle–hole and $2p$-$2h$ configurations alone.[42] It has been known for quite a long time[43] that residual interactions could lower four-particle, four-hole configurations well below their unperturbed energy of 46 MeV. This has been demonstrated[14] by diagonalizing the H.F. Hamiltonian (43) in ^{16}O for $M = 4$ particles in the $2s$-$1d$ shell and $N = 4$ holes in the p shell. Figure 1b shows the H.F. energy of oblate and prolate $4p$-$4h$ states and of the $2p$-$2h$ states plotted against the residual interaction strength V_0. It may be seen that a $4p$-$4h$ state at 6 MeV is more likely to occur than a $2p$-$2h$ state. Figure 1b also shows the single-particle spectrum of the $4p$-$4h$ solutions. Note that the filled $2s$-$1d$ shell orbit is depressed well below the empty $1p$ shell orbit. The Fermi levels of the deformed $4p$-$4h$ solution and the spherical ground state of ^{16}O are quite similar. The energy gap of the oblate solution suggests indeed that the $4p$-$4h$ solution is another equilibrium shape of ^{16}O. Recent H.F. calculations[44] have shown that there is a lower axially asymmetric solution for the $4p$-$4h$ state, in accordance with calculations[6] based on the SU_3 classification of states (see Sections 9 and 15). Such a state will give rise to $K = 0$ and $K = 2$ rotational bands, and the 2^+ (9.85 MeV) and 3^+ (11.08 MeV) states are assigned to the $K = 2$ band. The electromagnetic transitions between the excited states of ^{16}O cannot be accounted for unless some mixing between the closed-shell ground state and the $2p$-$2h$ and $4p$-$4h$ configurations is allowed for. Calculations which estimate such mixing[22,45] show that the 0^+ (6.05 MeV), 2^+ (6.92 MeV), and 4^+ (10.36 MeV) states are predominantly $4p$-$4h$ configurations. The mixing of various equilibrium shapes of nuclei will not be treated in this review. Hartree–Fock calculations of deformed excited states have also been made for ^{18}O and ^{19}F.[15] With the help of the angular momentum projection method (Section 14), they account quite well for the

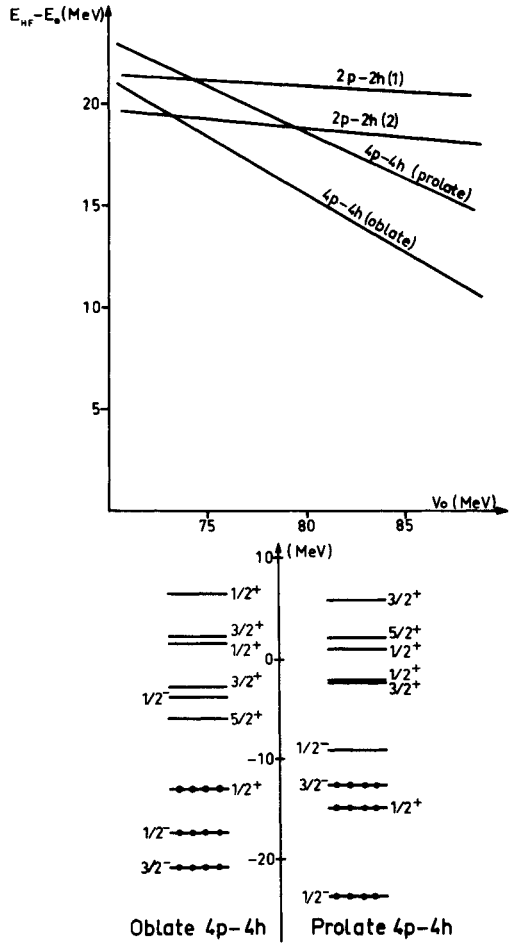

Fig. 1*b*. Variation of the H.F. energy of 2*p*-2*h* and 4*p*-4*h* H.F. states with the residual interaction strength V_0 of the Rosenfeld force [Eq. (52)]. The 2*p*-2*h* state of Eq. (1) consists of two proton particles and two proton holes in $m_\lambda = \frac{1}{2}^+$ and $m_\lambda = \frac{1}{2}^-$ orbits, respectively. The 2*p*-2*h* state of Eq. (2) consists of proton and neutron particles in the orbit $m_\lambda = \frac{1}{2}^+$ and proton and neutron holes in the orbit $m_\lambda = \frac{1}{2}^-$. The band head of the rotational band generated by the 4*p*-4*h* deformed state will lie approximately 4 MeV below the H.F. energy. Below, the spectra of the 2*s*-1*d* shell H.F. orbits of the oblate and prolate 4*p*-4*h* solutions are shown. Dots indicate occupied orbits.

low-lying positive- and negative-parity levels of ^{19}F which belong, respectively, to a $3p$, $K = 1/2^+$ and a $4p$-$1h$, $K = 1/2^-$ rotational band.

8. A SOLUBLE MODEL—THE EFFECTS OF THE EXCHANGE COMPONENTS OF THE INTERACTION

Some insight into the nature of the H.F. spectrum may be obtained by considering a model interaction with no radial dependence

$$v = W + BP_\sigma - HP_\tau + MP_x \tag{63}$$

and a degenerate $2s$-$1d$ shell in which the three single-particle energies ϵ_j assume a common value ϵ.[10,11]

As shown in Section 3, H.F. solutions can then be obtained such that the orbits factorize into space, spin, and isospin parts:

$$|\lambda\rangle = |\lambda_x\rangle\,|\sigma_\lambda\rangle\,|\tau_\lambda\rangle \tag{64}$$

The model interaction (63), having no radial dependence, cannot determine the spatial wave function $|\lambda_x\rangle$ of the H.F. orbits, so that the H.F. Hamiltonian is diagonal in any orthonormal representation of the spatial wave function. It is straightforward to obtain the energy e_α of any orbit α, because matrix elements of model interaction (63) reduce to overlaps between the orbital and spin wave functions:

$$\begin{aligned} e_\alpha &\equiv \langle \alpha_x \sigma_\alpha \tau_\alpha \,|\, h \,|\, \alpha_x \sigma_\alpha \tau_\alpha \rangle \\ &= \epsilon + W \sum_\lambda [1 - (\alpha_x \,|\, \lambda_x)^2\, \delta_{\sigma_\lambda,\sigma_\alpha}\, \delta_{\tau_\lambda,\tau_\alpha}] \\ &\quad + B \sum_\lambda [\delta_{\alpha,\sigma_\lambda} - (\alpha_x \,|\, \lambda_x)^2\, \delta_{\tau_\alpha,\tau_\lambda}] \\ &\quad - H \sum_\lambda [\delta_{\tau_\alpha,\tau_\lambda} - (\alpha_x \,|\, \lambda_x)^2\, \delta_{\sigma_\alpha,\sigma_\lambda}] \\ &\quad + M \sum_\lambda [(\alpha_x \,|\, \lambda_x)^2 - \delta_{\sigma_\lambda,\sigma_\alpha}\, \delta_{\tau_\lambda,\tau_\alpha}] \end{aligned} \tag{65}$$

The two terms in each bracket are the contributions of the direct and exchange terms of the interaction matrix element, respectively, and $(\alpha_x \,|\, \lambda_x)$ is the overlap between the spatial wave functions of the orbit α and the occupied orbit λ. The sums are extended over occupied orbits only.

Equation (65) may be used to check that H.F. solutions, constructed by filling each orbit $|\lambda_x\rangle$ with two protons and two neutrons of opposite spin

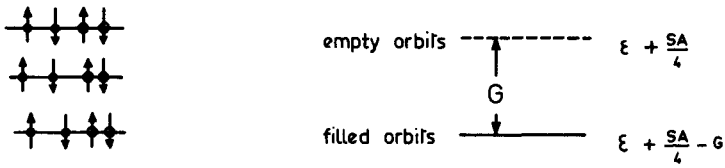

Fig. 2. The filling and the spectrum of the orbits in the case of a degenerate shell and model interaction (63) with no radial dependence.

(as shown in Fig. 2), have the special property that all the filled orbits λ are degenerate at the energy

$$e_\lambda = \epsilon + \frac{SA}{4} - G \qquad \text{filled orbits}$$

and all the empty orbits are degenerate at the energy

$$e_\alpha = \epsilon + \frac{SA}{4} \qquad \text{empty orbits} \tag{66}$$

Here A is the number of nucleons in the shell ϵ, and S and G are defined in Eq. (56). The empty orbits are depressed relative to the filled orbits, and an energy gap G is formed. The constancy of the Fermi level e_λ is ensured by the "saturating condition" $S = 0$, which is verified by a Rosenfeld force. The H.F. energy of the system is

$$E_{\mathrm{HF}} = A\epsilon + \frac{SA^2}{8} - \frac{GA}{2} \tag{67}$$

so that the saturating condition ensures a linear dependence of the energy upon the number of particles. The gap is determined by the combination G of the exchange mixture, which is dominated by the Majorana component of the interaction; a strong attractive Majorana force will produce a large gap. Note that with an attractive Wigner force the occupied orbits would lie above the empty orbits; the gap G would be negative.

When four nucleons fill each orbit $|\lambda_x\rangle$, the matrix elements of the H.F. Hamiltonian become

$$\langle\alpha \mid h \mid \beta\rangle = \langle\alpha \mid t \mid \beta\rangle + S \sum_{\lambda=1}^{n} \langle\alpha\lambda \mid v \mid \beta\lambda\rangle_D - G \sum_{\lambda=1}^{n} \langle\alpha\lambda \mid v \mid \lambda\beta\rangle_D$$

where $n = A/4$ is the number of orbits $|\lambda_x\rangle$ and $\langle\alpha\lambda \mid v \mid \beta\lambda\rangle_D$ is the direct (not antisymmetrized) matrix element

$$\langle\alpha\lambda \mid v \mid \beta\lambda\rangle_D = \int \mathbf{dr}_1\, \mathbf{dr}_2 \varphi_\alpha^*(\mathbf{r}_1)\, \varphi_\lambda^*(\mathbf{r}_2)\, v(\mathbf{r}_1, \mathbf{r}_2)\, \varphi_\beta(\mathbf{r}_1)\, \varphi_\lambda(\mathbf{r}_2)$$

This expression for the H.F. Hamiltonian is valid for a central force with an arbitrary radial dependence.

The H.F. Hamiltonian may be transformed to the configuration space representation

$$\langle \mathbf{r}_1 \mid h \mid \mathbf{r}_2 \rangle = -\delta(\mathbf{r}_1 - \mathbf{r}_2) \frac{\nabla^2}{2m} + S\delta(\mathbf{r}_1 - \mathbf{r}_2) \int \mathbf{dr} \sum_\lambda |\varphi_\lambda(\mathbf{r})|^2 v(\mathbf{r}_1, \mathbf{r})$$
$$- G \sum_\lambda \varphi_\lambda^*(\mathbf{r}_2)\, \varphi_\lambda(\mathbf{r}_1)\, v(\mathbf{r}_1, \mathbf{r}_2)$$

Thus S is the intensity of the local term of the H.F. field and G is the intensity of the nonlocal term. The depression of filled orbits compared with empty

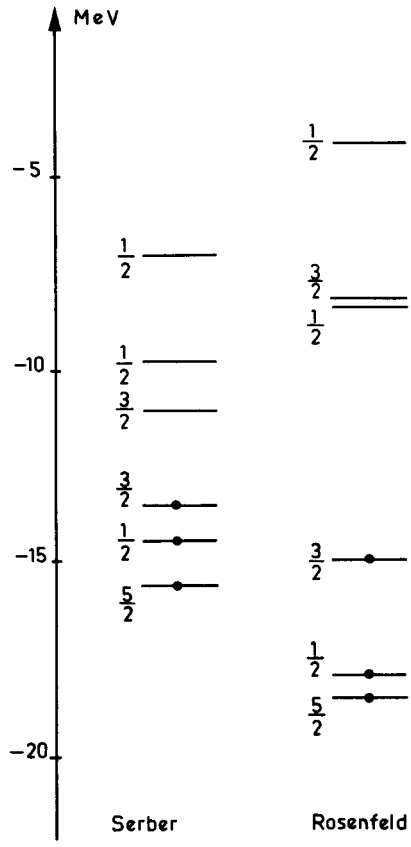

Fig. 3. The spectrum of the H.F. orbits of the oblate solution of ^{28}Si calculated with Serber and Rosenfeld forces.

orbits is an effect of the nonlocality of the H.F. field. One of the main differences between Nilsson orbits[4] and H.F. orbits resides in the large gap. There is no nonlocal term in the Nilsson Hamiltonian.

This model shows, e.g., that if the strengths of a Rosenfeld force ($S = 0, G > 0$) and of a Serber force ($S = -G$) are chosen so as to give similar binding energies in a nucleus, the Rosenfeld force will yield a larger gap. Indeed, let G_r and G_s be the values of G for the Rosenfeld and Serber forces. Then, if they give similar binding energies,

$$E_{\mathrm{HF}} = A\epsilon - \frac{G_r A}{2} = A\epsilon - \frac{G_s A}{2}\left[\frac{A}{4} + 1\right]$$

and

$$G_s = \frac{G_r}{(A/4) + 1} \tag{68}$$

The combination S of the mixture contributes to the binding energy but not to the gap. The combination G contributes to both. This result may be checked on a realistic single major-shell calculation. Figure 3 shows the H.F. spectrum of ^{28}Si calculated with the Rosenfeld force (52) and the Serber force (54). The H.F. energies are, respectively, -123 and -115 MeV. The gaps are, respectively, 6.67 and 2.5 MeV.

9. THE DEFORMATION OF THE HARTREE–FOCK FIELD—THE QUADRUPOLE–QUADRUPOLE INTERACTION

In the model of Section 8, only the monopole part of the force was considered and the wave functions of the orbits in configuration space remained completely undetermined. The model predicted degenerate filled and empty orbits separated by an energy gap, but in calculations which use the complete force the orbits are further split up by the deformation of the field. This additional lifting of the degeneracy of the orbits is very similar to the splitting of various Nilsson orbits as the deformation of the field is increased. It may be understood in terms of a quadrupole–quadrupole force $Q \cdot Q$ with arbitrary spin and isospin exchange components. The quadrupole–quadrupole force is defined as

$$Q \cdot Q \equiv \sum_{m=-2}^{+2} r_1^2 r_2^2 Y_{2m}(\Omega_1)\, Y_{2m}^*(\Omega_2) \equiv \sum_m Q_m Q_m^*$$

Consider the effect of adding the $Q \cdot Q$ force to monopole interaction (63)

in the case of vanishing spin–orbit splitting. The interaction may be written thus

$$v = [W + BP_\sigma - HP_\tau + MP_x](1 + fQ \cdot Q) \tag{69}$$

where f is the strength of the $Q \cdot Q$ force relative to the monopole force.

The orbits still factorize as in Eq. (64) so that the H.F. Hamiltonian is diagonal in spin and isospin space. It is quite straigthforward to obtain the matrix elements of the H.F. Hamiltonian

$$\langle \alpha_x \sigma\tau \mid h \mid \beta_x \sigma\tau \rangle = \delta_{\alpha\beta} h_0(\alpha, \sigma, \tau) + f \sum_m \langle \alpha_x \mid Q_m \mid \beta_x \rangle N_m^{\sigma\tau}$$
$$- f \sum_m \sum_\lambda \langle \alpha_x \mid Q_m \mid \lambda_x \rangle \langle \beta_x \mid Q_m \mid \lambda_x \rangle G_\lambda^{\sigma\tau} \tag{70}$$

In Eq. (70) the first term on the right-hand side is just the contribution of monopole–monopole interaction (63)

$$\langle \alpha_x \sigma\tau \mid h_0 \mid \beta_x \sigma\tau \rangle = \epsilon\, \delta_{\alpha\beta} + \delta_{\alpha\beta} \sum_\lambda S_\lambda^{\sigma\tau} - \delta_{\alpha\beta} \sum_\lambda (\alpha_x \mid \lambda_x)^2 G_\lambda^{\sigma\tau} \tag{71}$$

while

$$N_m^{\sigma\tau} = \sum_\lambda S_\lambda^{\sigma\tau} \langle \lambda_x \mid Q_m \mid \lambda_x \rangle$$
$$S_\lambda^{\sigma\tau} = \sum_{\sigma_\lambda \tau_\lambda} (W + B\delta_{\sigma,\sigma_\lambda} - H\delta_{\tau,\tau_\lambda} - M\delta_{\sigma,\sigma_\lambda}\, \delta_{\tau,\tau_\lambda}) \tag{72}$$
$$G_\lambda^{\sigma\tau} = \sum_{\sigma_\lambda \tau_\lambda} (W\delta_{\sigma,\sigma_\lambda}\, \delta_{\tau,\tau_\lambda} + B\delta_{\tau,\tau_\lambda} - H\delta_{\sigma,\sigma_\lambda} - M)$$

The sums over λ are limited to the occupied orbits only. When four nucleons fill each orbit as shown in Fig. 2, the quantities $S_\lambda^{\sigma\tau}$ and $G_\lambda^{\sigma\tau}$ become independent of σ, τ, and λ and they reduce to S and G defined by Eq. (56). In that case $N_m^{\sigma\tau}$ becomes independent of σ and τ and reduces to

$$N_m = S \sum_{\lambda_x} \langle \lambda_x \mid Q_m \mid \lambda_x \rangle$$

Finally, H.F. Hamiltonian (70) becomes simply

$$\langle \alpha_x \sigma\tau \mid h \mid \beta_x \sigma\tau \rangle = \epsilon \delta_{\alpha\beta} + S \left[n\delta_{\alpha\beta} + f \sum_m \langle \alpha_x \mid Q_m \mid \beta_x \rangle N_m \right]$$
$$- G \sum_{\lambda_x} \left[\delta_{\alpha\beta}\, \delta_{\alpha\lambda} + f \sum_m \langle \alpha_x \mid Q_m \mid \lambda_x \rangle \langle \beta_x \mid Q_m \mid \lambda_x \rangle \right] \tag{70a}$$

where $n = A/4$ is the number of accupied λ_x.

Consider now the states

$$|n_x, n_y, n_z\rangle \tag{73}$$

of the harmonic oscillator. Orbits (73) are defined in terms of the number of quanta in the x, y, and z directions. Let us assume that the orbits λ_x are linear combinations of states (73) which belong to one major shell only, $n_x + n_y + n_z =$ constant for each orbit λ_x. In the $2s$-$1d$ shell, $n_x + n_y + n_z = 2$. It is easy to check that the local term S of H.F. Hamiltonian (70a) is of the form $ax^2 + by^2 + cz^2$ which is diagonalized by harmonic-oscillator states (73). The exchange term requires special attention because, with saturating forces such as the Rosenfeld force ($S = 0$, $G > 0$), it is the only term which contributes. It is not diagonal in representation (73) except in special cases.

Consider ^{20}Ne which has one $2s$-$1d$ shell orbit λ_x filled by four nucleons. It is easy to check that, if the occupied orbit λ_x is a pure $(n_x, n_y, n_z) = (0, 0, 2)$ state, the exchange term of the H.F. Hamiltonian is also diagonal in the representation (73). It would be diagonal no matter which orbit is filled in ^{20}Ne. Thus in ^{20}Ne the H.F. orbits obtained with the model force (69) are pure harmonic-oscillator states (73).

Consider now ^{24}Mg in which eight nucleons fill two orbits λ_x of the $2s$-$1d$ shell. Consider the trial solution in which the filled orbits are the (002) and (011) states of the oscillator. With this trial solution the H.F. Hamiltonian has a nonzero off-diagonal matrix element between the filled (002) orbit and the empty (020) orbit. Indeed this comes from the $Q_1 + Q_{-1}$ contribution

$$(002 \mid yz \mid 011)(020 \mid yz \mid 011) \neq 0$$

But the mixing between the (020) and (002) states is expected to be small, because the diagonal matrix elements of the H.F. Hamiltonian in the states (002) and (020) are separated by the quantity

$$-fG(002 \mid Q_0 \mid 002)^2$$

Moreover the (011) orbit is an eigenstate of the H.F. Hamiltonian so that filling the (002) and (011) orbits is a good approximation to the H.F. solution.

Thus the deformation of the field produced by $Q \cdot Q$ force is very similar to that of a deformed oscillator. The H.F. Hamiltonian [Eq. (70)] consists of a monopole term and of a quadrupole deformation. Both are nonlocal. The monopole term is a constant for each orbit. It affects the energy of each orbit but not its wave function. The quadrupole–quadrupole force contributes a local term which is just a deformed oscillator and, because of the deformation of the field, the exchange term is also nearly diagonalized

by the oscillator wave functions. Note that this would remain true if the term ϵ in Eq. (71) for h_0 were replaced by the kinetic energy operator. The wave functions (but not the energies) obtained with H.F. Hamiltonian (70) are, in fact, similar to asymptotic Nilsson wave functions (obtained for vanishing spin–orbit splitting.) The relation[29] between orbits (73), the $|lm\rangle$ representation, and the $|jm\rangle$ basis is shown in Table VIII.

When single major-shell H.F. calculations are performed with a complete force, such as the Rosenfeld force with a Gaussian radial dependence, it is possible to check whether in the case of vanishing spin–orbit splitting the orbits obtained are similar to orbits (73) obtained with the quadrupole–quadrupole interaction. A vanishing spin–orbit splitting is obtained by replacing the single-particle energies $\epsilon_{d_{5/2}}$ and $\epsilon_{d_{3/2}}$ with a common energy

$$\epsilon = \tfrac{1}{5}(2\epsilon_{3/2} + 3\epsilon_{5/2}) \tag{74}$$

but keeping the $2s_{1/2}$ level at its original position. This method assumes that the splitting of the $d_{5/2}$ and $d_{3/2}$ states is due to a spin–orbit term of the type $a\,\mathbf{l}.\,\mathbf{s}$.

In the case of vanishing spin–orbit splitting, the wave function of the occupied orbit of ^{20}Ne becomes

$$\begin{aligned} |\lambda\rangle &= -0.6286d^{5/2}_{1/2} + 0.5843s^{1/2}_{1/2} + 0.5133d^{3/2}_{1/2} \\ &= -0.8115d_0\uparrow + 0.5843s_0\uparrow \\ &= -0.9999(002)\uparrow - 0.0060(020)\uparrow + 0.0060(200)\uparrow \end{aligned} \tag{75}$$

The ^{20}Ne orbit is very close to a pure (002) orbit of type (73). Figure 4*a* shows the spectrum of orbits in the ^{20}Ne field.

In ^{24}Mg four extra particles have to be placed in the d_1 and d_{-1} orbits which are degenerate in the ^{20}Ne field. If a neutron and a proton are placed in the $d_1\uparrow$ orbit, the time-reversal symmetry requires the other proton–neutron pair to fill the $d_{-1}\downarrow$ orbit. Thus the axially symmetric solution of ^{24}Mg shown in Fig. 4*a* is formed. In this solution the wave functions of the occupied orbits are

$$\begin{aligned} |\lambda_1\rangle &= -0.5964d^{5/2}_{1/2} + 0.6320s^{1/2}_{1/2} + 0.4870d^{3/2}_{1/2} \\ &= -0.7700d_0\uparrow + 0.6320s_0\uparrow \\ |\lambda_2\rangle &= -0.8944d^{5/2}_{3/2} + 0.4472d^{3/2}_{3/2} = d_1\uparrow \end{aligned} \tag{76}$$

The axially symmetric solution of ^{24}Mg does not share all the symmetries of the ^{20}Ne solution. It is invariant under a rotation $e^{-i\pi J_y}$, but not under the

TABLE VIII

Relation between $2s$-$1d$ Shell Harmonic-Oscillator Orbits in Various Representations[a]

(jm) Orbit $(n_x n_y n_z)$	$d^{5/2}_{-3/2}$	$d^{5/2}_{1/2}$	$d^{5/2}_{5/2}$	$s^{1/2}_{1/2}$	$d^{3/2}_{1/2}$	$d^{3/2}_{-3/2}$
$(002)\uparrow$	0	$\sqrt{\frac{2}{5}}$	0	$-\frac{1}{\sqrt{3}}$	$-\sqrt{\frac{4}{15}}$	0
$i(011)\downarrow$	$\sqrt{\frac{2}{5}}$	$\frac{1}{\sqrt{5}}$	0	0	$\sqrt{\frac{3}{10}}$	$\frac{1}{\sqrt{10}}$
$-(101)\downarrow$	$-\sqrt{\frac{2}{5}}$	$\sqrt{\frac{1}{5}}$	0	0	$\sqrt{\frac{3}{10}}$	$-\frac{1}{\sqrt{10}}$
$-i(110)\uparrow$	$-\frac{1}{\sqrt{10}}$	0	$\frac{1}{\sqrt{2}}$	0	0	$\sqrt{\frac{2}{5}}$
$(020)\uparrow$	$-\frac{1}{\sqrt{20}}$	$-\frac{1}{\sqrt{10}}$	$-\frac{1}{2}$	$-\frac{1}{\sqrt{3}}$	$\frac{1}{\sqrt{15}}$	$\frac{1}{\sqrt{5}}$
$(200)\uparrow$	$\frac{1}{\sqrt{20}}$	$-\frac{1}{\sqrt{10}}$	$\frac{1}{2}$	$-\frac{1}{\sqrt{3}}$	$\frac{1}{\sqrt{15}}$	$-\frac{1}{\sqrt{5}}$

$$(002) = -\frac{1}{\sqrt{3}} s_0 + \sqrt{\frac{2}{3}} d_0$$

$$(011) = -\frac{i}{\sqrt{2}} (d_1 + d_{-1})$$

$$(101) = -\frac{1}{\sqrt{2}} (d_1 - d_{-1})$$

$$(110) = \frac{i}{\sqrt{2}} (d_2 - d_{-2})$$

$$(020) = -\frac{1}{\sqrt{3}} s_0 - \frac{1}{\sqrt{6}} d_0 - \frac{1}{2} (d_2 + d_{-2})$$

$$(200) = -\frac{1}{\sqrt{3}} s_0 - \frac{1}{\sqrt{6}} d_0 + \frac{1}{2} (d_2 + d_{-2})$$

[a] Above, the $(n_x n_y n_z)$ σ orbits are expressed in terms of the $|jm\rangle$ basis used for ellipsoidal H.F. solutions. Below, the $(n_x n_y n_z)$ orbits are expressed in terms of the $|lm\rangle$ basis. The lm spectroscopic notation is used; d_1 is the $l = 2$, $m = 1$ state. Arrows pointing up and down indicate spins with projection $\frac{1}{2}$ and $-\frac{1}{2}$ along the z axis.[29]

rotations $e^{-i\pi L_y}$ and $e^{-i\pi S_y}$ separately. The ^{20}Ne solution is an L-S coupling wave function, but the axially symmetric solution of ^{24}Mg is not.

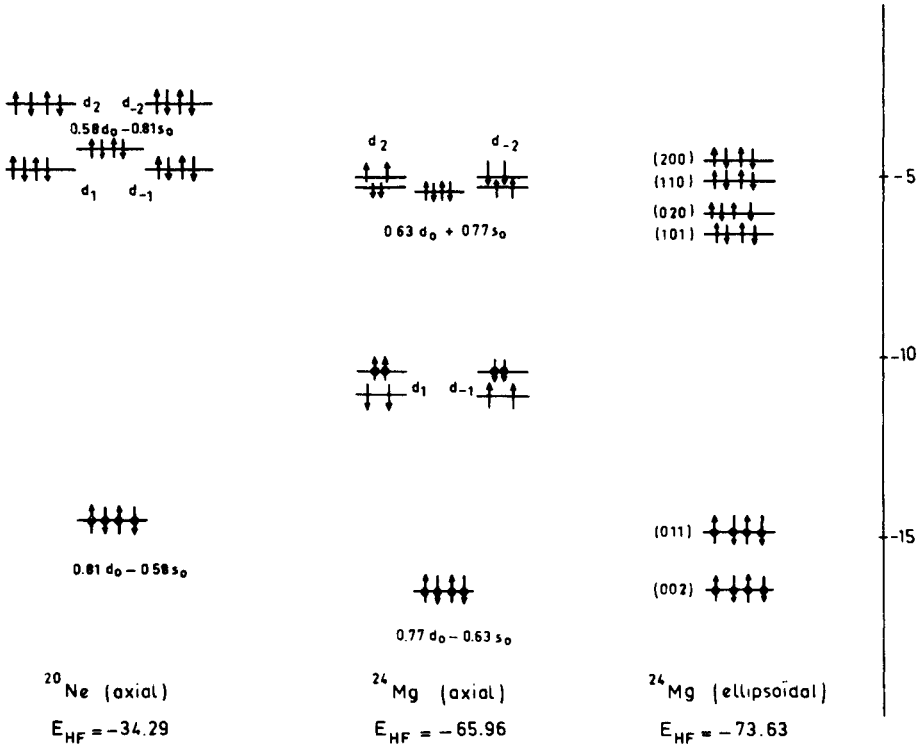

Fig. 4*a*. The spectrum of H.F. orbits of ^{20}Ne and ^{24}Mg in the case of vanishing spin–orbit interaction. The orbits are labeled by their wave function in configuration space and the orientation $\uparrow$ and $\downarrow$ of the spin. Neutrons and protons have similar orbits. Occupied orbits are marked by a dot. The notation d_1 means the $l = 2$, $m = 1$ state of the $2s$-$1d$ shell. The orbits of the ellipsoidal solution are labeled by the state (n_x, n_y, n_z) to which they approximate closely. The H.F. energy E_{HF} of each solution is indicated.

The ellipsoidal solution of ^{24}Mg is obtained by filling the $(d_1 + d_{-1})/=\sqrt{2}$ (011) orbit. The wave functions of the orbits are

$$\begin{aligned} |\lambda_1\rangle &= 0.7882 d_0\uparrow - 0.6526 s_0\uparrow - 0.1210(d_2 + d_{-2})\uparrow \\ &= 0.9795(002)\uparrow + 0.1964(020)\uparrow - 0.0456(200)\uparrow \qquad (77) \\ |\lambda_2\rangle &= \frac{1}{\sqrt{2}}(d_1 + d_{-1})\uparrow = (011)\uparrow \end{aligned}$$

The orbits of the ellipsoidal solution are very nearly pure (002) and (011) states. Figure 4*a* shows the spectrum of the two solutions of ^{24}Mg. Both have the proton–neutron and time-reversal symmetries. But they differ in the way

the second orbit is constructed from the d_1 and d_{-1} orbits which are degenerate and empty in the ^{20}Ne field. In the axially symmetric solution a neutron and a proton are placed in the $d_1\downarrow$ and $d_{-1}\uparrow$ orbits. In the ellipsoidal solution four nucleons fill the same $(d_1 + d_{-1})$ spatial orbit. The ellipsoidal solution, which has lower energy and a larger gap, has maximum spatial symmetry. Thus, in order of preferred symmetries, after the neutron–proton and time-reversal symmetries, a Rosenfeld force prefers H.F. solutions with maximum spatial symmetry to solutions with axial symmetry. In ^{20}Ne both are compatible, but not in ^{24}Mg. The ellipsoidal solution of ^{24}Mg is an L-S coupling wave function with $S = 0$.

In the prolate solution of ^{28}Si both the $d_1 - d_{-1}$ and the $d_1 + d_{-1}$ orbits are filled. Then axial symmetry is restored because the operator J_z simply transforms one occupied orbit into another and leaves the set of occupied orbits invariant. In ^{28}Si, exactly half the orbits of the $2s$-$1d$ shell are filled. The oblate solution of ^{28}Si may be obtained by exchanging empty and filled orbits of the prolate solution, as shown in Fig. 4*b*. The two solutions are orthogonal and nearly degenerate. The energies of the H.F. orbits are

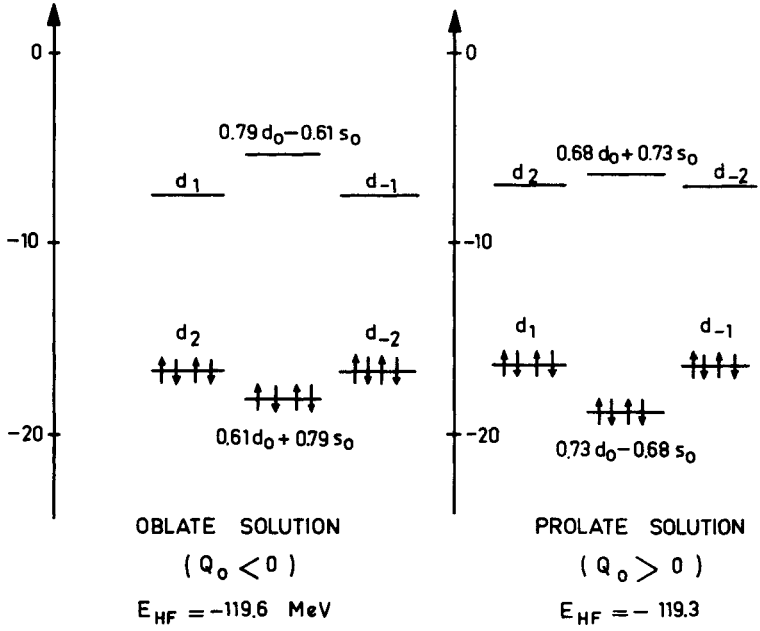

Fig. 4*b*. The spectrum of H.F. orbits of oblate and prolate solutions of ^{28}Si in the case of vanishing spin–orbit interaction. The arrows indicate the spins of nucleons that fill the orbits. The H.F. energy E_{HF} of each solution is shown below the spectrum.

completely reversed both by the monopole and the quadrupole part of the interaction. The deformation of the field changes sign.

The fact that H.F. orbits are very similar to orbits (73) of a deformed oscillator shows that the H.F. variational procedure essentially minimizes the energy of the quadrupole–quadrupole component of the two-body interaction. The other components act only in first-order perturbation in the sense that they affect the energy rather that the wave function. It should be born in mind that these conclusions are only shown to be valid for the solutions of even–even $N = Z$ nuclei with a given parity. Other cases need to be investigated separately. The similarity between H.F. and deformed oscillator orbits in the absence of spin–orbit splitting also shows that the H.F. wave functions are quite similar to the wave functions which diagonalize the quadrupole–quadrupole interaction and which are obtained by group theoretical methods.[13] J. P. Elliott has shown that the quadrupole–quadrupole interaction may be diagonalized among major-shell configurations by states which are obtained from a Slater determinant of orbits (73) by angular momentum projection. The Slater determinants are labeled by (λ, μ) where

$$\lambda = N_z - N_y \qquad \mu = N_y - N_x \tag{78}$$

and where N_x, N_y, and N_z are the total number of quanta in the Slater determinant $|\varphi(\lambda, \mu)\rangle$ along the three directions

$$N_x = \sum_{\lambda=1}^{A} (n_x^{(\lambda)} + \tfrac{1}{2}) \qquad N_y = \sum_{\lambda=1}^{A} (n_y^{(\lambda)} + \tfrac{1}{2}) \qquad N_z = \sum_{\lambda=1}^{A} (n_z^{(\lambda)} + \tfrac{1}{2}) \tag{79}$$

each orbit λ being of the type $(n_x^{(\lambda)}, n_y^{(\lambda)}, n_z^{(\lambda)})$. The states of highest weight

$$G = \lambda^2 + \lambda\mu + \mu^2 + 3(\lambda + \mu) \tag{80}$$

are lowest in energy.

States with good angular momentum L are obtained from the Slater determinant $|\varphi(\lambda, \mu)\rangle$ by angular momentum projection

$$|(\lambda, \mu)KLM\rangle = \int d\Omega\, D_{MK}^{*L}(\Omega)\, R(\Omega)|\, \varphi(\lambda, \mu)\rangle \tag{81}$$

where $K = \mu, \mu - 2, \ldots, 0$. It may be shown[13] that each state $|\varphi(\lambda, \mu)\rangle$ gives rise to rotational bands labeled by K and containing angular momenta $L = K, K + 1, \ldots, \lambda$. In Section 9 it will be shown that rotational bands are obtained from H.F. states $|\varphi\rangle$ by projecting angular momentum as in Eq. (81). Thus, if the H.F. orbits are similar to the (n_x, n_y, n_z) orbits from which the intrinsic state $|\varphi(\lambda, \mu)\rangle$ is constructed, the states obtained by the H.F. method are similar to the states in Eq. (81). This is certainly true for even–even nuclei in the case of vanishing spin–orbit splitting. In fact, the

H.F. calculations entirely confirm the results of J. P. Elliott and M. Moshinsky[13] in even–even nuclei. In particular the predictions concerning the symmetries of the lowest–energy solutions are confirmed by H.F. calculations. But the way of treating the spin–orbit interaction differs. The states (81) do not diagonalize the spin–orbit interaction, and they are used as a basis in which the spin–orbit interaction is diagonalized. In the H.F. method the spin–orbit interaction alters the wave functions of the orbits λ, but the H.F. state is still a Slater determinant. It will be seen that in ^{32}S, e.g., the spin–orbit interaction produces near degeneracies among various H.F. solutions so that neither the H.F. method nor the states in (81) provide an adequate description in this case.

The Slater determinants obtained by filling various (n_x, n_y, n_z) orbits with four nucleons are excellent states to begin the H.F. iteration process with.

10. THE EFFECT OF THE SPIN–ORBIT SPLITTING

The 5 MeV spin–orbit splitting between the $d_{5/2}$ and $d_{3/2}$ single–particle states produces important effects on the H.F. wave functions.

The spin–orbit splitting introduces an additional term of the type of $a\mathbf{l} \cdot \mathbf{s}$ into the H.F. Hamiltonian. This term mixes states with spins of opposite sign so that the orbits no longer factorize into spin and space parts as in Eq. (64). If the spin–orbit term were small, it would cause a very small perturbation in even–even nuclei, which are constructed with closed spin and isospin shells, as shown in Fig. 2. In such configurations the term $a\mathbf{l} \cdot \mathbf{s}$ perturbs the energy only in second order. The large gap caused by the central force reduces the amplitudes of the first-order particle–hole perturbation of the H.F. wave function. But, as shown in Table VII, the gap becomes smaller as the nucleus gets heavier, so that the spin–orbit perturbation becomes increasingly important as one proceeds through the $2s$-$1d$ shell. In the absence of spin–orbit splitting the wave functions of $2s$-$1d$ shell nuclei would be symmetrical with respect to ^{28}Si. ^{36}A and ^{20}Ne, ^{24}Mg and ^{32}S would have similar wave functions because the H.F. equations for holes in ^{40}Ca would be the same as those of particles outside ^{16}O, at least if a degenerate $2s$-$1d$ shell is assumed in the ^{16}O and ^{40}Ca field. The spin–orbit splitting introduces an asymmetry between properties of nuclei belonging to the first and second halves of the $2s$-$1d$ shell. For example, in ^{32}S the spherical solution shown in Table III lies very close in energy to the deformed solution shown in Table V. The spherical solution consists of filled $d_{5/2}$ and $s_{1/2}$ shells. But in ^{24}Mg the spherical solution is a closed $d_{3/2}$ shell, and it has a much higher energy than the deformed solutions because of the spin–orbit splitting. In fact the properties of ^{32}S are easier to understand in terms of vibrations, whereas the states of ^{24}Mg are known to have rotational properties.

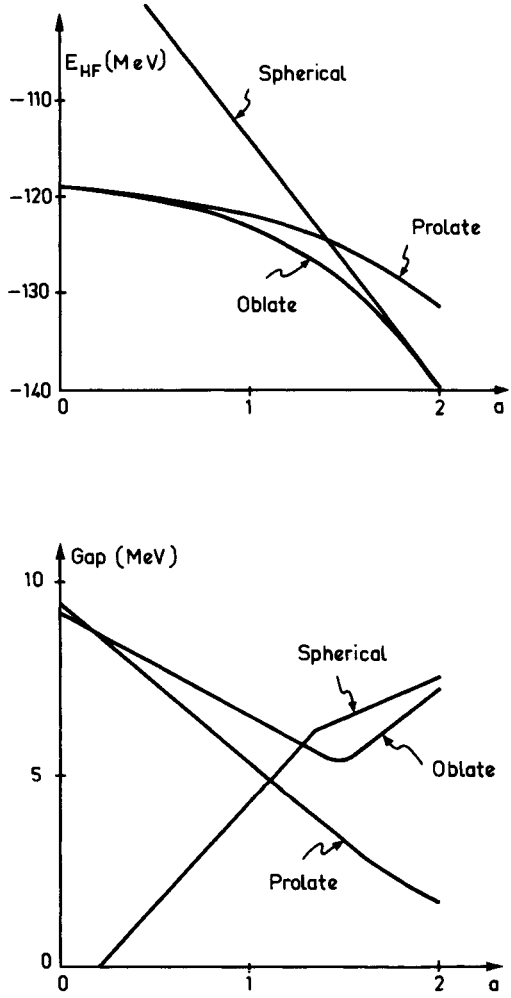

Fig. 5*a*. Variation of the H.F. energy and of the gap of the oblate, prolate, and spherical solutions of ^{28}Si with the spin–orbit strength a. The oblate and prolate solutions correspond to a filling of the $\frac{1}{2}$, $\frac{3}{2}$, $\frac{5}{2}$ and $\frac{1}{2}$, $\frac{1}{2}$, $\frac{3}{2}$ orbits as shown in Table IV. The spherical solution corresponds to a filled $d^{5/2}$ shell. The strength a of the spin–orbit splitting $a\mathbf{l}\cdot\mathbf{s}$ is measured in experimental units. The discontinuities in the gap are due to a change in the nature of the lowest empty orbit. For example, for $a > 1.35$ the lowest empty orbit of the spherical solution becomes the $2s^{1/2}$ state.

Appreciable deviations from the L-S coupling scheme, which results from the factorization of the orbits in Eq. (64), occur already in nuclei of the first half of the $2s$-$1d$ shell. The occupied orbits of ^{20}Ne given by Table IV can be written in the $|\, lm\sigma\rangle$ representation thus

$$|\,\lambda\rangle = (-0.8301d_0 + 0.5273s_0)\uparrow - 0.1812d_1\downarrow \tag{82}$$

The two occupied orbits of ^{24}Mg given by Table V are

$$\begin{aligned} |\,\lambda_1\rangle &= (-0.7014d_0 + 0.5327s_0 + 0.1213d_2 + 0.0479d_{-2})\uparrow \\ &\quad - (0.3733d_1 + 0.2608d_{-1})\downarrow \\ |\,\lambda_2\rangle &= (-0.2475d_0 + 0.3343s_0 + 0.0870d_2 + 0.1866d_{-2})\uparrow \\ &\quad + (0.4693d_1 + 0.7511d_{-1})\downarrow \end{aligned} \tag{83}$$

Orbits (82) and (83) of ^{20}Ne and ^{24}Mg should be compared with the orbits in Eqs. (75) and (77) obtained for vanishing spin–orbit splitting. The mixing of states with opposite spin affects the magnetic moments of odd-A nuclei (Section 13).

The spin–orbit splitting further affects the energies and the stability of the H.F. solutions. Figure 5a shows the variation of the H.F. energy and of the gap of the prolate, oblate, and spherical solutions of ^{28}Si with the spin–orbit splitting strength a. For zero spin–orbit splitting the prolate and oblate deformed solutions are lowest and degenerate. Their wave functions are very similar to the $(\lambda, \mu) = (12, 0)$ and $(0, 12)$ states of Eqs. (78). Figure 5a shows that this degeneracy is not significantly lifted for observed spin–orbit strengths. But the energy of the spherical solution is very sensitive to the spin–orbit strength. Indeed, if the spin–orbit strength is increased so as to lower the $d_{5/2}$ state by 1 MeV, the spherical state is lowered by 12 MeV. In fact, for spin–orbit strengths of about twice the observed value, the oblate solution merges into the spherical solution. The H.F. theory then predicts a closed-shell solution for ^{28}Si. Figure 5a also shows how the gaps of the deformed solutions decrease as the spin–orbit splitting is increased. The permanent deformation looses its stability against particle excitations.

The case of ^{32}S is shown in Fig. 5b. For vanishing spin–orbit splitting the ellipsoidal solution is strongly favored, as in ^{24}Mg. The ellipsoidal solution is similar to the state $(\lambda, \mu) = (4, 8)$ which has highest weight. But as the spin–orbit strength is switched on, the deformed solutions all merge into the spherical solution which consists of closed $d_{5/2}$ and $s_{1/2}$ shells. Around the observed spin–orbit strength, the solutions are nearly degenerate and they have overlaps with each other. Thus in ^{32}S the spin–orbit splitting apparently destroys the stability of the H.F. deformed state against β and γ vibrations e.g. It will be seen in Section 13 that the magnetic moment of ^{33}S

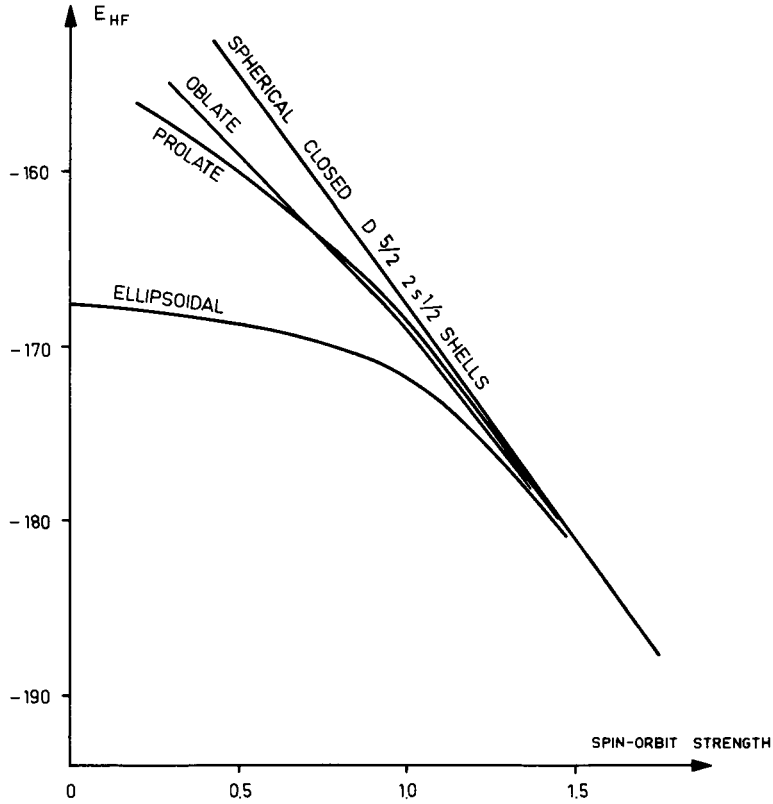

Fig. 5*b*. Variation of the energy of various solutions of ^{32}S with the spin–orbit strength *a* drawn in the same units as in Fig. 5*a*.

is not well explained in the strong coupling limit which should apply to a permanently deformed nucleus.

11. THE MULTIPLICITY OF HARTREE–FOCK SOLUTIONS

For each nucleus there are many solutions to the H.F. equations. They may be distinguished by the different filling of orbits and different symmetries. The near degenerate and orthogonal oblate and prolate solutions of ^{28}Si are a striking example.[21] The H.F. Hamiltonian depends on the nature of the filled orbits. Thus different H.F. solutions obtained by filling different orbits are not necessarily orthogonal, because they are not eigenstates of the same Hamiltonian. Ideally one would hope to find one solution with an energy much lower than the others and with a large gap. This solution

TABLE IX

Various H.F. Solutions of Even–Even $N = Z$ Nuclei[a]

Nucleus	Filled 2s-1d shell orbits $n_x n_y n_z$	(λ, μ)	$G = \lambda^2 + \mu^2 + \lambda\mu + 3(\lambda + \mu)$	$N_x N_y N_z$	E_{HF}	Gap
^{20}Ne	002 110	(8,0) (0,4)	88 28	539/8 567/8	−35.78 −31.44	8.00 4.89
^{24}Mg	002 011	(8,4)	148	140	−76.73	6.58
	002 020	(0,8)	88	144	−75.14	6.15
	002 110	(4,0)	28	150	−72.52	5.67
	101 011	(4,0)	28	150	−71.24	4.47
^{28}Si	200 020 110	(0,12)	180	2025/8	−123.00	6.67
	002 011 101	(12,0)	180	2057/8	−122.01	5.41
	002 101 110	(8,4)	148	2145/8	−118.46	5.07
	200 020 011	(4,8)	148	2145/8	−119.16	5.15
	002 020 200	(0,0)	0	2197/8	−118.20	4.79
	110 101 011	(0,0)	0	2197/8	−117.44	6.27

[a] The second column indicates the initial filling of the orbits with which the iteration process is begun. Four nucleons are placed in each orbit ($n_x n_y n_z$) indicated. The third and fourth columns are the values (λ, μ) and the weight G of the initial filling [see Eqs. (78) and (80)]. The fifth column gives the value of the product of N_x, N_y, and N_z defined by Eq. (79) by summing over all the occupied orbits of the 1s, 1p, and 2s-1d shells. The sixth and seventh columns give the H.F. energy and the gap of the H.F. solution.

TABLE IX (*continued*)

Nucleus	Filled 2s-1d shell orbits $n_x n_y n_z$	(λ, μ)	$G = \lambda^2 + \mu^2 + \lambda\mu + 3(\lambda + \mu)$	$N_x N_y N_z$	E_{HF}	Gap
^{32}S	200 020 101 110	(4,8)	148	432	−171.84	5.24
	200 110 101 011	(8,0)	88	441	−170.64	5.63
	200 020 002 110	(0,4)	28	448	−169.24	3.91
	200 020 011 101	(0,4)	28	448	−170.57	6.58
^{36}Ar	020 200 110 101 011	(0,8)	88	5415/8	−220.48	4.6
	002 020 200 101 011	(4,0)	28	5491/8	−218.24	1.84

might then be expected to represent a stable equilibrium shape of the nucleus. Unfortunately the H.F. calculations predict too many equilibrium shapes which lie closer in energy than experimental spectra suggest. A nucleus may of course have two or more equilibrium shapes. A well-known example of this is ^{16}O, which has a closed-shell ground state and an excited rotational band beginning at 6 MeV, which is due to a four-particle, four-hole H.F. state[14] of the type of Eq. (44). Electromagnetic transitions are observed between the states belonging to the rotational band and the ground state. This shows that there is some mixing between the two equilibrium shapes, which is not included in the H.F. theory as described here. It is certainly reasonable

to expect that the occurrence of too many H.F. solutions closely spaced in energy is an indication that there is further non-negligible configuration mixing which is not taken into account by the H.F. wave functions. One may be temped to take into account the extra configuration mixing by a subsequent diagonalization of the Hamiltonian among the H.F. solutions which lie lowest in energy. This may not be an easy task because the lowest solutions often differ by the displacement of four or more particles and they would only mix by introducing intermediate configurations of higher energy. The large number of the latter would make such a calculation clumsy except in a few simple cases.[22]

The multiplicity of H.F. solutions is illustrated in Table IX. The table gives the energy and the gap of various solutions which are labeled by the values (78) of (λ, μ) of the Slater determinant of orbits (n_x, n_y, n_z), from which the iteration process was begun. It is seen that by beginning the iteration process with states of highest weight, one converges toward the solution with lowest energy. But the different solutions thus obtained often lie very close in energy and the spacing between the solutions is reduced by the spin–orbit splitting.

12. HARTREE–FOCK SOLUTIONS OF OTHER NUCLEI

In the previous sections only even–even $N = Z$ nuclei have been discussed. In these nuclei the proton–neutron and time-reversal symmetries produce a fourfold degeneracy of the orbits. These symmetries no longer hold for H.F. solutions of odd-A nuclei. When a neutron is added to an even–even $N = Z$ nucleus to form, say, ^{21}Ne, an extra term is added to the H.F. Hamiltonian (43). The extra term affects the wave functions of all the orbits and produces a polarization of the ^{20}Ne core. A solution with axial symmetry may always be found, but in an odd-N or -Z nucleus time-reversal symmetry is not compatible with axial symmetry because the time-reversal operator reverses the sign of the projection m_λ of J_z of each orbit and hence cannot leave the set of occupied orbits invariant. Table X shows the H.F. solutions of ^{21}Ne obtained by adding one neutron to the $m_\lambda = \frac{1}{2}$, $\frac{3}{2}$, or $\frac{5}{2}$ orbits which are empty in ^{20}Ne. The extra neutron polarizes the ^{20}Ne core so that the orbits in ^{21}Ne are not the same as in ^{20}Ne. The H.F. energy of the ^{21}Ne solution may be compared with the unperturbed energy also shown in Table X. This is the energy of the state which would be obtained by neglecting the polarization of the ^{20}Ne core and using the wave functions of ^{20}Ne to describe ^{21}Ne. Table X shows that the polarization is small. It continues to be small in ^{29}Si. When an extra neutron is added to the empty $m_\lambda = \frac{3}{2}$ orbit of the oblate ^{28}Si solution, the H.F. energy of the ^{29}Si state

is −131.4 MeV and the unperturbed energy is −131.3 MeV. The overlap between the unperturbed solution and the exact H.F. solution is 0.973.

The polarization of the core discussed here is not the quadrupole polarization which produces effective charge (Section 15). Because of the limited expansion [Eq. (37)] of the orbits it is essentially a spin polarization produced by the Rosenfeld force.

TABLE X

Spin Polarization of the ^{20}Ne Core Due to an Extra Neutron[a]

	λ	e_λ	$d^{5/2}$	$s^{1/2}$	$d^{3/2}$	E_{HF}
$K = \frac{1}{2}$	p	−16.07	−0.7594	0.5408	0.3617	−42.39
	n	−14.00	−0.7666	0.5336	0.3572	
	$-p$	−15.11	0.7550	−0.5451	0.3644	
	$-n$	−15.23	0.7441	−0.5468	0.3838	
$K = \frac{3}{2}$	n	−6.63	−0.9925		0.1233	
$K = \frac{1}{2}$	p	−15.29	−0.7888	0.4671	0.3995	−40.98
	n	−14.14	−0.7891	0.4842	0.3781	
	$-p$	−14.68	0.7976	−0.4634	0.3862	
	$-n$	−14.84	0.7768	−0.4787	0.4092	
$K = \frac{5}{2}$	n	−5.28	1.0000			
$K = \frac{1}{2}$	p	−15.45	−0.7075	0.6125	0.3525	−41.08
	n	−14.52	−0.7313	0.5829	0.3540	
	$-p$	−15.32	0.7138	−0.6057	0.3516	
	$-n$	−14.58	0.7121	−0.5982	0.3675	
$K = \frac{1}{2}'$	n	−5.43	−0.6719	−0.7050	−0.2272	
				Neon 20		*E (unperturbed)*
$K = \frac{1}{2}$	p	−14.58	−0.7576	0.5273	0.3847	
$K = \frac{3}{2}$	p	−6.58	−0.9932		0.1167	−42.36
$K = \frac{5}{2}$	p	−5.14	1.0000			−40.92
$K = \frac{1}{2}'$	p	−5.19	−0.6357	−0.7298	−0.2516	−40.97

[a] The orbits of three ^{21}Ne solutions are shown. The odd neutron is placed in a $K = \frac{3}{2}$, $\frac{5}{2}$, and $\frac{1}{2}$, orbit, respectively. The wave functions and energies of every occupied orbit are shown for the three solutions. The third, the fourth, and the fifth columns show the components on the $d^{5/2}$, $s^{1/2}$, and $d^{3/2}$ states. The last column gives the H.F. energy of the ^{21}Ne state. The corresponding ^{20}Ne orbits of Table IV are shown below for comparison. The unperturbed energy is the energy which the ^{21}Ne state would have if it were made up of unpolarized ^{20}Ne orbits. This energy is equal to $E = E_0 + e_\lambda$, where E_0 is the ^{20}Ne H.F. energy and e_λ is the energy, in the ^{20}Ne field, of the orbit occupied by the odd neutron.

In ^{21}Ne the $K = \frac{1}{2}$, $\frac{3}{2}$, and $\frac{5}{2}$ H.F. states are very close in energy. They will mix when states of a given angular momentum are constructed in the strong coupling limit, because of the Coriolis term.[1] The Coriolis mixing of odd-A nuclei has already been evaluated for ^{23}Mg and ^{25}Mg.[8] In Section 14 it will be shown that the coriolis mixing in the strong coupling limit may not be very accurate in $2s$-$1d$ shell nuclei.

Nuclei with a neutron excess of two no longer have the neutron–proton symmetry, but they do have time-reversal symmetry in the ground state. Figure 6 shows the spectrum of H.F. orbits in ^{22}Ne. The neutron and proton gaps are, respectively, 2.2 and 6.0 MeV. The experimental values are 5.16 and 6.48 MeV. The neutron experimental gap is much larger than the Hartree–

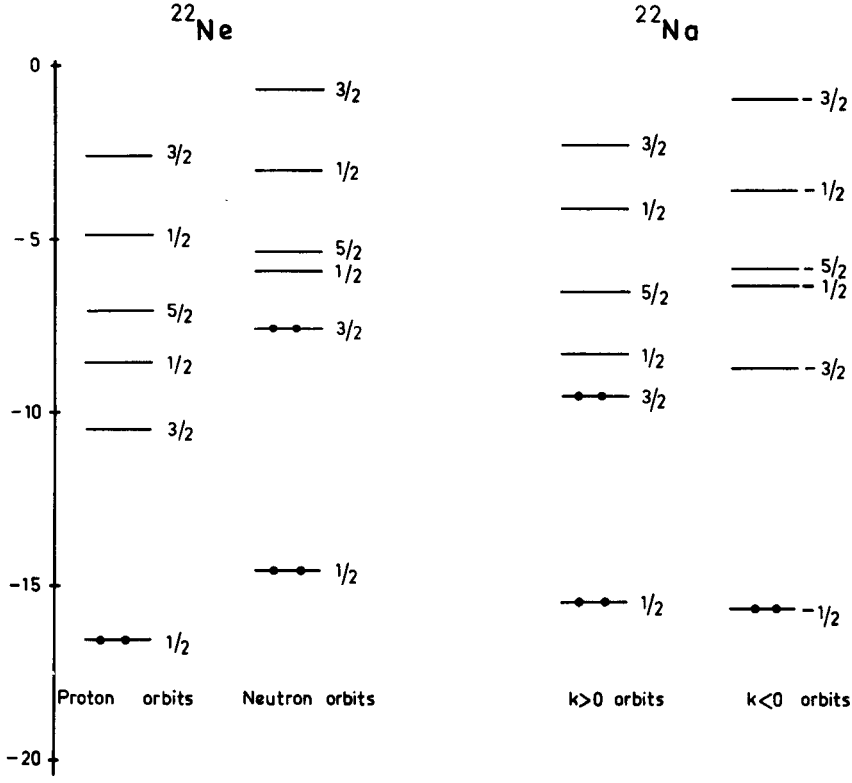

Fig. 6. Spectrum of H.F. orbits in the axially symmetric solution of ^{22}Ne and ^{22}Na. ^{22}Ne has two neutrons in the $K = \pm\frac{1}{2}$ orbit, two neutrons in the $K = \pm\frac{3}{2}$ orbit, and two protons in the $K = \pm\frac{1}{2}$ orbit. This solution has time-reversal symmetry, but neutrons and protons have different orbits. ^{22}Na has a neutron and a proton in the lowest $K = \frac{1}{2}$, $K = -\frac{1}{2}$, and $K = \frac{3}{2}$ orbits. Neutrons and protons are in the same orbits, but the solution does not have time-reversal symmetry.

Fock gap and, in fact pairing is expected to occur in nuclei with a neutron excess of two or more,[23] in which case the H.F. wave functions are not an adequate description of these nuclei. Figure 6 also shows the spectrum of the orbits in the ^{22}Na $K = 3$ state obtained by adding a neutron and a proton in the $m_\lambda = \frac{3}{2}$ orbit. This state has the neutron–proton symmetry, but not the time-reversal symmetry. Odd–odd nuclei such as ^{22}Na have a double Coriolis mixing problem,[46] and they have not yet been investigated thoroughly.

13. MAGNETIC MOMENTS OF ODD-*A* NUCLEI

The calculation of magnetic moments of odd-A nuclei is a useful check of the H.F. wave functions. These are calculated in the simplest strong coupling model,[4] neglecting band mixing.[30] A gyromagnetic ratio $g_R = 0.5$ is used for the core contribution. The results are shown in Table XI. The overall agreement with experiment is good, and the disagreements are significant. The magnetic moments are sensitive to the mixing of $d_{5/2}$, $s_{1/2}$, and $d_{3/2}$ states of the orbital wave functions, and they are therefore sensitive to the spin–orbit splitting. A detailed study of this has been made by Bohr and Mottelson.[1]

A good value is obtained for ^{29}Si when an oblate ^{28}Si core is assumed. Mavromatis, Zamick, and Brown[31] have calculated deviations of magnetic moments from the Schmidt value by calculating the contribution of particle–hole admixtures to closed–shell solutions of various nuclei. A poor value was obtained for ^{29}Si, and a better value is obtained with the H.F. wave function. This confirms the deformed nature of ^{28}Si. On the other hand, the H.F. wave function gives a poor result for ^{33}S. The fact that Mavromatis, Zamick, and Brown obtain a better value suggests that the strong coupling model is not applicable to ^{33}S. This reflects the fact, stressed in Section 10, that the H.F. theory predicts nearly degenerate spherical and deformed solutions for ^{32}S. In ^{27}Al a similar value of the magnetic moment is obtained whether one assumes the $\frac{5}{2}^+$ ground state to consist of a $K = \frac{5}{2}$ rotational-band head or a member of a $K = \frac{1}{2}$ band.

The case of ^{27}Al requires special attention. ^{27}Al is a proton hole in ^{28}Si; it has spin $\frac{5}{2}$ and a positive quadrupole moment. A natural way to obtain the ground-state spin and quadrupole moment (see Section 15) would be to consider the ground-state ^{27}Al as a band head of a $K = \frac{5}{2}$ rotational band, obtained by making an $m_\lambda = \frac{5}{2}$ hole in the prolate solution of ^{28}Si. But H.F. calculations show that, unless an unusually strong spin–orbit splitting is used, the prolate solution of ^{28}Si is made up of two $m_\lambda = \frac{1}{2}$ orbits and an $m_\lambda = \frac{3}{2}$ orbit, but no $m_\lambda = \frac{5}{2}$ orbit. An $m_\lambda = \frac{5}{2}$ hole in the oblate

solution would yield a quadrupole moment of the wrong sign in ^{27}Al. A hole in the $m_\lambda = \frac{1}{2}$ orbit of the oblate solution would yield a $K = \frac{1}{2}$ intrinsic state. The spin $\frac{5}{2}$ state of the rotational band generated by this intrinsic state has correct magnetic and quadrupole moments. Although the decoupling factor of the $m_\lambda = \frac{1}{2}$ hole state is of the right sign to lower the spin $\frac{5}{2}$ member of the rotational band, it is not certain whether the Coriolis effect could produce a spin $\frac{5}{2}$ ground state. A change in the shape of the ^{28}Si core when a particle is removed or added to form ^{27}Al and ^{29}Si may be observable, since it would result in a reduction of stripping or pickup amplitudes between the ground states of these nuclei.

TABLE XI

Magnetic Moments of Odd-A Nuclei[30] Obtained from Axially Symmetric Solutions[a]

Nucleus	K	J	Even core	Calc.	Expt.	Schmidt
^{11}B	$\frac{3}{2}^-$	$\frac{3}{2}^-$	^{12}C	2.57	2.69	3.79
^{13}C	$\frac{1}{2}^-$	$\frac{1}{2}^-$		0.86	0.72	0.64
^{19}F	$\frac{1}{2}^+$	$\frac{1}{2}^+$	^{20}Ne	2.82	2.63	2.79
	$\frac{1}{2}^+$	$\frac{5}{2}^+$		3.86	3.5 ± 0.5	4.79
^{21}Ne	$\frac{3}{2}^+$	$\frac{3}{2}^+$		-0.582	-0.66	1.14
^{23}Na	$\frac{3}{2}^+$	$\frac{3}{2}^+$	^{24}Mg	2.44	2.22	0.12
^{25}Mg	$\frac{5}{2}^+$	$\frac{5}{2}^+$		-1.01	-0.85	-1.91
^{27}Al	$\frac{5}{2}^+$	$\frac{5}{2}^+$	^{28}Si	3.78	3.64	4.79
	$\frac{1}{2}^+$	$\frac{5}{2}^+$	^{28}Si oblate	3.81		
^{29}Si	$\frac{1}{2}^+$	$\frac{1}{2}^+$	^{28}Si oblate	-0.47	-0.56	-1.91
			^{28}Si prolate	-1.689		
^{33}S	$\frac{3}{2}^+$	$\frac{3}{2}^+$	^{32}S oblate	0.05	0.64	1.14
			^{32}S prolate	1.317		
^{35}Cl	$\frac{3}{2}^+$	$\frac{3}{2}^+$	^{36}Ar	0.63	0.82	0.12

[a] The intrinsic states of the odd-A nucleus are labeled by K, the projection of J_z along the z axis of the intrinsic frame. The third column gives the spin J of the state. The fourth column indicates the nature of the underlying even–even core. The last three columns show the calculated, experimental, and Schmidt values of the magnetic moments.

14. ANGULAR MOMENTUM PROJECTION

The H.F. intrinsic states generate rotational bands in deformed nuclei. It is usual to describe the actual nuclear states with definite angular momentum J by a product wave function [Eq. (1)] in which the rotational motion is distinguished from the intrinsic motion. More precisely, the nuclear state of angular momentum J and projection M in the laboratory frame belonging to a rotational band generated by a deformed intrinsic state $|\varphi_K\rangle$, which has axial symmetry and projection K of J_Z on the z axis of the intrinsic frame, is written thus[1]

$$|\psi^J_{MK}\rangle = \sqrt{\frac{2J+1}{16\pi^2}}\{D^{J*}_{MK}(\Omega)|\varphi_K\rangle + (-)^{J+K} D^{J*}_{M-K}(\Omega)|\varphi_{-K}\rangle\} \tag{84}$$

where $|\varphi_{-K}\rangle = e^{-i\pi J_y}|\varphi_K\rangle$.

An alternative way of describing the state $|\psi^J_{MK}\rangle$ is provided by the projection method of Peierls and Yoccoz,[25] which uses the Hill–Wheeler integral[26]

$$|\psi^J_{MK}\rangle = \frac{2J+1}{8\pi^2 N^{1/2}_{JK}} \int d\Omega\, D^{J*}_{MK}(\Omega)\, R(\Omega)|\varphi_K\rangle \tag{85}$$

where $R(\Omega)$ is the rotation operator

$$R(\Omega) = e^{-i\alpha J_z} e^{-i\beta J_y} e^{-i\gamma J_z} \tag{86}$$

in which Ω stands as an abbreviation for the Euler angles α, β, and γ and the matrix elements of which are[2]

$$D^J_{MK}(\Omega) = \langle JM\,|\,R(\Omega)|\,JK\rangle \tag{87}$$

Wave function (85) has no redundant variables, in contrast to wave function (84). Indeed, the intrinsic wave function $|\varphi_K\rangle$ already contains all the variables of the system. Wave function (85) is the projection of the intrinsic deformed wave function on the subspace of angular momentum J. It is easy to check that

$$\frac{2J+1}{8\pi^2}\int d\Omega\, D^{*J}_{KK}(\Omega)\, R(\Omega) = \sum_\alpha |\alpha JK\rangle\langle\alpha JK| \tag{88}$$

where α is any complete set of quantum numbers other than J and K. N_{JK} is a normalization constant

$$N_{JK} = \frac{2J+1}{8\pi^2}\int d\Omega\, D^{J*}_{KK}(\Omega)\,\langle\varphi_K\,|\,R(\Omega)|\,\varphi_K\rangle \tag{89}$$

When strong coupling wave functions (84) are used, the matrix elements of a tensor operator T_q^k are given by [4]

$$\langle \psi^{J_1}_{M_1K_1} \mid T_q^k \mid \psi^{J_2}_{M_2K_2} \rangle = \sqrt{\frac{2J_2+1}{2J_1+1}} \begin{bmatrix} J_2 & k & J_1 \\ M_2 & q & M_1 \end{bmatrix} \times \sum_\nu \left\{ \begin{bmatrix} J_2 & k & J_1 \\ K_2 & \nu & K_1 \end{bmatrix} \langle \varphi_{K_1} \mid T_\nu^k \mid \varphi_{K_2} \rangle + (-)^{J_1+K_2} \begin{bmatrix} J_2 & k & J_1 \\ K_2 & \nu & -K_1 \end{bmatrix} \langle \varphi_{-K_1} \mid T_\nu^k \mid \varphi_{K_2} \rangle \right\} \tag{90}$$

In addition to the selection rules given by the first Clebsch–Gordan coefficient, which reflects simply the Wigner–Eckhart theorem, matrix element (90) also implies the well-known K selection rule

$$\mid K_1 - K_2 \mid \leqslant k \tag{91}$$

Expression (90) may only be used for operators which do not have an explicit dependence on the collective variable Ω. Expressions for operators which do, such as the magnetic moment operator, need to be modified.[4]

When projected wave functions (85) are used, the matrix element of an operator T_q^k is given by

$$\langle \psi^{J_1}_{M_1K_1} \mid T_q^k \mid \psi^{J_2}_{M_2K_2} \rangle = \frac{(2J_1+1)(2J_2+1)}{(8\pi^2)^2 N^{1/2}_{J_1K_1} N^{1/2}_{J_2K_2}} \times \int d\Omega_1\, d\Omega_2\, D^{J_1}_{M_1K_1}(\Omega_1)\, D^{*J_2}_{M_2K_2}(\Omega_2) \times \langle \varphi_{K_1} \mid R^{-1}(\Omega_1)\, T_q^k R(\Omega_2) \mid \varphi_{K_2} \rangle \tag{92}$$

The expression above may be reduced to a single integral by using the commutation rule[2] between the tensor operator T_q^k and the rotation operator $R(\Omega_2)$

$$T_q^k R(\Omega_2) = \sum_\nu D^{*k}_{q\nu}(\Omega_2)\, R(\Omega_2)\, T_\nu^k \tag{93}$$

Since rotations form a group, the rotation $R(\Omega_1)$ may be written thus

$$R(\Omega_1) = R(\Omega_2) R^{-1}(\Omega_3) \tag{94}$$

Taking the matrix element of Eq. (94) between states $\mid J_1M_1\rangle$ and $\mid J_1K_1\rangle$, one obtains

$$D^{J_1}_{M_1K_1}(\Omega_1) = \sum_\mu D^{J_1}_{M_1\mu}(\Omega_2)\, D^{J_1^*}_{K_1\mu}(\Omega_3) \tag{95}$$

Equations (93), (94), and (95) yield the desired matrix element

$$\langle \psi^{J_1}_{M_1K_1} \mid T_q^{\,k} \mid \psi^{J_2}_{M_2K_2} \rangle = \frac{2J_2+1}{8\pi^2 N^{1/2}_{J_1K_1} N^{1/2}_{J_2K_2}} \begin{bmatrix} J_2 & k & J_1 \\ M_2 & q & M_1 \end{bmatrix}$$

$$\times \sum_{\mu\nu} \begin{bmatrix} J_2 & k & J_1 \\ K_2 & \nu & \mu \end{bmatrix} \int d\Omega D^{*J_1}_{K_1\mu}(\Omega) \langle \varphi_{K_1} \mid R(\Omega)\, T_\nu^{\,k} \mid \varphi_{K_2} \rangle \tag{96}$$

Because of axial symmetry the intrinsic states $\mid \varphi_K \rangle$ are eigenstates of J_z with eigenvalue K, so that the normalization constant [Eq. (89)] and the integral in expression (96) reduce to

$$N_{JK} = \frac{2J+1}{2} \int_0^\pi d\beta \sin\beta\, d^J_{KK}(\beta) \langle \varphi_K \mid e^{-i\beta J_y} \mid \varphi_K \rangle$$

and

$$\frac{2J_1+1}{8\pi^2} \int d\Omega\, D^{*J_1}_{K_1\mu}(\Omega) \langle \varphi_{K_1} \mid R(\Omega)\, T_\nu^{\,k} \mid \varphi_{K_2} \rangle$$

$$= \frac{2J_1+1}{2} \int_0^\pi d\beta \sin\beta\, d^{J_1}_{K_1\mu}(\beta) \langle \varphi_{K_1} \mid e^{-i\beta J_y} T_\nu^{\,k} \mid \varphi_{K_2} \rangle \tag{97}$$

The reduced rotation matrix $d^J_{MK}(\beta)$ is defined by

$$d^J_{MK}(\beta) = \langle \alpha JM \mid e^{-i\beta J_y} \mid \alpha JK \rangle$$

Expression (96) is valid for the matrix element of any operator. In particular, when the nuclear Hamiltonian (7), which is a tensor operator of rank zero, is substituted for $T_q^{\,k}$ in expression (96), one obtains the energy E_J of the state of spin J belonging to the rotational band generated by the intrinsic state $\mid \varphi_K \rangle$

$$E_J \equiv \langle \psi^J_{MK} \mid H \mid \psi^J_{MK} \rangle = \frac{\int_0^\pi d\beta \sin\beta\, d^J_{KK}(\beta) \langle \varphi_K \mid e^{-i\beta J_y} H \mid \varphi_K \rangle}{\int_0^\pi d\beta \sin\beta\, d^J_{KK}(\beta) \langle \varphi_K \mid e^{-i\beta J_y} \mid \varphi_K} \tag{98}$$

When the integrals of Eq. (97) are substituted in expression (96), a check may be made to see that matrix element (96) between projected wave functions reduces to the strong coupling limit value of Eq. (90) provided the overlap functions

$$\langle \varphi_{K_1} \mid e^{-i\beta J_y} T_\nu^{\,k} \mid \varphi_{K_2} \rangle \quad \text{and} \quad \langle \varphi_K \mid e^{-i\beta J_y} \mid \varphi_K \rangle \tag{99}$$

have nonvanishing contributions only at the values $\beta \sim 0$ and $\beta \sim \pi$.[27]

The K selection rule (91) is strictly true only in this limit. In other words, the collective variable β is well defined provided overlap functions (99) have a much quicker variation than the weight functions $d^J_{MK}(\beta)$ which describe the collective rotational motion. When the overlap functions contribute only at the angles $\beta \sim 0$ and $\beta \sim \pi$, it may be checked directly[27] whether expression (98) for the energy yields a $J(J+1)$ spectrum for the members of a $K = 0$ rotational band and the well-known energy spectrum

$$\begin{aligned} E_J &= A[J(J+1) + (-)^{J+1/2} a(J+\tfrac{1}{2})] \\ a &= \sum_j |C_j^\lambda|^2 (j+\tfrac{1}{2})(-)^{j+1/2} \end{aligned} \tag{100}$$

for the members of a $K = \frac{1}{2}$ rotational band. Spectrum (98) obtained from projected wave functions contains decoupling effects of rotational bands, but no band mixing.

It is possible to calculate the overlap functions in Eq. (99) exactly[10,15] and to check at what angles they contribute to the integrals in Eq. (98). With the expansion (35) of the orbits, the rotated intrinsic state (3) may be written

$$e^{-i\beta J_y} | \varphi_K \rangle = b^\dagger_{\lambda_1'} b^\dagger_{\lambda_2'} \cdots b^\dagger_{\lambda_A'} | 0 \rangle \tag{101}$$

where $K = \sum_{\lambda=1}^{A} m_\lambda$ and λ' is the rotated orbit

$$| \lambda' \rangle = e^{-i\beta J_y} | \lambda \rangle = \sum_j C_j^\lambda \sum_m d^j_{mm_\lambda}(\beta) | jm \rangle \tag{102}$$

With the help of Wick's theorem, the overlap function $\langle \varphi_K | e^{-i\beta J_y} | \varphi_K \rangle$ becomes

$$\langle \varphi_K | e^{-i\beta J_y} | \varphi_K \rangle = \det [N_{\lambda\mu}(\beta)] \tag{103}$$

where $N_{\lambda\mu}(\beta)$ is the matrix of the scalar products of the orbits λ with the rotated orbits λ' of $| \varphi_K \rangle$,

$$N_{\lambda\mu}(\beta) = \sum_j C_j^{\lambda *} C_j^\mu d^j_{m_\lambda m_\mu}(\beta) \tag{104}$$

The functions $d^j_{mm'}(\beta)$ are known simple polynomials of $\sin\beta/2$ and $\cos\beta/2$ so that, once the C_j^λ coefficients are determined by the H.F. calculation, the matrix $N_{\lambda\mu}(\beta)$ and its determinant (103) are easily evaluated numerically.

Figure 7 shows the overlap functions $\langle \varphi_K | e^{-i\beta J_y} | \varphi_K \rangle$ of the $K = 0$ and $K = \frac{1}{2}$ intrinsic states of ^{20}Ne and ^{19}F compared with the $d^J_{KK}(\beta)$ functions. Clearly the overlap functions are not very peaked about $\beta = 0$

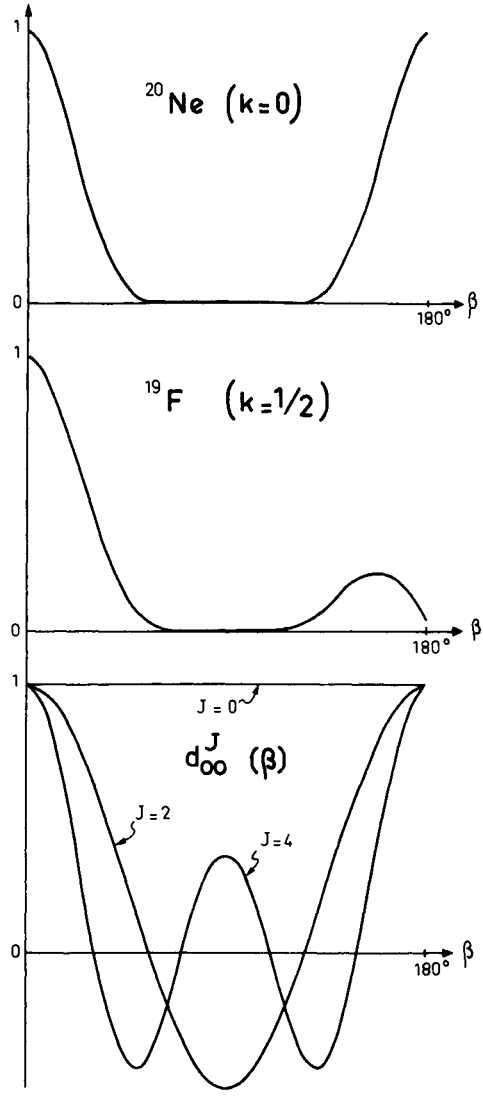

Fig. 7. The overlap functions $\langle \varphi_K \mid e^{i\beta J_y} \mid \varphi_K \rangle$ of the H.F. solutions of ^{20}Ne and ^{19}F. The lowest graph shows the reduced rotational matrices $d^J_{00}(\beta)$ for $J = 0$, 2, and 4, which are used in the angular momentum projection of the ^{20}Ne H.F. state.

and $\beta = \pi$. For values of $\beta < \pi/2$ the overlap function of ^{20}Ne is approximated quite well by

$$F(\beta) = e^{-(\beta^2/4)\langle\varphi_0|\mathbf{J}^2|\varphi_0\rangle} \tag{105}$$

so that the width of the overlap function is determined by the mean value of the square of the angular momentum operator in the intrinsic state. Table IV shows the mean value of $\mathbf{J}^2$ of all the axially symmetric solutions. They vary between 15 and 25. In heavy deformed nuclei the mean value of $\mathbf{J}^2$ is expected to exceed 100, so that the overlap functions are very peaked there. Thus in $2s$-$1d$ shell nuclei the collective variable β is not very well defined and the strong coupling model should be used with some caution.

The overlap function $\langle\varphi \mid e^{-i\beta J_y}H \mid \varphi\rangle$ may be calculated in a similar fashion[10] by introducing intermediate two-particle, two-hole states

$$\begin{aligned}\langle\varphi_K \mid e^{-i\beta J_y}H \mid \varphi_K\rangle &= \langle\varphi_K \mid e^{-i\beta J_y} \mid \varphi_K\rangle\langle\varphi_K \mid H \mid \varphi_K\rangle \\ &\quad + \sum_{2p2h}\langle\varphi_K \mid e^{-i\beta J_y} \mid 2p2h\rangle\langle 2p2h \mid H \mid \varphi_K\rangle\end{aligned} \tag{106}$$

When $\mid \varphi_K\rangle$ is a H.F. state, the $1p$-$1h$ intermediate states do not contribute because $\langle 1p1h \mid H \mid \varphi_K\rangle = 0$. Particle–hole configurations of higher order than 2 do not contribute, because H is a two-body operator only. The $2p$-$2h$ configurations are further limited to states of a given major shell because the rotation operator can only change the magnetic quantum number of a state $\mid jm\rangle$. The matrix element $\langle 2p2h \mid H \mid \varphi\rangle$ is easily computed

$$\begin{aligned}\mid 2p2h\rangle &= b^\dagger_{\mu_1} b^\dagger_{\mu_2} b_{\lambda_1} b_{\lambda_2} \mid \varphi_K\rangle \\ \langle 2p2h \mid H \mid \varphi_K\rangle &= \langle \mu_1\mu_2 \mid v \mid \lambda_1\lambda_2\rangle\end{aligned} \tag{107}$$

μ_1 and μ_2 are empty orbits belonging to the same major shell as the filled orbits λ_1 and λ_2. Since the $2p$-$2h$ state is also a Slater determinant, the overlap function $\langle 2p2h \mid e^{-i\beta J_y} \mid \varphi_K\rangle$ is given by Eq. (103). It is equal to the determinant of the scalar product matrix of the rotated orbits of $\mid \varphi_K\rangle$ with the unrotated orbits occupied in the $2p$-$2h$ state. The overlap function $\langle\varphi_K \mid e^{-i\beta J_y}H \mid \varphi_K\rangle$ has an angular dependence similar to those shown in Fig. 7.[10] By combining Eqs. (98) and (106), the following expression is obtained for the energy of a projected H.F. state:

$$E_J = E_{\mathrm{HF}} + \Delta_J$$

$$\Delta_J = \frac{\int_0^\pi d\beta \sin\beta\, d^J_{KK}(\beta) \sum_{2p2h} \langle\varphi_K \mid e^{-i\beta J_y} \mid 2p2h\rangle\langle 2p2h \mid H \mid \varphi_K\rangle}{\int_0^\pi d\beta \sin\beta\, d^J_{KK}(\beta)\langle\varphi_K \mid e^{-i\beta J_y} \mid \varphi_K\rangle} \tag{108}$$

Table XII shows the distribution N_{JK} of angular momenta in the

deformed intrinsic states of ^{12}C, ^{20}Ne, ^{28}Si, and ^{36}A. Distribution N_{JK} is just the mean value [Eq. (89)] of the projection operator [Eq. (88)] in the intrinsic state.

TABLE XII

The Distribution N_{JK} of Angular Momentum in the Deformed Intrinsic States of ^{12}C, ^{20}Ne, and the Oblate Solutions of ^{28}Si and ^{36}Ar[a]

J	^{12}C	^{20}Ne	^{28}Si	^{36}Ar
0	0.230	0.109	0.079	0.132
2	0.582	0.398	0.313	0.440
4	0.188	0.336	0.326	0.314
6	0	0.134	0.194	0.100
8	0	0.022	0.071	0.013

[a] Values of J are given up to 8 which is the natural cutoff for the ^{20}Ne and ^{36}Ar rotational bands. The natural cutoff for ^{12}C is $J = 4$.

By evaluating Δ_J from Eq. (108), the projected spectra shown in Fig. 8 are obtained. In ^{20}Ne the rotational band is cut off at $J = 8$ because this is the maximum angular momentum which two neutrons and two protons can have in the $2s$-$1d$ shell. All the levels of this band have been identified experimentally.[28] The projected H.F. state reproduces well the observed spectrum. But there are some systematic discrepancies between the projected and observed spectra. The spacing between the $J = 0$ and $J = 2$ states is always too small. This spacing is increased when a pairing interaction is added to a quadrupole–quadrupole interaction in exact diagonalization calculations.[32] The discrepancy may thus be due to a change in the wave function produced by the pairing effects. The projected H.F. spectrum of ^{28}Si is altogether too compressed by nearly a factor of 2. The projected prolate solution is similar. Apparently the H.F. solutions of ^{28}Si are too deformed.

Projected H.F. spectra may be compared with rotational spectra. The spacing of the levels is quite close to a $J(J + 1)$ spectrum except for high angular momenta near the band cutoff. The moments of inertia deduced from the spacing of the lowest levels of the projected spectra lie in between values obtained by the cranking formula and the Thouless–Valatin formula.[10] For example, in ^{28}Si the cranking model predicts a moment of inertia parameter $A = 0.18$ MeV, and the value deduced from the projected spectrum is $A = 0.11$ MeV. The cranking value of the moment of inertia is[33]

$$\theta = 2 \sum_{\mu\nu} \frac{|\langle \mu \mid J_x \mid \nu \rangle|^2}{e_\mu - e_\nu} \qquad A = \frac{1}{2\theta} \tag{109}$$

where μ and ν are filled and empty orbits, respectively, the energies of which are e_μ and e_ν.

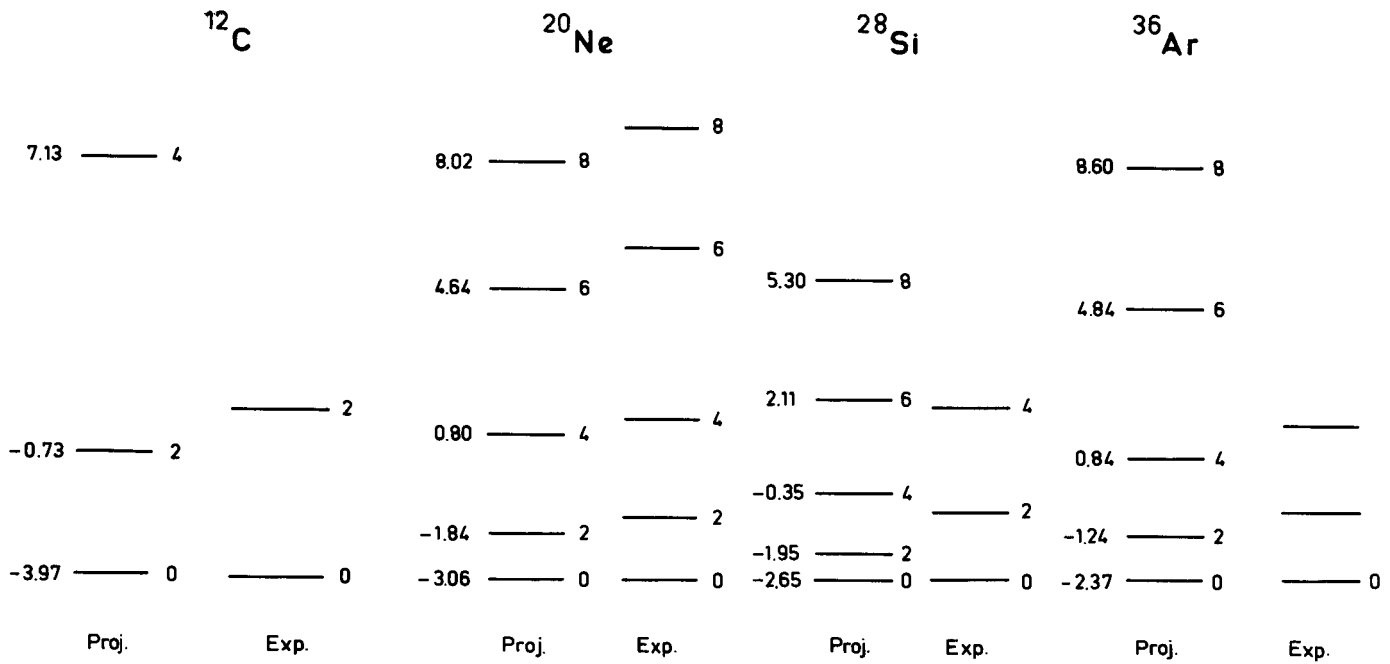

Fig. 8. Projected H.F. spectra of ^{12}C, ^{20}Ne, ^{28}Si, and ^{36}Ar. The oblate solution of ^{28}Si was used. The projected spectra are drawn to the left of the experimental spectra for each nucleus. The number on the right of each level is the spin of the level. The number on the left of the projected levels is the difference Δ_J between the energy of the projected level and the H.F. energy of the intrinsic state.

The gap between the filled and empty orbits affects the moment of inertia by increasing the denominators in Eq. (109). One may be lead to conclude that the moments of inertia are sensitive to the exchange mixture of the interaction, which has been shown to have an important effect on the energy gap (Section 8). In Fig. 3 the spectrum of the H.F. orbits of ^{28}Si obtained with a Serber and a Rosenfeld force is shown. The gaps are respectively 2.5 and 6.6 MeV. The moment of inertia parameters calculated by the cranking formula (109) are, respectively, $A = 0.10$ MeV and $A = 0.18$ MeV. The projected spectra are shown in Fig. 9. They are very similar, and so the gap does not have an important effect on projected H.F. spectra. Thus, in $2s$-$1d$ shell nuclei, cranking formulas should be used with some caution. For L-S coupling wave functions, the monopole force of Eq. (63), responsible for the gap, does not contribute to the splitting Δ_J of Eq. (108).

In the case of ^{19}F it is possible to compare the projected spectrum with the spectrum obtained by diagonalizing exactly the three-particle configurations in the $2s$-$1d$ shell.[15] The results are shown in Fig. 10. The agreement between the exact spectrum and the projected H.F. spectrum is very good for states up to spin 7/2. Both the exact and projected H.F. spectra are very similar to spectrum (100) of a $K = \frac{1}{2}$ rotational band. The decoupling parameter a may be extracted from the calculated spectra by the ratio

$$\frac{E_{3/2} - E_{1/2}}{E_{5/2} - E_{3/2}} = \frac{3(a+1)}{5(1-a)}$$

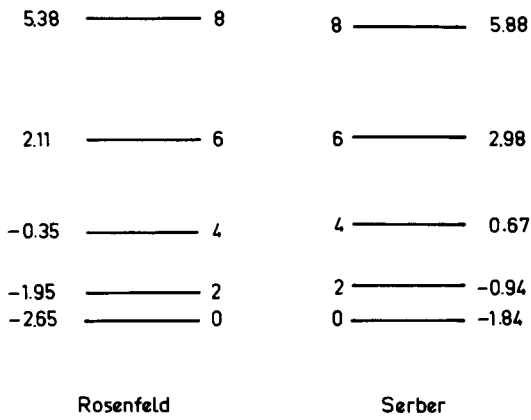

Fig. 9. A comparison between the projected H.F. spectra of the oblate solution of ^{28}Si using Rosenfeld and Serber forces. For each level the spin and the difference Δ_J defined in the caption of Fig. 8, are shown. The single-particle spectrum of the solutions using both forces is shown in Fig. 3.

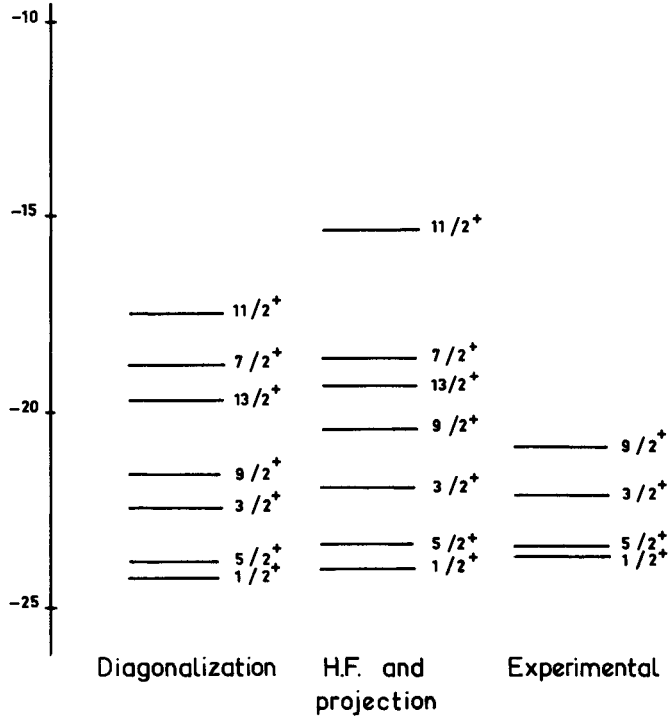

Fig. 10. A comparison between the spectrum of three particle states of ^{19}F obtained by the exact diagonalization of the Hamiltonian among all $2s$-$1d$ shell configurations, the H.F. projected spectrum, and the experimental spectrum.[10,15] Only the lowest states of each spin obtained by the diagonalization are shown.

The exact diagonalization and the projected spectrum give a value $a = 2.4$, whereas the value of Eq. (100) predicted from the strong coupling model is $a = 1.7$. Thus, in spite of the fact that projected H.F. spectra bear a strong resemblance to rotational bands and that, as in the case of ^{20}Ne, the projected spectrum agrees well with the observed one, the validity of the wave function (84) in $2s$-$1d$ shell nuclei is questionable.

15. MAJOR-SHELL-MIXING HARTREE–FOCK CALCULATIONS —QUADRUPOLE POLARIZATION OF CLOSED SHELLS

The single major-shell H.F. calculations discussed in the previous sections, although instructive, are necessarily limited. The H.F. wave functions obtained are not stable against particle–hole excitations from one

major shell to another. All the configurations belonging to a given major shell have the same kinetic energy so that a single major-shell calculation can at best minimize the potential energy. The kinetic energy of each orbit is determined by the oscillator constant, which in turn is determined by the mean square radius of the nucleus. It is well known that large quadrupole deformations are observed in $2s$-$1d$ shell nuclei. ^{17}O has a charge quadrupole moment of $-2.6\ \mathrm{fm}^2$ ($= -0.026$ barns). The neutron in the $2s$-$1d$ shell carries no charge, and the observed quadrupole moment is understood as a polarization of the closed ^{16}O shell by the odd neutron.[34] Also ^{21}Ne has a charge quadrupole moment of $9\ \mathrm{fm}^2$. In single major-shell calculations this quadrupole moment can only be due to the two protons in the $2s$-$1d$ shell. The maximum quadrupole moment of a two-proton configuration is the one obtained by placing both protons in the $(n_x, n_y, n_z) = (0, 0, 2)$ orbit. This yields an intrinsic quadrupole moment equal to

$$Q_0 = \langle \varphi_K | \sum_{i=1}^{z} (2z_i^2 - x_i^2 - y_i^2) | \varphi_K \rangle = \frac{6}{\alpha_0^2} \tag{110}$$

Using the value $\alpha_0 = 0.56\ \mathrm{fm}^{-1}$ for the oscillator constant, given in Table II, one finds $Q_0 = 19\ \mathrm{fm}^2$. In a deformed nucleus the measured quadrupole moment of a state of spin J belonging to a rotational band generated by an intrinsic state $|\varphi_K\rangle$ is given by[1]

$$Q = \frac{3K^2 - J(J+1)}{(J+1)(2J+3)} Q_0 \tag{111}$$

The above expression may be derived from Eq. (90). In ^{21}Ne, $J = K = \frac{3}{2}$, so that an intrinsic quadrupole moment of $19\ \mathrm{fm}^2$ implies a quadrupole moment of $3.8\ \mathrm{fm}^2$ for the ground state of ^{21}Ne. This is much less than the experimental value. The use of expression (111) for the quadrupole moment may be questioned in the light of the results of Section 14, but the discrepancy between the experimental and calculated quadrupole moment of ^{21}Ne is large enough to be significant. Equation (90) also implies a relation between the $B(E2)$ of the $2^+ \to 0^+$ transition in ^{20}Ne and the intrinsic quadrupole moment Q_0 of ^{20}Ne

$$B(E2) = \frac{5}{16\pi} e^2 Q_0^2 \tag{112}$$

The intrinsic quadrupole moment Q_0 deduced from the $B(E2)$ by Eq. (112) is $69\ \mathrm{fm}^2$. The value deduced from the static quadrupole moment of ^{21}Ne by Eq. (111) is $45\ \mathrm{fm}^2$. Both values are much larger than the maximum value of $19\ \mathrm{fm}^2$ which can be obtained from a single major-shell H.F. calculation. The

The difference between the value of Q_0 deduced from the $B(E2)$ of ^{20}Ne and the static moment of ^{21}Ne is not explained by the simplest rotational model.

In order to account for quadrupole deformations of closed shells, it is necessary to extend the expansion of the H.F. orbits beyond the restrictions of Eq. (37). It is necessary to admix to each orbit, whose main component belongs to a given major shell, components belonging to the neighboring major shells of the same parity. For nuclei up to ^{40}Ca, expansion (29) of the orbits must include the states

$$\begin{aligned} j &= 1s^{1/2}, 1d^{5/2}, 2s^{1/2}, 1d^{3/2}, 1g^{9/2}, 2d^{5/2}, 3s^{1/2}, 2d^{3/2}, 1g^{7/2} \\ &\qquad \text{for even parity orbits} \\ j &= 1p^{3/2}, 1p^{1/2}, 1f^{7/2}, 2p^{3/2}, 2p^{1/2}, 1f^{5/2} \\ &\qquad \text{for negative parity orbits} \end{aligned} \tag{113}$$

Many of the simplifications of single major-shell calculations (Section 5) are lost when the more complete expansion (113) is used. The mean square radius of the nucleus is no longer determined by the oscillator constant alone, because the mixing of states belonging to different major shells changes the mean square radius of each orbit. Therefore one is exposed to the problem of radial stability of the nucleus, and the radial dependence of the effective interaction becomes critical. It is well known that an interaction with a hard core cannot be used in H.F. calculations. The choice of an effective interaction is still a subject of much unsettled debate.[35] For this reason the energetics of major-shell-mixing H.F. calculations will not be discussed here. Since the deformation of the field is most probably due to the long-range quadrupole–quadrupole part of the interaction, it is reasonable to expect that similar results will be obtained with various forces which differ in the way the short-range effects are treated. Experimental single-particle energies ϵ_j may no longer be used in major-shell-mixing calculations, because in ^{17}O the closed-shell ^{16}O core may be polarized by the admixture of $2p$-$1f$ states to the filled $1p$ shell orbits, so that Eq. (38) is no longer valid. Thus the H.F. Hamiltonian equation (30) must be solved.

A major-shell-mixing H.F. calculation has been made using expansion (113) of the orbits.[17] A Volkov central interaction was used[5]

$$\begin{aligned} v &= v(r)(0.29 + 0.2P_\sigma - 0.05P_\tau + 0.71P_x) \\ v(r) &= -78\, e^{-(r/1.5)^2} + 82.5\, e^{-(r/0.8)^2} \qquad \text{MeV} \end{aligned} \tag{114}$$

This interaction, which is the sum of a longe-range attractive and a short-range repulsive interaction, was successfully used in p-shell nuclei.[5] The force of Eq. (114) does not have good saturation properties. Already in the

second half of the $2s$-$1d$ shell, it gives too small radii, so that only the results for quadrupole deformations will be discussed here. Central forces do not yield a spin–orbit splitting, and a spin–orbit term was added to the H.F. Hamiltonian (30)

$$\langle jm \mid h \mid j'm' \rangle = \langle jm \mid t' \mid j'm' \rangle + \sum_{\lambda=1}^{A} \langle jm, \lambda \mid v \mid j'm', \lambda \rangle$$
$$t' = \frac{p^2}{2m} + a\mathbf{l} \cdot \mathbf{s} \tag{115}$$

The spin–orbit strength a was chosen so as to reproduce the experimental splittings in ^{15}O and ^{17}O. The quadrupole deformations are not very sensitive to the spin–orbit strength a. The H.F. equations must be solved with successive values of the oscillator constant until the H.F. energy becomes minimum for infinitesimal variations of both the C_j^{λ} coefficients and the oscillator constant.

A convenient measure of the deformation is given by the ratio of the quadrupole moment Q_0 to the monopole moment $\langle r^2 \rangle$

$$Q_0 = \langle \varphi_K \mid \sum_{i=1}^{Z} (2z_i^2 - x_i^2 - y_i^2) \mid \varphi_K \rangle = \sum_{\lambda=1}^{Z} \langle \lambda \mid 2z^2 - x^2 - y^2 \mid \lambda \rangle$$
$$\langle r^2 \rangle = \langle \varphi_K \mid \sum_{i=1}^{Z} r_i^2 \mid \varphi_K \rangle = \sum_{\lambda=1}^{Z} \langle \lambda \mid r^2 \mid \lambda \rangle$$
$$\text{Deformation} = \frac{Q_0}{\langle r^2 \rangle} \tag{116}$$

For small deformations this is related to the deformation parameter β[4] by

$$\text{Deformation} = \frac{Q_0}{\langle r^2 \rangle} = 1.26\,\beta$$

The sums in (116) are over proton particles and proton orbits only. The deformation defined by Eq. (116) is a dimensionless number which does not vary much with the nuclear size. Figure 11 shows the variation of the H.F. energy, the deformation, and the monopole moment, with the oscillator constant α. In ^{20}Ne it is seen that the deformation is quite close to its maximum value at equilibrium.

The effect of closed-shell polarization on the quadrupole deformation is shown in Table XIII. The table compares the deformations [Eq. (116)] of axially symmetric solutions obtained by a single major-shell and a major-shell-mixing calculation. It is seen that the prolate deformations double their

value and that the oblate deformations increase by about 60%. Viewed as a microscopic calculation of the effective charge of a neutron, the calculation yields the value $\frac{1}{2}e$ for prolate shapes. The deformations are quite large. They may be visualized by comparing the H.F. intrinsic state with an axially symmetric ellipsoid, the major and minor axis of which are a and b (Fig. 12). The axes a and b are chosen such that the ellipsoid has the same monopole and quadrupole moments as the nucleus. The volume of the ellipsoid is $\frac{4}{3}\pi R^3$, where $R^3 = ab^2$ is the mean radius. Table XIV shows the ratio a/b of the

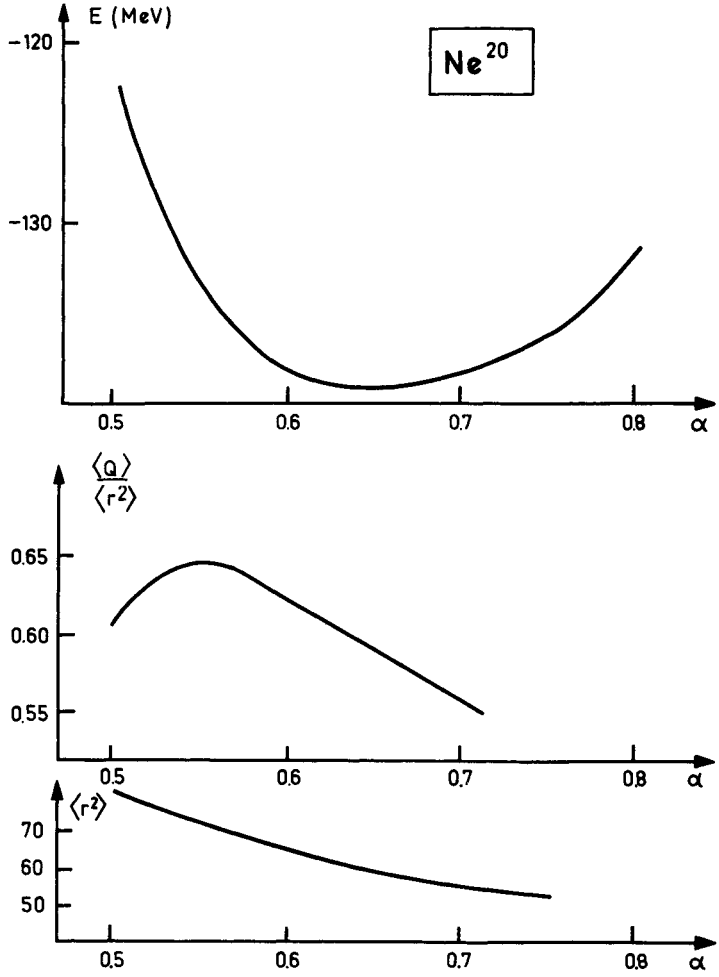

Fig. 11. Variation of the H.F. energy E, the deformation $\langle Q\rangle/\langle r^2\rangle$, and the monopole moment $\langle r^2\rangle$ of ^{20}Ne with the oscillator constant α. The curves are obtained by solving the H.F. equations successively for each value of α.

axes, and the mean radius R of the ellipsoid corresponding to the solutions of ^{16}O, ^{20}Ne, and ^{28}Si. In the case of ^{28}Si the ratio a/b varies by a factor of 2 between the oblate and prolate equilibrium shapes, yet R remains remarkably constant. The constancy of R is a measure of the incompressibility of the nucleus. In other words, the increase of the monopole moment with deformation is very similar to that of an incompressible liquid drop.

TABLE XIII

The Effect of Closed-Shell Polarization on the Quadrupole Deformations of Even–Even $N = Z$ Nuclei[a]

Nucleus	Single major shell	Major-shell mixing
^{12}C	−0.3	−0.47
^{20}Ne	0.31	0.59
^{24}Mg	0.30	0.63
^{28}Si oblate	−0.30	−0.49
^{28}Si prolate	0.30	0.75
^{32}S oblate	−0.08	−0.13
^{32}S prolate	0.17	0.35
^{36}Ar	−0.15	−0.24

[a] The second and third columns show the quadrupole deformation obtained from axially symmetric solutions of single major-shell and major-shell-mixing H.F. calculations.

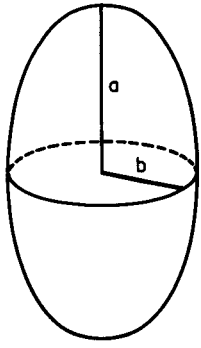

$$R^3 = ab^2$$

$$\langle r^2 \rangle = \frac{R^2}{5}\left[\left(\frac{a}{b}\right)^{4/3} + 2\left(\frac{b}{a}\right)^{2/3}\right]$$

$$Q_0 = \frac{2R^2}{5}\left[\left(\frac{a}{b}\right)^{4/3} - \left(\frac{b}{a}\right)^{2/3}\right]$$

Fig. 12. The axially symmetric ellipsoid with which H.F. solutions are compared. The monopole and quadrupole moments $\langle r^2 \rangle$ and Q_0 are expressed in terms of the equivalent radius R and the ratio a/b of the major to the minor axes.

TABLE XIV

Comparison of Deformed Nuclei with an Axially Symmetric Ellipsoid[a]

Nucleus		Configurations	$\langle r^2 \rangle$	$\langle Q \rangle / \langle r^2 \rangle$	E	a/b	R
^{16}O		Single shell	35.9	0	−109.2	1.0	7.75
		Shell mixing	35.5	0	−109.4	1.0	7.70
^{20}Ne		Single shell	56.4	0.31	−126	1.16	9.35
		Shell mixing	61.6	0.59	−139	1.31	9.30
^{28}Si	Oblate	Single shell	90.2	−0.30	−206	0.85	12.45
		Shell mixing	99.8	−0.49	−226	0.74	13.00
	Prolate	Shell mixing	124.7	0.75	−232	1.41	12.8

[a] The monopole moment $\langle r^2 \rangle$ and the deformation $Q_0/\langle r^2 \rangle$ are shown in the third and fourth columns for various solutions indicated in the second column. The H.F. energy is shown in the fifth column. The last two columns show the ratio a/b of major and minor axes and the equivalent radius $R = \sqrt[3]{ab^2}$ of an ellipsoid which has the same monopole and quadrupole moments as the H.F. solution. Lengths are given in fermi (10^{-13} cm) and energies in MeV.

The deformations obtained are compatible with the observed static quadrupole moments of odd-A nuclei as shown in Table XV. The static quadrupole moments were calculated with Eq. (111). In order not to be exposed to errors in the overall size of the nucleus, the intrinsic quadrupole

TABLE XV

Quadrupole Moments of Odd-A Nuclei[a]

Nucleus	K	J	Even core	Single shell	Shell mixing	Expt.
^{11}B	$\frac{3}{2}^-$	$\frac{3}{2}^-$	^{12}C	−1.52	−2.54	±3.1
^{21}Ne	$\frac{3}{2}^+$	$\frac{3}{2}^+$	^{20}Ne	4.83	9.65	9.0
^{23}Na	$\frac{3}{2}^+$	$\frac{3}{2}^+$	^{24}Mg	5.70	12.0	11.0
^{25}Mg	$\frac{5}{2}^+$	$\frac{5}{2}^+$		11.2	23.2	22.0
^{27}Al	$\frac{5}{2}^+$	$\frac{5}{2}^+$	^{28}Si oblate	−11.3	−20.0	15.0
	$\frac{1}{2}^+$	$\frac{5}{2}^+$		9.15	16.1	
^{33}S	$\frac{3}{2}^+$	$\frac{3}{2}^+$	^{32}S oblate	−2.52	−4.32	−5.5
	$\frac{3}{2}^+$	$\frac{3}{2}^+$	prolate	7.6	11.8	
^{35}Cl	$\frac{3}{2}^+$	$\frac{3}{2}^+$	^{36}Ar	−5.84	−9.8	−7.9

[a] The first four columns have the same meaning as those of Table XI. The quadrupole moments obtained using the deformation of single major-shell and major-shell-mixing calculations are shown in the fifth and sixth columns. The last column gives the experimental value. The quadrupole moments are expressed in units of $fm^2 = 0.01$ barn.

moments Q_0 were calculated by using the deformations obtained from the H.F. wave function and by using the experimental mean square radii for the monopole moment $\langle r^2 \rangle$. Of course the neutron carried no effective charge.

It is interesting to compare the results of major-shell-mixing H.F. calculations with the core polarization model proposed by Mottelson.[34] In this model the orbits are assumed to be the states (n_x, n_y, n_z) of a deformed harmonic oscillator. There are four nucleons in each orbit as shown in Fig. 2. Let ω_x, ω_y, and ω_z be the frequencies of the deformed oscillator along the three directions x, y, and z. Then the intrinsic quadrupole and monopole moments are given by

$$Q_0 = \frac{2\hbar}{m}\left[\frac{2N_z}{\omega_z} - \frac{N_x}{\omega_x} - \frac{N_z}{\omega_z}\right]$$

$$\langle r^2 \rangle = \frac{2\hbar}{m}\left[\frac{N_x}{\omega_x} + \frac{N_y}{\omega_y} + \frac{N_z}{\omega_z}\right]$$

N_x, N_y, and N_z being the total number of quanta in the three directions defined in Eq. (79). A comparison between this intrinsic state and the equivalent ellipsoid of Fig. 12 shows that the volume of the ellipsoid is determined by the product

$$\omega_0^3 = \omega_x \omega_y \omega_z \tag{117}$$

In the model of Mottelson, the axes of the oscillator potential are assumed to be in the same ratio as the axes of the mass distribution. The principal axes of the oscillator potential are proportional to $1/\omega_x$, $1/\omega_y$, and $1/\omega_z$ and the principal axes $\langle x^2 \rangle^{1/2}$, $\langle y^2 \rangle^{1/2}$, and $\langle z^2 \rangle^{1/2}$ of the mass distribution are proportional to $(N_x/\omega_x)^{1/2}$, $(N_y/\omega_y)^{1/2}$, and $(N_z/\omega_z)^{1/2}$. Thus in the Mottelson model

$$N_x\omega_x = N_y\omega_y = N_z\omega_z = \omega_0 \sqrt[3]{N_x N_y N_z} \tag{118}$$

while in an isotropic oscillator

$$\omega_x = \omega_y = \omega_z = \omega_0 \tag{119}$$

The quadrupole and monopole moments obtained with an isotropic oscillator are

$$\begin{aligned} Q_0 &= \frac{2\hbar}{m\omega_0}[2N_z - N_x - N_y] \\ \langle r^2 \rangle &= \frac{2\hbar}{m\omega_0}[N_x + N_y + N_z] \end{aligned} \tag{120}$$

The quadrupole and monopole moments obtained with a deformed oscillator in the Mottelson model are

$$Q_0 = \frac{2\hbar}{m\omega_0} \frac{1}{\sqrt[3]{N_x N_y N_z}} [2N_z^2 - N_y^2 - N_x^2]$$
$$\langle r^2 \rangle = \frac{2\hbar}{m\omega_0} \frac{1}{\sqrt[3]{N_x N_y N_z}} [N_x^2 + N_y^2 + N_z^2] \tag{121}$$

Quadrupole deformations obtained with an isotropic oscillator should be compared with those obtained in a single major-shell H.F. calculation. Quadrupole deformations obtained with a deformed oscillator should be compared with those obtained in a major-shell-mixing H.F. calculation. Such comparisons are shown in Table XVI in the case of ^{20}Ne. The product (117) of the oscillator axes was chosen such that the H.F. and oscillator wave functions should have corresponding ellipsoids of equal radius R. It has been seen that R does not vary significantly, so that ω_0 remains constant when the oscillator frequencies vary. Table XVI, shows the contribution of the $1s$, $1p$,

TABLE XVI[a]

Hartree-Fock Calculation

	Single major shell		Major-shell mixing	
Shell	$\langle r^2 \rangle$	Q_0	$\langle r^2 \rangle$	Q_0
$1s$	6.76	0	6.66	1.42
$1p$	33.78	0	35.10	9.41
$2s$-$1d$	15.78	17.23	19.82	26.29
Total	56.32	17.23	61.58	37.12

Mottelson Model

	Isotropic oscillator		Deformed oscillator	
Shell	$\langle r^2 \rangle$	Q_0	$\langle r^2 \rangle$	Q_0
$1s$	6.78	0	7.14	2.28
$1p$	33.81	0	35.69	11.42
$2s$-$1d$	15.78	18.09	17.70	27.20
Total	56.37	18.09	60.52	41.10

[a] A comparison between H.F. calculations and the model of Mottelson for ^{20}N. The contribution to the monopole moment $\langle r^2 \rangle$ and the quadrupole moment Q_0 of the orbits belonging to each major shell are shown.

and $2s$-$1d$ shells to the monopole and quadrupole moments of ^{20}Ne. The $1s$ and $1p$ shells have no quadrupole moment with wave functions of the isotropic oscillator, because they are closed shells, and only the $2s$-$1d$ shell orbit (0, 0, 2) contributes to the deformation. When the oscillator deforms (and in the major-shell-mixing H.F. calculations), the $1s$ and $1p$ shells are polarized and contribute about 30% of the total quadrupole moment. The $2s$-$1d$ shell orbit also increases its quadrupole moment by a mutual polarization effect.

There is good agreement between the quadrupole deformations obtained from the Mottelson model and the H.F. calculation. Similar quadrupole deformations can therefore by expected by expanding the H.F. orbits over states (n_x, n_y, n_z) belonging to a given major shell of a *deformed oscillator*. The variational parameters of the H.F. wave function are then the expansion coefficients of the orbits on the (n_x, n_y, n_z) states and the oscillator constants ω_x, ω_y, and ω_z. Such calculations have been done in the $1p$ shell by A. Volkov[5] and have begun in the $2s$-$1d$ shell.[24]

It is worth noting that the relation of Eq. (118), which gives the ratio of the oscillator axes for any configuration $\{N_x, N_y, N_z\}$, is also obtained by minimizing the kinetic energy of the system "at constant volume," i.e., keeping ω_0 constant. If ω_0 is constant, it is convenient to write

$$\omega_x = e^{\alpha}\omega_0 \qquad \omega_y = e^{\beta}\omega_0 \qquad \omega_z = e^{-(\alpha+\beta)}\omega_0 \tag{122}$$

The kinetic energy of the system is given by

$$T(\alpha, \beta) = 2\hbar\omega_0[N_x e^{\alpha} + N_y e^{\beta} + N_z e^{-(\alpha+\beta)}] \tag{123}$$

The minimum kinetic energy is obtained when

$$\frac{\partial T}{\partial \alpha} = \frac{\partial T}{\partial \beta} = 0 \tag{124}$$

which yields immediately relation (118) of the Mottelson model. Thus the model of Mottelson will predict the correct equilibrium deformation if the potential energy is independent of α and β,[1] because Eq. (124) will then minimize the total binding energy. Furthermore, at the minimum the kinetic energy is equal to

$$T_{\min} = 6\hbar\omega_0 \sqrt[3]{N_x N_y N_z} \tag{125}$$

[1] There are some indications that this may be so. It has been checked in H.F. calculations of $2s-1d$ shell nuclei in which the orbits are expanded on states (n_x, n_y, n_z) of a deformed oscillator and in which a Volkov force was used (A. Volkov, *private communication*) and in which a Kallio–Kolltveit force was used (A. Landé, "Variational calculations in light nuclei with realistic nucleon–nucleon interactions: ground state deformations," *to be published*).

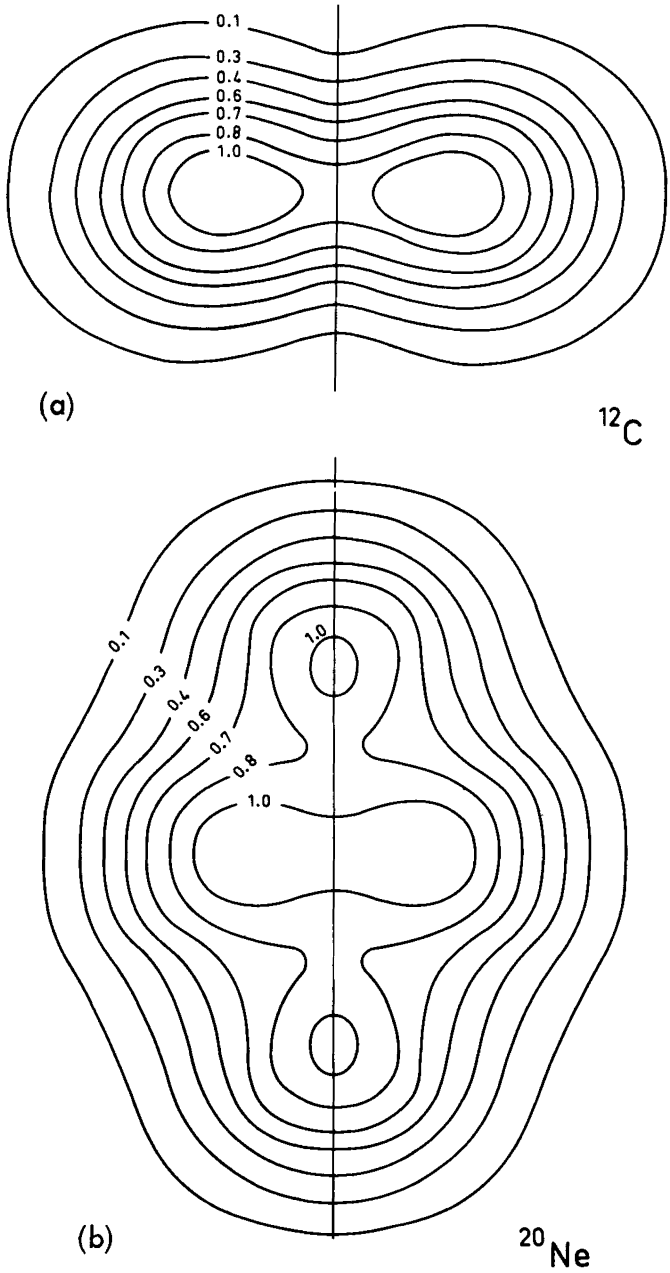

Fig. 13. Cross sections of equidensity surfaces cut by a plane containing the symmetry axis (vertical line) of axially symmetric H.F. solutions. Sections *a* to *d* represent, respectively, the oblate solution of ^{12}C, the prolate solution of ^{20}Ne, and the oblate and the prolate

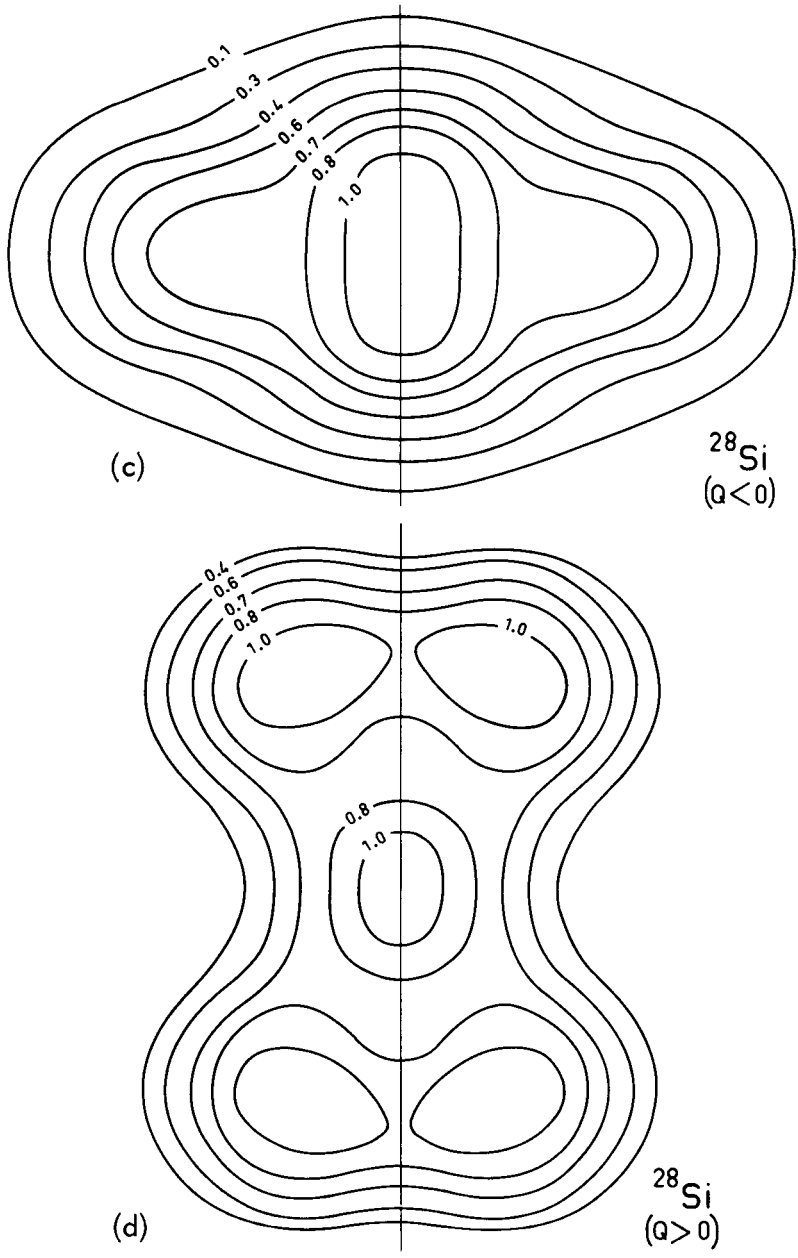

solutions of ^{28}Si. The contour line with highest density is arbitrarily normalized to 1. The scale of length of the vertical axis is 12% smaller than the scale of length of the horizontal axis.

Thus the kinetic energy is minimum for the configuration $\{N_x, N_y, N_z\}$ which has the product $N_xN_yN_z$ minimum. Table IX shows this product for various configurations of $2s$-$1d$ shell nuclei, and it is seen that in a given nucleus, whenever the product $N_xN_yN_z$ increases, the weight G of the state decreases. Now states (81) are constructed in such a way that the states with the highest weight G have minimum potential energy in an isotropic harmonic oscillator. All $2s$-$1d$ shell configurations have the same kinetic energy in an isotropic oscillator. Thus, if the potential energy does not change when the oscillator is deformed, the states with the highest weight continue to minimize the potential energy and the same configuration can minimize the kinetic *and* potential energies.

With $\hbar\omega_0 = 13$ MeV in ^{20}Ne, the kinetic energy gained by polarizing the closed shell is 7.6 MeV. Note that the prolate and oblate $(\lambda, \mu) = (12, 0)$ (0,12) shapes of ^{28}Si do not have the same kinetic energies at equal volumes. With $\hbar\omega_0 = 12.4$ MeV in ^{28}Si, the oblate (0,12) wave function has 2.5 MeV less kinetic energy than the prolate (12,0) wave function.

It is possible to visualize the equilibrium shapes obtained from the H.F. wave functions by drawing cross sections of equidensity surfaces. The density of nuclear matter is equal to the diagonal element of the density operator [Eq. (33)] in the **r** representation. Figures 13*a* to *d* show cross sections of equidensity surfaces of ^{12}C, ^{20}Ne, and ^{28}Si obtained from axially symmetric solutions of a major-shell-mixing H.F. calculation. The equidensity contours of single major-shell solutions have the same structure as major-shell-mixing solutions. The major-shell-mixing solution differs only by a more pronounced deformation.

16. CONCLUSION

The H.F. theory has proved to be a considerable help to the understanding of systems of interacting neutrons and protons in open shells. It is successful in accounting for the large neutron separation energies of even–even nuclei with equal numbers of neutrons and protons, as well as the large energy gap in the single-particle spectrum of these nuclei. The effect of the direct and exchange terms of the monopole and quadrupole components of the nuclear force on the single-particle spectrum has been made explicit, and the gap has been shown to be related to the nonlocality of the H.F. field. The spin–orbit interaction has been shown to become increasingly important in the second half of the $2s$-$1d$ shell, where it tends to destroy the stability of the H.F. wave functions. The validity of the adiabatic separation of the collective rotation and the intrinsic single-particle motion has been analyzed with the angular momentum projection method: The relatively small number

of nucleons in the open shells and the relatively low angular momenta of these shells make the collective variables of a light-deformed nucleus, such as the orientation in space of the intrinsic state, ill-defined. Applied to the quadrupole polarization of closed shells, the H.F. theory has allowed a microscopic calculation of the effective charge which agrees well with experiment. The main energy gain when closed shells are polarized is a kinetic energy gain, and it has been shown that the states which minimize the potential energy of the quadrupole–quadrupole interaction are also those which minimize the kinetic energy in the Mottelson model.

It is certain that the H.F. theory, i.e., the independent–particle model, cannot explain all the spectroscopic properties of light nuclei. As soon as a nucleus develops a neutron excess in the open shells, the H.F. theory gives a too small neutron gap, and it would be worth studying pairing effects there. The too large moments of inertia of nuclei in the middle of the $2s$-$1d$ shell and the multiplicity of the H.F. solutions still remain problems. The mixing of various equilibrium shapes also requires further study. It appears therefore that much of the improvement of the nuclear wave function lies outside the framework of the independent-particle model, and one of the great merits of the Hartree–Fock theory is that it allows a microscopic calculation of the parameters of this model, which is precise enough to show its limitations.

Acknowledgments

The author wishes to acknowledge the fruitful collaboration of W.H. Bassichis and B. Giraud in all the phases of this work. He wishes to thank Professor C. A. Levinson for a constant and stimulating exchange of ideas. He also wishes to thank Professors S. A. Moszkowski, M. Banerjee, and A. Volkov for many illuminating discussions. He is greatly indebted to Professor M. Baranger, who made many suggestions which improved the text of this article. He is extremely grateful to Miss C. Chevereau for her very efficient help in the numerical calculations.

REFERENCES

1. A. Bohr and B. Mottelson, *Kgl. Danske Videnskab. Selskab Mat. Fys. Medd.* **27** (16) (1953) (3rd ed., 1964).
2. A. Messiah, "Quantum Mechanics," North-Holland Publishing Co., Amsterdam, (1961) and Dunod, Paris (1959).
3. D. Kurath and L. Picman, *Nucl. Phys.* **10**:313 (1959).
4. S. G. Nilsson, *Kgl. Danske Videnskab. Selskab Mat. Fys. Medd.* **29** (16) (1955).
5. A. Volkov, *Nucl. Phys.* **74**:33 (1965).
6. J. Hayward, *Nucl. Phys.* **81**:193 (1966).

D. M. Brink, E. Boecker, *Nucl. Phys.* **A91**:1 (1967).
R. Muthukrishnan, *Nucl. Phys.* **A93**:417 (1967).
7. I. Kelson, *Phys. Rev.* **132**:2189 (1963).
8. I. Kelson and C. A. Levinson, *Phys. Rev.* **134**:B269 (1964).
9. W. H. Bassichis, C. A. Levinson, and I. Kelson, *Phys. Rev.* **136**:B380 (1964).
10. G. Ripka, "Lectures in Theoretical Physics," Vol. VIII C, University of Colorado Press, Boulder, 1966.
11. J. Bar-Touv and C. A. Levinson, *Phys. Rev.* **153**:1099 (1967).
12. J. Bar-Touv and I. Kelson, *Phys. Rev.* **138**:B1035 (1965).
13. J. P. Elliott, "Selected Topics in Nuclear Theory," *IAEA*, Vienna (1963).
M. Moshinsky, *in* "Group Theory and the Many Body Problem" Gordon and Breach, New York, 1965.
M. Harvey, review article in this volume.
14. W. H. Bassichis and G. Ripka, *Phys. Letters* **15**:320 (1965).
15. W. H. Bassichis, B. Giraud, and G. Ripka, *Phys. Rev. Letters* **15**:930 (1965).
16. I. Kelson, *Phys. Letters* **16**:143 (1965).
G. J. Stephenson and M. Banerjee, to be published in *Phys. Letters.*
17. G. Ripka, Lectures delivered at the Institute of Theoretical Physics in Trieste, *IAEA*, Vienna, 1966.
G. Ripka (Ref. 21).
18. K. T. R. Davies, S. J. Krieger, and M. Baranger, *Nucl. Phys.* **84**:545 (1966).
19. R. Hofstadter, "Electron Scattering and Nuclear and Nucleon Structure," W. A. Benjamin, Inc., New York (1963).
20. V. Gillet and E. Sanderson, *Nucl. Phys.* **31**:292 (1967).
21. G. Ripka, International Conference on Nuclear Physics Gaitlinburg, Tenn. (1966).
S. Das Gupta and M. Harvey, *Nucl. Phys.* **A94**:593 (1967).
22. G. E. Brown and A. M. Green, *Nucl. Phys.* **75**:401 (1966).
23. M. Banerjee, *private communication.*
24. A. Volkov, *private communication.*
R. Muthukrishnan (Ref. 6).
25. R. E. Peierls and J. Yoccoz, *Proc. Phys. Soc. (London)*, **A70**:381 (1957).
26. D. L. Hill and J. A. Wheeler, *Phys. Rev.* **89**:1106 (1953).
27. B. J. Verhaar, *Nucl. Phys.* **54**:641 (1964).
28. J. A. Kuehner and R. W. Ollerhead, *Phys. Letters* **20**:301 (1966).
29. J. N. Smirnov, *Nucl. Phys.* **39**:346 (1962).
30. L. Zamick and G. Ripka, *Phys. Letters* **23**:347 (1966).
31. H. A. Mavromatis, L. Zamick, and G. E. Brown, *Nucl. Phys.* **80**:545 (1966).
32. M. de Llano, P. A. Mello, E. Chacon, and J. Flores, *Nucl. Phys.* **72**:379 (1965).
33. D. R. Inglis, *Phys. Rev.* **96**:1059 (1954).
34. B. Mottelson, "The Many Body Problem," École d'Été de Physique Théorique, Les Houches, Dunod, Paris (1958) and John Willey and Sons, Inc., New York (1958).
35. C. W. Wong, *Nucl. Phys.* **A91**:399 (1967).
T. T. S. Kuo and G. E. Brown, *Nucl. Phys.* **85**:40 (1966).
B. H. Brandow, "The theory of Effective Interaction," Varenna Summer School Seminar (1965).
A. D. Mackellar and R. L. Becker, *Phys. Letters* **18**:308 (1965).
C. M. Shakin, J. P. Svenne, and Y. P. Waghmare, *Phys. Letters* **21**:209 (1966). See also the contributions of M. Baranger, H. A. Bethe, W. H. Bassichis, A. K. Kerman and J. P. Svenne to the International Conference on Nuclear Physics Gatlinburg, Tenn. (1966).

36. V. Gillet, *Nucl. Phys.* **51**:410 (1964) Thesis, University of Paris (1962).
37. J. P. Elliott and B. H. Flowers, *Proc. Roy. Soc. (London)* **A229**:536 (1965).
38. Carter, Mitchell, and Davis, *Phys. Rev.* **133**:B1421 (1964).
39. N. Vinh-Mau and G. Brown, *Phys. Rev. Letters* **1**:361 (1962).
40. J. M. Eisenberg, M. Spicer, and M. E. Rose, *Nucl. Phys.* **71**:273 (1965).
41. G. Ripka, *Proc. Paris Conf. Nucl. Structure* C174 (1964).
    L. Zamick, *Phys. Letters* **19**:580 (1965).
42. S. Gorodetzky, P. Mennrath, N. Benenson, P. Chevalier, and F. Scheibling, *J. Phys. Radium* **24** (1963).
43. I. Unna and I. Talmi, *Phys. Rev.* **112**:452 (1958).
44. M. K. Banerjee and G. J. Stephenson, Jr., "Shape of the four particle-four hole state of ^{16}O," *to be published.*
45. E. Boecker, *Phys. Letters* **21**:69 (1966).
    L. S. Celenza and A. Klein, *to be published.*
46. I. Kelson, *Phys. Rev.* **134**:B267 (1964).

THE STATISTICAL THEORY OF NUCLEAR REACTIONS

Erich Vogt

1. INTRODUCTION

The statistical theory of nuclear reactions has evolved from a rough tool, used for several decades to provide a global order to a large body of nuclear data, into one of the most quantitative tools we possess in nuclear physics. It is based on the compound nucleus picture of nuclear reactions. The closely spaced narrow resonances which are characteristic of compound nucleus processes are individually of interest only at low energies, say energies of a few million electron volts or less in all but the lightest nuclear systems. At higher energies, with increasing numbers of resonances, the physical interest (and usually the measurements themselves) concerns nuclear cross sections averaged over the resonances. The statistical theory of nuclear reactions deals with such average cross sections.

To a great extent the treatment of average cross sections employs an evaporation model with only a partial basis in nuclear reaction theory. The model depicts the nuclear reaction as proceeding in two stages. In the first stage a compound nucleus is formed by the collision of the projectile with a target nucleus. In the second the compound nucleus decays into one of the possible pairs of reaction products. The evaporation model assumes that the compound nucleus, in its decay, loses all memory of the way in which it was formed; the decay treats all possible decay products in the democratic fashion realized in evaporation from a classical liquid drop. The present review article aims at describing the modern form of the evaporation model (Section 2), illustrating its application to cross-section data (Section 3), and exploring its justification in the theory of resonance reactions (Section 4). The emphasis will be on the use of the model rather than on its foundation in theory. The treatment is intended to be didactic, concentrating on a few simple examples which illustrate how the theory is applied. The purpose is to make the statistical theory accessible to a large group of nuclear scientists who should be

using the modern statistical theory for straightforward and accurate predictions of compound nucleus processes.

The modern evaporation theory takes its main ideas from early evaporation models but modifies these models in several important ways. The early theories were used for several decades to describe many nuclear reactions and are still useful in providing quick order-of-magnitude estimates of many nuclear cross sections. We present the early models here to introduce main ideas which we shall employ later and to provide rough estimates of cross sections. The refinements of the early theory are based on fundamental conservation laws and on recent knowledge of the average interaction between nucleons and nuclei as described by the nuclear optical model and the shell model. The ideas tying the optical potential to the compound nucleus processes are similar to ideas which relate the compound nucleus processes to a whole class of competing mechanisms—the direct reactions.

1.1 Early Evaporation Models

The early forms of evaporation models were developed by Bethe,[1] Weisskopf,[2] and Weiskopf and Ewing[3] soon after the compound nucleus was proposed[4,5] to explain nuclear-resonance cross sections. Because the physical ideas underlying the resonance cross sections have guided so much of the thinking about average cross sections at higher energies, we examine them briefly. When neutrons are bombarded against almost any heavy element, the cross sections exhibit[6] resonances which are very narrow (typically about 0.03 to 0.10 eV in width) and very closely spaced (typically only 1 to 10 eV apart). The compound nucleus picture explained the width and spacing of the resonances in terms of the rapid sharing of energy of the neutron with the target nucleus. The energy sharing implied that resonance states excited by the neutron were not only the virtual single-particle states of a neutron in a simple potential well of nuclear size but also the many-particle states in which neutrons and protons of the target nucleus are excited. The spacing of the single-particle states is determined primarily by nuclear size and is of the order of several MeV or more. On the other hand, the many-particle states in a heavy nuclei are so numerous that they easily explain the observed spacing. The narrow width or long lifetime of the resonances was attributed to the long time required for an individual nucleon to obtain enough of the shared energy to escape from the nucleus. The independence of formation and decay of the evaporation models is often attributed to the long lifetime of compound states. In fact the validity of the models (Section 4) extends even to energies where the compound states are very short-lived.

The evaporation model first proposed by Bethe[1] and Weisskopf[2,3]

was fully developed a decade later into a rough workable model as described by Blatt and Weiskopf.[7] In this rough model a nuclear reaction of the following kind

> Initial projectile and target nucleus (labeled c) $\rightarrow$ compound nucleus $\rightarrow$ reaction products (labeled c')

is assumed to have an average cross section $\bar{\sigma}_{cc'}$ which may be factored

$$\bar{\sigma}_{cc'} = [\sigma_{\text{comp}}(c)] \left[\frac{G_{c'}}{G}\right] \tag{1}$$

The average of the cross section is over any resonance structure. The first factor of Eq. (1) depends only on the initial pair of particles c and is called a *cross section for the formation of the compound nucleus*: the second factor depends only on the final reaction products c' and is called a *branching ratio*. The denominator of the branching ratio is a sum of the factor $G_{c'}$ over all the pairs of reaction products (including c and c') available to the compound nucleus

$$G \equiv \sum_{c''} G_{c''} \tag{2}$$

Hence it is a property of the compound nucleus only—it does not depend on the particular choice of c and c'. The factorization assumed in Eq. (1) is an expression of the independence of formation and decay of the compound nucleus. It is frequently referred to as the *Bohr assumption*.

To complete the workable model based on Eq. (1) a reciprocity theorem is used to express each factor G_c in terms of the compound-nucleus-formation cross section for the same pair of particles c. Then a simple nuclear model is used to evaluate each $\sigma_{\text{comp}}(c)$. The reciprocity theorem is the following one:

$$k_c^2 \bar{\sigma}_{cc'} = k_{c'}^2 \bar{\sigma}_{c'c} \tag{3}$$

where k_c is the wave number for the relative motion of the pair c and $\bar{\sigma}_{c'c}$ is the average cross section for the reverse reaction. The factor k_c^2 on left side of Eq. (3) and the corresponding factor $k_{c'}^2$ on the right side are required to change the cross section, as conventionally defined, into a proper transition probability.[7]

The reciprocity theorem (3) then expresses the invariance of the physical process under time reversal together with the conservation of particle flux. Use of Eq. (1) and the corresponding expression for $\bar{\sigma}_{c'c}$ in Eq. (3) yields the result, for each c,

$$G_c = k_c^2 \sigma_{\text{comp}}(c) \tag{4}$$

The cross section for the formation of a compound nucleus is taken to be πR_c^2 for the collision of neutral particles, where R_c is the nuclear radius of the colliding pair. For the collision of charged particles the cross section is modified by a multiplicative penetration factor taking care of the penetration of the pair through the Coulomb barrier to the nuclear radius. This prescription for each $\sigma_{\text{comp}}(c)$ assumes that all particles reaching the target nucleus are absorbed by it.

Combining Eqs. (4), (2), and (1), we have

$$\bar{\sigma}_{cc'} = \sigma_{\text{comp}}(c) \frac{k_{c'}^2 \sigma_{\text{comp}}(c')}{\sum_{c''} k_{c''}^2 \sigma_{\text{comp}}(c'')} \tag{5}$$

In addition to the prescription above for σ_{comp} of each pair, the evaluation of the denominator of Eq. (5) requires an enumeration of all the possible reaction products. To carry out the enumeration, we describe each reaction alternative, c', by two labels. The first, p', labels the pair of particles (e.g., proton plus residual nucleus or alpha particle plus the corresponding residual nucleus, etc); the second, $E_{p'}^*$, labels the state of excitation of the pair. Alternatively, we can use the center-of-mass kinetic energy $E_{p'}$ of the pair p'. The excitation energy $E_{p'}^*$ of the residual nucleus is related to $E_{p'}$ in the following way. For each energy E of the incident beam there is a maximum value $E_{p'}^{\max}$ of energy available to the emitted projectile. If S_p is the separation energy of the incident pair from the compound system and $S_{p'}$ is that of the residual pair, then we have

$$E_{p'}^{\max} = E - S_{p'} + S_p \equiv E + Q_{pp'}$$

where $Q_{pp'}$ is the Q value of the reaction. The excitation energy of the residual nucleus is the difference between $E_{p'}^{\max}$ and $E_{p'}$

$$E_{p'}^* = E_{p'}^{\max} - E_{p'}$$

As an illustration of the reaction alternatives available to the compound nucleus, we show, in Fig. 1, all the pairs p and the excitation levels E_p^* available when the compound nucleus Mg^{24} has been excited to 25 MeV. The ground states of the various pairs are displaced above the ground state of Mg^{24} by the following known separation energies:

$$\begin{aligned} Mg^{24} &\rightarrow Na^{23} + H^1 \quad + 11.69 \text{ MeV} \\ &\rightarrow Mg^{23} + n \quad\;\; + 16.54 \text{ MeV} \\ &\rightarrow Na^{22} + H^2 \quad + 21.88 \text{ MeV} \end{aligned}$$

$$\rightarrow \mathrm{Ne}^{21} + \mathrm{He}^{3} + 23.13\ \mathrm{MeV}$$
$$\rightarrow \mathrm{Ne}^{20} + \mathrm{He}^{4} + 9.31\ \mathrm{MeV}$$
$$\rightarrow \mathrm{O}^{16} + \mathrm{Be}^{8} + 14.14\ \mathrm{MeV}$$
$$\rightarrow \mathrm{C}^{12} + \mathrm{C}^{12} + 13.93\ \mathrm{MeV}$$

As indicated by Fig. 1 the number of reaction alternatives can be very large and increases rapidly with energy.

When many different states of excitation are possible, a level density $w(E_p)$ is used to evaluate the sum in the denominator of (5). Therefore we write

$$\bar{\sigma}_{cc'} = \sigma_{\mathrm{comp}}(c) \frac{k_{c'}^2 \sigma_{\mathrm{comp}}(c')}{\sum_{p''} \int_0^{E_{p''}^{\max}} k_{p''}^2 w(E_{p''}^*)\, \sigma_{\mathrm{comp}}(E_{p''})\, dE_{p''}} \tag{6}$$

The level density formulas used in Eq. (6) were, at first,[7] the very simple formulas of a "degenerate Fermi gas"

$$w(E^*) = w_0 e^{2E^*/\theta} \tag{7}$$

where w_0 is a constant (varying from nucleus to nucleus), and θ, a constant [usually with a value near 1 MeV[12]] sometimes loosely referred to as the "nuclear temperature" (a more accurate temperature of the nuclear Fermi

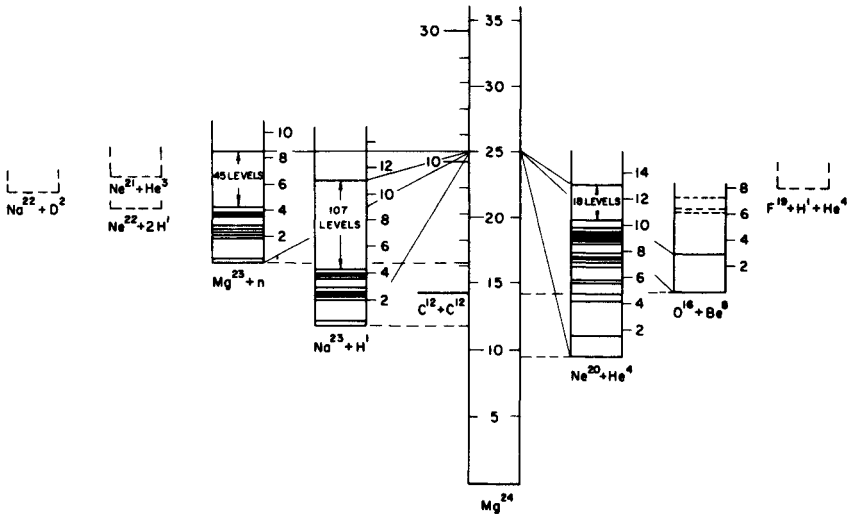

Fig. 1. The energy levels available for the decay of compound states of Mg^{24} at an excitation energy of ~25 MeV.

gas is given in Section 3.3). More recently the level density formulas have been modified to include the effects of the nuclear shell model[8] and other fashionable ideas about nuclear structure. Some of these effects are discussed below. To quite an extent the early work[9] with the evaporation models aimed at obtaining information about nuclear level densities directly from the energy spectra $N(E_{p'})$ of particles emitted from the compound nucleus. Thus we have

$$N(E_{p'})\,dE_{p'} \equiv \sum_{\Delta E_{p'}} \bar{\sigma}_{cc'} = w(E_{p'}^{*})\,\bar{\sigma}_{cc'}\,dE_{p'}$$

$$= \sigma_{\text{comp}}(c)\,G^{-1}k_{p'}^{2}w(E_{p'}^{*})\,\sigma_{\text{comp}}(E_{p'})\,dE_{p'} \tag{8}$$

in which G is the denominator of (6). $\Delta E_{p'}$ is the energy interval between $E_{p'}$ and $E_{p'} + dE_{p'}$.

Extensive tests of the early evaporation models were made in the decade 1945 to 1955 and resulted in the following substantial achievements:

1. The theory accounted for the general systematics of particle emission following the bombardment of a large variety of nuclei at many bombarding energies. For example, in the bombardment of nuclei throughout the periodic table with 14-MeV neutrons, Paul and Clarke[10] found very great variations in the yield of protons and alpha particles; most of the variations were accounted for by variations in the particle-separation energies.

2. Ghoshal[11] confirmed the central idea of the evaporation model—the Bohr assumption concerning the independence of formation and decay of the compound nucleus. In separate experiments he excited the compound nucleus Zn^{64} by the bombardment of Ni^{60} with alpha particles and the bombardment of Cu^{63} with protons. The cross-section ratios $\sigma(\alpha, n)/\sigma(\alpha, 2n)/\sigma(\alpha, pn)$ of the first reaction agreed with the ratios $\sigma(p, n)/\sigma(p, 2n)/\sigma(p, pn)$ of the second.

3. The energy spectra of particles emitted from the compound nucleus obtained from the use of Eq. (8) had the characteristic shapes shown in Fig. 2. For neutrons the compound-nucleus cross section is πR_c^2 for all energies so that the energy spectrum, according to (8), is directly proportional to $E_n e^{-2E_n/\theta}$, where E_n is the neutron energy. This spectrum shape is frequently referred to as a *Maxwellian spectrum.* For charged-particle emission the spectrum is changed because, for low particle energies, the penetration through Coulomb barriers inhibits particle emission. The yield of alpha particles or protons from heavy nuclei is therefore very small unless the neutron-separation energy is unusually large.

4. Nuclear level densities deduced from the energy spectra of emitted

particles[9,12] yielded moderate agreement with the predictions of nuclear models and with other data on level densities.

5. The theory explained the "boiling-off" of large numbers of neutrons from an excited heavy nucleus. For any excited heavy nucleus, the emission of a neutron is greatly favored over the emission of any charged particle. The mean energy of neutrons emitted by the compound nucleus is θ, the mean excitation energy imparted to the residual nucleus in neutron emission is $E - S_n - \theta$, where E is the excitation energy of the compound nucleus and S_n the neutron-separation energy (typically 6 to 10 MeV in a heavy nucleus). This excitation energy may itself be large enough that a second neutron may escape. The total number of neutrons which boil off is then roughly equal to $E/(S_n + \theta)$. For example, for Au^{197} excited to 140 MeV, the number of neutrons[13] which boil off lies between 5 and 8. For 1000-MeV protons incident on a lead or bismuth target each incident proton yields about 20 neutrons.[14] The excited compound nucleus behaves like a heated

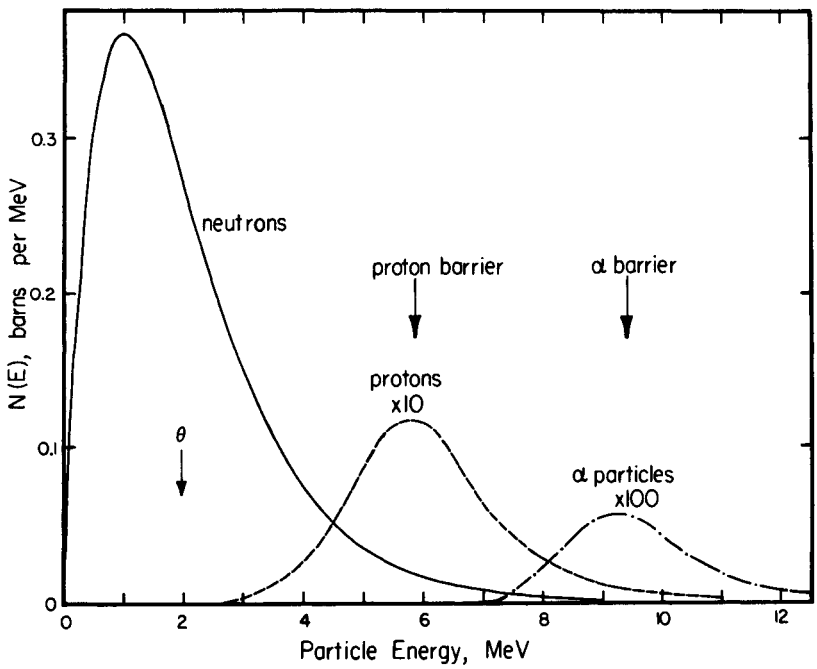

Fig. 2. Typical energy spectra of emitted particles as predicted by the early evaporation models. The proton spectrum has been multiplied by a factor of 10 and the alpha particle spectrum by a factor of 100. The choice of temperatures is one which might apply to moderate excitation energies of the compound nucleus (say, 10 to 50 MeV) and the choice of barrier positions to a moderately light nucleus ($A \sim 40$).

mixture of two liquids—neutrons and protons. Because of their Coulomb barriers, the protons have a higher boiling point so that all the heat escapes in the form of neutrons. This evaporation process may yet turn out to be the cheapest source of neutrons for the production of the fissionable isotopes required as fuel in the production of nuclear energy.[14]

1.2 Refinement of the Early Evaporation Models

There are two major defects in the early evaporation theory given above. The first concerns the lack of conservation of total angular momentum and parity in the cross-section formulas. Regardless of how long the compound nucleus lasts, there is no evidence that it can forget its total angular momentum. The improved theory, developed in Section 2, assumes that the factorization of the cross section, as in Eq. (1) above, holds for each total angular momentum and parity separately. The second major defect of the early theory concerns its use of compound-nucleus cross sections which do not exhibit the giant resonances or size resonances which are one of the dominant features of the interaction between a nucleon and a nucleus. This neglect is easily corrected by using absorption cross sections prescribed by the nuclear optical model. Both of these improvements are of great importance in some of the examples discussed in Section 3.

At the same time that the evaporation theory has improved, the wealth of new knowledge about nuclear energy levels has removed much of the arbitrariness present in early applications. As an example, consider the compound nucleus Mg^{24} excited to 25 MeV. Even though the number of possible final states exceeds 200 (see Fig. 1), enough is known about the energies of the final states and about their spins and parities that one does not need to use any level-density formula. The statistical theory can then be applied with essentially no adjustable parameters. In Section 3.2 below we shall see how well it works for this case.

The giant resonances accounted for by the optical model not only modify the absorption cross sections but also cast some doubt on the whole compound-nucleus picture. The giant resonances are the vestiges, in nuclear reactions, of the bound states or orbits of the nuclear shell model. The view of nuclear structure which they impart to us might be pictorially represented as in Fig. 3. The compound-nucleus picture and the early evaporation theory had in mind a "black-box" view of the nucleus: Any particle which appeared at the nuclear radius was absorbed into the black-box; what eventually emerged from the box was independent of its formation. On the other hand, the shell model has told us that neutrons and protons in the nucleus can be regarded as moving in individual orbits. Similarly, the optical model tells us that the mean free path of a nucleon in a nucleus

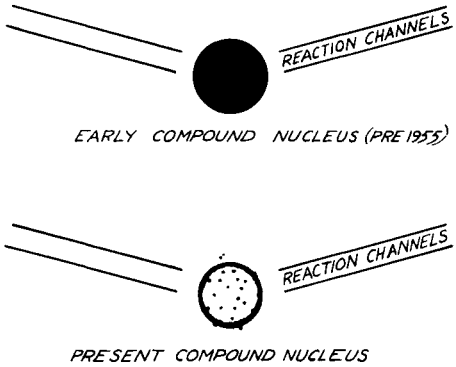

Fig. 3. A pictorial representation of the compound nucleus. The entrance channel is represented on the left of the nucleus.

is comparable to the nuclear radius. Consequently we have a microscopic view of the nucleus, such as that indicated in Fig. 3, which is far richer than the black-box picture.

Within the microscopic picture of the nucleus there are all kinds of simple nuclear reactions that can take place in which no compound nucleus is ever formed. For example, an incoming nucleon can pass right through a nucleus without being absorbed. Such a refracted wave interferes with the waves which pass around the nucleus and produces a diffraction pattern accounted for by the optical model. Alternatively, the incoming nucleon can strike a single nucleon in the target nucleus or excite a quantum of surface excitation, etc. There is a large variety of such simple direct reactions[15] which can be described in terms of the *distorted-wave Born Approximation.*

The justification of the modern statistical theory (Section 4) must be made in a way that describes the relation of the compound-nucleus processes to direct reactions. It is not likely that any completly satisfactory justification can be given. At high excitation energies the compound nucleus decays very quickly—more quickly than it takes a neutron or proton to cross the nucleus —and the idea of a compound state becomes somewhat artificial. Nonetheless, the theory of resonances provides a framework for discussing both the direct reactions and the compound-nucleus processes and illuminates the connection between the two. The physical conditions under which the model given in Section 2 holds are found to have little to do with the time for which the compound state lasts. Rather, they concern the time taken for the decay into any particular reaction channel. The statistical theory appears to fit data even under conditions for which it cannot be easily justified.

The applicability of the statistical theory is almost universal. There are many cases for which the direct-reaction cross sections are much smaller than those of the compound nucleus. In other cases the direct reactions predominate, but the compound-nucleus processes form a background which is usually neglected. The neglect is unnecessary and often unjustifiable: It leads to a distortion of the direct-reaction analysis. In many of these cases the statistical theory is a parameter-free, straightforward, quantitative theory, which should be used to subtract out the compound-nucleus processes before applying the direct-reaction theories.

2. THE MODEL FOR AVERAGE CROSS SECTIONS

2.1 Basic Evaporation Theory

A modern evaporation theory can be constructed along the same physical principles as the early evaporation theory except that we add conservation of total angular momentum and parity and we also compute absorption cross sections with the optical model. Since such an evaporation theory does not deal directly with the nuclear resonances over which the cross section is assumed to be averaged, we refer to it as a model. In Section 4 the justification of the model is discussed in terms of the theory of resonance reactions. The evaporation model in the form given here is often referred to as the *Hauser–Feshbach model* after the authors[16] who first added conservation of total angular momentum and parity to the neutron cross sections of the old theory. A complete statement of the model as described and used in this article was given by Thomas[17] and by Lane and Thomas.[18]

The requirement of conservation of total angular momentum in the model makes it necessary to be more explicit about what is meant by a reaction alternative (or channel). We shall use the label c to denote the following set of quantum numbers:

$$c = (\alpha, I, i, s, l, J, M_J, \Pi) \tag{9}$$

where α labels the pair of particles and their state of excitation (it combines the symbols p and E_p used in Section 1; thus each of the energy levels in Fig. 1 would correspond to a different α); I and i are the intrinsic spins of the pair of particles α (in units of $\hbar$); s is the channel spin

$$\mathbf{s} = \mathbf{I} + \mathbf{i} \tag{10}$$

l is the orbital angular momentum of the pair; J is the total angular momentum

$$\mathbf{J} = \mathbf{l} + \mathbf{s} = \mathbf{l} + \mathbf{I} + \mathbf{i} \tag{11}$$

M_J is the z component of J; and Π is the total parity (the product of $(-)^l$ with the intrinsic parities of the pair α). In everything that follows we shall assume that all reactions are independent of M_J and that M_J can be averaged over and ignored.

The result of the evaporation theory below for the cross section $\bar{\sigma}_{\alpha\alpha'}$ (integrated over all angles of the outgoing pair α' and averaged over any resonance structure) may be written

$$\bar{\sigma}_{\alpha\alpha'} = \frac{\pi}{k_\alpha^2} \sum_{J,\Pi} \frac{2J+1}{(2I+1)(2i+1)} \left\{\sum_{sl} T_l(\alpha)\right\} \left\{\frac{\sum_{s'l'} T_{l'}(\alpha')}{\sum_{\alpha''s''l''} T_{l''}(\alpha'')}\right\} \tag{12}$$

The unprimed quantities refer to the incoming channels of the reaction, the primed quantities refer to the outgoing channels, and the double-primed quantities in the denominator are summed over all channels to which the compound nucleus can decay. The functions $T_l(\alpha)$ are called *transmission functions* and are given by the optical-model phase shifts $\delta_{\alpha l}$ of the pair α

$$T_l(\alpha) \equiv 1 - |\, e^{2i\delta_{\alpha l}} \,|^2 \tag{13}$$

The optical potentials to be used are discussed below, and the connection of the transmission functions to the width and spacing of nuclear resonance states is given in Section 4. The sums of (12) run over the following values: Π is positive or negative; J has the values 0, 1, 2,... if the compound nucleus has even mass number and the values $\frac{1}{2}, \frac{3}{2}, \frac{5}{2}$,... otherwise; s takes on all integer values between $I - i$ and $I + i$ [cf. (10)]; and l runs all even values between $|\, J - s \,|$ and $J + s$ [cf. (11)] if the pair α has the same parity as Π and over all odd values otherwise.

The notation of Eqs. (12) and (13) implies that the transmission functions are independent of J and s. This is true only if the optical-model potential has no spin–orbit term. There is no evidence that such spin–orbit terms have any great effect on average cross sections (see Section 2-3). If they are to be included, then we must replace each $\sum_{sl} T_l(\alpha)$ in (12), and in the following, by $\sum_{jl} T_{lj}(\alpha)$, where

$$\mathbf{j} = \mathbf{i} + \mathbf{l}$$

and where $T_{lj}(\alpha)$ is related to the optical-model phase shifts $\delta_{lj\alpha}$ by

$$T_{lj}(\alpha) \equiv 1 - |\, e^{2i\delta_{lj\alpha}} \,|^2 \tag{14}$$

Since the choice of j or s as quantum numbers is a choice between angular momentum coupling schemes, we can, alternatively, define transmission fractions $T_{slJ}(\alpha)$, depending on s and J to be used in place of the $T_l(\alpha)$ of (12).

The dependence on s and J arises only if we have spin–orbit forces, and the $T_{slJ}(\alpha)$ are given in terms of optical-model phase shifts by

$$T_{slJ}(\alpha) \equiv \sum_j (2j+1)(2s+1)W^2(lIJi;js)\, T_{lj}(\alpha) \tag{15}$$

Here the $W(lIJi;js)$ are Racah coefficients.[21–23] With this choice of transmission functions, all of the evaporation formulas apply even when spin–orbit potentials are used, and we merely need to add the labels s and J to each transmission function in the text.

Before deriving the result [Eq. (12)] for the average cross section $\bar{\sigma}_{\alpha\alpha'}$ in terms of the evaporation theory, we display the terms which occur in a specific example. Consider the reaction $Na^{23}(p,\alpha)\,Ne^{20}$ at proton energies of less than 0.4 MeV. According to Fig.1 we then have the three values of α shown in Table I. With this definition of the three values of α, the cross section we want is $\bar{\sigma}_{12}$. The result for $\bar{\sigma}_{12}$ is given by Eq. (16) for the first few values of $J\Pi$, with each line corresponding to a different value $J\Pi$ as indicated.

$$\begin{aligned}
\bar{\sigma}_{12} = \frac{\pi}{8k_1^2}\Bigg\{ & [T_2(1)]\,\frac{[T_0(2)]}{T_2(1)+T_0(2)+T_2(3)} && J\Pi\ 0+\\
& + [T_1(1)]\,\frac{[\text{no terms}]}{T_1(1)} && 0-\\
& + 3[T_0(1)+2T_2(1)]\,\frac{[\text{no terms}]}{T_0(1)+2T_2(1)+T_2(3)} && 1+\\
& + 3[2T_1(1)+T_3(1)]\,\frac{[T_1(2)]}{2T_1(1)+T_3(1)+T_1(2)+T_1(3)+T_3(3)} && 1-\\
& + 5[T_0(1)+2T_2(1)+T_4(1)]\,\frac{[T_2(2)]}{\begin{pmatrix}T_0(1)+2T_2(1)+T_4(1)+T_2(2)\\ +T_0(3)+T_2(3)+T_4(3)\end{pmatrix}} && 2+\\
& + 5[2T_1(1)+2T_3(1)]\,\frac{[\text{no terms}]}{2T_1(1)+2T_3(1)+T_1(3)+T_3(3)} && 2-\\
& + 7[2T_2(1)+2T_4(1)]\,\frac{[\text{no terms}]}{2T_2(1)+2T_4(1)+T_2(3)+T_4(3)} && 3+\\
& + \text{terms for higher } J\Pi\Bigg\}
\end{aligned} \tag{16}$$

The display contains all the terms up to $J\Pi = 3+$ and all partial waves for each $J\Pi$; all higher terms will involve incoming partial waves of $l = 3$

or higher and will therefore be small at low proton energies. At higher energies the compound nucleus Mg^{24} has many more channels available for decay than the three values of α of our display. Cross-section calculations at higher energies are given in Section 3.2.

TABLE I

Channels for the Na^{23} (p, α) Ne^{20} Reaction at Low Proton Energies

	Description of channel	I	i	s	Parity
$\alpha = 1$	$p + Na^{23}$ (ground state)	$\frac{3}{2}$	$\frac{1}{2}$	1,2	+
$\alpha = 2$	alpha + Ne^{20} (ground state)	0	0	0	+
$\alpha = 3$	alpha + Ne^{20} (1st excited state)	2	0	2	+

The derivation of Eq. (12) is parallel to the derivation of the older evaporation theory described in Section 1. Since we wish to conserve total angular momentum J and parity Π, we consider the decomposition of $\bar{\sigma}_{\alpha\alpha'}$ into contributions from separate J, Π

$$\bar{\sigma}_{\alpha\alpha'} \equiv \sum_{J\Pi} \bar{\sigma}_{\alpha\alpha'}^{J\Pi} \tag{17}$$

Next we factor each $\bar{\sigma}_{\alpha\alpha'}^{J\Pi}$ into a compound-nucleus-formation cross section and a branching ratio

$$\bar{\sigma}_{\alpha\alpha'}^{J\Pi} \equiv [\sigma_{\text{comp}}^{J\Pi}(\alpha)] \frac{G_{\alpha'}^{J\Pi}}{\sum_{\alpha''} G_{\alpha''}^{J\Pi}} \tag{18}$$

The sum over α'' runs over all reaction alternatives available to the compound nucleus. Since Eq. (18) is now valid for each J, Π separately, the factorization of the cross section as in Eq. (18) does not imply that the compound nucleus forgets its total angular momentum and parity.

The connection between compound-nucleus cross sections and branching ratios is established by the following reciprocity theorem:

$$k_\alpha^2 \bar{\sigma}_{\alpha\alpha'}^{J\Pi} = k_{\alpha'}^2 \bar{\sigma}_{\alpha'\alpha}^{J\Pi} \tag{19}$$

Combining Eqs. (19) and (18), we find

$$G_\alpha^{J\Pi} = k_\alpha^2 \sigma_{\text{comp}}^{J\Pi}(\alpha) \tag{20}$$

Finally we obtain each $\sigma_{\text{comp}}(\alpha)$ from the optical-model absorption cross

section $\sigma_\alpha(\text{abs})$ for the pair α. In terms of the complex phase shifts $\delta_{\alpha l}$ of the optical model we have

$$\sigma_\alpha(\text{abs}) = \frac{\pi}{k_\alpha^2} \sum_l (2l+1)(1 - |e^{2i\delta_{\alpha l}}|^2)$$

$$\equiv \sum_{J\Pi} \frac{\pi}{k_\alpha^2} \frac{2J+1}{(2I+1)(2i+1)} \sum_{l=|J-s|}^{J+s} \sum_{s=|I-i|}^{I+i} (1 - |e^{2i\delta_{\alpha l}}|^2)$$

$$\equiv \sum_{J\Pi} \sigma_{\text{comp}}^{J\Pi}(\alpha) \tag{21}$$

Comparison of Eqs. (21), (20), (13) yields

$$G_\alpha^{J\Pi} = \sum_{sl} T_l(\alpha) \tag{22}$$

Use of Eqs. (22) and (21) in Eq. (18) yields the main result, Eq. (12), of our evaporation model. For each $J\Pi$ separately, the evaporation model of Eq. (12) has the same form as the old evaporation model (Section 1).

The evaporation model for average cross sections is based on a number of fashionable concepts which have only an indirect connection with nuclear theory. The use of optical-model transmission functions depends on the validity of the optical model for the description of absorption processes in nuclei; a justification of the optical model in terms of the nuclear properties of compound states is parallel to the justification of the evaporation model itself (Section 4). The general behavior of optical-model transmission functions is discussed in Section 2.3 and further properties are given in the examples, Section 3.

The factorization assumed in Eq. (18) is central to the evaporation model, but it will be shown to be justified only in special cases, e.g., when all the transmission functions are much smaller than unity. This circumstance applies to one of the examples discussed in Section 3, that of inelastic neutron scattering, but for another example the $C^{12} + C^{12}$ reactions, almost all of the transmission functions are very close to their maximum value of unity. Even in this case the evaporation model turns out to agree very well with the experiment. The magnitude of the transmission functions determines the leakage rate of the compound nucleus into the corresponding channel; a small transmission function means a small decay rate. Each of the transmission functions may be small, and still the compound nucleus may decay very rapidly because of the large number of decay alternatives [see the denominators of Eq. (16)]. The justification of the evaporation model by the resonance theory (Section 4) also yields some corrections to the model.

2.2 Extension of the Model to Differential Cross Sections

With a few additional approximations, the evaporation model can also be applied to average differential cross sections. The approximations which are made concern the noninterference of different incoming partial waves with each other and of outgoing partial waves with each other. To exhibit the approximations, we first sketch briefly the general connection between a differential cross section and the components of the collision matrix. The connection concerns the geometry of reaction measurements and does not concern the nuclear physics of the problem (which resides in the behavior of the collision matrix components themselves).

Any compound nucleus has a given number of reaction alternatives, such as those illustrated in Fig. 1. When all the nucleons of the system are close together, we have a compound nucleus; when any two groups of reaction products are separated from each other, we have a reaction channel. The whole system of the problem has a Schrödinger equation and a wave function in the region of space where we have a compound nucleus as well as where we have any of the reaction alternatives. The reaction cross sections and the collision matrix components are defined by the wave amplitudes in the reaction channels. The nuclear theory enters the problem when we try to connect the amplitudes by solving the wave equation in the whole space or by adopting phenomenological models for the collision matrix components.

Corresponding to our definition of a channel c, we define a channel wave function ψ_c, describing all of the properties of the channel except radial motion,

$$\psi_c = r_c^{-1}\Phi_\alpha \sum_{m_l} \sum_{m_s} (lsm_l m_s \mid Jm_J)\, i^l Y_{lm_l} X_{sm_s} \tag{23}$$

where r_c is the relative separation of the pair of particles in each channel; Φ_α is the state of internal motion of the two particles in the channel (e.g., for $\alpha = 2$ in Table I, Φ_α is the product of the Ne^{20} ground state and the He^4 ground state); $i^l Y_{lm_l}$ is a spherical harmonic describing their relative orbital angular momentum l and its z component m_l; X_{sm_s} is the wave function of the coupled intrinsic spins I and i of the two particles; $(lsm_l m_s \mid Jm_J)$ is a Clebsch–Gordan coefficient; and J is the total angular momentum of the system, and m_J, its z component.[19]

In the region of space outside of the compound nucleus where the channels exist, the whole wave function of the system can be written

$$\Psi = \sum_c \varphi_c \psi_c \tag{24}$$

where the φ_c are the radial wave functions in each channel. If we have only Coulomb and angular momentum barriers in the channel c the radial wave equation is

$$\frac{d^2\varphi_c}{dr_c^2} - \frac{l(l+1)}{r_c^2}\varphi_c - \frac{2\eta_c k_c}{r_c}\varphi_c + k_c^2\varphi_c = 0 \tag{25}$$

where $\eta_c(\equiv Z_1 Z_2 e^2/\hbar v_c)$ is the usual Coulomb parameter. The regular and irregular solutions of Eq. (25) are, respectively, F_c and G_c, which are tabulated[20] and normalized by their Wronskian

$$G_c \frac{dF_c}{dr_c} - F_c \frac{dG_c}{dr_c} = k_c \tag{26}$$

Alternatively we can define linear combinations of the F_c and G_c which are incoming waves I_c or outgoing waves O_c. These are[18]

$$I_c = O_c^* = (G_c - iF_c)\, e^{i\omega_c} \tag{27}$$

where ω_c is the Coulomb phase shift related to the orbital angular momentum quantum number l_c and the Coulomb parameter η_c by

$$\omega_c = \sum_{n=1}^{l_c} \tan^{-1}\frac{\eta_c}{n} \tag{28}$$

These incoming and outgoing waves have the following behavior at large distances:

$$I_c^* = O_c \approx \exp i(k_c r_c - \tfrac{1}{2} l_c \pi - \eta_c \ln 2k_c r_c) \tag{29}$$

In terms of the channel wave functions ψ_c and radial wave functions I_c and O_c, we are now ready to define the collision matrix used to describe a nuclear reaction. Since each φ_c of Eq. (27) can be written as a linear combination of incoming and outgoing waves, we have

$$\Psi = \sum_c v_c^{-1/2}(A_c I_c - B_c O_c)\,\psi_c \tag{30}$$

Here the A_c and B_c are amplitude coefficients, and the factor $v_c^{-1/2}$ is chosen so that $v_c^{-1/2} I_c$ (or $v_c^{-1/2} O_c$) correspond to unit incoming (or outgoing) flux. In a nuclear reaction we have incoming beams in some channels and outgoing beams in all channels for which the decay is allowed energetically. Whatever the incoming channels and their coefficients, the solution of the Schrödinger

equation everywhere (including the compound-nucleus region) would yield all the coefficients B_c of the outgoing waves. This fact is expressed by writing

$$B_c = \sum_{c'} U_{cc'} A_{c'} \tag{31}$$

where $U_{cc'}$ is the collision matrix. The collision matrix has many interesting properties[18] which follow either from general conservation theorems or from specific properties of the nucleus. Our aim here is at connecting the observed differential cross sections for nuclear reactions directly to the outgoing waves as parameterized by the collision matrix.

In a nuclear reaction we have an incident beam, or plane wave, of a given pair of particles α and an outgoing wave of some pair α' observed in a direction (θ, φ) relative to the incident beam. The total wave function can be written

$$\Psi = \Psi_{\text{inc}} + \Psi_{\text{reac}} \tag{32}$$

The incident plane wave is described by the wave function

$$\begin{aligned} \Psi_{\text{inc}} &\equiv \Phi_\alpha X_{sm_s} \exp(ik_\alpha z_\alpha) \\ &= \Phi_\alpha X_{sm_s} (4\pi)^{1/2} \sum_{l=0}^{\infty} (2l+1)^{1/2} j_l(k_\alpha r_\alpha)\, i^l Y_{l0}(\theta, \varphi) \end{aligned} \tag{33}$$

where the internal wave function Φ_α and the spin wave function, X_{sm_s} are those of Eq. (23). The expansion of the plane wave into spherical harmonics, as in the second step of Eq. (33), shows that a projectile beam implies a sum over relative orbital angular momenta. If the projectile and target are unpolarized, we shall also have a sum over the channel spin and its z component. Both types of sums mean that in any nuclear reaction we have nonzero coefficients A_c for a variety of l, s, and m_s. This fact introduces the quantum theory of angular momentum into the description of nuclear reactions. (If some ingenious experimentalist would complement present polarization methods with a tool to select individual orbital angular momenta, we might not need to teach nuclear physicists the quantum theory of angular momentum.)

To establish the coefficients A_c of the various incoming waves contained in the incident wave Ψ_{inc}, we compare Eq. (33) with the incoming and outgoing waves at distances so large that the Coulomb fields of the target and projectile are completely screened from each other. Then we have

$$j_l(k_\alpha r_\alpha) \simeq (k_\alpha r_\alpha)^{-1} F_l(k_\alpha r_\alpha) = (2k_\alpha r_\alpha)^{-1} i(I_l - O_l) \tag{34}$$

where F_l, I_l, and O_l are the radial wave functions defined in connection with Eq. (27). Using Eq. (34) in Eq. (33), we obtain

$$\Psi_{\text{inc}} = \Phi_\alpha \sum_{J=0}^{\infty} \sum_{m_J=-J}^{J} \sum_{l=|J-s|}^{J+s} ik_\alpha^{-1}\pi^{1/2}(ls0m_s \mid Jm_J)(2l+1)^{1/2} r_\alpha^{-1}$$

$$\times \sum_{m_l=-l}^{l} \sum_{m_s=-s}^{s} (lsm_lm_s \mid Jm_J)(I_l - O_l)\, Y_{l0}X_{sm_s} \qquad (35)$$

Since Ψ_{reac} contains only outgoing waves, the coefficients A_c of the total wave function are the coefficients of the incoming waves in Eq. (35)

$$A_c \equiv A_{\alpha sl}^{Jm_J} = ik_\alpha^{-1}(\pi v_\alpha)^{1/2}\,(ls0m_s \mid Jm_J)(2l+1)^{1/2} \qquad (36)$$

for the α, s, and m_s of the incident beam and $A_c = 0$ for all other channels. The amplitudes $B_{c'}$ of the outgoing waves are given by Eq. (31) to be

$$B_{c'} \equiv B_{\alpha' s' l'}^{Jm_J} = i(k_c)^{-1}(\pi v_c)^{1/2} \sum_{l=|J-s|}^{J+s} (ls0m_s \mid Jm_J)(2l+1)^{1/2}\, U_{\alpha sl;\alpha' s' l'}^{J} \qquad (37)$$

By means of Eqs. (37), (35), and (32), we can write Ψ_{reac} in the following way:

$$\Psi_{\text{reac}} = \sum_c \sum_{c'} (\delta_{cc'} - U_{cc'})\, A_{c'} O_{c'} \qquad (38)$$

The Kronecker delta function $\delta_{cc'}$ occurs in this expression because the incident plane wave contains outgoing waves as well as incoming waves.

The various possible cross sections are given by Ψ_{reac}. However Ψ_{reac} is not yet in a form suitable for the definition-of the cross sections observed in a laboratory. The channels c and c', as they have been defined, correspond to a definite J, m_J, and l as well as to α and s. The actual detectors in the laboratory are presumed to select a given pair particles, in a given state of excitation (possibly in a given state of polarization, $X_{s'm_{s'}}$, or alternatively with definite values of $m_{l'}$ and $m_{i'}$), and traveling in a direction θ, φ. We can write Ψ_{reac} to correspond with quantities that are observed, by changing Eq. (38) to

$$\Psi_{\text{reac}} \equiv i \sum_{\alpha', s', m_{s'}} k_\alpha^{-1}(v_\alpha/v_{\alpha'})^{1/2}\, r_{\alpha'}^{-1} e^{ik_{\alpha'}r_{\alpha'}}\, \Phi_{\alpha'} X_{s'm_{s'}} q_{\alpha' s' m_{s'};\alpha s m_s}(\theta, \varphi) \qquad (39)$$

where the amplitude $q_{\alpha' s' m_{s'};\alpha s m_s}$ is found by comparison with Eq. (38) to be

$$q_{\alpha' s' m_{s'};\alpha s m_s}(\theta, \varphi) = -\sum_{J=0}^{\infty} \sum_{m_J=-J}^{J} \sum_{l=|J-s|}^{J+s} \sum_{l'=|J-s'|}^{J+s'} \sum_{m_{l'}=-l'}^{l'}$$
$$\times \pi^{1/2}(2l+1)^{1/2} (ls0m_s \mid Jm_J)(l's'm_{l'}m_{s'} \mid Jm_J)$$
$$\times (\delta_{\alpha\alpha'}\delta_{ss'}\delta_{ll'} - U^J_{\alpha' s' l';\alpha s l})\, i^{l'} Y_{l' m_{s'}}(\theta, \varphi) \tag{39}$$

The sums over m_J and $m_{l'}$ are purely formal, since $m_J = m_s$ and $m_{l'} = m_J - m_{s'}$.

The differential cross section for the process $\alpha \to \alpha'$ can be expressed as follows:

$$\frac{d\sigma_{\alpha\alpha'}}{d\Omega} = k_\alpha^{-2} \sum_{m_s=-s}^{s} \sum_{m_{s'}=-s'}^{s'} \sum_{s=|I-i|}^{I+i} \sum_{s'=|I'-i'|}^{I'+i'} \frac{1}{(2I+1)(2i+1)} \mid q_{\alpha' s' m_{s'};\alpha s m_s}(\theta, \varphi)|^2 \tag{40}$$

which is the result we require. More commonly[21] this result is written in a form in which many of the sums over Clebsch–Gordan coefficients have been carried out and expressed in terms of tabulated recoupling coefficients. This form is

$$\frac{d\sigma_{\alpha\alpha'}}{d\Omega} = \frac{1}{k_\alpha^2} \sum_{L=0}^{\infty} B_L(\alpha, \alpha')\, P_L(\cos\theta) \tag{41}$$

with

$$B_L(\alpha, \alpha') = \sum_{m_s, m_{s'}, s, s', J_1, J_2, l_1, l_2, l_1', l_2'} \frac{(-)^{s-s'}}{4(2I+1)(2i+1)}$$
$$\times\, i^{l_1-l_2-L} Z(l_1 J_1 l_2 J_2; sL)\, i^{l_1'-l_2'-L} Z(l_1' J_1 l_2' J_2; sL)$$
$$\times\, \mathrm{RP}\, [(\delta_{\alpha\alpha'}\delta_{l_1 l_1'}\delta_{ss'} - U^{J_1}_{\alpha' s' l_1';\alpha s l_1})^* (\delta_{\alpha\alpha'}\delta_{ss'}\delta_{l_2 l_2'} - U^{J_2}_{\alpha' s' l_2';\alpha s l_2})] \tag{42}$$

Here RP stands for the real part of the bracket; the Z's are the Z coefficients defined by Biedenharn, Blatt, and Rose[22] and tabulated by many authors.[23] The phase correction due to Huby[24] corrects an error in the derivation given by Blatt and Biedenharn.[21]

The differential cross section given by Eq. (41) can be integrated over all angles to obtain the well-known result

$$\sigma_{\alpha\alpha'} = \frac{4\pi}{k_\alpha^2} B_0(\alpha, \alpha') = \frac{\pi}{k_\alpha^2} \sum_{s, s', J, l, l'} g_J \mid \delta_{\alpha\alpha'}\delta_{ss'}\delta_{ll'} - U^J_{\alpha' s' l';\alpha s l} \mid^2 \tag{43}$$

which no longer contains the Z coefficients.

In Eq. (43) g_J is a statistical spin factor

$$g_J \equiv \frac{(2J+1)}{(2I+1)(2i+1)} \tag{44}$$

The above results for differential and integrated cross sections are completely general. We have derived them to exhibit the coherence of partial waves and the consequent assumptions which must be made in the evaporation theory.

A general statement about the behavior of the collision matrix components for compound-nucleus processes serves to extend the model. As discussed in Section 4, the collision matrix components are complex numbers which vary rapidly with energy. Both the real and imaginary parts assume positive and negative values with a mean value of zero. In addition there is assumed to be no correlation between the variation with energy of different components of the collision matrix. Consequently, when we average the cross section over an energy interval in which the components have each varied a great deal, we can ignore all cross terms between various components.

The random phase of the collision matrix components together with the previous basic assumptions of the model (factorization of the cross section, conservation of total angular momentum and parity, reciprocity of cross sections, and use the optical model for compound-nucleus-formation cross sections) completes the evaporation model. According to the previous basic assumptions, each absolute square of collision matrix components takes the form

$$\overline{|\, U^J_{\alpha' s' l';\alpha s l} \,|^2} = \frac{T_l(\alpha)\, T_{l'}(\alpha')}{\sum_{\alpha'' l'' s''} T_{l''}(\alpha'')} \tag{45}$$

in which we have the optical-model transmission functions (13). If we take $\bar{\sigma}_{\alpha\alpha'}$ from Eq. (43) by ignoring the cross terms and use Eq. (45) for the energy averages of squares of collision matrix components we obtain the evaporation model, Eq. (12). The same procedure applied to the differential cross section yields

$$\frac{d\bar{\sigma}_{\alpha\alpha'}}{d\Omega} = \sum_L \frac{1}{4k_\alpha^2} \sum_{J\Pi} \frac{1}{(2I+1)(2i+1)} \left\{\sum_{sl} T_l(\alpha)\right\}$$
$$\times \sum_{s'l'} \left\{\frac{T_{l'}(\alpha')}{\sum_{s''l''\alpha''} T_{l''}(\alpha'')}\right\} Z(lJlJ;\, sL)\, Z(l'Jl'J;\, s'L)(-)^{s-s'} P_L(\cos\theta) \tag{46}$$

In obtaining Eq. (46), we have ignored all interference incoming partial waves with each other and of outgoing partial waves with each other. This lack of interference is attributed to the random phase of the components of the collision matrix. The lack of interference has a direct consequence on

the shape of the average angular distributions: They are not, in general, isotropic, but they are symmetric about 90°. This property of Eq. (46) is manifested through the coefficients $Z(lJlJ; sL)$, which vanish unless L is even. Under more restrictive conditions, which are not of physical interest, the average cross sections are also isotropic.[16,18] A number of illustrations of angular distributions predicted by the evaporation model are shown in Section 3.2.

The coherence or noncoherence of various partial waves is a property of the particular kind of cross section. For example, integration of the differential cross section over all angles removes the interference of orbital angular momentum waves. Similarly the result (40) has noncoherence of various channel spins because we have averaged over polarizations. If we have polarized incoming and outgoing particles, then the whole differential cross section would be a single absolute square; the sum over s and s' would go into the amplitude in Eq. (40).

The coherence of cross sections is of great importance in the theory of cross-section fluctuations.[25] The cross-section fluctuations concern the variation of the cross section about the average values which are the concern of the statistical theory. The variations arise from the same random-phase behavior of the collision matrix components which we employed in deriving the average cross sections. Since any sum of random elements is itself random, the magnitude of the fluctuations is determined principally by the number of incoherent cross-section contributions; the fluctuations are largest when the cross section is a single absolute square. For differential cross sections of unpolarized particles we therefore wish to know the mean value of the individual terms of Eq. (40). This can be obtained by the same methods as the differential cross section itself, and the result is

$$\frac{d\bar{\sigma}_{\alpha\alpha'}}{d\Omega} = \frac{1}{4k_\alpha^{\,2}(2I+1)(2i+1)} \sum_{s,s',m_s,m_{s'}} \times \left[\begin{array}{r} \sum_{J,l,l',L} (2l+1)(2l'+1)(lsm_lm_s \mid Jm_J)^2\,(l's'm_{l'}m_{s'} \mid Jm_J)^2 \\ (ll'00 \mid L0)(ll'm_l - m_{l'} \mid L0)\, P_L(\cos\theta) \dfrac{T_l(\alpha)\, T_{l'}(\alpha')}{\sum_{\alpha''l''s''} T_{l''}(\alpha'')} \end{array} \right] \tag{47}$$

An example is given in Section 3.2. The result (47) is identical to Eq. (46) except that Eq. (47) exhibits explicitly the separate contributions of the coherent cross sections for each s, m_s, s', $m_{s'}$.

2.3 Behavior of Transmission Functions

Nuclear transmission functions exhibit quantum wave properties analogous to the behavior of waves in classical optics. In the nuclear optical

model the interaction between a particle and a nucleus is made up of the three parts shown in Fig. 4:

1. The *Coulomb interaction* behaving at large separation distances like $Z_1Z_2e^2/r$, where Z_1e and Z_2e are the charges of the particle and target nucleus,

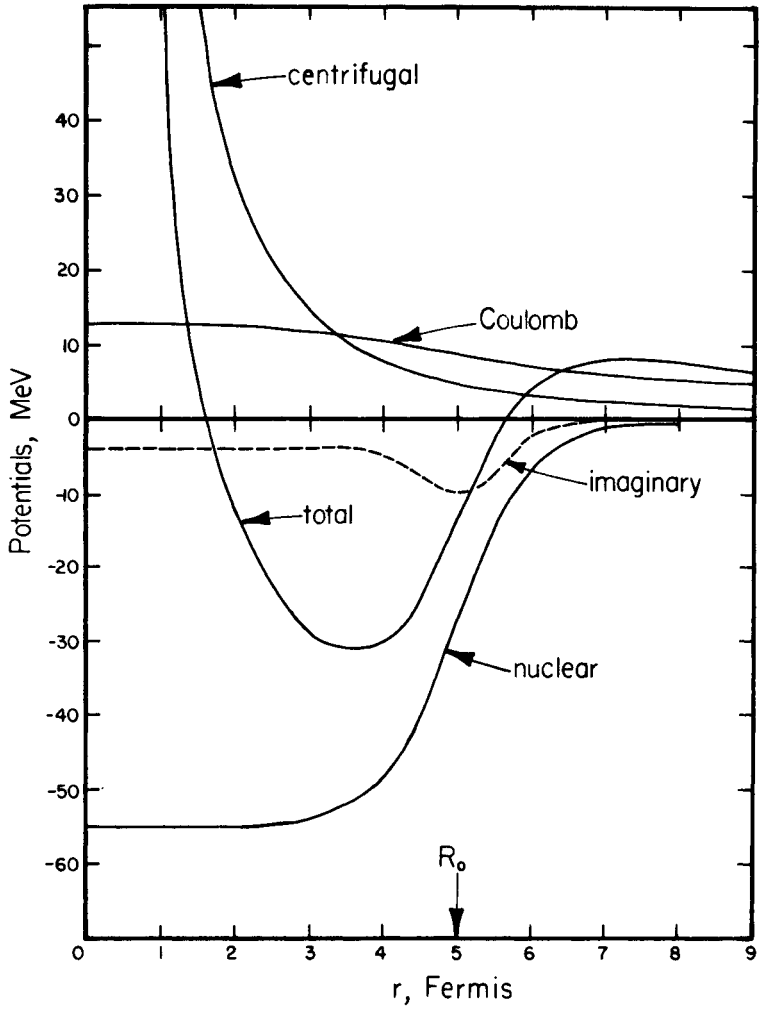

Fig. 4. The potentials which determine nuclear transmission functions. The choice of radius and charge are appropriate for protons and Cu^{64}. The surface thickness is $a = 0.5$ fm. The centrifugal potential is that for protons of $l = 2$. The potential marked *total* is the sum of the nuclear, Coulomb, and centrifugal potentials.

respectively; within the nucleus the finite size of the nuclear charge distribution reduces the Coulomb potential below the point-charge value

2. The *centrifugal potential* $l(l+1)\hbar^2/mr^2$, where m is the reduced mass of the pair and l their relative orbital angular momentum,

3. The *nuclear potential*, described below, which is roughly constant in the nuclear interior and falls to zero in the vicinity of the nuclear radius.

The nuclear potential is complex; its real part leads to wave refraction and its imaginary part to wave absorption. The sum of the three potentials has, as shown in Fig. 4, a real part which is strongly attractive in the nuclear interior and then repulsive in the barrier region beyond the nuclear radius. The imaginary part of the total potential is nuclear in origin and concentrated in the nuclear interior and in particular in the vicinity of the nuclear radius. The wave properties of the nuclear transmission functions are found by solving the Schrödinger equation, with such a potential, for the optical-model phase shifts.

The principal wave properties of the nuclear transmission functions are:

1. *Penetration* through the Coulomb and angular momentum region beyond the nuclear radius.
2. *Reflection* at the abrupt nuclear "surface" in the vicinity of the nuclear radius.
3. *Resonance* within the nuclear potential, dampened by the absorption which takes place in the nuclear interior.

The resonance effects, referred to as *giant resonances* or *size resonances* and exhibited below, are like those occurring in the excitation of a cavity by electromagnetic waves. The treatment of all three of these effects in the calculation of nuclear transmission functions is simplified by the abruptness of the nuclear surface—the rapidity with which the total potential falls from its value in the barrier to its value in the interior. As a consequence of this abruptness we shall show [e.g., Eq. (73) below] that the transmission functions can very nearly be written as a product of three factors, one referring to penetration, one to reflection, and one to resonance. The justification of this approximation will help to clarify the role of the nuclear optical potential in the theory of average cross sections.

The nuclear part, V_N, of the total can be written in the following way:

$$V_N(r) = (-V_0 - c_0E - iW_0)(1 + e^{(r-R)/a})^{-1} - i(W_g + c_1E)\, e^{-(R-r)^2/b^2} + V_{\text{spin-orbit}} \tag{48}$$

Here E is the relative kinetic energy of the interacting pair in MeV and V_0, c_0, W_0, R, a, W_g, c_1, and b are constants about which much is known

from the fits of the optical model to elastic-scattering data.[26,30] The shape of the nuclear potential as given by Eq. (18) is not the only shape that V_n might take, but it contains most of the effects of importance for the calculation of average cross sections. Values of the constants suitable for the calculation of transmission functions are given in Table II. The radius R of the potential is taken to be $r_0A^{1/3}$, where A is the mass number of the target nucleus.

TABLE II

Optical-Model Parameters for Compound-Nucleus Calculations[a]

Particle		V_0, MeV	W_0, MeV	W_g, MeV	r_0, 10^{-13} cm	a, 10^{-13} cm	b, 10^{-13} cm	c_0	c_1
Neutrons		51	3–5		1.25	0.5		−0.5	
	or	51		4–8	1.25	0.5	1.0	−0.5	0–0.5
Protons		55	3–5		1.25	0.5		−0.5	
	or	55		4–8	1.25	0.5	1.0	−0.5	0–0.5
D,		50–75	10		1.3	0.5			
He^3, T,	or	75–150	10		1.25	0.5			
other heavy ions									

[a] The various parameters are those of Eq. (48) and their application to evaporation calculations is discussed in the text. Although these optical-model parameters are usually good enough for evaporation calculations, they may only give rough results for other purposes.

The suitability of the tabulated optical-model parameters for the calculation of average cross sections is based in part on their effect on transmission functions, as discussed below, and in part on the physics underlying the optical parameters. For example, the real part of the optical potential is also the average potential for shell model orbitals; the position of shell model orbitals determines the value of V_0R^2 for neutrons and protons to within a percent or two. The product V_0R^2 may be regarded as the size of the well and V_0 and R can each vary by much more than a few percent if V_0R^2 is kept fixed. Similarly the measured mean absorption for many nuclei determines a rough value of the integral over the radial coordinate r, of the product of r and the imaginary part of the optical potential.[32] The second term on the right side of Eq. (48) is a Gaussian absorption term centered on the nuclear surface, whereas the term proportional to W_0 is a "volume absorption" distributed through the whole nucleus. The absorption in the nuclear interior is inhibited by the Pauli principle; the surface absorption is

based on the diminution of this effect in regions of lower density. There is usually no need to use more than one parameter to represent the absorption; either the term with W_0 or with W_g will do, although the use of the latter for neutrons and protons is perhaps more sound. The terms c_0E and c_1E roughly account for the known energy dependence of the optical potentials. The spin–orbit potential is concentrated on the nuclear surface (like all spin–orbit terms of the Thomas type). Its value is known from application of the nuclear shell model and the optical model to data. As discussed below, the effect of the spin–orbit term on average cross-section calculations is usually small. The language we employ, in which transmission functions are taken to be independent of channel spin (apart from the required conservation of total angular momentum), is valid only in the absence of a spin–orbit potential. The changes in transmission functions when a spin–orbit term is employed were given by Eq. (15) above.

The abruptness of the nuclear surface, on which our discussion of transmission functions is based, is manifested by the small value of the surface-thickness parameter a compared with the nuclear radius $r_0A^{1/3}$; $2a$ is approximately the distance in which the optical potential falls from three-quarters of its central value to one-quarter. The region $R - a < r < R + a$ is referred to as the nuclear surface and has a thickness of about 1 fm.

The optical model parameters of Table II are largely those which fit elastic-scattering data. There is almost no information on the optical model appropriate for calculating the transmission functions of excited states. There is no reason to believe that the optical potential should be very different for excited states. Perhaps W_0 should be slightly larger because the Pauli principle does not inhibit the two-nucleon forces so strongly when some of the target nucleons are excited. For all the calculations discussed below such differences have been ignored and the same potential has been used for all states.

The transmission functions are directly defined in terms of the absorption of each partial wave. The absorption, in turn, can be related to the elastic scattering in the same channel; e.g., the complex phase shifts of the optical model give both the scattering and absorption cross sections. However, the relation between the two goes much beyond the validity of a one-particle model such as the optical model. The following general statement of nuclear transmission functions in terms of the diagonal components of the collision matrix will aid us later in introducing potential well properties into the transmission functions.

The reaction cross section of a projectile by a target nucleus is the sum over all reaction cross sections with the exception of elastic scattering,

$$\sigma_{\text{reac}}(\alpha) \equiv \sum_{\alpha'}{}' \sigma_{\alpha\alpha'} = \frac{\pi}{k_\alpha^2} \sum_{\alpha'}{}' \sum_{Jsls'l'} g_J \mid U^J_{\alpha's'l';\alpha sl} \mid^2 \tag{49}$$

where the prime on the summation sign indicates that the incident pair α is omitted from the sum. The result, Eq. (49), follows from Eq. (43) above. From the conservation of flux and the invariance of the collision process under time reversal, the collision matrix is unitary and symmetric,[18]

$$\sum_{\alpha' s' l} (U^J_{\alpha' s' l';\alpha s l})(U^J_{\alpha' s' l';\alpha s l})^* = 1 \tag{50}$$

Using Eq. (50) in Eq. (49), we have a simple result for the reaction cross section, which follows directly from the general conservation properties.

$$\sigma_{\text{reac}}(\alpha) = \frac{\pi}{k_\alpha^2} \sum_{Jsl} g_J \{1 - | U^J_{\alpha s l;\alpha s l} |^2\} \tag{51}$$

More directly, the elastic-scattering cross section $\sigma_{el}(\alpha)$ of the same channel can be written

$$\sigma_{\text{el}}(\alpha) = \frac{\pi}{k_\alpha^2} \sum_{Jsl} g_J | 1 - U^J_{\alpha s l,\alpha s l} |^2 \tag{52}$$

Thus, at each energy one complex number—the diagonal component of the collision matrix—gives both the reactions and the scattering of each partial wave. In the optical model we also have a single complex number, the phase shift, which gives both the absorption and the scattering.

The general relation of transmission coefficients to the diagonal components of the collision matrix follows from taking energy averages of Eqs. (51) and (52) over any narrowly spaced compound nucleus resonances which would cause both $\sigma_{\text{reac}}(\alpha)$ and $\sigma_{\text{el}}(\alpha)$ to vary rapidly with energy. Indicating such energy averages by bars, we have

$$\overline{\sigma_{\text{reac}}}(\alpha) = \frac{\pi}{k_\alpha^2} \sum_{Jsl} g_J \{1 - \overline{| U^J_{\alpha s l;\alpha s l} |^2}\} \tag{53}$$

$$\overline{\sigma_{\text{el}}}(\alpha) = \frac{\pi}{k_\alpha^2} \sum_{Jsl} g_J \{| 1 - \overline{U^J_{\alpha s l;\alpha s l}} |^2 + \overline{| U^J_{\alpha s l;\alpha s l} |^2} - | \overline{U^J_{\alpha s l;\alpha s l}} |^2\} \tag{54}$$

The last two terms in Eq. (54) can be identified[31] as the part of the elastic-scattering cross sections proceeding through the compound nucleus. Combining this part with the mean reaction cross section, we obtain an average-absorption cross section

$$\overline{\sigma_{\text{abs}}}(\alpha) = \frac{\pi}{k_\alpha^2} \sum_{Jsl} g_J \{1 - | \overline{U^J_{\alpha s l;\alpha s l}} |^2\} \tag{55}$$

The remainder of the elastic-scattering cross section is referred to as the *shape elastic scattering* and it also depends only on $\overline{U^J_{\alpha sl;\alpha sl}}$

$$\overline{\sigma_{\text{shape el}}}(\alpha) = \frac{\pi}{k_\alpha^2} \sum_{Jsl} g_J \,|\, 1 - \overline{U^J_{\alpha sl;\alpha sl}} \,|^2 \tag{56}$$

The general result for the transmission functions follows from Eq. (55)

$$T_{slJ}(\alpha) = 1 - |\, \overline{U^J_{\alpha sl;\alpha sl}} \,|^2 \tag{57}$$

The optical-model cross sections and transmission functions are a special case of these results. The special case is obtained by replacing each $\overline{U^J_{\alpha sl;\alpha sl}}$ in Eqs. (55), (56), and (57) with the phase factor $\exp(2i\delta_{\alpha l})$ of a complex potential well.

The general results for cross sections or transmission functions or phase shift or collision matrix components all refer to the complex amplitudes of the outgoing waves in a nuclear reaction for separation distances of the reaction products larger than those at which any nuclear interaction takes place. The description of the quantum wave properties—penetration, reflection, and resonance—require that we extend the channel wave functions into the region of the nucleus. This can be done, e. g., if the nuclear interaction is taken to be a complex potential well, as in the optical model.

The conventional concept of barrier penetration, which we shall adopt, arises from a simple but extreme picture of a nuclear reaction. In this picture a compound nucleus is formed in two steps: (a) the incident pair of particles penetrate through their Coulomb and angular momentum barriers to the nuclear radius; (b) the compound nucleus is then formed at the nuclear radius. The picture is not necessarily tied to any potential model, such as the optical model, in describing the formation of the compound nucleus. It does, however, require the nuclear interaction to vanish beyond the nuclear radius. This latter unacceptable feature of the picture can be made unobjectionable (see below) by introducing the property of wave reflection.

In the two-step picture of nuclear absorption we can replace the average collision matrix component $\overline{U^J_{\alpha sl;\alpha sl}}$ with a complex number related directly to the nucleus. The channel wave function $\varphi_{\alpha slJ}$ appropriate for the discussion of average cross sections may be written

$$\varphi_{\alpha slJ} \equiv v_\alpha^{-1/2} A_{\alpha l}(I_l - \overline{U^J_{\alpha sl;\alpha sl}}\, O_l)\, \psi_{\alpha slJ} \tag{58}$$

where the incoming and outgoing waves, I_l and O_l, and the channel function $\psi_{\alpha slJ}$ are the same as in Eq. (30) above. Since the nuclear interaction is now assumed to vanish beyond the nuclear radius R_α, the channel wave function

is valid for separation distances down to R_α. We can therefore introduce a complex number, related to the nucleus at R_α, which we can use in place of $\overline{U^J_{\alpha sl:\alpha sl}}$. We define

$$f_{\alpha slJ} \equiv f^{Re}_{\alpha slJ} + i f^{Im}_{\alpha slJ} \equiv \left[\frac{r\, d\varphi_{\alpha slJ}/dr}{\varphi_{\alpha slJ}} \bigg|_{r=R_\alpha} - b_{\alpha l} \right]^{-1} \tag{59}$$

where $b_{\alpha l}$ is a real number to be chosen later (see below) in order to make $f^{Re}_{\alpha slJ}$ and $f^{Im}_{\alpha slJ}$ directly connected with the size-resonance properties of complex potentials. [The complex number $f_{\alpha slJ}$ is an R function in the R-matrix theory of nuclear reactions.[18,19]] Because $f_{\alpha slJ}$ is defined at the nuclear surface, it can easily be written in terms of the properties of nuclear potentials. For the moment we do not tie it down to any such realization.

Combining Eqs. (57), (58), and (59), we obtain an expression for the transmission function in terms of the complex number $f_{\alpha slJ}$

$$T_{slJ}(\alpha) = \frac{4P_l f^{Im}_{\alpha slJ}}{[(1 - S_l f^{Re}_{\alpha slJ} + P_l f^{Im}_{\alpha slJ})^2 + (P_l f^{Re}_{\alpha slJ} + S_l f^{Im}_{\alpha slJ})^2]} \tag{60}$$

Here P_l is the usual penetration factor used in nuclear reaction studies[18,19]

$$P_l \equiv \frac{kR_\alpha}{F_l^2(kR_\alpha) + G_l^2(kR_\alpha)} \tag{61}$$

and S_l is the usual *shift function* of nuclear reaction theory,

$$S_l \equiv -b_{\alpha l} + \left\{ \frac{rF_l\, dF_l/dr + rG_l\, dG_l/dr}{F_l^2 + G_l^2} \right\} \bigg|_{r=R_\alpha} \tag{62}$$

The F_l and G_l are, respectively, the regular and irregular Coulomb functions defined by Eq. (26).

The nuclear transmission function (60) is directly proportional to a conventional penetration factor. By suitable choice of the quantity $f_{\alpha slJ}$ we can bring other nuclear properties, including those of complex potentials, into the transmission functions. We illustrate the use of Eq. (60) first with the *black nucleus model* and secondly with complex potentials.

The black nucleus model is one of the oldest employed in nuclear reactions and has influenced much of the thinking about nuclear reactions. It was used in all the early calculations of average cross sections. For the black nucleus we assume that the nuclear interaction vanishes beyond the nuclear radius and that at $r = R_\alpha$ we have only incoming waves

$$\varphi_{\alpha slJ} \propto e^{-iKr} \qquad r \leqslant R_\alpha \tag{63}$$

where K is a wave number appropriate to the nuclear interior. If, e.g., we choose $b_{\alpha l} = 0$, we then obtain

$$f_{\alpha slJ} = \frac{i}{KR_\alpha} \tag{64}$$

and

$$T_{lsJ}(\alpha) = \frac{(4P_l/KR_\alpha)}{(1 + P_l/KR_\alpha)^2 + (S_l/KR_\alpha)^2} = \frac{4k/K}{(1 + k/K)^2} \qquad \text{for } s\text{-wave neutrons} \tag{65}$$

At low energies ($k < K$) all the transmission functions (even those for $l = 0$ neutrons) are very small because of wave reflection or penetration. At higher energies ($P \to kR_\alpha$, $k \to K$) the black-nucleus transmission functions approach their maximum value of unity.

The absorption of the black nucleus model may be compared to a wave guide problem[29] in classical electromagnetic theory. The incoming partial waves approach the nucleus, which is treated like a resonating cavity. The cavity is tuned so that waves propagate inward at the cavity entrance R_α with the given wave propagation number K. [This is not the tuning for optimum absorption. We can improve on it by choosing a nonzero value of $b_{\alpha l}$ whose value makes S_l vanish, while retaining Eq. (64) but not Eq. (63).] The tuning is not easily duplicated by a potential well model. Just as it is difficult to build resonating cavities which are tuned in a certain way for all wavelengths, it is impossible to make optical-model potentials for which the black-nucleus conditions apply at all energies. The optical-model transmission functions oscillate about the value of the black-nucleus transmission functions with the maxima corresponding to size resonances. Moreover the optical-model transmission functions are usually also larger on the average, because the sudden change in wave number at R_α, in the black nucleus model, implies too much wave reflection with a resultant loss in absorption.

The positions and widths of the nuclear size resonances depend on many of the properties of the optical-model potential. We describe their behavior for neutrons absorbed in a complex square well. The size resonances for other particles and other wells can be given in terms of the results for this example.

The absorption of neutrons by a complex square well (of radius R_0 and depth $-V_0 - iW_0$) is derived in Appendix A. For each partial wave l it is found that the value of $f_{\alpha slJ}$ (or f_l, dropping the subscripts α, s, and J) corresponding to a choice of $b_{\alpha l} = -l$ is

$$f_l = \sum_p \frac{\gamma_{lp}^2}{E_{lp} - E - iW_0} \tag{66}$$

with

$$\gamma_{lp}^2 = \frac{\hbar^2}{mR_0^2} \tag{67}$$

Here E_{lp} are *resonance energies* for each partial wave, and the numerators γ_{lp}^2 are often referred to as *single-particle reduced widths of the well* for reasons which will be evident below. The choice of $b_{\alpha l} = -l$ makes all the reduced widths have the same value $\hbar^2/mR_0^2$ and leads to the identification of the E_{lp} with the energies of the size resonances; at low energies the shift functions, Eq. (62), all vanish identically with this choice of $b_{\alpha l}$. From Eq. (66) we obtain

$$f_l^{Im} \equiv \pi s_l = \sum_p \frac{\gamma_{lp}^2 W_0}{(E_{lp} - E)^2 + W_0^2} \tag{68}$$

$$\begin{aligned} f_l^{Re} &= \sum_p \frac{(E_{lp} - E)\gamma_{lp}^2}{(E_{lp} - E)^2 + W_0^2} \\ &= P \int_{-\infty}^{\infty} \frac{s_l(E')\, dE'}{E' - E} \end{aligned} \tag{69}$$

where P stands for the principal value of the improper integral. The quantity s_l, proportional to f_l^{Im}, is usually referred to as the *neutron strength function*, a name derived from its identification with neutron level-widths and spacings (Section 4). The strength function s_l has "resonances" whenever $E \approx E_{lp}$. If we retain only one resonance, $p = p_0$, in the sums of f_l^{Im} and f_l^{Re}, we get the the following one-resonance approximation to the transmission function

$$T_l \approx \frac{2\Gamma_{lp_0} W_0}{(E_{lp_0} - E - S_l\gamma_{lp_0}^2)^2 + \frac{1}{4}(\Gamma_{lp_0} + 2W_0)^2} \tag{70}$$

where

$$\Gamma_{lp_0} \equiv 2P_l\gamma_{lp_0}^2 \tag{71}$$

is the "natural width" of the line which would obtain in a purely real potential. The result, Eq. (70), clearly exhibits the size resonances which occur in neutron transmission functions whenever the energy is near one of the single-particle energies E_{lp}. The level shift $S_l\gamma_{lp}^2$ vanishes in the zero energy limit for our choice of $b_{\alpha l}$.

The size resonances of strength functions or transmission functions are not necessarily exhibited as resonances in elastic-scattering data. As McVoy[27] and others have shown, the maximums and minimums of elastic-scattering data are, to a great extent, determined by the real potential-scattering phase shifts, and they behave like the Ramsauer effect of atomic physics. However, at low energies (see Figs. 6 and 7 below) the nucleon-absorption cross section can clearly exhibit the size resonances. Because of the rapid energy increase of the level density, the average cross sections of

the statistical theory are determined primarily by low-energy transmission functions. The average cross sections are often dominated by the straightforward size resonances of the absorption data.

The neutron size resonances undergo only minor modifications if we change the square well to a realistic optical potential such as Eq. (48). The positions E_{lp} of the size resonances at low energy are determined by the real part, $V(r)$, of the optical potential—more precisely, by the integral of $rV(r)$, over the region where the real potential (including the centrifugal potential) is attractive. The real potential with the parameters of Table II has size resonances very close to those of a square well with the same depth and radius. Figure 5 illustrates the positions of neutron giant resonances. The even partial waves resonate together, and the odd partial waves resonate together roughly halfway in between the even partial waves.

The width of the neutron size resonances [see Eq. (70)] are equal to $\Gamma_{lp} + 2W_0$. The natural width of the square well, Γ_{lp}, is usually less than 1 or 2 MeV (and much less when the penetration factor is much smaller than unity), while $2W_0$ is usually more than 6 MeV. Therefore the absorption determines the width. For $\Gamma_{lp} < 2W_0$ the transmission function has the same

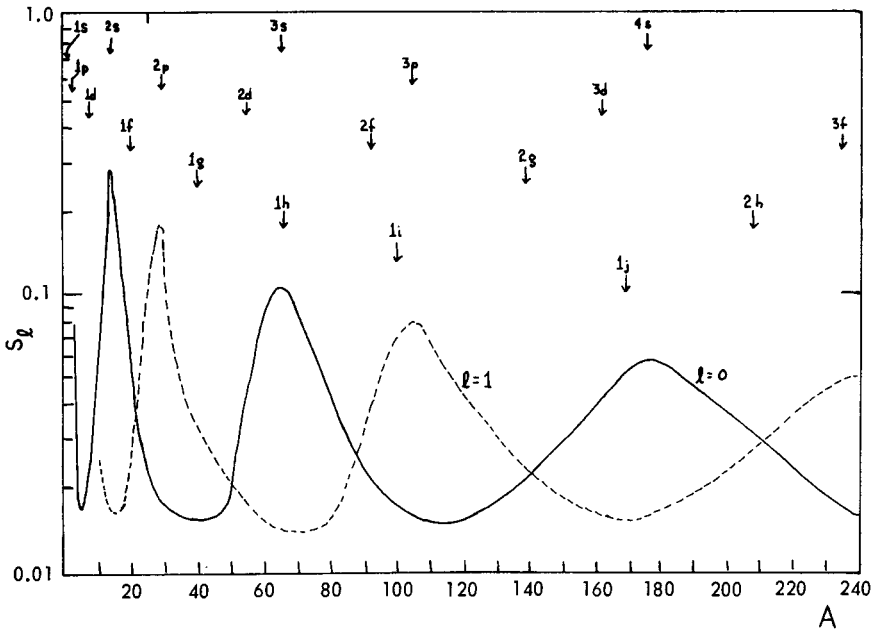

Fig. 5. The neutron strength function at zero energy as a function of the mass number A for a square well of depth -51 MeV. The s-wave and p-wave strength functions are shown, and the positions of the giant resonance of other partial waves are indicated.

shape as the strength function. If the imaginary part of the potential is given a realistic shape as in Eq. (48), the form of the strength function remains that of the square well; in place of W_0 we must use the integral of $W(r)$ over the region where the real part of the potential is attractive.[32]

Although the shape of the optical potential has no major effect on either the position of the size resonances or their width, the magnitude of the transmission function is increased if we change the square edge of the real part of the potential to a realistic nuclear surface of finite thickness. The increase is due to diminished reflection. It is accomodated by a reflection factor[28] that multiplies the penetrability whenever it occurs in either the exact transmission function, Eq. (60), or its approximate form, Eq. (70). However, the strength function or f_l^{Im} and f_l^{Re} retain their square-well values, Eqs. (68) and (69). The value of the reflection-factor f is given by[28]

$$f = \pi K_0 \alpha \coth \pi K_0 \alpha \tag{72}$$

where a is the surface thickness and K_0 the wave number corresponding to the well depth V_0. The reflection factor has a magnitude of about 2.6 for the neutron potentials of Table II and varies roughly quadratically with a. Therefore the size resonance of a realistic optical potential ($a = 0.5$) for neutrons should have the square-well widths Γ_{lp} in Eq. (70) multiplied by 2.6. Even the black-nucleus results, Eq. (65), suffer from too much reflection and too little absorption caused by the abrupt "switching-on" of the black-nucleus condition at the nuclear radius. In fact the black-nucleus transmission functions can be obtained from the square-well transmission functions by averaging out all of the size-resonance structure in the latter: the transmission functions, Eq. (70), oscillate about those of Eq. (65) when the two models have the same wave number.

The size resonances for protons have many properties similar to those for neutrons because the optical potentials are roughly the same for both neutrons and protons and the size resonances are a property of the potential wells, not of the barriers. The proton size resonances occur at somewhat different energies than those for neutrons because of the mean Coulomb energy of the protons. This effect is partly compensated for by a deeper nuclear potential for protons (see Table II). Typical proton size resonances are shown on Fig. 6 and may be compared with the neutron size resonances of Fig. 5. For protons, also, the width of the resonances is determined by the imaginary part of the potential and the reflection factor, Eq. (72), has the same value as for neutrons. The principal difference between the transmission functions of protons and neutrons is caused by the Coulomb barrier; proton penetrabilities, given by Eq. (61), are much smaller than those of neutrons when the energy is much below the barrier. This reduction is mirrored in a corresponding reduction of the transmission functions.

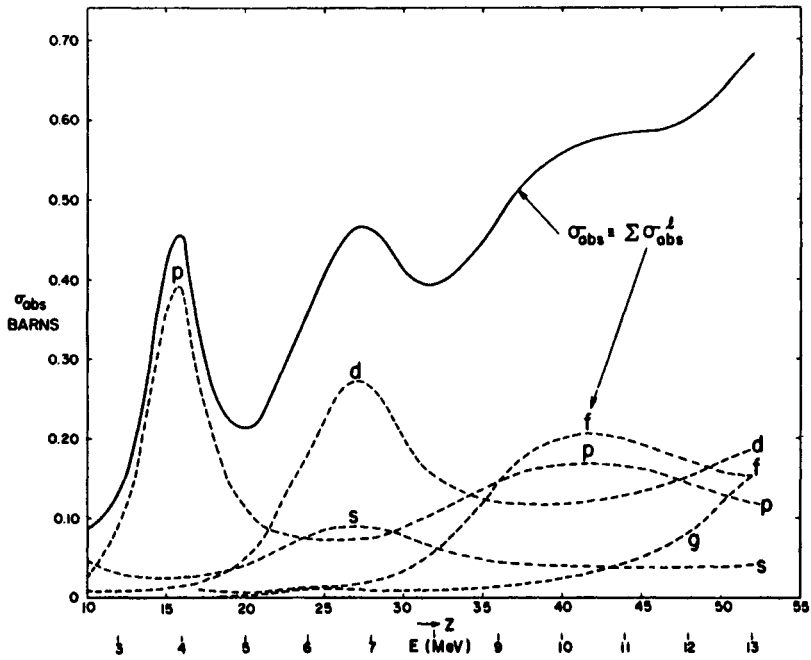

Fig. 6. The proton-absorption cross section at the top of the Coulomb barrier (i.e., $E_p = 0.25Z$ MeV) as a function of the atomic number Z of the target nucleus, calculated by using the Saxon–Woods potential [Eq. (48)] with $V_0 = -55$ MeV, $R = 1.25A$ fm, $W_0 = -5$ MeV, $a = 0.4$ fm. The contributions from various partial waves to the total absorption cross section are shown by dashed lines. They clearly exhibit the proton size resonances.

The nucleon size resonances are a striking manifestation of the same independent particle motion which underlies the shell model. The real part of the optical potential of nucleons should be equal to the average potential of the shell model. The positions of the giant resonances helps to determine the size of the shell-model potential. The width $2W$ of the size resonances compared with their spacing gives a measure of how long the independent particle motion persists. The spacing of the nucleon size resonances can be roughly estimated from the square-well potential applied to neutrons. If the real part of the potential has a depth $V_0(=\hbar^2K_0^2/2m)$ and a radius R_0, then the spacing of such resonances for s waves at zero energy (see Appendix A) is $(\hbar^2/mR_0^2)(\pi K_0R_0)$, which has a value of $170A^{-1/3}$ MeV for $V_0 = -51$ MeV and $R_0 = 1.25A^{1/3}$. For most nuclei the size resonances are therefore spaced 30 to 50 MeV apart. For nucleons the value of $2W_0$ is usually less than 10 MeV so that the size resonances do not overlap. Typically, the peak-to-

valley ratio of the transmission functions at low energy is about one hundred. The size resonances are manifested clearly in low-energy absorption and scattering. The transmission functions can never exceed unity; when the penetration factors get large, then the transmission function will be close to unity even if the strength function varies greatly. For nucleons the size resonance effects are of importance whenever the energy of the nucleons is below the angular momentum and Coulomb barriers of the partial wave being considered. When the transmission functions are much smaller than unity, we can approximate them by

$$T_l \approx 4\pi P_l s_l f \tag{73}$$

where P_l is the usual square-well penetration factor Eq. (61); s_l is the trength function, Eq. (68); and f is the reflection factor, Eq. (72). The factor f is nearly energy independent. The function s_l varies with energy only slowly; e.g., near resonance, s_l varies greatly in an energy interval W_0. However, P_l can vary strongly with energy.

Figure 7 shows data for the s-wave neutron size resonance observed in the bombardment of many heavy nuclei with zero-energy neutrons. The giant resonance is split or broadened by the nonspherical shape of the nuclei in the rare earth region.[33,34] For most problems involving average cross sections, this broadening of the size resonances is unimportant. Figure 7 also illustrates clearly the dependence of the strength function on the reflection factor and the variation of the reflection factor with the surface thickness.

For deuterons, tritons, H^3 nuclei, alpha particles, or heavier projectiles the size-resonance structure is absent because these particles are more strongly absorbed. The size resonances would be closer together for these particles because of their increased mass; the spacing is smaller than $2W_0$ so that any size resonances overlap strongly. The optical model yields this kind of absorption if we choose W_0 to be in the neighborhood of 10 MeV. When the resonance structure is washed out, the transmission functions are no longer greatly sensitive to the depth of the optical potential. The transmission functions are very nearly those of black nucleus *multiplied* by the appropriate reflection factor, Eq. (65), and increased to include the effect that the real part of the optical potential has in rounding off the Coulomb barriers. The scattering data for such projectiles, when fitted by optical potentials, yield information about the rounding-off and reflection-of the potential; like the transmission functions, the scattering data are not sensitive to any other feature of the optical potential. Since the validity of an optical model for such projectiles is greatly in question, it is fortunate that the use of optical models for their transmission functions merely gives a realistic treatment of the absorption of these particles in the nulear surface.

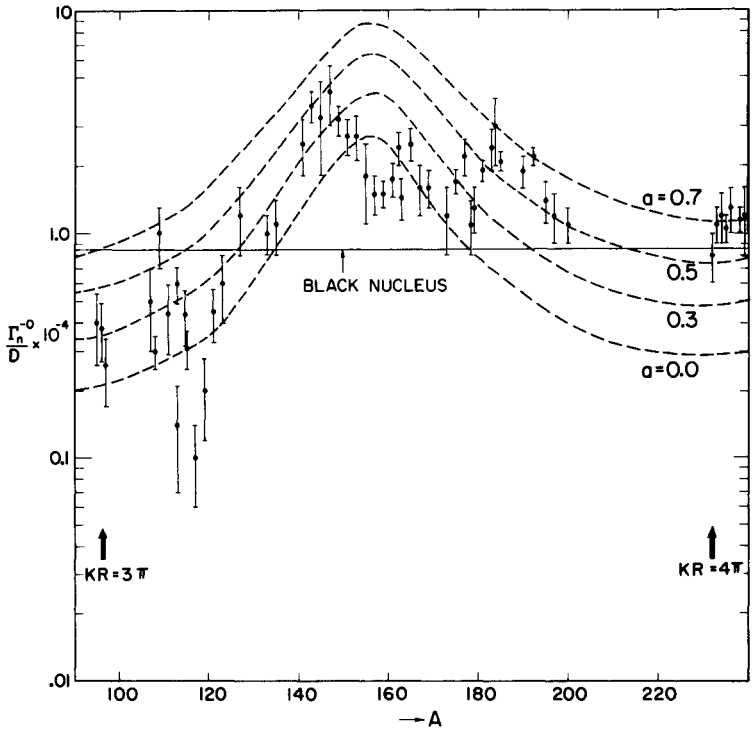

Fig. 7. The s-wave neutron strength function as a function of mass number A in the vicinity of the $4s$ size resonance. The points are data (see Reference 19), and the dashed curves are optical-model computations with a Saxon–Woods potential [Eq. (48)] having $W_0 = -3$ MeV, $R_0 = 1.25A^{1/3}$ fm, and V_0 adjusted slightly to make the $4s$ size resonances of each curve occur in the same place. Computations for various surface thicknesses a are shown, as well as the black-nucleus strength function. Shape deformations of the optical potential have been ignored in the computations, although they produce a better fit to the data. The data and curves are normalized to correspond with transmission functions evaluated at 1 eV and divided by 2π. In the language of Section 4, this is the ratio of the average level width $\langle \Gamma_\lambda \rangle$ divided by the level spacing D and reduced to 1 eV.

We have accounted for all the effects of the optical potential on nuclear transmission functions except for the spin–orbit potential, which was ignored in our average cross-section theory. The spin–orbit potential tends to split each giant resonance into one for $j = l + \frac{1}{2}$ and another for $j = l - \frac{1}{2}$. The data for p-wave neutrons absorbed by nuclei in the mass region of 80 to 110 give evidence of such splitting.[34,35] The spin–orbit splitting will be of importance for average cross sections only when we have low-energy nucleon transmission functions for nuclei which exhibit size resonances for $l \geqslant 1$.

3. APPLICATION OF THE EVAPORATION MODEL

The evaporation model developed in Section 2 can be applied to a wide variety of problems. We choose several problems of increasing complexity, which more or less cover the range of applicability of the evaporation model. The selected problems are ones with which the author is very familiar; other examples could have served as well.

In the first, that of inelastic neutron scattering (Section 3.1), we have only a few possible final states of known spin and parity. Furthermore, the optical potential for neutrons is known very well from studies of neutron elastic scattering and absorption. Consequently we have a simple situation with no adjustable parameters in the evaporation model. The model turns out to describe such cross sections very well. It not only predicts the variation of the cross-section shape with energy but also predicts the magnitude within about 10%. With this kind of accuracy it is possible to use the model to obtain new information about nuclear structure.

In the second, the $C^{12} + C^{12}$ reactions exciting the compound nucleus Mg^{24} to 25 MeV (Section 3.2), we have a more complex situation. The reaction alternatives are the large numbers shown in Fig. 1. Still, we know most of the final states and their spins and parities as well as the optical-model parameters required to calculate the transmission functions. Therefore the application of the evaporation model is still straightforward and almost free of adjustable parameters, even though the situation is no longer simple. The evaporation model still works very well—surprisingly well if one notices that most of the transmission functions of the problem are close to their maximum value of unity, in which case the basic theory (Section 4) is open to question. In both its abundance of final states and the straightforward way in which the evaporation model applies here, this problem is illustrative of the application of the evaporation model to a wide variety of problems, including the compound-nucleus background to many direct reactions.

The third kind of problem is one in which we have so many final states that we must employ level densities to enumerate them. The fundamental evaporation model, Eq. (12), is adapted to this case (Section 3.3). The level densities contain a large number of adjustable parameters. In fact the physical interest now lies in using the evaporation model to obtain information about level densities or in roughly describing cross-section observations with reasonable level densities.

In all three problems the conservation of total angular momentum and parity in the model is essential for some of the predictions. Thus the early evaporation theory is shown to be, at most, a rough guide. The use of the optical model for transmission functions is essential in inelastic neutron scattering—the cross sections are dominated by size resonances— but it is of only moderate importance in the other problems.

3.1 Inelastic Neutron Scattering at Low Energies

The low-lying levels of the nucleus In^{115} are shown in Fig. 8, together with their spin and parity assignments.[36] The first excited state is an isomeric level; it decays to the ground state with a half life of 4.5 hours. We have chosen an example of inelastic scattering involving an isomeric level because the application[37] of the evaporation model to it yields direct information about the neutron transmission function for d waves ($l = 2$). Such information is not presently available by any other means.

For neutron energies below 1 MeV, the reaction channels for the problem are those shown in Table III.

TABLE III

Reaction Channels for the Inelastic Neutron Scattering from In^{115}

	Excitation energy, MeV	I	i	s	Parity
$\alpha = 1$	0.0	$\frac{9}{2}$	$\frac{1}{2}$	4,5	+
$\alpha = 2$	0.335	$\frac{1}{2}$	$\frac{1}{2}$	0,1	−
$\alpha = 3$	0.595	$\frac{3}{2}$	$\frac{1}{2}$	1,2	−
$\alpha = 4$	0.825	$\frac{3}{2}$	$\frac{1}{2}$	1,2	−
$\alpha = 5$	0.858	$\frac{1}{2}$	$\frac{1}{2}$	0,1	−
$\alpha = 6$	0.935	$\frac{7}{2}$	$\frac{1}{2}$	3,4	+

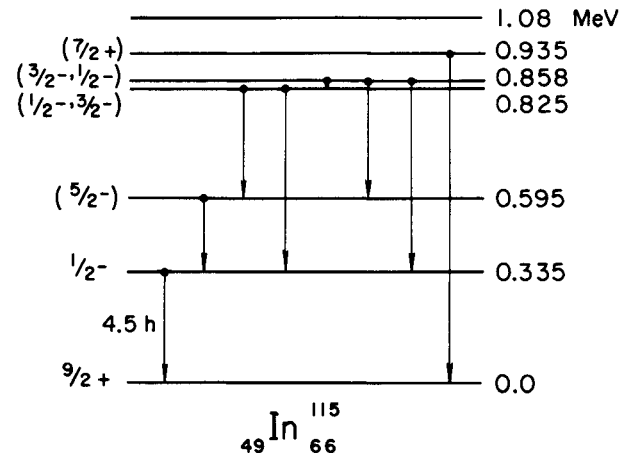

Fig. 8. The low-lying levels of In^{115} and their measured spins and parities. Bracketed spins and parities indicate doubtful assignments. The evaporation calculations[37] clearly indicate a $\frac{3}{2}^-$ assignment to the level at 0.595 MeV.

We have omitted the channels corresponding to capture gamma rays in the In^{116} compound nucleus. These can be shown to be unimportant in the problem because their transmission functions are so much smaller than those for neutron emission. As indicated by Fig. 8, the observed gamma rays from excited states of negative parity feed the isomeric level. Hence the isomeric activity after neutron bombardment is equal to the cross section σ_{isom} for inelastic scattering to all the negative-parity levels. According to Eq. (12), the average of σ_{isom} is

$$
\begin{aligned}
\bar{\sigma}_{\text{isom}} = \frac{\pi}{20k_n^2} \Big\{ & 5[T_2(1)] && J\Pi \\
& \times \frac{[T_1(2) + 2T_1(3) + 2T_1(4) + T_1(5)]}{T_2(1) + T_1(2) + 2T_1(3) + 2T_1(4) + T_1(5) + 2T_2(6)} && 2+ \\
& + 7[2T_2(1)] \frac{[T_1(3) + T_1(4)]}{2T_2(1) + T_1(3) + T_1(4) + T_0(6) + 2T_2(6)} && 3+ \\
& + 7[T_1(1)] \frac{[T_2(2) + 2T_2(3) + 2T_2(4) + T_2(5)]}{T_1(1) + T_2(2) + 2T_2(3) + 2T_2(4) + T_2(5) + 2T_1(6)} && 3- \\
& + 9[2T_1(1)] \frac{[T_2(3) + T_2(4)]}{2T_1(1) + T_2(3) + T_2(4) + 2T_1(6)} \Big\} && 4- \qquad (74)
\end{aligned}
$$

where we have shown all the contributions to the cross sections for neutron partial waves of low orbital angular momentum, $l \leqslant 2$. The higher partial waves ($l \geqslant 3$) are not important here because of their small penetration factors. The transmission functions of the problem are shown in Fig. 9.

The average cross section $\bar{\sigma}_{\text{isom}}$ is dominated by d wave transmission functions. We show how this fact arises from the structure of the average cross section and the gross behavior of neutron-section functions. The measurement of the average cross sections of this kind are the only accurate tool we have determining the value of d-wave neutron-strength functions.

For In^{115} the p-wave (and f-wave) strength functions are large and the s-wave and d-wave strength functions are small. A look at Fig. 5 confirms this fact; In^{115} is moderately near the size resonance for odd partial waves and near the minimums for even partial waves. The strength functions s_l of each partial wave do not vary appreciably with energy within the 1-MeV energy interval of our problem. Therefore we can regard each strength function as a constant which is the same for each of the states of In^{115}. The transmission functions vary with the energy as shown on Fig. 9, because they are proportional to a penetration factor [see Eq. (73) above]. Their relative magnitude is determined by the resonance of the strength functions.

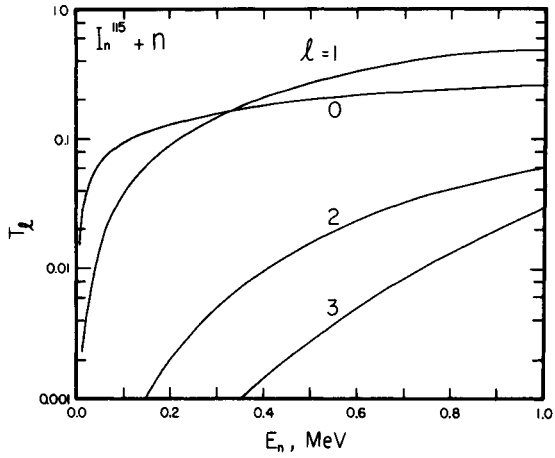

Fig. 9. The neutron transmission functions of In^{115} for various partial waves as a function of the neutron energy.

At all energies the $l = 1$ transmission functions greatly exceed those for $l = 2$.

The same parity difference and large angular momentum difference responsible for the long lifetime of the isomeric level also gives Eq. (74) a structure that makes it possible to factor out the d-wave strength function from the average cross section. Each term of Eq. (74) has a numerator with two factors: one containing only $l = 2$ transmission functions, and the other only $l = 1$ transmission functions. In the denominator of each term the $l = 1$ transmission functions dominate over those for $l = 2$ because of size-resonance effects. Therefore the $l = 1$ strength functions cancel out in numerator and denominator, and the whole average cross section is directly proportional to the strength function for $l = 2$.

The comparison of the calculated average cross section with the data[38] is shown in Fig. 10. The optical model employed to calculate the transmission functions was one which yielded a fit to the s-wave and p-wave absorption of neutrons by In^{115} measured at very low energies.[34] The calculated cross sections included higher partial waves in addition to those ($l \leqslant 2$) of Eq. (74).

The sensitivity of the calculated cross section to the value of the d-wave strength function is also shown by Fig. 10. As s_2 is decreased from the value given by the optical model by multiplying each transmission function by a factor smaller than unity, the average cross section decreases by about the same factor. A small fraction of the cross section involves partial waves greater than $l = 2$, as shown by the nonzero result of the calculation when all d waves were omitted.

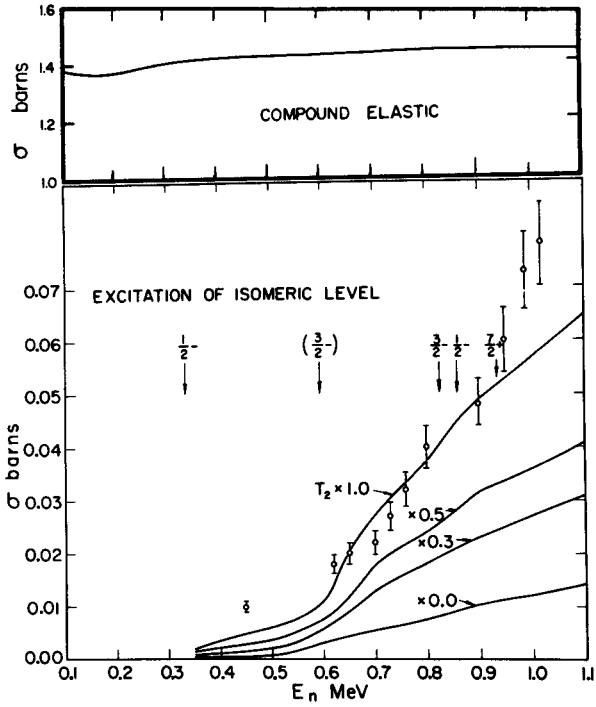

Fig. 10. The cross section for the excitation of the isomeric state in In^{115} by inelastic neutron scattering and for compound elastic scattering in the same nucleus. The points are the data of Reference 38. The curves represent calculations made with the statistical theory, as described in the text. The direct dependence of the isomeric cross section on the value of the *d*-wave transmission functions is shown by the variation of the computed curves when only T_2 is varied. The spin, parity, and positions of the excited states of In^{115} are shown in the figure.

Inelastic neutron scattering gives us the simplest test of the model of average cross sections. For this case, most of the transmission functions are much smaller than unity, the model has a sound basis in theory (Section 4), and only a few channels are involved. Even more, the optical potential for transmission functions is well known from elastic-scattering data. Therefore the model, as applied in Fig. 10 without any free parameters, should yield an accurate description of the cross section. The agreement between data and calculations provides confirmation of the theory.

The application of the model for average cross sections to inelastic neutron scattering usually depends strongly on the improvements in the

modern model. The conservation of total angular momentum and parity gave $\bar{\sigma}_{\text{isom}}$ for In^{115} the particular structure of Eq. (74). If we had neglected this conservation law, then $\bar{\sigma}_{\text{isom}}$ would be a major fraction of the total absorption cross section above 0.5 MeV; the calculation would have been wrong by an order of magnitude instead of by $\pm 10\%$. The use of the optical model for the transmission functions is also important. The minimum in the *d*-wave strength function is almost an order of magnitude below its average value. With black-nucleus transmission functions the calculated cross section would have been too large by an order of magnitude.

The particular example of inelastic neutron scattering which we have chosen has some interesting physics associated with it. First of all, the counting of isomeric activity makes this kind of experiment one of the simplest to carry out. It is so simple that there are almost no recent measurements of this kind, even though such measurements could provide us with almost our sole information on the strength functions of higher partial waves. Secondly, the *d*-wave strength function is here determined near its minimum value where it would be very hard to measure otherwise. The absorption in between size resonances is not at all sensitive to small changes in the depth of the real potential which change the position of the size resonances. The absorption [see Eq. (70)] is directly proportional to the strength of the imaginary part of the potential and to the reflection factor, which, in turn, depends on the surface thickness. Since the centrifugal barrier keeps *d*-waves out of the nuclear center, the measurement of $\bar{\sigma}_{\text{isom}}$ is directly proportional to the strength of the absorption in the nuclear-surface region. Such measurements could be valuable in distinguishing between volume and surface absorption. The behavior of $\bar{\sigma}_{\text{isom}}$ may be contrasted with the compound elastic-scattering cross section $\bar{\sigma}_{\text{c.e.}}$ for In^{115} which is also shown in Fig. 10. The latter is dominated by the *p*-wave giant resonance, and is large because of this and very sensitive to minor changes (by 1 or 2 MeV) in the depth of the real part of the optical potential.

The results for In^{115} are not very different from those for inelastic neutron scattering in general, as In^{115} is not particularly close to the *p*-wave size resonance. Inelastic neutron scattering for Rh^{103} and Y^{89} yields more striking size-resonance effects.[40] Most of the special features of our example apply to any case of inelastic neutron scattering to a level differing in parity from the ground state and lying near an even-*l* or odd-*l* giant resonance. In particular there are a large number of isomeric levels of this type. The long lifetime of the isomeric level ensures that the excitation of the level is not likely to occur through a direct reaction. In view of the great accuracy of the model of average cross sections for inelastic neutron scattering and of the physical interest in the analysis, it is surprising that there have been so few studies of this kind.

3.2 The $C^{12} + C^{12}$ Reactions

The reactions initiated by the bombardment of C^{12} on a C^{12} target[41] and similar heavy-ion reaction studies[42] constitute the most complete and complex test of the model for average cross sections. The channels involved in the $C^{12} + C^{12}$ reactions were shown in Fig. 1. Although the total number of final states is several hundred, recent measurement of nuclear-energy levels have provided the energies, spins, and parities of the levels which dominate the $C^{12} + C^{12}$ reactions. With this knowledge, with the optical models of Table II, and with the aid of computer programs, it is possible to calculate the transmission coefficients and to carry out the sums of Eqs. (12) and (46). The model for average cross sections can be applied in the straightforward fashion just illustrated for inelastic neutron scattering.

The complete study of the $C^{12} + C^{12}$ reactions was motivated in part by the simplicity of the cross-section fluctuations exhibited in this system. Figure 11 shows the kind of fluctuations which are observed in the $C^{12}(C^{12}, \alpha)\,Ne^{20}$ reaction as a function of the C^{12} bombarding energy.[43] The average cross sections are also shown. To remove the fluctuations, the averaging interval must be at least a few MeV. More quantitatively, the study of the fluctuations shows that the average differential cross section of the $C^{12}(C^{12}, \alpha)\,Ne^{20}$ for alpha particles emitted to the ground state of Ne^{20} will deviate from its true mean (in the absence of fluctuations) by about $50/\sqrt{I}\%$, where I is the averaging interval in MeV. Cross sections which are integrated over angles (and differential cross sections to other final states) generally have smaller deviations from the mean. A more complete treatment of the effect of a finite averaging interval on the average cross sections is given in Appendix B.

The $C^{12} + C^{12}$ reactions constitute a useful test of the model for average cross sections and illustrate most of the important features of the model. The heavy-ion transmission functions which dominate the problem are shown in Fig. 12 along with those for neutrons and protons. The majority of the transmission functions of importance are close to unity, so that the basis of the model in nuclear reaction theory is less sound (Section 4). In spite of this, the model is shown to be very successful in fitting the data. The range of particles emitted by the compound nucleus Mg^{24} makes it possible for us to show quantitatively how nucleons are much less successful at carrying off large angular momenta than heavy ions are, how the average angular distribution of various emitted particles varies with the excitation energy, how the magnitude of the evaporation cross section depends on the spin of the final state, etc. The fact that the compound nucleus is formed by heavy ions diminishes the effect of many competing direct-reaction mechanisms,

leads to a population of high angular momentum states in the compound nucleus, and therefore yields a semiclassical result for some of the observed angular distributions. We give some of the results and measurements which illustrate these points. A more complete treatment of the problem can be found in the work of Almqvist *et al.*[43,43]

The application of the evaporation model to the $C^{12} + C^{12}$ reactions is subject to one unusual modification. The incident particles are identical

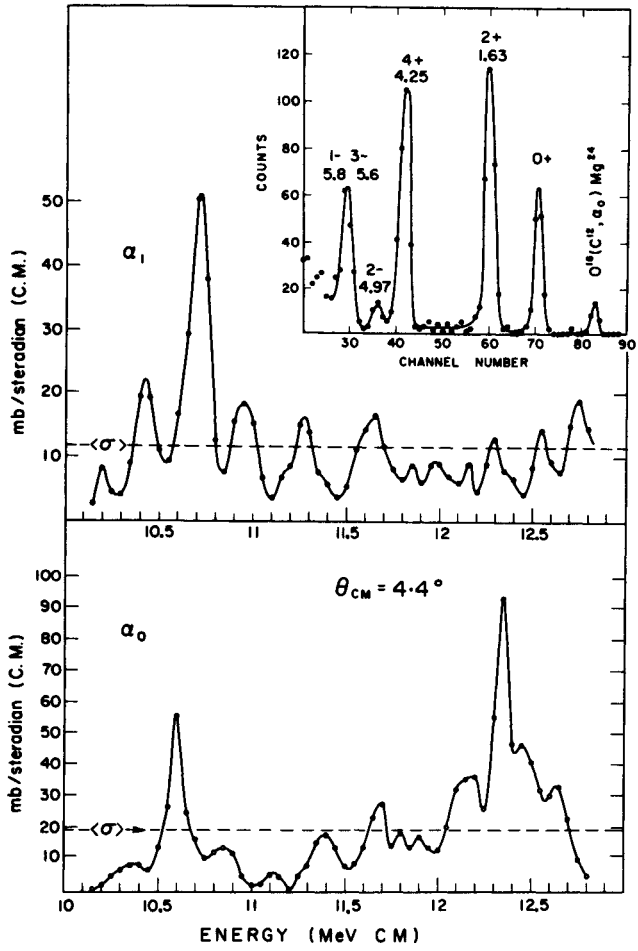

Fig. 11. The energy dependence of the differential cross sections of the reactions C^{12} (C^{12}, α) Ne^{20} (ground and 1.63-MeV states) at 4.4°.[43] The inset shows a pulse-height spectrum from the detector at 11.3 MeV. The average of the data over the whole energy interval is denoted by $\langle\sigma\rangle$.

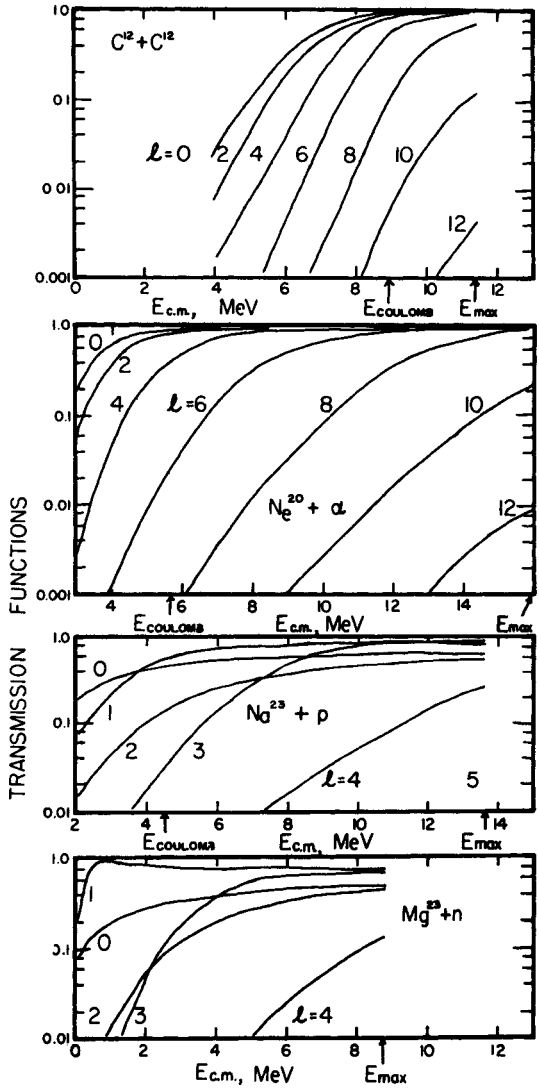

Fig. 12. The transmission functions for statistical theory calculations with the compound nucleus Mg^{24} excited to 25.3 MeV. The odd partial waves for $Ne^{20} + \alpha$ are not shown, nor the transmission functions for $O^{16} + Be^{8}$, but the maximum energy and the Coulomb barriers for each particle are shown. The neutron and proton transmission functions exhibit size resonances while those for heavy ions do not.

bosons of zero spin. Because of the zero spin the incident channel spin is zero and l and J are equal in Eqs. (12) and (46); because of the identity of the C^{12} nuclei all odd values of l (and J) are excluded, the total parity Π is positive, and Eqs. (12) and (46) must each be multiplied by a factor of 2. The absorption cross sections of the $C^{12} + C^{12}$ system are shown in Fig. 13 as a function of the center-of-mass bombarding energy. The optical-model parameters for these absorption cross sections and for all the transmission functions of the problem lie in the range of the parameters in Table II and are given in Reference 41. None of the calculated results below depend sensitively on the value of the optical-model parameters employed; there are no important size-resonance effects.

To show the relative importance of the various channels in the decay of the compound nucleus Mg^{24}, we give in Table IV the result of a statistical theory calculation carried out by using all the final states shown on Fig. 1. The tabulated results include all the final states involving heavy-ion emission and some of the final states involving nucleon emission. Calculated angular distributions for some of the final states are shown in Figs. 14 and 15. The cross-section calculations refer to an energy of 11.4 MeV of the $C^{12} + C^{12}$ system, lying in the middle of the region in which measurements were made (Fig. 11). Most of the partial cross sections are only moderately energy dependent, so that the calculated values can be taken as averages for the energy interval which we are considering.

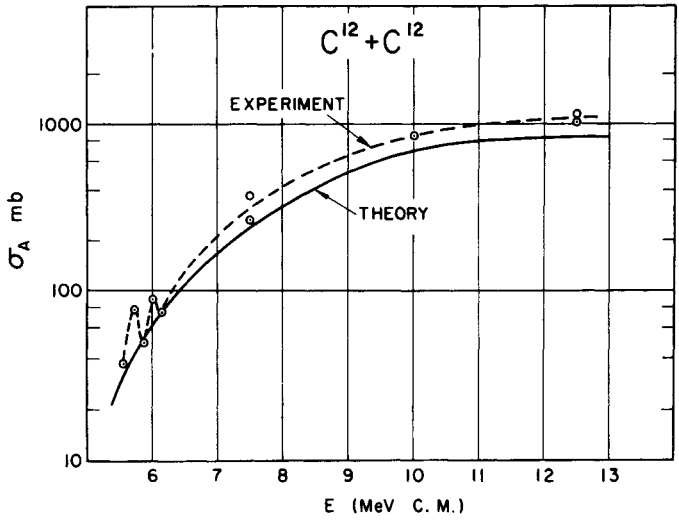

Fig. 13. Comparison of experimental and theoretical absorption cross sections of the $C^{12} + C^{12}$ system as a function of the center-of-mass bombarding energy.

TABLE IV

Results of the Statistical Theory Calculation for the Reaction Cross Sections of the $C^{12} + C^{12}$ System at a Center-of-Mass Energy of 11.4 MeV[a]

Residual state E^*, MeV	$J\Pi$	$\sigma_{cc'}$, mb	Residual state E^*, MeV	$J\Pi$	$\sigma_{cc'}$, mb
Ne^{20}			C^{12}		
ground	0+	16.7	ground	0+	13.5
1.63	2+	41.2	4.43	2+	2.6
4.25	4+	50.9			Sum = 16.1
4.97	2−	15.4			
5.63	3−	33.3	Be^8		
5.80	1−	12.9	ground	0+	13.2
6.75	0+	4.0	2.90	2+	11.4
7.02	4−	24.0			Sum = 24.6
7.19	3−	23.6			
7.23	0+	3.5	Na^{23}		
7.46	2+	13.4	ground	$\frac{3}{2}$+	2.9
7.86	2+	11.8	0.44	$\frac{5}{2}$+	4.1
8.52	5−	33.6	2.08	$\frac{7}{2}$+	6.2
8.60	0+	2.2	2.39	($\frac{1}{2}$+)	0.8
8.70	1−	4.7	2.64	($\frac{5}{2}$+)	2.7
8.80	2+	8.5	2.70	($\frac{3}{2}$+)	1.8
8.84	6+	41.4	2.98	($\frac{9}{2}$+)	7.4
8.91	1−	4.3	3.68	($\frac{3}{2}$−)	3.1
9.10	4+	20.4	3.85	($\frac{5}{2}$−)	6.3
9.18	3−	12.2	3.92	($\frac{3}{2}$+)	1.5
9.58	2+	6.2			
(10.30)	(2+)	4.4			
(10.50)	(0+)	1.1	Mg^{23}		
(10.50)	(1+)	0.8	ground	$\frac{3}{2}$+	2.0
(10.50)	(2+)	3.9	0.44	$\frac{5}{2}$+	2.7
(10.50)	(3+)	3.3	2.08	$\frac{7}{2}$+	3.6
(10.50)	(4+)	11.4	2.39	$\frac{1}{2}$+	0.5
(10.50)	(2−)	1.7	2.64	$\frac{5}{2}$+	1.5
(10.50)	(4−)	5.4	2.70	$\frac{3}{2}$+	1.1
11.08	(0+)	0.7	2.98	$\frac{9}{2}$+	4.0
11.16	(0−)	0.0	3.68	$\frac{3}{2}$−	2.5
11.30	(1+)	0.5			
11.39	(1−)	1.1			
11.66	(2+)	1.6			
11.84	(2−)	0.6			
12.16	(3+)	0.6			
12.24	(3−)	1.2			
12.48	(4+)	1.5			
13.06	(4−)	0.2			
13.10	8+	2.7			
		Sum = 426.8			

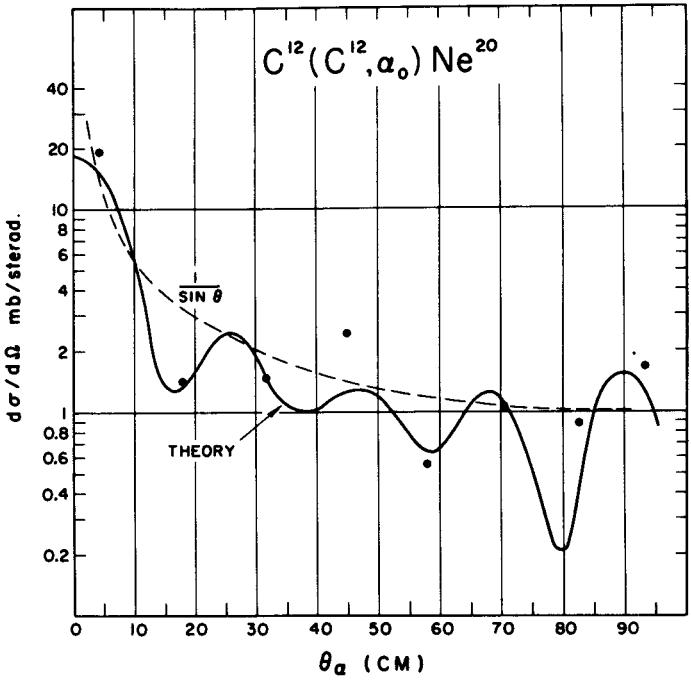

Fig. 14. The experimental and calculated values of the average differential cross section for the C^{12} (C^{12}, α_0) Ne^{20} reaction as a function of the center-of-mass angle θ_α of the emitted alpha particles. The experimental values are the solid points[41], which have an absolute error of $\pm 20\%$. The statistical theory curve (solid line) has a finite sample error at each angle of about $\pm 25\%$. Neither the experimental points near the theoretical curve have been multiplied by an arbitrary normalization factor. The angular distribution $(\sin \theta)^{-1}$ applicable in the limit of large angular momentum is also shown.

The main difficulty with the statistical theory calculations shown here is the lack of knowledge of the possible final states involved in nucleon emission. It happens that these levels do not play a dominant role in the

←

[a] The first column gives the residual nucleus and its state of excitation; the second, the spin and parity of each state; and the third, the angle-integrated cross section $\sigma_{cc'}$ in millibarns for each final state. Bracketed energies, spins, and parities refer to estimated values based on known level densities and spin distributions. Only a few of the levels for nucleon emission are listed. Results for the others are given in Ref. 41. The properties of the levels of Mg^{23} are taken to be the same as those of the mirror nucleus Na^{23}. Levels sufficiently far below the Coulomb barrier so that their cross sections are negligible are not listed in the table.

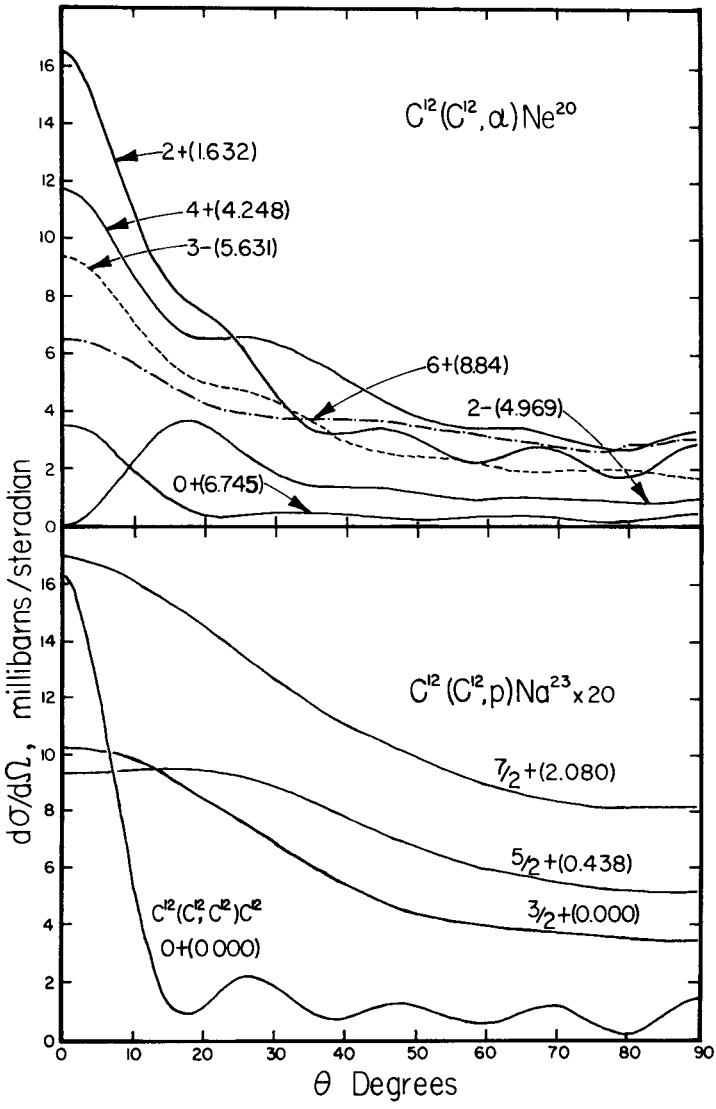

Fig. 15. Representative angular distributions calculated for the $C^{12} + C^{12}$ reactions at a center-of-mass energy of 11.4 MeV, as a function of the center-of-mass angle of the emitted particle. The integrated cross sections for these reactions and the others of the $C^{12} + C^{12}$ systems are shown in Table IV. The spin of each state is indicated, and its energy (in MeV) is in parentheses. The C^{12} (C^{12}, p) Na^{23} have been multiplied by a factor of 20.

$C^{12}(C^{12}, \alpha)\, Ne^{20}$ reactions for which measurements were made, even though the nucleon-emission channels far outnumber the levels of Ne^{20} available to alpha dacay. The feature of the present problem which overrides other considerations is the large amount of angular momentum imparted to the compound nucleus by the $C^{12} + C^{12}$ incident channel. The α particles carry off the angular momentum much more readily than nucleons do. The number of nucleon-emission channels estimated for the calculations is not subject to great uncertainty if one employs the information on level densities available from the $F^{19} + \alpha$ and $Ne^{22} + p$ reactions (allowing in each case for missed levels of high spin). The calculations[41] show that the only levels in Mg^{23} and Na^{23} which are fed appreciably are those of very high spin. The density of levels of spin I was assumed to be proportional to (see Section 3.3)

$$(2I + 1) \exp \frac{-I(I + 1)}{2\sigma^2}$$

with a spin cutoff parameter[1] $\sigma = 3.5$. In addition, the lowest level of spin I was assumed to be at an energy of $0.20[I(I + 1) - I_0(I_0 + 1)]$ MeV, where I_0 is the spin of the ground state of $Na^{23}(I_0 = \frac{3}{2})$. Without this latter assumption the cross sections of a small number of low-lying high-spin levels of Na^{23} and Mg^{23} are so large that the probability of nucleon emission is doubled. Such a large number of nucleon emissions is not in accord with experiment. The assumptions made to obtain the results of Table IV yield the prediction that neutrons and protons together contribute about 40% of the total yield from the compound nucleus. The total production of alpha particles is predicted to be approximately equal to the sum of proton and neutron production. This result of the calculation is in reasonable accord with the experimental results.[44]

The comparison of calculated and measured cross sections for the $C^{12} + C^{12}$ reactions is made without any variation of optical-model parameters to fit the data or any effort to adjust the number or properties of the levels to which Mg^{24} can decay. The agreement between calculated and absorption cross sections of $C^{12} + C^{12}$ as shown in Fig. 13 is a check on the $C^{12} + C^{12}$ transmission functions used in the theory.

The measured value of the average angle-integrated cross sections of $C^{12}(C^{12}, \alpha)\, Ne^{20}$ for the ground state and first excited state of Ne^{20} are, respectively, 19 ± 4 and 63 ± 14 mb. The corresponding calculated values are 16 ± 3 and 39 ± 3 mb, where the errors are those arising from the finite size of the averaging interval (Appendix B and Reference 41). The

[1] This value of the spin cutoff parameter is based on the observed spacings of high-spin levels in Mg^{24} as reported in Ref. 41.

observed and calculated angular distribution for each of these final states is shown in Fig. 14. Since neither the data nor the calculations have been renormalized in Fig. 14, the agreement in both shape and magnitude is of interest.

The calculations of the average cross sections illustrate a number of general features of the evaporation model.

3.2.1 *The Angular Momentum Carried Off by Various Particles*

The small cross sections for proton emission to the low excited states of Na^{23}, compared with the cross section for alpha-particle emission to the low excited states of Ne^{20}, is directly a result of angular momentum considerations. Table V gives the fraction of the $C^{12} + C^{12}$ absorption cross section

TABLE V

The Calculated Absorption Cross Section and the Branching Ratios for Each Value of $J\Pi$ of the Reactions of the $C^{12} + C^{12}$ System at 11.4-MeV Bombarding Energy of the Center of Mass

$J\Pi$	$\frac{\sigma_{abs}^{J\Pi}}{\sum_{J\Pi} \sigma_{abs}^{J\Pi}}$, %	$\sum_i T_i$	Branching ratios, %				
			Alpha Particles	Protons	Neutrons	B_e^8	C^{12}
0+	2.3	72.5	30.2	41.7	21.6	2.5	4.0
2+	11.6	219.0	26.9	45.9	23.5	1.6	2.1
4+	21.1	177.0	32.0	44.0	20.4	1.6	2.0
6+	30.2	75.5	46.7	35.5	12.0	2.6	3.2
8+	28.6	21.4	74.9	12.5	1.0	4.9	6.7
10+	5.9	5.54	91.7	0.7	0	3.3	4.2
12+	0.3	0.71	97.9	0	0	0.8	1.3
Totals	100.0		51.8	29.9	11.4	3.0	3.9

feeding each value of $J\Pi$ in the compound nucleus as well as the corresponding branching ratios from each $J\Pi$ for each pair of reaction products. For the low values of $J\Pi$, which are not strongly fed by the $C^{12} + C^{12}$ incident channel, nucleon emission predominates. For the high values of $J\Pi$, alpha particles and heavy ions dominate the decay. The variation of branching ratios with $J\Pi$ clearly demonstrates the need for a theory which considers conservation of J and Π.

3.2.2 The Lack of Isotropy of Angular Distributions

Various calculated angular distributions are shown in Fig. 15 for the same incident energy and choice of parameters used in connection with Table IV. All of the differential cross sections are symmetric about 90°, but they deviate greatly from isotropy and vary strongly with the spin of the final state and moderately with the excitation energy of the state. The angular distributions tend to show a classical "flywheel" effect[45] modulated by quantum wave oscillations. The flywheel effect makes the cross section large at forward and backward directions and has its origin in the large angular momentum brought into the system by the $C^{12} + C^{12}$ incident channel. If we view the reaction classically, the heavy-ion incident on the target nucleus sticks to it. With conservation of angular momentum the combined system spins about an axis perpendicular to the direction of the incident beam. A particle thrown off by the spinning system is thrown tangentially. Because the axis of rotation is perpendicular to the incident beam, the angular distribution of the particles is $(\sin \theta)^{-1}$, where θ is their angle relative to the incident beam. The results for alpha-particle emission to the ground state of Ne^{20} (Fig. 14) are very close to this classical result, apart from the wave modulation. The wave oscillations are those of the $l = 6$ and $l = 8$ partial waves which dominate the process. Changes in spin or parity of the final nucleus (or the replacement of the alpha particles by nucleons which have fewer partial waves) reduce the applicability of this classical treatment.

There are many striking quantum-mechanical features of the average angular distributions, such as the vanishing of the cross section for alpha-particle emission at 0° if the state in Ne^{20} has a parity $(-)^{I'+1}$, where I' is the spin of the state.

3.2.3 Effect of Spin on Decay

A general rule has frequently been stated[46] that, for states of different spin I at roughly the same energy in the residual nucleus, the decay probability is proportional to $2I + 1$. Some of the results for our problem roughly follow this rule (e.g., the proton emission to the first few states of Na^{23}), while others deviate from it strongly. The $2I + 1$ rule applies to a democratic regime in which all transmission functions for emission of a given particle are equal and all compound states contribute equally to the decay, i.e., have the same ratio of total-formation probability to total-decay probability (the ratio of the second and third columns of Table V). Under this regime only statistical weight factors affect the relative-decay probability. A state of greater spin has more magnetic substates and effectively comprises more channels available for decay. Table VI shows how the regime is established

TABLE VI

The Partial Waves for Alpha Decay from the Compound States of Various $J\Pi$ in Mg^{24} to States of Ne^{20} with Various $I\pi$

$J\Pi$	$I\pi = 0+$	$I\pi = 2+$	$I\pi = 4+$
0+	0	2	4
0−	–	–	–
1+	–	2	4
1−	1	1, 3	3, 5
2+	2	0, 2, 4	2, 4, 6
2−	–	1, 3	3, 5
3+	–	2, 4	2, 4, 6
3−	3	1, 3, 5	1, 3, 5, 7
4+	4	2, 4, 6	0, 2, 4, 6, 8
4−	–	3, 5	1, 3, 5, 7
5+	–	4, 6	2, 4, 6, 8
5−	5	3, 5, 7	1, 3, 5, 7, 9
6+	6	4, 6, 8	2, 4, 6, 8, 10
6−	–	5, 7	3, 5, 7, 9
7+	–	6, 8	4, 6, 8, 10
7−	7	5, 7, 9	3, 5, 7, 9, 11
8+	8	6, 8, 10	4, 6, 8, 10, 12
etc.			

in the alpha decay of Mg^{24} and displays the factors which tend to undermine it. For each possible $J\Pi$ in Mg^{24} the table shows the partial waves for alpha-particle emission to the ground state 0+, first excited state 2+, and second excited state 4+ of Ne^{20}. Each partial wave of greater orbital angular momentum than the intrinsic spin I occurs $2I + 1$ times in the table. Unfortunately for the success of the rule, the $C^{12} + C^{12}$ incident channel feeds only the sequence $J\Pi = 0+, 2+, 4+, 6+$, etc., and even these states do not all treat a given partial wave in the same manner. To take into account only the absence of compound states other than $J\Pi = 0+, 2+, 4+$, the $2I + 1$ rule should be modified to an $I + 1$ rule for the even-parity, even-I states of Ne^{20} and to an (I) rule for all other states. This modified rule applies fairly well to the tabulated cross sections. The most general and striking behavior of this kind is the complete forbiddenness of the decay to 0− states in Ne^{20}. The forbiddenness is a result of angular momentum conservation and applies to all reaction mechanisms.

3.2.4 Population of Various Magnetic Substates

The population of various magnetic substates is of importance in the analysis of cross-section fluctuations. Average cross sections for individual magnetic substates are given by Eq. (47). For the reaction $C^{12}(C^{12}, \alpha)\, Ne^{20}$ with alpha particles emitted to the first excited state 2+ of Ne^{20}, the separate

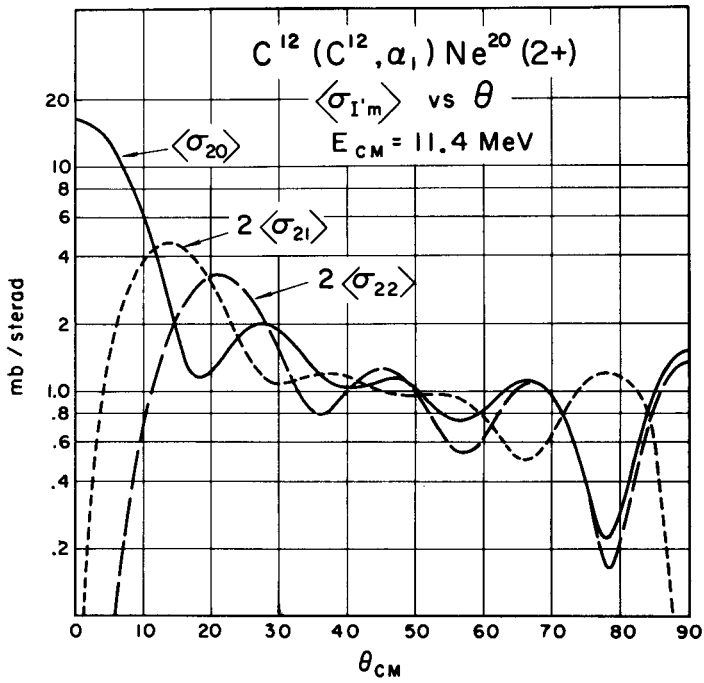

Fig. 16. The predicted angular distributions of the cross sections to particular magnetic substates m of the spin-2 state of Ne^{20} at 1.63 MeV. All quantities are in the center-of-mass system; $\langle\sigma_{20}\rangle$ is the average cross section for the spin-2, $m = 0$ component; $2\langle\sigma_{21}\rangle$ is the sum of the $m = 1$ and $m = -1$ components; and $2\langle\sigma_{22}\rangle$ is the sum of the $m = 2$ and $n = -2$ components. The cross sections are calculated by Eq. (47).

cross sections are shown in Fig. 16. Because of the identity of the C^{12} nuclei from which the compound nuclei are formed, the cross sections for $m_{I'}$ are identical with those for $-m_{I'}$. Figure 16 shows σ_0, $\sigma_1 + \sigma_{-1}$, $\sigma_2 + \sigma_{-2}$. Selection rules arising from angular momentum and parity conservation affect the various contributions. At 0° the spherical harmonies $Y_{lm_l}(0, \varphi)$ vanish for $m_l \neq 0$, so that at this angle we have only the contribution for $m_l = 0$. The factor $(l'I'00 \mid l0)$ of Eq. (47) vanishes unless $I' + l' + l$ is even. This leads to the selection rule, in our case, that at 0° the cross section vanishes unless the parity of the risidual state equals $(-)^{I'}$. The angular distributions of Fig. 15 illustrate this point.

3.3 Evaporation Model with Level Densities

As the excitation energy of the compound nucleus increases, the number of final states becomes very large, so large that statistical arguments need to

be invoked to apply the average cross-section model. The example of the $C^{12} + C^{12}$ reactions which we have just discussed is near the limit to which one might go at present with individual treatment of each final state. The problems at higher energy which require level densities suffer from the lack of knowledge of nuclear-level densities to the extent that they have not provided much new information about nuclear properties and have not posed a good test of the evaporation model. A large number of such studies have been made, prompted in part by the need for information about level densities and in part by an attempt to understand the gross features of a wide variety of problems by using reasonable guesses at nuclear-level densities. Progress on these studies has been aided by the success of the evaporation model at lower energies and by increasing information on the abundance of nuclear states.

The density $\rho_I(E^*)$ of states of spin I of a nucleus is usually assumed to depend on the excitation energy E^* of the states and on their spin but to be independent of the parity and other properties. A common practice is to assume that the energy dependence and the spin dependence are separate factors

$$\rho_I(E^*) = \rho(E^*)[(2I + 1)\, e^{-I(I+1)/2\sigma^2}] \tag{75}$$

where $\rho(E^*)$ is independent of the spin and σ is called a spin cutoff parameter. This form of the level density is convenient for calculations but has some unrealistic aspects to it. It yields the same proportion of high-spin and low-spin levels at all energies, even though we know that levels of high spin, which are usually formed by adding rotational energy to low-lying levels, do not make their appearance as early as levels of low spin. The usual practice is to work with Eq. (75) and to correct the calculations by makeshift methods when necessary. We discuss the kind of cross sections in which level densities are used before describing their detailed properties.

When final states are not discrete we are interested in the evaporation spectra of particles. The old evaporation theory provided results such as Eqs. (6) and (8) for such cases. Our intention is to improve on these old results by adding to them the conservation of total angular momentum and parity, the nuclear optical model for transmission functions, and level densities such as Eq. (75) to enumerate levels. As in Section 1, we now label a pair of particles p and their center-of-mass kinetic energy E_p separately; in our earlier results the index α labeled both these quantities,

$$\alpha = (p, E_p)$$

The results for energy spectra are obtained from our basic average cross section, Eq. (12).

The energy spectra are

$$N(E_{p'})\,dE_{p'} \equiv \sum_{\Delta E_{p'}} \bar{\sigma}_{\alpha\alpha'}$$

$$= \frac{\pi}{k_\alpha^2} \sum_{J\Pi} g_J \left\{\sum_{sl} T_l(\alpha)\right\} \frac{\sum_{l'} g_{l'Jp'} T_{l'}(E_{p'})\,\rho(E_{p'}^{\max} - E_{p'})\,dE_{p'}}{\sum_{p''l''} g_{l''Jp''} \int_0^{E_{p''}^{\max}} T_{l''}(E_{p''})\,\rho(E_{p''}^{\max} - E_{p''})\,dE_{p''}} \tag{76}$$

where

$$g_{l'Jp'} \equiv \sum_{\pi'=\pm} \sum_{s'=|J-l'|}^{J+l'} \sum_{I'=|i'-s'|}^{i'+s'} (2I'+1)\,e^{-(I'+1/2)^2/2\sigma^2} \tag{77}$$

is a sum over all the spin factors of the problem. In Eq. (77) i' is the intrinsic spin of the emitted particle of the pair p'. The advantage of a level density of the form of Eq. (75) is that it permits energy integrals of the transmission functions (multiplied by level density functions) and sums over the spin variables to be carried out separately. Lacking this advantage (e.g., by making σ energy dependent), the number of integrals which need to be evaluated is much greater.

Because the level density is assumed to be independent of parity, we can ignore the parity in Eq. (76). Ordinarily the sums over l values include only even or odd values of l, or the sum over s' in Eq. (77) includes only even or odd values of s', depending on the parity of the compound state and the channel under consideration. We can simply remove the sum over Π in Eq. (76) and each sum over π' in the factors $g_{l'Jp'}$ and compensate for this by letting l, l', l , s', s'', etc., run over *all* integral values compatible with the triangle conditions

$$\mathbf{J} = \mathbf{s} + \mathbf{l} = \mathbf{s}' + \mathbf{l}' = \mathbf{s}'' + \mathbf{l}'' \qquad \text{etc.}$$

Such an approximation would have been disastrous in the case of discrete final states discussed in Section 3.1 or 3.2.

The average cross section of a discrete final state singled out from the unenumerated spectra can be evaluated by means of Eq. (76) if we make the following replacement in the numerator of Eq. (76):

$$\sum_{l'} g_{l'Jp'} T_{l'}(E_{p'})\,\rho(E_{p'}^{\max} - E_{p'})\,dE_{p'} \to \sum_{s'l'} T_{l'}(\alpha') \tag{78}$$

The average differential cross sections, when we have unenumerated final states, can be calculated by the same kind of modifications of the basic cross sections of Section 2.

The variation of nuclear level densities with energy has been the subject of many investigations for several decades, but neither the functional form of the variation nor the value of the constants are very well known. The functional form is roughly given by some simple physical pictures of nuclear excitations. Experimental determination of resonance energies has provided a great deal of information about the density of levels at fixed points in the energy spectrum of most nuclei. Together, the rough theory and the aggregate of data allow one to extrapolate reasonable accurately the level densities which apply to average cross-section calculations. In part, such estimates were made in the $C^{12} + C^{12}$ calculations of Section 3.2, even though the final states were treated individually. More usually the cross-section calculations are subject to considerable uncertainty arising from the lack of knowledge of level densities.

In the Fermi gas model of the nucleus, the level density ρ may be written [according to Newton [8,47]]

$$\rho^{-1} = \text{const. } AG_Z^{1/2}G_N^{1/2}(2U + 3t)^2 \exp\left[-2\left(\frac{\pi^2 GU}{6}\right)^{1/2}\right] \tag{79}$$

where A is the atomic mass and $G = G_Z + G_N$ is the density of single-particle orbits at the Fermi energy U; the subscripts Z and N refer to the number of protons and neutrons, respectively. Effective values of the quantities G for various nuclei may be obtained from tabulations in papers by Newton[8] and Cameron.[48] The equivalent energy U of the Fermi gas is obtained by substracting, from the nuclear excitation energy E^*, the pairing correction. The nuclear temperature t is given by

$$t = \left(\frac{6U}{\pi^2 G}\right)^{1/2} = \left(\frac{U}{c}\right)^{1/2} \tag{80}$$

which also defines the constant c in terms of G. [The temperature t of Eq. (76) is not to be confused with the more empirical temperature concept of the old evaporation theory in Eq. (7).] We may then rewrite Eq. (79)

$$\rho^{-1} = B[2U + 3(U/c)^{1/2}]^2 \exp[-2(cU)^{1/2}] \tag{81}$$

where B and c are constants to be determined by experiment for any given nucleus. Much more complicated forms of the level densities have been proposed (e.g., see Reference 48), but for most average cross-section calculations Eq. (81) should be entirely adequate. As much as possible, the formula should be used as an extrapolation formula in which B is fixed by the known level density at some energy, such as the neutron-binding energy, and then physically reasonable values of c are used to extrapolate to the range of

energies which are important to the problem. A detailed review of the assumptions and limitations of the various level-density formules has been by Ericson.[49]

The constant c of the level-density formula is assumed to be proportional to the mass number A, or roughly so,[50] with a constant of proportionality in the neighborhood of 0.100. For example,[41] for the Mg^{24} compound nucleus of interest in the $C^{12} + C^{12}$ reactions of Section 3.2, the value of the level density is known at 12 MeV and 19 MeV, yielding $c/A = 0.108$. For this case Newton's prescription[8] yields $c/A = 0.129$, and Cameron's prescription[48] yields 0.095. Although the temperature t varies with the energy and the mass number of the compound nucleus, it lies between 1 and 10 MeV for the vast majority of situations.[12,48,49]

The spin dependence of the nuclear-level density, as in Eq. (75), has an exponential factor in which the exponent is related to the rotational energy of a nucleus E_{rot} and hence to its moment of inertia $\mathscr{I}$

$$\begin{aligned} E_{\text{rot}} &= \frac{\hbar^2}{2\mathscr{I}} I(I+1) \\ &= \frac{t^2}{2\sigma^2} I(I+1) \end{aligned} \tag{82}$$

Here t is the nuclear temperature of Eq. (80). For the compound nucleus Mg^{24}, the observed[41] spacing of spin $I = 8$ levels at 25-MeV excitation energy leads to a value of σ near 3.5. Combining this with the value of the temperature obtained from Eq. (80) and from $c/A = 0.108$, one obtains $(\hbar^2/2\mathscr{I}) = 108$ keV. This value is very close to the rigid-body value of the moment of inertia if one takes the shape of Mg^{24} as that found from the rotational bands of energy levels at low energy.[51] For the ground-state band, the value of $(\hbar^2/2\mathscr{I})$ is 237 keV. It is expected that the moments of inertia of nuclei will approach the rigid-body value at high energies. Such considerations serve to determine reasonable values of the spin-cutoff parameter for many nuclei. The value of $\sigma = 3.5$ is not at all untypical. If σ is not independent of the energy, then we cannot separate out the energy integrals and spin sums as in Eq. (76). The characteristic energy distributions of emitted particles, as in Fig. 2, ensures that σ needs to be assumed constant only over the relatively narrow peak region of the energy spectrum.

The level-density formula, Eq. (75), tends to predict too many levels of high spin at low energies. The spin distribution is based [Eq. (82)] on rotational characteristics of the levels.[49] The lowest-lying levels in most nuclei are shell model states of low angular momentum on which we can base rotational bands. The energy at which a level of high spin first appears is then

given by the moment of inertia, as in Eq. (82). For example, in Mg^{24} the lowest level of spin of spin 8 should be found at about 15 MeV. The level-density formula, Eq. (75), allows the same spin distribution of levels at all energies. It is more reasonable to exclude all levels of high spin at energies below which we cannot achieve them by adding rotational energy to the ground state.[51,52] Estimates of this lower limit require knowledge of the moment of inertia of the nucleus. This kind of correction is important whenever the compound nucleus has a lot of angular momentum. Without this correction the number of evaporated nucleons in the $C^{12} + C^{12}$ reactions of Section 3.2 would have been doubled—from the anomalous presence of a very few high spin levels in Na^{23} and Mg^{23} at low energy. Corrections of this kind have been made in other heavy-ion calculations.[52] Applying this correction makes it invalid to separate out the energy integrals of transmission functions, as in Eq. (76).

3.4 The Range of Recent Applications

Without attempting to describe each of the large number of statistical theory calculations which have been carried out, we attempt here to describe the range of problems to which the theory has been applied recently. A very comprehensive survey of calculations prior to 1962 has been given by Bodansky.[12] Most of the early calculations and only a few of the recent ones employ the simple evaporation models of Section 1.

3.4.1 Neutron Elastic and Inelastic Scattering

The earliest Hauser–Feshbach calculations[16,53,54] were applied to the elastic and inelastic scattering of neutrons of a few MeV or less. The example in Section 3.1 continues in this tradition and so does much other recent work.[34,55,57] Problems of this kind have all of the advantages of the In^{115} work described above: They involve only a few levels of known spin and parity, the optical model for transmission functions is well known, and the competition from direct-reaction mechanisms is often absent. At the same time the neutron cross sections exhibit the most striking effects of angular momentum conservation and of size resonances. The work on neutron cross sections at very low energies, where the compound-nucleus levels do not overlap, is subject to a small correction[58,59] arising from the statistical distribution of level parameters. This correction is discussed further in Section 4. For many of the neutron cross sections the transmission functions are all much smaller than unity and the average-cross-section theory here enjoys a firmer foundation in nuclear reaction theory (Section 4) than for any of the other problems.

3.4.2 Neutron Capture at Low Energies

This work is similar to the neutron elastic and inelastic scattering except that the outgoing particles are photons. Transmission functions for electric dipole transitions, which predominate for the capture gamma rays, can be found in many publications.[60,61] The interest of the work centers on the prediction of the relative population of ground states and near-lying spin states (e.g., isomeric levels) after gamma-ray cascades. For all heavy nuclei the number of final states available to photons following neutron capture is very large, usually several million or more. The calculation of capture cross sections requires level-density formulas. Such calculations are perhaps the best tool we have for determining the density of levels which are particle stable. It is a general feature of nuclear physics that gamma emission, even to an enormous number of final states, has difficulty in competing with particle emission. In the In^{115} problem of Section 3.1, the capture gamma rays were neglected because the sum of transmission coefficients for all the capture gamma rays was several orders of magnitude below the sum of the few neutron transmission functions of the problem. Exceptions to this rule occur, e.g., in multineutron cascades following formation of a compound nucleus by high-energy heavy ions.[62] The neutrons carry off little of the angular momentum of the system, and the last few neutrons which could be boiled off can have difficulty in competing with gamma-ray emission.

3.4.3 Heavy-Ion Formation of Compound Systems

A recent paper by Halbert *et al.*[42] reports work on the $C^{12} + O^{16}$ with results very similar to those of the $C^{12} + C^{12}$ reactions discussed in Section 3.2. Although this work required enumeration of the final states by means of level densities, the evaporation model fits the data about as successfully as in the case of the $C^{12} + C^{12}$ reactions. Calculations and measurements for the reaction $O^{16}(He^4, Be^8)\,C^{12}$ have been reported by a group at the University of Washington.[63] A large number of recent studies[64–67] of heavy-ion bombardment at moderately high energies have investigated the effect of angular momentum conservation on the energy spectra of emitted particles. At very high energies (several hundred MeV,) the angular momentum given to the compound nucleus can be very large[45] (in the neighborhood of $l \approx 100$) and the average angular distributions follow the classical flywheel law discussed in connection with Fig. 14.

3.4.4 Fission

Recent statistical theory calculations by Vandenbosch[68] for the neutron-induced fission of U^{234} and U^{236} have yielded information about the fission

barriers. Many other calculations concern the number of neutrons emitted from excited fission fragments.

3.4.5 Calculation of Cross-Section Fluctuations

There has been a great renewal of interest in compound-nucleus processes during the past 7 years arising from the study of cross-section fluctuations.[25] The nature and origin of the fluctuations is given, in part, in Section 4. When the levels of the compound nucleus overlap, the fine structure of the cross sections is that of fluctuations. The average cross sections of interest to us here deal with averages over the fine structure. Calculations of average cross sections have greatly supported the work on the fluctuations, e.g., by providing separate estimates, such as Eq. (47), of the individual coherent cross sections, each of which obeys a simple fluctuation law. The example in Section 3.2 supported work on fluctuations.[43] Many other recent examples occur in the literature.[42,69,70] In addition to providing estimates of the mean values about which the cross sections fluctuate, the statistical theory estimates aid in the determination of level spacings. The cross-section structure of the fluctuations yields direct estimates of the total width Γ_λ of the underlying compound levels. The transmission functions for each channel are related to the ratio $2\pi\langle\Gamma_{\lambda c}\rangle/D$ of the average partial width of that channel to the level spacing (see Section 4). For each spin and parity separately we can sum the individual transmission functions (or rather the values of $\langle\Gamma_{\lambda c}\rangle/D$) to obtain estimates of Γ_λ/D. Combining these with the width estimates from the fluctuation analysis, one can obtain very direct estimates of the spacing of compound levels. The spacing of high-spin states in Mg^{24} quoted in Section 3.3 were obtained in this way.

3.4.6 Competition between Direct Reactions and Compound-Nucleus Processes

This problem is the one with perhaps the greatest need of sound statistical theory calculations and with the fewest number of attempts. The $S^{32}(d, p)$ work recently reported by Leachman[71] uses a fluctuation analysis to indicate roughly how much of the measured cross section at 4.6 MeV corresponds to each mechanism. Statistical theory calculations are used to corroborate the findings and to provide estimates of level spacings. Cross and Clarke[72] estimated the amount of compound-nucleus background which might apply to their dominant direct reactions for inelastic scattering of 14-MeV neutrons on C^{12}. There are a great number of so-called direct reactions of all kinds for which there is a background arising from the compound nucleus. To a large extent this background is an independent contribution to the cross section. Both the magnitude and shape of the

compound-nucleus contribution to the differential cross section can be estimated with the accuracy illustrated by the example in Section 3.2. In certain cases the total of all direct-reaction amplitudes is so large that the compound-nucleus estimates need to be reduced. For example, in deuteron stripping, much of the stripping occurs at large radii. Only a fraction of the deuterons which might form the compound nucleus reach it. Typically the reduction factor lies between 1.0 and 0.5. The imaginary potential used in the optical model, in direct reactions, and in the calculation of transmission functions describes absorption of the incident beam by all processes—direct and compound-nucleus. Only the part of the absorption corresponding to compound-nucleus formation should be used in the calculation of transmission functions for the statistical theory.

4. BASIS OF THE EVAPORATION MODEL IN REACTION THEORY

The foundation of the evaporation models in the theory of nuclear reactions is a very difficult problem and only partial success has been achieved. The difficulty is caused by a large number of reaction alternatives (see Fig. 1) and the denumerable infinity of compound-nucleus resonances [see Eq. (75)]. To approach the problem, there is a discrete but large spectrum of reaction theories. An excellent comparison of the various theories has been made recently by Lane and Robson[73] based on the general treatment by Bloch.[74] The theories fall into three classes: (1) those[75–78] which define the resonances of the compound nucleus by means of imposed boundary conditions at the radius of each channel; (2) those[79–82] which use a modified Hamiltonian and projection operators to produce the resonances and avoid the use of channel radii; and (3) those[83] based on analytical properties of the scattering matrix. Each of these theories has its own particular advantages. Because of the multitude of channels and the multitude of levels, any theory needs to be approximate. The various theories lend themselves in different ways to the kind of approximations which need to be made. We choose to base our discussion on the Wigner–Eisenbud theory,[75] not only because it is widely used in the analysis of reaction data, but also because it is more easily amenable than any of the other theories to statements about the kind of statistical properties of level parameters which are needed to establish evaporation models. The general approach to the theory of average cross sections which we shall follow is that of Thomas[17] and of Lane and Thomas.[18]

In the Wigner and Eisenbud theory the collision matrix components $U_{cc'}$ are given by the widths and energies of compound states constructed for the theory. The compound states X_λ are characteristic states of the full nuclear

Hamiltonian. They exist in the region of configuration space of the compound nucleus, i.e., for separations of each pair of reaction products which are less than the channel radius. The compound-nucleus region and the channel region can be visualized much as a cavity for electromagnetic waves coupled to various channels through which the waves can enter or exit. Although the actual compound states of the nucleus are not stationary—they eventually decay be emitting particles or photons— the resonance theory makes them stationary in order to provide a framework for discussing reactions. The conditions which make them stationary are boundary conditions imposed at the channel radius R_c of each channel

$$\frac{r_c\, dX_\lambda}{dr_c} = b_c\, X_\lambda \,|_{r_c=R_c} \tag{83}$$

where the boundary-condition numbers b_c are real numbers, which turn out to modify the shift functions of the reaction theory, as in Eq. (62). These rather artificial boundary conditions can be chosen in a physical way[19] so that the stationary states of the resonance theory resemble as closely as possible the nonstationary states of the nuclear problem.

The characteristic energies E_λ of the compound states X_λ and their reduced widths $\gamma_{\lambda c}^2$ are the only nuclear quantities of the resonance theory. The amplitudes of the reduced widths are defined by

$$\gamma_{\lambda c} \equiv \left(\frac{\hbar^2}{2m_c R_c}\right)^{1/2} \int \psi_c^* X_\lambda\, dS \tag{84}$$

where the channel wave function ψ_c^* is the one defined by Eq. (23) and the integration is over all the coordinates of the channel wave function. The reduced widths give the coupling of the channel to the cavity; physically it corresponds to the ease with which the state X_λ accepts a pair of reaction products. In addition to the nuclear quantities, the reaction theory requires the penetration factors P_c and shift functions S_c described earlier.

The relation between the collision matrix and the nuclear quantities is made by matching, at each channel radius, the logarithmic derivative of the compound state to the logarithmic derivative of the wave function [Eq. (30)] for the reaction products. The matching is achieved[75,18,19] by observing that the compound states X_λ obey the same Schrödinger equation as the actual wave function and by a consequent application of Green's theorem. The result is often stated in terms of an auxiliary matrix, called the *R matrix*, but we give it in a form of greater direct use in most nuclear reactions[18,19]

$$U_{cc'} = e^{i(\Omega_c+\Omega_{c'})}\left(\delta_{cc'} + i\sum_{\lambda\lambda'} \Gamma_{\lambda c}^{1/2}\Gamma_{\lambda' c'}^{1/2} A_{\lambda\lambda'}\right) \tag{85}$$

The quantities in this expression of the collision matrix are

$$\Gamma_{\lambda c}^{1/2} \equiv (2P_c)^{1/2} \gamma_{\lambda c}$$

which is the square root of the partial width $\Gamma_{\lambda c}$; the level matrix $A_{\lambda\lambda'}$, which is a matrix whose rows and columns refer to levels, not channels, and is most easily defined by its inverse

$$(A^{-1})_{\lambda\lambda'} = (E_\lambda - E)\,\delta_{\lambda\lambda'} - \sum_{c''} (S_{c''} + iP_{c''})\,\gamma_{\lambda c''}\gamma_{\lambda' c''} \tag{86}$$

the Ω_c are potential scattering phase shifts of a hard sphere of radius R_c and are given by

$$\Omega_c \equiv \omega_c - \tan^{-1} \frac{F_c(k_c R_c)}{G_c(k_c R_c)} \tag{87}$$

in which the ω_c are the Coulomb phase shifts defined by Eq. (28).

The result, Eq. (85), is readily applied to a large variety of problems. If we have a single isolated resonance X_{λ_0} of the compound nucleus, then we ignore all other compound states in Eqs. (86) and (85); the use of such an approximate formula of the collision matrix in the general result for cross sections, Eq. (43), leads at once to the familiar Breit–Wigner formula. For situations involving a few overlapping compound levels, the cross-section formula[18,84] is more complicated but the shapes of the cross sections are very well reproduced by the theory. For average cross sections, we adapt the collision matrix with other approximations discussed below. The Wigner–Eisenbud theory is really a framework not a theory. In its most general form, Eq. (85), it is completely correct but completely intractable; however, the framework is one with which it is possible to make reasonable approximations based on the properties of compound states associated with cross-section resonances. These approximations range from situations involving single resonance lines to those of broadly overlapping levels.

For the theory of average cross sections a useful approximation to Eq. (85) is obtained by expanding the level matrix A about its diagonal. The lowest term in the expansion is

$$U_{cc'} \approx e^{i(\Omega_c + \Omega_{c'})} \left[\delta_{cc'} + i \sum_\lambda \frac{\Gamma_{\lambda c}^{1/2}\Gamma_{\lambda c'}^{1/2}}{E_\lambda - E - (i/2)\,\Gamma_\lambda}\right] \tag{88}$$

a very plausible result in which we have a simple sum of Breit–Wigner amplitudes. The total width of each resonance term is just the sum of the individual partial widths

$$\Gamma_\lambda \equiv \sum_\lambda \Gamma_{\lambda c} \tag{89}$$

The approximation Eq. (88), is valid if, for each channel, the following condition holds:

$$\frac{2\pi\langle\Gamma_{\lambda c}\rangle}{D^{J\Pi}} \ll 1 \tag{90}$$

where $\langle\Gamma_{\lambda c}\rangle$ is the average level width and $D^{J\Pi}$ is the average spacing of the compound states whose total angular momentum and parity are $J\Pi$. The condition is related below to the magnitude of nuclear transmission functions. It should be noted that the condition of Eq. (90) does not necessarily mean that we have individual nonoverlapping resonances. If we have many open channels, we can have each of them obey the condition of Eq. (90), while Γ_λ is nonetheless greater than $D^{J\Pi}$.

Approximation (88) has thrown out very little when condition (90) is valid. For example, it includes the direct reactions as well as the compound-nucleus processes. The former arise from sums over the small amplitudes of many resonances very distant from the energy E of the system; the latter arise from the resonances near E. A more precise definition of distant and near is given below. Some of the reaction theories[73] achieve the result for the collision matrix in the form of Eq. (88) by more direct means than those of the Wigner–Eisenbud theory. The price for this directness is, usually, an intractable energy dependence of the nuclear parameters or *ad hoc* assumptions about the behavior of collision matrix components.

Before performing the appropriate cross-section averages, using the collision matrix of Eq. (88) we sketch a simple and beautiful picture which contains most of the physics of nuclear reactions. Considered as a function of the energy in the complex energy plane, the sum of Breit–Wigner amplitudes in Eq. (88) gives the collision matrix a series of poles. There is one pole for each compound state at $E = E_\lambda - (i/2)\,\Gamma_\lambda$. Each pole gives rise to a resonance in the cross section. The resonances and poles are shown in Fig. 17. At higher energies the poles become closer together and farther removed from the real axis so that the resonances overlap. The spacing of the compound states D is usually much less than 1 MeV, sometimes 1 eV or less, which is much smaller than the characteristic spacing d of the size resonances of the optical model. In the language of the shell model, the size resonances are single-particle states, while the compound states include, in addition, states with many particles in excited orbits.

The size resonances have their origin in the variation in strength of the poles. If we consider the diagonal element of the collision matrix, the numerator of each Breit–Wigner term in Eq. (88) is $\Gamma_{\lambda c}$. The mean pole strength per unit of energy interval is

$$\frac{\langle\Gamma_{\lambda c}\rangle}{D} = 2P_c\,\frac{\langle\gamma_{\lambda c}^2\rangle}{D} \equiv 2P_c s_c \tag{90}$$

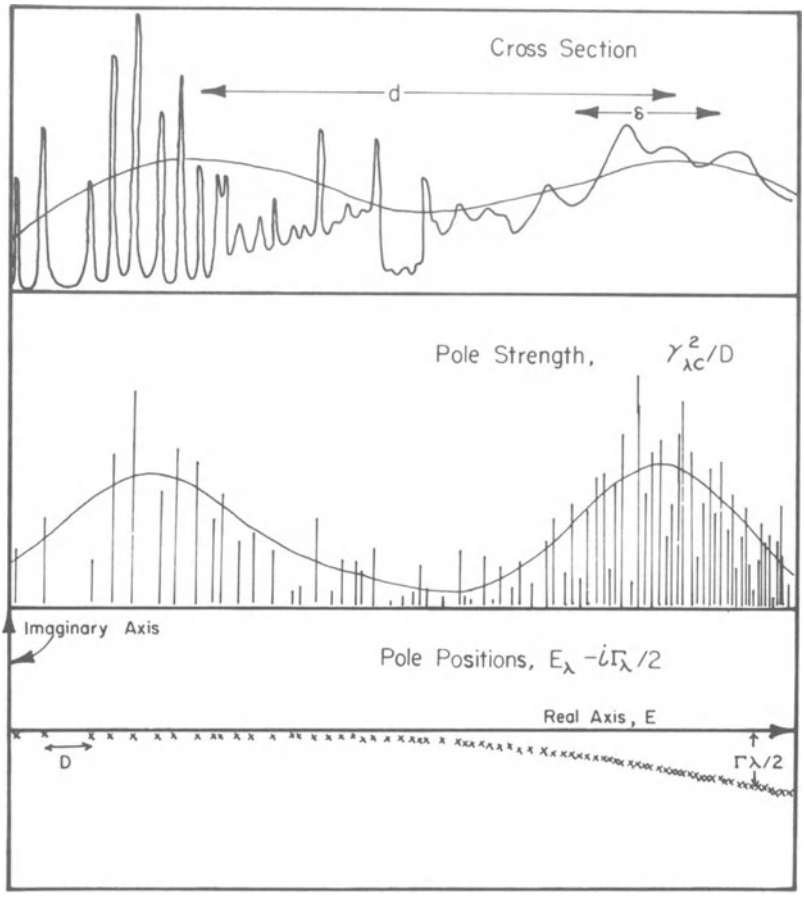

Fig. 17. A schematic representation of the poles of the collision matrix, of the corresponding strength function, and of the cross sections, as a function of energy. The poles are shown in the complex energy plane with the origin corresponding roughly to the threshold for neutron emission. Although the scale of the figure is arbitrary and not realistic, it does indicate the relative magnitude of the level widths Γ_λ, level spacings (D), size-resonance spacings (d), and averaging interval (δ). The average of the pole strength and cross section are also shown. The cross section in a given nucleus sometimes indicates a single size resonance (see Figs. 6 and 7); the cross section for elastic scattering, however, does not have simple size resonances as shown, even if the pole strength function has such size resonances (see Section 2.3 and Reference 27).

which defines the nuclear strength function

$$s_c \equiv \frac{\langle \gamma^2_{\lambda c} \rangle}{D} \tag{91}$$

The gross structure which modulates the mean size of the resonances in Fig. 17 is attributed to the behavior of nuclear reduced widths.[85] Because the channel wave function ψ_c^* in Eq. (84) is a wave function with a particle moving independently, the reduced width amplitudes of Eq. (84) are directly proportional to the single-particle component contained in each compound state. Single-particle states for nucleons are mixed into other shell model states by the residual interaction of the shell model. The mixing is appreciable only within an energy interval of a few MeV around the positions of the single-particle states.[85,19] Hence, for nucleons, the strength function exhibits size resonances. We have not yet associated the strength function defined by Eq. (91) with the strength function of the nuclear transmission functions (see Section 2.3), but we shall do so below.

The theory of cross-section fluctuations is based on a collision matrix of the form of (88). An angle-integrated reaction cross section is proportional to $|U_{cc'}|^2$. The fluctuations arise because the sum over Breit–Wigner amplitudes is under the square; no matter how strongly the resonances overlap, all of the Breit–Wigner amplitudes are added up coherently

$$\begin{aligned} |U_{cc'}|^2 &= \left| \sum_\lambda \frac{\Gamma_{\lambda c}^{1/2}\Gamma_{\lambda c'}^{1/2}}{E_\lambda - E - (i/2)\,\Gamma_\lambda} \right|^2 \\ &= \left| 2P_c^{1/2}P_{c'}^{1/2} \sum_\lambda \frac{\gamma_{\lambda c}\gamma_{\lambda c'}[E_\lambda - E + (i/2)\,\Gamma_\lambda]}{(E_\lambda - E)^2 + \frac{1}{4}\Gamma_\lambda^2} \right|^2 \\ &\equiv |u_{cc'} + iv_{cc'}|^2 = u_{cc'}^2 + v_{cc'}^2 \end{aligned} \tag{92}$$

If the reduced-width amplitudes $\gamma_{\lambda c}$ are assumed to have a Gaussian distribution with a mean value of zero (as befits small nuclear overlap integrals), then the real and imaginary parts $u_{cc'}$ and $v_{cc'}$ of the sum over Breit–Wigner amplitudes separately have the same distribution. It is shown in Appendix B that the mean values of $u_{cc'}^2$ and $v_{cc'}^2$ are equal. From this it follows that $U_{cc'}^2$ has a chi-squared distribution for two degrees of freedom. The basic distribution law for cross-section fluctuations is then

$$P(x)\,dx = e^{-x}\,dx \tag{93}$$

with

$$x \equiv \frac{|U_{cc'}|^2}{\overline{|U_{cc'}|^2}} \tag{94}$$

In Eq. (93), $P(x)\,dx$ is the probability that x has a value between and $x + dx$. The two degrees of freedom are a consequence of the equal mean value of $u_{cc'}^2$ and $v_{cc'}^2$. Much work on cross-section fluctuations[25] has demonstrated

the validity of this law. For many cross sections the basic fluctuation law is altered because the cross section is a sum of incoherent terms (see Section 2.2). The cross-section fluctuations have a structure related to the total width Γ_λ of the underlying levels. Whenever we change the energy by about Γ_λ, we effectively take a whole new set of overlapping levels, because the Breit–Wigner amplitudes fall off in the distance Γ_λ. The sum of Breit–Wigner resonances at $E + \Gamma_\lambda$ should be independent of the sum at E. The structure of Fig. 11 arises from the fluctuations of compound nucleus which overlap strongly ($\Gamma_\lambda \approx 150$ keV, $D \approx 25$ keV).

The sum of Breit–Wigner amplitudes can be divided into two parts, one yielding the direct reactions and the other the compound-nucleus processes

$$\sum_\lambda \frac{\Gamma_{\lambda c}^{1/2}\Gamma_{\lambda c'}^{1/2}}{E_\lambda - E - (i/2)\,\Gamma_\lambda} = \sum{}' \frac{\Gamma_{\lambda c}^{1/2}\Gamma_{\lambda c'}^{1/2}}{E_\lambda - E - (i/2)\,\Gamma_\lambda} + \sum_{\text{local levels}} \frac{\Gamma_{\lambda c}^{1/2}\Gamma_{\lambda c'}^{1/2}}{E_\lambda - E - (i/2)\,\Gamma_\lambda} \tag{95}$$

The local levels are those lying in the neighborhood of the energy E, within an energy interval of the order of Γ_λ. It is these poles or compound states which produce individual resonances or cross-section fluctuations. The prime on the first sum indicates that the local levels are omitted. The sum required to convert the first sum into the amplitude for direct reactions has its important contributions from as far away as the nearby size resonances.[18,74] Since usually $\Gamma_\lambda < d$, the removal of the local resonances from the sum is of no importance. For elastic scattering, the sum over distant resonances changes the hard-sphere phase shifts Ω_c of Eq. (88) into the phase shifts of a diffuse-edge potential well.[18,19] The Wigner–Eisenbud theory is an awkward one for describing direct processes, but it exhibits clearly the relation between the direct and compound processes. In the calculation of average cross sections for the compound nulceus, we drop the first term (the direct-reaction term) on the right of Eq. (95).

In order to obtain average cross sections, we must average the squares of collision matrix components over an energy interval δ containing the local levels; δ must be much larger than either the level spacing D or the level width Γ_λ (see Fig. 17). We illustrate the calculation of the average for the reaction cross section ($c \neq c'$) using a method first employed by Bethe.[1] We need the average of

$$|\,U_{cc'}\,|^2 = 4P_cP_{c'} \sum_{\lambda\lambda'} \frac{\gamma_{\lambda c}\gamma_{\lambda c'}\gamma_{\lambda' c}\gamma_{\lambda' c'}}{[E_\lambda - E - (i/2)\,\Gamma_\lambda][E_{\lambda'} - E + (i/2)\,\Gamma_{\lambda'}]} \tag{96}$$

where the levels λ, λ' lie in the averaging interval δ. We can ignore the terms in the double sum from levels outside δ because the denominators of Eq. (96) make such contributions small, although the very distant terms would yield

the direct-reaction amplitude. We also assume that the energy interval δ is small enough that the penetrabilities P_c and P_c' may be regarded as constants. The average of Eq. (96) taken over the energy is found by multiplying Eq. (96) by δ^{-1} and integrating over the energy E from $-\infty$ to $+\infty$. The integral is evaluated by completing a contour in the upper half of the complex energy plane, and the result is $2\pi i$ times the sum of the residues of Eq. (96) at the poles located at $E = E_{\lambda'} + (i/2)\,\Gamma_{\lambda'}$

$$\overline{|U_{cc'}|^2} = \frac{4\pi P_c P_{c'}}{\delta} \sum_{\lambda\lambda' \text{ in } \delta} \frac{\gamma_{\lambda c}\gamma_{\lambda c'}\gamma_{\lambda' c}\gamma_{\lambda' c'}(\Gamma_\lambda + \Gamma_{\lambda'})}{(E_\lambda - E_{\lambda'})^2 + \frac{1}{4}(\Gamma_\lambda + \Gamma_{\lambda'})^2} \tag{97}$$

For each term in the sum over λ of Eq. (97) there will be about $\langle\Gamma_\lambda\rangle/D$ contributions from the λ' sum and therefore about $\delta\langle\Gamma_\lambda\rangle/D^2$ pairs altogether. The reduced-width amplitudes are assumed to have random sign fluctuations.[87,88] so that the contribution from the terms with $\lambda \neq \lambda'$ will be proportional to the square root $[\delta\langle\Gamma_\lambda\rangle/D^2]^{1/2}$ of the number of pairs, while the corresponding contribution from the diagonal terms ($\lambda = \lambda'$) is δ/D. With $\delta > \Gamma_\lambda$ we can neglect the cross-product terms and obtain

$$\begin{aligned} \overline{|U_{cc'}|^2} &= \frac{\delta}{D}\, 8\, \frac{\pi}{\delta}\, P_c P_{c'}\, \frac{\langle\gamma_{\lambda c}^2\rangle\langle\gamma_{\lambda c'}^2\rangle}{\langle\Gamma_\lambda\rangle} \\ &= \frac{T_c T_{c'}}{\sum_{c''} T_{c''}} \end{aligned} \tag{98}$$

where

$$\begin{aligned} T_c &\equiv \frac{2\pi\,\langle\Gamma_{\lambda c}\rangle}{D^{J\Pi}} \\ &= \frac{4\pi P_c\,\langle\gamma_{\lambda c}^2\rangle}{D^{J\Pi}} \\ &\equiv 4\pi P_c s_c \end{aligned} \tag{99}$$

in which s_c is the strength function of the channel c. The result, Eq. (98), has the same form as Eq. (45), and we therefore have the connection, Eq. (99) between transmission functions and nuclear-level widths and spacings. Because of condition (90), the connection holds only when the transmission functions are much smaller than unity. Comparison of Eqs. (73) and (99) now identifies the nuclear strength function as that of the optical potential, apart from a reflection factor which we might well incorporate into the penetration factor of Eq. (99).

It is an interesting exercise for the reader to use the averaging methods used in deriving Eq. (98) to obtain the corresponding result for the elastic-

scattering cross section. According to the discussion following Eq. (54), the average compound elastic scattering is proportional to

$$\overline{|U_{cc}|^2} - |\overline{U_{cc}}|^2$$

A small numerical correction must be applied to result (98) when we have nonoverlapping compound levels and only a few channels open. The $\gamma_{\lambda c}^2$ have a Porter–Thomas size distribution:[87,88] if the $\gamma_{\lambda c}$ are random matrix elements with a Gaussian distribution about the mean value of zero, then the distribution of the $\gamma_{\lambda c}^2$ is that of a chi-squared distribution with *one* degree of freedom

$$P(y)\,dy = (2\pi y)^{-1/2}\,e^{-y/2}\,dy \tag{100}$$

$$y \equiv \frac{\gamma_{\lambda c}^2}{\langle \gamma_{\lambda c}^2 \rangle} \tag{101}$$

The distribution law differs from Eq. (93) because the $\gamma_{\lambda c}$ are real, unlike the sum of Breit–Wigner amplitudes. If, e.g., we had only two channels open (c and c'), then the size distribution of Γ_λ would be correlated (because $\Gamma_\lambda = 2P_c\gamma_{\lambda c}^2 + 2P_{c'}\gamma_{\lambda c'}^2$) with that of $\gamma_{\lambda c}^2$ and $\gamma_{\lambda c'}^2$. In general we shall have

$$\left\langle \frac{\gamma_{\lambda c}^2 \gamma_{\lambda c'}^2}{\Gamma_\lambda} \right\rangle = \theta\,\frac{\langle \gamma_{\lambda c}^2 \rangle \langle \gamma_{\lambda c'}^2 \rangle}{\langle \Gamma_\lambda \rangle} \tag{102}$$

with θ being a correction factor to the basic evaporation formula, (98) or (12). With very few open channels the value of θ may be as small as one-half (inelastic scattering) or as large as three (elastic scattering), but it rapidly approaches unity when the number of channels becomes large, Moldauer[58] has discussed this and other similar corrections to the basic evaporation formulas. This correction was not used in the calculations for inelastic neutron scattering by In^{115} given in Section 3.1. It would have slightly reduced the calculated cross sections of Fig. 10 at neutron energies below 0.5 MeV.

When the transmission functions are not small compared with unity, the average cross-section theory becomes much more difficult. In the case of only one channel (which is a good approximation to compound elastic scattering of neutrons by many elements for neutron energies in the keV region), we can derive a connection between optical-model transmission functions and nuclear-level widths which is more general than the approximate result of (98). The restriction to a single channel changes the collision matrix to a collision function U_l for each partial wave. Since there is no reaction cross section, the compound elastic scattering is the absorption cross section given in terms of the square of the average value of U_l by Eq. (55). Since we have only one channel, we can describe the nuclear

collision function by the same methods that are used in Section 2.3 to describe the average collision function by an optical potential. If f_l for the partial wave l is given by Eq. (59), we have the following completely general connection between U_l and f_l

$$U_l = (O_l/I_l)[1 - (S_l - iP_l)f_l]/[1 - (S_l + iP_l)f_l] \tag{103}$$

where O_l/I_l is a phase factor of no importance to the absorption cross section (it is the ratio of the outgoing waves of Eq. (27) to the incoming waves evaluated at the nuclear radius), S_l is the shift function of Eq. (62), and P_l is the penetration factor of Eq. (61). The derivation Eq. (103) follows directly from Eqs. (58) and (59).

The nuclear collision function, Eq. (59), has closely spaced resonances. The theory of nuclear reactions[18,19] gives the following result for f:

$$f_l = \sum \gamma_\lambda^2/(E_\lambda - E) \tag{104}$$

where the γ_λ^2 are the reduced widths of the compound states, and E_λ, their energies. (In the Wigner–Eisenbud theory, f_l would be called an R function.) To obtain the average cross section for our one-channel problem, we must average U_l over the resonances.

The averaging procedure which we use is that of Thomas.[17] We move the averaging interval δ up into the complex plane by an amount ϵ

$$\delta \gg \epsilon \gg D \tag{105}$$

where D is the average spacing of the compound levels. The new average, with E replaced by $E + i\epsilon$, is equal to the old because the new interval can be connected with the old to form a closed contour containing no poles. If $\delta \gg \epsilon$ holds, then the integral over the two connecting ends is negligible. When E is replaced by $E + i\epsilon$ (with $\epsilon \gg D$, as assumed), then the collision function U_l and f_l no longer vary rapidly with the energy. Therefore we have

$$\begin{aligned} f_l = f_l(E + i\epsilon) &= \sum_\lambda \frac{\gamma_\lambda^2}{E_\lambda - E - i\epsilon} \\ &= \int_{-\infty}^{\infty} \frac{\langle \gamma_\lambda^2 \rangle}{D} (E_2 - E - i\epsilon)^{-1}\, dE_\lambda \\ &= i\pi s_l + P \int s_l (E_\lambda - E)^{-1}\, dE_\lambda \end{aligned} \tag{106}$$

where s_l is the nuclear strength function (91). The beautiful feature of this result is that the real and imaginary parts of f_l are related to each other in

exactly the same way as the optical model f_l^{Re} and f_l^{Im} of Eqs. (68) and (69). Moreover, Lane, Thomas, and Wigner[85] showed that the optical-model strength function of Eq. (68) gave a reasonable description of the behavior with energy of the nuclear strength function. If so, we have then provided a justification for using the optical model to prescribe the average cross sections of our one-channel problem.

By use of Eq. (60) and with the shift functions chosen to be zero (by choice of the boundary-condition-numbers), we obtain

$$T_l \approx \frac{4\pi P_l s_l}{1 + \pi P_l s_l} \tag{107}$$

To change this square-well result to that of a diffuse-edge potential, we should multiply each P_l by the reflection factor f. Equation (107) is a generalization of Eq. (99) or (73) which hold only for small values of the transmission functions. The transmission function of Eq. (107) does not exceed unity and is equal to unity for $\pi P_l s_l = 1$. Unfortunately the connection between T_l and $\pi P_l s_l$ is two valued. To help resolve any ambiguity, we note that for a black nucleus $\pi P_l s_l$ increases to the value of unity as the penetrability approaches its maximum value. Therefore there is only one possible value of $\pi P_l s_l$ for each value of T_l in the black-nucleus model. For an optical potential at low energy the transmission functions are very small and $\pi P_l s_l$ might be very small or very large; however, the penetrability makes $\pi P_l s_l$ small, so that no ambiguity exists. At high energies the value of $\pi P_l s_l$ for the optical model can exceed unity so that the connection of (107) is approximate and uncertain. In practice[41] no great uncertainty is encountered, and Eq. (107) is useful in estimating level spacings from transmission function calculations combined with total widths measured from cross-section fluctuations. Moldauer[89] has recently suggested that a better connection is given by

$$T_l = 1 - e^{-4\pi P_l s_l} \tag{108}$$

This equation and Eq. (107) both yield Eq. (99) at low values of $\pi P_l s_l$, and the next term in the Taylor series expansion of both about the value $\pi P_l s_l = 0$ are the same. However, both are also open to question concerning the validity of the compound-nucleus picture when the transmission functions are large.

Attempts to develop the average cross-section theory in the case of more than one channel run into difficulties of mathematics and of physical interpretation. Some interesting approaches to this problem have been made,[89] but many questions remain. When the transmission function of a channel approaches unity, this implies that the channel entrance should really be regarded as part of the cavity, the coupling is so large. The compound nucleus

decays very rapidly into the entrance channel. In the early days of evaporation theory one spoke of partial heating of a small area on the nucleus surface. At present one speaks of sharing the energy between only a few nucleons [forming only "doorway" states[90]]. Griffin[91] has recently given an interesting analysis of neutron emission which is not compatible with the normal compound-nucleus picture. In the language of nuclear reaction theory, these questions concern the randomness of the reduced widths and the uniform convergence of expansions of the level matrix, Eq. (86), particularly for terms in the expansion of the collision matrix of higher order than Eq. (88). These questions affect the meaning of the "total width" underlying fluctuations. When the partial widths $\Gamma_{\lambda c}$ of a single channel exceed the level spacing, then the analysis of the reactions in terms of compound states may not be the simplest one possible. The resolution of such questions will require much more confrontation of cross-section data with theory.

5. CONCLUSIONS

The modern evaporation theory has been shown to predict with great accuracy a wide variety of nuclear cross sections. Quite typically it requires no fitting to be accurate within about 20%. It achieves this success by employing the optical potential to incorporate modern ideas about nuclear structure into the evaporation theory and by taking care of the conservation of total angular momentum and parity. The early evaporation models which ignored these details are only a rough-and-ready tool in comparison. They are still adequate in giving quick estimates of evaporation cross sections which are accurate to within an order of magnitude. Such quick estimates can be made by dividing the geometric area of the nucleus (or the total absorption cross section if it is significantly smaller) by the number of open channels. The modern theory not only improves the estimated value of the angle-integrated decay rate but also predicts the shape of the average differential cross section. The estimates with the modern theory are straightforward and should be applied much more widely than at present, particularly to estimate the background noise of direct processes.

Just as the compound nucleus theory has achieved such success in confronting nuclear data, a large number of questions about its validity have arisen. The picture as applied above is extreme. By incorporating the optical model into the theory we have assumed that in the nuclear interior we have either single-particle motion or complete energy sharing, but nothing in between. A large amount of recent work has suggested a hierarchy of states through which one proceeds to the compound nucleus.[90] For example, a single incident nucleon (single-particle motion before it reacts) first excites

a nucleon of the target nucleus and leaves a hole in the core (the two-particle, one-hole state is called a doorway state), which might be followed by a further excitation (a three-particle, two-hole state called a hallway state), etc., until one finally attains sharing of the initial energy (a compound-nucleus state). This view of the process is picturesque, but does it have any effect on the cross sections? The answer is that it does if, e.g., the doorway state has a greater probability of decaying back into the entrance channel than of proceeding into the hallway state. In this case one would expect to see an intermediate structure, an energy variation with a spacing intermediate between that of the compound-nucelus resonances and the size resonances. There is no completely convincing evidence that such a structure exists, although the idea is so compelling that the search for it should continue.

Fortunately the doorway states have a spacing Δ, such that the intermediate structure does not always wash out when one averages over the closely spaced compound-nucleus resonances. If d is the spacing of the size resonances, D that of the compound-nucleus resonances, and δ the averaging interval, then we must have

$$d \text{ or } \Delta \gg \delta \gg \Gamma_\lambda \text{ or } D \tag{109}$$

A glance at Fig. 17 shows that d is of the order of 10 MeV and D (in heavy nuclei) of the order of 1 eV. Typically Γ_λ can vary from a few electron volts to hundreds of keV depending on how high above the neutron-emission threshold the energy of the system is. The intermediate structure has a typical spacing of hundreds of keV. This allows Eq. (109) to be satisfied in some situations.

The simple evaporation process discussed in this article forms a reasonable zero-order picture of how a complex nuclear system interacts. Further theory and experiment concerning the reaction processes are likely to be based on this zero-order picture.

Acknowledgments

The author is greatly indebted to Dr. D. McPherson of the Chalk River Nuclear Laboratories for assistance with many parts of the calculations carried out for this article.

APPENDIX A. ABSORPTION CROSS SECTION OF A COMPLEX SQUARE WELL

To begin the calculation of the absorption cross section of a complex square well, we demonstrate first the single-particle resonances of a real square well. The radial equation of the problem is

$$\left[\frac{d^2}{dr^2} + \frac{2m}{\hbar^2}(E - V) - \frac{l(l+1)}{r^2}\right] u_l(r) = 0 \tag{A.1}$$

We define a set of stationary states $X_{\lambda l}$ which satisfy the Schrödinger equation (A.1) and the following boundary condition at the square-well radius R_0

$$r\frac{dX_{\lambda l}}{dr} = b_l X_{\lambda l}\,|_{r=R_0} \tag{A.2}$$

Because the well is square and spherical the stationary states are spherical Bessel functions

$$X_{\lambda l} \equiv c_{\lambda l} r j_{\lambda l}(\rho) \tag{A.3}$$

where $c_{\lambda l}$ is a normalization constant and $\rho \equiv Kr \equiv [(\hbar^2/2m)(E + V_0)]^{1/2} r$ in which V_0 is the depth of the square well. The radial wave functions $X_{\lambda l}$ are assumed to be normalized by

$$\int_0^{R_0} X_{\lambda l} X_{\lambda' l}\, dr = \delta_{\lambda\lambda'} \tag{A.4}$$

This yields for the normalization constants

$$c_{\lambda l}^2 = 2R_0^{-3}[j_l^2(K_{\lambda l}R_0) - j_{l-1}(K_{\lambda l}R_0)\, j_{l+1}(K_{\lambda l}R_0)] \tag{A.5}$$

in which $K_{\lambda l}$ is the wave number corresponding to the characteristic energy $E_{\lambda l}$ of the stationary state $X_{\lambda l}$.

The exact radial wave functions of the square-well problem can be expanded in terms of the stationary states

$$u_l(\rho) = \sum_\lambda A_{\lambda l} X_{\lambda l}(\rho) \tag{A.6}$$

To find the expansion coefficients $A_{\lambda l}$ which depend on the energy E of the

actual wave function, we multiply Eq. (A.1) by $X_{\lambda l}$ and multiply the same radial equation for $X_{\lambda l}$ by u_l, subtract, and integrate. The result is

$$A_{\lambda l} \equiv \int_0^{R_0} X_{\lambda l} u_l \, dr = \frac{\hbar^2}{2m} \frac{1}{E_{\lambda l} - E} \left[X_{\lambda l} \frac{1}{r} \left(r \frac{du_l}{dr} - b_l u_l \right) \right]_{r=R_0} \tag{A.7}$$

Using (A.7) in (A.6), we have the actual wave function u_l at any point $r(\leqslant R_0)$ in terms of the value and derivative of u_l at $r = R_0$. Evaluating (A.6) at $r = R_0$, we find

$$u_l(KR_0) = f_l \left(r \frac{du_l}{dr} - b_l u_l \right) \Big|_{r=R_0} \tag{A.8}$$

where

$$f_l \equiv \sum_\lambda \frac{\gamma_{\lambda l}^2}{E_{\lambda l} - E} \tag{A.9}$$

$$\gamma_{\lambda l}^2 \equiv \frac{\hbar^2}{2mR_0} X_{\lambda l}^2(K_{\lambda l} R_0) \tag{A.10}$$

The surface quantity f_l can be directly connected to the collision matrix. Outside the square well the radial wave function is written

$$u_l = I_l - U_l O_l \tag{A.11}$$

where I_l and O_l are incoming and outgoing radial waves and U_l is the collision function. By matching the logarithmic derivative of (A.11) with the logarithmic derivative of the interval wave function (A.8) at $r = R_0$, we find

$$U_l = \frac{I_l}{O_l} \frac{1 - (S_l - iP_l) f_l}{1 - (S_l + iP_l) f_l} \tag{A.12}$$

[see Eq. (103)]. The calculation of scattering and absorption cross sections follows from the use of (A.12) in

$$\sigma_{\text{scatt}} \equiv \frac{\pi}{k^2} \sum_l (2l + 1) \mid 1 - U_l \mid^2 \tag{A.13}$$

$$\sigma_{\text{abs}} \equiv \frac{\pi}{k^2} \sum_l (2l + 1)(1 - \mid U_l \mid^2) \tag{A.14}$$

For real square wells f_l is real, and we have no absorption.

The $\gamma_{\lambda c}^2$ of Eq. (A.10) are the reduced width of the single-particle levels. Their direct evaluation yields

$$\gamma_{\lambda l}^2 = \frac{\hbar^2}{m R_0^2} \left[1 - \frac{j_{l-1}(K_{\lambda l} R_0) j_{l+1}(K_{\lambda l} R_0)}{j_l^2(K_{\lambda l} R_0)} \right]^{-1} \tag{A.15}$$

where $\hbar^2/mR_0^2$ is the usual single-particle reduced width used in nuclear physics and the square bracket is a correction factor. The correction factor can be made equal to unity with a suitable choice of the boundary-condition number. The choice is one which makes $j_{l-1}(K_{\lambda l}R_0)$ vanish and can be found from the following recursion formula for spherical Bessel functions:

$$\frac{\rho}{2l+1} j_{l-1} = (l+1) j_l + \rho \frac{dj_l}{d\rho}$$
$$= (l+1) j_l + (b_l - 1) j_l \tag{A.16}$$

The desired choice of b_l is therefore $b_l = -l$. With it each $\gamma_{\lambda l}^2$ is equal to $\hbar^2/mR_0^2$ for all partial waves. This choice of boundary-condition number is also physical in another sense[19]; it makes the Breit–Wigner formula into an accurate approximation to the scattering cross section by the real square well when the energy is close to a low-energy resonance $E_{\lambda l}$. The above resonance analysis is useful in the description of the scattering of particles by a real square well and clearly exhibits the resonances of the problem.

The size resonances of the optical-model strength function are found by generalizing the above results to those for a complex square well. From the radial equation (A.1) we see that replacing V_0 by $V_0 + iW_0$ is equivalent to evaluating the solution for a real square well at the complex energy $E \to E - iW_0$. This is true only for the square well in which the imaginary part of the potential has no radial dependence. We therefore find

$$f_l = \sum_\lambda \frac{\gamma_{\lambda l}^2}{E_{\lambda l} - E + iW_0} \tag{A.17}$$

which is the result used in Section 2.3 in the discussion of size resonances.

The spacing of the size resonances is given, very nearly, by the positions of the resonances in the real square well. For s waves we have the following characteristic energies:

$$E_{\lambda 0} = \frac{\hbar^2}{2m} K_{\lambda 0}^2 = \frac{\hbar^2}{2mR_0^2} \pi^2 (\lambda + \tfrac{1}{2})^2 \tag{A.18}$$

measured from the bottom of the square well. The spacing d between adjacent resonances is

$$d \equiv E_{\lambda 0} - E_{\lambda-1,0} = \frac{\hbar^2}{mR_0^2} \pi^2 \lambda \tag{A.19}$$

If the resonances occur at zero energy in a square well of depth V_0, we have

$$\frac{E_{\lambda 0} + E_{\lambda-1,0}}{2} = V_0 \approx \frac{\hbar^2}{mR_0^2} \pi^2 \lambda^2 \tag{A.20}$$

Combining (A.19) and (A.20), we obtain

$$d = \left(\frac{\hbar^2 \pi V_0}{m R_0^2}\right)^{1/2} \tag{A.21}$$

For other partial waves the spacing of resonances is similar (see Fig. 5).

APPENDIX B. EFFECT OF FINITE AVERAGING INTERVAL

An estimate of the energy interval required to obtain true average cross sections can be made by calculating the fluctuations about the average. The fluctuations of the compound-nucleus cross sections in the case of overlapping levels ($\Gamma_\lambda > D$), as discussed in the text (Sections 3.2 and 4), arise from the reaction theory through the same random-sign fluctuations of the $\Gamma_{\lambda c}^{1/2}$ used in the derivation of average cross sections. Thus Eq. (88) is a complex amplitude

$$U_{cc'} \alpha \sum_\lambda \frac{\Gamma_{\lambda c}^{1/2} \Gamma_{\lambda c'}^{1/2}}{E_\lambda - E - (i/2)\,\Gamma_\lambda} \equiv u_{cc'} + i v_{cc'} \tag{B.1}$$

whose average square $\langle u_{cc'}^2 \rangle + \langle v_{cc'}^2 \rangle$ was evaluated by Eq. (98). If the numerators of Eq. (B.1) have random signs and if $u_{cc'}$ and $v_{cc'}$ then have Gaussian distributions about the average value zero

$$\langle u_{cc'} \rangle = \langle v_{cc'} \rangle = 0 \tag{B.2}$$

then both $u_{cc'}^2$ and $v_{cc'}^2$ have chi-squared distributions with one degree of freedom. To find the probability distribution of $\langle | U_{cc'} |^2 \rangle$, we must first find the relative values of $\langle u_{cc'}^2 \rangle$ and $\langle v_{cc'}^2 \rangle$. From (B.1) we have

$$v_{cc'}^2 = \tfrac{1}{4} \sum_{\lambda\lambda'} \frac{\Gamma_{\lambda c}^{1/2} \Gamma_{\lambda' c'}^{1/2} \Gamma_{\lambda c'}^{1/2} \Gamma_{\lambda c'}^{1/2} \Gamma_\lambda \Gamma_{\lambda'}}{[(E_\lambda - E)^2 + \frac{1}{4}\Gamma_\lambda^2][(E_{\lambda'} - E)^2 + \frac{1}{4}\Gamma_{\lambda'}^2]} \tag{B.3}$$

To obtain the average of (B.3) over an energy interval $\delta (\delta \gg \Gamma_\lambda, D)$, we again restrict the sum in (B.3) to the levels in δ, multiply by δ^{-1}, and integrate over E_λ from $-\infty$ to $+\infty$. As in Eq. (97), the contribution of the diagonal terms ($\lambda = \lambda'$) in Eq. (B.3) to the integral is larger than the contribution of the cross-product terms ($\lambda \neq \lambda'$). The former can be integrated directly and yields

$$\begin{aligned} \langle v_{cc'}^2 \rangle &= \frac{\delta}{D} \frac{\pi}{\delta} \frac{\Gamma_{\lambda c} \Gamma_{\lambda c'}}{\Gamma_\lambda} \\ &= \tfrac{1}{2} \langle | U_{cc'} |^2 \rangle \\ &= \langle u_{cc'}^2 \rangle \end{aligned} \tag{B.4}$$

The equality of $\langle v_{cc'}^2 \rangle$ and $\langle u_{cc'}^2 \rangle$ means that $U_{cc'}^2$, which is the sum of the two, has a chi-squared with two degrees of freedom.

It should be noted that, if the total level width Γ_λ is not much larger than the average level spacing, then the fluctuations of $u_{cc'}^2$ and $v_{cc'}^2$ are not independent and the distribution of $|U_{cc'}|^2$ becomes closer to that of a chi-squared distribution with one degree of freedom. The study of the fluctuations of the $C^{12}(C^{12}, \alpha)\,Ne^{20}$ reactions[43] showed no evidence of such an effect.

The averaging interval ΔE required to obtain true average cross sections must be considerably larger than the full width Γ_λ of the compound levels. In the discussion of fluctuations the ratio $\Delta E/\pi\Gamma_\lambda$ is referred to as the sample size S. The sample size S together with the basic distribution law (an exponential distribution, i.e., a chi-squared distribution with two degrees of freedom) of the fluctuating cross sections permits a quantitative estimate of the effect of the finite size of the averaging interval.

To distinguish finite-sample averages of cross sections from true averages, we shall write the former as $\langle \sigma \rangle_S$ and the latter as $\bar{\sigma}$ (or, equivalently, $\langle \sigma \rangle$), and we use the generic symbol σ to denote either $\sigma_{cc'}$ or $d\sigma_{cc'}/d\Omega$. In the case of overlapping levels, each fluctuating cross section may be written as

$$\sigma = \sum_j C_j x_j \tag{B.5}$$

where the x_j is a fluctuating quantity whose probability distribution $P(x_j)$ is

$$P(x_j) = e^{-x_j} \tag{B.6}$$

and the C_j are weight coefficients calculated from the statistical theory of average cross sections. For example, if σ is the integrated cross section $\sigma_{cc'}$, then the index j of Eq. (B.5) runs over all combinations of the quantum numbers $J\Pi sls'l'$ and the value of C_j for each value of j is given by the corresponding term on the right side of Eq. (12) in the text. If σ is the differential cross section of the $C^{12}(C^{12}, \alpha)\,Ne^{20}$ reaction to the ground state of Ne^{20}, then the index j contains only one term and the corresponding value of C_j is given by the right-hand side of Eq. (46). For more general differential cross sections, the index j runs over all combinations of s, m_s, s', and $m_{s'}$, and the value of C_j is then given by Eq. (47) of the text.

The sample average of σ is

$$\langle \sigma \rangle_s = s^{-1} \sum_{i=1}^{S} \sum_j C_j x_{ij} \tag{B.7}$$

where each x_{ij} has the exponential distribution in (B.6). Tke corresponding true averages of σ are then

$$\langle\langle\sigma\rangle_S\rangle = \bar{\sigma} = \sum_j C_j \tag{B.8}$$

in agreement with Eq. (12) or Eq. (46) or both.

The distribution of $\langle\sigma\rangle_S$ rapidly approaches a normal distribution as S becomes large. For example, if the sum over j contains only one term $C_j = C$, then $\langle\sigma\rangle_S$ is a chi-squared distribution of $2S$ degrees of freedom. This distribution has its maximum at $(S - 1)\, C/S$, although the true average value of $\langle\sigma\rangle_S$ is still C. Moreover, if we choose a probable error so that the probability of finding $\langle\sigma\rangle_S/\bar{\sigma}$ within $1 + \epsilon_S$ is 50%, then

$$\epsilon_S \equiv d_S S^{-1/2} \tag{B.9}$$

where $d_\infty = 0.6745$ (the value for a normal distribution) and $d_{10} = 0.6714$ and $d_{50} = 0.6739$. Thus, for even fairly small values of the sample size, the tendency toward the normal distribution enables one to use the usual estimate of the probable error.

For cross sections, Eq. (B.5) with more than one weight coefficient C_j, we estimate the probable error of $\langle\sigma\rangle_S$ by means of the second moment of the distribution about its mean value (B.8). The result is

$$\epsilon_S \approx 0.6745 S^{-1/2} \frac{(\sum_j C_j^2)^{1/2}}{\sum_j C_j} \tag{B.10}$$

The probable errors quoted in Section 3.2 are based on Eq. (B.10) with weight coefficients obtained from the calculated average cross sections and with sample-size values from the fluctuation analysis.[43]

REFERENCES

1. H. A. Bethe, *Rev. Mod. Phys.* **9**:69 (1937).
2. V. F. Weisskopf, *Phys. Rev.* **52**:295 (1937).
3. V. F. Weisskopf and D. H. Ewing, *Phys. Rev.* **57**:472 (1940).
4. N. Bohr, *Nature* **137**:344 (1936).
   N. Bohr and F. Kalckar, *Danske Videnskab. Selskab Mat. Fys. Medd.* **14**:10 (1937).
5. G. Breit and E. P. Wigner, *Phys. Rev.* **49**:519 (1936).
6. T. Bjerge and C. H. Westcott, *Proc. Roy. Soc. (London), Ser.* **A150**:709 (1935).
   P. Moon and J. Tillman, *Nature* **135**:904 (1935).
   L. Szilard, *Nature* **136**:849 and 950 (1935).
   E. Fermi and E. Amaldi, *Ric. Sci.* **A6**:544 (1935).
   O. Frisch and G. Placzek, *Nature* **137**:357 (1936).
   L. R. Hafstad and M. A. Tuve, *Phys. Rev.* **48**:306 (1935).
7. J. Blatt and V. F. Weisskopf, "Theoretical Nuclear Physics," John Wiley and Sons, Inc., New York (1952).
8. T. D. Newton, *Can. J. Phys.* **34**:804 (1956) and further references given in Section 3.3.

9. P. C. Gugelot, *Phys. Rev.* **93**:425 (1954).
R. M. Eisberg, G. Igo and H. E. Wegner, *Phys. Rev.* **100**:1309 (1955).
Other early references can be found in the review article by K. J. Le Couteur *in* "Nuclear Reactions" (P. M. Endt and M. Demeur eds.) North-Holland Publishing Company, Amsterdam (1959).
10. E. Paul and R. L. Clarke, *Can. J. Phys.* **31**:267 (1953).
11. S. N. Ghoshal, *Phys. Rev.* **80**:939 (1950).
12. A very thorough survey of nuclear temperatures can be found in the review article by D. Bodansky, *Ann. Rev. Nucl. Sci.* **12**:79 (1962).
13. N. Poffe, G. Albouy, and M. Gusakow, *J. Phys. Radium* **23**:213A (1962).
14. "The AECL Study for an Intense Neutron Generator" (G. A. Bartholomew and P. R. Tunnicliffe, *At. Energy Can. Ltd., AECL Report* 2600 (1966).
15. N. Austern, *in* "Fast Neutron Physics" (J. B. Marion and J. L. Fowler, eds.) J. Wiley and Sons, Inc., New York (1963).
W. Tobocman, "Theory of Direct Nuclear Reactions," Oxford University Press, London (1961).
16. W. Hauser and H. Feshbach, *Phys. Rev.* **87**:366 (1952).
An important earlier contribution to the same problem was made by L. Wolfenstein, *Phys. Rev.* **82**:690 (1951).
17. R. G. Thomas, *Phys. Rev.* **97**:224 (1955).
18. A. M. Lane and R. G. Thomas, *Rev. Mod. Phys.* **30**:257 (1958).
19. E. W. Vogt, *Rev. Mod. Phys.* **34**:723 (1962).
20. M. H. Hull and G. Breit, "Handbuch der Physik," Vol. XLI, 1, p. 408, Springer-Verlag, Berlin (1959). These authors discuss the theory of Coulomb functions and provide a list of tables.
21. J. M. Blatt and L. C. Biedenharn, *Rev. Mod. Phys.* **24**:528 (1952).
22. L. C. Biedenharn, J. M. Blatt, and M. E. Rose, *Rev. Mod. Phys.* **24**:249 (1952).
23. A "Directory to Tables and Reviews of Angular Momentum and Angular Correlation Coefficients" has recently been prepared by K. Way and F. W. Hurley, Oak Ridge National Laboratory, Nuclear Data Sec. A1:473–86, July (1966).
24. R. Huby, *Proc. Phys. Soc. (London)* **A67**:1103 (1954).
25. T. Ericson and T. Mayer-Kuckuk, *Ann. Rev. Nucl. Sci.* **16** (1966), a recent review of the work on cross-section fluctuations.
26. G. R. Satchler, *in* "Proceedings of the International Conference on Nuclear Physics, Gatlinburg" (R. L. Becker, ed.) Academic Press, New York (1967).
P. E. Hodgson, *in* "Comptes Rendues du Congrès International de Physique Nucléaire" (P. Gugenberger, ed.) Éditions du Centre National de la Recherche Scientifique, Paris (1964).
27. K. McVoy, *Phys. Letters*, **17**:42 (1965). See also *Ann. Phys.* **43**:91 (1967).
28. E. W. Vogt, H. Reeves, and G. Michaud, *Phys. Letters* **19**:570 (1965). See also Ref. 19. The earliest treatment of nuclear reflections was given by D. C. Peaslee, *Nucl. Phys.* **3**:255 (1957).
29. N. Austern, A. Prakash, and R. M. Drisko, *Ann. Phys. (N.Y.)* **39**:253 (1966).
30. H. Feshbach, C. E. Porter, and V. F. Weisskopf, *Phys. Rev.* **96**:448 (1954) established the foundations of the optical model.
31. Weisskopf and Friedman, *in* "Niels Bohr and the Development of Physics," McGraw-Hill, New York (1955).
32. C. E. Porter, *Phys. Rev.* **100**:935 (1955). See also
T. K. Krueger and B. Margolis, *Nucl. Phys.* **28**:578 (1961).
33. B. Margolis and E. S. Troubetskoy, *Phys. Rev.* **106**:105 (1957).

34. D. J. Hughes, R. L. Zimmermann, and R. E. Chrien, *Phys. Rev. Letters* **1**:461 (1958).
35. H. W. Newson, *in* "Proceedings of the International on the Study of Nuclear Structure with Neutrons" (M. Neve de Mevergnies, P. Van Assche, and J. Vervier, eds.) North Holland Publishing Company, Amsterdam (1966).
36. Landolt-Bornstein, Zahlenwerte und Funktionen aus Physik, Chemie, Astronomie, Geophysik, und Technik, Group I, Vol. I. "Energy Levels of Nuclei: A = 5 to A = 257," Springer-Verlag, Berlin (1961).
37. E. W. Vogt, *Phys. Letters* **7**:61 (1963).
38. A. Ebel and C. Goodman, *Phys. Rev.* **93**:197 (1954).
39. H. C. Martin, B. C. Diven, and R. F. Taschek, *Phys. Rev.* **93**:199 (1954).
40. W. G. Cross, D. McPherson, and E. W. Vogt, *to be published.*
41. E. W. Vogt, D. M. McPherson, J. Kuehner, and E. Almqvist, *Phys. Rev.* **136**:B99 (1964). See also
J. Bondorff and R. Leachman, *Kgl. Danske Videnskab. Selskab, Mat. Fys. Medd.* **34**(10) (1965).
42. M. L. Halbert, F. E. Durham, C. D. Moak, and A. Zucker, *to be published.*
M. L. Halbert, F. E. Durham, and A. van der Woude, *to be published.*
43. E. Almqvist, J. A. Kuehner, D. McPherson, and E. W. Vogt, *Phys. Rev.* **136**:B84 (1964).
44. E. Almqvist, J. A. Kuehner, D. McPherson, E. W. Vogt, and J. D. Prentice, *in* "Proceedings of the Third Conference on Reactions between Complex Nuclei, Asilomar, California" (A. Ghiorso, R. M. Diamond, and H. E. Conzett, eds.) University of California Press (1963).
45. V. E. Viola, H. M. Blann, and T. D. Thomas, *in* "Proceedings of the Second Conference on Reactions between Complex Nuclei, 1960" (A. Zucker, F. T. Howard, and E. C. Halbert, eds.) J. Wiley and Sons, Inc., New York (1960), p. 224.
46. N. MacDonald, *Nucl. Phys.* **33**:110 (1961).
47. A review of early work on level densities can be found in an article by K. J. Le Couteur, *in* "Nuclear Reactions" (P. M. Endt and M. Demeur, eds.) North Holland Publishing Company, Amsterdam (1959).
48. A. G. W. Cameron, *Can. J. Phys.* **36**:1040 (1958).
49. T. Ericson, *Advan. Phys.* **9**:425 (1960).
50. J. M. B. Lang and K. J. Le Couteur, *Proc. Phys. Soc. (London)* **A67**:586 (1954).
51. H. E. Gove and C. Broude, *in* "Proceedings of the Second Conference on Reactions between Complex Nuclei, 1960" (A. Zucker, F. T. Howard, and E. C. Halbert, eds.) John Wiley and Sons, Inc., New York (1960), p. 57.
I. Kh. Lemberg, *ibid.*, p. 112.
52. D. W. Lang, *Nucl. Phys.* **77**:545 (1965).
53. B. Margolis, *Phys. Rev.* **88**:327 (1952).
54. H. Feshbach, *in* "Statistical Aspects of the Nucleus," Brookhaven Conference Report *BNL* 333 (C.21) (1955).
55. D. M. Van Patter, N. Nath, S. M. Shafroth, S. S. Malik, and A. Rothman, *Phys. Rev.* **128**:1246 (1962). Similar measurements and calculations for some simple (p, p') reactions can be found, e.g., in a paper by
R. K. Mohindra and D. M. Van Patter, *Phys. Rev.* **139**:B274 (1965).
56. A. T. G. Ferguson, *in* "Proceedings of the International Conference on the Study of Nuclear Structure with Neutrons" (M. Neve de Mevergnies, P. Van Assche, and J. Vervier, eds.) North Holland Publishing Company, Amsterdam (1966).
57. A. V. Malyshev, *in* "Proceedings of the International Conference on the Study of Nuclear Structure with Neutrons" (M. Neve de Mevergnies, P. Van Assche, and J. Vervier, eds.) North Holland Publishing Company, Amsterdam (1966).

58. P. A. Moldauer, *Rev. Mod. Physics* **36**:1079 (1964).
59. G. R. Satchler, *Phys. Letters* **7**:55 (1963).
60. A. K. Chaubey and M. L. Sehgal, *Phys.* **152**:1055 (1966).
61. M. L. Sehgal, *Phys. Rev.* **128**:761 (1962).
62. T. D. Thomas, *Nucl. Phys.* **53**:577 (1963).
63. R. E. Brown, J. S. Blair, D. Bodansky, N. Cue, and C. D. Kavaloski, *Phys. Rev.* **138**:B1394 (1965). See also
R. Vandenbosch, J. C. Norman, and C. J. Bishop, *Phys. Rev.* **158**:887 (1967) for an analysis of the Si^{28} (He^4, O^{16}) O^{16} reaction.
64. D. C. Williams and T. D. Thomas, *Nucl. Phys.* **A92**:1 (1967).
65. R. A. Esterlund and B. D. Pate, *Nucl. Phys.* **69**:401 (1965).
66. D. G. Sarentites, *Nucl. Phys.* **A93**:567 (1967) and *Nucl. Phys.* **A93**:576 (1967).
67. See many papers presented at the Second and Third Conferences on Reactions between Complex Nuclei, Refs. 45 and 46.
68. R. van den Bosch, *in* "Proceedings of the International Conference on Nuclear Physics, Gatlinburg" (R. L. Becker, ed.) Academic Press, Inc., New York (1967).
69. W. R. Gibbs, P. Fessenden, and R. B. Leachman, *in* "Proceedings of the International Conference on Nuclear Physics, Gatlinburg" (R. L. Becker, ed.) Academic Press, Inc., New York (1967).
70. V. Bobyr, M. Corti, G. M. Marcazzan, L. Milazzo-Colli, and M. Milazzo, *in* "Proceedings of the International Conference on Nuclear Physics, Gatlinburg" (R. L. Becker, ed.) Academic Press, Inc., New York (1967).
71. R. B. Leachmann, *in* "Proceedings of the International Conference on Nuclear Physics, Gatlinburg" (R. L. Becker, ed.) Academic Press, Inc., New York (1967).
72. R. L. Clarke and W. G. Cross, *Nucl. Phys.* **53**:177 (1964).
73. A. M. Lane and D. Robson, *Phys. Rev.* **151**:774 (1966).
74. C. Bloch, *Nucl. Phys.* **4**:503 (1957).
75. E. P. Wigner and L. Eisenbud, *Phys. Rev.* **72**:29 (1947).
76. P. L. Kapur and R. E. Peierls, *Proc. Roy. Soc. (London)* **A166**:277 (1938).
77. G. E. Brown and C. T. De Dominicis, *Proc. Phys. Soc. (London)* **A72**:70 (1958).
78. M. Sano, S. Yoshida, and T. Terasawa, *Nucl. Phys.* **6**:20 (1958).
79. H. Feshbach, *Ann. Phys.* **5**:357 (1958); *ibid.* **19**:287 (1962).
R. Lemmer and C. Shakin, *Ann. Phys.* **27**:13 (1964).
80. L. Rodberg, *Phys. Rev.* **124**:210 (1961).
81. W. M. MacDonald, *Nucl. Phys.* **54**:393 (1964); *ibid.* **56**:636 and 647 (1964); see also W. MacDonald and A. Mekjian, *Phys. Rev.* **160**:730 (1967).
82. A. Herzenberg, K. L. Kwok, and F. Mandl, *Proc. Phys. Soc. (London)* **84**:477 (1964).
83. J. Humblet and L. Rosenfeld, *Nucl. Phys.* **26**:529 (1961) and a series of subsequent papers in the same journal.
84. J. B. French, S. Iwao, and E. W. Vogt, *Phys. Rev.* **122**:1248 (1961).
85. A. M. Lane, R. G. Thomas, and E. P. Wigner, *Phys. Rev.* **98**:693 (1955).
86. See various papers in "Proceedings of the International on the Study of Nuclear Structure with Neutrons" (M. Neve de Mevergnies, P. Van Assche, and J. Vervier, eds.) North Holland Publishing Company, Amsterdam (1966).
87. C. E. Porter and R. G. Thomas, *Phys. Rev.* **104**:483 (1956).
88. C. E. Porter, *Rev. Mod. Phys.* **36**:1094 (1964).
89. P. A. Moldauer, *Phys. Rev.* **157**:907 (1967).
90. H. Feshbach, *in* "Proceedings of the International Conference on Nuclear Physics, Gatlinburg" (R. L. Becker, ed.) Academic Press, Inc., New York (1967).
91. J. J. Griffin, *Phys. Rev. Letters* **17**:478 (1966).

THREE-PARTICLE SCATTERING A REVIEW OF RECENT WORK ON THE NONRELATIVISTIC THEORY*

Ian Duck

1. INTRODUCTION

This review is intended to be an exposition of recent work in three-particle scattering. Our discussion is restricted to the nonrelativistic regime—in fact almost exclusively to the three-nucleon problem—and we emphasize comparison with experiment rather than the formalism itself. We shall meet the three-body bound-state problem only coincidentally as it occurs in our discussion of scattering. The major portion of this article will be a discussion of recent successful calculations of low-energy neutron–deuteron elastic and inelastic scattering. In this discussion we shall follow most closely the elegant and lucid work of Amado and his co-workers. Following the discussion of Amado's work[1–5] we turn to the formal, general work of Faddeév,[6–9] which is based upon the original discussions of rearrangement collisions due to Ekstein[10] and Gerjuoy.[11] Faddeév's equations reduce to those of Amado when we make special assumptions on the two-particle interaction following Lovelace,[12] but they also provide a basis for a more detailed treatment of the problem using unrestricted two-particle interactions. Having obtained Faddeév's equations, we next use them in a few applications of special interest and discuss: Hetherington and Schick's work[13–15] on rescattering corrections in kaon–deuteron (K–D) scattering; Lovelace and Phillips' work[16] on n–D scattering; three-meson scattering in a pseudo-relativistic generalization[17]; and three-particle correlation energies in nuclear matter.[18–20]

The theoretical work on three-particle scattering divides naturally into two eras. The historical era is characterized by Born approximation calculations, variation calculations, high-energy impulse approximations, and, generally, attempts to treat the two-particle interactions exactly, at the

* Work supported in part by U.S. Atomic Energy Commission.

expense of ignoring the three-particle aspects of the problem except perhaps through a bound-state target wave function. The modern era, dating from the work of Faddeév and Amado and others, is concerned with an exact treatment of the three-particle aspects of the problem, which are made tractable only by the sacrifice of some fidelity in the two-particle interactions. This review will be devoted to work of the modern era. For a summary of the earlier work we refer to Verde's Handbuch der Physik article[21] and to Schick's more recent review article on rescattering corrections in three-body scattering[22] and comprehensive articles on the impulse approximation in nucleon–deuteron scattering by Feldman and Kowalski[23] and by Koehler and Mann.[24]

We have confined our attention to the Faddeév theory, which is an exact theory, equivalent in all respects to the Schrödinger equation with appropriate boundary conditions; and to the Amado theory, which is derivable from it, which treats the three-particle aspects exactly and can be improved in a systematic way to include the two-particle scattering amplitude with arbitrary precision, and which, furthermore, has the advantage of simplicity. We have excluded entirely any discussion of a number of treatments which are approximate from the outset and do not provide the basis for a systematic, fundamental, and general theory.

Some readers might wish for a profound reason for studying three-particle scattering beyond the intrinsic interest of solving the Schrödinger equation for a situation a great deal more complicated than usual. There certainly have been such reasons. The hope of extracting the neutron–neutron scattering length prompted much of the inelastic neutron–deuteron scattering. Some vague hope of discovering effects explicable only through a three-body force underlies some of the work. A determination to test proposed two-particle potentials has led to exhaustive variational calculations of three-particle bound states. It seems to us that most of these profound hopes are forlorn and that for a long time to come uncertainties in three-particle calculations and experiments are going to preclude any detailed tests of the two-particle interaction. However, it also seems clear that the challenge of the three-body problem *per se* is quite intriguing enough, and its further study will increase our knowledge of the structure of scattering amplitudes and is even now leading to methods useful in the relativistic theory of strong interactions.

1.1 Resumé of Two-Particle Scattering Theory

Let us briefly review the theory of two-particle scattering before we turn to three-particle scattering. Schrödinger's equation for two particles interacting through a potential V, which depends only on their separation,

can be separated into a trivial equation for the center-of-mass (*c-m*) motion and a Schrödinger equation for the relative motion of the two particles, which is the same as that for the scattering of a single particle by a fixed potential V. Let this single particle have mass m and momentum $\mathbf{k}$ (with $\hbar = 1$). We shall assume that the potential is spherically symmetric, independent of spin, and of finite range (which excludes only Coulomb potentials of practical interest). Choose the origin of coordinates at the center of the scattering potential with the z axis parallel to $\mathbf{k}$. Shrödinger's equation for the scattering wave function ψ is

$$\left[-\frac{\nabla^2}{2m} + V(r)\right] \psi_{\mathbf{k}}(\mathbf{r}) = \frac{k^2}{2m} \psi_{\mathbf{k}}(\mathbf{r}) \tag{1}$$

The solution which satisfies the asymptotic conditions that it should correspond to an incident plane wave with momentum $\mathbf{k}$ plus only outgoing spherical waves due to the scattering has the form at large distances r

$$\psi_{\mathbf{k}}(\mathbf{r}) = e^{ikz} + f_k(\theta) \frac{e^{ikr}}{r} \tag{2}$$

The scattering amplitude $f_k(\theta)$ is a function of the scattering angle θ between $\mathbf{r}$ and $\hat{z}$ and can be expressed in terms of the individual partial-wave scattering amplitudes $f_L(k)$ for the partial wave with orbital angular momentum L by

$$f_k(\theta) = \sum_{L=0}^{\infty} (2L + 1) f_L(k) P_L(\cos \theta) \tag{3}$$

The partial-wave scattering amplitudes $f_L(k)$ in turn can be expressed in terms of the partial-wave phase shifts $\delta_L(k)$ by

$$f_L(k) = e^{i\delta_L(k)} \sin \delta_L(k)/k \tag{4}$$

The differential cross section for the scattering of a particle through an angle θ is

$$\frac{d\sigma}{d\Omega} = |f_K(\theta)|^2 \tag{5}$$

and the total cross section σ for the elastic scattering of a particle of momentum $\mathbf{k}$ by a short-range potential $V(r)$ is

$$\sigma = \frac{4\pi}{k^2} \sum_{L=0}^{\infty} (2L + 1) \sin^2 \delta_L \tag{6}$$

We can note some simple properties of the phase shifts. First of all, at threshold (i.e., as $k \to 0$, or the bombarding energy of the incident particle goes to zero) the phase shifts satisfy

$$\tan \delta_L(k) \to -(ka_L)^{2L+1} \tag{7}$$

where a_L is a constant. This threshold behavior is simply a property of the centrifugal barrier. Next, let us recall the scattering-length effective-range approximation for the S-wave ($L = 0$) phase shift, valid for k sufficiently small, which states that

$$\cot \delta_0(k) = -\frac{1}{ka_0} + \frac{1}{2} r_0 k \tag{8}$$

in terms of the scattering length a_0 and effective range r_0. For a repulsive potential the phase shift starts at zero and goes negative, and the scattering length is positive. For an attractive potential which is too weak to have a bound state, the phase shift starts at zero and goes positive, requiring a negative scattering length. If we imagine the strength of the attractive potential to increase until there is almost a zero-energy bound state, then the scattering length goes to $-\infty$ and switches to $+\infty$ as the potential is increased enough to just bind the first bound state. Thereafter the scattering length decreases to zero, goes negative, and repeats the cycle as the strength of the potential is increased enough to produce a second bound state. The zero-energy phase shift, meanwhile, skips from zero to $\pi/2$ when there is a zero-energy bound state, to π when there is one bound state, to 2π when there are two bound states, etc. At high energies the phase shift decreases to zero. These properties of the scattering length have a graphic interpretation in terms of the zero-energy wave function outside the interaction potential. We refer to the textbook of Blatt and Weisskopf[25] for further details. The behavior of the zero-energy phase shift is summarized in Levinson's theorem

$$\delta_L(0) - \delta_L(\infty) = N_L \pi \tag{9}$$

where N_L is the number of bound states in the particular partial wave and $\delta_L(\infty)$ is zero.

The $^1S_0$ and $^3S_1$ neutron–proton phase shifts exemplify the above discussion with[26]

$$a_0(^3S_1) = 5.41 \text{ fm} \qquad \text{and} \qquad a_0(^1S_0) = -23.78 \text{ fm}$$

corresponding to the facts that the deuteron is the one bound state in the $^3S_1$ partial wave and that there is almost a bound state in the $^1S_0$ partial wave so the $^1S_0$ scattering length is large and negative. The effective ranges for neutron–proton S-wave scattering are[26]

$$r_0(^3S_1) = 1.78 \text{ fm} \qquad \text{and} \qquad r_0(^1S_0) = 2.67 \text{ fm}$$

So far we have only parametrized the scattering by the phase shifts but have not related the δ_L to the scattering potential. This can be done by solving Schrödinger's equation (1) for the individual partial-wave radial wave function $\psi_L(k, r)$ which, for S waves, e.g., has the asymptotic form (outside the scattering potential)

$$\psi_0(k, r) = e^{i\delta_0(k)} \sin (kr + \delta_0)/kr \tag{10}$$

and, by matching logarithmic derivatives of the actual radial wave function and the asymptotic radial wave function at some point outside the potential, we could determine the phase shift δ_0. Alternatively, it is possible to recast the Schrödinger equation into an integral equation—the Lippmann–Schwinger equation—directly for the quantity of interest, the partial-wave scattering amplitudes $f_L(k)$. The Lippmann–Schwinger integral equation is equivalent to the Schrödinger equation plus a prescribed asymptotic behavior for the wave function, so it cannot offer any essential advantages over the direct use of the differential equation, but it does have great formal advantages which will become clear as we proceed. Furthermore, we shall need these Lippmann–Schwinger techniques to follow Faddeév's discussion of three-particle scattering.

If we rewrite Eq. (1) as

$$(H_0 - E_k)\psi_k = -V\psi_k \tag{11}$$

with $E_k = k^2/2m$ and $H_0 = -\nabla^2/2m$, then we can obtain a formal solution by operator manipulations as

$$\psi_k = \phi_k - \frac{1}{H_0 - E_k} V\psi_k \tag{12}$$

where ϕ_k is a solution of the homogeneous equation with $V = 0$,

$$(H_0 - E_k)\phi_k = 0 \tag{13}$$

The operator manipulations are given meaning by inserting a complete set of momentum eigenstates which diagonalize H_0. The momentum states with momentum $\mathbf{p}$

$$\langle \mathbf{r} \mid \mathbf{p} \rangle = e^{i\mathbf{p}\cdot\mathbf{r}} \tag{14}$$

are orthonormal over all space

$$\langle \mathbf{p}' \mid \mathbf{p} \rangle = \int d^3r\, e^{i(\mathbf{p}-\mathbf{p}')\cdot\mathbf{r}} = (2\pi)^3\, \delta^3(\mathbf{p} - \mathbf{p}') \tag{15}$$

and are complete

$$\langle \mathbf{r} \mid \mathbf{p} \rangle \langle \mathbf{p} \mid \mathbf{r}' \rangle = \int \frac{d^3p}{(2\pi)^3} e^{i\mathbf{p}\cdot(\mathbf{r}-\mathbf{r}')} = \delta^3(\mathbf{r} - \mathbf{r}') \tag{16}$$

Then the second term in Eq. (12) becomes

$$\begin{aligned} -(H_0 - E_k)^{-1} V\psi_k &= -(H_0 - E_k)^{-1} \langle \mathbf{r} \mid \mathbf{p} \rangle \langle \mathbf{p} \mid V\psi_k \rangle \\ &= -\int \frac{d^3p}{(2\pi)^3} \frac{2m}{p^2 - k^2} e^{i\mathbf{p}\cdot(\mathbf{r}-\mathbf{r}')} V(\mathbf{r}') \psi_k(\mathbf{r}') \, d^3r' \end{aligned} \tag{17}$$

We have given the operator manipulations meaning, but to completely specify the solution $\psi_k(\mathbf{r})$ we must specify ϕ_k, the solution of the homogeneous ($V = 0$) equation, and also we must specify how to treat the singularity in the integrand at $p^2 = k^2$. If we are looking for negative-energy bound states, ϕ would be zero and there would be no singularity in the integrand since $k^2 < 0$ and $p^2 \geqslant 0$. If we are looking for a positive-energy solution with the asymptotic form, Eq. (2), of an incident plane wave and outgoing spherical waves, we shall need

$$\phi_k(\mathbf{r}) = e^{ikz} \tag{18}$$

and the prescription for treating the singularities in the integrand is that we give k^2 a small positive imaginary part which eventually approaches zero. We can get this result from Eq. (17) by examining the asymptotic form as $r \to \infty$. Then (17) becomes

$$\begin{aligned} &-2m \int \frac{d^3p}{(2\pi)^3} \frac{1}{p^2 - k^2} e^{i\mathbf{p}\cdot(\mathbf{r}-\mathbf{r}')} V(r') \psi_k(\mathbf{r}') \, d^3r' \\ &= \frac{-m}{8\pi^2 ik} \int_{-\infty}^{\infty} \frac{p\,dp}{y} (e^{ipy} - e^{-ipy}) \left\{ \frac{1}{p-k} - \frac{1}{p+k} \right\} V(r') \psi_k(\mathbf{r}') \, d^3r' \end{aligned} \tag{19}$$

where $y = |\mathbf{r} - \mathbf{r}'|$. We do the integration over e^{+ipy} by completing the contour around the upper half of the complex p plane, and over e^{-ipy} by going around the lower half plane. If we include the pole at $p = +k$ in the upper half plane and the one at $p = -k$ in the lower half plane, the residues at both poles will contain the factor

$$\frac{e^{iky}}{y}$$

which for $r \gg r'$ is approximately

$$\frac{e^{ikr}}{r} e^{-i\mathbf{k}_f\cdot\mathbf{r}'}$$

with $\mathbf{k}_f = k\hat{r}$. This is just the asymptotic outgoing spherical-wave behavior required in the scattering wave function, Eq. (2), and it has been obtained by moving the poles at $p = \pm k$ to $p = \pm(k + i\eta)$, where η is a small positive quantity which eventually goes to zero. So, by giving k (or k^2 or E_k) a small positive imaginary part, we have built in the prescription for outgoing scattered waves. With Eqs. (18), and comparing (19), and (2), we find the scattering amplitude

$$\begin{aligned} f_k(\theta) &= -\frac{m}{2\pi}\int d^3r\, e^{-i\mathbf{k}_f\cdot\mathbf{r}} V(r)\,\psi_k(r) \\ &\equiv -\frac{m}{2\pi}\langle \mathbf{k}_f \mid V \mid \psi_k\rangle \\ &\equiv -\frac{m}{2\pi}\langle \mathbf{k}_f \mid t(E) \mid \mathbf{k}_i\rangle \end{aligned} \tag{20}$$

where we have written the scattering amplitude as a matrix element of the scattering potential V between the full wave function for the initial state $\psi_k(r)$ and a plane wave $e^{i\mathbf{k}_f\cdot\mathbf{r}}$ for the final state. We also introduced the scattering matrix $t(E)$ so that the scattering amplitude is a matrix element of the t matrix between initial and final plane-wave states e^{ikz} and $e^{i\mathbf{k}_f\cdot\mathbf{r}}$. Equation (20) expresses the scattering amplitude in terms of the wave function ψ and also in terms of the operator t. We could solve the Schrödinger equation for ψ and get the scattering amplitude from Eq. (20), or, equivalently, we can find an equation for the matrix elements of t, which give the scattering amplitude directly.

Now that the operator manipulations have been given meaning by inserting complete sets of states to diagonalize the operators, and the integrands have been arranged to give outgoing scattered waves only, a host of formal—and sometimes even useful—relations can be derived. We shall present a sampling of these relations.

Call

$$E^+ = E + i\eta \tag{21}$$

where it is understood that η is a small positive quantity which will eventually approach zero. The operator appearing in Eq. (12) is the free two-particle Green's function

$$g_0(E) = (H_0 - E^+)^{-1} \tag{22}$$

and Eq. (12) can be written

$$\psi = \phi - g_0 V\psi \tag{23}$$

suppresing all variables. Solving Eq. (23) by iteration, we obtain

$$\begin{aligned}\psi &= \phi - g_0 V\phi + g_0 V g_0 V\phi + \cdots \\ &= \phi - gV\phi \end{aligned} \tag{24}$$

introducing the full two-particle Green's function

$$\begin{aligned} g &= g_0 - g_0 V g_0 + \cdots \\ &= g_0(1 + Vg_0)^{-1} = (1 + g_0 V)^{-1} g_0 \end{aligned} \tag{25}$$

which we obtain by formally summing the series. From Eq. (24) it is clear that knowledge of the full Green's function g is equivalent to a solution for the scattering wave function ψ. Equation (25) can also be expressed

$$g^{-1} = g_0^{-1} + V = H - E^+ \tag{26}$$

We can get these results without iteration. From Eq. (23)

$$(1 + g_0 V)\psi = \phi \tag{27}$$

and

$$\begin{aligned}\psi &= \phi + \left(\frac{1}{1 + g_0 V} - 1\right)\phi \\ &= \phi - gV\phi \end{aligned} \tag{24a}$$

using Eq. (26). If we multiply Eq. (27) on the left with g_0^{-1}, we obtain

$$g^{-1}\psi = g_0^{-1}\phi$$

or

$$\psi = g g_0^{-1}\phi$$

but

$$g_0^{-1}\phi = (H_0 - E - i\eta)\phi = -i\eta\phi$$

hence

$$\psi = \lim_{\eta \to 0^+} - i\eta g\phi \tag{28}$$

Recall the definition of the t matrix in terms of the scattering amplitude

$$\langle \mathbf{p} \mid t(E) \mid \mathbf{k} \rangle = \langle \mathbf{p} \mid V \mid \psi_k \rangle = \frac{-2\pi}{m} f_k(\theta) \tag{20a}$$

From Eq. (23) we get (making variables explicit)

$$\langle \mathbf{p} \mid V \mid \psi_k \rangle = \langle \mathbf{p} \mid V \mid \mathbf{k} \rangle - \langle \mathbf{p} \mid V \mid \mathbf{q} \rangle \langle \mathbf{q} \mid g_0(E_k) \mid \mathbf{q}' \rangle \langle \mathbf{q}' \mid V \mid \psi_k \rangle \tag{29}$$

which is an integral equation for t matrix elements of a slightly more general form than originally introduced in Eq. (20). In Eq. (20) we only need matrix elements of the scattering matrix $t(E)$ between initial and final states which conserve energy, so $p^2/2m = k^2/2m = E$. The t-matrix element giving the scattering amplitude is said to be *on the energy shell* at both ends. This is not the case for the matrix elements occuring in the second term of Eq. (29), because the intermediate states $|\,\mathbf{q}'\rangle$ do not conserve energy and in the matrix element $\langle \mathbf{q}' \mid V \mid \psi_k(E)\rangle$

$$\frac{q'^2}{2m} \neq \frac{k^2}{2m} = E$$

and this is a t-matrix element only in the extended sense that we introduce *off-energy-shell* matrix elements of the t matrix between initial and final states which do not conserve energy. Then

$$\langle \mathbf{q}' \mid V \mid \psi_k(E)\rangle = \langle \mathbf{q}' \mid t(E) \mid \mathbf{k}\rangle$$

is a t-matrix element which is off the energy shell at one end. Equation (29) becomes

$$\langle \mathbf{p} \mid t(E) \mid \mathbf{k}\rangle = \langle \mathbf{p} \mid V \mid \mathbf{k}\rangle - \langle \mathbf{p} \mid V \mid \mathbf{q}\rangle\langle \mathbf{q} \mid g_0(E) \mid \mathbf{q}'\rangle\langle \mathbf{q}' \mid t(E) \mid \mathbf{k}\rangle \tag{29a}$$

If we allow $|\,\mathbf{p}\rangle$ to go off the energy shell also, then Eq. (29a) is the Lippmann–Schwinger equation defining t-matrix elements off the energy shell at one end. If $|\,\mathbf{k}\rangle$ also goes off the energy shell so that $p^2/2m$ and $k^2/2m$ are allowed to differ from E, Eq. (29a) defines t-matrix elements off the energy shell at both ends. If we leave the energy variable implicit and understand that matrix elements between plane-wave states are to be taken to define operator manipulations, then Eq. (29a) becomes

$$t = V - Vg_0t \tag{30}$$

and, either by iteration or inversion, we get

$$t = V - VgV \tag{30a}$$

Once again we see that knowledge of the full Green's function g is equivalent to a solution of the scattering problem since, knowing g, we can recover the t matrix from Eq. (30a) and the scattering amplitude from Eq. (20). If we formally solve Eq. (30) by iteration, we obtain the perturbation, or multiple-scattering, series

$$t = V - Vg_0V + Vg_0Vg_0V + \cdots \tag{31}$$

which is just the first, second, etc., Born approximation to the t matrix and represents t as the amplitude due to the particles interacting once, twice, etc., through the scattering potential V.

It is useful to make a quantitative (as distinct from qualitative) graphical, or diagrammatic, representation of the integral equation (30) and the iterative solution, Eq. (31). The two interacting particles (whose reduced mass is m) are represented by horizontal lines which can be labeled with the particles' momenta and which can have an arrow pointing in the direction of increasing time. A single interaction through the potential V is represented by a vertical line connecting the two horizontal particle lines. Figure 1a corresponds to the matrix element in the c-m system

$$\langle \mathbf{p} \mid V \mid \mathbf{k} \rangle$$

An interaction through the full scattering matrix t is represented by a blob connecting the two particle lines. Figure 1b corresponds to the matrix element

$$\langle \mathbf{p} \mid t \mid \mathbf{k} \rangle$$

The two particles propagate from one interaction to the next with the amplitude $(-g_0)$. The second-order Born approximation

$$\langle \mathbf{p} \mid V \mid \mathbf{q} \rangle \langle \mathbf{q} \mid -g_0(E) \mid \mathbf{q} \rangle \langle \mathbf{q} \mid V \mid \mathbf{k} \rangle$$

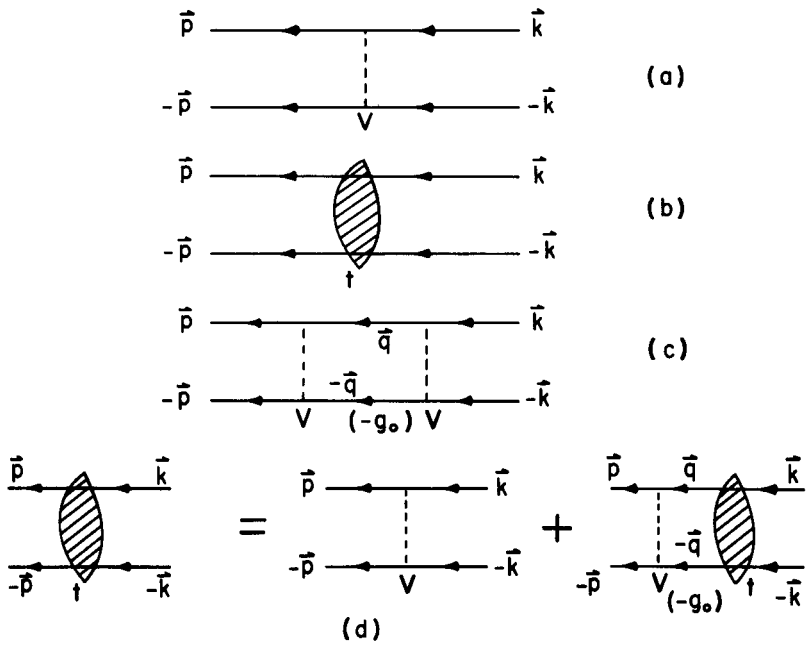

Fig. 1. (a) Diagram representing the two-particle matrix element $\langle \mathbf{p} \mid V \mid \mathbf{k} \rangle$; (b) diagram of $\langle \mathbf{p} \mid t \mid \mathbf{k} \rangle$; (c) diagram of $\langle \mathbf{p} \mid -Vg_0V \mid \mathbf{k} \rangle$; (d) Diagrams representing the matrix elements of the full Lippmann–Schwinger equation $t = V - Vg_0t$.

is represented by the diagram of Fig. 1*c*. The diagrams corresponding to the integral equation (30) are shown in Fig. 1*d*.

The integral equation (29) can be reduced to a one-dimensional integral equation for individual partial-wave t-matrix elements $t_L(p, k, E)$ defined through the expansion

$$\langle \mathbf{p} \mid t(E) \mid \mathbf{k} \rangle = \sum_{L=0}^{\infty} (2L + 1)\, t_L(p, k, E)\, P_L(\cos\theta) \tag{32}$$

where the P_L are Legendre polynomials and θ is the the angle between $\mathbf{p}$ and $\mathbf{k}$. A similar expansion can be made for the scattering potential V. Then Eq. (29) becomes

$$t_L(p, k, E) = V_L(p, k) + \int_0^{\infty} dq K_L(p, q; E)\, t_L(q, k, E) \tag{33}$$

where the $V_L(p, k)$ are analogous to the $t_L(p, k, E)$ of Eq. (32) and the kernel

$$K_L(p, q; E) = -\frac{q^2}{2\pi^2} \frac{V_L(p, q)}{q^2/2m - E^+} \tag{34}$$

The kernel becomes singular as E^+ approaches positive real values and a cut appears in the complex energy plane—the unitarity or right-hand cut—in $t_L(p, k, E)$.[12,25] On the energy shell, $t_L(p, k, E)$ has the phase (δ_L) for p^2 just above the positive real axis and $(-\delta_L)$ just below it. The cut connects two complex energy sheets, the physical sheet, where the observed scattering amplitude is the value of t just above the cut, and the unphysical sheet. The physical sheet maps into the upper half of the complex momentum plane; the unphysical, into the lower half. The physical sheet is that part of the Riemann surface for which the wave function is normalizable. Bound states appear as simple poles at negative real energies on the physical sheet; virtual states and resonances, as poles on the unphysical sheet.

Equation (33) is an integral equation of the Fredholm type, and sufficient conditions for it to have a unique solution are discussed by Courant and Hilbert[27] for the condition in which the energy is negative or complex and the kernel is nonsingular. The extension of this discussion to real positive energies has been made by Lovelace,[12] Weinberg,[28] and others.[29,30] The proofs for negative or complex energy require that the kernel be square integrable

$$\int_0^{\infty} \mid K_L(p, q; E)|^2\, dp\, dq < \infty$$

and that the integrals

$$\int_0^{\infty} \mid K_L(p, q; E)|^2\, dp \qquad \text{and} \qquad \int_0^{\infty} \mid K_L(p, q; E)|^2\, dq$$

be bounded functions of q and p, respectively, which will be the case if the scattering potential is square integrable

$$\int d^3r V^2(r) < \infty$$

Courant and Hilbert show that the square integrable or $L^{(2)}$ kernel can be uniformly approximated with arbitrary precision by a degenerate kernel $A_N(p, q)$, which is one that can be written

$$A_N(p, q) = \sum_{ij=1}^{N} C_{ij}\omega_i(p)\,\omega_j(q) \tag{35}$$

where the C_{ij} are expansion coefficients and the ω_i can be chosen orthogonal and normalized

$$\int_0^\infty \omega_i^*(p)\,\omega_j(p)\,dp = \delta_{ij}$$

i.e., they are in the Hilbert space $L^{(2)}$ of square integrable functions. Kernels which can be so approximated are termed *compact* or *completely continuous*. For any finite N the integral equation (33) with the approximate kernel, Eq. (35), becomes a system of algebraic equations for the expansion coefficients α_i in an expansion of the form

$$t_L^{(N)} = \sum_{i=1}^{N} \alpha_i\omega_i$$

and we are assured that the sequence converges uniformly and absolutely, as $N \to \infty$, to the unique solution t. The extension of these proofs to the case of integral equations of more than one dimension is straightforward. The extension to the case of real positive energy and a singular kernel can be made most easily[12,29,30] by generalizing from the Hilbert space of square integrable functions to the Banach space of continuous functions for the ω_i and with the same conclusions, that Eq. (33) has a unique solution in the Banach space of continuous functions for all energies E provided the kernel is square integrable for complex E.

Practically speaking, the compactness of the kernel ensures that we can turn the integral equation into a matrix equation and solve by matrix inversion. Alternatively, we can approximate the kernel by a degenerate kernel, as in Eq. (35), with N small—as small as 1 or 2 in actual applications—and convert the integral equation (33) into a system of N linear algebraic equations in N unknowns. The construction of an approximate separable or

degenerate kernel is accomplished physically by the assumption of a nonlocal separable potential of the form

$$V_L(p, q) = v_L(p)\, v_L(q)$$

A detailed discussion of scattering by separable potentials is contained in Appendix B.

1.2 Difficulties in Three-Particle Scattering Theory

There are two difficulties which distinguish the problem of three-particle scattering from that of two-particle scattering. One of these is the practical problem of the proliferation of the number of degrees of freedom so that, even after partial-wave analysis, the integral equations for the partial-wave scattering amplitudes are integral equations for functions of two variables. A numerical solution of these equations is beyond the scope of present-day electronic computers and some reduction in the complexity is necessary if any progress is to be made. The current fashion, and the trick which has made all recent progress possible, is to assume that the two-particle scattering amplitude is separable in initial and final relative coordinates. In this way the two-dimensional integral equations are reduced to one-dimensional equations of no greater essential complexity than those arising in two-particle scattering. This separable assumption can be justified for two-particle scattering amplitudes in the neighborhood of a bound state or resonance, as Lovelace has shown[12] in his definitive paper on the application of the Faddeév equations. Also, the two-particle scattering amplitude can be made separable if the actual scattering amplitude is parameterized by nonlocal separable potentials (see Appendix B). Nonlocal separable potentials can reproduce the experimental nucleon–nucleon phase shifts with considerable precision,[31–34] and indications are that they can also reproduce the off-energy-shell matrix elements.[35–37]

The second and fundamental difficulty of three-particle scattering appears if one uses the Lippman–Schwinger equation to formulate the three-particle scattering problem. One readily discovers that the homogeneous equation has nonzero solutions for a continuum of energies when there are two-particle bound states, so the inhomogeneous equation has no unique solution.[11,6] The Lippman–Schwinger equation in this case is not an integral equation with a unique solution satisfying the Schrödinger equation and prescribed boundary conditions and is not even a formal solution to the scattering problem. The reason for the failure of the Lippman–Schwinger equation can be expressed in a number of ways.[38,17] In perturbation theory diagrams, disconnected diagrams occur in which two particles interact and the third is disconnected from the other two. These diagrams lead to delta-

function singularities in the kernel of the Lippmann–Schwinger equation, and they make the kernel not square-integrable and noncompact and preclude a unique solution of these integral equations. These facts are illustrated by the Lippmann–Schwinger equations for the two- and three-particle Green's functions.[12,38] For two particles interacting through the potential V, the Green's function introduced in Eq. (25) satisfies the Lippmann–Schwinger equation

$$g = g_0 - g_0 V g = g_0 + Kg \tag{36}$$

and a solution exists and can be found, as we have just discussed for Eq. (33), if the kernel is compact, which in turn is the case if it is square integrable or $L^{(2)}$. This is in fact the case in two-particle scattering, where Eq. (36) becomes

$$\langle \mathbf{q} \mid g(E) \mid \mathbf{q}' \rangle = \frac{-(2\pi)^3\, \delta^3(\mathbf{q} - \mathbf{q}')}{E - E_q} + \int đ^3q'' \frac{\langle \mathbf{q} \mid V \mid \mathbf{q}'' \rangle \langle \mathbf{q}'' \mid g \mid \mathbf{q}' \rangle}{E - E_q} \tag{37}$$

(where we use $đq = dq/2\pi$). The condition that the kernel be square integrable may be written

$$\int d^3q\, d^3p \left| \frac{\langle \mathbf{q} \mid V \mid \mathbf{p} \rangle}{E - E_p} \right|^2 < \infty \tag{38}$$

As discussed Section 1.1, this will be true (for complex or negative E) provided the potential itself is square integrable

$$\int d^3r V^2(\mathbf{r}) < \infty \tag{39}$$

The situation is essentially different for the three-particle Green's function G defined by

$$G \equiv G_0 - G_0 V G = G_0 + KG \tag{40}$$

where $V = V_1 + V_2 + V_3$ is the total interaction potential between the three particles with, e.g., V_1 the interaction between the pair (2, 3); the free three-particle Green's function is $G_0 = (H_0 - E^+)^{-1}$ with $H_0 = p_1^2/2m_1 + p_2^2/2m_2 + p_3^2/2m_3$, the kinetic energy of the three particles. The kernel has matrix elements which contain delta functions even after factoring out one overall, and the matrix element of the kernel between three-particle states $\mid \mathbf{p}_1' \mathbf{p}_2' \mathbf{p}_3' \rangle$ and $\mid \mathbf{p}_1 \mathbf{p}_2 \mathbf{p}_3 \rangle$ is

$$\begin{aligned} \langle \mathbf{p}_1\mathbf{p}_2\mathbf{p}_3 \mid K \mid \mathbf{p}_1'\mathbf{p}_2'\mathbf{p}_3' \rangle = (2\pi)^3 \big(E - E(p)\big)^{-1} \{ & \delta^3(\mathbf{p}_1 - \mathbf{p}_1') \langle \mathbf{p}_2\mathbf{p}_3 \mid V_1 \mid \mathbf{p}_2'\mathbf{p}_3' \rangle \\ & + \delta^3(\mathbf{p}_2 - \mathbf{p}_2') \langle \mathbf{p}_1\mathbf{p}_3 \mid V_2 \mid \mathbf{p}_1'\mathbf{p}_3' \rangle \\ & + \delta^3(\mathbf{p}_3 - \mathbf{p}_3') \langle \mathbf{p}_1\mathbf{p}_2 \mid V_3 \mid \mathbf{p}_1'\mathbf{p}_2' \rangle \} \end{aligned} \tag{41}$$

where $E(p)$ is the kinetic energy of the three particles of momenta $\mathbf{p}_1$, $\mathbf{p}_2$, and $\mathbf{p}_3$. This kernel cannot be made $L^{(2)}$ or compact by any nontrivial choice of interactions. In a condition corresponding to Eq. (38), we always obtain the integral of the square of a delta function, which is infinite.

It is this problem which Faddeév recognized and solved in such a clever way by writing a system of coupled integral equations for elements of the three-particle Green's function, each of which has a characteristic compact kernel corresponding to a series of completely connected perturbation diagrams and each of which is inhomogeneous and has, therefore, a unique solution.

We shall return to the Faddeév equations in Section 3, but, first, in Section 2 we present a discussion of the detailed comparison of the Amado model with the experimental results on neutron–deuteron scattering. We discuss the Amado model first because, in spite of the fact that it is couched in field theoretic terms unfamiliar to many, it is really simple. If readers unacquainted with field theory will ignore these aspects of the discussion and understand the Amado model as simply the summation of connected diagrams in a multiple-scattering expansion of three-particle scattering, using a simplified two-particle interaction, then there need be no difficulty. Section 4 is devoted to a few applications of the Faddeév equations. Following a summary in Section 5 are appendices containing notation, a discussion of two-particle scattering in the separable potential approximation, a calculation of spin–isospin factors in n–D inelastic scattering, a derivation from the Faddeév equation of the integral equation for K–D elastic scattering, and a derivation of the Amado equation from the Faddeév equation.

2. THE AMADO MODEL

2.1 Construction of the Model

Amado, in a beautifully lucid series of papers[1–5] has constructed a soluble model three-body problem which has a strong similarity to the real problem of scattering from a composite target in spite of the simplifications necessary to make it tractable. The artifice employed is to introduce an "elementary" particle for the two-particle bound state, or resonance, for all strengths of the interaction. Then, if the two-particle interaction is approximated by just a reduced interaction effective in only the one angular momentum state required to couple the two particles to the elementary particle, a soluble one-dimensional linear integral equation for the scattering amplitude is obtained. The equation represents an exact three-dimensional model of three-body scattering and breakup reactions. In a limit in which the elementary particle becomes a bound state, the two-particle interaction

is a one-component separable potential. The equations obtained for the elastic scattering amplitude are of the Lippmann–Schwinger form for an optical model with an energy-dependent complex potential and are linear integral equations for off-energy-shell scattering amplitudes.

The elementary-particle theory is constructed so that it has the same Born approximation as the bound-state theory,[1,39] in which the two-particle interaction is explicitly described by a potential. Integral equations for scattering and reactions via the reduced interaction are readily obtained. One can conceive of improving the model by taking account of the actual two-body interactions through a perturbation theory using the elementary-particle theory with its reduced interaction as a basis and the rest of the two-particle interaction (the residual interaction) as a perturbation. If the residual interaction has no bound states (as is the case for the nucleon–nucleon force), a perturbation theory presumably is convergent. This would certainly not be the case for the full interaction, since the target particle is a bound state in the potential one wishes to treat as a perturbation and the scattering amplitude cannot change smoothly as the potential is turned off, so presumably an expansion of the scattering amplitude in powers of the potential would not converge.[40,41]

As a simple first example to discuss by the Amado technique, consider a model of neutron–deuteron scattering in which the neutron is a spinless boson and the deuteron is an S-wave composite of two neutrons. Call these n and D. If the n–n interaction was an ordinary local potential acting in all partial waves and the D was a bound state in this potential, we should have the full three-body problem and should be forced to resort to some of the unsatisfactory classical procedures. However, by replacing the D with an elementary particle and imagining the n–n interaction to be only through the D,

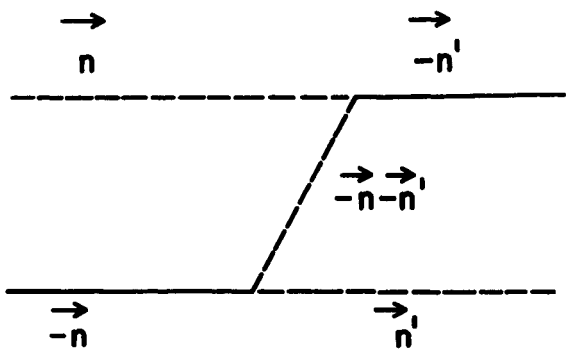

Fig. 2. One-nucleon-exchange amplitude for n–D elastic scattering. Broken lines represent nucleons, and solid lines represent the deuteron.

i.e., just an S-wave interaction separable in initial and final momenta in the bound-state limit, we find a tractable model with a wealth of physical features.

We need to make a correspondence between our model, in which the n–n interaction is solely through the D, and a potential model. In our model the first term in a multiple scattering expansion of n–D elastic scattering is the amplitude corresponding to the diagram of Fig. 2. This $1n$-exchange amplitude occurs only in the exhange or rearrangement amplitude of scattering from a composite target in which the D is a bound state of two n's. We shall construct the elementary-particle theory so that the $1n$-exchange amplitudes of the two theories coincide.

In Fig. 2, let us suppose for the moment that we have distinguishable particles lableled (1, 2, 3). Let particle (1) of momentum $\mathbf{n}$ be incident on the bound state (2, 3); particle (2) is exchanged, and a bound state (1, 2) plus particle (3) with momentum $\mathbf{n}'$ are outgoing. The normalized bound-state wave function ψ_1 of the pair (2, 3), e.g., satisfies

$$(p_1^2 + \alpha^2)\,\psi_1 = -V_1\psi_1 \tag{42}$$

where p_1^2 is the kinetic energy of relative motion of the pair (2, 3) (with the n mass equal to 1), V_1 is the interaction potential between the pair (2, 3), and $-\alpha^2$is the binding energy. Then the Born approximation for the rearrangement scattering amplitude for the reaction $(1) + (2, 3) \to (1, 2) + (3)$ is the matrix element between initial and final states of

$$-V_3 G_0(E)\, V_1$$

with E, the total energy, and $G_0(E)$, the free three-particle Green's function. Note that we label a pair by the number of the particle not included in the pair. The matrix element can be evaluated to give the Born approximation

$$\begin{aligned}(\mathbf{n}' \mid B(E) \mid \mathbf{n}) &\equiv -(\mathbf{n}'\psi_3 \mid V_3 G_0(E)\, V_1 \mid \psi_1\mathbf{n}) \\ &= (\psi_3 \mid V_3 \mid \mathbf{p}_3)\left[E - \frac{\mathbf{n}'^2}{2} - \frac{\mathbf{n}^2}{2} - \frac{(\mathbf{n}+\mathbf{n}')^2}{2} + i\eta\right]^{-1} \\ &\quad \times (\mathbf{p}_1 \mid V_1 \mid \psi_1)\end{aligned} \tag{43}$$

with $\mathbf{p}_3 = \mathbf{n} + \mathbf{n}'/2$ and $\mathbf{p}_1 = +\mathbf{n}' + \mathbf{n}/2$, the relative momenta of the pairs (3) and (1). The potentials can be eliminated by using Eq. (42) to get

$$(\mathbf{p}_1 \mid V_1 \mid \psi_1) = -(\alpha^2 + p_1^2)\,\psi(p_1^2) \tag{44}$$

where $\psi(p_1^2)$ is the Fourier transform of the bound-state wave function,

which is a function only of p_1^2 since we are dealing with an S-wave bound state. The Born amplitude, Eq. (43), becomes

$$(\mathbf{n}' \mid B(E) \mid \mathbf{n}) = \frac{\Gamma_0^2 v([\mathbf{n}' + \mathbf{n}/2]^2)\, v([\mathbf{n} + \mathbf{n}'/2]^2)}{E^+ - \mathbf{n}^2/2 - \mathbf{n}'^2/2 - (\mathbf{n} + \mathbf{n}')^2/2} \tag{45}$$

in units where $\hbar = M_n = c = 1$. We have introduced the vertex function v and coupling constant Γ_0, whose product is related to the Fourier transform of the D bound-state wave function ψ by

$$\Gamma_0 v(q^2) = \sqrt{2}\,(\alpha^2 + q^2)\,\psi(q^2) \tag{46}$$

A factor of $\sqrt{2}$ arises from the identity of the two n's. Equation (45) is just the Born amplitude that would be obtained if the D were considered an elementary particle with the only interaction permitted the $D \rightleftharpoons 2n$ process with the vertex function $\Gamma v(q^2)$ replacing $\Gamma_0 v(q^2)$ of the above bound-state theory. It has been shown[1] that such an elementary-particle theory has meaning for all Γ in the range $0 < \Gamma < \Gamma_0$ and in the limit of $\Gamma = \Gamma_0$ yields the same predictions as a model in which the D is a bound state in an n–n interaction separable in momentum space and acting only in S waves.

There is one more step required in the construction of the elementary-particle theory. The n–n scattering amplitude must be made to coincide with the potential model where the D is an n–n bound state and scattering takes place through the n–n potential. We can simply impose this equality by writing the off-energy-shell matrix elements of the two-particle t matrix in a separable form [see Appendix B, especially Eq. (B.19)]

$$(p \mid t_K \mid p') = \Gamma^2 v(p^2)\, v(p'^2)\, P(k^2) \tag{47}$$

where Γ and v are the same coupling constant and vertex function of Eq. (46), and Eq. (47) defines the full propagator $P(k^2)$ for D particles in intermediate states that is required for the elementary-particle theory to reproduce the

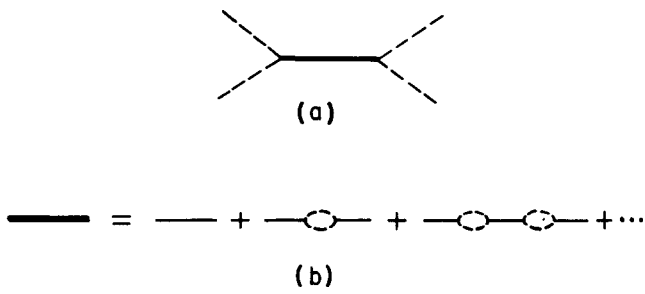

Fig. 3. Diagrams contributing to the full D propagator.

off-energy-shell matrix elements of a separable potential. Figure 3*a* is the diagram corresponding to the amplitude, Eq. (47). A factor Γv occurs at each n–n–D vertex. The heavy solid line represents the full D in the intermediate state and corresponds to the full D propagator defined by Eq. (47).

This is actually all we need to know about the propagator, coupling constant, and vertex function of the Amado model. We have completely specified them in terms of the n–n scattering amplitude as determined by a separable potential. We could even allow some freedom to adjust the theory by recalling that the S-wave part of the deuteron wave function is normalized to something less than 1, because the deuteron is partly D state, and we could permit the same freedom in the model. Then Γ would be an adjustable parameter with a maximum value of Γ_0 for a D which is 100% an S-wave n–n bound state. This modification is discussed in greater detail in Appendix B following Eq. (B.19).

Amado actually arrived at these results in a different way, by treating the n–n–D interaction as a model field theory. The full n–n scattering amplitude (Fig. 3*a*) then arises as the sum of a series of processes pictured in Fig. 3*b*, which are the repeated spontaneous disassociation and reassociation of the virtual bare D particle. The sum of all these "bubble" diagrams is performed in Appendix B. The result is that each bare D line plus the bare D

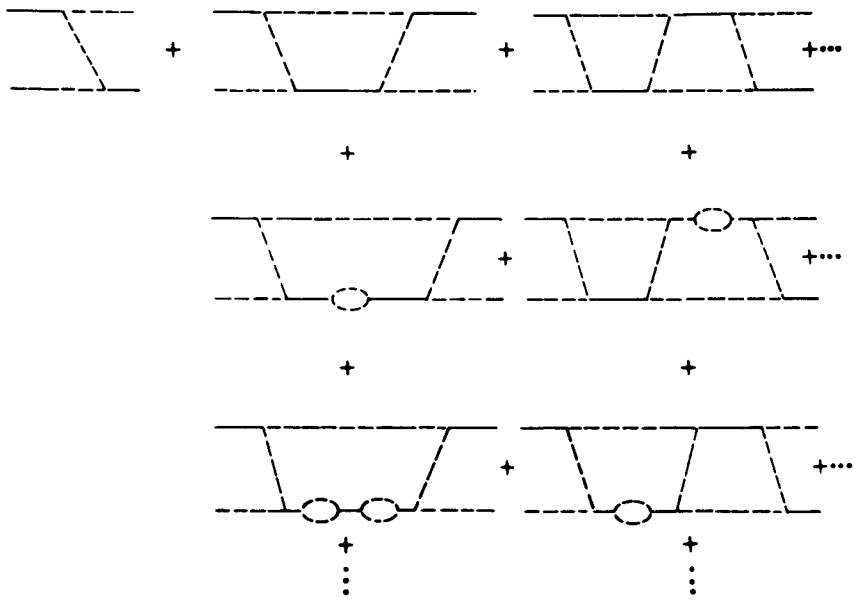

Fig. 4. Diagrams contributing to n–D elastic scattering amplitude in a theory with only a basic $D \rightleftharpoons 2n$ vertex, including multiple-n-exchange amplitudes and all possible deuteron polarization diagrams.

Fig. 5. Diagrams representing integral equation for n–D elastic scattering with renormalized D propagator in intermediate states.

line with all bubbles sums up to a full D line, as in Fig. 3b, which corresponds to the full D propagator of Eq. (47). Now we can immediately construct an integral equation for the n–D scattering amplitude by a direct summation of the diagrams appearing in a perturbation expansion that permits only the basic $D \rightleftharpoons 2n$ vertex. (The perturbation expansion presumably converges for sufficiently small Γ, and after the series is summed we can let $\Gamma \to \Gamma_0$, independent of the D binding energy.) The diagrams can be ordered in the following way, as shown in Fig. 4: Each column consists of a basic ladder graph (with multiple-n-exchange) plus the same basic graph with all possible bubble insertions in internal D lines. We can sum these bubble insertions separately to get the full D propagator, which we represent, as in Fig. 3b, by a heavy line. The reordered perturbation series is just a sum of ladder graphs with the full D propagator in internal lines, and the series can be summed into an exact Bethe–Salpeter equation[1] for n–D scattering, as in Fig. 5. Call the full scattering amplitude $(\mathbf{n}' \mid t(E) \mid \mathbf{n})$, the Born amplitude $(\mathbf{n}' \mid B(E) \mid \mathbf{n})$, and the full D propagator $P(k^2)$. If we work in the c-m system, then we need the D propagator at an internal momentum $k^2 = E - \frac{3}{4}n^2$. [For a discussion of the full D propagator, see Appendix B and especially the derivation of Eq. (B.25).] Then our integral equation for the n–D scattering amplitude is [with $\bar{d}^3q = d^3q/(2\pi)^3$]

$$(\mathbf{n}' \mid t(E) \mid \mathbf{n}) = (\mathbf{n}' \mid B(E) \mid \mathbf{n}) + \int \bar{d}^3q_\delta (\mathbf{n}' \mid B(E) \mid \mathbf{q})\, P(E - \tfrac{3}{4}q^2)(\mathbf{q} \mid t(E) \mid \mathbf{n}). \tag{48}$$

Equation (48) can be recast in the form of a Lippmann–Schwinger equation with a complex, energy-dependent optical potential and can be solved by standard methods. Amado proves that, even in the singular limit $\Gamma = \Gamma_0$, Eq. (48) has solutions that can be found by the use of Fredholm methods.

Let us devote a brief discussion to the solution of this integral equation for scattering parameters chosen to simulate actual neutron–deuteron scattering.[2] We shall next turn to the more complicated problem including spin, which is necessary to get a detailed understanding of the real n–D problem, albeit the present model of spinless bosons possesses many features of the full problem. Make a partial-wave analysis [compare Eq. (32)]

$$(\mathbf{n}' \mid t(E) \mid \mathbf{n}) = \sum_L (2L + 1)\, P_L(\hat{n} \cdot \hat{n}')(n' \mid t_L(E) \mid n) \tag{49}$$

and similarly for $(\mathbf{n}' \mid B(E) \mid \mathbf{n})$, to get a set of uncoupled one-dimensional linear integral equations for each partial-wave amplitude

$$(n' \mid t_L(E) \mid n) = (n' \mid B_L(E) \mid n) + \int_0^\infty dq (n' \mid K_L(E) \mid q)(q \mid t_L(E) \mid n) \tag{50}$$

with the kernel

$$(n' \mid K_L(E) \mid n) = \frac{q^2}{2\pi^2} (n' \mid B_L(E) \mid q) P(E - \tfrac{3}{4}q^2) \tag{51}$$

Throughout these calculations, a Hulthén wave function[26,31] for the deuteron is used. The vertex function corresponding to the Hulthén wave function is, according to Eq. (46),

$$v(q^2) = (q^2 + \beta^2)^{-1} \tag{52}$$

with β^{-1} the range of the n–n interaction (and an adjustable parameter independent of the D binding energy ϵ in this theory), and the coupling constant from Eq. (46) is, with $\alpha^2 = \epsilon < \beta^2$,

$$\Gamma^2 = 32\pi\alpha\beta(\alpha + \beta)^3(1 - Z) \tag{53}$$

with Z, the D wave-function renormalization constant (see Appendix B), equal to zero in the limit of a pure S-wave n–n bound state. From Eq. (B.25) we see that $P(E - \frac{3}{4}q^2)$ has a cut in the complex E plane along the real axis from $E = 0$ to ∞ due to the possibility at positive energy of the breakup process $n + D \rightleftharpoons 3n$. The Born term itself possesses logarithmic and pole singularities for $E > 0$ (and off the energy shell) corresponding to the exhange of a real n on its mass shell. The kernel of Eq. (50), $(n' \mid B_L(E) \mid q) S(E - \frac{3}{4}q^2)$ [see Eq. (B.25)] plays the role of an energy-dependent optical potential with an imaginary part starting at the inelastic threshold $E = 0$. With proper care for these singularities, the integral equation can be converted to a matrix equation and solved numerically.

Three-body bound states appear as solutions to Eq. (50) without the inhomogeneous term $(n' \mid B_L(E) \mid n)$, which are possible at $E < -\alpha^2$ when the matrix equation is singular, i.e., when the Fredholm determinant $D_L(E)$[27] vanishes. The potential $(n' \mid B_L(E) \mid q) S(E - \frac{3}{4}q^2)$ is attractive in even partial waves and repulsive in odd. There are $L = 0$ bound states for a range of parameters (Z, β), and of course there is no possibility of bound states with $L = 1$; furthermore, the interaction with reasonable (Z, β) is too weak for bound states with $L \geqslant 2$. For $L = 0$, there is one tightly bound state for a wide range of (Z, β) and also a loosely bound state for some (Z, β), which becomes a virtual state when the interaction is weakened. Choose $\beta = 5.75\alpha$ [near Yamaguchi's choice[31] of 6.25α for a best fit to triplet n–p scattering

with this form of separable potential]. Then, visually interpolating Amado's results, we see the following behavior of the three-particle bound states. For E large and negative, the Fredholm determinant for $L = 0$, $D_0(E)$, starts at 1, curves down through one bound-state zero, goes negative, and then goes through another zero just below threshold where a square-root singularity drives D positive. In the separable-potential $Z = 0$ limit, the binding energy of the tightly bound state is $+12\alpha^2$; the other one, $1.2\alpha^2$. When the interaction is weakened by increasing Z, the weakly bound state disappears at $Z = 0.1$ and the binding energy of the other state approaches zero as $Z \to 1$ and it passes through the triton binding energy at $Z = 0.145$. An interesting test of the importance of three-body propagation in intermediate states is made by setting $S = 1$ in the deuteron propagator so that deuterons are always on the mass shell. There is a really significant effect on the tightly bound state. For $Z = 0$, its binding energy is reduced from $12\alpha^2$ to $2.3\alpha^2$, which indicates the necessity of including the three-body nature of the intermediate states. Increasing β has the effect of increasing the binding energy of both bound states. Since the deuteron binding energy is being kept constant, the strength of the interaction must increase as its range β^{-1} is decreased. The zero range limit is a pathological one in which the equations cease to be of the Fredholm type.[1]

The on-energy-shell scattering amplitude (with $n' = n = k$, $E = \frac{3}{4}k^2 - \alpha^2$) for each partial wave can be obtained from Eq. (50) and the results summarized in terms of a phase shift $\delta_L = \mathrm{Re}\delta_L + i\mathrm{Im}\delta_L$ such that

$$(k \mid t_L(E) \mid k) \equiv T_L(E) = -\frac{2\pi}{\mu}\frac{e^{2i\delta_L} - 1}{2ik} \tag{54}$$

with μ, the reduced mass, equal to $\frac{2}{3}$. Here δ is real below the inelastic threshold $E = 0$, and $\mathrm{Re}\delta$ turns out to be as simple as can be imagined, compatible with Levinson's theorem and what we know about the interaction. Only the S wave possesses any noteworthy structure. We shall return to it in a moment, but first let us dispense with the featureless higher L waves, still for $\beta = 5.75\alpha$. The real part of the P-wave phase shift is negative, since the $1n$-exchange potential is repulsive in odd partial waves, falls through $-30°$ at $E = 0$, and reaches $-60°$ at $E = 3\alpha^2$; $\mathrm{Re}\delta_2$ is positive and rises slowly to $20°$ at $E = 3\alpha^2$. These phase shifts are quite insensitive to the choice of Z, being practically indistinguishable for $Z = 0$ and $Z = 0.145$. Higher L phase shifts are well represented by their Born approximation. The S-wave phase shift is just what one would expect on the basis of Levinson's theorem and shows evidence of a cusp at the inelastic threshold. For $Z = 0$, when there are two bound states, $\mathrm{Re}\delta_0$ falls rapidly from 2π at threshold, cusps at $E = 0$, falls through π at $E = 1.5\alpha^2$, and eventually falls to zero. Increasing β

decreases the rate at which the phase shift falls. Increasing Z removes the weakly bound state, and the phase shift for $Z = 0.1$ starts at π, rises rapidly at very low energies, where it is dominated by the nearby virtual state, and then falls through π at $E = 0$ and eventually to zero. Further increase of Z to 0.145 reduces the effect of the virtual state at threshold and, generally, uniformly reduces the phase shift. The contribution of each partial wave to the total (solid line) and elastic (dotted line) cross sections are shown in Fig. 6 for $\beta = 5.75\alpha$. The sensitivity of the low-energy S wave to the choice of Z is apparent, as is the cusp in the S-wave cross section at the inelastic

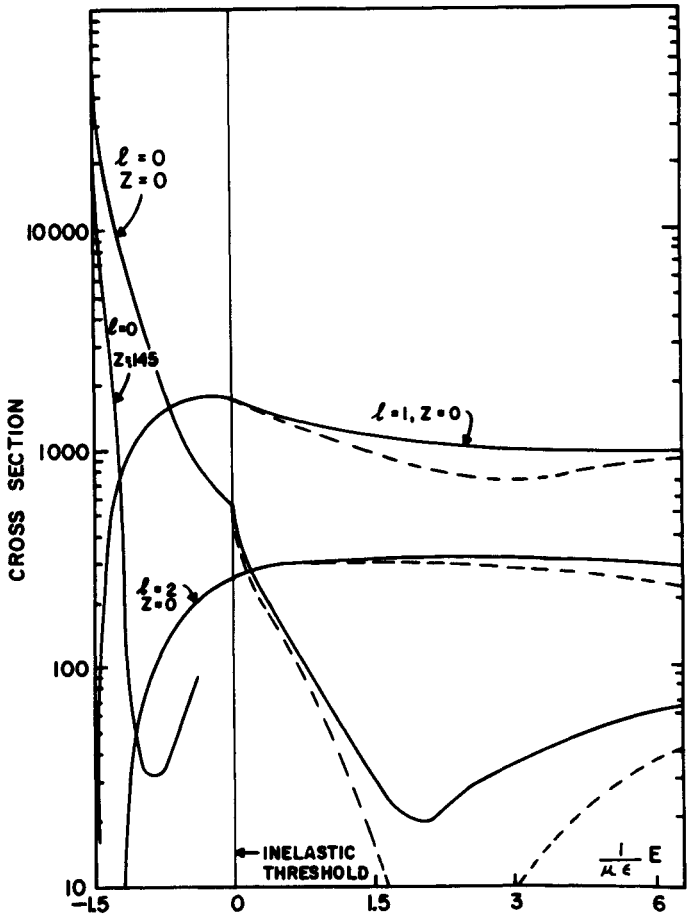

Fig. 6. $L = 0, 1, 2$ partial-wave contributions to n–D scattering cross section for a model with identical spinless nucleons. Solid line represents total cross section, broken line represents elastic cross section.

threshold. At energies significantly above $E = 0$, the S-wave phase shift is near π and the P wave is left to dominate the cross section. The angular distribution below the inelastic threshold ($E = -0.61\alpha^2$) and above ($E = +3.22\alpha^2$) are shown in Fig. 7 and 8 along with the Born-approximation cross section. The Born cross section has a backward peak characteristic of the exchange reaction, decreases monotonically to the forward direction, and is about an order of magnitude too large. The near symmetry around 90° is due to the dominance of the P wave and results in nearly equal forward and backward peaks in the cross section. All of these features are found in the actual n–D scattering problem. We turn now to a detailed discussion of that problem, including the spin–isospin structure of the nucleons.

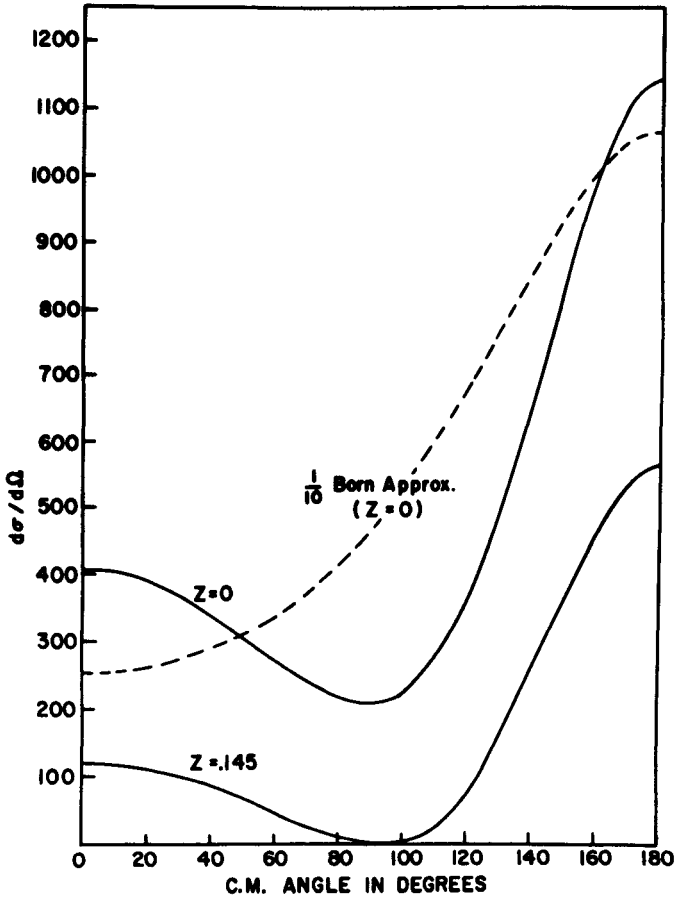

Fig. 7. Angular distribution for n–D elastic scattering at $E = -0.61\alpha^2$, below the inelastic threshold, for model with identical spinless nucleons.

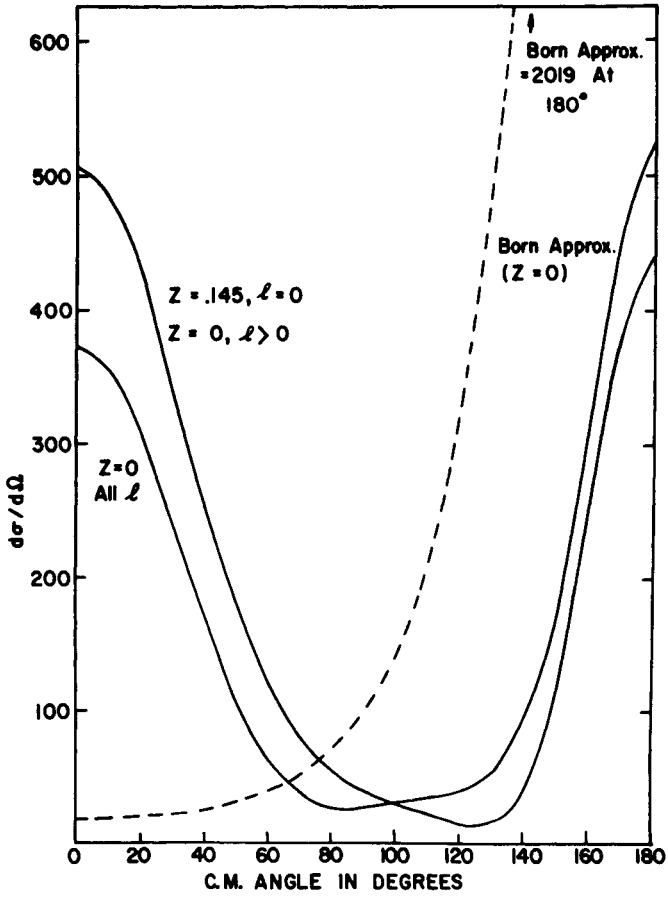

Fig. 8. Angular distribution for n–D elastic scattering at $E = 3.22\alpha^2$, above the inelastic threshold.

2.2 Nucleon–Deuteron Elastic Scattering

We deal now with real nucleons interacting differently in the spin–triplet and spin–singlet states and introduce particles D and φ to represent the two nucleons interacting in ^3S or ^1S states.[3] Since there is no $^1S_0$ bound state, it is more precise to refer to the φ as a quasi-particle. We shall use the expression quasi-particle for φ and D hereafter. The parameters of the nn–D and nn–φ interactions are chosen to fit the low-energy nucleon–nucleon scattering in these channels. Since we are including only S-wave interactions and no tensor forces, both L and S are good quantum numbers and we can use an L-S representation of the three-particle scattering amplitude with uncoupled

equations for spin $\frac{1}{2}$ and $\frac{3}{2}$ channels. For n–D scattering the isotopic spin state is $T = \frac{1}{2}$, $T_Z = -\frac{1}{2}$. The two-channel generalization of Eq. (48) can be written down directly by reference to Fig. 9 representing n–D scattering with D and φ intermediate states. We have for $S = \frac{1}{2}$ or $\frac{3}{2}$ in the c-m system

$$(\mathbf{k}, i \mid t(E) \mid \mathbf{k}', j) = \chi_{ij}(\mathbf{k}, i \mid B(E) \mid \mathbf{k}', j) + \sum_l \int d^3p (\mathbf{k}', i \mid B(E) \mid \mathbf{p}, l) P_l(E - \tfrac{3}{4}p^2)(\mathbf{p}, l \mid t(E) \mid \mathbf{k}', j) \tag{55}$$

where $(i, j, l) = D$ or ϕ for the triplet or singlet nucleon–nucleon quasi-particle. Here the χ's are spin–isospin factors derived in Appendix C. For $S = \frac{3}{2}$, $\chi_{DD} = -1$ and all the rest are zero; for $S = \frac{1}{2}$, $\chi_{DD} = \chi_{\phi\phi} = \frac{1}{2}$ and $\chi_{D\phi} = \chi_{\phi D} = -\frac{3}{2}$. For example, $(\mathbf{k}, \phi \mid B(E) \mid \mathbf{k}', D)$ is the Born amplitude for $1n$ exchange between a nucleon of momentum $\mathbf{k}'$ incident on a D to a nucleon of momentum $\mathbf{k}$ and a ϕ outgoing; P_D and P_ϕ are the full quasi-particle propagators. These equations give exact one-dimensional linear integral equations for the three-particle scattering amplitude obtained at the expense of using quasi-particles (i.e., one-component separable potentials) to represent the two-particle interaction. A more faithful representation of the two-particle scattering amplitude is conceivable, but at the cost of introducing a new quasi-particle and coupled-integral equation for each

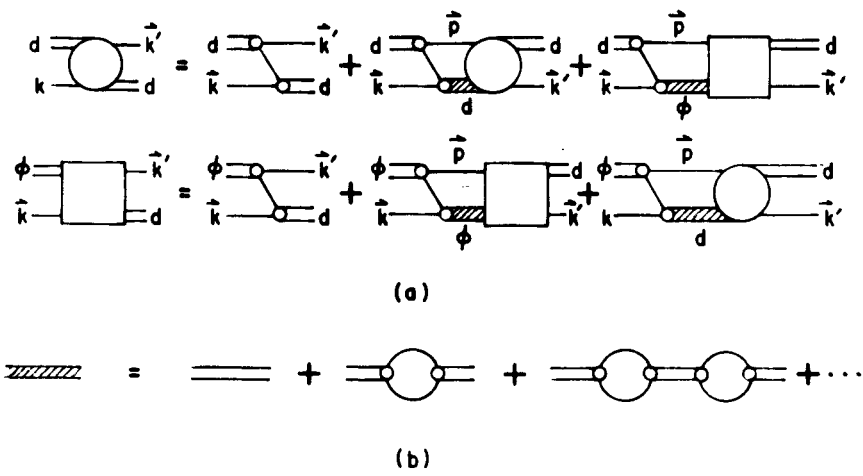

Fig. 9. (a) Diagrams representing coupled integral equations for n–D elastic scattering in a theory with real nucleons interacting only in ^3S and ^1S states through deuteron and singlet-deuteron quasi-particles; (b) the full quasi-particle propagator as the sum of bubble diagrams.

new separable-potential term. The Born amplitudes with the Hulthén form factor of Eq. (44) are [compare Eq. (45)]

$$(\mathbf{k}, i \mid B(E) \mid \mathbf{k}', j) = \frac{\Gamma_i \Gamma_j v_i([\mathbf{k}' + \mathbf{k}/2]^2)\, v_j([\mathbf{k} + \mathbf{k}'/2]^2)}{E - \mathbf{k}^2/2 - \mathbf{k}'^2/2 - (\mathbf{k} + \mathbf{k}')^2/2 + i\eta} \tag{56}$$

and the quasi-particle propagators [compare Eq. B.25)] are

$$[P_D(k^2)]^{-1} = -(k^2 + \alpha^2)\left[-Z + \Gamma_D{}^2 \int \frac{đ^3 q v_D{}^2(q^2)}{(\alpha^2 + q^2)(k^2 - q^2 + i\eta)}\right]$$

and

$$[P_\phi(k^2)]^{-1} = -\left[1 + \Gamma_\phi{}^2 \int \frac{đ^3 q v_\phi{}^2(q^2)}{(k^2 - q^2 + i\eta)}\right] \tag{57}$$

As before, Z is the probability that D is a pure elementary particle and not a two-particle S-wave bound state or, alternatively, Z is the probability of non-S-wave components in the D bound-state wave function and is a variable independent of the binding energy α^2. We include the ϕ only in the full separable-potential $Z = 0$ limit. By comparison with Eq. (B.19) we can express the (D, ϕ) parameters in terms of the ^3S and ^1S scattering parameters[42]: $r_s = 2.67$ fm, $a_S = -23.78$ fm, $r_T = 1.78$ fm, $a_T = 5.41$ fm, and $\alpha^2 = 2.226$ MeV. Then,

$$\beta_\phi = \frac{3}{2r_s}\left[1 + \left(1 - \frac{16 r_s}{9 a_s}\right)^{1/2}\right]$$

$$\Gamma_\phi{}^2 = \frac{8\pi\beta_\phi{}^4 a_s}{a_s\beta_\phi - 2}$$

and

$$\frac{1}{a_T} = \frac{4\pi\alpha^2\beta_D{}^2 Z}{\Gamma_D{}^2} + \frac{\alpha\beta_D(\alpha + 2\beta_D)}{2(\alpha + \beta_D)^2}$$

with

$$\Gamma_D{}^2 = 16\pi\alpha\beta_D(\alpha + \beta_D)^3(1 - Z) \tag{58}$$

Equations (55) can be solved numerically, after partial-wave analysis, by matrix inversion techniques and sometimes by iteration. Experimentally, the triton binding energy is 8.49 MeV and the quartet and doublet scattering lengths are $a_4 = 6.38$ fm and $a_2 = 0.7$ fm. A calculation with $Z = 0$ leads to $a_4 = 6.32$ fm (positive because the quartet-channel effective potential is repulsive), which is excellent agreement; however, the triton is too tightly bound at $E_T = 11.0$ MeV and the doublet scattering length is negative, $a_2 = -1.0$ fm, as a second bound state approaches. It is not surprising that the interaction is too attractive, since repulsive effects due to hard cores and

tensor forces have been left out. These can be simulated by weakening the ^3S interaction by increasing Z. A value $Z = 0.0496$ gives $a_2 = 0.7$ fm and $E_T = 8.53$ MeV without significantly affecting the agreement found for a_4, i.e., $a_4 = 6.20$ fm. The percentage of non-S-wave deuteron is very reasonable.

The solutions at higher energies are best displayed through angular distributions, and these are shown for a series of energies in Figs. 10 to 12. Figure 10 shows the calculated angular distribution and (dotted line) the Born approximation, which has a characteristic backward peak and no forward peak and is clearly inadequate. The agreement with experiment at all energies is quite remarkable; the only possible criticism is that the forward peak is generally too small. This discrepancy could perhaps be corrected by including high-momentum components of the two-particle force in some

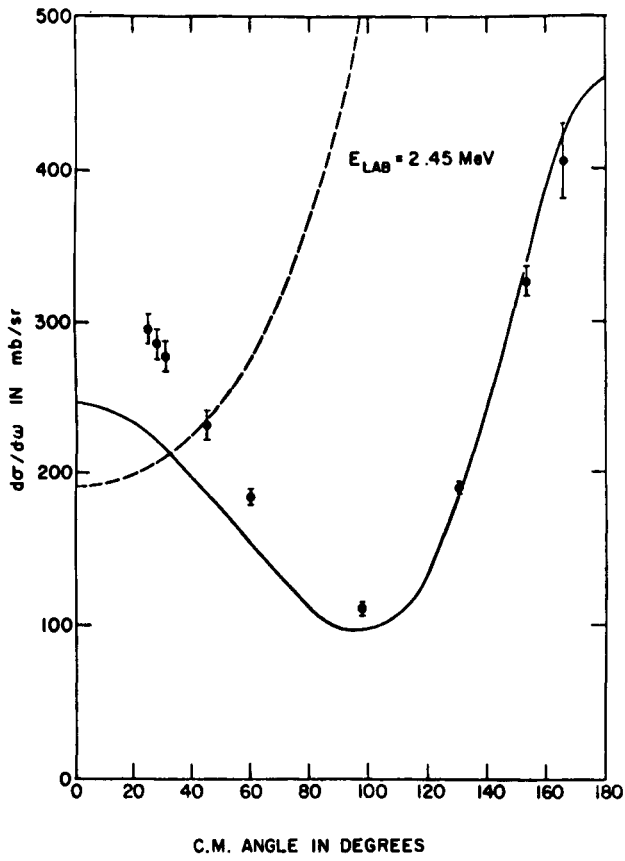

Fig. 10. Angular distribution in n–D elastic scattering at $E_{\mathrm{LAB}} = 2.45$ MeV.

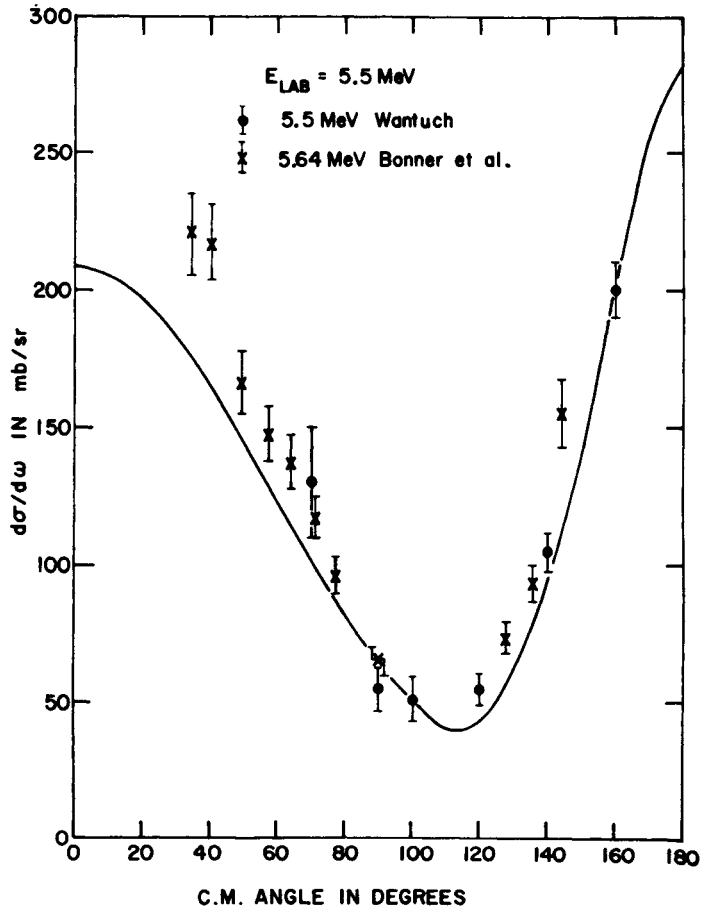

Fig. 11. Angular distribution in n–D elastic scattering at $E_{LAB} = 5.5$ MeV.

kind of impulse approximation. The total and reaction cross sections in Fig. 13 are also in excellent agreement, although the discrepancy in the forward direction is reflected here also. Figure 12 shows the doublet contribution to the scattering at $E_L = 14.4$ MeV and shows to what extent the quartet channel dominates the scattering.

The impressive success of the Amado model shows that n–D elastic scattering up to 14.4 MeV is well understood on the basis of an S-wave effective-range approximation for the nucleon–nucleon interaction. As experiments are pushed to higher energy, the discrepancies already apparent in the forward direction will provide stimulus to treat the problem with a full nucleon–nucleon interaction such as the Tabakin potentials.[33,34] In the next

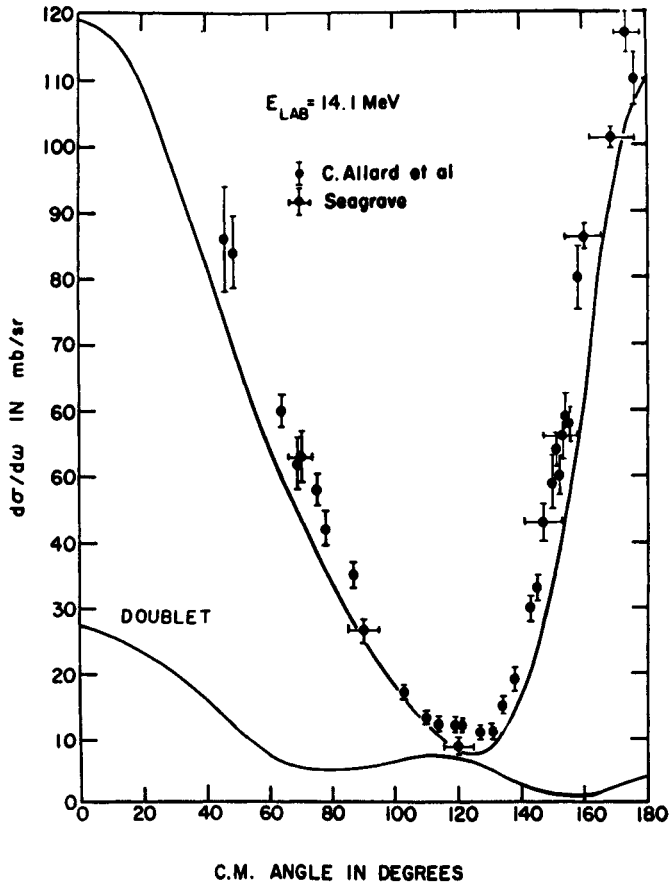

Fig. 12. Angular distribution in n–D elastic scattering at $E_{LAB} = 14.4$ MeV.

section we see that, even at 14.4 MeV, the inelastic scattering requires a more refined treatment.

2.3 Neutron–Deuteron Inelastic Scattering

The amplitude for $n + D \to n + n + p$ can be obtained[4] from the off-energy-shell amplitudes for $n + D \to n + D$ or $n + \phi$ already obtained with Eq. (55) by allowing the off-shell quasi-particle D or ϕ to propagate and then disassociate. We must append to the off-shell amplitude a propapator and off-shell vertex function and must take account of particle identity by doing this in all possible ways so that the matrix element is antisymmetric in the exchange of particles in the final state. Label the neutrons (1) and (2) and the proton (3). Then the matrix element from an initial state $|\mathbf{k}', D\rangle$ with spin

(S, S_Z) and isospin $(\frac{1}{2}, -\frac{1}{2})$ to a final state $|\mathbf{k}_1, \mathbf{k}_2, \mathbf{k}_3, m_1, m_2, m_3, i_1, i_2, i_3\rangle$ in the c-m system is

$$M_S = M_{S,D} + M_{S,\phi} \tag{59}$$

and

$$M_{S,j} = M_{S,j}(1, 2; 3) + M_{S,j}(3, 1; 2) + M_{S,j}(2, 3; 1) \tag{60}$$

where, e.g., $M_{S,\phi}(1, 2; 3)$ is the amplitude for particles (1, 2) to emerge from the quasi-particle ϕ and is antisymmetric in the exchange $(1 \rightleftharpoons 2)$. The spin-isospin dependence of one of these terms can be made explicit through Clebsch–Gordan coefficients as

$$M_{S,j}(1,2;3) = \left(\begin{matrix} m_1 & m_2 \\ \frac{1}{2} & \frac{1}{2} \end{matrix}\middle|\begin{matrix} m_j \\ S_j \end{matrix}\right)\left(\begin{matrix} i_1 & i_2 \\ \frac{1}{2} & \frac{1}{2} \end{matrix}\middle|\begin{matrix} t_j \\ T_j \end{matrix}\right)\left(\begin{matrix} m_3 & m_j \\ \frac{1}{2} & S_j \end{matrix}\middle|\begin{matrix} S_z \\ S \end{matrix}\right)\left(\begin{matrix} i_3 & t_j \\ \frac{1}{2} & T_j \end{matrix}\middle|\begin{matrix} T_z \\ T \end{matrix}\right) A_{s,j} \tag{61}$$

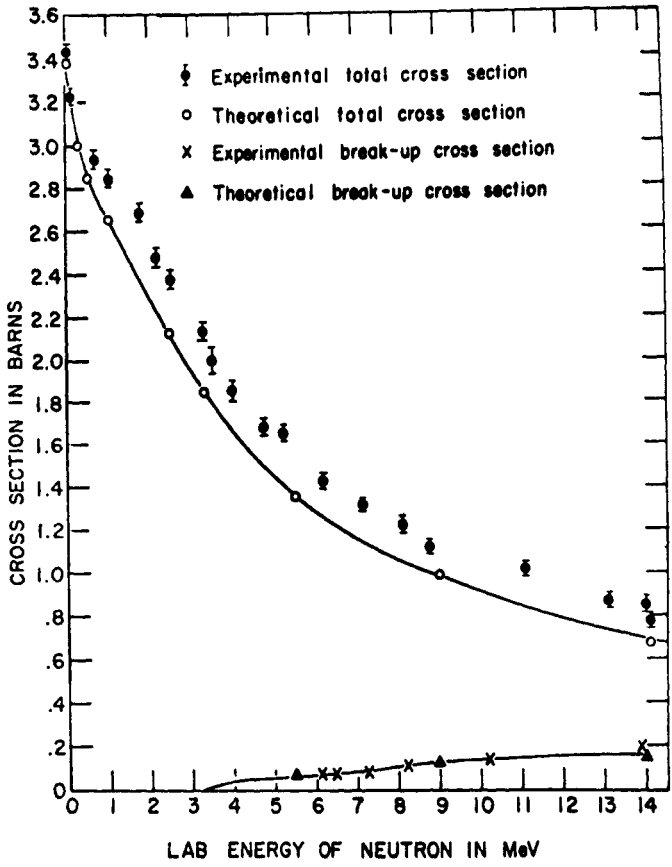

Fig. 13. Total and breakup cross sections in n–D scattering.

summed over (m_j, t_j); and the amplitude with no spin factors, symmetric in $(1 \rightleftharpoons 2)$, is

$$A_{S,j}(1,2;3) = \Gamma_j v_j \left(\left[\frac{\mathbf{k}_1 - \mathbf{k}_2}{2}\right]^2\right) P_j(k_3^2)(\mathbf{k}_3, j \mid t_S(E) \mid \mathbf{k}', D) \tag{62}$$

The matrix element squared and summed over spins is

$$M^2 = \tfrac{1}{3} \mid M_{1/2} \mid^2 + \tfrac{2}{3} \mid M_{3/2} \mid^2$$

with

$$\mid M_S \mid^2 = \sum_{ji,\text{spins}} M_{S,i} M_{S,j}^*$$

which can be evaluated from Eq. (61) by using Racah algebra. The cross section σ is (with v the relative velocity)

$$\sigma v = \int đ^3k_1\, đ^3k_2\, đ^3k_3 (2\pi)^4\, \delta^3(\mathbf{k}_1 + \mathbf{k}_2 + \mathbf{k}_3)\, \delta(E_f - E_i) \mid M \mid^2 \tag{63}$$

and we have compared with the experimental proton-energy spectrum at $E_L = 14.4$ MeV, so we require $d\sigma/d\Omega_p\, dE_p$ and must integrate Eq. (63) over neutron momenta. Here θ_p is measured with respect to the incident beam, and (E_p, θ_p) are both laboratory variables.

A major difficulty in the numerical solution of the integral equations is the treatment of singularities of the kernel, arising from the propagator and the Born term. Straightforward integration of the integral equations leads to ill-conditioning and large uncertainties in the solutions of the equations for the off-energy-shell amplitudes. It is possible to deform the contour of integration and transform to a very smooth kernel provided the deformed contour does not cross any singularities of the integrand. In fact, Amado was only able to locate the singularities of the Born term and the propagator but not of the off-energy-shell scattering amplitude itself. He rotated the contour into the lower half plane to avoid the propagator singularity but not far enough to cross the Born singularities, solved the integral equations for complex momenta, and recovered the desired off-energy-shell scattering amplitudes by one more integration along the deformed contour.

The calculated differential cross section is compared with experiment in Figs. 14, 15, and 16 for $E_L = 14.4$ MeV. The theoretical cross section is in general agreement with experiment, although it is too low at small angles and too high at large ones (consistent with a correct total cross section) owing, presumably, to neglect of high-momentum components in the nucleon–nucleon interaction, which are significant for collisions in which the proton is projected straight ahead. It is important to realize, however, that this good agreement is obtained with *no* adjustable parameters, since the effect of

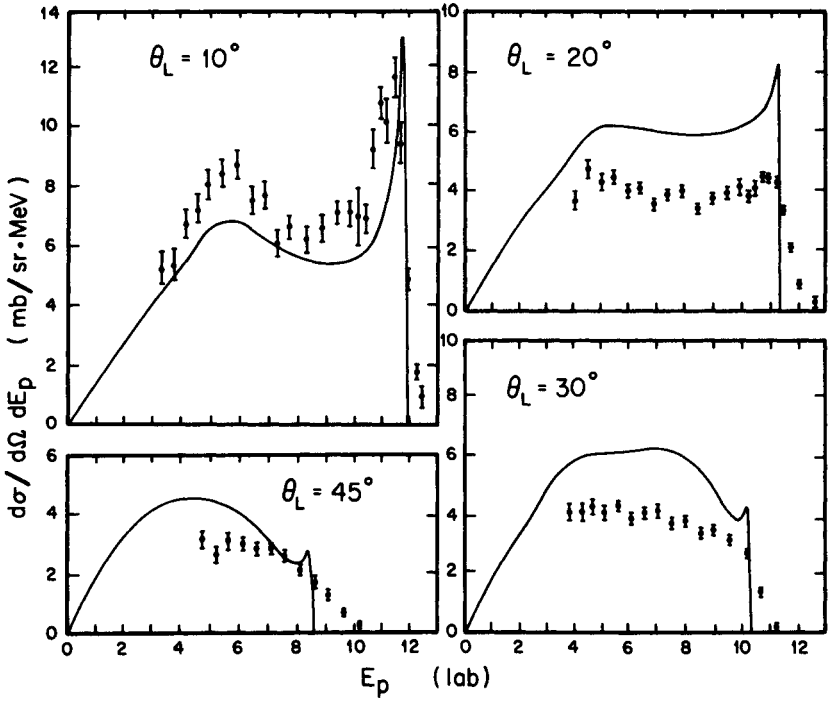

Fig. 14. Proton distributions in n–D inelastic scattering at $E_{\mathrm{LAB}} = 14.4$ MeV.

$Z \neq 0$ is negligible at these energies and Z has been set equal to zero. Furthermore, no effect of finite experimental resolution has been included. Figure 15 shows the cross section at small angles where the neutron–neutron relative momentum is near zero for maximum proton energy and the strong n–n final-state interaction results in a sharp peak in the proton spectrum. Efforts to determine the n–n $^1S_0$ scattering length a_{nn} from the shape of this peak provide a major source of interest in the breakup reaction. It is not easy to relax isospin invariance exactly and introduce a_{nn} independent of a_{np} in the full calculation, since this would necessitate another quasi-particle and another coupled-integral equation. However, it turns out to be sufficient to vary a_{nn} only in the final n–n interaction, i.e., in the final vertex and propagator of Eq. (62). Spectrum shapes for $a_{nn} = -23.78$ fm and -17.0 fm are shown in Fig. 15 , and in fact it appears difficult to distinguish the two experimentally. Quartet and doublet contributions to the differential cross sections are shown in Fig. 16 , where we see that the quartet spectrum is nearly featureless and almost the same as the phase space factor. The doublet spectrum even up to large angles $\theta_p \sim 45°$ is dominated by the final-state interaction peaks.

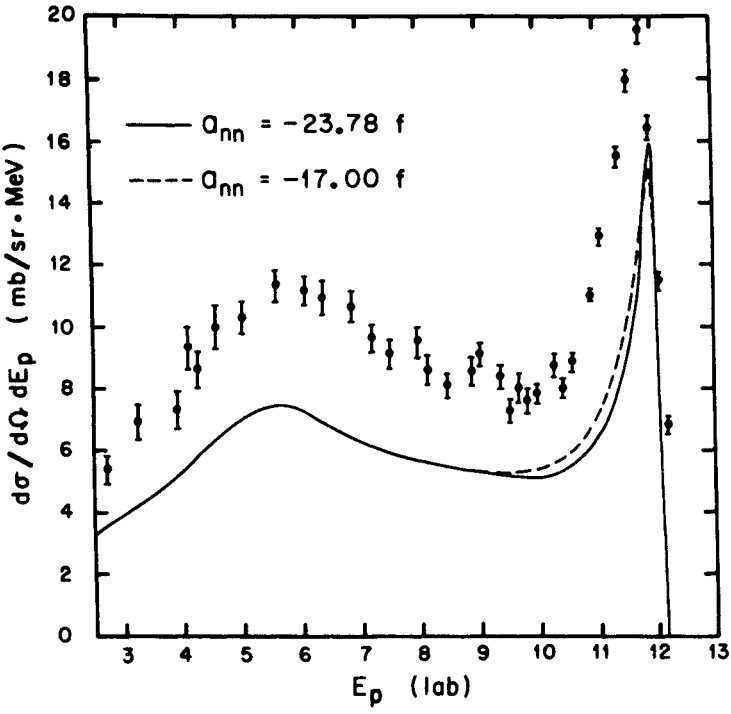

Fig. 15. Proton distribution in n–D inelastic scattering at $E_{LAB} = 14.4$ MeV with two choices of neutron–neutron $^1S_0$ scattering length a_{nn} in the final interaction.

Previous attempts to extract a_{nn} from the spectrum shape[43] have been based on the Watson theory of final-state interactions,[44] in which the full momentum dependence of the matrix element [Eq. (59)] is assumed to be in the final vertex function and propagator of $M_{1/2,\phi}(1, 2; 3)$, with the spectrum near the maximum proton energy proportional simply to $\sin^2 \delta_{nn}$, where δ_{nn} is the $^1S_0$ n–n phase shift at the appropriate n–n relative momentum. Owing to finite experimental resolution it is not possible to determine a_{nn} simply from the location of the peak in the proton-energy spectrum, or from the slope of the high-energy side, but one must use the slope of the spectrum on the low-energy side of the peak. Figure 17 shows the shape of the peak for the full doublet cross section and for the Watson approximation and shows that the Watson theory predicts too broad a peak and would interpret the experimental spectrum in terms of too large a scattering length. In fact, $nD \to nnp$ experiments analyzed this way do predict a_{nn} larger than that obtained from $\pi^- D \to \gamma nn$[45] and inconsistent with $a_{np} = -23.78$ fm and charge independence. The situation is even

worse in comparison with the full (doublet and quartet) cross section, because both these terms are rapidly varying with energy at the spectrum end point and, furthermore, the part of the doublet amplitude in which a proton and neutron interact last also turns out to be important. Evidently the simple Watson theory is very misleading in this case.

The Amado model has also been applied to discussions of the triton wave function and charge and magnetic form factors[5] and, in a different form, to the problems of deuteron stripping by heavy nuclei[46] and pion–nucleon scattering in the static limit.[47] Rosenberg[48] has derived the Amado equations from a Lippmann–Schwinger equation for the elastic scattering of a particle from a bound state of two identical particles, assuming separable S-wave potentials, and Lovelace[12] has derived the Amado equations for rearrangement scattering from the Faddeév integral equations, also assuming separable S-wave interactions. This last development is presented in Appendix E.

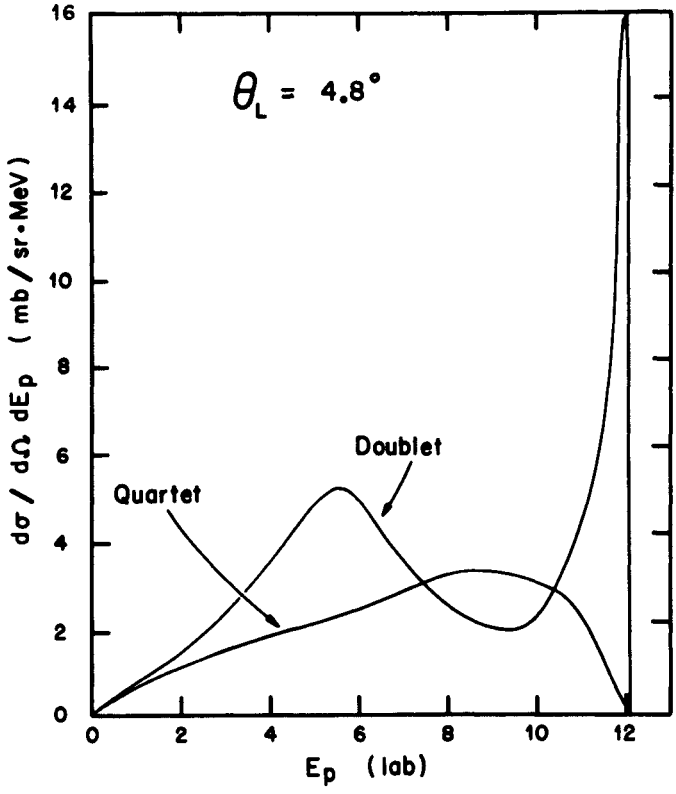

Fig. 16. Doublet and quartet state contributions to proton differential cross section in n–D inelastic scattering at E_{LAB} = 14.4 MeV.

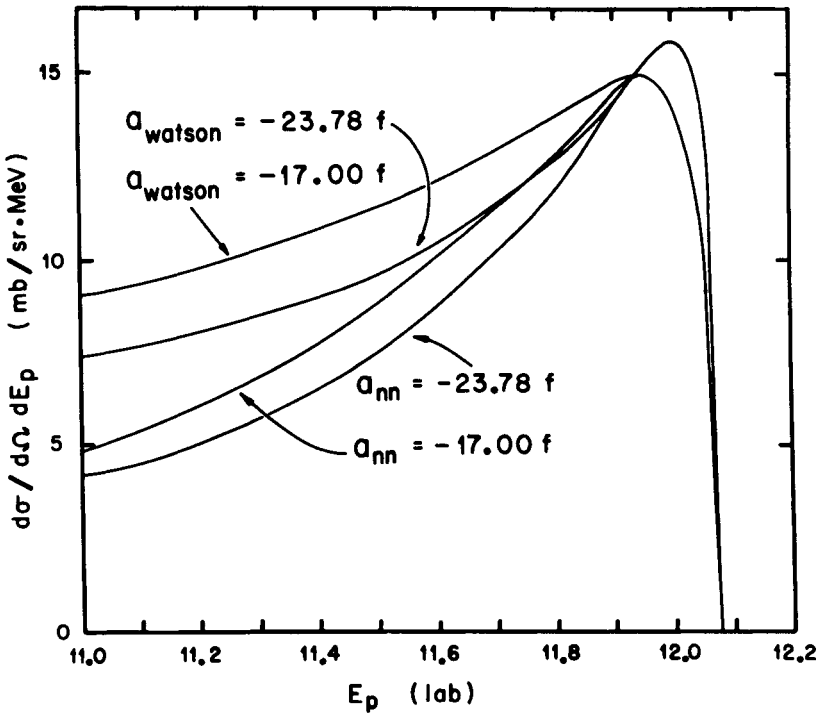

Fig. 17. Comparison of the Watson theory of final-state interactions with the full Amado theory for the proton distribution in n–D inelastic scattering at $E_{LAB} = 14.4$ MeV.

The n–D bound-state and scattering problem has been solved in a similar way by Mitra and his co-workers,[49–55] who base their theory directly on the Schrödinger equation with separable potentials. This approach has a definite advantage when more complicated potentials with tensor forces, hard cores, or $\mathbf{L} \cdot \mathbf{S}$ couplings are included. Mitra and his co-workers have obtained good agreement with experiment except for uncertainties in the value a_2, which is extremely sensitive to the details of the potentials used.

We turn now to the general formulation of three-body scattering as developed by Ekstein, Faddeév, and others.

3. THE FADDEÉV EQUATIONS

3.1 Rearrangement Scattering

We begin this section with a discussion from Ekstein[10] of the S-matrix formalism for rearrangement collisions, in which Ekstein carefully defines

channels and corresponding channel wave functions that are eigenfunctions of various asymptotic Hamiltonians for which one or more interaction terms vanish. [This definition of channel wave functions is distinctly different from that used in nuclear reaction theory,[25] where channel wave functions are defined only outside a reaction volume and have the same asymptotic value as the unknown exact wave function to which they are matched at the (somewhat arbitrary) interaction radius.] Then, as is intuitively evident, the actual time-dependent wave function describing the rearrangement collision of the compound system approaches a time-independent superposition of these channel wave functions at times far removed from the collision. The time-independent absolute square of the amplitude in any one of the channels is the observed cross section for a given initial configuration. Next, we summarize the work of Lovelace,[12] who employs the operator relations for Ekstein's scattering amplitudes to give a succinct derivation of integral equations of the Faddeév form for the experimentally observed amplitudes in three-body collisions. Finally, we turn to the original work of Faddeév,[6] who overcomes the difficulties inherent in a Lippmann–Schwinger approach to three-body scattering amplitudes and finds a system of integral equations for the Green's functions and full wave functions for the three-particle system, from which the Ekstein scattering amplitudes can be constructed.

Ekstein defines channels and corresponding systems of basis functions by which the various transition amplitudes for rearrangement collisions in a three-particle system can be expressed in forms familiar from potential-scattering theory. The basis functions are of four classes and are labeled (0, 1, 2, 3) so that channel (0) corresponds to the free motion of all three particles and the channel-(0) basis functions Φ_0 are the complete set of plane-wave eigenfunctions of the Hamiltonian H_0 for the noninteracting system. Channel (1) corresponds to the free motion of particle (1) and the bound pair (2, 3), and the channel-(1) basis functions Φ_1 are the (incomplete set of) eigenfunctions of the Hamiltonian H_1 (including the (2, 3) interaction exactly), which are products of plane waves for both the motion of particle (1) and the *c-m* motion of (2, 3) and the bound-state wave functions for the relative motion of (2, 3). Similar definitions hold for channels (2) and (3). For the sake of clarity we shall suppose our three particles are distinguishable and that bound states exist for each pair. This will create no difficulty in our eventual discussion. In fact, Ekstein does incorporate the effects of particle identity in his definition of channels and basis functions. Our notation is, hopefully, self-explanatory, but the definitions of H_0, H_1, etc., are collected in Appendix A.

Steady-state solutions of the Schrödinger equation which are asymptotically equal to the channel wave functions Φ_i plus only outgoing waves in all

channels are defined by the operator equation [compare Eq. (23) for the two-particle case]

$$\Psi_i^+ = \Phi_i - G\tilde{V}_i\Phi_i \tag{64}$$

where G is the full three-particle Green's function of Eq. (40) and Appendix A and $\tilde{V}_i$ is the interaction *not* included in channel (i). The ingoing wave solution Ψ_i^- is obtained by using the adjoint to G [with $E + i\eta$ replaced by $E - i\eta$ in Eq. (40)] in Eq. (64). Ekstein establishes the validity of a result formally identical with that of potential scattering, namely, the S-matrix element for a transition-from an incident channel (j) to an outgoing channel (i) is

$$S_{ij} = (\Psi_i^-, \Psi_j^+) \tag{65}$$

Using Eq. (64) and the orthonormality of the Ψ_j^+ (and, separately, of the Ψ_j^-), which Ekstein also establishes, we can express the S-matrix element as

$$S_{ij} = \delta_{ij} - 2\pi i\,\delta(E_i - E_j)\,R_{ij}^{\pm} \tag{66}$$

with

$$R_{ij}^+ = (\Phi_i\,,\,\tilde{V}_i\Psi_j^+) \qquad \text{and} \qquad R_{ij}^- = (\Psi_i^-,\,\tilde{V}_j\Phi_j) \tag{67}$$

where R_{ij}^+ and R_{ij}^- are equal on the energy shell but not off. Lovelace defines transition operators $U_{ij}^{\pm}$ such that

$$R_{ij}^{\pm} = (\Phi_i\,,\,U_{ij}^{\pm}\Phi_j) \tag{68}$$

which satisfy the operator relations [using Eq. (64)]

$$U_{ij}^+ = \tilde{V}_i - \tilde{V}_i G\tilde{V}_j$$

and

$$U_{ij}^- = \tilde{V}_j - \tilde{V}_i G\tilde{V}_j \tag{69}$$

These equations can be recast into a system of linear integral equations by using

$$GV_\delta = Gg_\delta^{-1}g_\delta V_\delta = Gg_\delta^{-1}G_0t_\delta \tag{70}$$

and

$$Gg_\delta^{-1} = 1 - G\tilde{V}_\delta \tag{71}$$

so

$$\begin{aligned} U_{ij}^+ &= \tilde{V}_i - \sum_{\delta\neq j} \tilde{V}_i(1 - G\tilde{V}_\delta)\,G_0t_\delta \\ &= \tilde{V}_i - U_{i\delta}^+G_0F_{\delta j} \end{aligned} \tag{72}$$

and

$$U_{ij}^{-} = \tilde{V}_j - F_{i\delta}^{T} G_0 U_{\delta j}^{-} \tag{73}$$

Here we have used the characteristic Faddeév kernel F (and its transpose F^T) which is defined by (see also Appendix A)

$$F_{ij} = t_i(1 - \delta_{ij}) \tag{74}$$

In Eqs. (71) and (72) the repeated index δ is summed over.

The Green's functions that we use in Eq. (70) have the following meanings: G is the full three-particle Green's function

$$G(E) = (H - E^{+})^{-1} \tag{75}$$

with H, the full Hamiltonian for the three-particle system; G_0 is the free three-particle Green's function

$$G_0(E) = (H_0 - E^{+})^{-1} \tag{76}$$

with H_0, the free Hamiltonian for the three particles, just the kinetic energy. The Green's function g_1, e.g., is slightly different from the two-particle Green's function for the pair (2, 3) introduced in Eqs. (25) and (26), in that the Hamiltonian now includes the kinetic energy of particle (1) in addition to the full Hamiltonian for the pair (2, 3). It is the two-particle Green's function in the three-particle Hilbert space. Similarly, the t matrix t_1 is the two-particle t matrix in the three-particle Hilbert space and satisfies an equation identical in form with Eq. (30) with g replaced with g_1. It has matrix elements

$$\begin{aligned}
&\langle \mathbf{p}_1'\mathbf{p}_2'\mathbf{p}_3' \mid t_1(E) \mid \mathbf{p}_1\mathbf{p}_2\mathbf{p}_3\rangle \\
&\quad = (2\pi)^3\, \delta^3(\mathbf{p}_1 - \mathbf{p}_1') \left\langle \mathbf{p}_2'\mathbf{p}_3' \,\middle|\, t_1\left(E - \frac{p_1^{\,2}}{2m_1}\right) \middle|\, \mathbf{p}_2\mathbf{p}_3 \right\rangle \\
&\quad = (2\pi)^3\, \delta^3(\mathbf{p}_1 - \mathbf{p}_1')(2\pi)^3\, \delta^3\,(\mathbf{p}_2' + \mathbf{p}_3' - \mathbf{p}_2 - \mathbf{p}_3)\langle \mathbf{p}_{23}' \mid t_1(E_{23}) \mid \mathbf{p}_{23}\rangle
\end{aligned} \tag{77}$$

where $\mathbf{p}_{23}$ and $\mathbf{p}_{23}'$ are the relative momenta of particles (2) and (3) in the initial and final states and E_{23} is the total energy minus the kinetic energy of particle (1) and minus the kinetic energy of the c-m of (2, 3). The remaining matrix element in Eq. (77) is an off-energy-shell matrix element of the two-particle t matrix defined in Eq. (20).

Faddeév[9] and Lovelace[12] demonstrate the desired compactness of the kernel of the integral equation (72), which means that, at least in principle, its unique solution can be found by numerical methods such as matrix inversion, in which the kernel is approximated by an operator of finite rank.

Weinberg[38] also discusses the conditions under which this Faddeév kernel is compact. Recall that the square of the Lippmann–Schwinger kernel[41] contains the square of delta functions corresponding to a succession of interactions, in which one of the particles does not interact with the other two (disconnected diagrams) and is therefore not $L^{(2)}$ and not compact. The iterated Faddeév kernel does not suffer from this disease and includes only those processes in which successive interactions take place between different pairs (connected diagrams). The iterated Faddeév kernel contains terms like

$$t_1 \quad G_0 \quad t_2$$

which will never give the square of a delta function, and is $L^{(2)}$ (for negative or complex E) provided the interactions themselves are.[7,8] Faddeév is able to show that after five iterations the kernel is compact even for real, positive E.

3.2 The Faddeév Equations

Let us leave these equations temporarily while we discuss the original work of Faddeév and demonstrate the equivalence of his results with the transition amplitudes $U^{\pm}$, which are the experimentally measured S-matrix elements.

The full three-particle wave functions in the various channels are determined by the Schrödinger equation written in integral form to display the asymptotic conditions as [recall Eq. (28) for two-particle scattering]

$$\Psi_n = \lim_{\eta \to 0^+} - i\eta G \Phi_n \tag{78}$$

and one readily obtains equations of the Lippmann–Schwinger variety by expressing the full Green's function G in terms of G_0. Then for channel (0)

$$\begin{aligned} \Psi_0 &= \lim_{\eta \to 0^+} - i\eta (G_0 - G_0 V G)\, \Phi_0 \\ &= \Phi_0 - G_0 V \Psi_0 \end{aligned} \tag{79}$$

where we have used $\Phi_0 = \lim - i\eta G_0 \Phi_0$. However, if we look at the channel-(1) wave function, e.g., we obtain

$$\Psi_1 = \lim(-i\eta G_0 \Phi_1) - G_0 V \Psi_1$$

But the first term here is zero, since $(H_0 - E)\, \Phi_1 \neq 0$ and Ψ_1 satisfies a homogeneous equation with the same kernel as in the equation for Ψ_0. This means that the solution of Eq. (79) is not uniquely determined by the inhomogeneous term and Eq. (79) is not an integral equation in this usual

sense. The kernel is noncompact with a number of delta-function singularities, as discussed in the introduction. Faddeév succeeded in finding a system of integral equations for the three-particle wave functions, each of which is inhomogeneous and for all of which the kernel is compact and the solutions uniquely determined.

Faddeév begins his derivation[6] by writing the complete Green's function in terms of an operator T

$$G = G_0 - G_0 T G_0 \tag{80}$$

so that T satisfies

$$T = V - V G_0 T \tag{81}$$

If we simply write out the terms generated by iterating this equation

$$\begin{aligned} T &= V_1 + V_2 + V_3 - (V_1 + V_2 + V_3)\, G_0 (V_1 + V_2 + V_3) + \cdots \\ &= V_1 - V_1 G_0 V_1 + \cdots + V_2 - V_2 G_0 V_2 + \cdots - V_1 G_0 V_2 + \cdots \end{aligned} \tag{82}$$

we can identify the various subseries of terms and write this in terms of the two-particle t matrices (see Appendix A) as

$$T = t_1 + t_2 + t_3 - t_1 G_0 t_2 - t_1 G_0 t_3 + \cdots \tag{83}$$

which Faddeév recognizes as terms in an integral equation for T. Provided we write

$$T = T_1 + T_2 + T_3 \tag{84}$$

then Eq. (83) is just

$$T_1 = t_1 - t_1 G_0 (T_2 + T_3) \tag{85}$$

and similarly for T_2 and T_3. We can write these succinctly in matrix form in terms of the Faddeév kernel, Eq. (74), as

$$T_i = t_i - F_{ij} G_0 T_j \tag{86}$$

where the index (j) is summed over. These equations can be derived without recourse to a perturbation expansion,[9] but this is sufficient for our purposes. Evidently T_i is the term in the T operator corresponding to the pair (i) interacting last [here we label a pair equivalently as (2, 3) or (1), e.g.]. We can further write

$$T_i = \sum_k T_{ik} \tag{87}$$

where

$$T_{ik} = t_i \delta_{ik} - F_{ij} G_0 T_{jk} \tag{88}$$

and identify T_{ik} as the term in T corresponding to the pair (k) interacting first and the pair (i) interacting last.

The Faddeév equation (86) for T can be deduced as well from the diagrams of Fig. 18*a* and *b*, which makes clear the significance of the T_i as terms in $\dot{T}$ corresponding to the pair (i) interacting last. In Fig. 18 solid lines represent the particles (1, 2, 3) and connecting dotted lines represent the full off-energy-shell two-particle scattering amplitude. The blobs represent the full three-particle T matrix. The further breakdown of the T matrix into the T_{ij} is expressed in Fig. 18*c*, and the diagrammatic representation of Eq. (88) in Fig. 18*d*.

We shall make use of the T_{ik} later to demonstrate the equivalence of the Lovelace and Faddeév transition operators, and in fact we find for the elastic scattering amplitude

$$U_{ii}^{(+)} = \sum_{jk \neq i} T_{jk} \tag{89}$$

Combining Eqs. (80) and (86), we can write the complete Green's function as

$$G = G_0 + G_1 + G_2 + G_3 \tag{90}$$

with

$$G_i = (g_i - G_0) - G_0 F_{ij} G_j \tag{91}$$

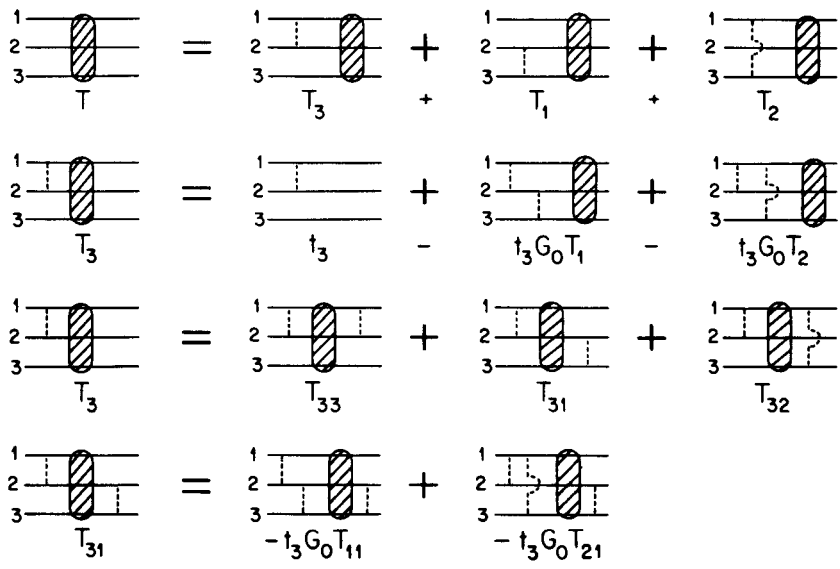

Fig. 18. Diagrams representing the Faddeév decomposition of the three-particle T matrix, and the terms in the various forms of the Faddeév integral equation.

where $(i, j) = 1, 2, 3$ and g_i is the two-particle Green's function. We are now ready to write inhomogeneous integral equations of the Lippmann–Schwinger type for the eigenfunctions in each of the four channels. For any channel (n)

$$\Psi_n = \lim_{\eta \to 0} - i\eta G \Phi_n$$

where the Φ_n are the basis functions described at the beginning of this section. For channel (0) with Eq. (90) for G and writing

$$\Psi_0 = \Phi_0 + \sum_{i=1}^{3} \Psi_0^{\,i} \tag{92}$$

we obtain (with $\lim \eta \to 0^+$ understood)

$$\Psi_0 = -i\eta G_0 \Phi_0 - i\eta \sum_{i=1}^{3} G_i \Phi_0 \tag{93}$$

Since $-i\eta G_0 \Phi_0 = \Phi_0$, we can identify

$$\begin{aligned} \Psi_0^{\,i} &= -i\eta G_i \Phi_0 \\ &= -i\eta g_i \Phi_0 - \Phi_0 - G_0 F_{ij} \Psi_0^{\,j} \\ &= (\Phi_i^{\,c} - \Phi_0) - G_0 F_{ij} \Psi_0^{\,j} \end{aligned} \tag{94}$$

For $i = 1, 2, 3$, Eq. (94) becomes a system of integral equations coupling the components $\Psi_0^{\,i}$ of the channel-(0) wave function Ψ_0. Here the $\Phi_1^{\,c} = -i\eta g_1 \Phi_0$ are closely related to the channel-(1) basis functions Φ_1, which are eigenfunctions of the Hamiltonian H_1 and products of plane waves for both the motion of (1) and the c-m motion of (2, 3) and the bound-state wave function for (2, 3). $\Phi_1^{\,c}$ has the pair (2, 3) in a positive-energy outgoing-wave scattering state. Equations (92) and (94) determine the exact channel-(0) wave function for the three-particle system.

The virtue of the Faddeév formulation becomes clear when we find inhomogeneous equations also for the wave functions in the other channels. The Faddeév integral equations have the essential property that the solutions are uniquely determined by the inhomogeous term and the kernel, properties which are not possessed by the equations obtained from a straightforward manipulation of the Lippmann–Schwinger equations. From Eq. (91), with the channel-$(i \neq 0)$ basis function

$$\Psi_i = \sum_{j=1}^{3} \Psi_i^{\,j} \tag{95}$$

we obtain

$$\Psi_i = -i\eta G_0 \Phi_i - i\eta \sum_{j=1}^{3} G_j \Phi_i$$

Now $-i\eta G_0\Phi_i = 0$, so with Eq. (87)

$$\begin{aligned}\Psi_i^j &= -i\eta g_j\Phi_i - G_0F_{jk}(-i\eta G_k)\,\Phi_i \\ &= \delta_{ij}\Phi_j - G_0F_{jk}\Psi_i^k\end{aligned} \tag{96}$$

Let us collect these Faddeév equations for the three-particle wave functions:

a. In channel (0)

$$\Psi_0 = \Phi_0 + \sum_{j=1}^{3} \Psi_0^j \tag{97}$$

$$\Psi_0^i = (\Phi_i^c - \Phi_0) - G_0F_{ij}\Psi_0^j \tag{98}$$

b. In channel ($i \neq 0$)

$$\Psi_i = \sum_{j=1}^{3} \Psi_i^j \tag{99}$$

$$\Psi_i^j = \delta_{ij}\Phi_j - G_0F_{jk}\Psi_i^k \tag{100}$$

and reiterate the virtue of the Faddeév integral equations: The wave functions in all channels satisfy inhomogeneous equations with the Faddeév kernel, and the solutions are uniquely determined by the inhomogeneous term. Furthermore Faddeév has shown that the Faddeév kernel is compact except on the positive-energy branch cuts and that even here the singularities of the kernel are sufficiently innocuous so that the kernel becomes compact after a number of iterations.

We can readily recover the Lovelace expression (69) for the Ekstein transition amplitude, Eq. (68). Write the full channel wave function, Eq. (100), for $i \neq 0$

$$\Psi_i = \Phi_i - \sum_j G_0t_j\tilde{\Psi}_i^j \tag{101}$$

where $\tilde{\Psi}_i^j = \sum_{k\neq j} \Psi_i^k$ and we have used the Faddeév kernel. Now

$$G_0^{-1}\Psi_i = -V\Psi_i \qquad \text{and} \qquad G_0^{-1}\Phi_i = -V_i\Phi_i$$

so

$$V\Psi_i = V_i\Phi_i + \sum_j t_j\tilde{\Psi}_i^j \tag{102}$$

We can use Eq. (102) to undo the Faddeév expansion of the wave function, and obtain

$$\Psi_i = \Phi_i - G_0V\Psi_i - G_0V_i\Phi_i$$

or

$$\begin{aligned}\Psi_i &= (1 + G_0V)^{-1}(1 + G_0V - G_0\tilde{V}_i)\,\Phi_i \\ &= (1 - G\tilde{V}_i)\,\Phi_i \qquad (103)\end{aligned}$$

and we recover just Ekstein's operator relation, Eq. (64) for the full channel wave function, from which we readily obtain Lovelace's integral equation for the transition amplitudes U.

For the elastic scattering amplitude in particular, the relation between the Lovelace transition operator U and the terms in the decomposed Faddeév T operator T_{lm} is direct and expressed in Eq. (89). To prove this relation go back to Eq. (69)

$$\begin{aligned}U_{ii}^{(+)} &= \tilde{V}_i - \tilde{V}_i G \tilde{V}_i \\ &= \tilde{V}_i - \tilde{V}_i g_i U_{ii}^{(+)} \qquad (104)\end{aligned}$$

just the Lippmann–Schwinger equation for the elastic scattering amplitude, which has the formal solution

$$U_{ii}^{(+)} = \sum_{lm \neq i} T_{lm} \qquad (89)$$

with

$$T_{lm} = V_l\,\delta_{lm} - V_l(1 + G_0V)^{-1}\,G_0V_m \qquad (105)$$

where Eq. (105) must be recognized as the solution to

$$T_{lm} = V_l\,\delta_{lm} - V_lG_0 \sum_k{}' T_{km} \qquad (106)$$

We can recast Eq. (106) into the Faddeév equation (88) by collecting all the terms T_{lm} on the left and multiplying by $(1 - V_lG_0)^{-1}$ to get

$$T_{lm} = t_l\,\delta_{lm} - F_{lk}G_0T_{km} \qquad (88)$$

A multiple-scattering expansion of Eq. (88) gives

$$T_{lm} = t_l\,\delta_{lm} - t_lG_0t_m + t_lG_0t_kG_0t_m + \cdots \qquad (107)$$

where $l \neq m$ in the double-scattering term and $k \neq l, m$ in the triple-scattering term. The expansion (107) justifies the interpretation of T_{lm} as the term in T with the pair (m) interacting first and (l) last.

We turn now to some specific applications of the Faddeév formalism.

4. APPLICATION OF THE FADDEÉV EQUATIONS

4.1 Hetherington–Schick Analysis of the Multiple-Scattering Series

Hetherington and Schick (referred to as HS)[13,14] have solved the Faddeév integral equations (88) with separable S-wave two-particle potentials chosen to simulate (K–D) elastic scattering, with a view to comparing the previously used impulse approximation (IA) and double-scattering approximation (DSA) with the full multiple-scattering (MS) solution including all rescattering corrections. They find significant corrections to the IA and DSA at kaon laboratory energies of 11.2, 38.2, and 91.5 MeV where they performed their calculations. In their work they take full account of the spin–isospin complexity of the problem including, eventually, the kaon and n–p mass splitting. For the sake of clarity in illustrating the calculation techniques required, we have paraphrased their work, using spinless isoscalar particles, in Appendix D where we take appropriate matrix elements and partial-wave projections of the Faddeév integral equation (88) for the elements of the operator T_{ij} which make up the elastic scattering operator $U_{11}^{(+)}$. Hetherington and Schick take account of the K–n interaction through a separable S-wave potential with a complex strength parameter chosen to give the experimental isotopic singlet and triplet scattering lengths ($\tan\delta = +kA$, opposite to the usual choice of sign)

$$\begin{aligned} A_0 &= (-0.50 + i.96)\ \text{fm} \\ A_1 &= (1.20 + i.56)\ \text{fm} \end{aligned} \tag{108}$$

and an assumed range parameter in the Hulthén form factor, Eq. (52),

$$\beta^{-1} = 0.4\ \text{fm} \tag{109}$$

They choose Yamaguchi's original n–p ^3S nucleon–nucleon interaction.[31]

The kernel of the integral equation (D.12) in Appendix D has a number of singularities due to the vanishing of denominators in Eq. (D.13a) which, for energies above the inelastic threshold, come close to the real axis and make numerical integration of Eq. (D.12) difficult. Hetherington and Schick circumvent this problem by rotating the contour of integration into the fourth quadrant and as far away from these singularities as possible (without crossing any of them) in order to find a contour along which the kernel is a slowly varying function and the numerical solution of the integral equation is possible with a small number of mesh points. Scattering amplitudes for real momenta are then recovered by one further integration of Eq. (D.12). In rotating the integration contour it has been necessary to assume that no singularities of the full three-particle amplitude $\langle \hat{T} \rangle$ get in the way, since its analyticity properties are not well understood.

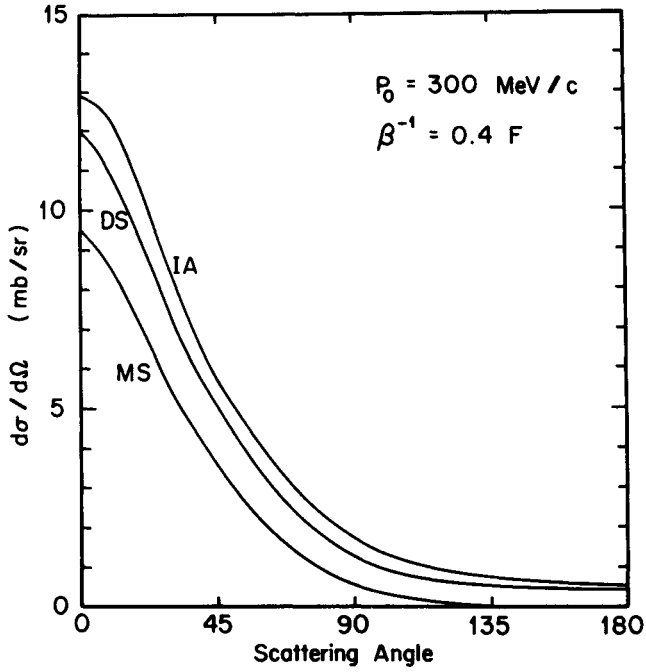

Fig. 19. K^-–D elastic-scattering cross section at $E_{LAB} = 91.5$ MeV in the impulse, double scattering, and full multiple scattering theory.

The results of these calculations are illustrated in Fig. 19, 20, and 21 were the elastic differential (K–D) cross section at kaon laboratory energies of 91.5, 38.2, and 11.2 MeV (kaon laboratory momentum $p_0 = 300$, 194, 105 MeV/c) are shown in the IA, DSA, and full MS. The IA is obtained with just the $t_i\,\delta_{ik}$ term in Eq. (88), and the DSA with the first iteration of this. In all cases it was sufficient to treat partial waves $L = 0,1$ in MS; $L = 2, 3$ in DSA; $L = 4, 5, 6, 7$ in IA and to neglect partial waves with $L > 7$ to obtain a precision better than 1% in any of the amplitudes. Figures 19, 20, and 21 show that rescattering effects are large at all these energies. The IA produces the correct angular distribution but fails by factors of 2 or 3 to produce the correct magnitude of cross section. The DSA does not improve the IA and can give a correction in the wrong direction or one that is deceptively small. All these results are found to be insensitive to the range parameter for $0.1 < \beta^{-1} < 0.4$ fm. Successive terms in the S-wave amplitude

$$\eta_0 = e^{i\delta} \sin \delta / p = \eta_{IA} + \eta_{DSA} + \eta_{MS} \tag{110}$$

are shown in Fig. (22).

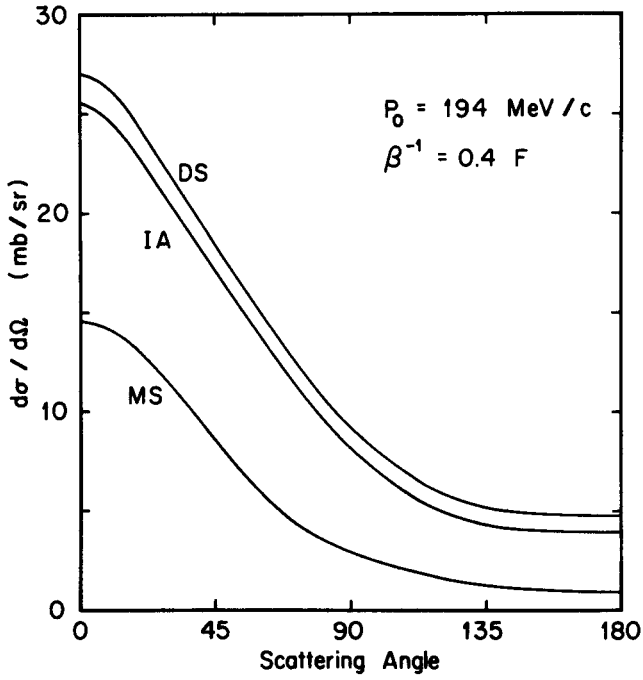

Fig. 20. K^-–D elastic-scattering cross section at $E_{LAB} = 38.2$ MeV in the impulse, double scattering, and full multiple-scattering theory.

These calculations illustrate clearly the inadequacy of the IA and DSA in understanding the actual cross section and demonstrate the importance of a full MS, at least in the S-wave amplitude.

4.2 Lovelace–Phillips' Calculations of Neutron–Deuteron Scattering

Lovelace[12] has derived Lippmann–Schwinger type of equations for the rearrangement scattering amplitude for three particles interacting through separable S-wave potentials, starting from the Faddeév integral equation (72) for the scattering operator U_{ij}. These equations, presented in Appendix E for the simple case of distinguishable particles with one bound state for each pair, are the same as those deduced by Amado in the limit $Z = 0$.

Phillips[16] has solved these equations numerically for the case of n–D elastic and inelastic scattering, taking account of the deuteron and singlet deuteron quasi-particles, and gets results in reasonable agreement with those obtained by Amado. He finds it necessary to include a repulsive three-body force in the doublet channel to get agreement with the triton binding energy and the n–D scattering length a_2. Without the three-body force the results

are in close agreement with the $Z = 0$ limit of Amado's calculations and give a too tightly bound triton and a negative doublet scattering length.

4.3 Relativistic Faddeév Equations

A number of authors[56–59] have made *ad hoc* modifications of the Faddeév equations to make them relativistically invariant. In practice this modification, which is by no means unique,[60] amounts to the replacement of the nonrelativistic three-body Green's function with a relativistic three-body propagator, a covariant normalization of state vectors, and a covariant definition of phase space and to the use of relativistic kinematics.[60,61] The resulting equations are relativistically invariant and guarantee three-body elastic unitarity and reduce to the Faddéev equations in the nonrelativistic limit. They are, in an approximate sense, a sum of connected relativistic three-body ladder diagrams. However, they have the essential drawbacks of not being crossing symmetric and of containing only elastic processes, so that they are only a model of a true relativistic theory, though one that contains two features otherwise difficult to incorporate[12]: three-body unitarity and

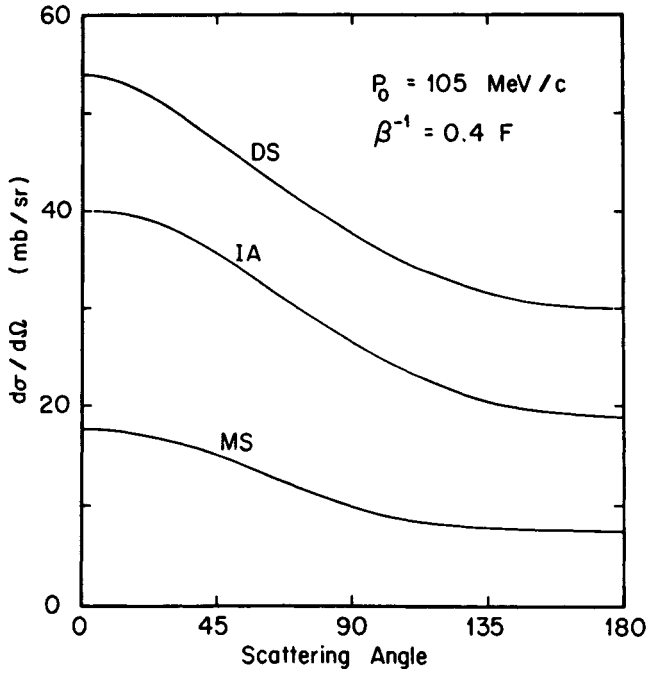

Fig. 21. K^-–D elastic-scattering cross section at $E_{LAB} = 11.2$ MeV in the impulse, double scattering, and full multiple-scattering theory.

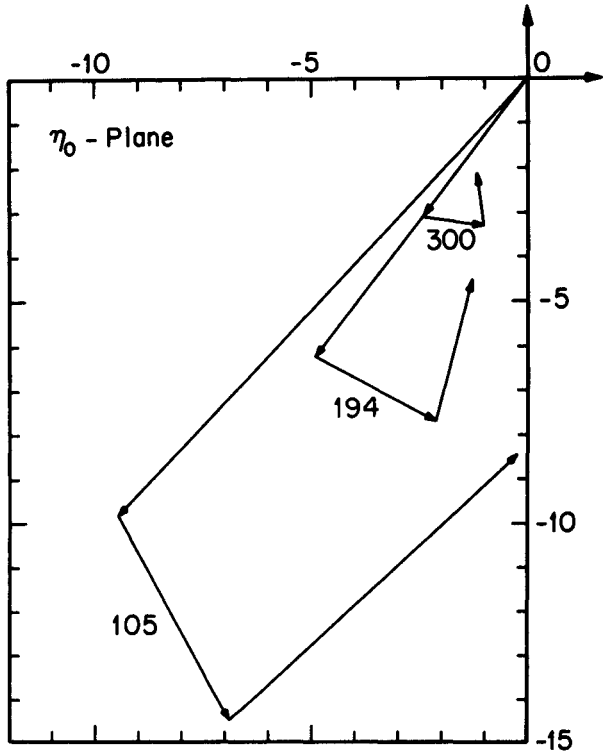

Fig. 22. Contributions to the complex K^-–D elastic-scattering amplitude coming from the impulse approximation (first arrow), double-scattering approximation (second arrow), and all other rescatterings (final arrow) at K^- incident momentum $P_0 = 300$, 194, and 105 MeV/c.

unstable two-particle states. These two features have made their use attractive in efforts to understand the many heavy mesons which decay into three-pion states[62,63] dominated by two-particle resonances and to study the effect of spin and overlapping two-body resonances on the Dalitz distributions of the three final-state pions. These model calculations can succeed only if the effects of overlapping resonances and three-body unitarity are sufficient to dominate the other dynamical processes causing three-body bound states and resonances.

Two great simplifications must be made to recast the relativistic three-body Bethe–Salpeter equation into the form of the Faddeév equations. First, the Bethe–Salpeter equation for the three-particle T matrix involves six amplitudes instead of three, because the kernel contains two-body amplitudes with one initial and one final particle off the mass shell. All these

amplitudes are in general distinct, and this leads to six coupled equations instead of three. The simplifying assumption that the two-body off-shell amplitude depends only on the relative momentum in the initial and final states and on the invariant energy reduces the six coupled equations to three. This restrictive assumption is dictated both by a desire to simplify the equations and by a complete lack of knowledge of the off-shell amplitudes. Second, the Bethe–Salpeter equation contains, in place of the free three-particle Green's function, two relativistic single-particle propagators which are functions of two off-shell four-momenta and would lead to an eight-dimensional integral. It is necessary to put these two intermediate particles on their mass shells and to replace the product of relativistic propagators with a three-particle propagator which can be defined in a number of ways. The simplest way is to replace the nonrelativistic kinetic energies in G_0 with relativistic kinetic energies.[60] Alessandrini and Omnes[58] write a dispersion integral in the three-body invariant energy (s) and obtain in place of $t_i G_0$

$$t_i A_i(s) = t_i \left[\frac{2}{\omega_j \omega_k} \frac{\sum_{n=1}^{3} \omega_n}{(\sum_{n=1}^{3} \omega_n)^2 - s} \right] \tag{111}$$

where $\omega_i^2 = (k_i^2 + 1)$ and (i, j, k) are cyclic $(1, 2, 3)$. All masses are set equal to 1. Less symmetrical generalizations of the nonrelativistic G_0 are possible[59,61] based on a dispersion representation in two-body and one-body invariant energies. After these simplifications it is necessary, following a partial-wave analysis,[60,17] to make the separable approximation on the two-particle scattering amplitudes to reduce the integral equations to one dimension.

The limitations of the relativistic Faddeév equations in the separable pole approximation have been carefully examined by Basdevant and Omnes,[64] who conclude that they have a limited region of applicability and that a number of calculations, particularly on three-pion bound states and resonances, are invalid. The separable pole approximation in the two-particle scattering amplitude is a weakness that casts doubt on the calculation of bound states of three particles, since it is only presumed valid when the two-particle energy $\sigma^{1/2}$ is in the neighborhood of the resonance mass m_R. However, in the integrations

$$\sigma = s - 2\omega \sqrt{s} + m^2 \tag{112}$$

and $m \leqslant \omega \leqslant \infty$, so σ varies from $(\sqrt{s} - m)^2$ to $-\infty$. For a three-body bound state with $s < (m_R + m)^2$, the integration is completely over a region where the two-particle amplitude is unreliable. Basdevant and Omnes maintain that this precludes the calculation of the ω meson as a π–ρ bound state, but does

not rule out the calculation of meson resonances near the π–ρ threshold,[62,63] where the ρ resonance pole does dominate the two-particle amplitude.

Basdevant and Omnes[64] point out another flaw characteristic of the relativistic Faddeév type of linear integral equations in three-momentum variables obtained from the Bethe–Salpeter equations, i.e., a spurious singularity at $s = 0$. The spurious singularities are claimed to dominate the eigenvalues near $s = 0$ and even to give rise to an infinite number of zero-energy bound states in special circumstances.

There are still a number of problems such as $\pi n \to n\pi\pi$, $K \to 3\pi$, the A mesons, etc., where these equations can be used to investigate intermediate energy problems.

4.4 Three-Particle Correlation Energy in Nuclear Matter

Bethe[18] has introduced the use of the Faddeév integral equations to sum a class of terms entering the Breuckner–Goldstone (BG) perturbation series for the groundstate energy of nuclear matter. In diagrams we can represent the BG series as in Fig. 23. Solid horizontal lines represent holes in the Fermi sphere, broken vertical lines represent an interaction through the two-particle scattering (or reaction) matrix t. (The diagrams are frequently drawn with hole lines as closed loops, but the method we use here makes comparison with the multiple-scattering series clearer.) The first term in the BG series (Fig. 23*a*) includes all two-hole interactions and is exact to second order in the density of nuclear matter ρ. That is, in an expansion of the interaction energy per particle in powers of the nuclear density ρ, these are the terms proportional to ρ. In order to test the convergence of the BG series, it is not sufficient to include just the terms of order t^3 since, as Rajaraman[65] has pointed out, there are a series of higher-order terms which make important contributions. In fact, all terms with three-hole lines and any number of two-particle interactions between successively different pairs must be included. The sum of these three–hole diagrams gives the ρ^2 term in the ground-state energy. Typical three-hole diagrams of order t^3 and higher are shown in Fig. 23*b*. Four-hole diagrams of order t^4, which are not included but would enter the ρ^3 term in the energy, are shown in Fig. 23*c*.

The diagrams of Fig. 23*b* correspond closely to the three-particle scattering diagrams of Fig. 18. The difference is that each of these diagrams has a first and last two-particle interaction separated from the rest of the diagram by a *two*-hole propagator. For example, the diagram of Fig. 23*d* can be written

$$t_3 \frac{Q}{e} \phi_{32} \frac{Q}{e} t_2 \tag{113}$$

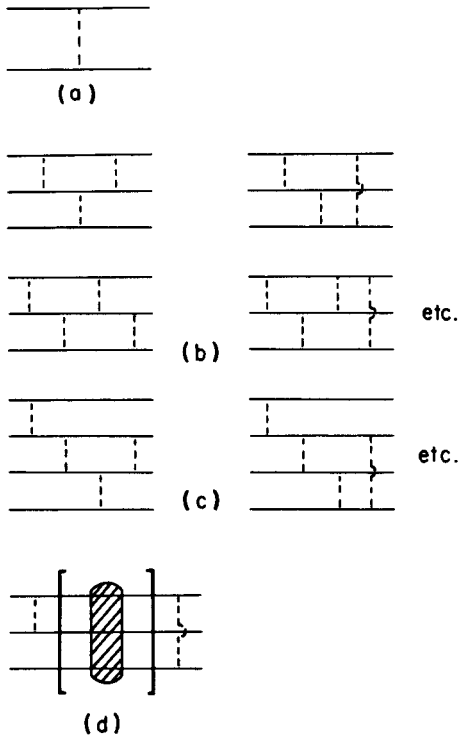

Fig. 23. (a) Two-hole diagram in the Brueckner–Goldstone perturbation expansion of the ground-state energy of nuclear matter; (b) 3-hole diagrams summed by the Faddeév integral equation to give three-particle correlation energy contribution to the ground-state energy of nuclear matter; (c) 4-hole diagrams of order ρ^3 in the ground-state energy of nuclear matter; and (d) the general structure of three-hole diagrams in the Brueckner–Goldstone expansion. The amplitude ϕ_{32} sums all contributions between the first and last interactions.

where t_3, the scattering matrix for particles 1 and 2 interacting through the potential v_3 in the nuclear medium, is

$$t_3 = v_3 - v_3 \frac{Q}{e} t_3 \tag{114}$$

Here e is the energy denominator in the nuclear medium with ground-state energy W; Q is the Pauli exclusion operator, which allows intermediate states outside the Fermi sphere only; and ϕ_{ij} is the sum of all diagrams with

three-hole lines where the first interaction is *not* between pair (j) and the last is *not* between the pair (i). The contribution of three-hole diagrams to the ground-state energy is[18]

$$W_3 = \tfrac{1}{3} \sum_{ij} \int d^3x_1\, d^3x_2\, d^3x_3 \Phi_0^* \left\{ t_i \frac{Q}{e} \phi_{ij} \frac{Q}{e} t_j \right\} \Phi_0 \tag{115}$$

where Φ_0 is the wave function of the unperturbed ground-state.

We have already expressed the sum of all connected three-particle diagrams in Fig. 18 as

$$T = \sum_i T_i = \sum_{ij} T_{ij} \tag{87}$$

where T_{ij} is the amplitude with pair (j) interacting first and pair (i) last, and for the scattering problem

$$T_{ij} = t_i \delta_{ij} - F_{ik} G_0 T_{kj} \tag{88}$$

Evidently we need to modify the Faddeév equation in the presence of nuclear matter by changing the free-particle Green's function G_0 to Q/e and by using the two-particle scattering matrix t calculated in the nuclear medium. The operator ϕ_{ij} can be identified as

$$\phi_{ij} = \sum_{m \neq i, n \neq j} T_{mn} \tag{116}$$

These are an exact system of equations for the three-particle correlation energy and could be attacked numerically. However, Bethe has obtained an approximate analytical solution starting from a zero-energy plane-wave unperturbed wave function Φ_0 for the three particles. He is then able to reduce the integral equation for the exact three-particle wave function to a system of linear algebraic equations and finally express W_3 as an integral over products of two-particle correlation functions. A careful examination of his procedure by subsequent authors[19,20,66] has not altered his conclusion that the three-particle correlation energy is in the neighborhood of 1 MeV compared with a two-particle correlation energy of —30 MeV per particle.

5. CONCLUDING REMARKS

The Faddeév theory provides an exact, systematic procedure for attacking any nonrelativistic three-body problem, and, with the simplifying assumption of separable potentials between the interacting pairs, the resulting integral equations can often be solved numerically.

The Amado model of neutron–deuteron elastic and inelastic scattering,

which is equivalent to the Faddeév equations with one-component separable S-wave potentials between pairs of nucleons, reproduces the low-energy experimental results with great success. However, Mitra[53] points out that Amado's success in obtaining the experimental triton binding energy and n–D doublet scattering length with S-wave forces and a single adjustable parameter Z is not a satisfactory solution to the problem because it masks the real mechanisms—hard cores, tensor forces, and relativistic effects—upon which these quantities, especially the doublet scattering length, depend in an extremely sensitive way. Mitra and his colleagues[49–55] have incorporated the effects of tensor forces and hard cores in his three-body theory based directly on the Schrödinger equation with separable potentials.[49] They are able to solve these equations, including the tensor force but neglecting the hard core, and find that acceptable two-particle forces which give the correct triton binding energy give the wrong magnitude and even the wrong sign for the doublet length. Mitra conjectures that this discrepancy is due to the effect of hard cores in the ^1S potential, an effect that was masked in Amado's treatment (and also in Phillips') by the use of a large effective range in the ^1S potential, which does not give a good fit to the p–p phase shift even at 30 MeV. Since n–D scattering is perhaps the most fundamental three-body problem, it is clearly important to surmount the computational barriers in the way of a simultaneous evaluation of the tensor and hard-core effects and the eventual inclusion of higher partial waves in the two-particle interaction.

The way is now clear to apply the Faddeév techniques to other problem, including the photodisintegration of the triton; three-alpha particle breakup of C^{12}, which is an example of a three-particle state with overlapping two-particle resonances; and many other less fundamental but nonetheless interesting reactions in low-energy nuclear physics.

Acknowledgments

I am particularly indebted to Professor G. C. Phillips, who encouraged me to study three-body problems, and to my colleagues, Dr. Faqir Khanna and Dr. Balram Singh Bhakar, who have been so generous in sharing their knowledge of the subject.

REFERENCES

1. R. Amado, *Phys. Rev.* **132**:485 (1963).
2. R. Aaron, R. Amado, and Y. Yam, *Phys. Rev.* **136**:B650 (1964).
3. R. Aaron, R. Amado, and Y. Yam, *Phys. Rev.* **140**:B1291 (1965).
4. R. Aaron and R. Amado, *Phys. Rev.* **150**:857 (1966).
5. R. Amado, *Phys. Rev.* **141**:902 (1966).
6. L. Faddeév, *Soviet Phys. JETP (English Transl.)* **12**:1014 (1961).

7. L. Faddeév, *Soviet Phys. "Doklady" (English Transl.)* **6**:384 (1961).
8. L. Faddeév, *Soviet Phys. "Doklady" (English Transl.)* **7**:600 (1963).
9. L. Faddeév, "Mathematical Problems of the Quantum Theory of Scattering for a Three-Particle System." Publication of the Steklov Mathematical Institute, Leningrad (1963); and H. M. Stationery Office, Harwell, Eng. (1964).
10. H. Ekstein, *Phys. Rev.* **101**:880 (1956).
11. E. Gerjuoy, *Phys. Rev.* **109**:1806 (1958).
12. C. Lovelace, *Phys. Rev.* **135**:B1225 (1964).
13. J. Hetherington and L. Schick, *Phys. Rev.* **137**:B935 (1965).
14. J. Hetherington and L. Schick, *Phys. Rev.* **139**:B1164 (1965).
15. J. Hetherington and L. Schick, *Phys. Rev.* **141**:1314 (1966).
16. A. Phillips, *Phys. Rev.* **142**:984 (1966).
17. R. Omnes, *Phys. Rev.* **134**:B1358 (1964).
18. H. Bethe, *Phys. Rev.* **138**:B804 (1965). See also H. Bethe, *Phys. Rev.* **158**:941 (1967), for modifications of the first results.
19. A. Petschek, *Phys. Rev.* **154**:934 (1967).
20. B. Day, *Phys. Rev.* **151**:826 (1966).
21. M. Verde, *in* "Handbuch der Physik" (S. Flugge, ed.) Vol. 34, Springer-Verlag, Berlin (1957).
22. L. Schick, *Rev. Mod. Phys.* **33**:608 (1961).
23. D. Feldman and K. Kowalski, *Phys. Rev.* **130**:276 (1963).
24. D. Koehler and R. Mann, *Phys. Rev.* **135**:B91 (1964).
25. J. Blatt and V. Weisskopf, "Theoretical Nuclear Physics," John Wiley and Sons, Inc., New York (1952).
    S. Frautschi, "Regge Poles and S-Matrix Theory," W. A. Benjamin, Inc., New York (1963).
26. M. Moravcsik, "The Two-Nucleon Interaction," Oxford University Press, New York (1963).
27. R. Courant and D. Hilbert, "Methods of Mathematical Physics," Interscience Publishers, Inc. (now John Wiley and Sons, Inc.), New York (1963).
28. M. Scadron, S. Weinberg, and J. Wright, *Phys. Rev.* **135**:B202 (1964).
29. W. Hunziker, *Helv. Phys. Acta* **34**:593 (1961).
30. A. Grossmann and T. T. Wu, *J. Math. Phys.* **2**:710 (1961).
31. Y. Yamaguchi, *Phys. Rev.* **95**:1628 (1954).
32. Y. Yamaguchi and Y. Yamaguchi, *Phys. Rev.* **95**:1635 (1954).
33. F. Tabakin, *Ann. Phys. (N.Y.)* **30**:51 (1964).
    F. Tabakin, *Phys. Rev.* **137**:B75 (1965).
34. J. Naqvi, *Nucl. Phys.* **58**:289 (1964).
35. E. Baranger, M. Baranger, and T. Kuo, *Nucl. Phys.* **81**:241 (1966).
36. I. Duck and W. Pearce, *Phys. Rev. Letters* **21**:669 (1966).
37. D. Wong and G. Zambotti, *Phys. Rev.* **154**:1540 (1967).
    J. Gillespie, *Phys. Rev.* **160**:1432 (1967).
38. S. Weinberg, *Phys. Rev.* **133**:B232 (1964).
39. S. Weinberg, *Phys. Rev.* **130**:776 (1963).
40. M. Vaughn, R. Aaron, and R. Amado, *Phys. Rev.* **124**:1258 (1961).
41. K. Greider and L. Dodd, *Phys. Rev.* **146**:671 (1966).
42. R. Wilson, "The Nucleon–Nucleon Interaction," Interscience Publishers, Inc. (now John Wiley and Sons, Inc.), New York (1961). Also,
    M. Moravcsik, "The Two-Nucleon Interaction," Oxford University Press, New York (1963).

43. M. Cerineo, K. Ilakovac, I. Slaus, P. Tomas, and V. Velkovic, *Phys. Rev.* **133**:B948 (1964).
44. K. Watson, *Phys. Rev.* **88**:1163 (1952).
45. R. Haddock, R. Salter, Jr., M. Zeller, J. Czin, and D. Nygren, *Phys. Rev. Letters* **14**:318 (1965).
46. P. Shanley, Thesis, Northeastern University, Chicago, Ill. (1966).
R. Aaron and P. Shanley, *Phys. Rev.* **142**:608 (1966).
47. R. Aaron, *Phys. Rev.* **151**:1293 (1966).
48. L. Rosenberg, *Phys. Rev.* **134**:B937 (1964).
49. A. Mitra, *Nucl. Phys.* **32**:529 (1962).
50. A. Mitra and V. Bhasin, *Phys. Rev.* **131**:1265 (1963).
51. V. Bhasin, G. Schrenk, and A. Mitra, *Phys. Rev.* **137**:B398 (1965).
52. B. Bhakar and A. Mitra, *Phys. Rev. Letters* **14**:143 (1965).
53. A. Mitra, G. Schrenk, and V. Bhasin, *Ann. Phys. (N.Y.)* **40**:357 (1966).
G. Schrenk and A. Mitra, *Phys. Rev. Letters* **19**:530 (1967).
54. B. Bhakar, *Nucl. Phys.* **46**:572 (1963).
55. V. Bhasin, *Nucl. Phys.* **58**:636 (1964).
56. D. Stojanov and A. Tavkhelidze, *Phys. Rev. Letters* **13**:76 (1964).
57. U. Shelest and D. Stojanov, *Phys. Rev. Letters* **13**:253 (1964).
58. V. Alessandrini and R. Omnes, *Phys. Rev.* **139**:B167 (1965).
59. D. Freedman, C. Lovelace, and J. Namyslowski, *Nuovo Cimento* **43**:258 (1966).
60. A. Ahmadzadeh and J. Tjon, *Phys. Rev.* **139**:B1085 (1965).
A. Ahmadzadeh and J. Tjon, *Phys. Rev.* **147**:1111 (1966).
W. Dunn and R. Ramachandran, *Phys. Rev.* **153**:1558 (1967).
I. Barbour and R. Schult, *Phys. Rev.* **155**:1712 (1967).
61. J. Basdevant and R. Kreps, *Phys. Rev.* **141**:1398 (1966).
62. J. Basdevant and R. Kreps, *Phys. Rev.* **141**:1404 (1966).
63. J. Basdevant and R. Kreps, *Phys. Rev.* **141**:1409 (1966).
64. J. Basdevant and R. Omnes, *Phys. Rev. Letters* **17**:774 (1966).
65. R. Rajaraman, *Phys. Rev.* **131**:1244 (1963).
66. S. Moszkowski, *Phys. Rev.* **140**:B283 (1965).
B. Bhaker and R. McCarthy, *Phys. Rev., to be published.*

APPENDIX A

In this appendix we define our notation for three-particle scattering and collect a number of basic formulas which are useful primarily in the Faddeév and Lovelace discussions of three-particle scattering. We label the particles 1, 2, and 3 and define the following quantities:

1. $K_1 = p_1^2/2m_1$	Kinetic energy of particle 1 of momentum p_1 and mass m_1 (and similarly for K_2, K_3)
2. $K = K_1 + K_2 + K_3$	The total kinetic energy
3. V_1	Interaction potential energy between the pair (2, 3); also $V_0 = 0$
4. $V = V_1 + V_2 + V_3$	The total potential
5. $\tilde{V}_1 = V_2 + V_3$	Also $\tilde{V}_0 = V$
6. $\tilde{K}_1 = K_2 + K_3$	
7. $H_0 = K$	The Hamiltonian for the noninteracting system
8. $H = K + V$	The total Hamiltonian
9. $h_1 = \tilde{K}_1 + V_1$	The Hamiltonian for the pair (2, 3) only
10. $H_1 = K + V_1$	The Hamiltonian including the (2, 3) pair interaction only
11. $G = (H - E^+)^{-1}$	(With $E^+ = E + i\eta$ and $\eta \to 0^+$) the Green's function for the three-particle system of energy E
12. $G_0 = (H_0 - E^+)^{-1}$	The free three-particle Green's function with $G = G_0 - G_0VG = G_0 - GVG_0$
13. $g_1 = (H_1 - E^+)^{-1}$	The two-particle Green's function for the pair (2, 3) in the three-particle Hilbert space and $G = g_1 - g_1V_1G = g_1 - GV_1g_1$
14. $t_1 = V_1 - V_1G_0t_1$	The two-particle t-matrix for the pair (2, 3) again in the three-particle Hilbert space; also $t_0 = 0$

15. $F_{\alpha\beta} = t_\alpha(1 - \delta_{\alpha\beta})$ The Faddeév kernel $= \begin{pmatrix} 0 & t_1 & t_1 \\ t_2 & 0 & t_2 \\ t_3 & t_3 & 0 \end{pmatrix}$ and its transpose F_{ij}^T.

These few definitions will expedite our discussion of the Faddeév equations in Section 3.

APPENDIX B

In this appendix we collect some formulas for two-particle scattering by a separable potential and also define the propagator of a two-particle state for a one-component separable potential.

The Schrödinger equation with a nonlocal potential

$$(E - H_0)\,\psi(\mathbf{r}) = \int d^3r'\,V(\mathbf{r}, \mathbf{r}')\,\psi(\mathbf{r}') \tag{B.1}$$

reduces to a system of linear algebraic equations if the nonlocal potential is also separable[31–34]

$$V(\mathbf{r}, \mathbf{r}') = -v(\mathbf{r})\,\lambda v(\mathbf{r}') \tag{B.2}$$

Consider a multicomponent separable potential acting only in S waves. Then

$$V(\mathbf{r}, \mathbf{r}') = -\sum_i v_i(r)\,\lambda_i v_i(r')$$

where (i) labels the different terms in the separable potential and $\lambda_i = +1(-1)$ corresponds to an attractive (repulsive) potential. Write this in matrix notation

$$V(\mathbf{r}, \mathbf{r}') = -\tilde{v}(r)\,\lambda v(r') \tag{B.3}$$

with λ a diagonal matrix, and the Fourier transform

$$(\mathbf{p} \mid V \mid \mathbf{p}') = -\tilde{v}(p)\,\lambda v(p') \tag{B.4}$$

with

$$v(p) = \int d^3r\, e^{-i\mathbf{p}\cdot\mathbf{r}} v(r) \tag{B.5}$$

For the interaction of equal mass particles of mass $M = 1$ (we take $\hbar = c = 1$ also), in the c-m system, the momentum space wave function satisfies (with $E = k^2$)

$$(k^2 - p^2)\,\psi_k(p) = -\tilde{v}(p)\lambda N \tag{B.6}$$

with

$$N_i = \int đ^3p\, v_i(p)\, \psi_k(p)$$

(where we use $đp = dp/2\pi$).

For a bound state with energy $E = k^2 = -\alpha^2$, the wave function is

$$\psi_k(p) = \frac{\tilde{v}(p)\,\lambda N}{(\alpha^2 + p^2)} \tag{B.7}$$

and the eigenvalue condition which must be satisfied for the bound state is

$$N = \Lambda N$$

with

$$\Lambda_{ij} = \int đ^3p\, \frac{v_i(p)\,\lambda_j v_j(p)}{(\alpha^2 + p^2)} \tag{B.8}$$

which determines the eigenvalue α^2. The eigenvector N determines the unnormalized boundstate wave function. The normalization condition can be written

$$\tilde{N}\Omega N = 1$$

with

$$\Omega_{ij} = \int đ^3p\, \frac{v_i(p)\,\lambda_i\lambda_j v_j(p)}{(\alpha^2 + p^2)^2} \tag{B.9}$$

For a single-component separable potential, we can adjust λ and v so that $\lambda N = 1$. Then the bound-state wave function is

$$\psi_\alpha(p) = \frac{v(p)}{(\alpha^2 + p^2)} \tag{B.7a}$$

and the normalization condition is

$$\int đ^3p\, \frac{v^2(p)}{(\alpha^2 + p^2)^2} = 1 \tag{B.8a}$$

Now turn to the scattering problem. We still have (B.6) with $k^2 \to k^2 + i\eta$ and $\eta \to 0^+$. The momentum space wave function asymptotic to a plane wave of momentum $\mathbf{k}$ and energy k^2 is

$$\psi_{\mathbf{k}}(\mathbf{p}) = (2\pi)^3\, \delta^3(\mathbf{k} - \mathbf{p}) - \frac{\tilde{v}(p)\,\lambda N}{k^2 - p^2 + i\eta} \tag{B.10}$$

For the simplest case when we have just a one-component separable potential

$$\lambda N = \frac{\lambda v(k)}{1 + \lambda \int đ^3p \, \dfrac{v^2(p)}{k^2 - p^2 + i\eta}} \tag{B.11}$$

whereas in general we have a matrix equation for N

$$(1 + \Delta)\, \lambda N = \lambda v(k) \tag{B.12}$$

with

$$\Delta_{ij} = \int đ^3p \, \frac{v_i(p)\, \lambda_i v_j(p)}{k^2 - p^2 + i\eta} \tag{B.13}$$

which we write

$$\lambda N = \Omega \lambda v \qquad \text{with} \qquad \Omega = (1 + \Delta)^{-1}$$

then

$$\psi_{\mathbf{k}}(\mathbf{p}) = (2\pi)^3\, \delta^3(\mathbf{k} - \mathbf{p}) - \frac{\tilde{v}(p)\, \Omega \lambda v(k)}{k^2 - p^2 + i\eta} \tag{B.14}$$

The off-energy-shell matrix elements of the t matrix, which are defined by the Lippmann–Schwinger equation

$$(\mathbf{p} \mid t_k \mid \mathbf{p}') = (\mathbf{p} \mid V \mid \mathbf{p}') + \int đ^3q \, \frac{(\mathbf{p} \mid V \mid \mathbf{q})(\mathbf{q} \mid t_k \mid \mathbf{p}')}{k^2 - q^2 + i\eta} \tag{B.15}$$

become, for an S-wave separable potential,

$$\begin{aligned}(p \mid t_k \mid p') &= -\tilde{v}(p)\, \lambda v(p') - \int \frac{đ^3q \tilde{v}(p)\, \lambda v(q)(q \mid t_k \mid p')}{k^2 - q^2 + i\eta} \\ &= \tilde{v}(p)\, \chi_k(p')\end{aligned} \tag{B.16}$$

and in terms of the previously defined matrices Δ and Ω,

$$\chi_k(p') = -\Omega_k \lambda v(p')$$

so

$$(p \mid t_k \mid p') = -\tilde{v}(p) \Omega \lambda v(p') \tag{B.17}$$

On the energy shell,

$$(k \mid t_k \mid k) = -\frac{2\pi}{\mu}\, e^{i\delta}\, \frac{\sin \delta}{k} \tag{B.18}$$

with δ the S-wave phase shift and μ, the reduced mass $= \frac{1}{2}$.

For a single-component separable potential Eq. (B.17) reduces to

$$(p \mid t_k \mid p') = \frac{-\lambda v(p)\, v(p')}{1 + \lambda \int \dfrac{d^3q[v(q)]^2}{k^2 - q^2 + i\eta}} = \Gamma^2 v(p)\, v(p')\, P(k^2) \qquad \text{(B.19)}$$

which defines $\Gamma^2 = \lambda$ and $P(k^2)$ the propagator for the pair representing a sum of bubble diagrams.[1] Bound-state poles in the propagator at $k^2 = -\alpha^2$, the binding energy, can be made explicit by a subtraction using Eq. (B.8)

$$\lambda \int \frac{d^3q v^2(q)}{(\alpha^2 + q^2)} = 1$$

and then the propagator becomes

$$[P(k^2)]^{-1} = -(k^2 + \alpha^2)\, \lambda \int \frac{d^3q v^2(q)}{(\alpha^2 + q^2)(k^2 - q^2 + i\eta)} \qquad \text{(B.20)}$$

These are the n–D coupling constant Γ, form factor v, and propagator P of the Amado theory in the limit of a purely S-wave composite deuteron.

Amado finds it necessary to relax the condition that the deuteron is a purely composite S-wave n–n bound state without at the same time complicating the n–n interaction by the introduction of spin-dependent forces. This is done by introducing the deuteron wave-function renormalization constant Z which can be viewed as the probability of non S-wave amplitudes in the deuteron bound-state wave function, so that $0 \leqslant Z \leqslant 1$. Alternatively, in a soluble model field theory of the n–D reaction, Z is the probability that the deuteron is a purely elementary particle. $Z = 1$ corresponds to the elementary particle limit, $Z = 0$ to the limit of a composite deuteron, which is a pure S-wave n–n bound state. In effect, the introduction of Z allows one to vary the n–D coupling without affecting the D binding energy.

In the model field theory the unrenormalized propagator is the sum of bubble diagrams of Fig. 3 . Define the bare propagator

$$P_0(k^2) = (k^2 + \alpha_0^2)^{-1} \qquad \text{(B.21)}$$

in the deuteron c-m system, with k^2 the c-m energy with a small positive imaginary part and α_0^2 the unrenormalized D binding energy. Then the renormalized propagator is

$$\begin{aligned} P &= \frac{1}{Z}(P_0 + P_0 I P_0 + P_0 I P_0 I P_0 + \cdots) \\ &= \frac{1}{Z}(P_0^{-1} - I)^{-1} \end{aligned} \qquad \text{(B.22)}$$

with

$$I = \Gamma_\mu^{\,2} \int \frac{đ^3 q v^2(q)}{k^2 - q^2 + i\eta} \tag{B.23}$$

and Γ_μ is an unrenormalized n–D coupling constant. The renormalized propagator has a pole at $k^2 = -\alpha^2$, the physical D binding energy, so

$$\alpha_0^{\,2} = \alpha^2 - \Gamma_\mu^{\,2} \int đ^3 q \frac{v^2(q)}{(\alpha^2 + q^2)} \tag{B.24}$$

With the D pole explicit, the propagator, Eq. (B.22), takes the form

$$\begin{aligned}[P(k^2)]^{-1} &= -(k^2 + \alpha^2)\left[-Z + \Gamma^2 \int \frac{đ^3 q v^2(q)}{(\alpha^2 + q^2)(k^2 - q^2 + i\eta)}\right] \\ &\equiv (k^2 + \alpha^2)\, S^{-1}(k^2)\end{aligned} \tag{B.25}$$

with $\Gamma^2 = Z\Gamma_\mu^{\,2}$, the renormalized coupling constant. The wave-function renormalization factor Z, which has been introduced into the renormalized propagator of Eq. (B.22) and in a compensating place in the renormalized coupling constant, gives the freedom necessary to impose the condition of unit residue at the bound-state pole in the renormalized propagator. The condition of unit residue at the bound-state pole gives

$$Z = 1 - \Gamma^2 \int đ^3 q \frac{v^2(q)}{(\alpha^2 + q^2)^2} \tag{B.26}$$

The Amado model for identical n's differs from the above development by the replacement $\Gamma \to \Gamma_0 = \sqrt{2}\Gamma$.

APPENDIX C

The spin–isospin factors χ appearing in the Amado integral equations (55) are most easily obtained[4] by recoupling to the appropriate channel spins the matrix elements of the Born amplitude for an interaction

$$\begin{aligned}\mathscr{H}_{\text{INT}} = \frac{1}{\sqrt{2}} \sum_{j,k,q} \Gamma_j v_j(q^2) \left(\begin{matrix} i_1 & i_2 \\ \frac{1}{2} & \frac{1}{2}\end{matrix} \middle| \begin{matrix} t_j \\ T_j \end{matrix}\right)\left(\begin{matrix} m_1 & m_2 \\ \frac{1}{2} & \frac{1}{2}\end{matrix} \middle| \begin{matrix} M_j \\ S_j \end{matrix}\right) \\ \times \left[\Phi_j(\mathbf{k})\, \Psi_1^{+}\left(\frac{\mathbf{k}}{2} - \mathbf{q}\right) \Psi_2^{+}\left(\frac{\mathbf{k}}{2} + \mathbf{q}\right) + HC\right]\end{aligned} \tag{C.1}$$

Here $\Phi_j(\mathbf{k})$ is the renormalized field operator for the quasi-particle (j) of momentum $\mathbf{k}$ and spin–isospin (S_j, M_j) and (T_j, t_j); $\Psi_1(\mathbf{k})$ is that for a

nucleon of momentum $\mathbf{k}$ and spin–isospin $(\frac{1}{2}, m_1)$ and $(\frac{1}{2}, i_1)$. HC is the Hermitian conjugate of the first term. The spin–isospin dependence of a Born amplitude can be expressed in terms of the χ_{ij} of the text and the Born amplitudes of Eq. (56), as

$$\begin{aligned}(\mathbf{k}, i\,; S, S_z\,; T, T_z \mid B(E) \mid \mathbf{k}', j\,; S, S_z\,; T, T_z) \\ = \chi_{ij}(\mathbf{k}, i \mid B(E) \mid \mathbf{k}', j)\end{aligned} \tag{C.2}$$

with

$$\begin{aligned}\chi_{ij}^{s} = 2 \left(\begin{matrix} i_1 & i_3 \\ \frac{1}{2} & \frac{1}{2}\end{matrix}\middle|\begin{matrix} t_i \\ T_i\end{matrix}\right)\left(\begin{matrix} m_1 & m_3 \\ \frac{1}{2} & \frac{1}{2}\end{matrix}\middle|\begin{matrix} M_i \\ S_i\end{matrix}\right)\left(\begin{matrix} m_2 & M_i \\ \frac{1}{2} & S_i\end{matrix}\middle|\begin{matrix} S_z \\ S\end{matrix}\right)\left(\begin{matrix} i_2 & t_i \\ \frac{1}{2} & T_i\end{matrix}\middle|\begin{matrix} T_z \\ T\end{matrix}\right) \\ \times \left(\begin{matrix} i_2 & i_3 \\ \frac{1}{2} & \frac{1}{2}\end{matrix}\middle|\begin{matrix} t_j \\ T_j\end{matrix}\right)\left(\begin{matrix} m_2 & m_3 \\ \frac{1}{2} & \frac{1}{2}\end{matrix}\middle|\begin{matrix} M_j \\ S_j\end{matrix}\right)\left(\begin{matrix} m_1 & M_j \\ \frac{1}{2} & S_j\end{matrix}\middle|\begin{matrix} S_z \\ S\end{matrix}\right)\left(\begin{matrix} i_1 & t_j \\ \frac{1}{2} & T_j\end{matrix}\middle|\begin{matrix} T_z \\ T\end{matrix}\right)\end{aligned} \tag{C.3}$$

summed over $(i_1, i_2, i_3, m_1, m_2, m_3, M_i, M_j, t_i, t_j)$ with $T = \frac{1}{2}$, $T_z = -\frac{1}{2}$ leads to the χ's of the text expressed in terms of Racah coefficients.

APPENDIX D

In this appendix we develop explicitly the integral equations for the elastic scattering of particle (1) off the bound state of the pair (1) by using the Faddeév formalism and following Hetherington and Schick.[13] For the sake of simplicity we consider these to be spinless isoscalar distinguishable particles. We work on the total c-m system, where plane-wave states can be labeled equivalently

$$\mid \mathbf{p}_1, \mathbf{p}_2, \mathbf{p}_3\rangle = \mid \mathbf{p}_1, \mathbf{k}_1\rangle = \mid \mathbf{p}_2, \mathbf{k}_2\rangle = \mid \mathbf{p}_3, \mathbf{k}_3\rangle \tag{D.1}$$

where $\mathbf{p}_i$ is the momentum of particle (i) and $\mathbf{k}_i$ is the relative momentum of the pair (i) defined as

$$\tilde{m}_i \mathbf{k}_i = \epsilon_{ijk} m_j \mathbf{p}_k \tag{D.2}$$

with $\tilde{m}_i = M - m_i$ and $M = m_1 + m_2 + m_3$, the total mass. The plane-wave states are normalized

$$\langle \mathbf{p}_1 \mid \mathbf{p}_1'\rangle = (2\pi)^3\, \delta^3(\mathbf{p}_1 - \mathbf{p}_1') \tag{D.3}$$

The elastic scattering amplitude from an initial incident momentum $\mathbf{p}_{1i}$ to a final momentum $\mathbf{p}_{1f}$ at a total c-m energy E is

$$M_{fi} = \langle \mathbf{p}_{1f}, \phi_1 \mid U_{11}^{(+)} \mid \phi_1, \mathbf{p}_{1i}\rangle \tag{D.4}$$

with $|p_{1f}| = |p_{1i}| = p$ and ϕ_1, the bound-state wave function for the pair (1). A partial-wave analysis defines the complex phase shifts δ_L through

$$M_{fi} = \sum_L \left(\frac{-2\pi}{\mu_1}\right) \frac{e^{i\delta_L} \sin \delta_L}{p} (2L + 1) P_L(\hat{p}_f \cdot \hat{p}_i) \tag{D.5}$$

where $\mu_1 = m_1\tilde{m}_1/M$ is the reduced mass. We require the appropriate matrix elements of Eq. (89)

$$U_{11}^{(+)} = \sum_{ij \neq 1} T_{ij} \tag{89}$$

and

$$T_{ij} = t_i\delta_{ij} - F_{il}G_0T_{lj} \tag{88}$$

Matrix elements of the two-body t matrix are

$$\langle \mathbf{p}_i', \mathbf{k}_i' \mid t_i \mid \mathbf{p}_i, \mathbf{k}_i \rangle = (2\pi)^3\, \delta^3(\mathbf{p}_i' - \mathbf{p}_i) \langle \mathbf{k}_i' \mid t_i(p_i\,; E) \mid \mathbf{k}_i \rangle \tag{D.6}$$

where we have factored out an overall momentum-conserving delta function $(2\pi)^3\, \delta^3(\mathbf{p}' - \mathbf{p})$. The matrix element is the off-energy-shell scattering amplitude for the scattering of the pair (i) at a pair c-m energy of $E - p_i^2/2m_i - p_i^2/2\tilde{m}_i$. Similarly we have the matrix element of $F_{il} = (1 - \delta_{il})\, t_i$ and G_0. Finally the matrix element of Eq. (88) is

$$\begin{aligned}\langle \mathbf{p}_i', \mathbf{k}_i' \mid T_{ij} \mid \mathbf{p}_j, \mathbf{k}_j \rangle = {} & (2\pi)^3\, \delta^3(\mathbf{p}_i - \mathbf{p}_i') \langle \mathbf{k}_i' \mid t_i(p_i\,; E) \mid \mathbf{k}_i \rangle\, \delta_{ij} \\ & - \sum_l (1 - \delta_{il}) \int d^3p_l''\, d^3k_l'' \langle \mathbf{k}_i' \mid t_i(p_i\,; E) \mid \mathbf{k}_i'' \rangle \\ & \times (2\pi)^3\, \delta^3(\mathbf{p}_i' - \mathbf{p}_i'')\, G_0(\mathbf{p}_1''\,; \mathbf{p}_2'', \mathbf{p}_3'') \\ & \times \langle \mathbf{p}_l'', \mathbf{k}_l'' \mid T_{lj} \mid \mathbf{p}_j, \mathbf{k}_j \rangle \end{aligned} \tag{D.7}$$

where we have labeled intermediate states by various sets of momentum variables and do the integrations over $\mathbf{k}_l''$ using

$$\mathbf{k}_i'' = -S_{il} \left(\mathbf{p}_l'' + \frac{m_l}{\tilde{m}_i}\, \mathbf{p}_i''\right) \tag{D.8}$$

and

$$\mathbf{p}_i'' = S_{il}\mathbf{k}_l'' - m_i/\tilde{m}_l\, \mathbf{p}_l'' \tag{D.9}$$

where $S_{il} = +1(-1)$ for (il) a cyclic (anticyclic) pair of (1, 2, 3). Now choose separable S-wave two-particle interactions of the form of Eq. (B.19) to reduce (D.7) to a system of coupled one-dimensional linear integral equations. Use

$$\langle \mathbf{k}_i' \mid t_i(p_i\,; E) \mid \mathbf{k}_i \rangle = \lambda_i v_i(k_i'^2)\, P_i(p_i^2; E)\, v_i(k_i^2) \tag{B.19}$$

then we can factor $\langle T_{ij}\rangle$ to

$$\langle \mathbf{p}_i', \mathbf{k}_i' \mid T_{ij} \mid \mathbf{p}_j, \mathbf{k}_j\rangle = v_i(k_i'^2)\, P_i(p_i'^2; E)\, v_j(k_j^2)\langle \mathbf{p}_i' \mid \hat{T}_{ij} \mid \mathbf{p}_j\rangle \tag{D.10}$$

and get

$$\begin{aligned}\langle \mathbf{p}_i' \mid \hat{T}_{ij} \mid \mathbf{p}_j\rangle = {} & (2\pi)^3\, \delta^3(\mathbf{p}_i' - \mathbf{p}_i)\, \lambda_i\, \delta_{ij} \\ & - \sum_l (1 - \delta_{il}) \int đ^3p_l''\lambda_i v_i(k_i''^2)\, G_0(p_1'', p_2'', p_3'') \\ & \times v_l(k_l''^2)\, P_l(p_l''^2; E)\langle \mathbf{p}_l'' \mid \hat{T}_{lj} \mid \mathbf{p}_j\rangle \end{aligned} \tag{D.11}$$

After a partial-wave expansion, Eq. (D.5), we obtain a set of coupled integral equations in the partial-wave amplitudes

$$\begin{aligned}\langle p_i' \mid \hat{T}_{ij}(L; E) \mid p_j\rangle = {} & 2\pi^2\, \delta(p_i' - p_i)\, \frac{\lambda_i}{p_i^2} - \sum_l (1 - \delta_{il}) \int_0^\infty p_l''^2\, dp_l''\lambda_i Z_L(ilj) \\ & \times P_l(p_l''^2; E)\langle p_l'' \mid \hat{T}_{lj}(L; E) \mid p_j\rangle \end{aligned} \tag{D.12}$$

with

$$Z_L(ilj) = \int \frac{dx}{(2\pi)^2}\, P_L(x)\, v_i(k_i''^2)\, G_0(p_1'', p_2'', p_3'')\, v_l(k_l''^2) \tag{D.13}$$

where $x = \hat{p}_l'' \cdot \hat{p}_j$. This is an integral of the form

$$Z_L(ilj) \sim \int \frac{dx}{(2\pi)^2}\, P_L(x)(a_{ij} - x)^{-1}\, (b_{lj} - x)^{-1}\, (c_j - x)^{-1}$$

provided we use Hulthén form factors, Eq. (52), for $v_i(k^2)$. Finally, after numerical solution, we need to fold these off-energy-shell amplitudes into the initial and final bound-state wave functions of Eq. (B.7) as

$$\begin{aligned} M_{fi} = {} & \sum_{L, ij \neq 1} \int đ^3p_1'\, đ^3k_1'\, đ^3p_1\, đ^3k_1 (2\pi)^3\, \delta^3(\mathbf{p}_1' - \mathbf{p}_{1f}) \\ & \times \phi_1^*(\mathbf{k}_1')(2\pi)^3\, \delta^3(\mathbf{p}_1 - \mathbf{p}_{1i})\, \phi_1(\mathbf{k}_1)\, v_i(k_i'^2)\, v_j(k_j^2) \\ & \times P_i(p_i^{12}; E)\, P_L(\hat{p}_i' \cdot \hat{p}_j)(2L + 1)\langle p_i' \mid \hat{T}_{ij}(L; E) \mid p_j\rangle \end{aligned} \tag{D.14}$$

which is most conveniently done by integrating in terms of $(\mathbf{p}_i', \mathbf{k}_i')$ and $(\mathbf{p}_j, \mathbf{k}_j)$.

APPENDIX E

In this appendix we present the Lovelace derivation[12] of the Amado equations from the Faddeév integral equation for the rearrangement scattering operator $U_{ij}^{(-)}$, assuming one-component separable S-wave interactions between distinguishable particles. We require the matrix element

$$(\phi_i\,,\, U_{ij}^{(-)}\phi_j) = (\phi_i\,,\, \tilde{V}_j\phi_j) - (\phi_i\,,\, F_{ik}^T G_0 U_{kj}^{(-)}\phi_j) \tag{E.1}$$

at an energy E which is eventually put on the energy shell for the initial and final bound states. The two-particle interaction between the pair (i) is

$$V_i = -|\, i\rangle\, \lambda_i \langle i\,| \tag{B.4}$$

with $\langle p \mid i\rangle = v_i(p)$ the form factor, and the two-particle scattering operator is

$$t_i(E) = |\, i\rangle\, P_i(E) \langle i\,| \tag{B.19}$$

in terms of the propagator P_i. The two-particle wave function at energy (E) is

$$\begin{aligned} \phi_i(E; p^2) &= \langle p \mid G_0(E) |\, i\rangle \\ &= (p^2 - E)^{-1} \langle p \mid i\rangle \end{aligned} \tag{B.7}$$

and the bound-state wave function for the pair

$$\phi_i(-\alpha^2; p) = (p^2 + \alpha^2)^{-1} \langle p \mid i\rangle \tag{B.7a}$$

is correctly normalized if we choose $|\, i\rangle$ according to (B.8a). The eigenvalue condition for the bound state is

$$\lambda_i \langle i \mid \phi_i(-\alpha^2)\rangle = 1 \tag{B.8}$$

Write the matrix elements of (E.1) as

$$\langle \phi_i\,,\, U_{ij}^{(-)}\phi_j\rangle = T_{ij}(E) \tag{E.2}$$

and

$$-\langle \phi_i F_{ik}^T G_0 U_{kj}^{(-)}\phi_j\rangle = B_{ik} P_k T_{kj} \tag{E.3}$$

where we define a Born amplitude

$$B_{ik} = -\langle \phi_i(E) |\, k\rangle (1 - \delta_{ik}) = -\langle i \mid G_0(E) |\, k\rangle (1 - \delta_{ik}) \tag{E.4}$$

Next, write

$$\langle \phi_i\,,\, \tilde{V}_j\phi_j\rangle = B_{ij} - B_{ik}\lambda_k B_{kj} - \{1 - \lambda_i(i \mid G_0(E) |\, i)\}\, B_{ij} \tag{E.5}$$

Then after some rearrangement (E.1) becomes

$$T_{ij} + (1 - \lambda_i \langle i \mid G_0 \mid i \rangle) B_{ij} = B_{ij} + B_{ik} P_k (T_{kj} - P_k^{-1} \lambda_k B_{kj}) \tag{E.6}$$

Using the Lippman–Schwinger equation for t_i, we can show

$$1 - \lambda_i \langle i \mid G_0 \mid i \rangle = -P_i^{-1} \lambda_i \tag{E.7}$$

so, if we define

$$\hat{T}_{ij} = T_{ij} - P_i^{-1} \lambda_i B_{ij} \tag{E.8}$$

equal to T_{ij} on the energy shell where P_i^{-1} has a zero, then (E.6) reduces to a Lippman–Schwinger equation for the rearrangement amplitude, just the Amado relation, Eq. (48), in the bound-state limit

$$\hat{T}_{ij} = B_{ij} + B_{ik} P_k \hat{T}_{kj} \tag{E.9}$$

The references will be found on page 397 preceding the Appendixes.

INDEX

A

Adiabaticity parameter ξ, 8, 13, 50
Adjoint symmetry of nuclear wave functions, 77
Angular momentum,
  conservation in compound nucleus processes, 268, 273
  distribution in deformed intrinsic states, 241
  expression for the energy of a state of spin J, 237
  mean value of $\mathbf{J}^2$ in Hartree–Fock intrinsic state, 240
  projection in Hartree–Fock calculation, 235
  projection in Hartree–Fock calculation, accuracy of, 243–244
Approximate symmetry groups for shell model Hamiltonians, 76
Average nuclear reaction cross sections,
  differential, 280
  integrated over angles, 271

B

Black nucleus model, 268, 288
Bohr assumption, 263, 266
Born approximation,
  distorted wave, 269
  first, 351
  second, 351–352
Broken symmetry groups,
  for SU_3, 104
  for shell model Hamiltonians, 76

C

Channel for three-particle scattering,
  definition, 379
  wave function, 379
Channel for two-particle reactions,
  definition, 270
  wave function, 275
Classification of nuclear states,
  according to U_3 and SU_3, 83
  according to S_A and SU_3 simultaneously, 85
  according to SU_3 and R_3, 89
  according to SU_3 and $SU_2 \times SU_1$, 90
Collision matrix,
  definition, 277, 322
  schematic representation, 324
Compact kernel, 354
Compact property of Faddeév kernel, 381, 386
Completely continuous kernel, 354
Compound nucleus,
  formation cross section, 273
  qualitative features, 261, 269, 274, 322, 332
Coulomb wave functions, definition, 276
Cross section fluctuations, 281, 303, 320, 326, 337–339
Cross section in reorientation experiments,
  formula for first-order, 51
  measurement of, 32, 35
Cross sections, general connection to the collision matrix, 279
Cross sections of the evaporation model, 271, 280
Creation and destruction operators for oscillator quanta, 80

D

Deformation,
  definition, 247
  due to closed-shell polarization, 247
  of Hartree–Fock field, 216
Deformation parameter β related to quadrupole moment, 3, 48
Deformed excited states of spherical nuclei, 210
Density matrix, 189

Deorientation, 41
Dimension of representation,
of U_s, 88
of U_3 and SU_3, 89
Dipole polarization of target in Coulomb excitation, 24
Direct reactions, competition with compound nucleus reactions, 262, 269, 320, 327
Distance of closest approach, 49
Doorway states in nuclear reactions, 333
Double scattering approximation, validity, 388–390

E

Effective interaction of shell model Hamiltonian, 99
Effective range,
definition, 346
numerical values for two nucleons, 369
Eight-fold way, and SU_3 for elementary particles, 181
Electric multipole transition, 7
Energy gap in single-particle spectrum, 207, 214, 216
influence on projected Hartree–Fock spectra, 243
Energy shell, on and off, 351
Energy spectrum of evaporated particles, 266, 315
Evaporation models,
early, 262
modern, 270
Excitation probability of a multipole,
first-order approximation, 8, 15
interference term, 15, 16, 23

F

Final-state interactions, Watson theory of, 376
Finite-averaging interval, effect on nuclear reactions, 302, 337
Flywheel effect in compound nucleus reactions, 311, 317
Fission and compound nucleus processes, 319

G

Gamma rays,
angular distribution of de-excitation gamma rays, 16, 36, 39, 41
circular polarization of de-excitation gamma rays, 42
Generating matrices, 80
Generating operators,
definition, 79
of the group U_s, 162
Giant dipole resonance,
excitation via, 21
excitation via interpreted as polarization effect, 24
Giant resonances of nuclear transmission functions, 283–295
Green's function for three particles,
free, 356, 381
full, 356, 380–381
Green's function for two particles,
free, 349
full, 350
in three-particle problem, 381
Groups and their properties, 154

H

Harmonic oscillator for nuclei,
Cartesian oscillator, 153
compared with Hartree–Fock, 216–224
cylindrical oscillator, 153
general properties, 152
many-particle Hamiltonian, 81
single-particle Hamiltonian, 80
orbits, relation between various representations in (s,d) shell, 220
spherical oscillator, 152
size of (oscillator parameter), 153, 199
Hartree–Fock calculations,
basis for, 187, 192
choice of single-particle energies, 199
compared with calculations using SU_3, 144, 145, 223
effect of the exchange mixture, 213
iterative procedure for, 188
major-shell mixing, 196, 244
major-shell mixing compared with Mottelson's core-polarization model, 251–253
of magnetic moments, 233
phase conventions for, 195
radial, 184, 246
single major-shell, 196
use of a reference closed-shell nucleus, 197
Hartree–Fock calculations of specific nuclei (in order of increasing mass),
^{11}B, magnetic moment, 234
^{11}B, quadrupole moment, 250
^{12}C, deformation, 249

Hartree–Fock calculations of specific nuclei *(continued)*,
^{12}C, distribution of angular momentum in deformed state, 241
^{12}C, equidensity surfaces, 254
^{12}C, projected Hartree–Fock spectrum, 242
^{12}C, solutions, 203–205, 208–210
^{13}C, magnetic moment, 234
^{16}O, deformed excited states, 210
^{16}O, solutions, 203, 208–209, 210
^{19}F, accuracy of projected Hartree–Fock spectrum, 243–244
^{19}F, magnetic moment, 234
^{19}F, overlap functions, 239
^{20}Ne, deformation, 249
^{20}Ne, distribution of angular momentum in deformed state, 241
^{20}Ne, equidensity surfaces, 254
^{20}Ne, overlap functions, 239
^{20}Ne, projected Hartree–Fock spectrum, 242
^{20}Ne, solutions, 204–205, 208–209, 219, 226, 228
^{21}Ne, magnetic moment, 234
^{21}Ne, quadrupole moment, 250
^{21}Ne, solutions, 230
^{22}Ne, solutions, 232
^{23}Na, magnetic moment, 234
^{23}Na, quadrupole moment, 250
^{24}Mg, deformation, 249
^{24}Mg, solutions, 204–205, 207, 208–209, 219, 221, 226, 228
^{25}Mg, magnetic moment, 234
^{25}Mg, quadrupole moment, 250
^{27}Al, magnetic moment, 233–234
^{28}Si, deformation, 249
^{28}Si, distribution of angular momentum in deformed state, 241
^{28}Si, equidensity surfaces, 255
^{28}Si, projected Hartree–Fock spectrum, 242
^{28}Si, solutions, 203–205, 208–210, 222, 225, 226, 228
^{29}Si, magnetic moment, 233–234
^{32}S, deformation, 249
^{32}S, solutions, 203–205, 207, 208–209, 226, 229
^{33}S, magnetic moment, 234
^{33}S, quadrupole moment, 250
^{35}Cl, magnetic moment, 234
Hartree–Fock calculations of specific nuclei *(continued)*,
^{35}Cl, quadrupole moment, 250
^{36}Ar, deformation, 249
^{36}Ar, distribution of angular momentum in deformed states, 241
^{36}Ar, projected Hartree–Fock spectrum, 242
^{36}Ar, solutions, 203–205, 208–209, 229
^{40}Ca, solutions, 203, 208–209
Hartree–Fock energy, 187
Hartree–Fock energy, stationary properties of, 187
Hartree–Fock equations, 187
Hartree–Fock Hamiltonian, 188
Hartree–Fock Hamiltonian compared with harmonic oscillator, 216–224
Hartree–Fock Hamiltonian, symmetries of,
axial symmetry, 191, 194
ellipsoidal symmetry, 194
isospin invariance, 191
mixed parity, 195
order of preferred symmetries, 222
parity, 191
spherical symmetry, 191, 194
spin–isospin invariance, 192
time-reversal invariance, 190, 194, 195
Hartree–Fock orbits,
choice of an expansion for, 192
compared with deformed oscillator orbits, 216, 223
compared with Nilsson orbits, 216
hole orbits, 197
particle orbits, 197
spectrum of, 207
Hartree–Fock solutions,
angular momentum projection, 235, 242
angular momentum projection, accuracy of, 243
angular momentum projection compared with rotational model, 241–243
axially symmetric, 204–206, 219, 222, 228–229
deviations from *L-S* coupling, 226
effect of spin–orbit splitting, 224
ellipsoidal, 206–207, 221, 228–229
equidensity surfaces, 254–256
for even–even $N = Z$ nuclei, 203
for even–even $N \neq Z$ nuclei, 232

Hartree–Fock solutions *(continued)*,
for odd-A nuclei, 230
for quadrupole force, 216
multiplicity of, 227
single-particle energies, 207
spherical, 196, 203
Hartree–Fock theory and SU_3 model, 144, 145
Hauser–Feshbach, model, 270
Heavy-ion formation of compound systems, 319
Hermitian generating operators, 81
Hulthén wave function, 363

I
Impulse approximation, validity, 388–390
Inner product of groups, 161
Interaction strength, choice of in Hartree–Fock calculations, 199
Interaction strength, $\chi_{i\to f}^{(\lambda)}$ of an $E\lambda$ transition, 7, 13, 31, 50
Interaction, two-body (see Two-body)
Intermediate states in Coulomb excitation, 10, 18, 20, 21
Intermediate states in Coulomb excitation, giant dipole resonance, 21
Intermediate structure in nuclear reactions, 333
Intrinsic state, 95, 184, 195, 235
Invariance properties of shell model Hamiltonian, 73–76
Isospin and nuclear states, 77

K
Kaon–deuteron elastic scattering, 388–391

L
Leading representation, 93, 104
Level density of nuclei, 265, 314
Levinson's theorem, 346
Lippmann–Schwinger integral equation, 347

M
Magnetic dipole reorientation, 19
Magnetic moments of odd-A nuclei, 233
Model, nuclear SU_3 (see SU_3 model of nuclei)
Moldauer corrections to basic evaporation formulas, 329
Moments of inertia in Hartree–Fock calculations, 243
Multiple Coulomb excitation, 10, 20

N
Neutron boil off, 267
Neutron capture at low energies, 319
Neutron–deuteron scattering (see Scattering)
Neutron inelastic scattering, 297–301, 318
Nilsson orbits, 185
compared with Hartree–Fock orbits, 216
Notation for three-particle scattering, 400
Nuclear interactions, effect on reorientation experiments, 28

O
Optical model for nuclear reactions,
parameters, 283
phase shifts, 271
strength functions, 290
transmission functions, 271, 274, 281, 287, 294
Orbital integrals,
symmetries of, 12
tables of, 51
Oscillator (see Harmonic oscillator)
Outer product of groups, 160
Overlap of rotated deformed intrinsic states, 238–240

P
Parity conservation in compound-nucleus processes, 268, 273
Penetration factor, definition, 288
Perturbation theory of Coulomb excitation,
first order, 7, 15
interference term, 15, 16
interference term via the giant dipole resonance, 23
second order, 9
Physical sheet of Riemann surface, 353
Poles of the transition matrix, 353
Porter–Thomas distribution of nuclear widths, 329
Potential scattering phase shift of resonance theories, 323
Projectile excitation in reorientation experiments, 43
Propagator of the deuteron,
bare, 404
discussion, 401–405
full, 360

Q
Quadrupole moment, definition, 3
Quadrupole moment of excited 2^+ state, 33
Quadrupole moments of odd-A nuclei, 250
Quadrupole orientation energy, 3
Quadrupole polarization of closed shells, 244
Quadrupole moment of closed shells, effect on deformation, 247, 249
Quadrupole–quadrupole interaction,
in Hartree–Fock calculations, 216
in the SU_3 model, 100

R
Raising and lowering operators of the group SU_3, 166
Reciprocity theorem for nuclear reactions, 263, 273
Reduced width of nuclear resonance lines, definition, 322
Reorientation experiments,
experimental methods, 44
list of, 45
results, 46
Residual interaction, 74
Resonance theories, 321
Root mean square radii, 200
Rotational bands,
comparison of Hartree–Fock and rotational models, 241–243
energies in Hartree–Fock calculations, 237
obtained from Hartree–Fock calculations, 235
Rotational model,
and results of reorientation experiments, 48
and the nuclear ($1p$) shell, 77–79
validity of, 244

S
Safe bombarding energies in reorientation experiments, 28
Scattering,
amplitude, two-body, 345
by a separable potential, 401
length, definition, 346
length, neutron–neutron, 375
length, numerical values for two nucleons, 369
matrix, 380 (see also Collision matrix)
Scattering *(continued)*,
neutron–deuteron, idealized, 358
neutron–deuteron, idealized, higher L waves, 364
neutron–deuteron, idealized, integral equation for, 362
neutron–deuteron, idealized, partial wave analysis, 362
neutron–deuteron, idealized, s-wave phase shifts, 364
neutron–deuteron, with real nucleons, angular distributions, 370
neutron–deuteron, with real nucleons, elastic, 367, 390
neutron–deuteron, with real nucleons, inelastic, 372, 390
Semiclassical approximation in Coulomb excitation, 6
validity of, 30
Separable potentials, 359–361
direct solution, 378, 397
theory of scattering, 401
Shell model, general theory, 69–73
Shift function in nuclear reactions, definition, 288
Shift operators, 79, 80, 164
Single-particle energies,
resulting from Hartree–Fock calculations, 207
spherical, 196
spherical, choice of, 199
Single-particle Hamiltonian, 74, 185, 188
Single-particle potential, 69
Size resonances of nuclear transmission functions, 283–295
Spin cutoff parameter, 309, 314
Spin-orbit splitting, effect on Hartree–Fock calculations, 224
Spurious states,
rotational motion, 97
center-of-mass, 131
Square integrable or $L^{(2)}$ kernel, 353–354
Square well (complex), absorption of, 334
Statistical theory of nuclear reactions,
applications, 296
basic formulas, 271, 280
basis in resonance theory, 321
Strength function,
definition, 290
derived from optical model, 290–295
derived from resonance properties, 328–330
SU_3 group for elementary particles, 180

SU_3 model for nuclei,
accuracy in the $(2s, 1d)$ shell, 106
and Hartree–Fock theory, 144, 145, 223
application to light nuclei, 105
Casimir operators of bilinear form, 103
Casimir operators of trilinear form, 105
deformation of intrinsic state, 95–96
energy matrix, 174
$E2$ transition probability, 176
expansion coefficients, $a((\lambda\mu)\gamma\varepsilon\Lambda v,\alpha LK_L)$, 94
intrinsic state, 95
J-projected states, 98
L-projected states, 98
matrix elements between states, 170
maximum weight state, 95
multi-excitation states in the $(1p)$ shell, 142
multi-excitation states in the $(2s, 1d)$ shell, 139
negative-parity states in the $(2s, 1d)$ shell, 128
particle probability density distribution, 96
positive-parity states in the $(2s, 1d)$ shell, 109, 123
raising and lowering operators, 166
Symmetric group, S_k,
classification of states according to, 157
dimensions of representations, 158
Symmetrization of Coulomb excitation parameters, 13

T
Tamm–Dancoff states and SU_3, 148
Target nucleus,
corrections due to its recoil motion, 41
effect of its spectrum on reorientation experiments, 32
Temperature of nuclei, 265, 316
Tensor shift operators, 165
Three-pion interactions, 392
Transition matrix,
three-particle, 380
two-particle, 350–353
two-particle in the three-particle problem, 381
Transmission functions for nuclear reactions,
connection to resonance parameters, 328, 331
general properties, 281–295
in terms of optical model phase-shifts, 271
modified for spin–orbit coupling, 271
use in basic compound nucleus formulas, 271, 272, 280
Two-nucleon interaction,
choice of strength of, 199
effect of tensor force and hard core on the three-nucleon problem, 397
Rosenfeld force, 201, 206
Serber force, 202, 216
symmetries of its matrix elements, 189
Wigner, Bartlett, Heisenberg, Majorana components, 202, 213

U
Unitary group, U_3, classification of states according to, 159
Unphysical sheet of the Riemann surface, 353

V
Vibrational model compared with results of reorientation experiments, 48

W
Wigner supermultiplet theory, 76

Y
Young pattern of the symmetric group, 158